



**STRUCTURAL SYSTEMS
RESEARCH PROJECT**

Report No.
SSRP-06/20

**EXPERIMENTAL VERIFICATION OF
THE INFLUENCE OF TIME-
DEPENDENT MATERIAL
PROPERTIES ON LONG-TERM
BRIDGE CHARACTERISTICS**

by

**MICHAEL LEWIS
VISTASP M. KARBHARI**

Interim Report Submitted to the California Department of
Transportation Under Contract No. 59A0420.

August 2006

Department of Structural Engineering
University of California, San Diego
La Jolla, California 92093-0085

University of California, San Diego
Department of Structural Engineering
Structural Systems Research Project

Report No. SSRP-06/20

**Experimental Verification of the Influence of Time-
Dependant Material Properties on Long-Term Bridge
Characteristics**

by

Michael Lewis

Graduate Student Researcher

Vistasp M. Karbhari

Professor of Structural Engineering

Interim Report Submitted to the California Department of Transportation
Under Contract No. 59A0420

Department of Structural Engineering
University of California, San Diego
La Jolla, California 92093-0085

August 2006

1. Report No. FHWA/CA/ES-2006/24		2. Government Accession No.		3. Recipient's Catalog No.	
4. Title and Subtitle Experimental Verification of the Influence of Time-Dependent Material Properties on Long-Term Bridge Characteristics				5. Report Date August 2006	
				6. Performing Organization Code	
7. Author(s) Michael Lewis and Vistasp M. Karbhari				8. Performing Organization Report No. UCSD / SSRP-06/20	
9. Performing Organization Name and Address Department of Structural Engineering School of Engineering University of California, San Diego La Jolla, California 92093-0085				10. Work Unit No. (TRAIS)	
				11. Contract or Grant No. 59A0420	
12. Sponsoring Agency Name and Address California Department of Transportation Division of Engineering Services 1801 30 th St., West Building MS-9-2/51 Sacramento, California 95807				13. Type of Report and Period Covered Interim Report	
				14. Sponsoring Agency Code	
15. Supplementary Notes Prepared in cooperation with the State of California Department of Transportation. This report is one of a series of reports and should be read in conjunction with SSRP 2006/21					
16. Abstract Post-tensioned cast-in-place box girder bridges are commonly used in California. Losses in tension in the steel prestressing tendons used in these bridges occur over time due to creep and shrinkage of concrete and relaxation of the tendons. The use of existing methods in bridge specifications used to predict these long-term losses often result in inaccurate estimate of losses leading to severe serviceability problems. The current research program aims at developing a more precise method for predicting the long-term prestress loss in concrete bridges. Two spans in a recently constructed post-tensioned concrete bridge were instrumented with vibrating wire strain gages to monitor the long-term deformations and determine prestress loss. The recorded measurements of prestress loss were compared with the available equations from several bridge specifications as well as with analytical models developed for long-term deformations of concrete structures. To ensure accuracy in the values of the input material parameters, creep and shrinkage of concrete were simultaneously determined experimentally. This research has shown that shrinkage is highly dependent on environmental influences. Additionally, measured creep and shrinkage appeared to reach asymptotes faster than was indicated by best-fit equations, thus ultimate values may be closer to the minimum extrapolated values. It is noted that the available specifications equations for predicting prestress loss may not be sufficiently accurate. The analytical predictions of prestress loss exceed the monitored values in some cases and further investigation is being continued and will be reported in the final report for this project.					
17. Key Words Prestress loss, creep, shrinkage, experimental verification, box girder			18. Distribution Statement No restrictions. This document is available to the public through the National Technical Information Service, Springfield, Virginia 22161		
19. Security Classification (of this report) Unclassified		20. Security Classification (of this page) Unclassified		21. No. of Pages 498	22. Price

Disclaimer

The contents of this report reflect the views of the authors who are responsible for the facts and the accuracy of the data presented herein. The contents do not necessarily reflect the official views or policies of the State of California or the Federal Highway Administration. This report does not constitute a standard, specification, or regulation.

The United States Government does not endorse products or manufacturers. Trade and manufacturers' names appear in this report only because they are considered essential to the object of the document.

Table of Contents

Disclaimer	i
Table of Contents.....	ii
List of Symbols.....	viii
List of Figures	x
List of Tables	xxvii
Acknowledgements.....	xxx
Abstract.....	xxxi
1. Introduction	1
1.1. Background	2
1.1.1. Problems Resulting from Inaccurate Prestress Loss Estimation	2
1.1.2. Problems with Existing Methods.....	2
1.2. Research Objectives	3
1.3. Report Outline	4
1.4. Research Significance	4
2. Literature Review.....	5
2.1. Material Properties	5
2.1.1. Creep of Concrete	6
2.1.2. Shrinkage of Concrete.....	7
2.1.3. Relaxation of Prestressed Steel	7
2.2. Methods for Predicting Creep and Shrinkage	8
2.2.1. Inputs to the Specifications.....	9
2.2.2. AASHTO.....	12
2.2.3. ACI/PCI	14

2.2.4.	CEB-FIP	16
2.2.5.	CHBDC.....	20
2.2.6.	GL2000.....	23
2.2.7.	NCHRP.....	25
2.3.	Methods for Predicting Prestress Loss	28
2.3.1.	Input Parameters to the Specifications.....	29
2.3.2.	AASHTO Approximate Lump Sum Estimate of Time-Dependent Losses.....	31
2.3.3.	AASHTO Refined Estimates of Time-Dependent Losses.....	33
2.3.4.	CEB-FIP	34
2.3.5.	CHBDC.....	35
3.	Material Tests	37
3.1.	Motivation	37
3.2.	Testing Methodology	37
3.2.1.	Factors Influential to Tests	41
3.3.	Test Setup	43
3.3.1.	Curing.....	43
3.3.2.	Attachment of DEMEC points.....	44
3.3.3.	Hydrostone cap	44
3.3.4.	Creep Test Setup	45
3.4.	Processed Data	47
3.4.1.	Shrinkage Strain.....	48
3.4.2.	Creep Coefficient.....	49
3.5.	Calculation of Experimental Creep and Shrinkage	50

3.5.1.	Shrinkage	50
3.5.2.	Creep.....	59
3.6.	Curve-fitting	79
3.6.1.	Curve-fit for Shrinkage.....	81
3.6.2.	Curve-fit for Creep at First Loading	88
3.6.3.	Curve-fit for Creep at Second Loading	92
3.6.4.	Curve-fit for Creep at Third Loading	96
3.7.	Specifications Predictions of Creep and Shrinkage: Test Specimen	97
3.7.1.	Shrinkage Strain.....	100
3.7.2.	Creep from First Loading.....	105
3.7.3.	Creep from Second Loading.....	109
3.7.4.	Creep from Third Loading.....	113
3.8.	Specifications Predictions of Creep and Shrinkage: Bridge.....	114
3.8.1.	Shrinkage Strain.....	121
3.8.2.	Creep at First Loading.....	124
3.8.3.	Creep at Second Loading.....	127
3.8.4.	Creep at Third Loading.....	130
3.9.	Commentary on Creep and Shrinkage	132
4.	Analysis of I5/805 Truck Connector	134
4.1.	Introduction.....	134
4.2.	Description of I5/805 Truck Connector	134
4.2.1.	Frame 4	137
4.2.2.	Frame 5	137
4.3.	Capabilities of CPF	140

4.4.	Analysis Assumptions and Approximations	145
4.4.1.	Structural and Geometrical Assumptions	145
4.4.2.	Input Material Parameter Assumptions.....	148
4.5.	Frame Idealization	149
4.5.1.	Frame 4	150
4.5.2.	Frame 5	152
4.6.	Loading Events.....	153
4.6.1.	Loading Case 50/50	154
4.6.2.	Loading Case 100/0	156
5.	Field Measurements	158
5.1.	Introduction.....	158
5.2.	Instrumentation.....	159
5.3.	Data Monitoring	161
5.3.1.	Data Analysis	163
5.3.2.	Strain Results from Monitoring	184
5.3.3.	Discussion on Strains	217
5.4.	Strains from Analysis and Field Monitoring.....	218
5.4.1.	Frame Analysis.....	220
5.4.2.	Analysis Results of Frame 4.....	224
5.4.3.	Analysis Results of Frame 5.....	232
5.5.	Commentary for Frame 4 and Frame 5	238
6.	Long-Term Prestress Loss.....	243
6.1.	Introduction.....	243
6.2.	Prestress Loss obtained from Monitored Data.....	243

6.2.1.	Frame 4 Midspan.....	245
6.2.2.	Frame 4 Near the Bent.....	248
6.2.3.	Frame 5 Midspan.....	249
6.2.4.	Frame 5 Near the Bent.....	252
6.3.	Prestress Loss: Proposed Method.....	253
6.3.1.	Strain Profiles Determined Using the Proposed Method	254
6.3.2.	Proposed Method Prestress Loss	257
6.4.	Long-Term Prestress Loss: Specifications Predictions.....	259
6.5.	Prestress Loss from Analysis	261
6.5.1.	Initial Prestress Losses at Transfer	262
6.5.2.	Frame 4 Midspan.....	265
6.5.3.	Frame 4 Near the Bent.....	269
6.5.4.	Frame 5 Midspan.....	272
6.5.5.	Frame 5 Near the Bent.....	275
6.5.6.	Commentary on Predicted Long-Term Prestress Loss.....	278
6.5.7.	Total Long-Term Prestress Losses from all Influences.....	281
6.6.	Concrete Stresses	287
6.6.1.	Frame 4 Midspan.....	289
6.6.2.	Frame 4 Near the Bent.....	294
6.6.3.	Frame 5 Midspan.....	300
6.6.4.	Frame 5 Near the Bent.....	305
6.6.5.	Commentary on Long-Term Concrete Stress Predictions	310
7.	Conclusions	312
7.1.	Project Summary	312

7.2. Significant Findings	313
7.3. Research Discussion.....	315
7.4. Recommendations for Future Research.....	317
Appendix A	318
Appendix B	350
Appendix C	356
Appendix D	416
Appendix E	422
Appendix F.....	428
Appendix G	434
Appendix H	463
References	465

List of Symbols

A_c	Area of net concrete section
A_p	Area of prestressed steel
A_s	Area of non-prestressed reinforcement
E_c	Modulus of elasticity of concrete
E_s	Modulus of elasticity of non-prestressed steel
E_p	Modulus of elasticity of prestressed steel
f'_c	Characteristic concrete compressive strength at 28 days
f_{cgp}	Concrete stress at the level of the prestress centroid due to all permanent loads
f_{p0}	Initial stress in prestressed steel
f_{pu}	Ultimate stress in prestressed steel
f_{py}	Yield stress of prestressed steel
f_y	Yield stress of non-prestressed steel
Δf_{cdp}	Change in stress at the level of prestress imposed by loads applied after prestress transfer
h_0	Notional thickness
I_c	Second moment of inertia of net concrete section about its centroid
RH	Average relative humidity
t	Concrete age after casting
t_0	Concrete age at loading
t_s	Concrete age at the end of the curing period

V / S	Volume to surface area ratio for the concrete element
y_p	Depth of prestressed steel centroid measured downwards positive from centroid of net concrete section
α	Modular ratio of prestressed steel and concrete; E_p / E_c
χ	Aging coefficient of concrete
χ_r	Reduced relaxation coefficient
$\Delta\sigma_{cp}$	Change in concrete stress at level of prestress imposed by loads applied after prestress transfer
$\Delta\sigma_{pr}$	Intrinsic relaxation of prestressed steel
$\overline{\Delta\sigma_{pr}}$	Reduced relaxation of prestressed steel
$\Delta\sigma_{ps}$	Long-term change in prestress
$\varepsilon_{cs}(t, t_s)$	Free shrinkage of concrete between t_s and t
ϕ	Creep coefficient of concrete
$\phi(t, t_0)$	Creep coefficient of concrete between t_0 and t .
σ_{cg}	Initial stress in concrete at centroid of prestress tendons due to permanent loads after prestressing
σ_{cp0}	Initial stress in concrete at level of prestress tendons due to prestressing and self-weight

List of Figures

Figure 2.1: Creep of concrete under sustained load.	6
Figure 2.2: Values of coefficient k_s (Figure 8.4.1.5 from [9]).	22
Figure 2.3: Values of coefficient k_0 (Figure 8.4.1.6 (a) from [9]).	22
Figure 2.4: Values of coefficient β_d (Figure 8.4.1.6 (b) from [9]).	23
Figure 2.5: Values of coefficient k_f (Figure 8.4.1.6 (c) from [9]).	23
Figure 3.1: Layout of F4 with casting times of specific portions of the bridge cross section.	38
Figure 3.2: Concrete locations in the F4 superstructure cross section.....	38
Figure 3.3: Layout of F5 with casting times of specific portions of the bridge cross section.	39
Figure 3.4: Concrete locations in the F5 superstructure cross section.....	39
Figure 3.5: Map of UCSD and I5/805 Bridge locations.	40
Figure 3.6: Relative humidity recorded over the monitoring period.....	43
Figure 3.7: Locations of DEMEC points as positioned on a test specimen.....	44
Figure 3.8: Hydrostone cap placed on a test specimen.	45
Figure 3.9: Setup of creep test fixtures.	46
Figure 3.10: All creep test setups.....	47
Figure 3.11: Measuring with DEMEC gage.....	48
Figure 3.12: Experimental data collection timeline.....	48
Figure 3.13: Measured shrinkage strain from April batch concrete.....	54
Figure 3.14: Thermal strain during strain measuring of the April batch concrete.	55
Figure 3.15: True shrinkage strain from April batch concrete.	56

Figure 3.16: True shrinkage from October batch concrete.....	57
Figure 3.17: True shrinkage from November batch concrete.....	57
Figure 3.18: True shrinkage from March batch concrete.	58
Figure 3.19: True shrinkage from April batch concrete.	58
Figure 3.20: True shrinkage from May batch concrete.....	59
Figure 3.21: Measured creep strain from April batch concrete.	63
Figure 3.22: Average measured shrinkage (shrinkage and thermal) strain beginning at the end of curing from April batch concrete.....	64
Figure 3.23: Average shrinkage and thermal strains beginning after loading from April batch concrete.	65
Figure 3.24: Measured creep strain less shrinkage and thermal strains from April batch concrete.	66
Figure 3.25: Creep strain including initial elastic deformation from the April batch concrete.....	67
Figure 3.26: True creep strain (measured creep strain less shrinkage, thermal, and elastic strains) from April batch concrete.	68
Figure 3.27: Creep coefficient from the April batch concrete.	69
Figure 3.28: Creep coefficient from the October batch concrete (using measured shrinkage) from first loading (prestressing).....	71
Figure 3.29: Creep coefficient from the October batch concrete (using F5 shrinkage) from first loading (prestressing).....	71
Figure 3.30: Creep coefficient from the November batch concrete (using measured shrinkage) from first loading (prestressing).....	72
Figure 3.31: Creep coefficient from the November batch concrete (using F5 shrinkage) from first loading (prestressing).....	72
Figure 3.32: Creep coefficient from the March batch concrete (using measured shrinkage) from first loading (prestressing).....	73

Figure 3.33: Creep coefficient from the March batch concrete (using F5 shrinkage) from first loading (prestressing).....	73
Figure 3.34: Creep coefficient from the April batch concrete from first loading (prestressing).....	74
Figure 3.35: Creep coefficient from the May batch concrete from first loading (prestressing).....	74
Figure 3.36: Creep coefficient from the October batch concrete (using measured shrinkage) from second loading (removal of falsework).....	75
Figure 3.37: Creep coefficient from the October batch concrete (using F5 shrinkage) from second loading (removal of falsework).....	75
Figure 3.38: Creep coefficient from the November batch concrete (using measured shrinkage) from second loading (removal of falsework).....	76
Figure 3.39: Creep coefficient from the November batch concrete (using F5 shrinkage) from second loading (removal of falsework).....	76
Figure 3.40: Creep coefficient from the March batch concrete (using measured shrinkage) from second loading (removal of falsework).....	77
Figure 3.41: Creep coefficient from the March batch concrete (using F5 shrinkage) from second loading (removal of falsework).....	77
Figure 3.42: Creep coefficient from the April batch concrete from second loading (removal of hinge supporting falsework).	78
Figure 3.43: Creep coefficient from the May batch concrete from second loading (removal of hinge supporting falsework).	79
Figure 3.44: Average true shrinkage (F4 experimental) for the October batch concrete with best-fit curve.	82
Figure 3.45: Average true shrinkage (F5 experimental) for the October batch concrete.	83
Figure 3.46: Average true shrinkage for the October batch concrete.....	83

Figure 3.47: Average true shrinkage (F4 experimental) for the November batch concrete with best-fit curve.	84
Figure 3.48: Average true shrinkage (F5 experimental) for the November batch concrete.	84
Figure 3.49: Average true shrinkage for the November batch concrete.	85
Figure 3.50: Average true shrinkage (experimental) for the March batch concrete with best-fit curve.	85
Figure 3.51: Average true shrinkage (F5 experimental) for the March batch concrete.	86
Figure 3.52: Average true shrinkage for the November batch concrete.	86
Figure 3.53: Average true shrinkage for the April batch concrete with best-fit curve.	87
Figure 3.54: Average true shrinkage for the May batch concrete with best-fit curve.	87
Figure 3.55: Average creep coefficient from the October batch concrete (measured shrinkage) from first loading (prestressing).	88
Figure 3.56: Average creep coefficient from the October batch concrete (F5 shrinkage) from first loading (prestressing).	89
Figure 3.57: Average creep coefficient from the November batch concrete (measured shrinkage) from first loading (prestressing).	89
Figure 3.58: Average creep coefficient from the November batch concrete (F5 shrinkage) from first loading (prestressing).	90
Figure 3.59: Average creep coefficient from the March batch concrete (measured shrinkage) from first loading (prestressing).	90
Figure 3.60: Average creep coefficient from the March batch concrete (F5 shrinkage) from first loading (prestressing).	91

Figure 3.61: Average creep coefficient from the April batch concrete (measured shrinkage) from first loading (prestressing).....	91
Figure 3.62: Average creep coefficient from the May batch concrete (measured shrinkage) from first loading (prestressing).....	92
Figure 3.63: Average creep coefficient from the October batch concrete (measured shrinkage) from second loading (removal of falsework).....	93
Figure 3.64: Average creep coefficient from the October batch concrete (F5 shrinkage) from second loading (removal of falsework).....	93
Figure 3.65: Average creep coefficient from the November batch concrete (measured shrinkage) from second loading (removal of falsework).....	94
Figure 3.66: Average creep coefficient from the November batch concrete (F5 shrinkage) from second loading (removal of falsework).....	94
Figure 3.67: Average creep coefficient from the March batch concrete (measured shrinkage) from second loading (removal of falsework).....	95
Figure 3.68: Average creep coefficient from the March batch concrete (F5 shrinkage) from second loading (removal of falsework).....	95
Figure 3.69: Average creep coefficient from the April batch concrete (measured shrinkage) from second loading (removal of hinge supporting falsework). ..	96
Figure 3.70: Average creep coefficient from the May batch concrete (measured shrinkage) from second loading (removal of hinge supporting falsework). ..	96
Figure 3.71: Experimental and predicted test specimen shrinkage for the F4 October concrete at first loading (prestressing) using measured shrinkage.	101
Figure 3.72: Experimental and predicted test specimen shrinkage for the F4 October concrete at first loading (prestressing) using F5 shrinkage.	101
Figure 3.73: Experimental and predicted test specimen shrinkage for the F4 November concrete at first loading (prestressing) using measured shrinkage.	102

Figure 3.74: Experimental and predicted test specimen shrinkage for the F4 November concrete at first loading (prestressing) using F5 shrinkage.102

Figure 3.75: Experimental and predicted test specimen shrinkage for the F4 March concrete at first loading (prestressing) using measured shrinkage. 103

Figure 3.76: Experimental and predicted test specimen shrinkage for the F4 March concrete at first loading (prestressing) using F5 shrinkage..... 103

Figure 3.77: Experimental and predicted test specimen shrinkage for the F5 April concrete at first loading (prestressing)..... 104

Figure 3.78: Experimental and predicted test specimen shrinkage for the F5 May concrete at first loading (prestressing)..... 104

Figure 3.79: Experimental and predicted test specimen creep coefficient (using measured shrinkage) for the F4 October concrete at first loading (prestressing).....105

Figure 3.80: Experimental and predicted test specimen creep coefficient (using F5 shrinkage) for the F4 October concrete at first loading (prestressing). .105

Figure 3.81: Experimental and predicted test specimen creep coefficient (using measured shrinkage) for the F4 November concrete at first loading (prestressing).....106

Figure 3.82: Experimental and predicted test specimen creep coefficient (using F5 shrinkage) for the F4 November concrete at first loading (prestressing). 106

Figure 3.83: Experimental and predicted test specimen creep coefficient (using measured shrinkage) for the F4 March concrete at first loading (prestressing)..... 107

Figure 3.84: Experimental and predicted test specimen creep coefficient (using F5 shrinkage) for the F4 March concrete at first loading (prestressing)..... 107

Figure 3.85: Experimental and predicted test specimen creep coefficient (using measured shrinkage) for the F5 April concrete at first loading (prestressing).
..... 108

Figure 3.86: Experimental and predicted test specimen creep coefficient (using measured shrinkage) for the F5 May concrete at first loading (prestressing).
..... 108

Figure 3.87: Experimental and predicted test specimen creep coefficient (using measured shrinkage) for the F4 October concrete at second loading (removal of falsework). 109

Figure 3.88: Experimental and predicted test specimen creep coefficient (using F5 shrinkage) for the F4 October concrete at second loading (removal of falsework). 110

Figure 3.89: Experimental and predicted test specimen creep coefficient (using measured shrinkage) for the F4 November concrete at second loading (removal of falsework). 110

Figure 3.90: Experimental and predicted test specimen creep coefficient (using F5 shrinkage) for the F4 November concrete at second loading (removal of falsework). 111

Figure 3.91: Experimental and predicted test specimen creep coefficient (using measured shrinkage) for the F4 March concrete at second loading (removal of falsework). 111

Figure 3.92: Experimental and predicted test specimen creep coefficient (using F5 shrinkage) for the F4 March concrete at second loading (removal of falsework). 112

Figure 3.93: Predicted test specimen creep coefficient for the F5 April concrete at second loading (removal of falsework). 112

Figure 3.94: Predicted test specimen creep coefficient for the F5 May concrete at second loading (removal of falsework). 113

Figure 3.95: Experimental and predicted test specimen creep coefficient for the F5 April concrete at second loading (removal of hinge supporting falsework).	114
Figure 3.96: Experimental and predicted test specimen creep coefficient for the F5 May concrete at second loading (removal of hinge supporting falsework).	114
Figure 3.97: Example representative range of shrinkage for the concrete used in the material tests.	118
Figure 3.98: Example representative range of creep for the concrete used in the material tests.	121
Figure 3.99: Experimental and predicted bridge shrinkage strain for the F4 October concrete.	122
Figure 3.100: Experimental and predicted bridge shrinkage strain for the F4 November concrete.	122
Figure 3.101: Experimental and predicted bridge shrinkage strain for the F4 March concrete.	123
Figure 3.102: Experimental and predicted bridge shrinkage strain for the F5 April concrete.	123
Figure 3.103: Experimental and predicted bridge shrinkage strain for the F5 May concrete.	124
Figure 3.104: Experimental and predicted bridge creep coefficient for the F4 October concrete at first loading (prestressing).	125
Figure 3.105: Experimental and predicted bridge creep coefficient for the F4 November concrete at first loading (prestressing).	125
Figure 3.106: Experimental and predicted bridge creep coefficient for the F4 March concrete at first loading (prestressing).	126
Figure 3.107: Experimental and predicted bridge creep coefficient for the F5 April concrete at first loading (prestressing).	126

Figure 3.108: Experimental and predicted bridge creep coefficient for the F5 May concrete at first loading (prestressing).....	127
Figure 3.109: Experimental and predicted bridge creep coefficient for the F4 October concrete at second loading (removal of falsework).	128
Figure 3.110: Experimental and predicted bridge creep coefficient for the F4 November concrete at second loading (removal of falsework).	128
Figure 3.111: Experimental and predicted bridge creep coefficient for the F4 March concrete at second loading (removal of falsework).....	129
Figure 3.112: Experimental and predicted bridge creep coefficient for the F5 April concrete at second loading (removal of falsework).....	129
Figure 3.113: Experimental and predicted bridge creep coefficient for the F5 May concrete at second loading (removal of falsework).....	130
Figure 3.114: Experimental and predicted bridge creep coefficient for the F5 April concrete at third loading (removal of hinge supporting falsework).	131
Figure 3.115: Experimental and predicted bridge creep coefficient for the F5 May concrete at third loading (removal of hinge supporting falsework).	131
Figure 4.1: Layout of I5/805 Bridge and surrounding highways.	136
Figure 4.2: Layout of F4.....	137
Figure 4.3: Layout of F5.....	138
Figure 4.4: Example representative range of shrinkage for the concrete used in the material tests.	142
Figure 4.5: Example representative range of creep for the concrete used in the material tests.	142
Figure 4.6: Layout of actual bridge cross sections.	149
Figure 4.7: Layout of idealized bridge cross sections.	150
Figure 4.8: Idealization of F4.	151
Figure 4.9: Idealized cross sections of F4 at midspan and near the bent.	152

Figure 4.10: Idealization of F5.	152
Figure 4.11: Idealized cross sections of F5 at midspan and near the bent.	153
Figure 4.12: Loads applied on F4 initially at prestressing for the LC50/50 load case.....	154
Figure 4.13: Loads applied on F4 at the removal of falsework for the LC50/50 load case..	155
Figure 4.14: Loads applied on F5 initially at prestressing for the LC50/50 load case.....	155
Figure 4.15: Loads applied on F5 at the removal of falsework for the LC50/50 load case..	155
Figure 4.16: Loads applied on F5 at the removal of falsework supporting the hinge (hinge loading) for the LC50/50 load case.	156
Figure 4.17: Loads applied on F4 at prestressing for the LC100/0 load case. ...	157
Figure 4.18: Loads applied on F5 at prestressing for the LC100/0 load case. ...	157
Figure 5.1: Elevation view of typical placement of VW strain gages affixed to longitudinal reinforcement.....	159
Figure 5.2: Typical locations of strain gages as mounted through the superstructure cross-section for both F4 and F5 and cardinal orientation.	160
Figure 5.3: Correlation between change in temperature and change in strain.	165
Figure 5.4: Average temperature in F4 and ambient air temperature during the monitoring period.	168
Figure 5.5: Average temperature in F5 and ambient air temperature during the monitoring period.	168
Figure 5.6: Maximum daily variation in strain in Stem A of F4 and F5.	170
Figure 5.7: Daily variation in concrete temperature in Stem A of F4 and F5 at 3:00 am.....	171
Figure 5.8: Strain in Stem A of F5 in the soffit.	173

Figure 5.9: Temperature in Stem A of F5 in the soffit.	173
Figure 5.10: Strain in Stem A of F5 in the deck.	174
Figure 5.11: Temperature in Stem A of F5 in the deck.	174
Figure 5.12: Strain in Stem A of F5 in the web.	174
Figure 5.13: Temperature in Stem A of F5 in the web.	175
Figure 5.14: Strain in Stem C of F5 in the deck.	176
Figure 5.15: Temperature in Stem C of F5 in the deck.	176
Figure 5.16: Strain in Stem C of F5 in the web.	177
Figure 5.17: Temperature in Stem C of F5 in the web.	177
Figure 5.18: Strain in Stem C of F5 in the soffit.	178
Figure 5.19: Temperature in Stem C of F5 in the soffit.	178
Figure 5.20: Temperature profile over a 24-hour period 100 days after prestressing in Stem A of F5 at midspan.	180
Figure 5.21: Temperature profile over a 24-hour period 100 days after prestressing in Stem C of F5 at midspan.	181
Figure 5.22: Temperature profile over a 24-hour period 150 days after prestressing in Stem A of F5 at midspan.	182
Figure 5.23: Temperature profile over a 24-hour period 150 days after prestressing in Stem C of F5 at midspan.	182
Figure 5.24: Determination of the change in moment from monitored data.	184
Figure 5.25: Change in moment for F4 at midspan.	186
Figure 5.26: Monitored strain in the deck at 3:00 am in F4 at the midspan section.	186
Figure 5.27: Monitored strain in the web at 3:00 am in F4 at the midspan section.	187

Figure 5.28: Monitored strain in the soffit at 3:00 am in F4 at the midspan section.	188
Figure 5.29: Monitored strains in Stem A in F4 at midspan.	189
Figure 5.30: Monitored strains in Stem B in F4 at midspan.	189
Figure 5.31: Monitored strains in Stem C in F4 at midspan.	190
Figure 5.32: Monitored strains in Stem D in F4 at midspan.	190
Figure 5.33: Monitored strain profile at prestressing and at T363 in F4 at midspan without faulty gage readings at 3:00 am.	191
Figure 5.34: Vertical displacement of F4 at midspan.	192
Figure 5.35: Monitored strain in the deck at 3:00 am in F4 at the near-bent section.	193
Figure 5.36: Monitored strain in the web at 3:00 am in F4 at the near-bent section.	194
Figure 5.37: Monitored strain in the soffit at 3:00 am in F4 at the near-bent section.	195
Figure 5.38: Change in moment for F4 at midspan and near the bent.....	197
Figure 5.39: Monitored strains in Stem A in F4 near the bent.....	198
Figure 5.40: Monitored strains in Stem B in F4 near the bent.....	199
Figure 5.41: Monitored strains in Stem C in F4 near the bent.....	199
Figure 5.42: Monitored strains in Stem D in F4 near the bent.....	199
Figure 5.43: Monitored strains at prestressing and T363 in F4 near the bent at 3:00 am.....	200
Figure 5.44: Monitored strain profile at prestressing and T363 in F4 near the bent without faulty gage readings at 3:00 am.	201
Figure 5.45: Change in moment for F5 at midspan.....	203

Figure 5.46: Monitored strain in the deck at 3:00 am in F5 at the midspan section.	204
Figure 5.47: Monitored strain in the web at 3:00 am in F5 at the midspan section.	204
Figure 5.48: Monitored strain in the soffit at 3:00 am in F5 at the midspan section.	205
Figure 5.49: Monitored strains in Stem A in F5 at midspan.	206
Figure 5.50: Monitored strains in Stem B in F5 at midspan.	206
Figure 5.51: Monitored strains in Stem C in F5 at midspan.	207
Figure 5.52: Monitored strains in Stem D in F5 at midspan.	207
Figure 5.53: Monitored strain profile at prestressing and T303 in F5 at midspan without faulty gage readings at 3:00 am.	208
Figure 5.54: Vertical displacement of F5 at significant intervals during monitoring.	209
Figure 5.55: Monitored strain in the deck at 3:00 am in F5 at the near-bent section.	210
Figure 5.56: Monitored strain in the web at 3:00 am in F5 at the near-bent section.	211
Figure 5.57: Changes in moment for F5 at midspan and near the near-bent....	212
Figure 5.58: Monitored strain in the soffit at 3:00 am in F5 at the near-bent section.	213
Figure 5.59: Vertical displacement of span 16 in F5.	214
Figure 5.60: Monitored strains in Stem A in F5 near the bent.	215
Figure 5.61: Monitored strains in Stem B in F5 near the bent.	215
Figure 5.62: Monitored strains in Stem C in F5 near the bent.	215
Figure 5.63: Monitored strains in Stem D in F5 near the bent.	216

Figure 5.64: Monitored strain profile at prestressing and T303 in F5 near the bent from gage readings at 3:00 am.	217
Figure 5.65: Cross-section of F4 at midspan.	225
Figure 5.66: Strain profile in F4 at midspan immediately after prestressing.....	225
Figure 5.67: Strain profile in F4 at midspan at T363.	225
Figure 5.68: Strain profile in F4 at midspan at a theoretical end of service life .	225
Figure 5.69: Cross-section of F4 near the bent.....	226
Figure 5.70: Strain profile of F4 near the bent immediately after prestressing. .	226
Figure 5.71: Strain profile of F4 near the bent at T363.	226
Figure 5.72: Strain profile of F4 near the bent at a theoretical end service life. .	226
Figure 5.73: Typical development of long-term creep of concrete in F4 and F5.	228
Figure 5.74: Typical development of long-term shrinkage of concrete in F4 and F5	229
Figure 5.75: Cross-section of F5 at midspan.	233
Figure 5.76: Strain profile of F5 at midspan immediately after prestressing.	233
Figure 5.77: Strain profile of F5 at midspan at T303.....	233
Figure 5.78: Strain profile of F5 at midspan at a theoretical end of service life. .	233
Figure 5.79: Cross-section of F5 near the bent.....	234
Figure 5.80: Strain profile of F5 near the bent immediately after prestressing. .	234
Figure 5.81: Strain profile of F5 neat the bent at T303.....	234
Figure 5.82: Strain profile of F5 near the bent at a theoretical end of service life.	234
Figure 6.1: Prestress losses resulting from creep and shrinkage in F4 at midspan between prestressing and T363.....	245

Figure 6.2: Intrinsic relaxation of tendons used in F4 between prestressing and T363.	246
Figure 6.3: Reduced relaxation of tendons used in F4 between prestressing and T363.	247
Figure 6.4: Prestress losses resulting from creep, shrinkage, and relaxation in F4 at midspan between prestressing and T363.	247
Figure 6.5: Prestress losses resulting from creep and shrinkage in F4 near the bent between prestressing and T363.....	248
Figure 6.6: Prestress losses resulting from creep, shrinkage, and relaxation in F4 near the bent between prestressing and T363.....	249
Figure 6.7: Prestress losses resulting from creep and shrinkage in F5 at midspan between prestressing and T303.....	250
Figure 6.8: Intrinsic relaxation of tendons used in F5 between prestressing and T303.	250
Figure 6.9: Reduced relaxation of tendons for F5 between prestressing and T303.	251
Figure 6.10: Prestress losses resulting from creep, shrinkage, and relaxation in F5 at midspan between prestressing and T303.....	251
Figure 6.11: Prestress losses resulting from creep and shrinkage in F5 near the bent between prestressing and T303.....	252
Figure 6.12: Prestress losses resulting from creep, shrinkage, and relaxation in F5 near the bent between prestressing and T303.	253
Figure 6.13: Strain profiles for the monitored midspan section in F4 at prestressing, T363, and the theoretical end of service life using CEB-FIP material property inputs.	255
Figure 6.14: Strain profiles for the monitored section near the bent in F4 at prestressing, T363, and the theoretical end of service life using CEB-FIP material property inputs.	256

Figure 6.15: Strain profiles for the monitored midspan section in F5 at prestressing, T303, and the theoretical end of service life using CEB-FIP material property inputs.	256
Figure 6.16: Strain profiles for the monitored section near the bent in F5 at prestressing, T303, and the theoretical end of service life using CEB-FIP material property inputs.	257
Figure 6.17: Prestress loss in F4 at midspan.	267
Figure 6.18: Prestress loss in F4 near the bent.	270
Figure 6.19: Prestress loss in F5 at midspan.	273
Figure 6.20: Prestress loss in F5 near the bent.	276
Figure 6.21: Stress profiles at prestressing and the theoretical end of service life obtained using CPF; 50% self-weight applied at prestressing and remaining 50% applied with the removal of falsework in F4 at midspan.	290
Figure 6.22: Stress profiles at prestressing and the theoretical end of service life obtained using CPF and the Proposed Method; 100% self-weight applied at prestressing in F4 at midspan.	291
Figure 6.23: Stress profiles determined with the specifications using the full self-weight at prestressing in F4 at midspan.	292
Figure 6.24: Stress profiles determined with the specifications using 50% of the self-weight at prestressing in F4 at midspan.	292
Figure 6.25: Stress profiles at prestressing and the theoretical end of service life obtained using CPF; 50% self-weight applied at prestressing and remaining 50% applied with the removal of falsework in F4 near the bent.	295
Figure 6.26: Stress profiles at prestressing and the theoretical end of service life obtained using CPF and the Proposed Method; 100% self-weight applied at prestressing in F4 near the bent.	296
Figure 6.27: Stress profiles determined with the specifications using the full self-weight at prestressing in F4 near the bent.	297

Figure 6.28: Stress profiles determined with the specifications using 50% of the self-weight at prestressing in F4 near the bent. 298

Figure 6.29: Stress profiles at prestressing and the theoretical end of service life obtained using CPF; 50% self-weight applied at prestressing and remaining 50% applied with the removal of falsework in F5 at midspan..... 301

Figure 6.30: Stress profiles at prestressing and the theoretical end of service life obtained using CPF and the Proposed Method; 100% self-weight applied at prestressing in F5 at midspan..... 302

Figure 6.31: Stress profiles determined with the specifications using the full self-weight at prestressing in F5 at midspan. 303

Figure 6.32: Stress profiles determined with the specifications using 50% of the self-weight at prestressing in F5 at midspan..... 303

Figure 6.33: Stress profiles at prestressing and the theoretical end of service life obtained using CPF; 50% self-weight applied at prestressing and remaining 50% applied with the removal of falsework in F5 near the bent. 306

Figure 6.34: Stress profiles at prestressing and the theoretical end of service life obtained using CPF and the Proposed Method; 100% self-weight applied at prestressing in F4 near the bent. 307

Figure 6.35: Stress profiles determined with the specifications using the full self-weight at prestressing in F5 near the bent. 307

Figure 6.36: Stress profiles determined with the specifications using 50% of the self-weight at prestressing in F5 near the bent. 308

List of Tables

Table 2.1: Input parameters to specifications for determining creep.....	11
Table 2.2: Input parameters to specifications for determining shrinkage.	11
Table 2.3: Values of coefficients ε_b and k_r . (After Table 8.4.1.5 from [9]).....	21
Table 2.4: Inputs used in considered specifications to calculate prestress loss..	30
Table 3.1: Concrete casting dates and reference names.....	37
Table 3.2: Table of values associated with the calculation of shrinkage from the April batch concrete from F5.....	52
Table 3.3: Table of values associated with the calculation of creep from the April batch concrete from F5.....	61
Table 3.4: Coefficients for the curve-fit [15] equations for each concrete type....	81
Table 3.5: Inputs as used in specifications for prediction of creep and shrinkage for the test specimens and bridge.....	98
Table 3.6: Values associated with the calculation of experimental shrinkage for the bridge.....	117
Table 3.7: Values associated with the calculation of experimental creep for the bridge.....	119
Table 4.1: Dates and ages of significant construction events of F4.	139
Table 4.2: Dates and ages of significant construction events of F5.	139
Table 4.3: Material properties used in the analysis of F4 at significant construction events.....	143
Table 4.4: Material properties used in the analysis of F5 at significant construction events.....	144
Table 5.1: Gage depths for F4.	160
Table 5.2: Gage depths for F5.	161
Table 5.3: Thermal expansion coefficients for all gage locations.....	166

Table 5.4: Material property inputs used for analysis of F4.....	222
Table 5.5: Material property inputs used for analysis of F5.....	223
Table 5.6: Monitored and analytical strains at the level of the centroid of the prestressing tendons in F4.....	230
Table 5.7: Monitored and analytical strains at the level of the centroid of the prestressing tendons in F5.....	237
Table 6.1: Inputs used in the Proposed Method [29].....	254
Table 6.2: Comparison of prestress loss values determined using the Proposed Method and CPF at significant instances during the life of the structure (LC100/0).....	258
Table 6.3: Input parameters used in the specifications for predicting prestress loss in F4 and F5.	260
Table 6.4: Prestress loss values for F4 at the end of service life determined using the specifications.	261
Table 6.5: Prestress loss values for F5 at the end of service life determined using the specifications.	261
Table 6.6: Prestress losses before and after stress transfer in F4.....	264
Table 6.7: Prestress losses before and after stress transfer in F5.....	265
Table 6.8: Prestress loss values calculated for F4 at midspan for points in time at T363 and the theoretical end of service life.	268
Table 6.9: Prestress loss values calculated for F4 near the bent for points in time at T363 and the theoretical end of service life.	271
Table 6.10: Prestress loss values calculated for F5 at midspan for points in time at T303 and the theoretical end of service life.	274
Table 6.11: Prestress loss values calculated for F5 near the bent for points in time at T303 and the theoretical end of service life.....	277

Table 6.12: Total prestress losses from all influences in F4 at midspan at the end of service life.....	282
Table 6.13: Total prestress losses from all influences in F4 near the bent at the end of service life.....	283
Table 6.14: Total prestress losses from all influences in F5 at midspan at the end of service life.....	285
Table 6.15: Total prestress losses from all influences in F5 near the bent at the end of service life.....	286
Table 6.16: Stresses from all considered methods at the theoretical end of service life in F4 at midspan.	294
Table 6.17: Stresses from all considered methods at the theoretical end of service life in F4 near the bent.....	299
Table 6.18: Stresses from all considered methods at the theoretical end of service life in F5 at midspan.	304
Table 6.19: Stresses from all considered methods at the theoretical end of service life in F5 near the bent.....	309

Acknowledgements

I would like to express my most sincere gratitude to my advisor, Professor Vistasp M. Karbhari. He questioned my rationale for attacking problems, in effect forcing me to develop better solutions to many of the issues encountered. I am appreciative of him allowing me the opportunity to conduct research under his tutelage.

I must acknowledge the assistance and direction received from Dr. Samer A. Youakim. His expertise in this field and ability to assist me with many of the issues encountered within this research is much appreciated.

Appreciation is deserved by Caltrans for supporting this research, in particular, Bob Dougherty, Sampson Engeda, Jay Gittin, and their support staff for enabling the placement of instruments and monitoring devices in the field as well as Dr. Charles Sikorsky and Susan Hida for technical discussions.

Thanks must be given to my friends Don Phillippi, Patrick Wilcox, Stephanie Svetlik, Johnson Lee, Ali Shirazi, and Jason Delaney. These individuals provided much needed support and were always willing to lend themselves to assisting me with various issues.

Of most importance, I would like to articulate my loving appreciation to my parents. Had they not reinforced my curiosity with building things when I was young, I would not have developed an acute curiosity for this field that I so wholeheartedly enjoy or arrived where I am today.

ABSTRACT OF THE REPORT

Experimental Verification of the Influence of Time-Dependent Material Properties on Long-Term Bridge Characteristics

Post-tensioned cast-in-place box girder bridges are commonly used in California. Losses in tension in the steel prestressing tendons used in these bridges occur over time due to creep and shrinkage of concrete and relaxation of the tendons. The use of existing methods in bridge specifications used to predict these long-term losses often result in inaccurate estimate of losses leading to severe serviceability problems.

The current research program aims at developing a more precise method for predicting the long-term prestress loss in concrete bridges. Two spans in a recently constructed post-tensioned concrete bridge were instrumented with vibrating wire strain gages to monitor the long-term deformations and determine prestress loss.

The recorded measurements of prestress loss were compared with the available equations from several bridge specifications as well as with analytical models developed for long-term deformations of concrete structures. To ensure accuracy in the values of the input material parameters, creep and shrinkage of concrete were simultaneously determined experimentally.

This research has shown that shrinkage is highly dependent on environmental influences. Additionally, measured creep and shrinkage appeared to reach asymptotes faster than was indicated by best-fit equations, thus ultimate values may be closer to the minimum extrapolated values. It is noted that the available specifications equations for predicting prestress loss may not be sufficiently accurate. The analytical predictions of prestress loss exceed the monitored values in some cases and further investigation is being continued and will be reported in the final report for this project.

1. Introduction

Post-tensioned cast-in-place box girder bridges are the most popular bridge type in California. The majority of these bridges incorporate several spans that form a continuous frame. Frame construction is preferred in California for the increased ability to resist and dissipate seismic loads. As a result, continuity created by the frame imposes several restraints that cannot be treated simply in analysis. The steel prestressing tendons used for prestressing in these bridges lose some of their initial tension over time as a result of creep and shrinkage of concrete and tendon relaxation.

Although several bridge specifications are available for the prediction of long-term prestress losses, these methods often result in inaccurate estimate of losses. The loss in prestress is generally considered not to affect the ultimate capacity of a prestressed member; however, such inaccuracies can lead to severe serviceability problems, such as cracking and excessive deflection, and uneconomic design.

There are two main sources of error in the current specifications. The first is the inaccurate use or representation of the long-term material properties including the creep coefficient and shrinkage of concrete and the relaxation of prestressing steel. The second source of error is inaccuracy in the method of analysis. Although some advanced methods exist for making more accurate predictions than those available through specifications, industry is reluctant to adopt such methods primarily because they are not backed by experimental proof.

Current research at UCSD aims at developing a more precise method to predict the long-term prestress loss in concrete bridges. This method is to be verified against field measurements of prestress loss in concrete bridges in California. As part of the monitoring program, two spans in a recently completed post-tensioned bridge, as part of the Interstate 5 to Interstate 805 (I5/805) Truck Connector in San Diego, California, were instrumented to monitor the long-term deformations; one span from Frame 4 (F4) and the other from Frame 5 (F5).

Further research will be done on several spans in a new bridge being constructed in Riverside, California.

1.1. Background

1.1.1. Problems Resulting from Inaccurate Prestress Loss

Estimation

Serviceability problems may exist as a result of incorrect estimate of prestress loss. Both over- and under-estimation of the prestress loss can have adverse impact. Underestimation of the prestress loss can lead to cracking and excessive deflection. Overestimation of the loss might lead to excessive camber or uneconomic design because of an increased number of prestressing tendons and requisite stress. Increased prestress load can also result in excessive shortening of the bridge members. Attempts to rectify these serviceability problems might lead to additional or excessive costs.

1.1.2. Problems with Existing Methods

Many methodologies exist for the determination of prestress loss. Several major problems exist in these methods, which makes them unsuitable. The main sources of error in these specifications procedure are the inaccurate use or representation of the long-term material properties (creep, shrinkage, and relaxation) and inaccuracy in the methods of analysis used.

Some of the methodologies developed for the specifications were formulated from tests of concrete members. These tests are dependent on material properties and environmental conditions used in the tests, which vary considerably on a nationwide basis. Some of the design equations do not include factors for adjusting the equations for local constituents, making some of the equations unsuitable for use in an area with different conditions as those from the testing procedure. The influence of creep, shrinkage, and relaxation are accounted for through empirical coefficients determined experimentally. Such

coefficients are valid only for the conditions and geometry in which tests or analytical procedures were conducted.

Several specifications that provide estimates for prestress loss also include formulations for creep and shrinkage prediction; however, in separate portions of the written specifications. There is no association between the calculated material properties and the inputs to the prestress loss equations. Material properties included in the prestress loss equations are only treated through coefficients developed through the testing regime

These specifications ignore the non-prestressed steel or account for its presence through incorrect assumptions. In such a condition, equilibrium and compatibility are not satisfied. The resultant of stress change in concrete, non-prestressed steel and prestressed steel must sum to zero. Neglecting the presence of non-prestressed steel would underestimate the change in concrete stresses, which are often tensile, and overestimate the remaining compressive stress in the concrete.

1.2. Research Objectives

The aim of this research is two-fold, corresponding to the two major problematic areas in current practice. The first objective is to examine the current specifications available for predicting the creep coefficient and shrinkage strain. These predictions are compared to the experimentally derived creep and shrinkage in an effort to disclose any major discrepancies. The second part of the research examines prestress loss in the monitored portions of the bridge. Computer analyses are performed on the monitored spans of the bridge and to examine the influence of creep and shrinkage on the prestress loss and the influence of these factors on continuous framed configurations of the bridge. The results of these analyses are compared to the predictions in current specifications and the results of monitoring.

1.3. Report Outline

Chapters are laid out such that the experimental procedures described, then comparisons between experimental and predicted behavior is made. Chapter 2 is a literature review of the available methods that can be used to predict creep and shrinkage in concrete and the methods available for predicting prestress loss. This is followed with the introduction of the material tests conducted on several test specimens composed of the concrete taken on the days concrete was cast in the bridge. Further in this chapter are the predictions of material test properties made by the specifications reviewed in Chapter 2. This chapter concludes with comparisons between the experimental and predicted material test properties. Refined methods for predicting prestress losses are covered in as well as the loss indicated through use of specifications. The instrumentation of the bridge frames is described in Chapter 5 in addition to the indicated stress and strain obtained through monitoring. Research conclusions and recommendations are presented in Chapter 7.

1.4. Research Significance

A considerable number of available methods for predicting the prestress loss are unsatisfactory. In design, the correct prestress loss must be accounted to ensure acceptable service performance. The motive for this research is to utilize advanced methods to accurately predict the long-term deformation of the bridge. Material tests were conducted to provide experimental creep and shrinkage to avoid using the specifications that are not accurate in every case. Several bridge spans were instrumented to record the strain occurring within the bridge over time. These monitored strains were used to verify the accuracy of the advanced computer analyses.

2. Literature Review

The methods for predicting specific time-dependent material properties – creep and shrinkage of concrete and prestressing steel relaxation, and prestress loss of a bridge, outlined in this chapter – represent the current state of the art. Though not exhaustive of all methods, those covered represent the general state of understanding of these issues. The methods reviewed are those that will typically be selected for use in design.

This chapter is laid out to first present the material properties that are of key importance to the time-dependent material changes in bridges that are often misunderstood and misinterpreted in use. Several of the available specifications for predicting creep and shrinkage are presented. The next portion of this chapter discusses several of the available specifications for predicting the prestress loss and identifies the inherent differences among the methods. These specifications are used in subsequent chapters as a basis of comparison with advanced analysis predictions of prestress loss as well as the loss obtained from the field monitoring of the I5/805 Bridge.

2.1. Material Properties

The material characteristics of creep, shrinkage, and relaxation are generally accepted as having the most significant influence on the long-term loss of prestress. Although these properties are regarded as having significant influence on the loss, the accommodation of these properties is not comprehensively treated in most available specifications commonly employed in practice. These properties are time-dependent and their influence on a prestressed member occurs gradually as a result of many influences. A simple gross estimate of these properties is not appropriate for every bridge in reflecting the imposed conditions. Material properties must be accommodated, as they actually occur to result in accurate prediction.

2.1.1. Creep of Concrete

Creep of concrete is the characteristic in which increase in strain occur as a result of sustained stress or load, as shown schematically in Figure 2.1. Creep of concrete is generally regarded as occurring independent of the applied stress for a magnitude up to 40% of the concrete compressive strength. Creep occurs rapidly during the early period after loading but this rate decreases over time until a constant value is approached asymptotically after many years. Creep is dependent on the age of the concrete at loading as well as the mix proportions, strength, humidity, volume-to-surface area ratio (V/S), curing regime, and elapsed time from loading. Depending on these factors, the creep strain can be several times the elastic strain – the strain that occurs upon application of load. Under sustained load, over time the strain in the concrete increases as a result of creep. For the duration of applied stress, the creep coefficient is defined as the ratio of creep strain to instantaneous strain

$$\phi = \frac{\epsilon_{creep}}{\epsilon_{instantaneous}} \quad (2.1)$$

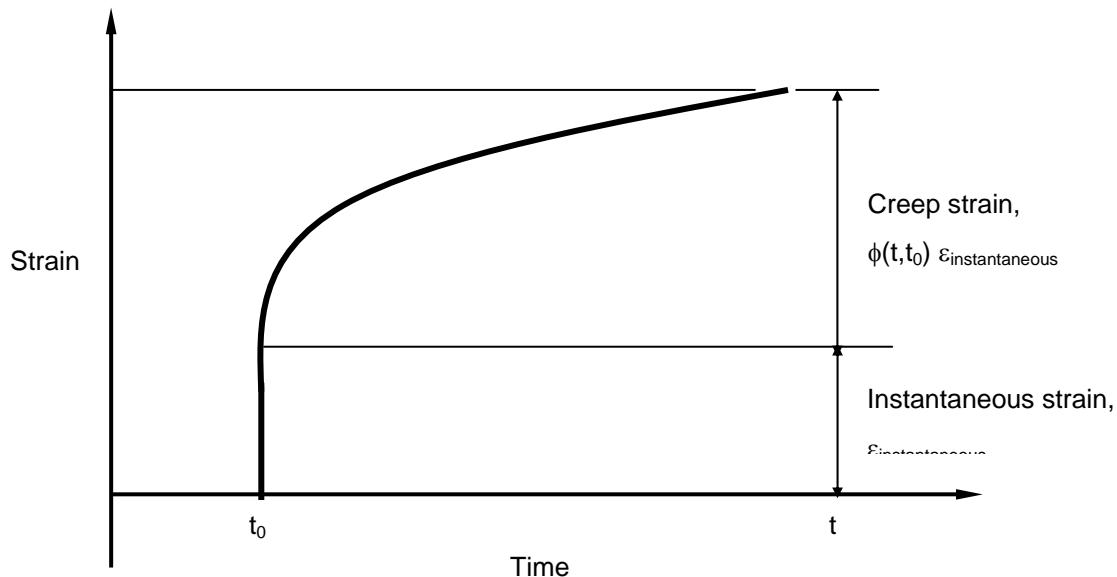


Figure 2.1: Creep of concrete under sustained load.

2.1.2. Shrinkage of Concrete

Shrinkage begins at the onset of drying, when curing of concrete ends. Shrinkage is categorized by the change in volume of the concrete through evaporation of water. The rate at which shrinkage occurs is rapid initially and decreases over time until a constant value is reached asymptotically after many years. In the absence of restraint, such as that provided by reinforcing steel, the shrinkage that occurs is referred to as the free shrinkage ε_{sh} .

2.1.3. Relaxation of Prestressed Steel

When stretched between two fixed points, a steel-prestressing tendon will maintain a constant strain. Over time, the prestressing steel will relax losing some of its initial tension while remaining at a constant strain when the applied stress is greater than 50% of its ultimate strength. This loss in stress is referred to as intrinsic relaxation $\Delta\sigma_{pr}$ and, for low relaxation steel, is frequently expressed through

$$\Delta\sigma_{pr} = -\frac{\log(24t)}{45} \left(\frac{\sigma_{p0}}{\sigma_{py}} - 0.55 \right) \sigma_{p0} \quad (2.2)$$

A prestressed concrete member constantly shortens over its life as a result of creep and shrinkage of concrete. This shortening results in the ends of the member moving towards one another slowly over time. A bonded prestressed tendon that reacts on the ends of the member will be subject to the same change in strain as that of the member and shortening results in loss of initial tension. The loss in tension resulting from creep and shrinkage has the same influence on the member as if the initial stress in the tendon were lower, thus creating reduced relaxation [18, 22]. The reduced relaxation $\overline{\Delta\sigma_{pr}}$ is accommodated by reducing the intrinsic relaxation by a factor χ_r , less than unity, typically on the order of 0.7 to 0.8 [18]. A value of χ_r taken as 0.8 was used in this research.

$$\overline{\Delta\sigma_{pr}} = \chi_r \Delta\sigma_{pr} \quad (2.3)$$

2.2. Methods for Predicting Creep and Shrinkage

This section reviews several current specifications available for predicting the creep coefficient and shrinkage strain. The values of creep and shrinkage have been determined using the AASHTO [2], ACI/PCI [3, 23], CEB-FIP [10], Gardner and Lockman (GL2000) [12], and NCHRP [21] methods, as several of these are commonly used in design. The CHBDC [9] specification is examined; however, this method was not used to produce creep and shrinkage for reasons explained later. The GL2000 [12] model was selected, among many methods developed by researchers, for the reason that it is the prime candidate for adoption in the upcoming revised version of the ACI-209 Committee Report [3]*.

The review of specifications is conducted in an attempt to examine one of the two possible sources of error in the predictions of prestress loss: the accurate use of material properties. To provide accurate estimates of prestress loss, values representative of the creep and shrinkage of concrete need to be used as input in prestress loss equations. To validate the appropriateness of the specifications for predicting creep and shrinkage, these specifications are compared to the creep and shrinkage obtained through the material tests conducted as part of this research.

Material tests are rarely conducted before a structure is erected. When creep and shrinkage values are needed, a design engineer would normally obtain these values from available specifications. Inaccurate input values of creep and shrinkage would invariably lead to incorrect estimates of prestress loss. The material tests discussed in the following chapter compare the actual measured values of creep and shrinkage with the predictions from the available specifications.

The development of creep and shrinkage is dependent on many factors. In several instances, complex variations are accommodated linearly or treated as constants in an effort to reduce the complexity of such methods and of

*Personal communication: Professor Walter Dilger, University of Calgary.

subsequent equations. Though unique in form, each of the considered specifications is formulated using some combination of the same six standard inputs in the prediction of creep and shrinkage. These inputs are usually known at the design stage of most new structures. Several of the specifications utilize additional inputs that accommodate concrete composition.

2.2.1. Inputs to the Specifications

Each of the specifications uses some combination of the same six inputs. These inputs are equivalent in quantity within each of the specifications; however, the equations, and use of the inputs in generating creep and shrinkage predictions, vary between specifications. The inputs used in each of the specifications are tabulated in Table 2.1 and Table 2.2. The inputs are described below with comments on the significance of the input on the development of creep and shrinkage with time.

- Concrete strength (f'_c) – This quantity, and in turn the modulus of elasticity, varies with time and directly influences the amount of creep and shrinkage that occurs over any period of time under consideration. The development of creep and shrinkage is dependent on the material consistency – aggregate, cement, and air content, cement and aggregate type – of the concrete. Since these parameters are often difficult to classify in specifications, the concrete strength is used, representative of the behavior as influenced by consistency.
- Relative humidity (RH) – The amount of moisture in the air impacts the rate at which the concrete hydrates. The rate of hydration influences the hardening rate and subsequently the development of creep and shrinkage.
- Age (t) – The age of the concrete at the point of time under consideration allows determination of the creep and shrinkage at that point in time, or at any other, though the life of the structure.

- Age at loading (t_0) – This term only affects the amount of creep that occurs in concrete. Terms provided in the specifications for the age at loading account for the amount of drying that has occurred in the concrete before load is applied. The age at loading influences the creep that occurs, as older concrete is less compliant than concrete younger in age.
- Length of moist cure ($t-t_s$) – The amount of time that the concrete is allowed to cure while kept in a moist environment. If the concrete is moist cured, this process begins immediately after the concrete has been stripped of any formwork. The rate of development of creep and shrinkage is dependent on the amount of water that remains in the concrete when drying commences. As the primary influence of shrinkage takes place in the early stage after casting, maintaining a moist environment for the concrete ensures the lowest amount of creep and shrinkage will take place.
- Volume to surface area ratio (V/S) – The ratio of the concrete volume to total surface area exposed to the environment. This ratio affects the rate at which the concrete hydrates and the influence of relative humidity is dependent on the element size. For structures with larger volume to surface areas, the rate of hydration will occur at a lower rate, developing lower ultimate creep and shrinkage values. Some specifications use, instead of the V/S ratio, the notional thickness of the element h_0 considered, which is twice the V/S ratio.

The inputs listed above are certainly not exhaustive of the total parameters that influence creep and shrinkage. Rather, each of the specifications uses these six inputs because they are known or can be reasonably assumed at the design stage. Furthermore, concrete consistency can vary significantly within different geographic regions; therefore, it is difficult to include in equations that are accurate in all cases.

Table 2.1: Input parameters to specifications for determining creep.

		Input Parameter					
		V/S	Relative Humidity	28-day Characteristic Compressive Strength	Concrete age	Concrete age at loading	Concrete age at end of curing
Specification	AASHTO	x	x	x	x	x	
	ACI/PCI	x	x	x	x	x	
	CEB-FIP	x	x	x	x	x	
	CHBDC	x	x		x	x	
	GL2000	x	x		x	x	x
	NCHRP	x	x	x	x	x	

Table 2.2: Input parameters to specifications for determining shrinkage.

		Input Parameter					
		V/S	Relative Humidity	28-day Characteristic Compressive Strength	Concrete age	Concrete age at loading	Concrete age at end of curing
Specification	AASHTO	x	x		x		
	ACI/PCI	x	x	x	x		x
	CEB-FIP	x	x	x	x		x
	CHBDC	x	x		x		x
	GL2000	x	x	x	x		x
	NCHRP	x	x	x	x		

The AASHTO [2], CEB-FIP [10], and CHBDC [9] specifications utilize SI units for the values of the inputs. The ACI [3], PCI [23], and NCHRP [21] specifications use Imperial units for the values of the inputs. Units will be indicated for particular input values when appropriate.

2.2.2.AASHTO

The following equations appear in the AASHTO [2] specifications and are appropriate for the calculation of creep and shrinkage to be used in the determination of such influences on the loss of prestress in bridges that are not constructed segmentally. This specification mentions that it is acceptable to approximate the shrinkage at 200 $\mu\text{m/m}$ after 28 days and 500 $\mu\text{m/m}$ after one year, and, if more accurate methods are desired, to consult the ACI [3] or CEB-FIP [10] specifications.

Creep

As can be seen in the Eq. 2.4, the creep coefficient $\phi(t, t_0)$ over an interval of time varies significantly with the concrete age at loading, k_{la} . Modification factors are included to correct for variations in concrete strength, k_f ; V/S, k_c ; and the average relative humidity, k_{hc} .

$$\phi(t, t_0) = 3.5k_f k_c k_{hc} k_{la} \left(\frac{(t - t_0)^{0.6}}{10 + (t - t_0)^{0.6}} \right) \quad (2.4)$$

t = Time (in days) from the date concrete was cast

t_0 = Age of the concrete at stressing (in days) from the date concrete was cast

From Eq. 2.4, it can be observed that the factor k_f reduces the ultimate creep coefficient as the concrete strength increases. No accommodation is made for the strength development with time.

$$k_f = \frac{62}{42 + 6.9f'_c} \quad (2.5)$$

f'_c = Concrete compressive strength at 28 days

The modification factor k_c reduces the ultimate creep with an increase in V/S.

$$k_c = \left(\frac{\frac{t}{26e^{0.0142(V/S)} + t}}{\frac{t}{45+t}} \right) \left(\frac{1.80 + 1.77e^{-0.0213(V/S)}}{2.587} \right) \quad (2.6)$$

V/S = Volume to surface area ratio, mm

A linear relation imposes accommodation for the influence of relative humidity. As the relative humidity increases, the correction k_{hc} decreases, and thus decreases the ultimate creep. The following correction k_{hc} is applicable for all relative humidity percentages.

$$k_{hc} = 1.58 - 0.0083RH \quad (2.7)$$

RH = Average relative humidity in percent

The term k_{la} accounts for the concrete age at loading. The ultimate creep decreases with the increase in concrete age.

$$k_{la} = t_0^{-0.118} \quad (2.8)$$

Shrinkage

The prediction of concrete shrinkage is determined using time and modifications for the element size and relative humidity.

$$\varepsilon_{sh}(t, t_s) = -k_s k_{hs} \left(\frac{t}{35+t} \right) 510(10)^{-6} \quad (2.9)$$

k_s = Correction factor for the V/S of the concrete

k_{hs} = Correction factor for the relative humidity influence on shrinkage

The correction factor for the influence of the element size k_s is given by

$$k_s = \left(\frac{\frac{t}{26e^{0.0142(V/S)} + t}}{\frac{t}{45+t}} \right) \left(\frac{1064 - 3.70(V/S)}{923} \right) \quad (2.10)$$

The relative humidity is represented through a bilinear curve, representing humidity from zero to 100%. Like that for the modification of creep, the modification k_{hs} for shrinkage also decreases with an increase in relative humidity, decreasing the ultimate shrinkage.

$$k_{hs} = 2.00 - 0.0143RH \text{ for } RH \leq 80\% \quad (2.11a)$$

$$k_{hs} = 4.286 - 0.0429RH \text{ for } 80 < RH \leq 100\% \quad (2.11 b)$$

Of significant interest is the use of a bilinear curve to represent the influence of humidity on the shrinkage, but a single linear curve for the relative humidity influence on the development of creep. Relative humidity affects shrinkage more than it does for creep. This is probably why a more accurate bilinear equation is adopted for shrinkage.

2.2.3.ACI/PCI

The equations from ACI 209: Predictions of Creep, Shrinkage, and Temperature Effects in Concrete Structures [3] for creep and shrinkage were adopted for use in the PCI Bridge Design Manual [23]. There exist minor differences in the equations, found in the coefficients of the equations, but the ACI [3] and PCI [23] methods are in essence the same and produce equivalent predictions of creep and shrinkage. The equations are written for concrete subject to “standard conditions.” The standard conditions include RH of 40% (70% in PCI [23]), V/S of 38 mm (1.5 in.), and average temperature of 21.1 °C (70 °F). The difference in the relative humidity standard condition between ACI [3] and PCI [23] does not affect the values of creep and shrinkage. Different coefficients in the equations result in equivalent predictions of creep and shrinkage at corresponding time; the equations for relative humidity presented here are from the PCI [23] specification. To adjust the equations for concrete subject to conditions that deviate from these standards, correction factors, presented below, are applied.

Creep

The general form of the creep equation is applicable for concrete with strengths in the range of 4 to 12 ksi.

$$\phi(t, t_0) = \frac{(t - t_0)^{0.6}}{(12 - 0.5f'_c) + (t - t_0)^{0.6}} (1.18 - 0.045f'_c) 1.88k_{la}k_{hc}k_s k_{\alpha}k_{sl}k_p \quad (2.12)$$

f'_c = Concrete compressive strength, ksi

The modifiers k_{la} , k_{hc} , and k_s are correction factors for concrete age at loading, relative humidity, and member size, respectively. These modification factors are determined by equations that are presented below. The modifiers k_{α} , k_{sl} , and k_p in these equations are intended to accommodate for air content, slump, and aggregate percentage in the concrete, respectively. If no data is available for these values, they can be taken as 1.0, which was done for the current research.

$$k_{la} = 1.25(t_0)^{-0.118} \quad (2.13)$$

$$k_{hc} = 1.586 - 0.0084RH \text{ for } 40 \leq RH \leq 100\% \quad (2.14)$$

$$k_s = 2/3(1 + 1.13e^{-0.54V/S}) \quad (2.15)$$

V/S = Volume to surface area ratio, in.

It is noted that Eq. 2.14 is similar to Eq. 2.7. These equations produce nearly identical results for the humidity modification factor on the influence of creep.

Shrinkage

The general equation for predicting shrinkage within the ACI [3] and PCI [23] specifications appears as the following, which can be utilized for the range of concrete strengths, from 4 to 12 ksi.

$$\varepsilon_{sh}(t, t_s) = \frac{(t - 7)}{(45 - 2.5f'_c) + (t - 7)} (1.2 - 0.05f'_c) 545(10)^{-6} k_{cp}k_{hs}k_s k_c k_{\alpha}k_{sl}k_p \quad (2.16)$$

The correction factors k_{cp} , k_{hs} , and k_s are adjustments for length of moist cure, $t - t_s$, relative humidity and size, respectively. The modifiers k_α , k_{sl} , and k_p are the same as those for creep; k_c modifies the equations to account for cement content. If no data exists for these modifications, they are taken as unity, which was done for the current research.

$$k_{cp} \text{ may be taken as } 1.0 \text{ for a moist curing period of seven days.} \quad (2.17)$$

$$k_{hs} = 2.00 - 0.0143RH \text{ for } 40 \leq RH \leq 80\% \quad (2.11a)$$

$$k_{hs} = 4.286 - 0.0429RH \text{ for } 80 < RH \leq 100\% \quad (2.11b)$$

$$k_s = 1.2e^{-0.12V/S} \quad (2.18)$$

Eqs. 2.11a and 2.11b for k_{hs} are identical for both AASHTO [2] and ACI/PCI [3,23].

2.2.4.CEB-FIP

The CEB-FIP [10] equations are written to account for several complex interdependencies of inputs that are not similarly treated in other specifications. The influence of notional thickness on rate at which relative humidity changes the development rate of creep is accounted. Additionally, the modulus of elasticity is calculated based on time-development rates of the concrete strength and hardening. The terms f'_c and h_0 must be input in MPa and mm, respectively, to uphold consistent units for all calculations.

The mean concrete compressive strength at 28 days f_{cm} may be calculated from Eq. 2.19.

$$f_{cm} = f'_c + 8 \text{ (MPa)} \quad (2.19)$$

The concrete strength at any point in time can be calculated by the following equations.

$$f_{cm}(t) = \beta_{cc}(t)f_{cm} \quad (2.20)$$

$f_{cm}(t)$ = Concrete compressive strength at any point in time

$\beta_{cc}(t)$ = Factor for the time-development rate of concrete strength

$$\beta_{cc}(t) = \exp\left(s\left(1 - \sqrt{\frac{28}{t}}\right)\right) \quad (2.21)$$

s = Factor for the influence of concrete hardening rate

The value s in Eq. 2.21 equals 0.2, 0.25 and 0.38 for rapidly hardening high strength cements, normal or rapidly hardening cements, and slowly hardening cements, respectively. Normal hardening cement was used in the bridge; a value of $s = 0.25$ was used in the present analysis.

The modulus of elasticity for concrete at 28 days $E_c(28)$ may be estimated by the following equation, using the mean 28-day compressive strength:

$$E_c(28) = 21500 \left(\frac{f_{cm}}{10}\right)^{1/3} \quad (2.22)$$

At any point in time, the modulus of elasticity for concrete can be calculated from

$$E_c(t) = \beta_E(t)E_c(28) \quad (2.23)$$

$E_c(t)$ = Concrete modulus of elasticity at any point in time

$\beta_E(t)$ = Factor for the time development rate of modulus of elasticity

$$\beta_E(t) = \sqrt{\beta_{cc}(t)} \quad (2.24)$$

Creep

Creep is expressed in Eq. 2.25.

$$\phi(t, t_0) = \phi_0 \beta_c(t - t_0) \beta_E(t_0) \quad (2.25)$$

The term ϕ_0 accounts for the influence of relative humidity, concrete strength, and the age at loading on creep.

$$\phi_0 = \phi_{RH} \beta(f_{cm}) \beta(t_0) \quad (2.26)$$

$$\phi_{RH} = 1 + \frac{1 - \frac{RH}{100}}{0.46 \left(\frac{h_0}{100} \right)^{1/3}} \quad (2.27)$$

ϕ_{RH} = Factor for the influence of relative humidity on the concrete

$$h_0 = \text{Notional thickness of the concrete} = \frac{2A_c}{p}, \text{ mm}$$

A_c = Cross sectional area of concrete

p = Perimeter of concrete exposed to the atmosphere

$$\beta(f_{cm}) = \frac{5.3}{\sqrt{\frac{f_{cm}}{10}}} \quad (2.28)$$

$\beta(f_{cm})$ = Factor for the influence of concrete strength on the ultimate
creep

$$\beta(t_0) = \frac{1}{0.1 + t_0^{0.2}} \quad (2.29)$$

$\beta(t_0)$ = Factor for the influence of the age at loading on the ultimate
creep

The $\beta_c(t - t_0)$ term accounts for the development of creep after the application of load.

$$\beta_c(t - t_0) = \left(\frac{t - t_0}{t - t_0 + \beta_H} \right)^{0.3} \quad (2.30)$$

A correction β_H , for element V/S and relative humidity influence on creep, is provided by

$$\beta_H = \frac{150h_0}{100} \left(1 + (0.012RH)^{18}\right) + 250 \leq 1500 \quad (2.31)$$

Creep is further influenced by the ratio of the modulus of elasticity at loading to the modulus at 28 days.

$$\beta_E(t_0) = \frac{E_c(t_0)}{E_c(28)} \quad (2.32)$$

Shrinkage

The general form of the shrinkage producing equation for any age of the concrete appears as

$$\varepsilon_{sh}(t, t_s) = \varepsilon_{cs0} \beta_s(t - t_s) \quad (2.33)$$

The term β_s accounts for the development of shrinkage with time and is influenced by the V/S ratio and duration of moist cure, $t - t_s$.

$$\beta_s(t - t_s) = \left(\frac{t - t_s}{350 \left(\frac{h_0}{100} \right)^2 + t - t_s} \right)^{0.5} \quad (2.34)$$

The terms ε_{cs0} , $\varepsilon_s(f_{cm})$, and β_{RH} in Eqs. 2.35, 2.36, and 2.37 adjust the development of shrinkage to account for the strength of the concrete, hardening rate and relative humidity.

$$\varepsilon_{cs0} = \varepsilon_s(f_{cm}) \beta_{RH} \quad (2.35)$$

$\varepsilon_s(f_{cm})$ = Factor for the influence of concrete strength and cement type
on shrinkage

β_{RH} = Factor for the influence of relative humidity on shrinkage

$$\varepsilon_s(f_{cm}) = \left(160 + 10 \beta_{sc} \left(9 - \frac{f_{cm}}{10} \right) \right) 10^{-6} \quad (2.36)$$

β_{sc} = Factor for the influence of cement hardening rate

$$\beta_{RH} = -1.55 \left(1 - \left(\frac{RH}{100} \right)^3 \right) \text{ for } 40 \leq RH \leq 99\% \quad (2.37)$$

$$\beta_{RH} = 0.25 \text{ for } RH > 99\% \quad (2.38)$$

The term β_{sc} is taken as 4, 5, or 8 for slowly hardening cements, normal or rapidly hardening cements, and rapidly hardening, high-strength cements, respectively. A value of $\beta_{sc} = 5$ was used in the current research as normal hardening cement was used within the bridge.

2.2.5. CHBDC

Though this method was not used for generating predictions of creep and shrinkage, the Canadian Highway Bridge Design Code (CHBDC) [9] method is as well suited for making predictions as any of the methods used. This method was not used for the prediction of creep and shrinkage because many of the necessary coefficients could only be taken from tables. These tables are reproduced from the CHBDC [9] manual and included herein. To provide a suitable representation of the development of creep and shrinkage with time, these coefficients would need to be read from tables (Table 2.3) and graphs (Figure 2.2 to Figure 2.5) at each point in time corresponding to the points at which measurements were made, discussed in an earlier chapter. Not only laborious, but this procedure could result in many errors, and as such, was not utilized.

Creep

The prediction for creep appears as

$$\phi(t, t_0) = \left(0.8(1 - k_0) + 0.4\beta_d + k_r(k_{f(t)} - k_{f(t_0)}) \right) \quad (2.39)$$

k_0 = Coefficient for the concrete age at stressing

β_d = Coefficient for the concrete age after stressing

k_r = Coefficient for the influence of average relative humidity

$k_{f(t)}$ = Coefficient for the notional thickness if the concrete at any time, t

$k_{f(t_0)}$ = Coefficient for the notional thickness if the concrete at stressing

Shrinkage

The equation for predicting shrinkage is

$$\varepsilon_{sh}(t, t_s) = \varepsilon_b (k_{s(t)} - k_{s(t_0)}) \quad (2.40)$$

ε_b = Maximum shrinkage in the concrete for average relative humidity

$k_{s(t)}$ = Coefficient for the notional thickness of the concrete at any time, t

$k_{s(t_0)}$ = Coefficient for the notional thickness of the concrete at stressing

Table 2.3: Values of coefficients ε_b and k_r . (After Table 8.4.1.5 from [9])

Mean relative humidity	ε_b ($\mu\varepsilon$)	k_r
40%	-520	3.0
70%	-320	2.0
90%	-130	1.0

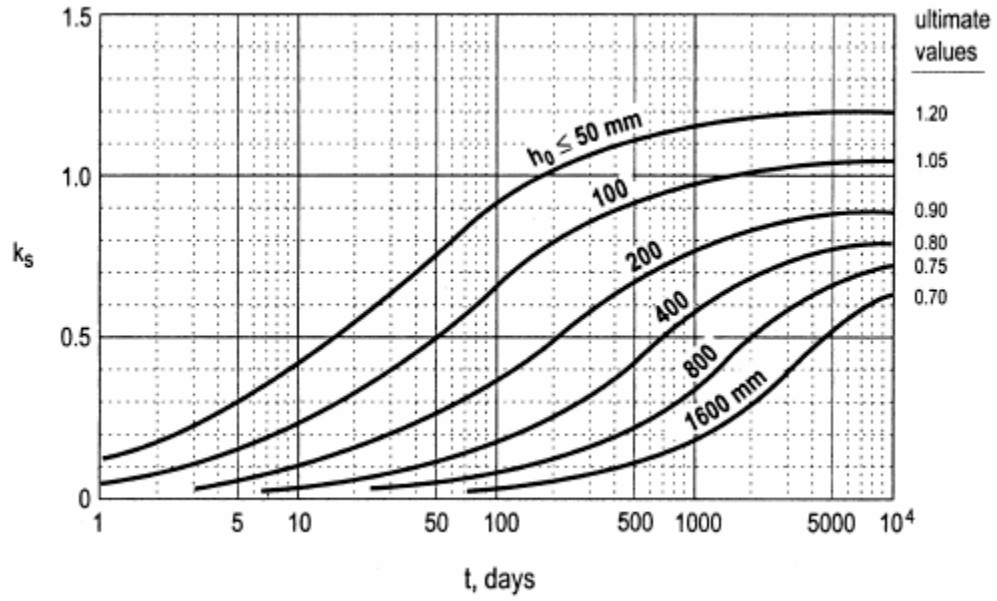


Figure 2.2: Values of coefficient k_s (Figure 8.4.1.5 from [9]).

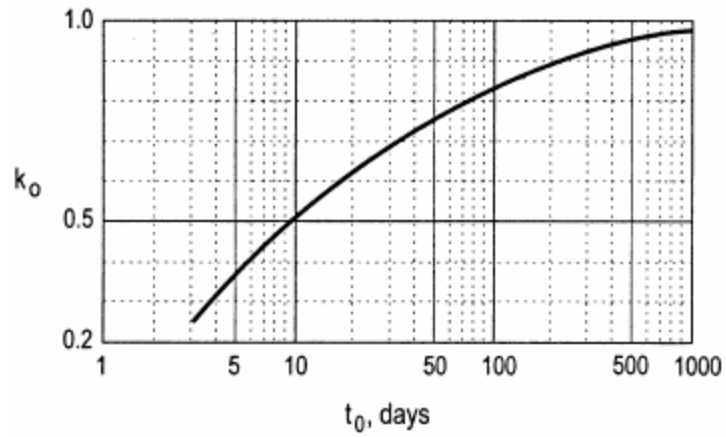


Figure 2.3: Values of coefficient k_0 (Figure 8.4.1.6 (a) from [9]).

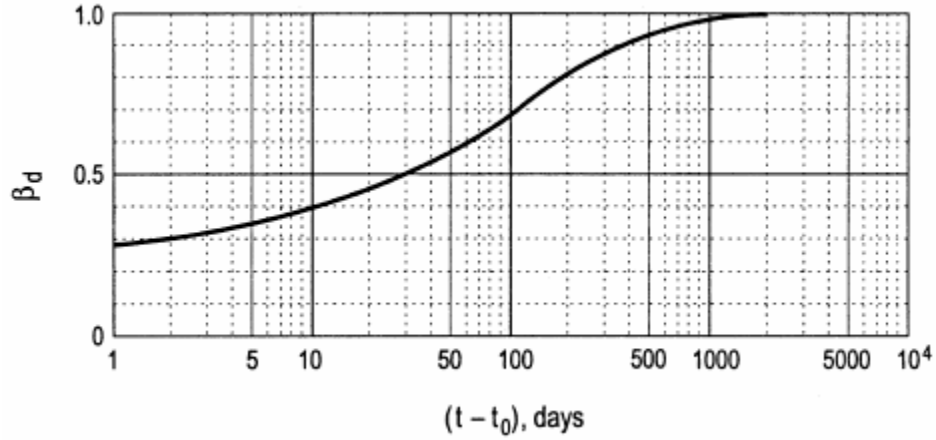


Figure 2.4: Values of coefficient β_d (Figure 8.4.1.6 (b) from [9]).

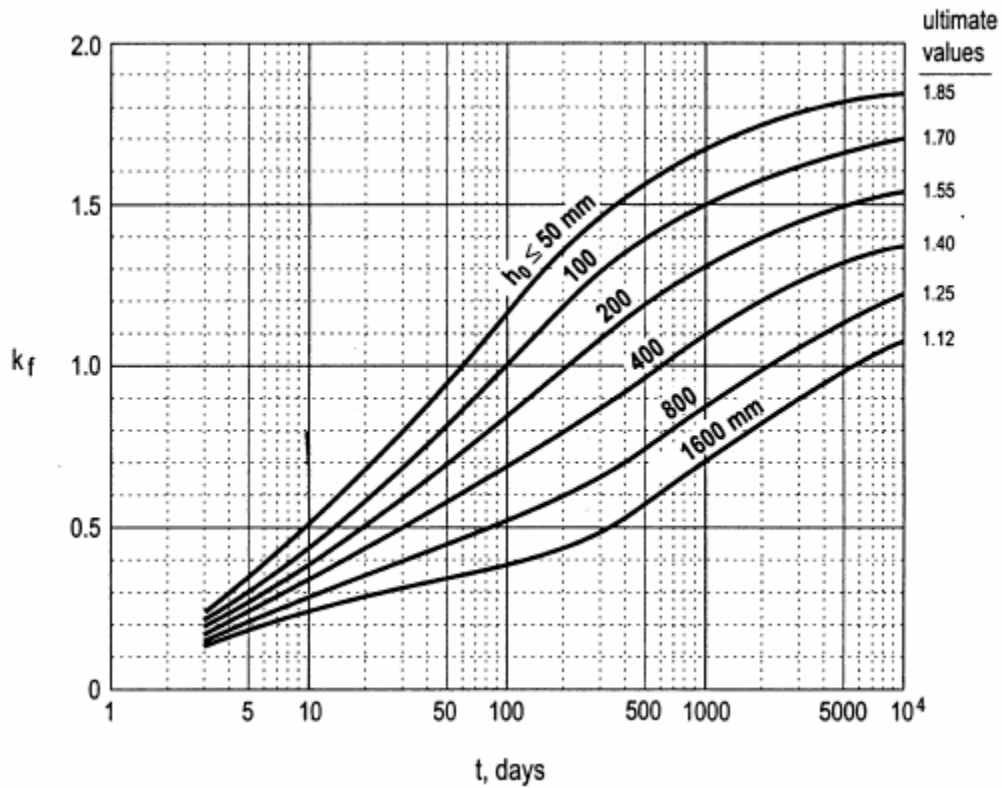


Figure 2.5: Values of coefficient k_f (Figure 8.4.1.6 (c) from [9]).

2.2.6. GL2000

The GL2000 [12] method developed by Gardner and Lockman is applicable for creep and shrinkage predictions in concrete with strength up to 12 ksi. The

method was formulated and verified [12] through comparisons to data from the RILEM Data Bank.

Creep

Creep is expressed in Eq. 2.41.

$$\phi(t, t_0) = \Phi(t_c) \left[2 \left(\frac{(t-t_0)^{0.3}}{(t-t_0)^{0.3} + 14} \right) + \left(\frac{7}{t_0} \right)^{0.5} \left(\frac{t-t_0}{t-t_0+7} \right) + 2.5 \left(1 - 1.086 \left(\frac{RH}{100} \right)^2 \right) \left(\frac{t-t_0}{t-t_0 + 0.15(V/S)^2} \right)^{0.5} \right] \quad (2.41)$$

V/S = Volume to surface area ratio, mm

The term $\Phi(t_c)$ accounts for the amount of drying that occurs in the concrete before the application of load.

$$\Phi(t_c) = \left(1 - \left(\frac{t_0 - t_s}{t_0 - t_s + 0.15(V/S)^2} \right)^{0.5} \right)^{0.5} \quad (2.42)$$

The concrete strength is used in the development of shrinkage over time. The mean concrete compressive strength is expressed in terms of the characteristic compressive strength, as shown in Eq. 2.43. Of course, if the actual 28-day compressive strength is available at the time of design, this value may be used to produce a better estimate of the shrinkage.

$$f_{cm} = 1.1f'_c + 5 \text{ (MPa)} \quad (2.43)$$

f'_c = Concrete compressive strength, MPa

Shrinkage

The general form of the shrinkage-prediction equation is

$$\varepsilon_{sh}(t, t_s) = \varepsilon_{shu} \beta(h) \beta(t) \quad (2.44)$$

The term ε_{shu} accounts for the ultimate concrete shrinkage and is dependent on the concrete strength at 28 days and the type of concrete, represented

through K , which is taken as 1, 0.7 or 1.15 for concrete Type I, II, and III, respectively. For the present research, a value of $K = 1.0$ was selected as the concrete in the bridge is Type I.

$$\varepsilon_{shu} = 1000K \left(\frac{30}{f_{cm}} \right)^{0.5} 10^{-6} \quad (2.45)$$

The $\beta(h)$ term adjusts the development of shrinkage to accommodate the influence of relative humidity.

$$\beta(h) = 1 - 1.18 \left(\frac{RH}{100} \right)^4 \quad (2.46)$$

The V/S and the length of moist cure, $t - t_s$, are represented through the $\beta(t)$ term.

$$\beta(t) = \left(\frac{t - t_s}{t - t_s + 0.15(V/S)^2} \right)^{0.5} \quad (2.47)$$

2.2.7.NCHRP

The NCHRP Report 496 [21] predictions for creep and shrinkage are reviewed herein. The developed equations for prestress loss in pretensioned girders are not presented here since this research is only concerned with post-tensioned members.

The NCHRP Report [21] discusses the standard conditions that are considered in the development of the equations. The ACI-209 [3] equations assume the standard relative humidity at 40%, which represents the low-end of average relative humidity in the United States. Most areas are subject to an average relative humidity around 70% [2]. Several specifications consider a V/S ratio of 38 mm (1.5 in.) to be a standard member size; most pre-tensioned members have a V/S ratio of about 89 mm (3.5 in.) (post-tensioned members typically exceed this). The standards in ACI-209 [3] are not standards for most structures; the NCHRP [21] equations use standards appropriate for most

bridges, as discussed here. In this method, an average relative humidity of 70% is selected. Additionally, a V/S ratio of 89 mm (3.5 in.) is considered along with loading ages of 1 day for pre-tensioned members and 7 days for cast-in-place elements. No accommodation for other influences as slump, cement content, fines percentage, and air content are included, as these result in minor changes to creep and shrinkage [3].

Creep

The creep coefficient for any point in time occurring in the concrete after loading is determined through

$$\phi(t, t_0) = 1.90k_{td}k_{la}k_{hc}k_s k_f K_1 K_2 \quad (2.48)$$

k_{td} = Modification for time-development of creep

k_{la} = Modification for concrete age at loading

k_{hc} = Modification for relative humidity

k_s = Modification for V/S

k_f = Modification for concrete strength

K_1, K_2 = Modifications for influence of local materials on creep and shrinkage

The 1.90 in Eq. 2.48 represents the ultimate creep that could be expected for standard conditions. This is very similar to the ultimate creep coefficient of 1.88 presented in the ACI/PCI [3, 23] section, Eq. 2.12. Values of K_1 and K_2 are intended to represent average, upper, and lower bound values to correct for the influence of local materials on the development of creep and shrinkage. These values were not developed for the NCHRP [21] project for all areas in North America, but may be developed through subsequent research. Values for these coefficients were proposed for the areas that tests were conducted, but these

areas are outside of California and are not well suited for the environment. These corrections may be taken as unity for the purposes herein.

The modifier k_{td} provides correction for the time-development of creep and shrinkage for concrete age other than of time at infinity.

$$k_{td} = \frac{t}{61 - 4f'_c + t} \quad (2.49)$$

f'_c = Concrete compressive strength, ksi

The term k_{la} corrects for the age of the concrete at loading.

$$k_{la} = t_0^{-0.118} \quad (2.8)$$

A linear relation, defined by Eq. 2.50, expresses the influence of relative humidity.

$$k_{hc} = 1.56 - 0.008RH \text{ for } 30 \leq RH \leq 80\% \quad (2.50)$$

The k_{hc} correction factor is nearly identical to the corresponding corrections in AASHTO [2] and ACI/PCI [3,23], given previously in Eqs. 2.7 and 2.14, respectively.

The correction factor to account for the V/S ratio

$$k_s = \frac{1064 - 94V/S}{735} \quad (2.51)$$

V/S = Volume to surface area ratio, in.

The correction factor k_s in Eq. 2.51 is similar to the corresponding correction factor in the AASHTO [2] section, Eq. 2.10 without a time-development factor.

The factor accounting for concrete strength is

$$k_f = \frac{5}{1 + f'_c} \quad (2.52)$$

Shrinkage

The general form of the shrinkage-predicting equation appears in Eq. 2.53. The 480 microstrain represents the maximum shrinkage strain that can be expected in the concrete.

$$\varepsilon_{sh}(t, t_s) = 480(10)^{-6} k_{td} k_s k_{hs} k_f K_1 K_2 \quad (2.53)$$

The modifiers k_{td} , k_s , and k_f used for predicting shrinkage are determined through the same equations as those for creep, as given in Eqs. 2.49, 2.51, and 2.52, respectively, with the addition of k_{hs} (for relative humidity), which is given by

$$k_{hs} = 2.00 - 0.0143RH \text{ for } 30 \leq RH \leq 80\% \quad (2.11a)$$

It is emphasized that the corrections for k_{hs} are the same as those found in AASHTO [2] and ACI/PCI [3]. The only difference is the range of applicable humidity to which the modifiers can be applied. The NCHRP Report [21] mentions that the range 30 to 80% is typical of what is experienced in the United States. No equation accommodating humidity above 80% is presented. Aside from a few coastal locations, most areas in the United States rarely experience average relative humidity above 80%.

2.3. Methods for Predicting Prestress Loss

The methods presented herein for determining the loss in prestress are those typically used in design. They include only a few inputs in the determination of the prestress loss to minimize complication and time involved in application. It is for this reason that these methods are not suitable for accurate prediction of the prestress loss in all bridges. The methods are kept too simple to reasonably predict the long-term behavior of all types of bridges in different environments. Most importantly, direct and logical representation of the influence of creep and shrinkage of concrete and prestress relaxation are not included.

It should be mentioned that only specifications that are widely used and accepted by practicing engineers are reviewed here. The methods selected for this research are the AASHTO Approximate Lump Sum Estimate of Time-Dependent Losses [2], AASHTO Refined Estimates of Time Dependent Losses [2], CEB-FIP Model Code 90 [10], and Canadian Highway Bridge Design Code (CHBDC) [9]. The PCI Bridge Design Manual [23] and Caltrans [8] have adopted the AASHTO Refined Method [2], which includes several inputs that are not represented by AASHTO Approximate [2], relative humidity and concrete stress. The CEB-FIP [10] specification is widely used in Europe and uses several inputs not accounted in other specifications, most importantly the concrete creep and shrinkage. Other inputs used include the moment of inertia, of the concrete, the concrete area, depth of prestress, prestress area, and prestress relaxation.

This research is concerned with the initial prestress, the loss that occurs after the transfer of stress. Anchor-set, elastic shortening, and frictional losses are not appropriate for inclusion. Components of the equations that determine the loss before transfer have been eliminated from presentation here. Several of the equations may appear slightly different from their presentation in the specifications such that symbols and signs would be consistent among the different methods as they are presented here. This was done to avoid confusion in the signs of input values and make the inputs for each of the specifications, as they are produced here, equivalent.

2.3.1. Input Parameters to the Specifications

Most of the specifications considered are developed empirically from experimental results. The inputs used in the examined specifications appear in Table 2.4. All specifications used herein for predicting the prestress loss are to be used with inputs in SI units.

Table 2.4: Inputs used in considered specifications to calculate prestress loss.

Input Parameter	Specification			
	CEB-FIP	AASHTO App.	AASHTO Ref.	CHBDC
Initial concrete stress at prestress centroid imposed by prestressing and self-weight	x		x	x
Change in concrete stress at prestress centroid from permanent loads			x	x
Prestressing steel ultimate stress				x
Prestressing steel initial stress			x	x
Stress change in prestressed steel, relaxation	x			
Yield stress of prestressed steel		x		
Yield stress of non-prestressed steel		x		
Prestressing steel modulus	x		x	x
Concrete modulus	x		x	x
Area, prestressed steel	x	x		
Area, non-prestressed steel		x		
Concrete area	x			
Concrete moment of inertia	x			
Depth of prestress from centroid of concrete section	x			
Shrinkage strain	x			
Creep coefficient	x			
Aging coefficient	x			
Relative humidity			x	x
Wobble coefficient			x	x
Curvature coefficient			x	x

2.3.1.1. Use of Material Properties in Specifications

Most of the specifications reviewed in this chapter include, in different sections, methods of calculating material properties and methods for calculating prestress loss. Although many of the specifications provide means of calculating material properties, the calculated creep, shrinkage, and relaxation are not used as input in most of the equations for predicting loss, with the exception of the CEB-FIP [10] specification. Alternatively, creep and shrinkage are accounted for through the presence of empirical constants obtained from experiments. The constants are only valid for the specific conditions, concrete type and geometry of the tested specimens. Shrinkage is commonly accounted for through only the relative humidity. The absence of creep and shrinkage inputs to the specifications hinders the overall suitability and robustness of the equations for general application.

As has been discussed previously, the specifications selected for use in this research were reasonably capable of predicting the creep and shrinkage that occurred within the material test specimens. The methods for predicting prestress loss should include a means to account for the predicted values of creep and shrinkage to yield improved results. It is of considerable importance to understand the deficiencies in available specifications in order to provide adequate justification for the implementation of refined methods.

2.3.2. AASHTO Approximate Lump Sum Estimate of Time-Dependent Losses

The AASHTO Approximate Method [2] can be applied to bridge members whose spans do not exceed 48.8 m (160 ft.). The equations predict the loss for members stressed at an age between 10 and 30 days and subjected to conditions in which the concrete strength is 24.1 MPa (3.5 ksi) or higher at stressing, the relative humidity is between 40 to 100%, the shrinkage strain is between 400 to 600 microstrain, and the creep coefficient is between 1.6 and

2.4. The range of the relative humidity alone would have substantial influence on the creep and shrinkage. Here, the creep and shrinkage create no alteration of the prestress loss determined with this method for the ranges specified. These ranges of conditions and concrete properties would cause substantial differences in the prestress loss, yet, these equations yield the same prediction for loss for bridges constructed in entirely different climates or subject to different construction schedules. Additionally, these equations would predict the same loss for two members with the same reinforcement ratio, but takes in no consideration the span and geometry of the actual member.

The loss is calculated using a partial prestress ratio (PPR):

$$PPR = \frac{A_p f_{py}}{A_p f_{py} + A_s f_y} \quad (2.54)$$

A_p = Area of prestressed steel

A_s = Area of non-prestressed steel

f_{py} = Yield stress of prestressed steel

f_y = Yield stress of non-prestressed steel

The equations 2.55a and 2.55b predict the upper-bound and average values of loss, respectively. These equations were developed from a computerized time-step model [2] that considered many different box-girder section geometries utilizing the above range of inputs.

$$\Delta\sigma_{ps} = -(21 + 4PPR) \quad (2.55a)$$

$$\Delta\sigma_{ps} = -(19 + 4PPR) \quad (2.55b)$$

For box-girders stressed with low-relaxation strands, the calculated prestress loss in equations 2.55a and 2.55b may be reduced by 28 MPa.

Eqs. 2.55a and 2.55b were developed in conjunction with other equations [2] for predicting the prestress loss in several common bridge members such as I-

girders and double-T's. Several of these equations include input for the concrete compressive strength. NCHRP [21] mentions this fact and raises the question as to why the equations for box-girders are not inclusive of such influence.

2.3.3. AASHTO Refined Estimates of Time-Dependent Losses

The AASHTO Refined Method [2vv] is applicable for predicting prestress loss in bridges whose span length is not greater than 76.2 m (250 ft.). There is no limit on the concrete age at stressing; however, the concrete strength must not be less than 24.1 MPa (3.5 ksi) when stressing occurs. Creep and shrinkage are accommodated through multipliers to the applied stress and relative humidity, respectively. A multiplier to RH expresses the influence of shrinkage; however, though relative humidity is a major influence, it is not the only factor. The duration and type of curing (moist or steam) is a significant influence on the development of shrinkage.

In this method, each component that influences prestress loss is computed individually. The sum of the individual components is the total prestress loss $\Delta\sigma_{ps}$ that can be expected at the end of service life for the structure.

$$\Delta\sigma_{ps} = \Delta\sigma_{ps,CR} + \Delta\sigma_{ps,SH} + \Delta\sigma_{ps,R} \quad (2.56)$$

The terms $\Delta\sigma_{ps,CR}$, $\Delta\sigma_{ps,SH}$, and $\Delta\sigma_{ps,R}$ represent the loss components as a result of creep, shrinkage, and relaxation, respectively.

The creep component of loss $\Delta\sigma_{ps,CR}$ is determined from the initial stress in the concrete at the centroid of prestressing tendons as provided through all permanent loads.

$$\Delta\sigma_{ps,CR} = 12f_{cgp} - 7\Delta f_{cdp} \geq 0 \quad (2.57)$$

f_{cgp} = Concrete stress at the level of the prestress centroid due to all

permanent actions including prestressing

Δf_{cdp} = Change in stress at the level of the prestress centroid due to all loads not included in f_{cgp}

The component of shrinkage on the loss $\Delta\sigma_{ps,SH}$ is dependent solely on the relative humidity.

$$\Delta\sigma_{ps,SH} = (93 - 0.85RH) \quad (2.58)$$

The prestress loss as a result of relaxation is given by:

$$\Delta\sigma_{ps,R} = k_l (20 - 0.2(\Delta\sigma_{ps,SH} + \Delta\sigma_{ps,CR})) \quad (2.59)$$

In Eq. 2.59, $k_l = 0.3$ and 1.0 for low-relaxation and stress-relieved tendons, respectively, and are set coefficients for particular tendon types [2].

2.3.4.CEB-FIP

The CEB-FIP [10] equation allows for the input of calculated creep and shrinkage. Additionally, the equations have been developed to account for the intrinsic relaxation of prestressing steel and apply a fixed reduced relaxation coefficient χ_r of 0.8, which is not impractical for most applications as it is a conservative value. A value for χ_r of 0.7 is commonly used in design.

$$\Delta\sigma_{ps} = \frac{\alpha\phi(t, t_0)f_{cgp} + E_p\varepsilon_{sh} + 0.8\Delta\sigma_{pr}}{1 + \alpha \frac{A_p}{A_c} \left(1 + \frac{A_c y_p^2}{I_c} \right) (1 + \chi\phi(t, t_0))} \quad (2.60)$$

α = Modular ratio of prestressed steel and concrete, E_p/E_c

E_p = Modulus of elasticity of prestressed steel

E_c = Modulus of elasticity of concrete

y_p = Depth of prestressed steel centroid from the centroid of the net concrete section

I_c = Moment of inertia of net concrete section

χ = Aging coefficient of concrete

$\Delta\sigma_{pr}$ = Loss in tendon stress due to steel relaxation

Eq. 2.60 is significant because on inspection it appears to make accommodations for the primary influences of prestress loss: concrete creep and shrinkage and prestressing steel relaxation. Examination of the equation indicates that the non-prestressed reinforcement has been neglected from the formulation and that only one layer of prestressing is considered. Several prestress layers may exist; however, this method takes only one input for the tendon, which can be taken at the tendon centroid, effectively creating one prestress layer. Although a single prestressing layer may be practical for short-span bridges, longer bridges typically utilize several layers of prestressing. Multiple tendons can be accommodated through a lumped equivalent tendon if it is to be considered. Not considering the presence of non-prestressed steel can lead to non-conservative estimate of prestress loss. While precast pretensioned girders contain negligible amounts or no non-prestressed steel, post-tensioned girders, the type of bridge considered in this study, contain considerable amounts of non-prestressed steel that cannot be neglected.

2.3.5. CHBDC

The CHBDC [9] method for predicting prestress loss calculates the loss using individual components, as is the case of the AASHTO Refined Method [2]. The total loss that occurs is the sum of the following components.

$$\Delta\sigma_{ps} = \Delta\sigma_{ps,CR} + \Delta\sigma_{ps,SH} + \Delta\sigma_{ps,R} \quad (2.61)$$

The equation for loss caused by creep is determined from the relative humidity and tendon stress imposed by dead loads.

$$\Delta\sigma_{ps,CR} = 1.6 \left(1.37 - 0.77(0.01RH)^2 \right) \frac{E_p}{E_c} (f_{cgp} - \Delta f_{cdp}) \quad (2.62)$$

The term $\Delta\sigma_{ps,CR}$ is dependent on the applied stress and relative humidity, an improvement and step forward compared to AASHTO [2].

The component accounting for the loss as a result of shrinkage is dependent entirely on the relative humidity. This equation is very similar to Eq. 2.58 from the AASHTO Refined Method [2].

$$\Delta\sigma_{ps,SH} = (94 - 0.85RH) \quad (2.63)$$

The relaxation component is calculated including the components of creep and shrinkage. The ultimate and initial stresses in the tendon are used for the calculation. The accommodation for intrinsic relaxation is accommodated in the following equation.

$$\Delta\sigma_{ps,R} = \left(\frac{f_{p0}}{f_{pu}} - 0.55 \right) \left(0.34 - \frac{\Delta\sigma_{ps,CR} + \Delta\sigma_{ps,SH}}{1.25f_{pu}} \right) \frac{f_{pu}}{3} \geq 0.002f_{pu} \quad (2.64)$$

f_{p0} = Initial stress in the prestressed steel

f_{pu} = Ultimate stress of the prestressed steel

3. Material Tests

3.1. Motivation

Material tests were conducted to obtain the creep coefficient and shrinkage strain for the specific concrete used in the bridge. The specifications, reviewed in the previous chapter use material properties, environmental conditions, physical geometry, and concrete age as input data to generate predictions of creep and shrinkage and some include procedures for accommodating concrete composition. While the specifications predictions for the case of the bridge under consideration will be shown to be acceptable, the objective is to eliminate possible margins of error in the inputs to the computer analysis (described in Chapter 4) by accurately characterizing the material properties.

3.2. Testing Methodology

Two frames from the I5/805 Bridge were selected for use in this research. On the Caltrans Contract Drawings, these frames are referred to as Frame 4 and Frame 5 and will be designated in as F4 and F5, respectively, for the remainder of this Report. The five different concrete types if F4 and F5 are assigned the names of the months that they were cast (

Table 3.1), as no duplicate months exist, and will be referenced by these names throughout the remainder of the report.

Table 3.1: Concrete casting dates and reference names.

Concrete Casting Date	Concrete Reference Name
October 5, 2004	October
November 2, 2004	November
March 3, 2005	March
April 5, 2005	April
May 3, 2005	May

The concrete in different portions of the superstructure of F4 was poured on three different days on October 5, 2004, November 2, 2004, and March 3, 2005.

These locations of the concrete and the components that the different types comprise are identified in Figure 3.1 and Figure 3.2.

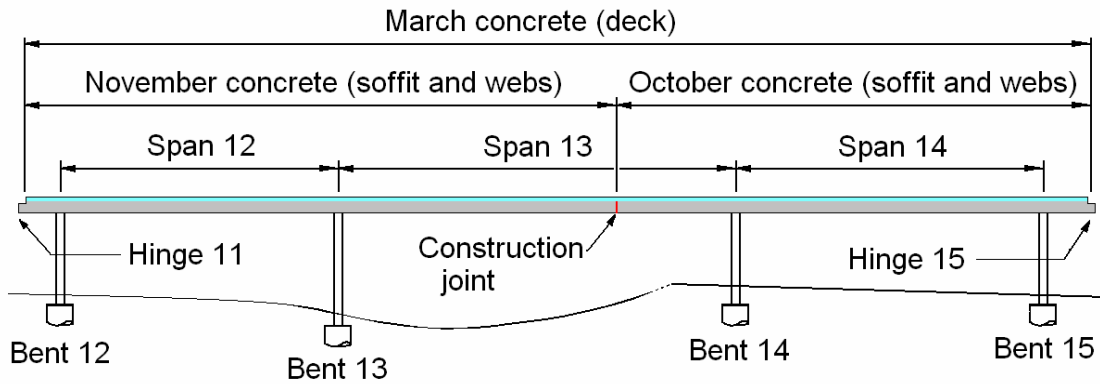


Figure 3.1: Layout of F4 with casting times of specific portions of the bridge cross section.

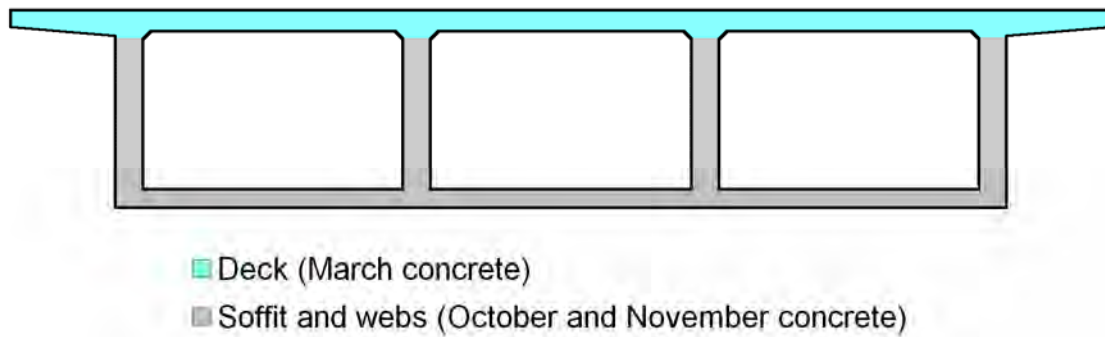


Figure 3.2: Concrete locations in the F4 superstructure cross section.

The concrete in F5 was poured on two different days on April 5, 2005 and May 3, 2005. The locations of the concrete comprising F5 are identified in Figure 3.3 and Figure 3.4.

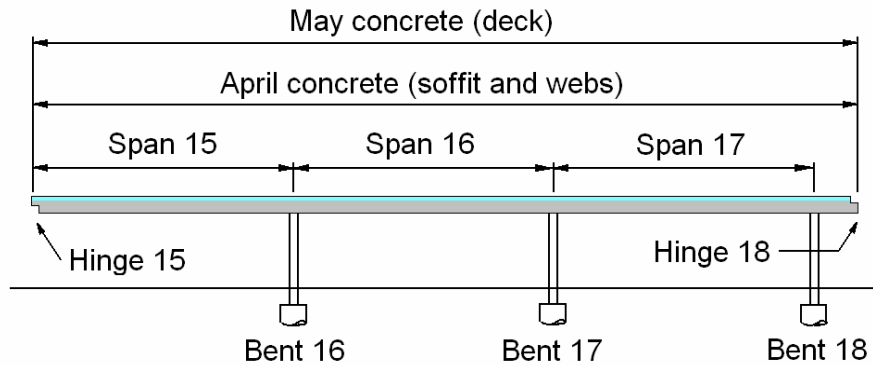


Figure 3.3: Layout of F5 with casting times of specific portions of the bridge cross section.

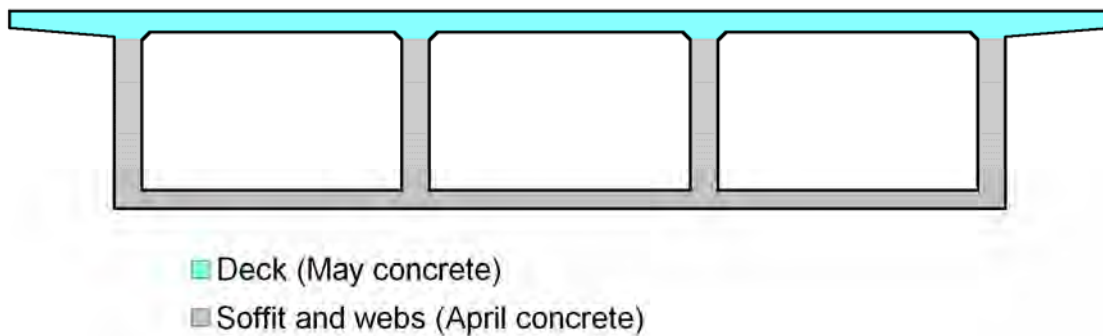


Figure 3.4: Concrete locations in the F5 superstructure cross section.

On each of the concrete pour days for the selected section of the I5/805 Bridge, concrete cylinders were cast for use in the material tests. The concrete cylinders (specimens) are 300 mm in length with a 150 mm diameter. A total of sixteen specimens, divided into three sets, were cast on each of the pour days. One set of two specimens is not loaded and is used in the determination of shrinkage. The second set of three specimens is used for determining creep and is placed under constant stress at about 30% of the concrete compressive strength at 28 days. The third set contains the remaining specimens not used in the testing of creep and shrinkage, which are used for determining concrete strength and modulus of elasticity at various ages after curing.

The preferred location of the test specimens for the duration of testing was at the bridge site. This would subject the specimens to the exact environmental conditions as those at the bridge. The actual placement of the specimens at the

UCSD campus was deemed acceptable due to the similar environmental conditions and proximity to the bridge site, Figure 3.5.

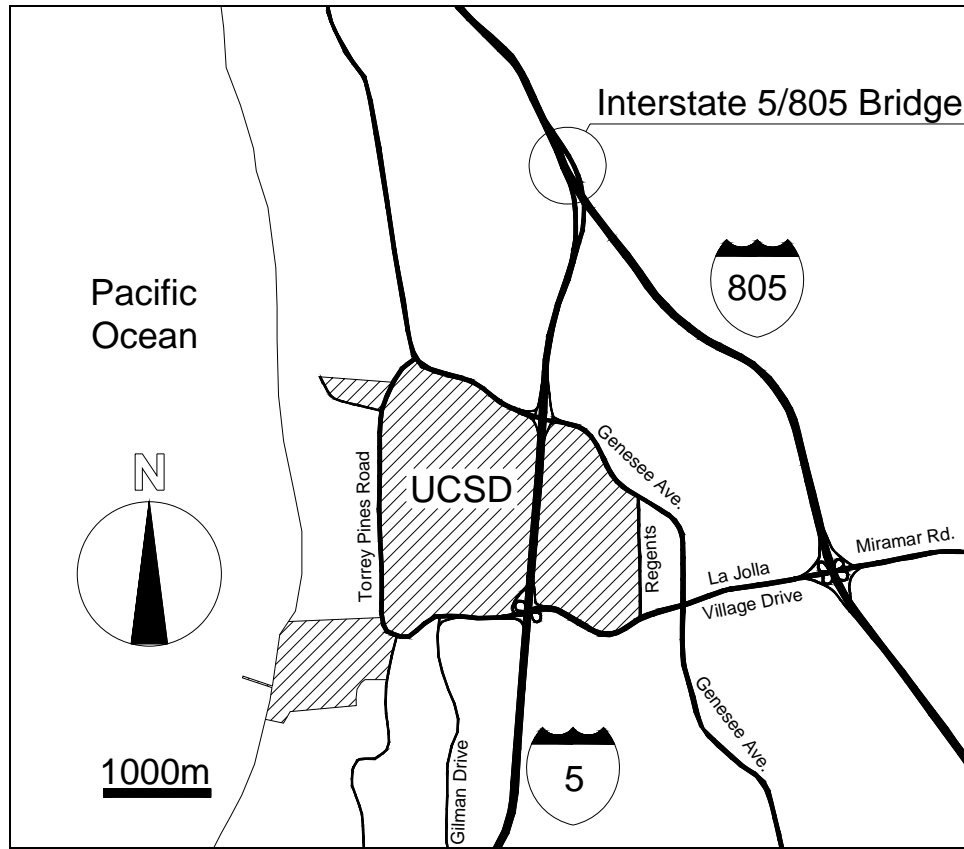


Figure 3.5: Map of UCSD and I5/805 Bridge locations.

The change in strain of the test specimens was measured at routine intervals; the procedure for measuring will be described in Section 3.4. The free shrinkage measured from the first set of cylinders is taken to represent the true shrinkage of the concrete after isolating the temperature effect.

$$\varepsilon_{shrinkage} = \varepsilon_{shrinkage,measured} - \varepsilon_{thermal} \quad (3.1)$$

Creep strain is determined by subtracting the elastic and shrinkage strains from the total measured strain.

$$\varepsilon_{creep} = \varepsilon_{creep,measured} - \varepsilon_{elastic} - \varepsilon_{shrinkage} \quad (3.2)$$

The ratio of the resulting creep strain to the elastic strain yields the creep coefficient.

$$\phi = \frac{\mathcal{E}_{creep}}{\mathcal{E}_{instantaneous}} \quad (2.1)$$

3.2.1. Factors Influential to Tests

As the material test specimens are located outdoors, they are subject to environmental conditions that influence the measured strains. To characterize the actual creep and shrinkage developed in the concrete, these influences had to be isolated from the measured experimental data, as described in the following.

3.2.1.1. Temperature

To evaluate the influence of thermal strain in the material tests, the creep and shrinkage strains were measured several times over the course of the same day on several occasions. This was done by measuring the strain in the specimens at several intervals over the day and recording the temperature at the times these measurements were made. After several months, creep and shrinkage do not occur rapidly enough to alter the strain in the concrete over the course of the day [3, 5, 15] and the change in strain is the result of thermal influence only. The measured strain over the day was divided by the change in temperature to generate the thermal expansion coefficient, determined to be 12 microstrain/°C, which is similar to common published values [19].

By taking measurements at approximately the same time of day at every measuring interval, the thermal influence could be minimized. Measurements taken between 8:00 am to 9:00 am allowed the data to be almost free of thermal influence. The physical location of the test specimens provided shading until roughly 9:00 am, maintaining the ambient temperature close to that of the reference temperature for each concrete. The strain data showed that as long as the test specimens had not been subject to direct solar radiation after a night of cooling, the thermal influence was small and could be corrected through a thermal expansion coefficient.

As a result of the observed behavior, from Eq. 3.1, the strain that occurs in the shrinkage test specimens is

$$\varepsilon_{shrinkage} = \varepsilon_{shrinkage,measured} - \varepsilon_{thermal} \quad (3.1)$$

While the strain that occurs in the loaded test specimens

$$\varepsilon_{creep} = \varepsilon_{creep,measured} - \varepsilon_{elastic} - \varepsilon_{shrinkage} - \varepsilon_{thermal} \quad (3.3)$$

Since the measured shrinkage includes the influence of shrinkage and thermal strain,

$$\varepsilon_{creep} = \varepsilon_{creep,measured} - \varepsilon_{elastic} - \varepsilon_{shrinkage,measured} \quad (3.4)$$

The measured shrinkage strain includes the influence of shrinkage and thermal strain; subtracting the thermal strain from the measured shrinkage strain yields the actual shrinkage. At the application of load, the ambient temperature at the location of the test specimens was recorded and served as the reference temperature for subsequent measurements, recorded at the time initial measurements were made. The deviation in temperature was corrected through use of an appropriate thermal expansion coefficient and resulting strain, as in

$$\varepsilon_{thermal} = \Delta T \alpha = (T - T_{ref}) \alpha \quad (3.5)$$

3.2.1.2. Relative Humidity

The relative humidity influences the development and ultimate values of creep and shrinkage over time. No correction was found in the literature to be applicable for correcting the variation of relative humidity. The equations of the specifications, on the other hand, include the relative humidity as input for calculating the development of creep and shrinkage. The average recorded relative humidity, 67% (Figure 3.6), was used in the specifications equations.

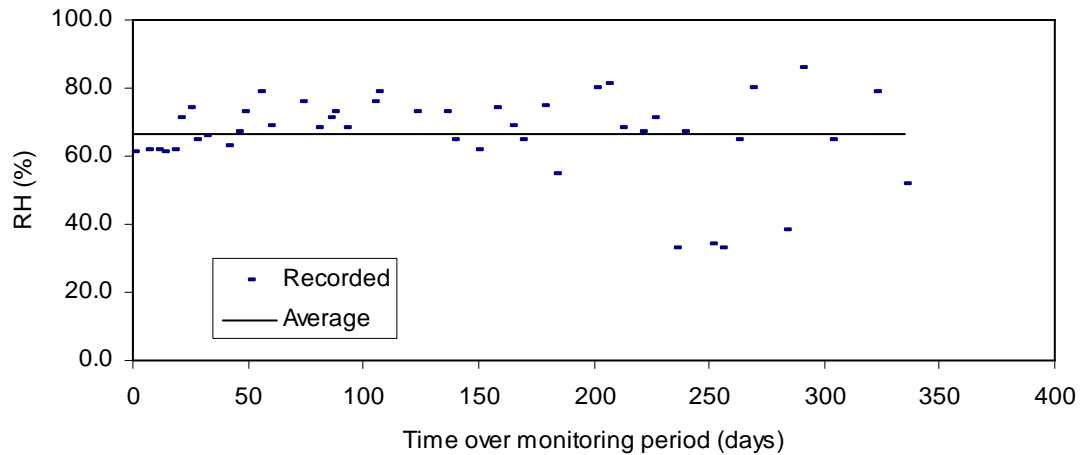


Figure 3.6: Relative humidity recorded over the monitoring period.

Altering the relative humidity for a lengthy period may result in significant changes in both creep and shrinkage [3]. Short abrupt changes in relative humidity would not result in significant changes to material behavior.

Bažant et al [4] examined the influence of cyclic relative humidity on creep and shrinkage. In their tests, they showed that a test specimen exposed to cyclic relative humidity can exhibit up to twice the creep of a specimen exposed to a relative humidity equal to the average of the cyclic humidity. Cyclic relative humidity was shown to not influence the shrinkage considerably from a specimen exposed to a constant relative humidity equal to the average of the cyclic relative humidity.

3.3. Test Setup

This section outlines the procedure used for the preparation of the test specimens for the material tests.

3.3.1. Curing

To simulate the bridge curing conditions, the test specimens were moist cured for a period of seven days at the bridge site. After concrete was placed in the plastic cylinder molds, the lids were placed and the cylinders were stored in a cool place maintaining a temperature similar to the reference of 15°C. After this

period, the molds were stripped. A piece of burlap was placed over the fresh specimens and was continually saturated with water for seven days.

3.3.2. Attachment of DEMEC points

To capture the change in strain, detachable mechanical (DEMEC) strain gage points were attached to the test specimens to serve as reference positions to measure the change in length, and hence strain, as shown in Figure 3.7. The DEMEC points were permanently adhered in pairs diametrically opposite of one another on the concrete cylinders. To ensure positive adhesion of the DEMEC points to the concrete, the area to receive the DEMEC points was sanded and cleaned. DEMEC points were affixed to the roughened and cleaned areas with adhesive. An Invar gage bar of 200 mm was used to establish the initial distance between the two DEMEC points while the adhesive set.

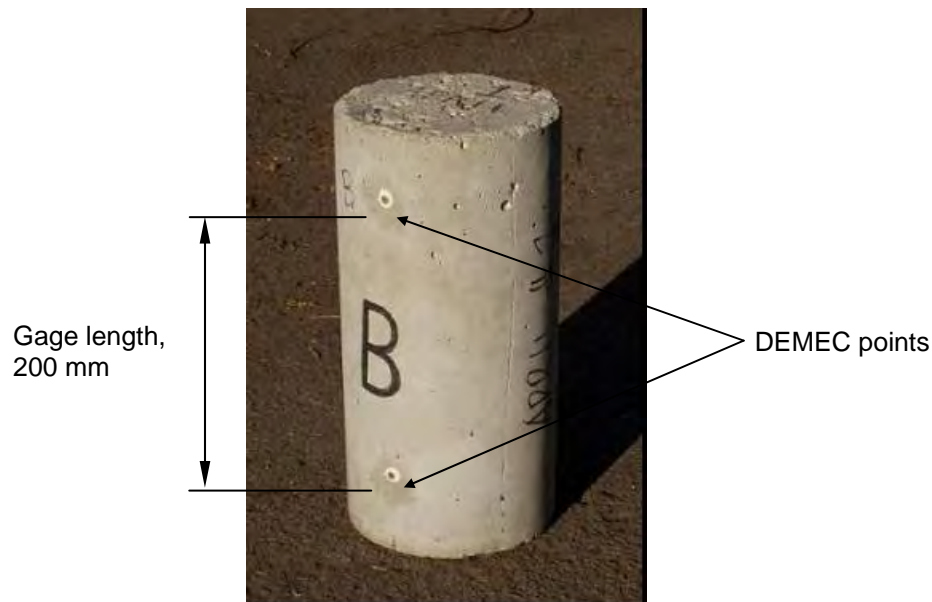


Figure 3.7: Locations of DEMEC points as positioned on a test specimen.

3.3.3. Hydrostone cap

As the ends of the concrete cylinders usually contain surface imperfections, a Hydrostone cap was placed on both ends of each specimen to create a level surface, as shown in Figure 3.8. The Hydrostone cap also helps distribute the compressive force evenly to the specimens when they are stacked in the setup.

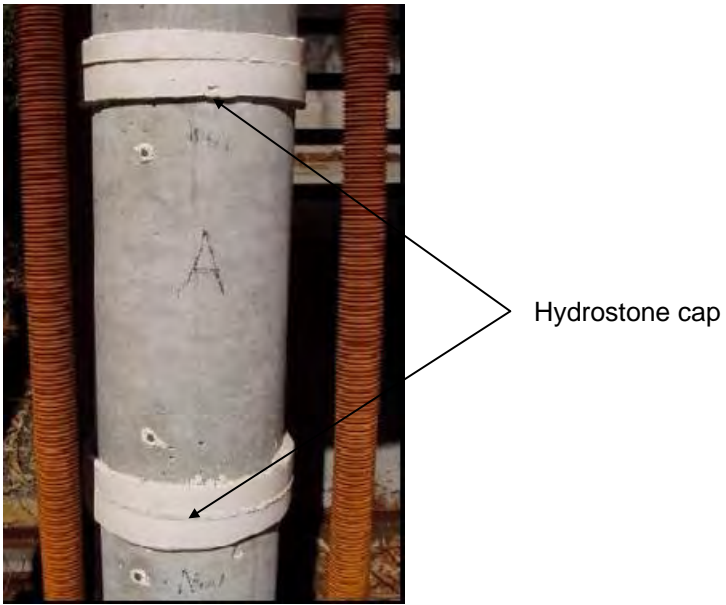


Figure 3.8: Hydrostone cap placed on a test specimen.

3.3.4. Creep Test Setup

A special test setup was designed to apply permanent load, as shown in Figure 3.9. These fixtures were designed to contain three test specimens stacked end-to-end vertically in the fixture. A hydraulic jack was used to compress a spring placed between the two lower steel plates. At the desired level of load, nuts were tightened on the all-threaded bars to retain the load on the specimens. A ball-joint assembly was used to ensure concentric loading on the specimens.

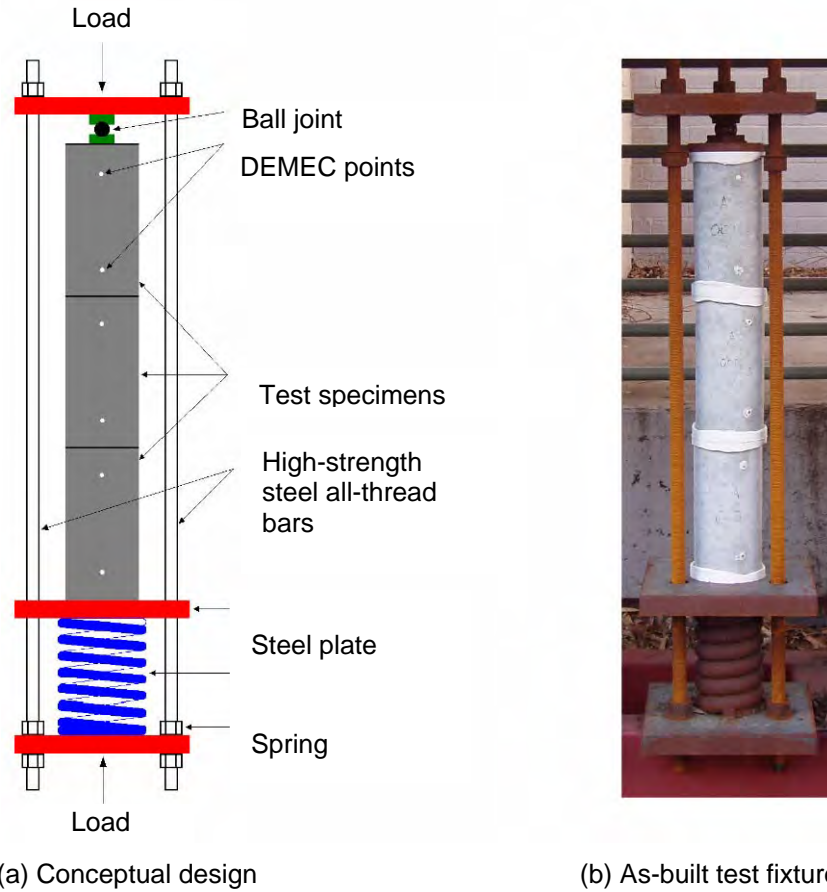


Figure 3.9: Setup of creep test fixtures.

Creep tests were performed at major loading instants to the bridge. Figure 3.10 shows all of the creep test setups for all of the material tests.



Figure 3.10: All creep test setups.

3.4. Processed Data

A DEMEC gage was used to measure the distance between the two DEMEC points on each test specimen as shown in Figure 3.11. The calculation of shrinkage strain and creep strain from the measured data is fundamentally the same; the differences arise from the procedures taken to isolate the required strains from other influences. The shrinkage strain readings should be measured at the same time as the creep strain readings in order to allow for appropriate isolation of the creep strain from its shrinkage counterpart. The timeline indicating the data collection intervals is indicated in Figure 3.12



Figure 3.11: Measuring with DEMEC gage.



Figure 3.12: Experimental data collection timeline.

3.4.1. Shrinkage Strain

The initial DEMEC reading $DR_{initial}$ serves as the baseline for subsequent shrinkage calculations. The measured change in strain, designated as ST DEMEC readings, is a result of two sources: shrinkage and thermal strains. The ST strain $\varepsilon_{ST,i}$ at any time instant is the difference between DEMEC readings at any instant DR_i and the initial DEMEC reading $DR_{initial}$, divided by the $DR_{initial}$ plus the gage length of 200 mm,

$$\varepsilon_{ST,i} = \frac{DR_i - DR_{initial}}{DR_{initial} + 200} \quad (3.6)$$

To isolate the shrinkage strain $\varepsilon_{sh,i}$ from the thermal influences $\varepsilon_{th,i}$, the calculated thermal strain must be subtracted from the ST strain. The thermal strain is calculated using Eq. 3.7.

$$\varepsilon_{thermal,i} = \Delta T_i \alpha = -(T_{ref} - T_i) \alpha \quad (3.7)$$

The true shrinkage strain $\varepsilon_{sh,i}$ is provided by Eq. 3.8.

$$\varepsilon_{sh}(t_i, t_s) = \varepsilon_{ST,i} - \varepsilon_{thermal,i} \quad (3.8)$$

This results in the shrinkage strain for the interval bounded by the onset of drying t_s to any point in time t_i during monitoring. The difference between initial and final measured shrinkage yields the total shrinkage strain, which is used later in this chapter for each of the concrete types.

3.4.2. Creep Coefficient

Similar to shrinkage measurements, before the specimens of the creep test are loaded, the initial distance between the DEMEC points $DR_{initial}$ was measured. Once load has been applied, a second DEMEC measurement DR_0 is made to determine the elastic strain $\varepsilon_{elastic}$.

$$\varepsilon_{elastic} = \frac{DR_0 - DR_{initial}}{DR_{initial} + 200} \quad (3.9)$$

Creep measurements are subject to the influence of creep, shrinkage, and thermal strains, thus the designation *CST* is adopted and the strain $\varepsilon_{CST,i}$ is determined at each interval, between loading and some later time instant. The change in strain within an interval is the difference between the DEMEC *CST* reading at any point in time DR_i and the initial reading $DR_{initial}$. Dividing the incremental change in length by the baseline length ($DR_{initial}$ plus 200 mm) yields the strain occurring within any time interval. The total *CST* strain occurring between loading and any point in time t_i , at which data was collected, is expressed as

$$\varepsilon_{CST,i} = \frac{DR_i - DR_{initial}}{DR_{initial} + 200} \quad (3.10)$$

To isolate the creep strain $\varepsilon_{cre,i}$ (which includes elastic shortening) from the ST influence, the strain resulting from $\varepsilon_{ST,i}$ is subtracted from $\varepsilon_{CST,i}$.

$$\varepsilon_{cre,i} = \varepsilon_{CST,i} - \varepsilon_{ST,i} \quad (3.11)$$

The elastic strain is removed, resulting in the true creep strain $\varepsilon_{cr,i}$

$$\varepsilon_{cr,i} = \varepsilon_{cre,i} - \varepsilon_{elastic} \quad (3.12)$$

The ratio of the creep strain measured between the time of loading t_0 and a later time t_i to the instantaneous elastic strain at t_0 , is referred to as the creep coefficient $\phi(t_i, t_0)$, as given by:

$$\phi(t_i, t_0) = \frac{\varepsilon_{cr,i}}{\varepsilon_{elastic}} \quad (3.13)$$

3.5. Calculation of Experimental Creep and Shrinkage

This section presents the experimental creep and shrinkage obtained from the measured data collected from the material tests. The influence of temperature is removed from the measured shrinkage to present the true shrinkage for the concretes used in the bridge. The shrinkage, thermal, and elastic strains are removed from the measured creep to determine the true creep for the concrete in the bridge. An example calculation using the collected data and the equations in Section 3.4 will be presented. Additional data and figures from the material testing are presented in the Appendix A.

3.5.1. Shrinkage

This section contains the shrinkage that was determined from the concrete test specimens used for this research. Additionally, the method of calculating the shrinkage using the equations in Section 3.4 will be illustrated through example calculations to illustrate the required steps necessary for isolating the true shrinkage.

3.5.1.1. Determination of Experimental Shrinkage

An example of the steps taken to calculate the shrinkage from the data from the material tests data is included. Since the concrete shrinkage from F4 was not measured until load was applied and appears to be unreliable (as will be shown later) the measured shrinkage from the April batch concrete in F5 will be used to illustrate the method of determining the true shrinkage of the concrete. It is noted that this is an approximation but given that the two frames are in close proximity to each other and that the climatic conditions and other factors are not likely to change between these two locations the approximation is considered to be justifiable.

The measured shrinkage includes components of temperature, which must be eliminated before revealing the true shrinkage of the concrete, as in Eq. 3.1. Table 3.2 displays the data corresponding to the measured shrinkage for the April concrete from the soffit and stems in F5.

Table 3.2: Table of values associated with the calculation of shrinkage from the April batch concrete from F5.

Time (days)	Demecc Readings (DR)					Measured shrinkage strain (m/m)					Thermal strain					True shrinkage (m/m)				
	1	2	3	4	5	6	7	8	9	10	11	12	13	14	15	16	17			
0/initial	0.018	-0.023	0.025	0.028	0.028	0.000000	0.000000	0.000000	0.000000	0.000000	20.0	0.000000	0.000000	0.000000	0.000000	0.000000	0.000000			
7	-0.014	-0.033	-0.005	0.012	0.012	-0.000160	-0.000050	-0.000150	-0.000080	-0.000110	14.0	-0.000072	-0.000088	-0.000022	-0.000078	-0.000008	-0.000038			
10	-0.029	-0.056	-0.021	-0.008	-0.008	-0.000235	-0.000165	-0.000230	-0.000180	-0.000203	16.5	-0.000042	-0.000193	-0.000123	-0.000188	-0.000138	-0.000161			
13	-0.034	-0.056	-0.019	-0.009	-0.009	-0.000260	-0.000165	-0.000220	-0.000185	-0.000208	16.0	-0.000048	-0.000207	-0.000117	-0.000172	-0.000137	-0.000160			
17	-0.033	-0.058	-0.020	-0.013	-0.013	-0.000255	-0.000175	-0.000225	-0.000205	-0.000215	16.0	-0.000048	-0.000207	-0.000127	-0.000177	-0.000157	-0.000167			
27	-0.066	-0.081	-0.049	-0.038	-0.038	-0.000420	-0.000290	-0.000370	-0.000330	-0.000353	18.0	-0.000024	-0.000396	-0.000266	-0.000346	-0.000306	-0.000329			
29	-0.067	-0.087	-0.052	-0.044	-0.044	-0.000425	-0.000320	-0.000385	-0.000360	-0.000373	16.9	-0.000037	-0.000388	-0.000283	-0.000348	-0.000323	-0.000335			
31	-0.069	-0.091	-0.059	-0.046	-0.046	-0.000435	-0.000340	-0.000420	-0.000370	-0.000391	20.4	0.000005	-0.000440	-0.000345	-0.000425	-0.000375	-0.000396			
34	-0.073	-0.093	-0.067	-0.048	-0.048	-0.000455	-0.000350	-0.000460	-0.000380	-0.000411	17.2	0.000034	-0.000422	-0.000317	-0.000427	-0.000346	-0.000378			
38	-0.074	-0.093	-0.062	-0.045	-0.045	-0.000460	-0.000350	-0.000435	-0.000365	-0.000403	19.7	-0.000004	-0.000457	-0.000347	-0.000432	-0.000361	-0.000399			
38	-0.074	-0.093	-0.062	-0.045	-0.045	-0.000460	-0.000350	-0.000435	-0.000365	-0.000403	19.7	-0.000004	-0.000457	-0.000347	-0.000432	-0.000361	-0.000399			
41	-0.081	-0.102	-0.072	-0.059	-0.059	-0.000495	-0.000395	-0.000485	-0.000435	-0.000453	16.0	-0.000048	-0.000447	-0.000347	-0.000437	-0.000387	-0.000405			
45	-0.089	-0.107	-0.072	-0.069	-0.069	-0.000535	-0.000420	-0.000485	-0.000485	-0.000481	17.2	-0.000034	-0.000502	-0.000387	-0.000452	-0.000452	-0.000448			
59	-0.098	-0.114	-0.084	-0.071	-0.071	-0.000580	-0.000455	-0.000545	-0.000495	-0.000519	18.4	-0.000019	-0.000561	-0.000436	-0.000526	-0.000476	-0.000500			
66	-0.106	-0.117	-0.091	-0.083	-0.083	-0.000620	-0.000470	-0.000580	-0.000555	-0.000557	19.0	-0.000012	-0.000608	-0.000458	-0.000568	-0.000543	-0.000545			
71	-0.110	-0.123	-0.095	-0.080	-0.080	-0.000640	-0.000500	-0.000600	-0.000540	-0.000570	21.0	0.000012	-0.000652	-0.000512	-0.000612	-0.000552	-0.000582			
72	-0.115	-0.121	-0.094	-0.085	-0.085	-0.000665	-0.000490	-0.000595	-0.000565	-0.000579	18.0	-0.000024	-0.000641	-0.000466	-0.000571	-0.000541	-0.000555			
73	-0.118	-0.123	-0.095	-0.083	-0.083	-0.000680	-0.000500	-0.000600	-0.000555	-0.000584	17.5	-0.000030	-0.000650	-0.000470	-0.000570	-0.000525	-0.000554			
78	-0.117	-0.125	-0.102	-0.086	-0.086	-0.000675	-0.000510	-0.000635	-0.000570	-0.000588	19.0	-0.000012	-0.000663	-0.000498	-0.000623	-0.000558	-0.000586			
90	-0.124	-0.130	-0.111	-0.089	-0.089	-0.000710	-0.000535	-0.000680	-0.000585	-0.000628	18.6	-0.000017	-0.000694	-0.000519	-0.000664	-0.000568	-0.000611			
92	-0.129	-0.129	-0.104	-0.086	-0.086	-0.000735	-0.000530	-0.000645	-0.000570	-0.000620	21.0	0.000024	-0.000711	-0.000506	-0.000621	-0.000546	-0.000596			
108	-0.113	-0.122	-0.096	-0.083	-0.083	-0.000655	-0.000495	-0.000605	-0.000555	-0.000578	18.1	0.000013	-0.000669	-0.000509	-0.000618	-0.000568	-0.000591			
125	-0.127	-0.132	-0.108	-0.094	-0.094	-0.000725	-0.000545	-0.000665	-0.000610	-0.000637	19.4	-0.000007	-0.000718	-0.000538	-0.000658	-0.000603	-0.000629			
135	-0.124	-0.129	-0.106	-0.092	-0.092	-0.000710	-0.000530	-0.000655	-0.000600	-0.000624	22.0	0.000024	-0.000734	-0.000554	-0.000679	-0.000624	-0.000648			
143	-0.131	-0.135	-0.117	-0.095	-0.095	-0.000745	-0.000560	-0.000710	-0.000615	-0.000642	18.4	-0.000019	-0.000726	-0.000541	-0.000691	-0.000596	-0.000639			
150	-0.133	-0.132	-0.113	-0.098	-0.098	-0.000756	-0.000545	-0.000690	-0.000630	-0.000655	20.0	0.000000	-0.000756	-0.000545	-0.000690	-0.000630	-0.000655			
154	-0.136	-0.139	-0.122	-0.104	-0.104	-0.000771	-0.000580	-0.000735	-0.000660	-0.000687	18.3	-0.000020	-0.000750	-0.000560	-0.000715	-0.000640	-0.000666			
164	-0.137	-0.134	-0.124	-0.099	-0.099	-0.000776	-0.000555	-0.000745	-0.000635	-0.000678	17.2	-0.000034	-0.000742	-0.000522	-0.000712	-0.000602	-0.000644			
169	-0.136	-0.145	-0.121	-0.103	-0.103	-0.000771	-0.000610	-0.000730	-0.000655	-0.000692	21.0	0.000012	-0.000783	-0.000522	-0.000742	-0.000667	-0.000704			
186	-0.142	-0.145	-0.135	-0.106	-0.106	-0.000801	-0.000610	-0.000801	-0.000670	-0.000720	17.8	-0.000026	-0.000774	-0.000584	-0.000774	-0.000644	-0.000694			
192	-0.117	-0.142	-0.142	-0.122	-0.122	-0.000675	-0.000595	-0.000836	-0.000600	-0.000652	17.1	-0.000035	-0.000641	-0.000561	-0.000801	-0.000465	-0.000617			
198	-0.121	-0.137	-0.123	-0.084	-0.084	-0.000695	-0.000570	-0.000740	-0.000560	-0.000642	17.0	-0.000036	-0.000659	-0.000534	-0.000704	-0.000524	-0.000606			
206	-0.140	-0.145	-0.137	-0.097	-0.097	-0.000791	-0.000610	-0.000811	-0.000625	-0.000709	15.1	-0.000059	-0.000732	-0.000552	-0.000752	-0.000567	-0.000650			
212	-0.144	-0.149	-0.140	-0.100	-0.100	-0.000811	-0.000630	-0.000826	-0.000640	-0.000727	16.0	-0.000048	-0.000763	-0.000582	-0.000778	-0.000592	-0.000679			
221	-0.156	-0.157	-0.146	-0.116	-0.116	-0.000871	-0.000671	-0.000856	-0.000720	-0.000779	18.5	-0.000018	-0.000853	-0.000653	-0.000838	-0.000702	-0.000761			
225	-0.148	-0.152	-0.139	-0.112	-0.112	-0.000831	-0.000645	-0.000821	-0.000700	-0.000749	18.0	-0.000024	-0.000807	-0.000621	-0.000797	-0.000676	-0.000725			
237	-0.168	-0.165	-0.152	-0.127	-0.127	-0.000931	-0.000711	-0.000886	-0.000775	-0.000826	11.5	-0.000102	-0.000829	-0.000609	-0.000784	-0.000673	-0.000724			
241	-0.155	-0.160	-0.143	-0.122	-0.122	-0.000866	-0.000686	-0.000841	-0.000750	-0.000786	15.0	-0.000060	-0.000806	-0.000626	-0.000781	-0.000690	-0.000726			
248	-0.163	-0.163	-0.155	-0.128	-0.128	-0.000906	-0.000701	-0.000901	-0.000780	-0.000822	11.4	-0.000103	-0.000803	-0.000597	-0.000797	-0.000677	-0.000719			
254	-0.140	-0.141	-0.125	-0.103	-0.103	-0.000791	-0.000590	-0.000750	-0.000630	-0.000697	17.5	-0.000030	-0.000761	-0.000560	-0.000720	-0.000625	-0.000667			
269	-0.136	-0.112	-0.095	-0.098	-0.098	-0.000771	-0.000445	-0.000600	-0.000530	-0.000612	15.0	-0.000060	-0.000711	-0.000385	-0.000540	-0.000570	-0.000552			
276	-0.148	-0.124	-0.109	-0.124	-0.124	-0.000831	-0.000505	-0.000670	-0.000760	-0.000692	10.0	-0.000120	-0.000711	-0.000385	-0.000550	-0.000640	-0.000572			
289	-0.155	-0.136	-0.127	-0.115	-0.115	-0.000866	-0.000565	-0.000760	-0.000715	-0.000727	11.0	-0.000084	-0.000758	-0.000447	-0.000652	-0.000607	-0.000619			
308	-0.148	-0.129	-0.120	-0.108	-0.108	-0.000831	-0.000530	-0.000725	-0.000680	-0.000692	13.0	-0.000084	-0.000747	-0.000446	-0.000641	-0.000596	-0.000608			
321	-0.141	-0.119	-0.123	-0.091	-0.091	-0.000796	-0.000480	-0.000740	-0.000595	-0.000653	18.9	-0.000013	-0.000782	-0.000467	-0.000727	-0.000582	-0.000640			
325	-0.116	-0.158	-0.112	-0.122	-0.122	-0.000670	-0.000676	-0.000685	-0.000750	-0.000695	11.7	-0.000100	-0.000571	-0.000576	-0.000586	-0.000651	-0.000596			
339	-0.131	-0.138	-0.126	-0.089	-0.089	-0.000745	-0.000575	-0.000755	-0.000585	-0.000665	13.4	-0.000079	-0.000666	-0.000496	-0.000676	-0.000506	-0.000586			

As mentioned in Section 3.4, the DEMEC gage measures the change in length of the test specimens from a gage length of 200 mm. The time (in days) is listed in column 1 of Table 3.2 and represents the time after the onset of drying, thus the 0/initial row designates the first DEMEC reading that was made after the DEMEC points were adhered to the concrete specimens.

To illustrate an example of how the calculation of strains is performed, the illustration is presented for the data of the 1A DEMEC point position. The procedure for calculating the strains for the other positions of the DEMEC points as placed on the other surfaces of the test specimens is the same as that performed here.

Eq. 3.6 determines the strain based on the initial length between the DEMEC points, accommodated by the $DR_{initial} + 200$ terms in the denominator.

$$\varepsilon_{ST,i} = \frac{DR_i - DR_{initial}}{DR_{initial} + 200} \quad (3.6)$$

As an example, the shrinkage that occurred in the specimens between the onset of drying (0/initial) and 339 days later, is calculated as the following.

$$\varepsilon_{ST,339} = \frac{DR_{339} - DR_{initial}}{DR_{initial} + 200} = \frac{-0.131 - 0.018}{0.018 + 200} (10^6) = -745$$

The strain $\varepsilon_{ST,339}$ of -745 can be seen in column 6 corresponding to the row in which time i is 339 days after the onset of drying. The value is also indicated (as circled) in Figure 3.13. The measured strain (including the influence of temperature) was calculated for each of the specimens (1A, 1B, 2A, and 2B) and located in columns 6 through 9. The average of all the calculated shrinkage strains is presented in column 10. The calculated strains and the average in columns 6 through 10 correspond to the strains in presented in Figure 3.13.

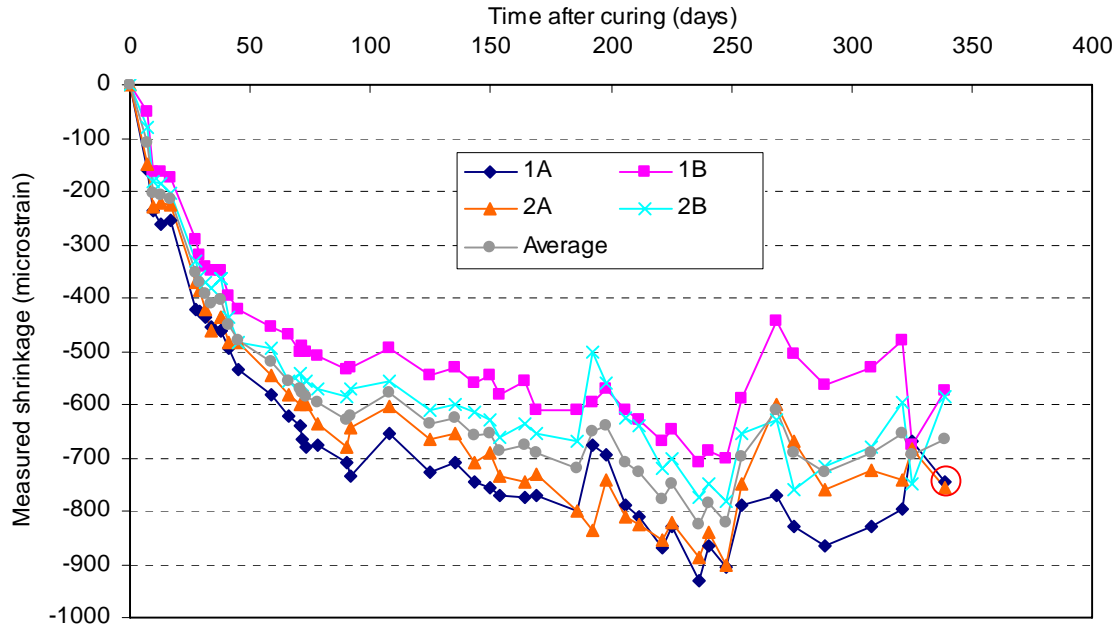


Figure 3.13: Measured shrinkage strain from April batch concrete.

The strains presented in Figure 3.13 are the measured strains and include thermal influences. The ambient air temperatures were collected at the times the readings were taken and are included in column 11 of Table 3.2. The reference temperature T_{ref} occurs in the 0/initial row and is 20.0 °C. The component of thermal strain is accommodated using Eq. 3.7.

$$\varepsilon_{thermal,i} = \Delta T_i \alpha = (T_i - T_{ref}) \alpha \quad (3.7)$$

Over the same time period as the previous calculation, the temperature at 339 days after the onset of curing T_{339} was 13.4 °C. The thermal expansion coefficient used, as mentioned previously, was taken as 12 microstrain/°C. Thus, the thermal strain within this period is as follows:

$$\varepsilon_{thermal,7} = \Delta T_7 \alpha = (T_7 - T_{ref}) \alpha = -(20.0 - 13.4) 12 = -79$$

The thermal strain $\varepsilon_{thermal,339}$ of -79 microstrain is located in Table 3.2 in the time i 339 row in column 12. This value can also be located in Figure 3.14, which displays the thermal strain at each of the measuring points in time during the period over which data were collected.

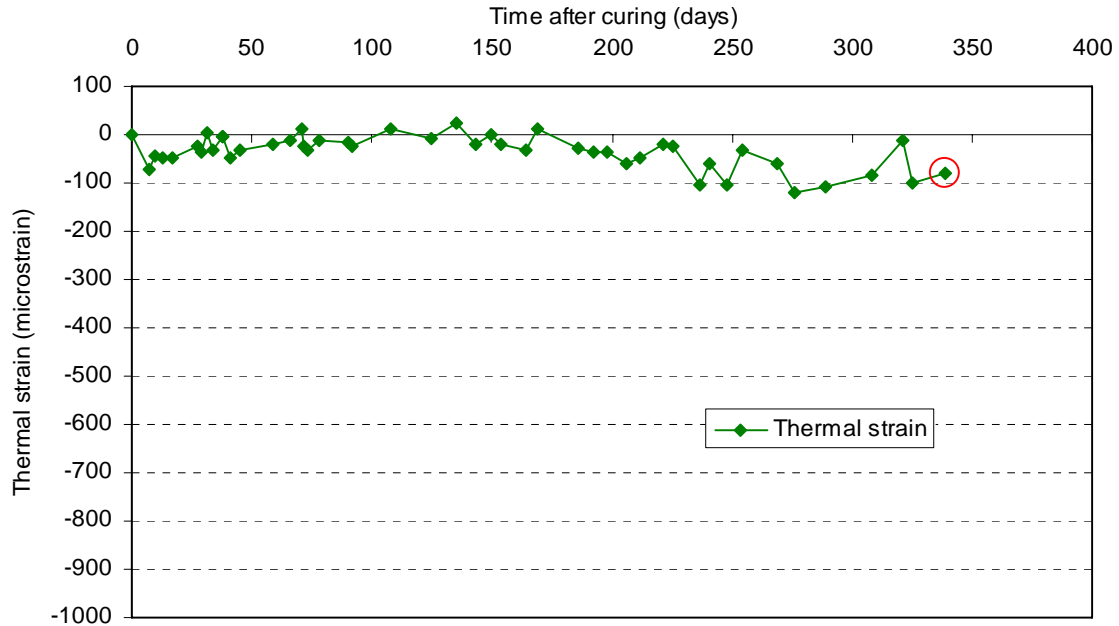


Figure 3.14: Thermal strain during strain measuring of the April batch concrete.

The measured shrinkage strain, which includes true shrinkage and thermal strains, are separated to result in the true shrinkage only, which is accommodated by Eq. 3.8.

$$\varepsilon_{sh}(t_i, t_s) = \varepsilon_{ST,i} - \varepsilon_{thermal,i} \quad (3.8)$$

$$\varepsilon_{sh}(t_{339}, t_0) = \varepsilon_{ST,339} - \varepsilon_{thermal,339} = -745 - (-79) = -666$$

The $\varepsilon_{sh}(t_7, t_0)$ term calculated above of -666 microstrain is located in time i of 339 days row in column 13 of Table 3.2 as well as indicated in Figure 3.15. The calculated true shrinkage values are presented in Figure 3.15 for each of the concrete specimens from the April batch concrete.

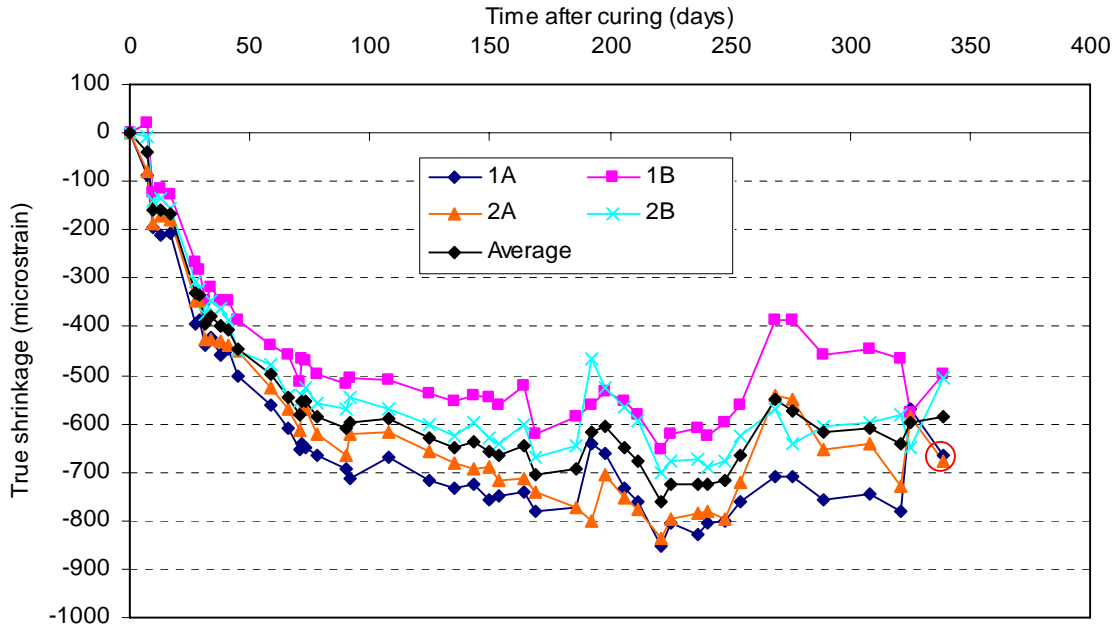


Figure 3.15: True shrinkage strain from April batch concrete.

The procedure for calculating the true shrinkage from the DEMEC readings of all specimens is the same as that performed above. The measured data (DEMEC readings), measured shrinkage, and true shrinkage, as determined in the previous example, are included for all concrete specimens in Appendix A. The calculated true shrinkage for each of the specimens is included in Figure 3.16 through Figure 3.20.

3.5.1.2. Experimental Shrinkage for all Concrete Specimens

The figures presented in this section display the experimental true shrinkage that was obtained through testing for each of the five batches of concrete.

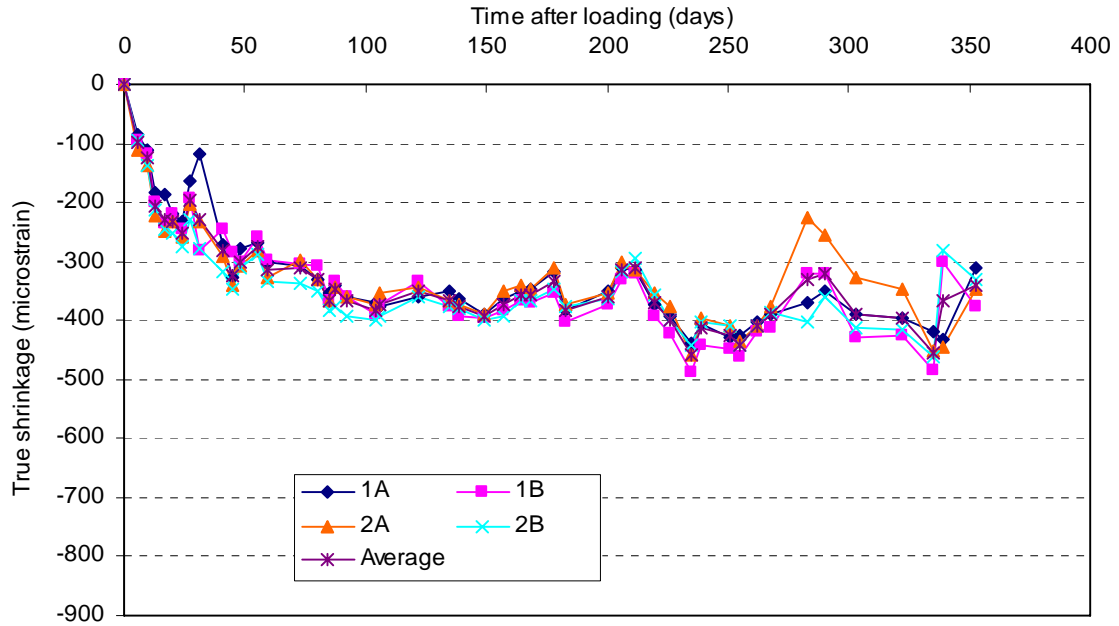


Figure 3.16: True shrinkage from October batch concrete.

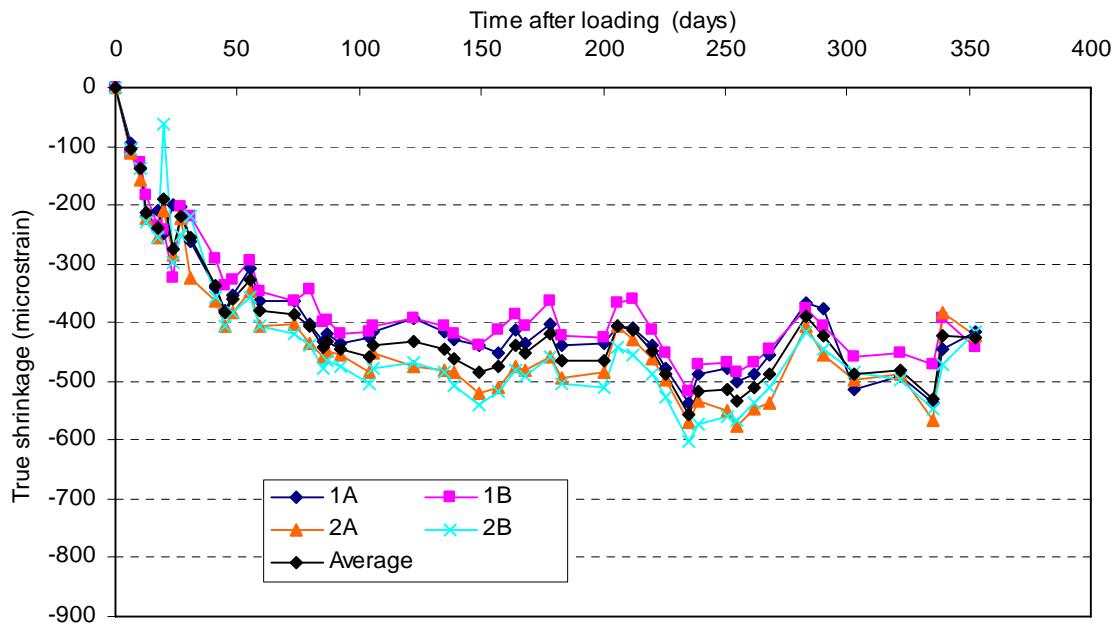


Figure 3.17: True shrinkage from November batch concrete.

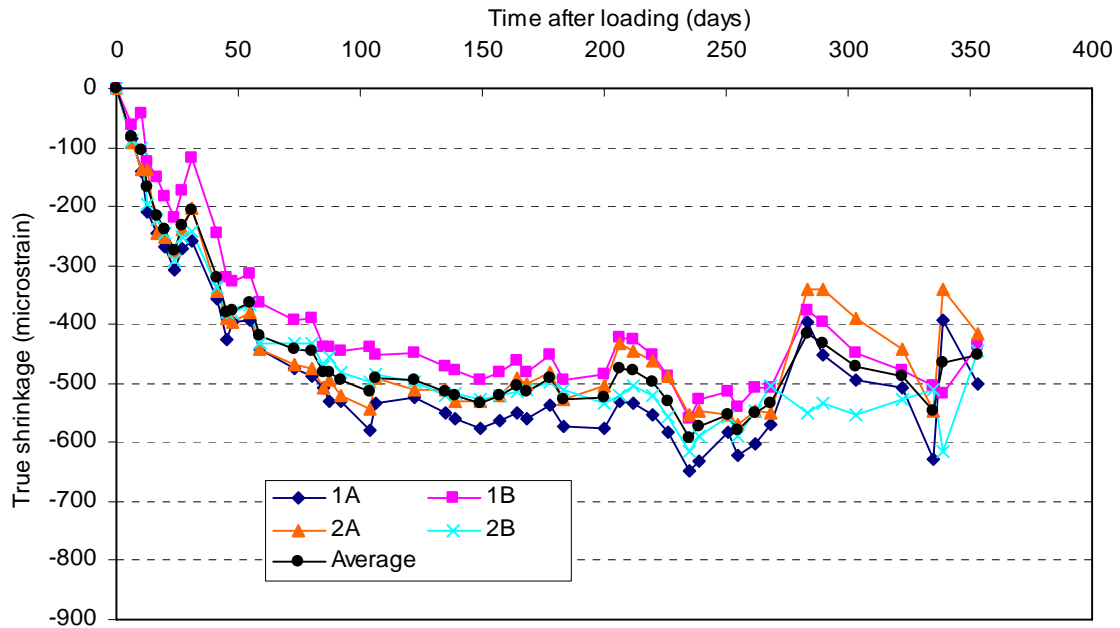


Figure 3.18: True shrinkage from March batch concrete.

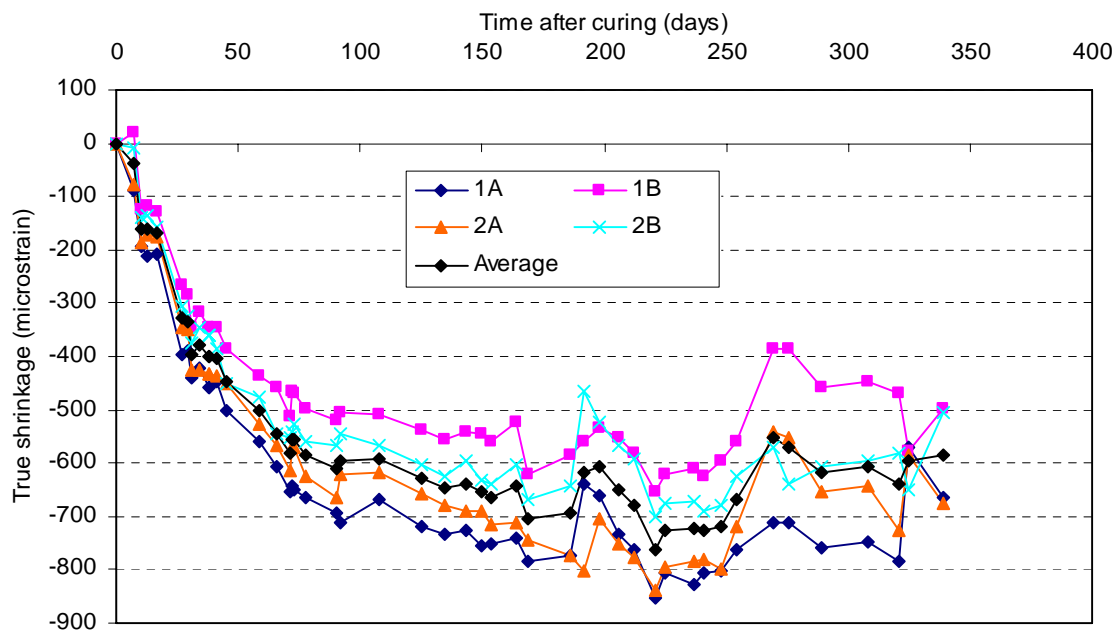


Figure 3.19: True shrinkage from April batch concrete.

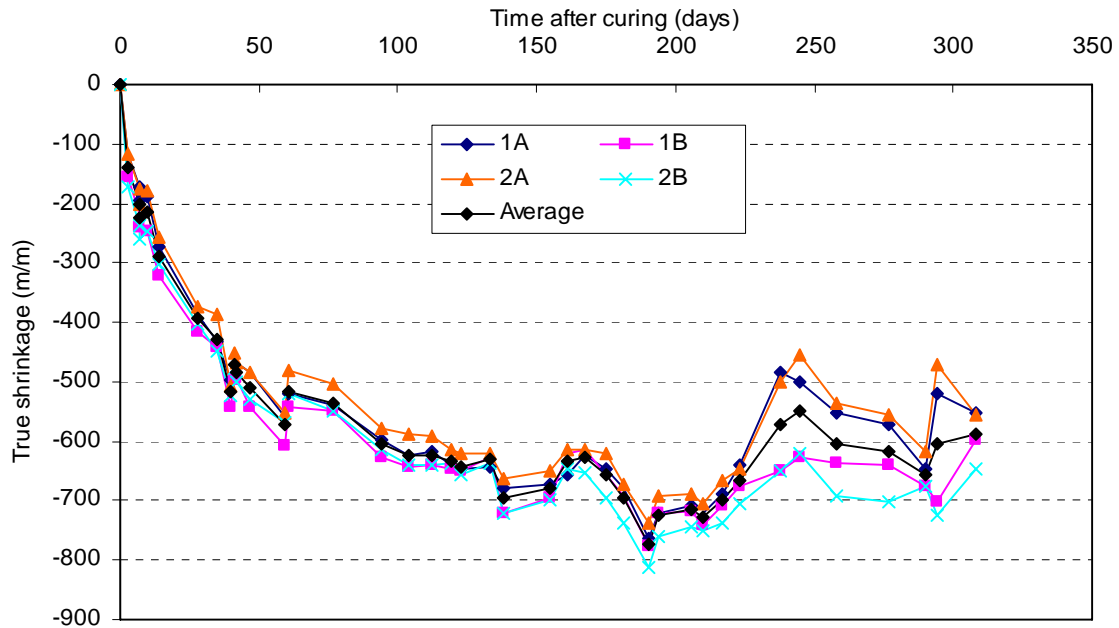


Figure 3.20: True shrinkage from May batch concrete.

3.5.2. Creep

The creep was determined from the measured data from the creep specimens. Similar to the example that was performed for determining the true shrinkage in the previous section, the creep coefficient is determined for each of the concretes. The procedure used to calculate the creep coefficient is illustrated through an example calculation that performs all of the steps taken to isolate the external influences from the true creep.

3.5.2.1. Determination of Experimental Creep

An example of the calculations illustrating the procedure used for isolating the creep strain, and hence the creep coefficient, is illustrated here. The test specimen and DEMEC point positions designated 1A will be used for this example and can be followed consistently through the calculations. The times at which DEMEC measurements were taken are listed in column 1 of Table 3.3.

The measured strain associated with creep is calculated from the DEMEC readings from the creep test specimens. As mentioned in Section 3.2 and 3.4,

the measured creep strain includes components of shrinkage, thermal, and elastic strains. The measured creep strain is calculated from the data obtained from measuring using the DEMEC gage and is determined from Eq. 3.10, as follows.

$$\varepsilon_{CST,i} = \frac{DR_i - DR_{initial}}{DR_{initial} + 200} \quad (3.10)$$

The measured creep strain (including shrinkage, thermal, and elastic strain) is calculated for this example at 301 days after loading. The difference between the DEMEC readings in the numerator $DR_i - DR_{initial}$ represents the change in length of the specimens. The initial length accommodated by the terms in the denominator, as the DEMEC gage indicates the change in length from an initial gage reading, hence $DR_{initial} + 200$.

$$\varepsilon_{CST,301} = \frac{DR_{301} - DR_{initial}}{DR_{initial} + 200} = \frac{-0.434 - (-0.111)}{-0.111 + 200} (10^6) = -1616$$

Table 3.3: Table of values associated with the calculation of creep from the April batch concrete from F5.

Time (days)	DEMEC Reading (DR)						Measured creep strain ($\mu\text{m/m}$) $\epsilon_{\text{CST},1}$						Thermal/ Shrinkage strain ($\mu\text{m/m}$)
	1A	1B	2A	2B	3A	3B	1A	1B	2A	2B	3A	3B	
1													
initial	-0.111	-0.091	-0.100	-0.041	-0.040	-0.107	0	0	0	0	0	0	0
0	-0.208	-0.184	-0.207	-0.117	-0.154	-0.182	-485	-465	-535	-380	-570	-375	-50
3	-0.253	-0.217	-0.252	-0.150	-0.199	-0.218	-710	-630	-760	-545	-795	-555	-79
7	-0.264	-0.223	-0.263	-0.155	-0.208	-0.223	-765	-660	-815	-570	-840	-580	-116
21	-0.287	-0.240	-0.284	-0.168	-0.231	-0.240	-880	-745	-920	-635	-955	-665	-154
28	-0.291	-0.247	-0.292	-0.171	-0.237	-0.243	-900	-780	-960	-650	-985	-680	-168
33	-0.297	-0.251	-0.299	-0.173	-0.244	-0.257	-931	-800	-995	-660	-1020	-750	-176
34	-0.305	-0.258	-0.306	-0.180	-0.251	-0.257	-971	-835	-1031	-695	-1055	-750	-181
35	-0.305	-0.261	-0.306	-0.186	-0.253	-0.262	-971	-850	-1031	-725	-1065	-775	-195
40	-0.311	-0.264	-0.312	-0.191	-0.258	-0.264	-1001	-865	-1061	-750	-1090	-785	-218
52	-0.320	-0.272	-0.319	-0.197	-0.267	-0.272	-1046	-905	-1096	-780	-1135	-825	-175
54	-0.325	-0.271	-0.324	-0.195	-0.272	-0.271	-1071	-900	-1121	-770	-1160	-820	-224
70	-0.324	-0.271	-0.331	-0.194	-0.277	-0.274	-1066	-900	-1156	-765	-1185	-835	-231
87	-0.345	-0.289	-0.351	-0.209	-0.298	-0.290	-1171	-990	-1256	-840	-1290	-915	-255
97	-0.342	-0.286	-0.351	-0.207	-0.298	-0.287	-1156	-975	-1256	-830	-1290	-900	-253
105	-0.358	-0.300	-0.365	-0.221	-0.310	-0.298	-1236	-1045	-1326	-900	-1350	-956	-284
112	-0.353	-0.292	-0.357	-0.212	-0.303	-0.292	-1211	-1005	-1286	-855	-1315	-925	-275
116	-0.361	-0.301	-0.363	-0.220	-0.308	-0.297	-1251	-1050	-1316	-895	-1340	-951	-289
126	-0.357	-0.299	-0.363	-0.217	-0.316	-0.296	-1231	-1040	-1316	-880	-1380	-946	-318
131	-0.354	-0.300	-0.350	-0.217	-0.307	-0.296	-1216	-1045	-1251	-880	-1335	-946	-249
148	-0.389	-0.325	-0.399	-0.240	-0.352	-0.321	-1391	-1171	-1496	-995	-1560	-1071	-239
154	-0.377	-0.316	-0.392	-0.231	-0.350	-0.290	-1331	-1126	-1461	-950	-1550	-915	-307
160	-0.371	-0.314	-0.388	-0.231	-0.341	-0.296	-1301	-1116	-1441	-950	-1505	-946	-324
168	-0.396	-0.330	-0.412	-0.246	-0.360	-0.317	-1426	-1196	-1561	-1025	-1600	-1051	-377
174	-0.393	-0.324	-0.408	-0.241	-0.357	-0.310	-1411	-1166	-1541	-1000	-1585	-1016	-347
183	-0.405	-0.342	-0.421	-0.258	-0.367	-0.327	-1471	-1256	-1606	-1085	-1635	-1101	-423
187	-0.420	-0.341	-0.425	-0.256	-0.368	-0.333	-1546	-1251	-1626	-1075	-1640	-1131	-419
199	-0.437	-0.354	-0.445	-0.269	-0.385	-0.350	-1631	-1316	-1726	-1140	-1725	-1216	-294
203	-0.435	-0.354	-0.441	-0.268	-0.383	-0.350	-1621	-1316	-1706	-1135	-1715	-1216	-209
210	-0.438	-0.353	-0.445	-0.268	-0.386	-0.351	-1636	-1311	-1726	-1135	-1730	-1221	-289
216	-0.416	-0.342	-0.428	-0.255	-0.371	-0.340	-1526	-1256	-1641	-1070	-1655	-1166	-250
231	-0.406	-0.346	-0.400	-0.264	-0.342	-0.324	-1476	-1276	-1501	-1115	-1510	-1086	-293
238	-0.431	-0.355	-0.427	-0.270	-0.361	-0.336	-1601	-1321	-1636	-1145	-1605	-1146	-324
251	-0.454	-0.363	-0.448	-0.275	-0.381	-0.346	-1716	-1361	-1741	-1170	-1705	-1196	-289
270	-0.444	-0.354	-0.446	-0.262	-0.380	-0.337	-1666	-1316	-1731	-1105	-1700	-1151	-250
283	-0.432	-0.347	-0.449	-0.254	-0.389	-0.318	-1606	-1281	-1746	-1065	-1745	-1056	-293
287	-0.445	-0.357	-0.460	-0.266	-0.406	-0.324	-1671	-1331	-1801	-1125	-1830	-1086	-263
301	-0.434	-0.349	-0.447	-0.259	-0.389	-0.326	-1616	-1291	-1736	-1090	-1745	-1096	

Table 3.3(cont): Table of values associated with the calculation of creep from the April batch concrete from F5.

Time (days)	Measured creep strain less shrinkage and thermal strain ($\mu\text{m/m}$) ϵ_{crel}						True creep strain ($\mu\text{m/m}$) ϵ_{crl}						Creep coefficient $\phi(t_i, t_0)$							
	1A	1B	2A	2B	3A	3B	1A	1B	2A	2B	3A	3B	1A	1B	2A	2B	3A	3B	Average	
1																				
0	-485	-465	-535	-380	-570	-375	0	0	0	0	0	0	0	0	0	0	0	0	0	0
3	-660	-580	-710	-495	-745	-505	-175	-115	-175	-115	-175	-130	0.36	0.25	0.33	0.30	0.31	0.35	0.32	0.32
7	-687	-581	-737	-491	-761	-501	-201	-116	-201	-111	-191	-126	0.41	0.25	0.38	0.29	0.34	0.34	0.33	0.33
21	-764	-629	-804	-519	-839	-549	-279	-164	-269	-139	-269	-174	0.57	0.35	0.50	0.36	0.47	0.46	0.45	0.45
28	-747	-626	-807	-496	-831	-526	-261	-161	-271	-116	-261	-151	0.54	0.35	0.51	0.31	0.46	0.40	0.43	0.43
33	-763	-633	-828	-492	-853	-583	-278	-167	-293	-112	-282	-208	0.57	0.36	0.55	0.30	0.50	0.55	0.47	0.47
34	-794	-659	-854	-519	-879	-574	-309	-194	-319	-139	-309	-199	0.64	0.42	0.60	0.36	0.54	0.53	0.51	0.51
35	-789	-669	-849	-544	-884	-594	-304	-204	-314	-164	-314	-219	0.63	0.44	0.59	0.43	0.55	0.58	0.54	0.54
40	-805	-670	-865	-555	-895	-590	-320	-205	-330	-175	-325	-215	0.66	0.44	0.62	0.46	0.57	0.57	0.55	0.55
52	-820	-680	-870	-555	-910	-600	-335	-215	-335	-175	-340	-225	0.69	0.46	0.63	0.46	0.60	0.60	0.57	0.57
54	-853	-683	-903	-552	-943	-603	-368	-217	-368	-172	-372	-228	0.76	0.47	0.69	0.45	0.65	0.61	0.60	0.60
70	-890	-725	-980	-590	-1010	-660	-405	-260	-445	-210	-440	-285	0.83	0.56	0.83	0.55	0.77	0.76	0.72	0.72
87	-937	-756	-1022	-606	-1056	-682	-451	-291	-486	-226	-486	-306	0.93	0.63	0.91	0.59	0.85	0.82	0.79	0.79
97	-934	-754	-1034	-609	-1069	-679	-449	-289	-499	-229	-499	-304	0.93	0.62	0.93	0.60	0.87	0.81	0.79	0.79
105	-980	-790	-1070	-645	-1095	-700	-495	-325	-535	-265	-525	-325	1.02	0.70	1.00	0.70	0.92	0.87	0.87	0.87
112	-958	-753	-1033	-602	-1063	-673	-473	-287	-498	-222	-492	-298	0.97	0.62	0.93	0.58	0.86	0.79	0.79	0.79
116	-967	-766	-1032	-611	-1056	-666	-481	-301	-496	-231	-486	-291	0.99	0.65	0.93	0.61	0.85	0.78	0.80	0.80
126	-955	-765	-1040	-605	-1105	-670	-470	-300	-505	-225	-535	-295	0.97	0.64	0.94	0.59	0.94	0.79	0.81	0.81
131	-927	-756	-962	-591	-1046	-656	-441	-291	-426	-211	-476	-281	0.91	0.63	0.80	0.56	0.84	0.75	0.75	0.75
148	-1073	-853	-1178	-677	-1242	-753	-588	-387	-643	-297	-672	-378	1.21	0.83	1.20	0.78	1.18	1.01	1.04	1.04
154	-1082	-877	-1212	-701	-1301	-666	-596	-411	-676	-321	-731	-291	1.23	0.88	1.26	0.84	1.28	0.78	1.05	1.05
160	-1062	-877	-1202	-711	-1266	-707	-576	-411	-666	-331	-696	-331	1.19	0.88	1.25	0.87	1.22	0.88	1.05	1.05
168	-1119	-889	-1254	-719	-1294	-744	-634	-424	-719	-339	-724	-369	1.31	0.91	1.34	0.89	1.27	0.98	1.12	1.12
174	-1087	-841	-1217	-676	-1261	-691	-601	-376	-681	-296	-691	-316	1.24	0.81	1.27	0.78	1.21	0.84	1.03	1.03
183	-1094	-879	-1229	-709	-1259	-724	-609	-414	-694	-328	-689	-349	1.25	0.89	1.30	0.86	1.21	0.93	1.07	1.07
187	-1199	-904	-1279	-729	-1294	-784	-714	-439	-744	-349	-724	-409	1.47	0.94	1.39	0.92	1.27	1.09	1.18	1.18
199	-1208	-893	-1303	-717	-1302	-793	-723	-427	-768	-337	-732	-417	1.49	0.92	1.43	0.89	1.28	1.11	1.19	1.19
203	-1238	-933	-1323	-752	-1332	-833	-753	-467	-788	-372	-762	-458	1.55	1.00	1.47	0.98	1.34	1.22	1.26	1.26
210	-1217	-891	-1307	-716	-1311	-801	-731	-426	-771	-336	-741	-426	1.51	0.92	1.44	0.88	1.30	1.14	1.20	1.20
216	-1232	-962	-1347	-776	-1361	-872	-747	-496	-811	-396	-791	-496	1.54	1.07	1.52	1.04	1.39	1.32	1.31	1.31
231	-1267	-1067	-1292	-906	-1301	-877	-782	-601	-757	-526	-731	-501	1.61	1.29	1.41	1.38	1.28	1.34	1.39	1.39
238	-1312	-1032	-1347	-856	-1316	-857	-827	-566	-811	-476	-746	-481	1.70	1.22	1.52	1.25	1.31	1.28	1.38	1.38
251	-1392	-1037	-1417	-846	-1381	-872	-907	-571	-882	-466	-811	-496	1.87	1.23	1.65	1.23	1.42	1.32	1.45	1.45
270	-1377	-1027	-1442	-816	-1411	-862	-892	-561	-907	-436	-841	-486	1.84	1.21	1.69	1.15	1.48	1.30	1.44	1.44
283	-1356	-1030	-1496	-815	-1495	-805	-870	-565	-960	-435	-925	-430	1.79	1.21	1.79	1.14	1.62	1.15	1.45	1.45
287	-1378	-1038	-1508	-832	-1538	-793	-893	-573	-973	-452	-967	-418	1.84	1.23	1.82	1.19	1.70	1.11	1.48	1.48
301	-1353	-1028	-1473	-827	-1483	-833	-868	-563	-938	-447	-912	-458	1.79	1.21	1.75	1.18	1.60	1.22	1.46	1.46

The measured creep strain from the above calculation of -1616 microstrain is presented in Figure 3.21. The measured creep strains calculated from the data are presented in Table 3.3. The progression of strains in each of the test specimens is represented graphically for all of the April batch concrete specimens in Figure 3.21.

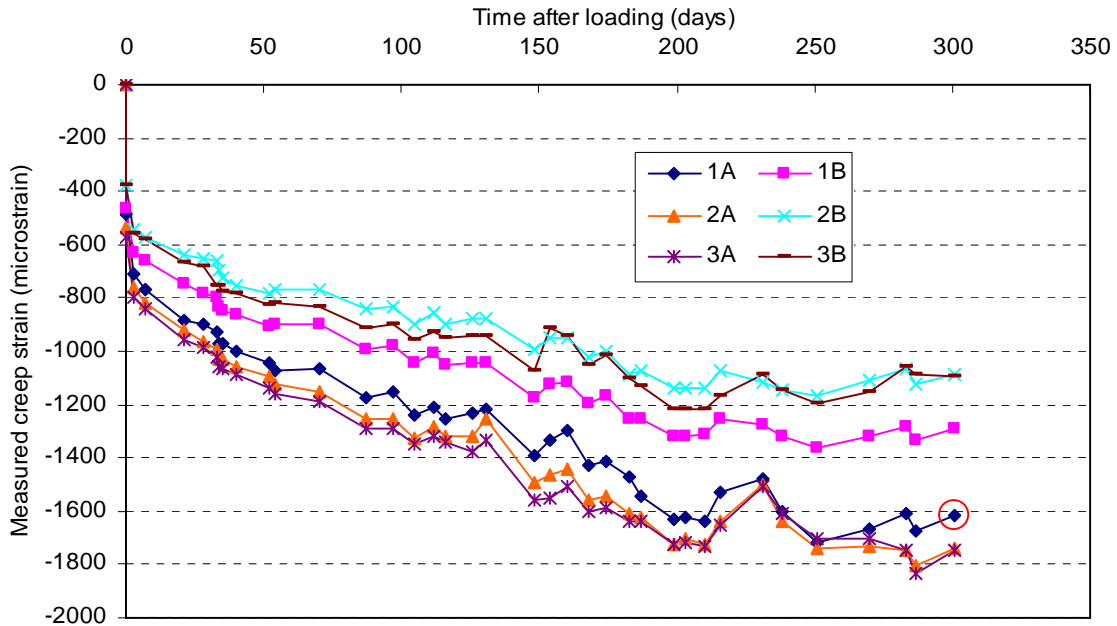


Figure 3.21: Measured creep strain from April batch concrete.

The measured creep strain includes the influences of true shrinkage and temperature. The measured shrinkage strain for each of the test specimens is presented in Figure 3.13. The average measured shrinkage (beginning from the point at which drying in air commenced, 7 days after casting) is presented in Figure 3.13 as well. The average measured shrinkage strain (from Figure 3.13) is reproduced in Figure 3.22. The end of curing period and prestressing do not coincide at the same point in time. The shrinkage that occurred prior to loading the specimens (corresponding to prestressing in the bridge) was subtracted from the total measured shrinkage to yield the shrinkage and thermal influences taking effect beginning at loading. When prestress was applied 38 days after the commencement of drying, shrinkage of -403 microstrain had occurred. This value

appears in the row corresponding to 38 days after the commencement of drying in column 10 in Table 3.2. This was subtracted from the measured shrinkage strain to yield the shrinkage that took place after loading. This is shown in Figure 3.22. In Figure 3.23, the time scale is adjusted to correspond to the age of the concrete after loading. At 301 days after loading, the average measured shrinkage strain (shrinkage and thermal) was $\varepsilon_{ST,301} = -263$ microstrain, as indicated column 14 in Table 3.3 and shown in Figure 3.22 and Figure 3.23.

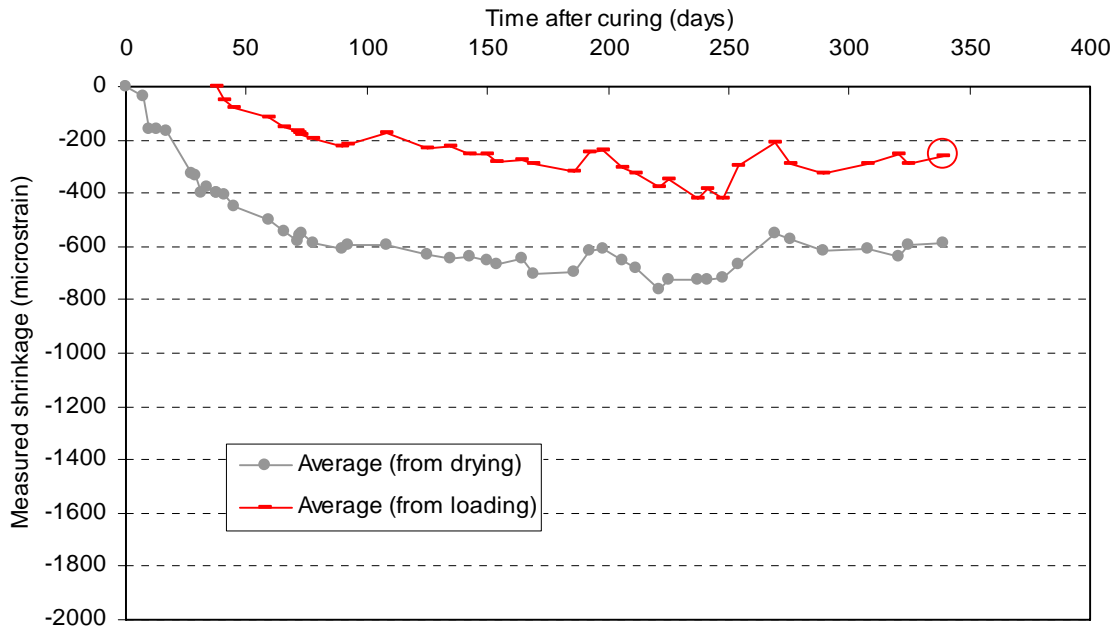


Figure 3.22: Average measured shrinkage (shrinkage and thermal) strain beginning at the end of curing from April batch concrete.

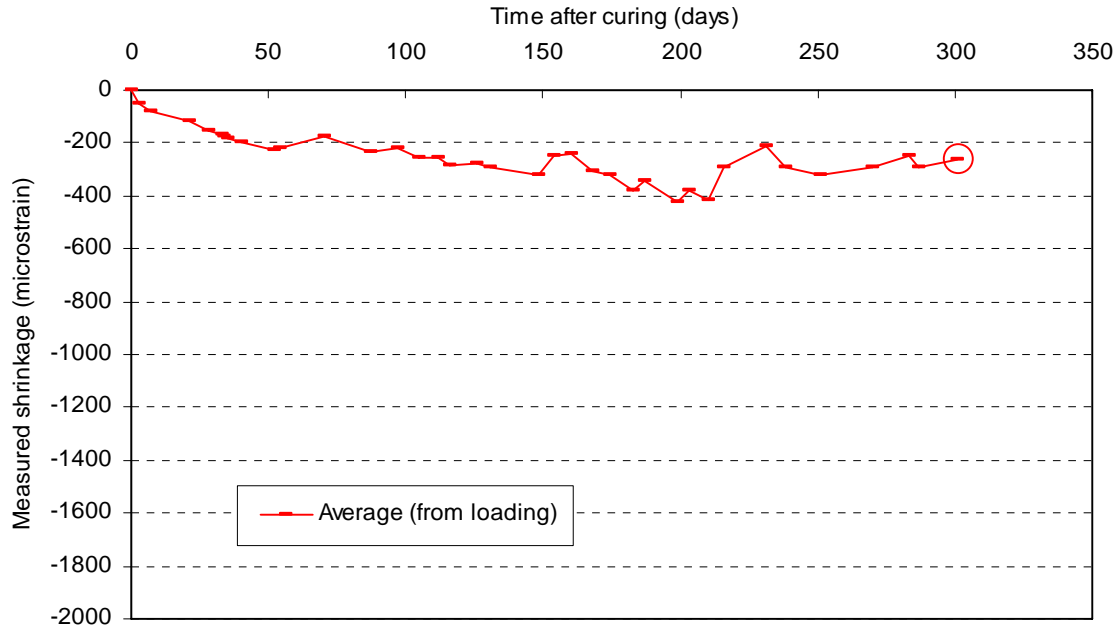


Figure 3.23: Average shrinkage and thermal strains beginning after loading from April batch concrete.

The measured shrinkage strain is subtracted from the measured creep strain to remove the influences of shrinkage and temperature. This is accommodated using Eq. 3.11.

$$\varepsilon_{cre,i} = \varepsilon_{CST,i} - \varepsilon_{ST,i} \quad (3.11)$$

$$\varepsilon_{cre,301} = \varepsilon_{CST,301} - \varepsilon_{ST,301} = -1616 - (-263) = -1353$$

The creep strain now only includes the elastic shortening component, thus the designation $\varepsilon_{cre,i}$. These values are presented in Figure 3.24 for each specimen and for all points in time during measuring.

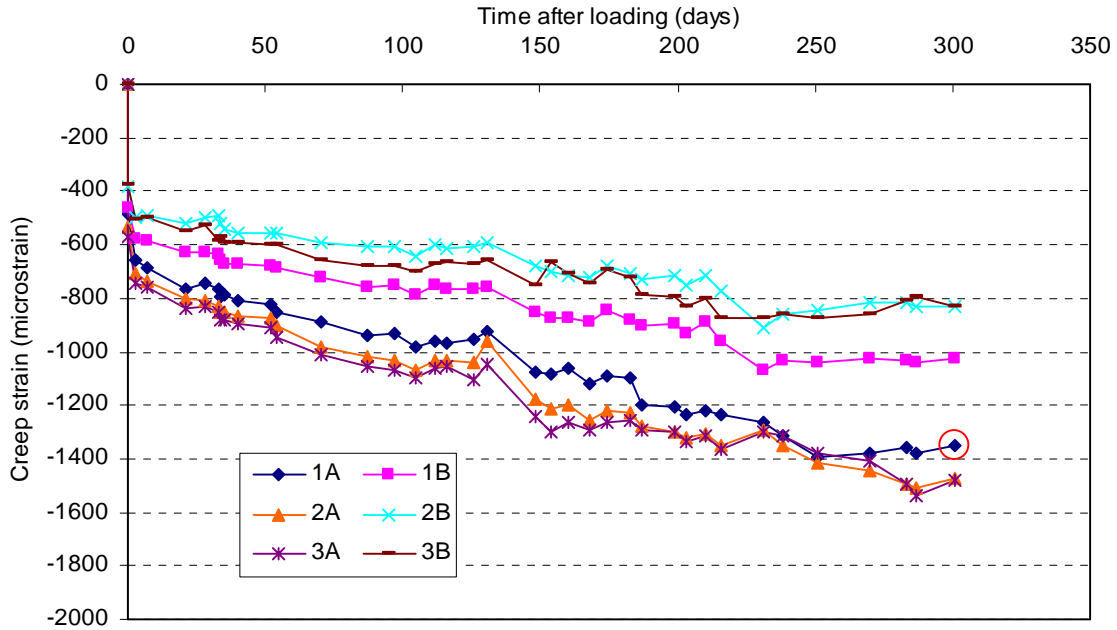


Figure 3.24: Measured creep strain less shrinkage and thermal strains from April batch concrete.

The strains in Figure 3.24 are the result of subtracting the strains in Figure 3.23 from those in Figure 3.21 for corresponding points in time. It is for this reason, that the progression of strain in Figure 3.24 is considerably smoother than that in Figure 3.21.

The elastic strains are calculated for each test specimen. Since all strain that occurs after the application of load is strain induced by creep, the elastic strain is a single value that occurs instantaneously with the application of load. The elastic shortening is calculated using Eq. 3.9.

$$\varepsilon_{elastic} = \frac{DR_0 - DR_{initial}}{DR_{initial} + 200} = \frac{-0.208 - (-0.111)}{-0.111 + 200} (10^6) = -485 \quad (3.9)$$

The strain caused by elastic shortening is provided in the 0 time row of Table 3.3 in columns 8 through 13 of the measured creep strain columns. This is represented in Figure 3.25 and is a constant value that must be subtracted from the creep strain, as will be shown in the next step of calculating the creep.

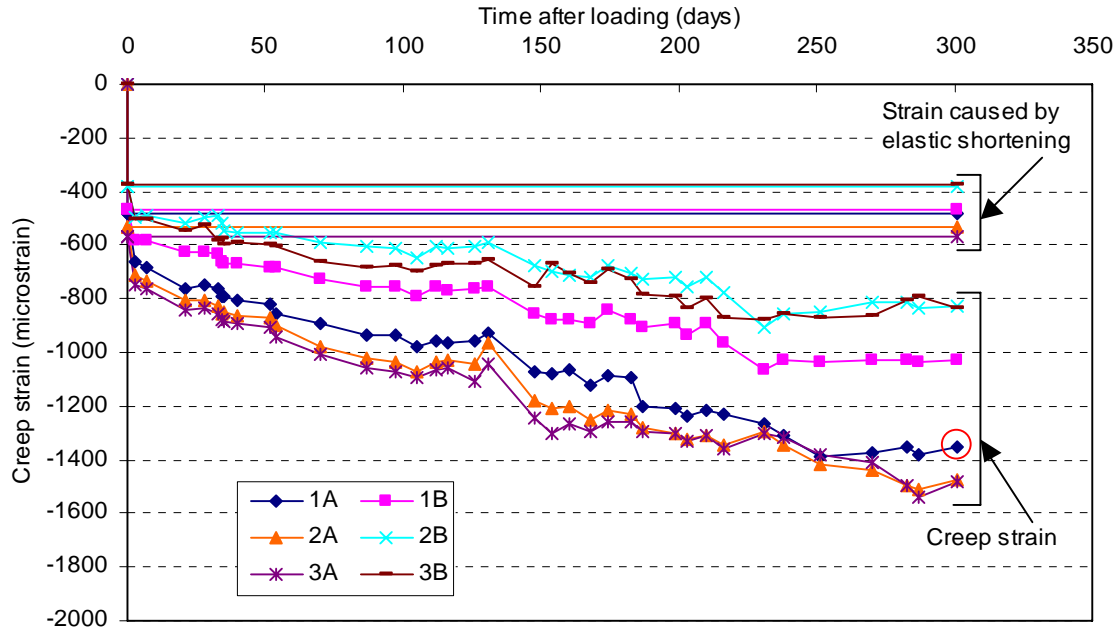


Figure 3.25: Creep strain including initial elastic deformation from the April batch concrete.

Removing the elastic strain $\varepsilon_{elastic}$ from the creep strain $\varepsilon_{cre,i}$ results in the true creep strain $\varepsilon_{cr,i}$. The true creep strain is isolated from the elastic shortening strain using Eq. 3.12.

$$\varepsilon_{cr,i} = \varepsilon_{cre,i} - \varepsilon_{elastic} \quad (3.12)$$

$$\varepsilon_{cr,301} = \varepsilon_{cre,301} - \varepsilon_{elastic} = -1353 - (-485) = -868$$

At 301 days after loading, the true creep strain $\varepsilon_{cr,301}$ is -868, which is located in column 21 in Table 3.3 as well as all true creep strains for the test specimens from the April batch concrete.

The elastic strain in show in Figure 3.25 is subtracted from the creep strain to yield the true shrinkage in Figure 3.26

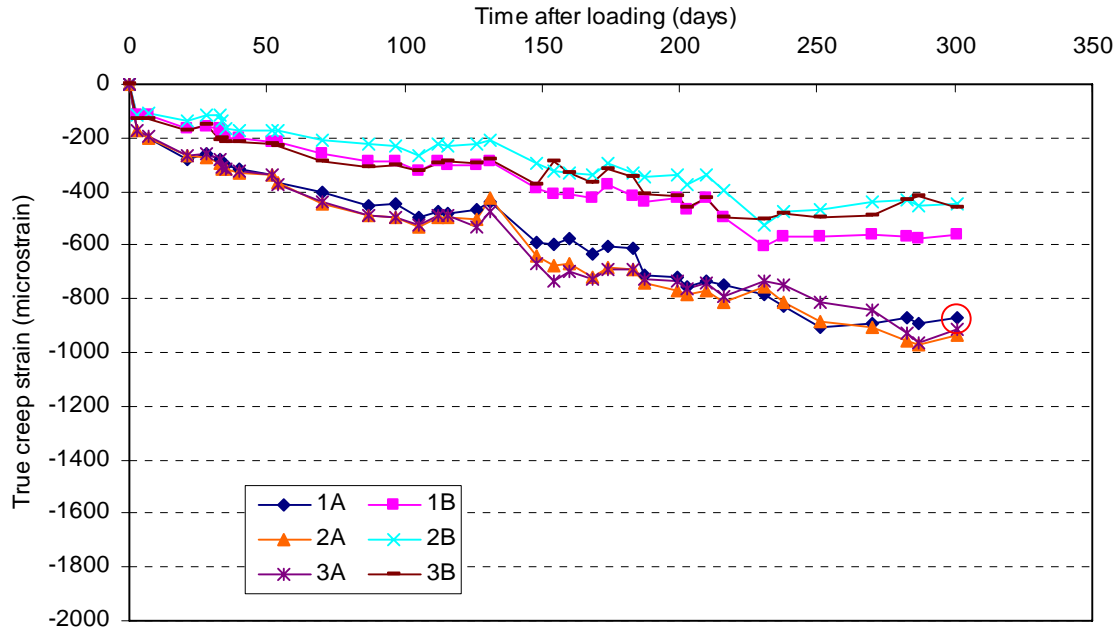


Figure 3.26: True creep strain (measured creep strain less shrinkage, thermal, and elastic strains) from April batch concrete.

The true creep strain is used to determine the creep coefficient, as the creep coefficient is the ratio of true creep strain to the elastic strain, as accommodated in Eq. 3.13.

$$\phi(t_i, t_0) = \frac{\varepsilon_{cr,i}}{\varepsilon_{elastic}} \quad (3.13)$$

For the point in time 301 days after prestressing, the creep coefficient is calculated for the 1A specimen, as follows.

$$\phi(t_{301}, t_0) = \frac{\varepsilon_{cr,301}}{\varepsilon_{elastic}} = \frac{-868}{-485} = 1.79$$

The creep coefficients for all specimens in the April batch concrete are presented in columns 27 through 32 in Table 3.3. The average creep coefficient is presented in column 33. The calculated creep coefficients are presented graphically in Figure 3.27 for all points in time during measuring.

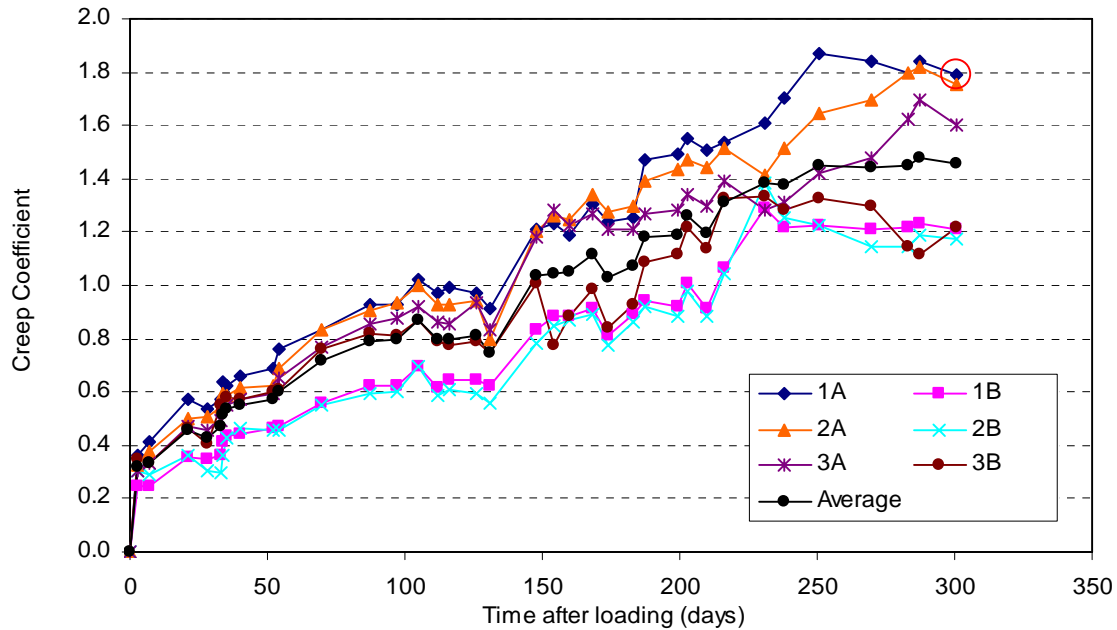


Figure 3.27: Creep coefficient from the April batch concrete.

3.5.2.2. Experimental Creep Coefficients from First Loading

It was determined that the shrinkage obtained through testing in the F4 and F5 concrete was not reliable. The shrinkage in the October, November, and March concrete specimens exhibited unreasonably high values of shrinkage long after curing had ended. The shrinkage in the April and May specimens exceeded predictions; however, not as much as the concrete in F4. For this reason, the true creep, and hence creep coefficient, was calculated using two methods. The first method used subtracted the measured shrinkage from the corresponding batch of shrinkage specimens. The second method subtracted the shrinkage that was determined using the shrinkage from the F5 concrete. The reasoning and justification for the second method follows.

The shrinkage in the F4 concrete was only measured beginning at the point load was applied, corresponding to the application of prestress in the bridge. The fact that the shrinkage was not measured during this time contributes to the lack of full understanding of the concrete behavior through this period. The shrinkage in the F5 concrete (April and May batches) was measured from the onset of drying, thus the full progression of experimental shrinkage is available for these

two concretes. As no anomalies were observed in the F5 concrete, the data for the April and May concrete batches was deemed acceptable, thus the reason for using the April batch concrete to illustrate the method of calculating the creep and shrinkage in the previous example calculations.

All concrete in the bridge is exposed to nominally equivalent environmental influences and is comparable in composition. It can be assumed with reasonable reliability that the concrete in F5 is representative of the concrete in F4. The shrinkage from the F5 concrete was taken to be representative of the concrete in F4.

As will be described in Section 3.6, a curve-fitting method was adopted to fit the creep and shrinkage data to produce a smooth curve and ultimate values. The curve fit to the shrinkage data for F5 was used to produce shrinkage values that could be expected for the F4 concrete, based on the ages of the concrete when load was applied.

The procedure used to isolate the influences of shrinkage, temperature, and elastic shortening from the creep strain for all concretes is the same as that presented using the April batch concrete presented previously. The primary difference that must be noted is that for the October, November, and March batch concretes, the measured shrinkage was taken as the value measured from the corresponding shrinkage tests for each concrete batch as well as the value determined using the concrete in F5. Since the points in time of measure in the F4 and F5 test specimens did not coincide, the measured shrinkage from F5 was taken as from the best-fit to the F5 shrinkage. For this reason, though the second method is being treated as the measured shrinkage for F4, it is a smooth progression of shrinkage values.

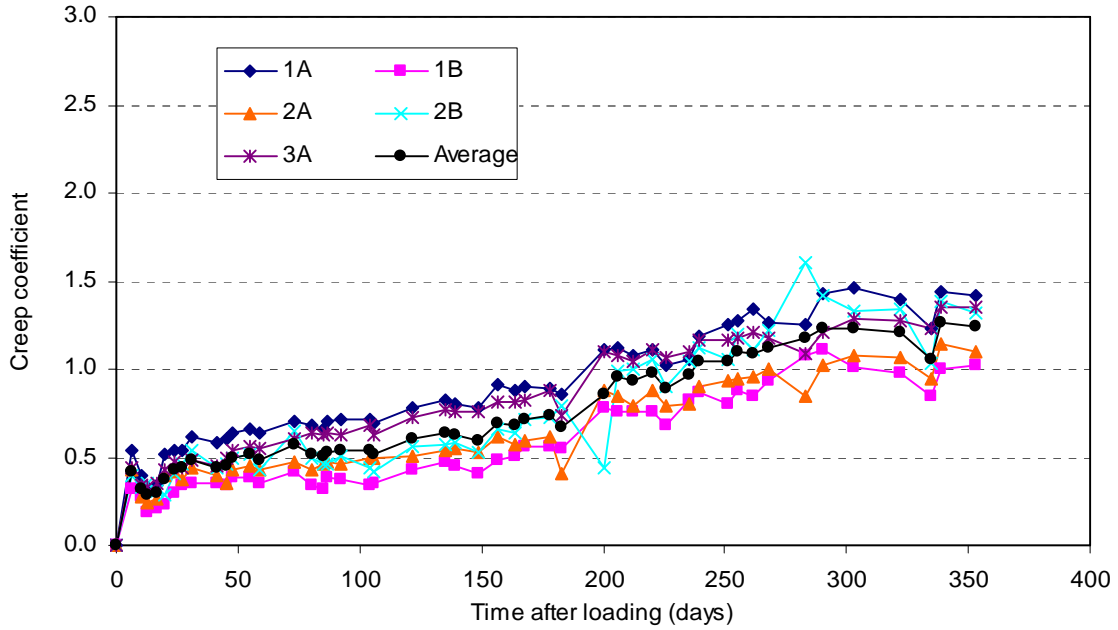


Figure 3.28: Creep coefficient from the October batch concrete (using measured shrinkage) from first loading (prestressing).

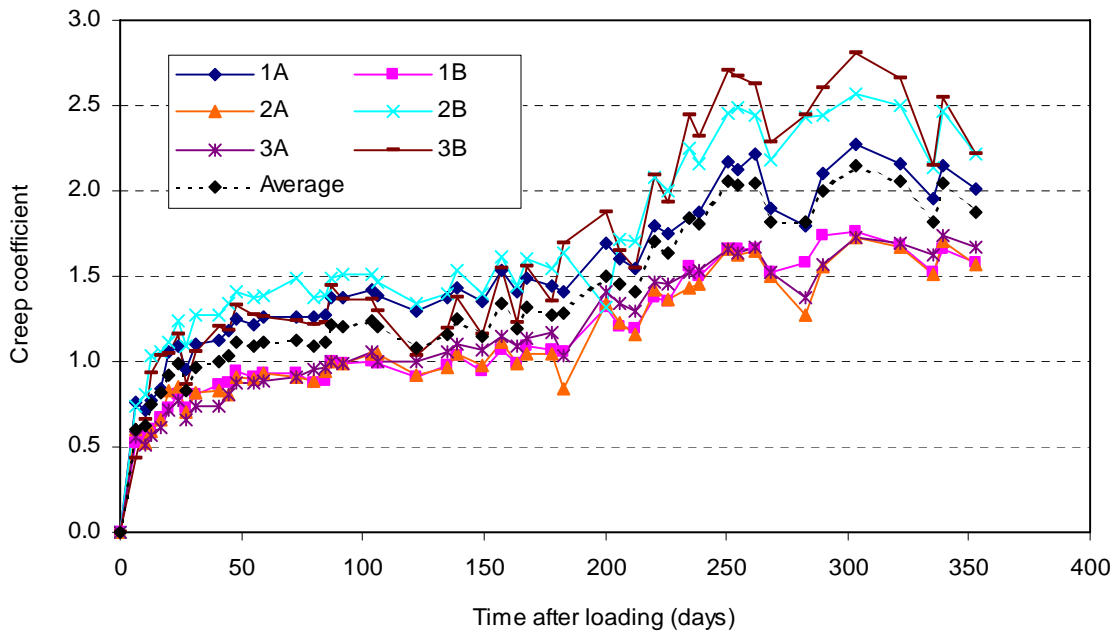


Figure 3.29: Creep coefficient from the October batch concrete (using F5 shrinkage) from first loading (prestressing).

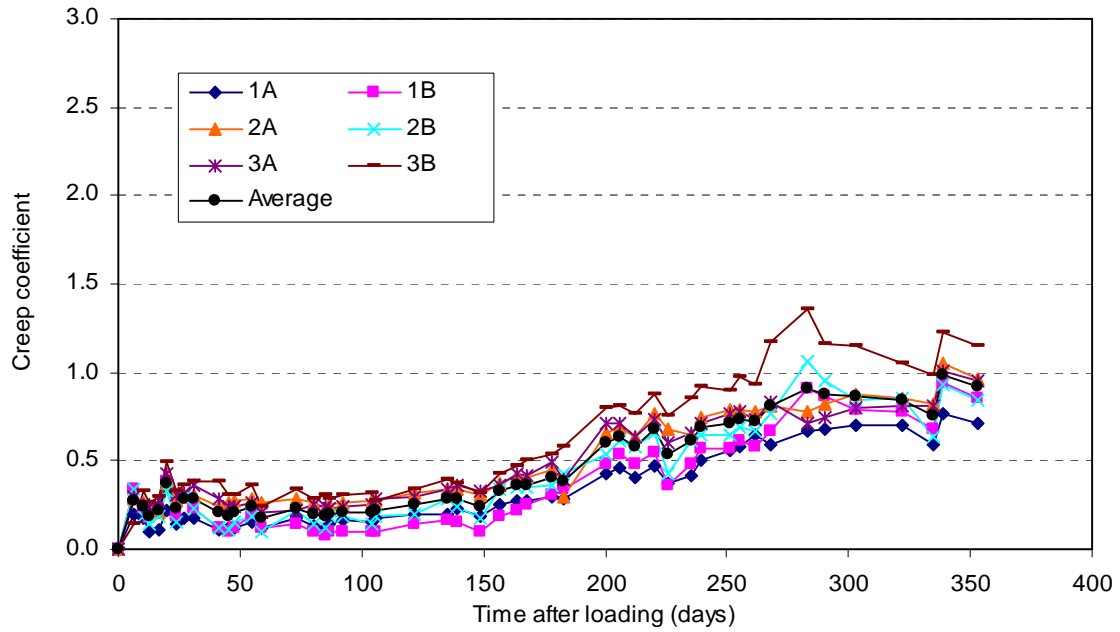


Figure 3.30: Creep coefficient from the November batch concrete (using measured shrinkage) from first loading (prestressing).

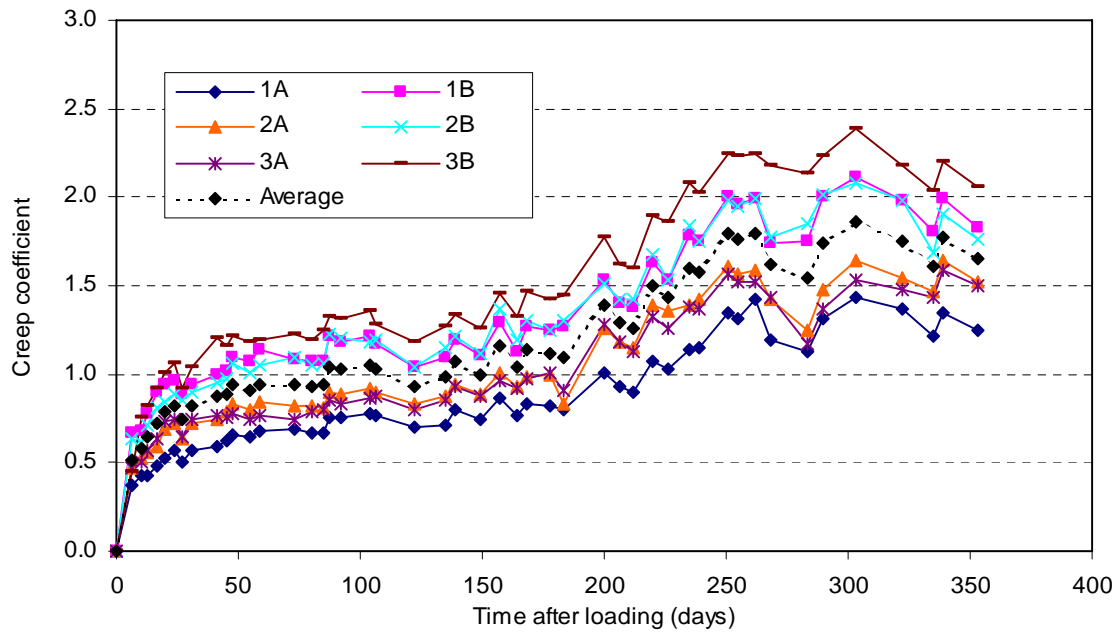


Figure 3.31: Creep coefficient from the November batch concrete (using F5 shrinkage) from first loading (prestressing).

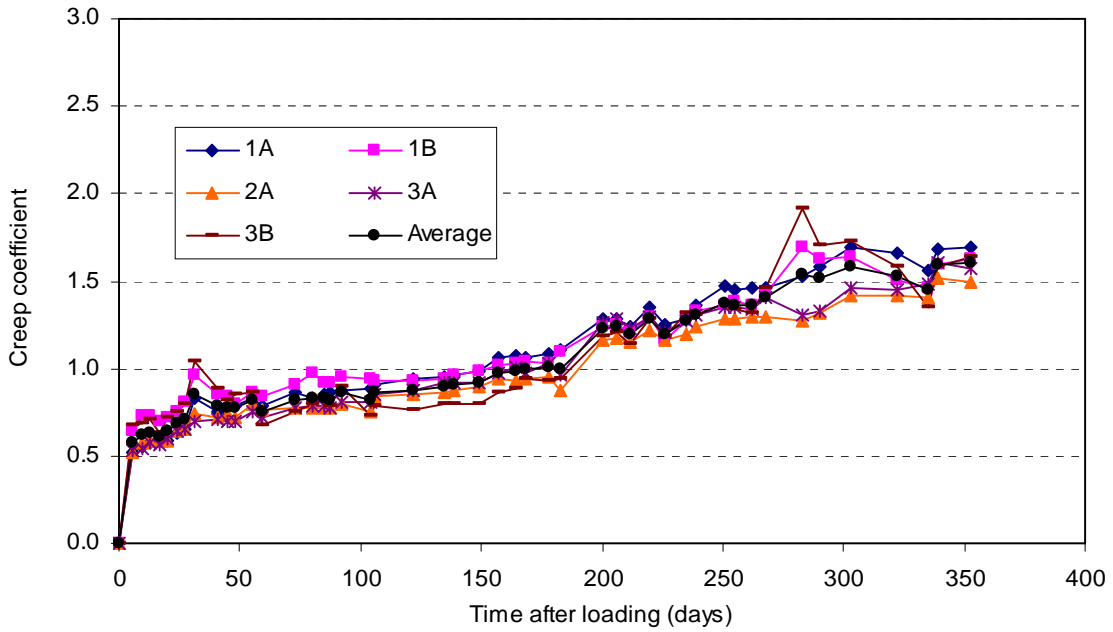


Figure 3.32: Creep coefficient from the March batch concrete (using measured shrinkage) from first loading (prestressing).

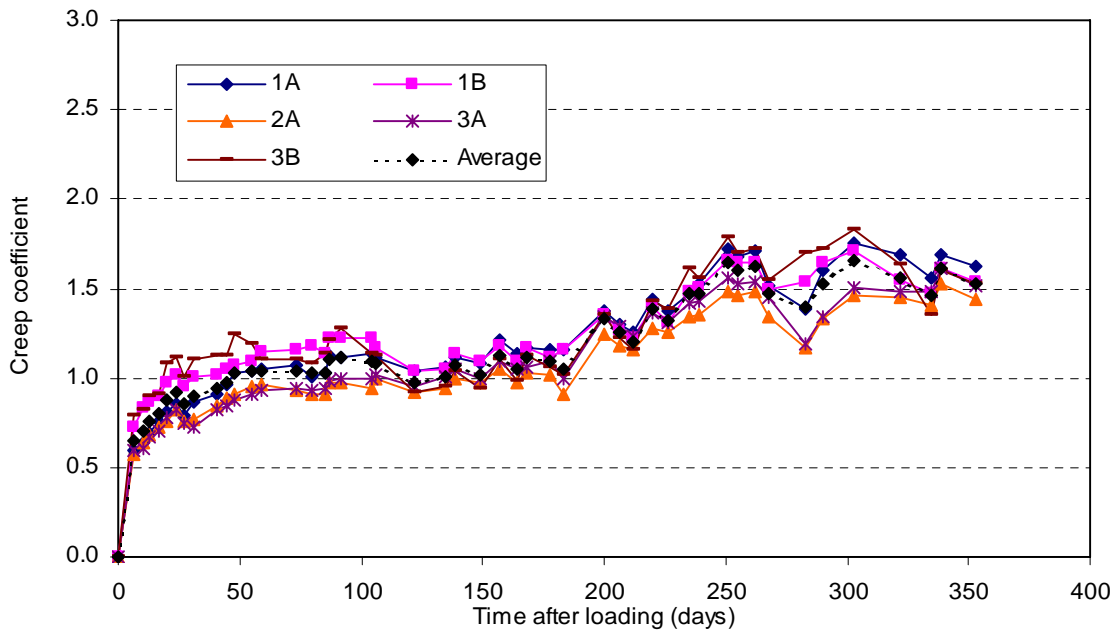


Figure 3.33: Creep coefficient from the March batch concrete (using F5 shrinkage) from first loading (prestressing).

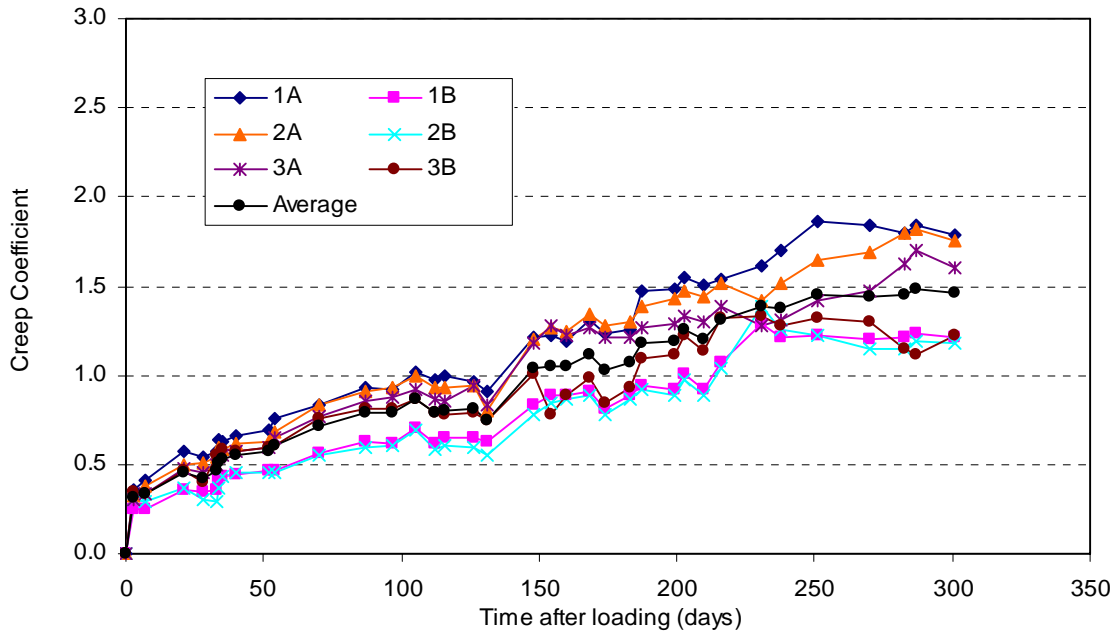


Figure 3.34: Creep coefficient from the April batch concrete from first loading (prestressing).

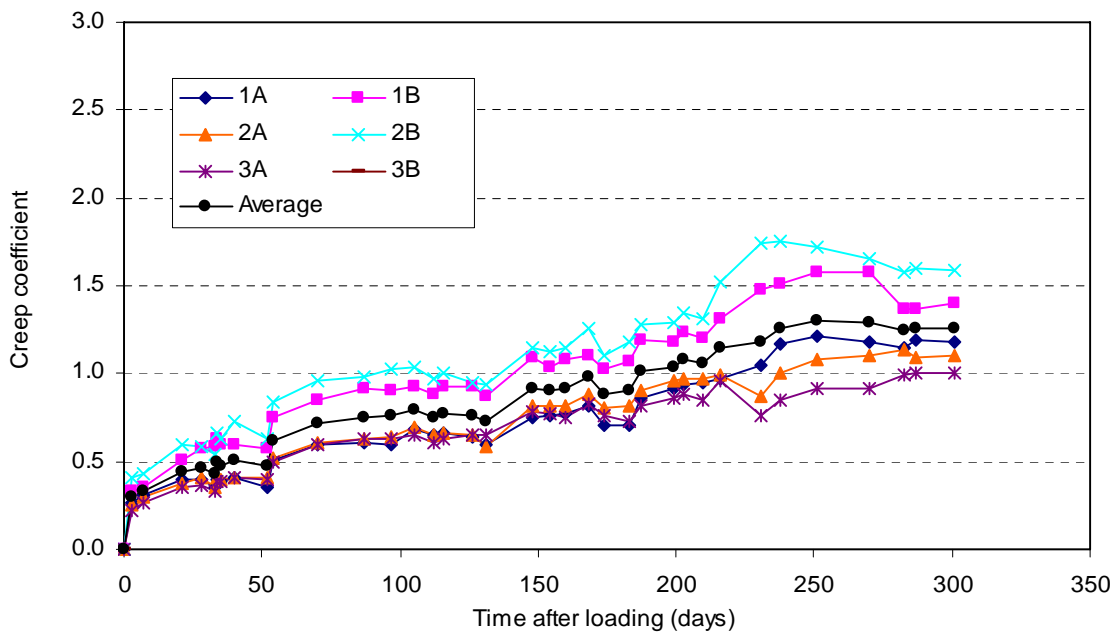


Figure 3.35: Creep coefficient from the May batch concrete from first loading (prestressing).

3.5.2.3. Experimental Creep Coefficients from Second Loading

The experimental creep coefficients from second loading correspond to the instant at which the falsework was removed – 121 and 69 days after prestressing in F4 and F5, respectively. The removal of falsework activates additional self-

weight imposing additional load on the concrete and causing creep. The experimental creep coefficients from testing are presented in this section.

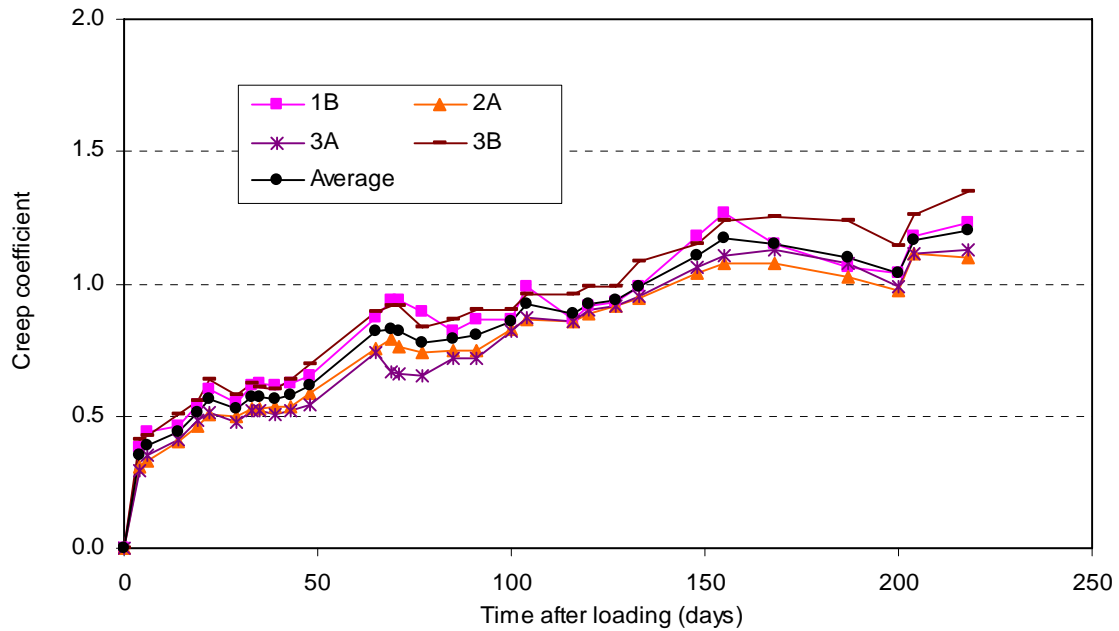


Figure 3.36: Creep coefficient from the October batch concrete (using measured shrinkage) from second loading (removal of falsework).

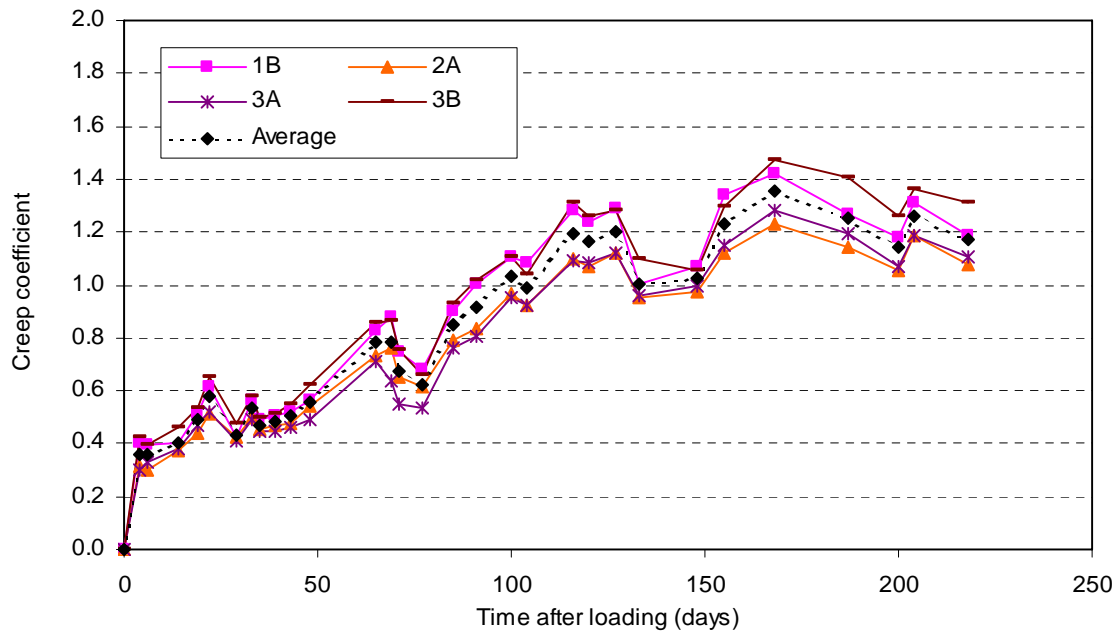


Figure 3.37: Creep coefficient from the October batch concrete (using F5 shrinkage) from second loading (removal of falsework).

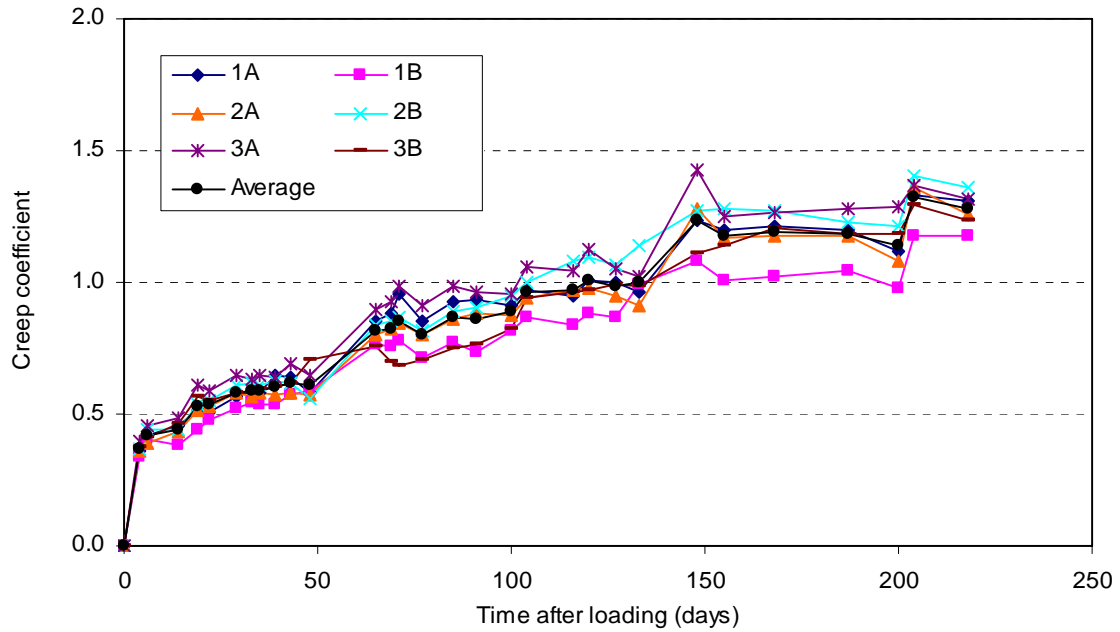


Figure 3.38: Creep coefficient from the November batch concrete (using measured shrinkage) from second loading (removal of falsework).

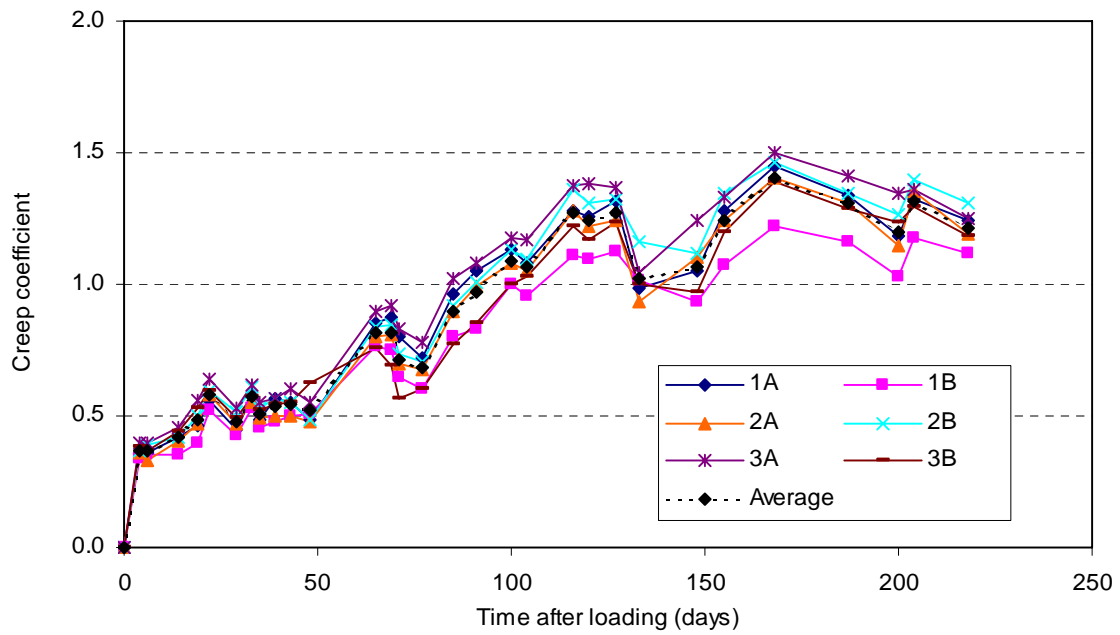


Figure 3.39: Creep coefficient from the November batch concrete (using F5 shrinkage) from second loading (removal of falsework).

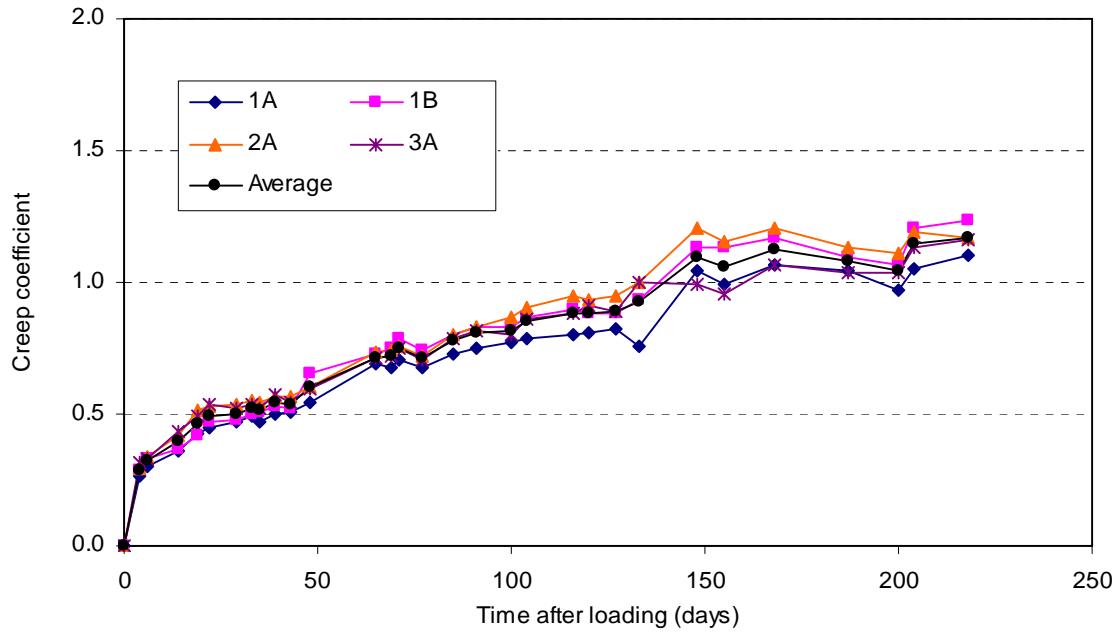


Figure 3.40: Creep coefficient from the March batch concrete (using measured shrinkage) from second loading (removal of falsework).

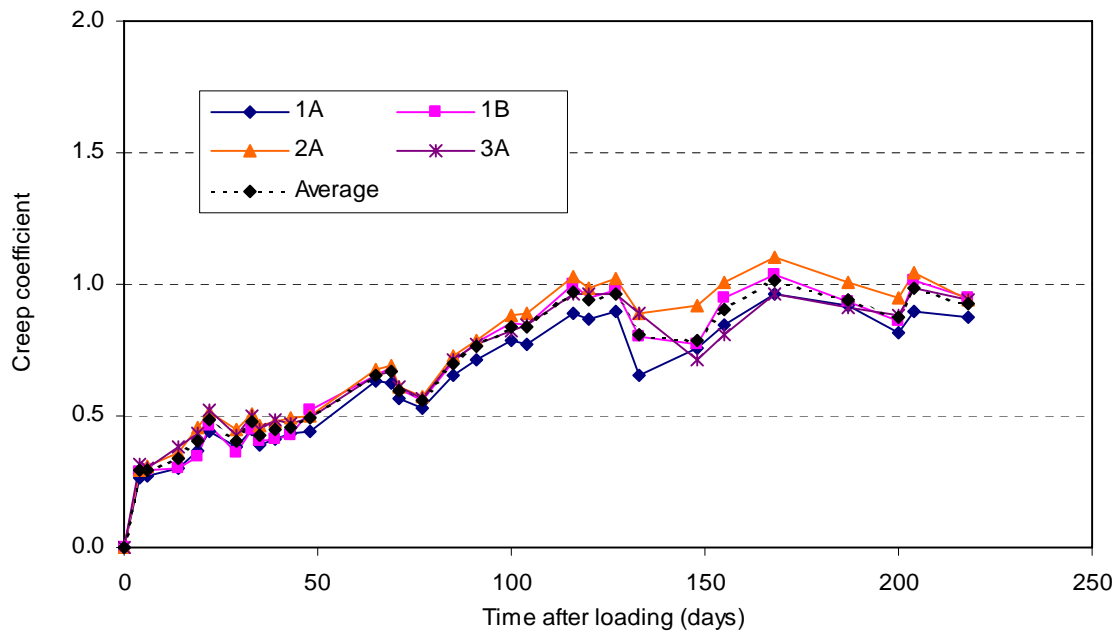


Figure 3.41: Creep coefficient from the March batch concrete (using F5 shrinkage) from second loading (removal of falsework).

3.5.2.4. Experimental Creep Coefficients from Third Loading

The experimental creep coefficient from third loading corresponds to the instant at which the hinges were loaded – 156 days after prestressing in F5. The adjacent frames react at the hinges and the additional load at the hinges causes creep. The figures for the creep coefficients at third loading are presented in this section.

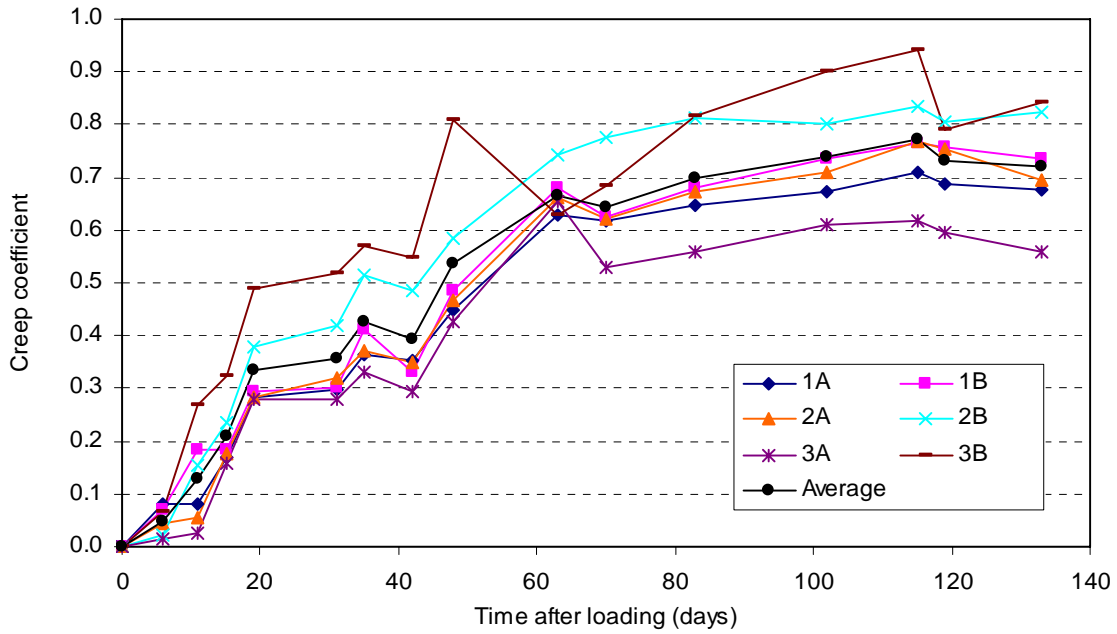


Figure 3.42: Creep coefficient from the April batch concrete from second loading (removal of hinge supporting falsework).

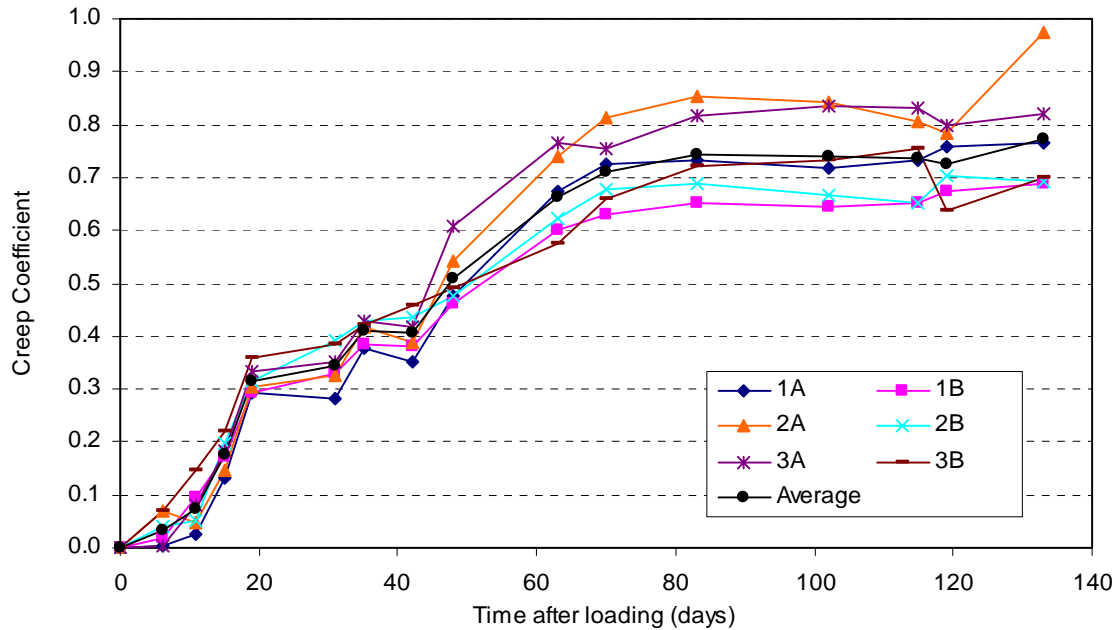


Figure 3.43: Creep coefficient from the May batch concrete from second loading (removal of hinge supporting falsework).

3.6. Curve-fitting

Using the measured data, the creep and shrinkage were determined for each concrete using the method of processing the measured data presented in Section 3.4 and shown for each concrete batch in Section 3.5. A method of curve fitting, developed by Ghali et al [15], was adopted using calibration of the CEB-FIP [10] equations for the collected data to provide a smooth progression of creep and shrinkage over the monitoring period as well as to project ultimate values. The CEB-FIP [10] equations off which the curve-fitting method is based are provided in Section 2.2.4. The measured data were used to derive equations for creep and shrinkage based on the CEB-FIP [10] equations. This curve-fitting method [15] provided the creep and shrinkage for any point in time during the life of the bridge.

Eq. 3.14 provides the general equation for the curve-fit for shrinkage and is based on Eq. 2.33 of the CEB-FIP [10] specification.

$$\varepsilon_{sh}(t, t_s) = a \left(\frac{t - t_s}{350 \left(\frac{h_0}{100} \right)^2 + t - t_s} \right)^b \quad (3.14)$$

The experimental shrinkage ε_{sh} is obtained through material testing, as described in Section 3.4.1. Eq. 3.14 can be rewritten in the form

$$\log a + b \log[\beta_s(t - t_s)] = \log \varepsilon_{sh} \quad (3.15)$$

Eq. 3.15 can be written in matrix form

$$\begin{bmatrix} 1 & \log[\beta_s(t - t_s)] \\ 1 & \dots \\ 1 & \dots \end{bmatrix} \begin{Bmatrix} \log a \\ b \end{Bmatrix} = \begin{Bmatrix} \log \varepsilon_{sh} \\ \dots \\ \dots \end{Bmatrix} \quad (3.16)$$

Eq. 3.16 is solved for coefficients a and b to accommodate the development of shrinkage with time.

The equation to determine creep is provided using Eq. 2.25 of the CEB-FIP [10]. The curve-fit for the creep coefficient is provided by the general equation:

$$\phi(t, t_0) = c \phi_{RH} \left(\frac{1}{0.1 + t_0^{0.2}} \right)^d \left(\frac{t - t_0}{\beta_H + t - t_0} \right)^e \beta_E(t_0) \quad (3.17)$$

The values of $\beta_E(t_0)$, ϕ_{RH} , and β_H are determined from the equations of the CEB-FIP in Section 2.2.4, Eqs. 2.24, 2.27, and 2.31, respectively. Eq. 3.17 equation can be written in the form of Eq. 3.18.

$$\begin{aligned} & \log c + d \log \left(\frac{1}{0.1 + t_0^{0.2}} \right) + e \log \left(\frac{t - t_0}{\beta_H + t - t_0} \right) \\ &= \log \phi(t, t_0) - \log \phi_{RH} - \log \beta_E(t_0) \\ &= \log \left(\frac{\phi(t, t_0)}{\phi_{RH} \beta_E(t_0)} \right) \end{aligned} \quad (3.18)$$

Eq. 3.18 can be rewritten in matrix form as Eq. 3.19.

$$\begin{bmatrix} 1 & \log\left(\frac{1}{0.1+t_0^{0.2}}\right) & \log\left(\frac{t-t_0}{\beta_H+t-t_0}\right) \\ 1 & \dots & \dots \\ 1 & \dots & \dots \end{bmatrix} \begin{Bmatrix} \log c \\ d \\ e \end{Bmatrix} = \begin{Bmatrix} \log\left(\frac{\phi(t,t_0)}{\phi_{RH}\beta_E(t_0)}\right) \\ \dots \\ \dots \end{Bmatrix} \quad (3.19)$$

The creep coefficient $\phi(t, t_0)$ is obtained through material testing, as described in Section 3.4.2. Eq. 3.19 is solved for coefficients c , d , and e to provide the curve-fit [15] equation to the creep data.

The values of a through e are provided for each concrete type in Table 3.4.

Table 3.4: Coefficients for the curve-fit [15] equations for each concrete type.

Concrete Type	Coefficients										
	Shrinkage		Creep: First Loading			Creep: Second Loading			Creep: Third Loading		
	a	b	c	d	e	c	d	e	c	d	e
October	433.92	0.58	0.72	0.01	0.45	0.65	-0.02	0.38	-	-	-
November	548.62	0.69	0.40	0.00	0.37	0.79	0.05	0.39	-	-	-
March	630.63	0.86	1.00	0.14	0.32	0.19	-1.22	0.42	-	-	-
April	880.41	1.09	0.96	0.01	0.47	-	-	-	1.50	0.66	0.59
May	796.29	0.65	0.84	0.05	0.43	-	-	-	0.57	-0.25	0.62

The curves fit to each set of data for shrinkage and creep are presented in the following sections, 3.6.1, 3.6.2, and 3.6.3. The average of the true shrinkage and creep coefficients from the first and second loadings are presented for each concrete batch on the same figures as the curve-fit for each specimen. The averages presented in the figures in this section (Section 3.6) correspond to the averages that are presented in the figures in Section 3.5. The average is presented to show the correlation of the true shrinkage and creep coefficients to the curve fit to each set of data.

3.6.1. Curve-fit for Shrinkage

Figure 3.44 displays the experimental shrinkage that was measured through testing for the October batch concrete from F4. As mentioned previously, the shrinkage from F4 was not reliable, especially for the October and November concrete batches. For this reason, the decision was made to determine the creep coefficients for the F4 concrete using two methods. The first method removes the

experimental shrinkage from the creep strain. The second method used the shrinkage from F5 to provide approximate shrinkage values for the concrete in F4, since it was determined that the F5 concrete was more reliable. In Figure 3.45 the shrinkage that could be expected in the October concrete beginning from loading is presented. It will be shown in Section 3.7.1 that the expected shrinkage for the F4 concrete using the experimental shrinkage values from F5 correlates well with the predicted shrinkage. Figure 3.46 compares the F4 experimental shrinkage and the F5 shrinkage adjusted for the F4 construction schedule. Similar curves for shrinkage are presented for the November and March concrete batches in Figure 3.47 to Figure 3.52.

To avoid confusion, the creep for the F4 concrete batches (October, November, and March) was determined using both the F4 experimental shrinkage and F5 expected shrinkage. Each creep curve will be noted as F4 shrinkage (measured) or F5 shrinkage, denoting the shrinkage strains that were removed from the creep strains. The shrinkage from F5 was reliable, thus only one creep curve is presented for the April and May concrete batches.

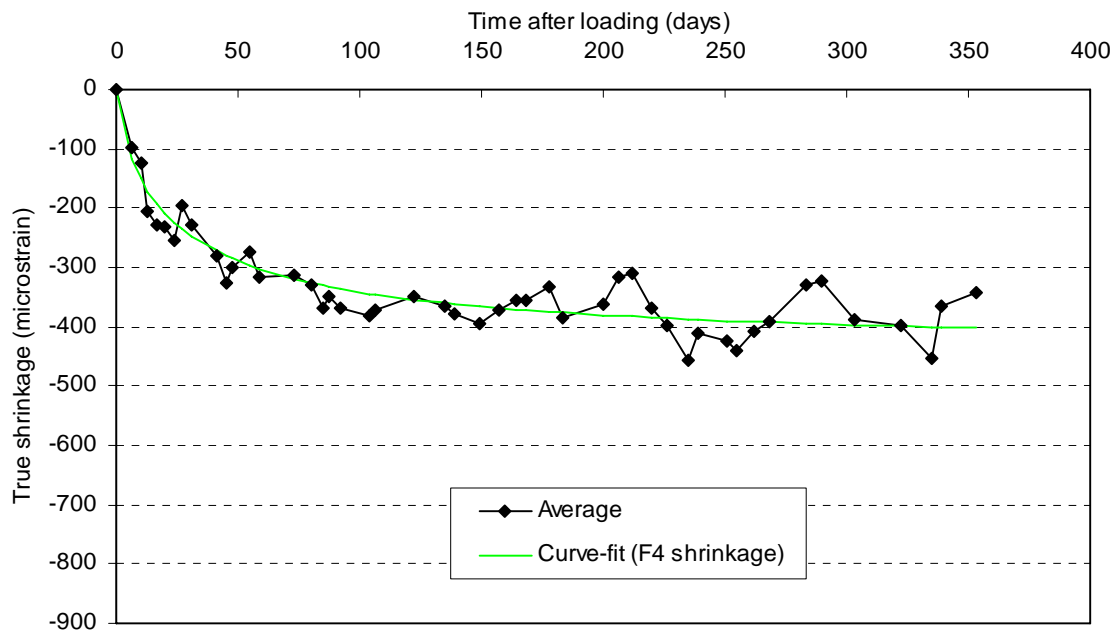


Figure 3.44: Average true shrinkage (F4 experimental) for the October batch concrete with best-fit curve.

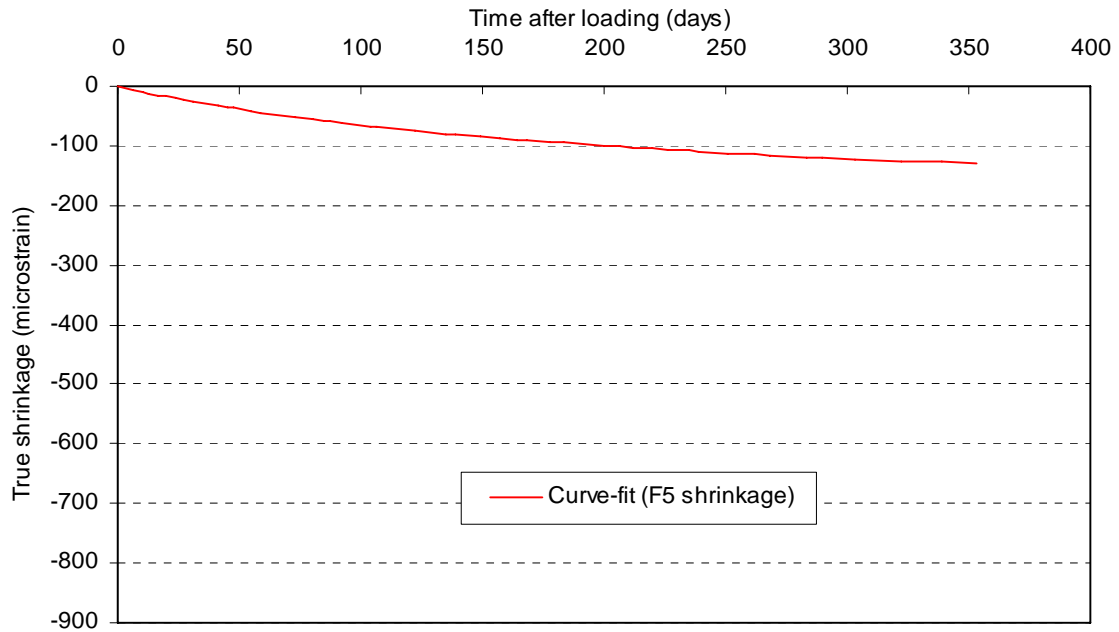


Figure 3.45: Average true shrinkage (F5 experimental) for the October batch concrete.

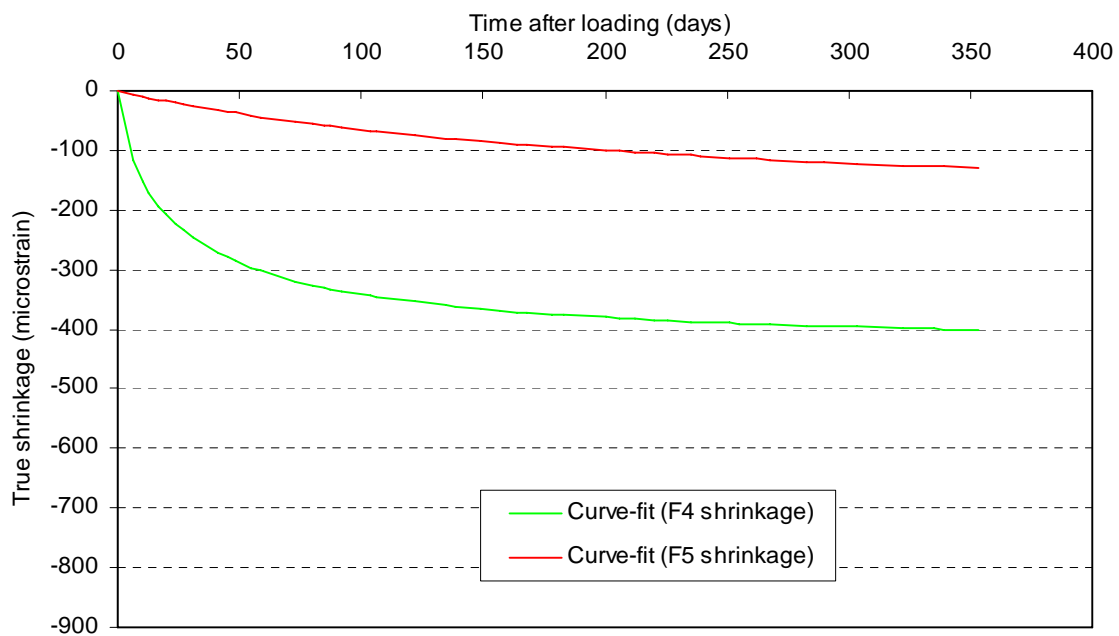


Figure 3.46: Average true shrinkage for the October batch concrete.

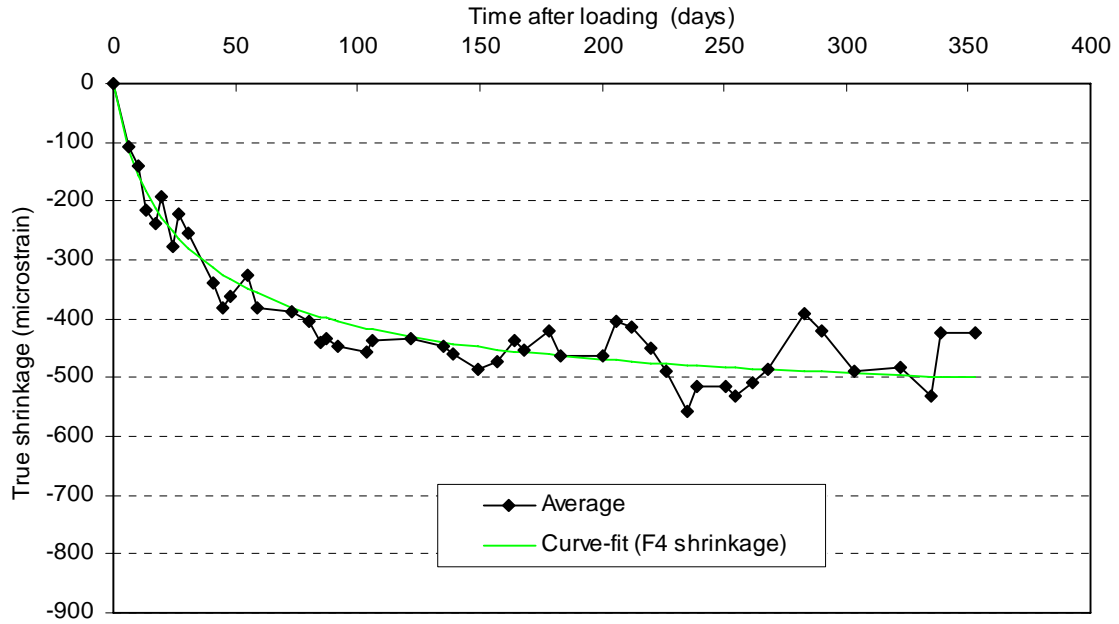


Figure 3.47: Average true shrinkage (F4 experimental) for the November batch concrete with best-fit curve.

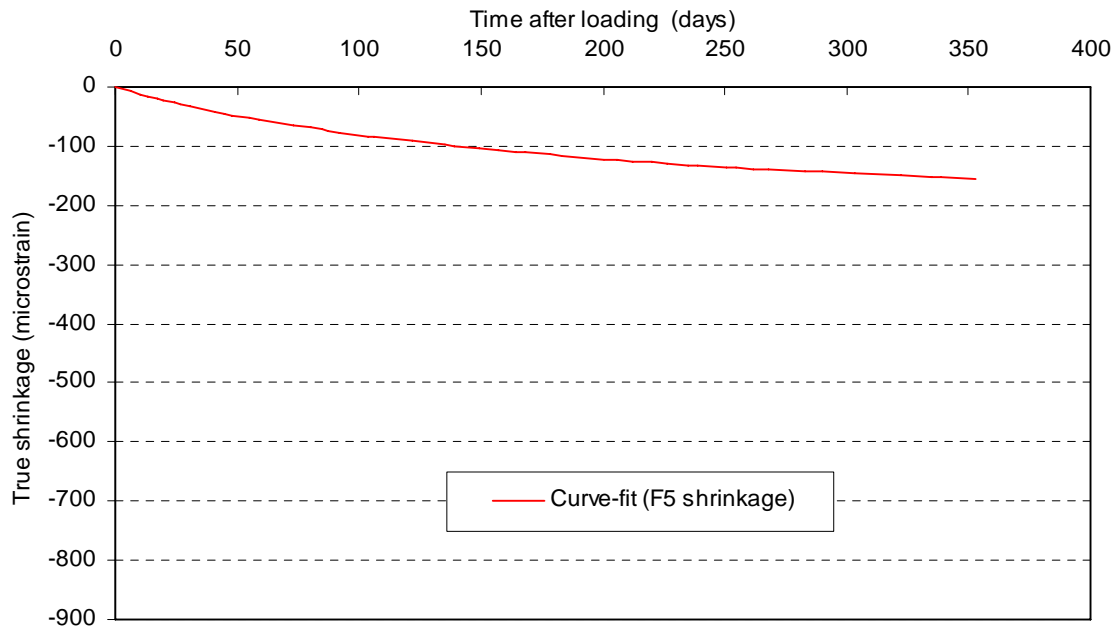


Figure 3.48: Average true shrinkage (F5 experimental) for the November batch concrete.

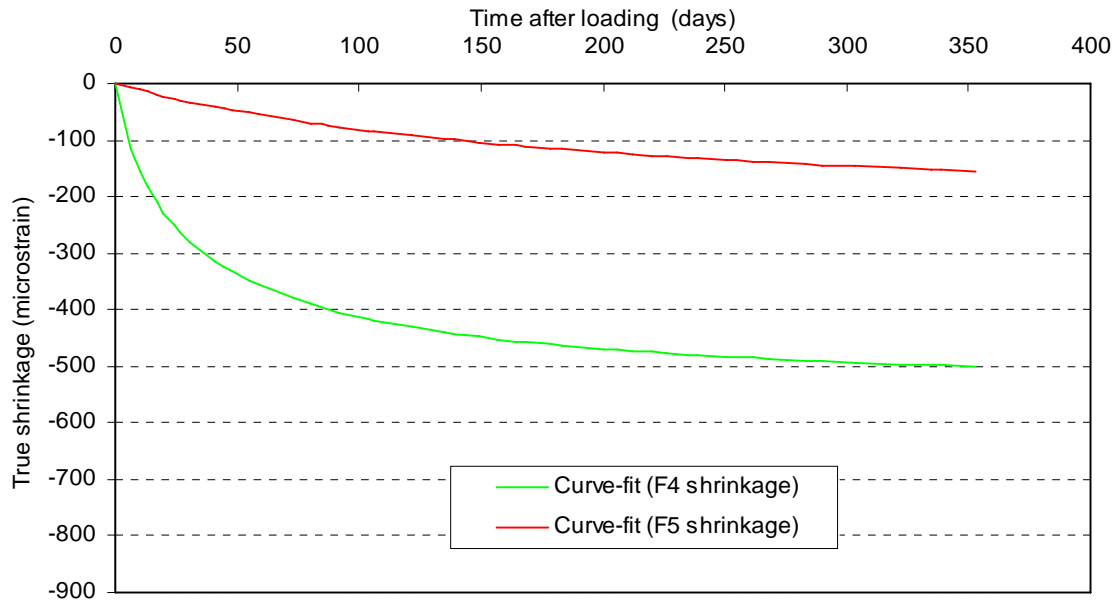


Figure 3.49: Average true shrinkage for the November batch concrete.

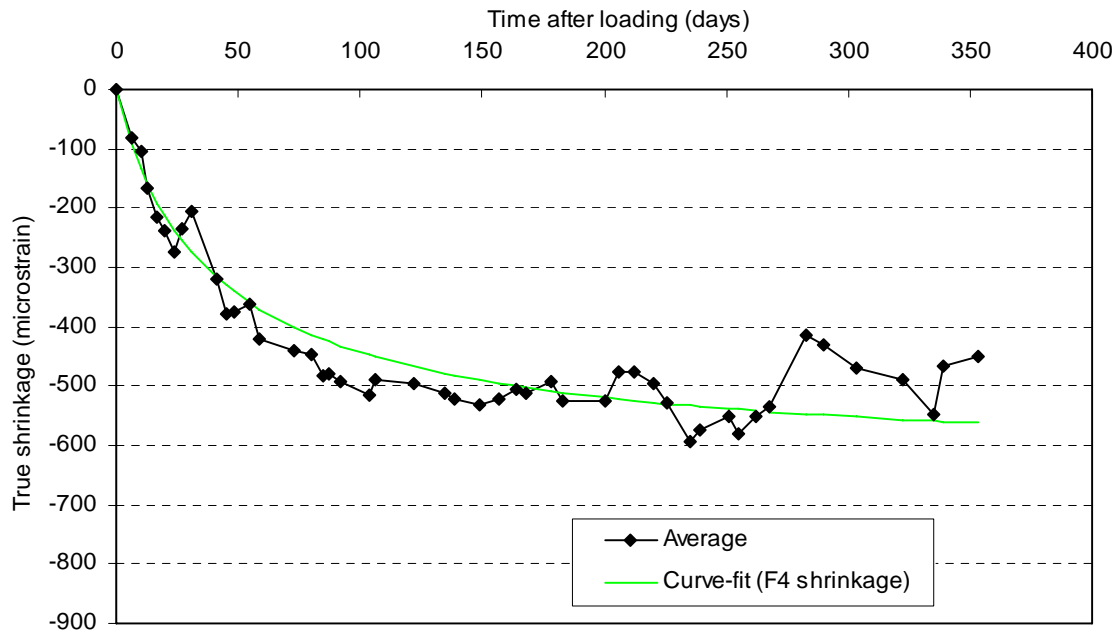


Figure 3.50: Average true shrinkage (experimental) for the March batch concrete with best-fit curve.

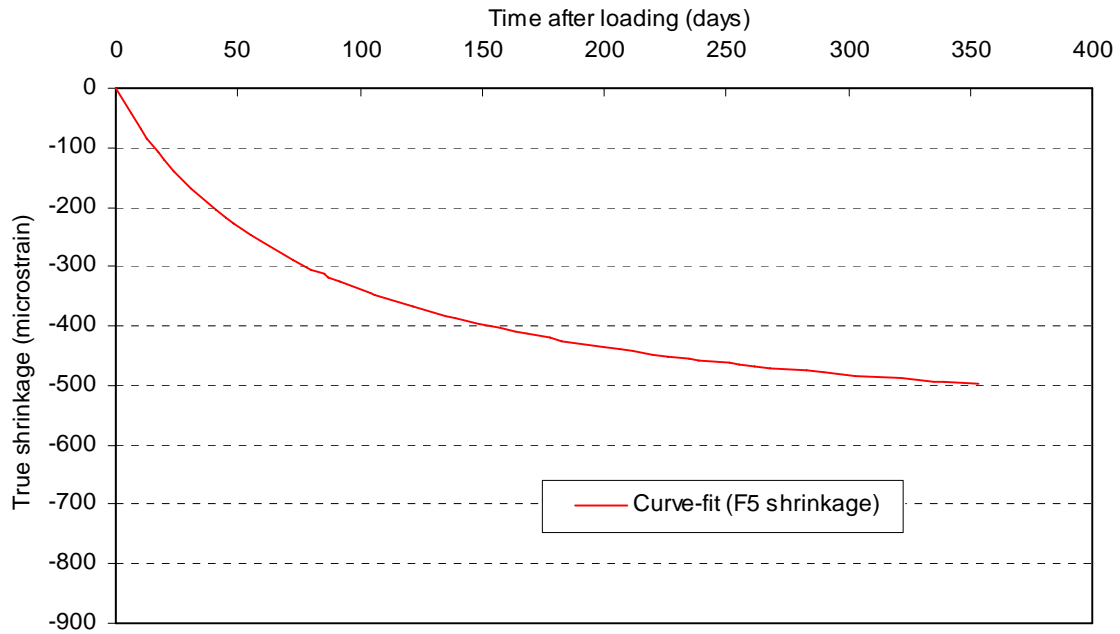


Figure 3.51: Average true shrinkage (F5 experimental) for the March batch concrete.

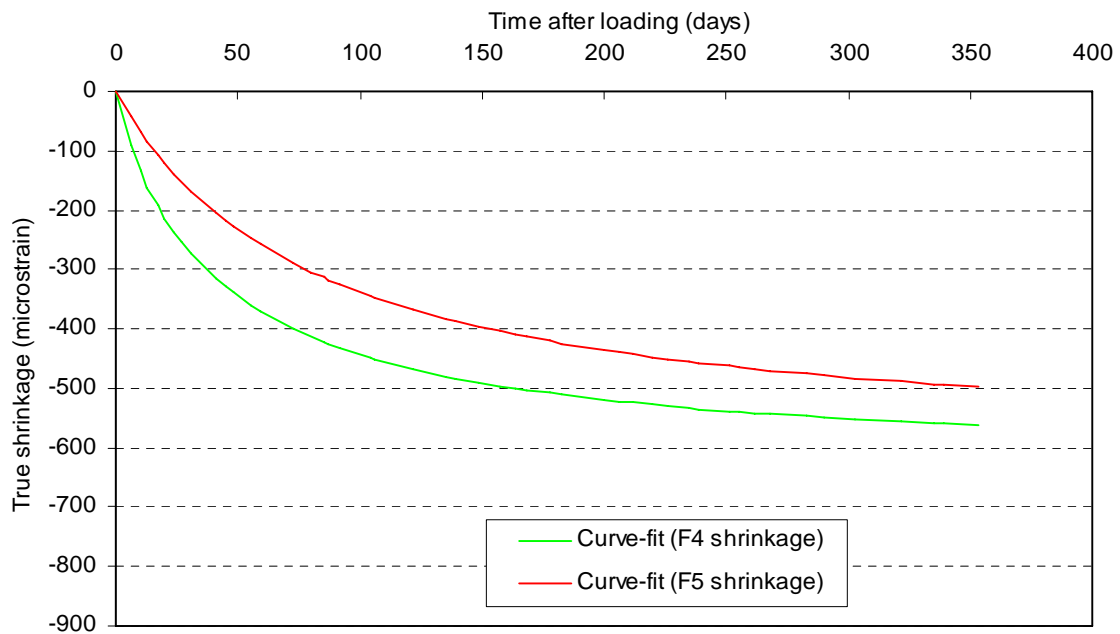


Figure 3.52: Average true shrinkage for the November batch concrete.

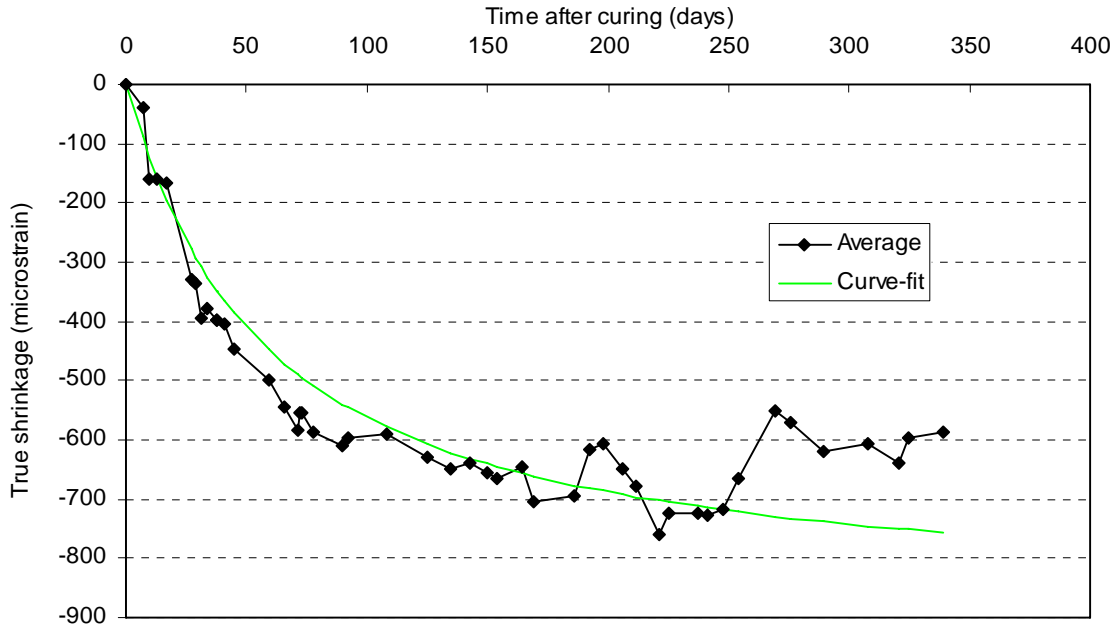


Figure 3.53: Average true shrinkage for the April batch concrete with best-fit curve.

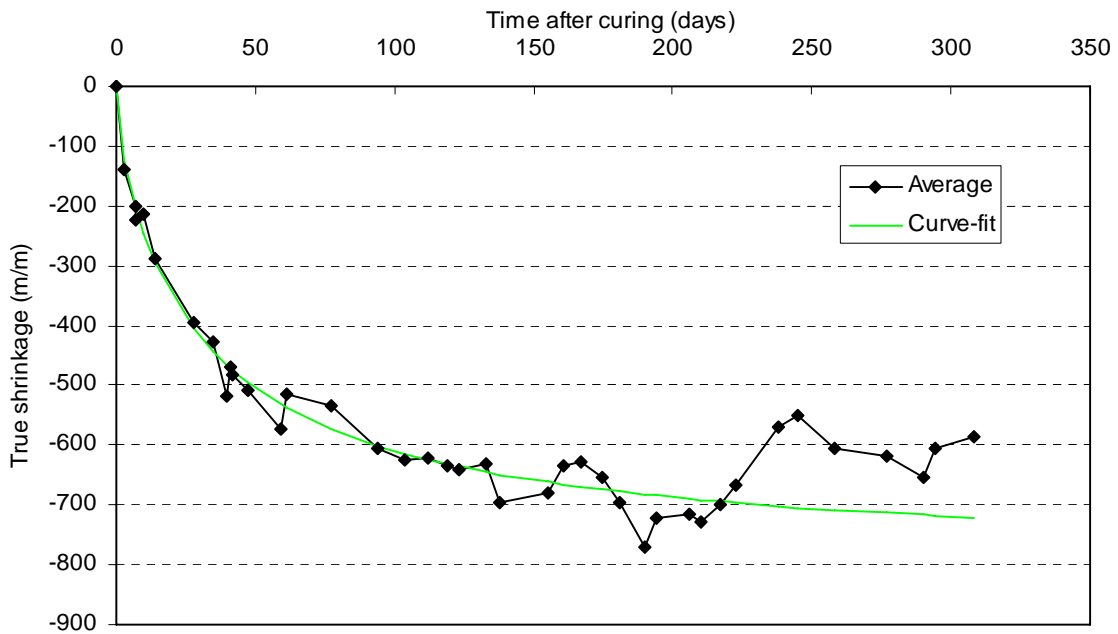


Figure 3.54: Average true shrinkage for the May batch concrete with best-fit curve.

3.6.2. Curve-fit for Creep at First Loading

As mentioned previously, the experimental shrinkage from the F4 concrete batches was not reliable. For this reason, the creep was determined removing either the measured shrinkage or the shrinkage that could be expected from the F5 concrete batches. For the F4 concretes, creep is provided for both methods of calculation and is designated with F4 shrinkage or F5 shrinkage to signify the shrinkage that was removed from the creep strain to provide the values presented here.

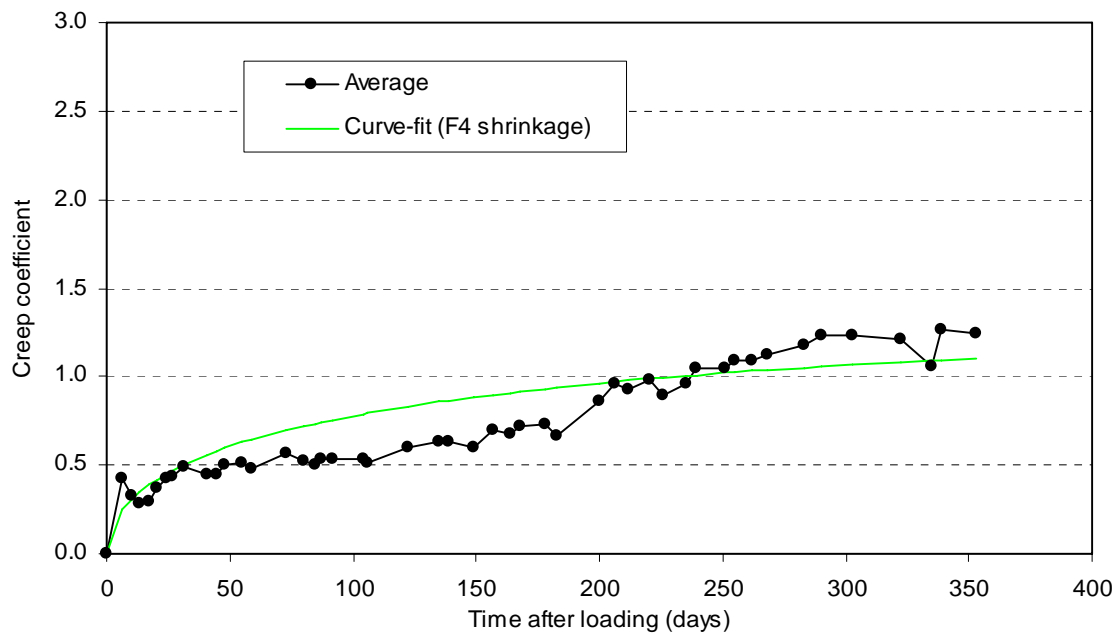


Figure 3.55: Average creep coefficient from the October batch concrete (measured shrinkage) from first loading (prestressing).

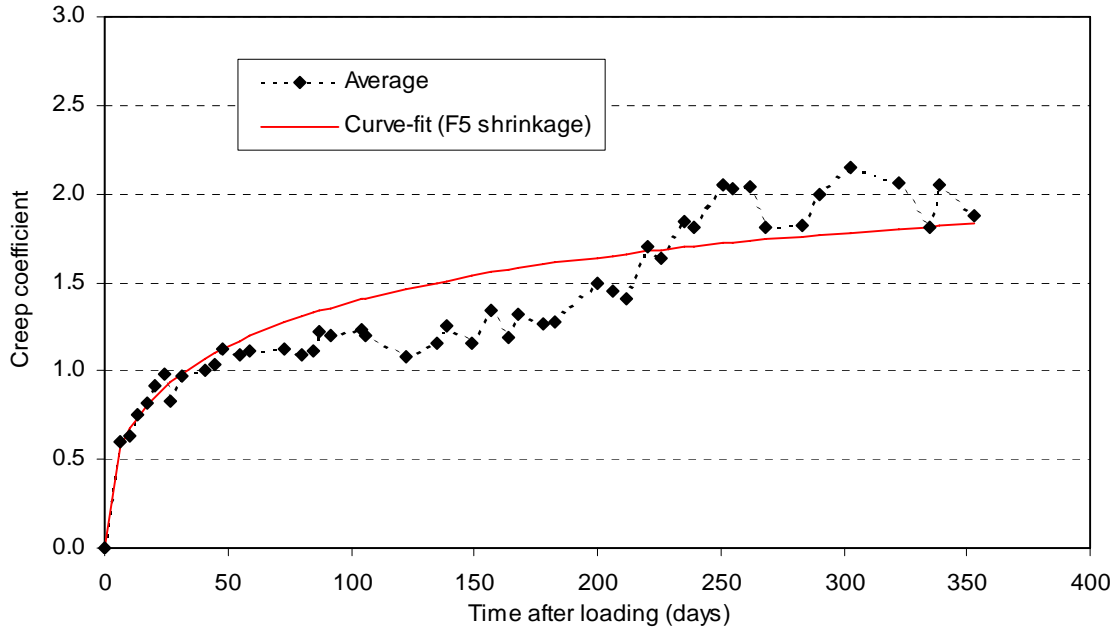


Figure 3.56: Average creep coefficient from the October batch concrete (F5 shrinkage) from first loading (prestressing).

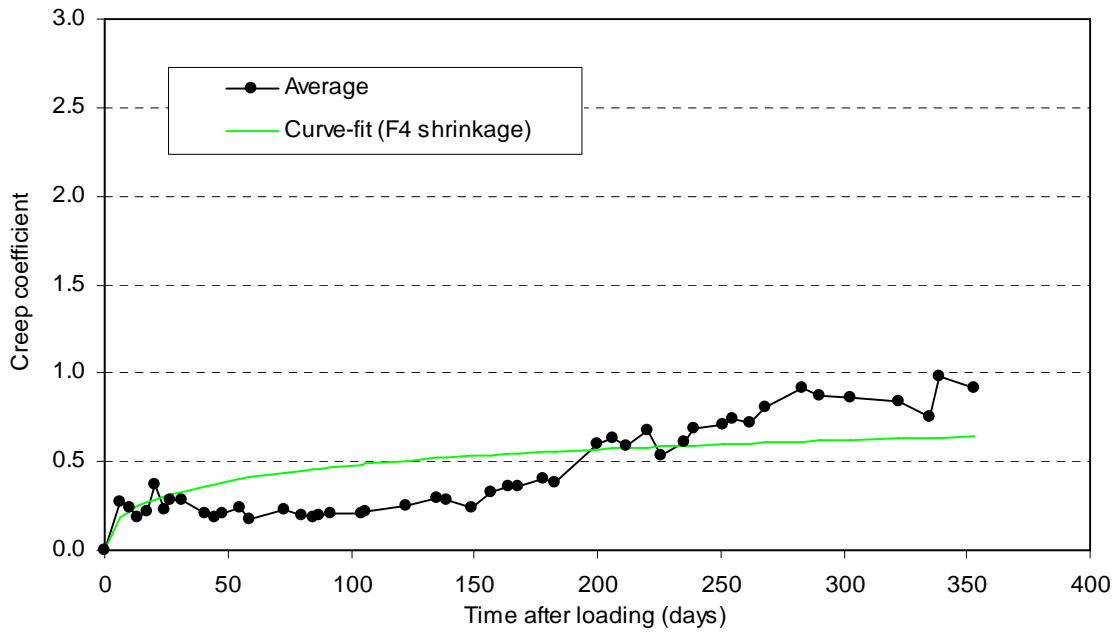


Figure 3.57: Average creep coefficient from the November batch concrete (measured shrinkage) from first loading (prestressing).

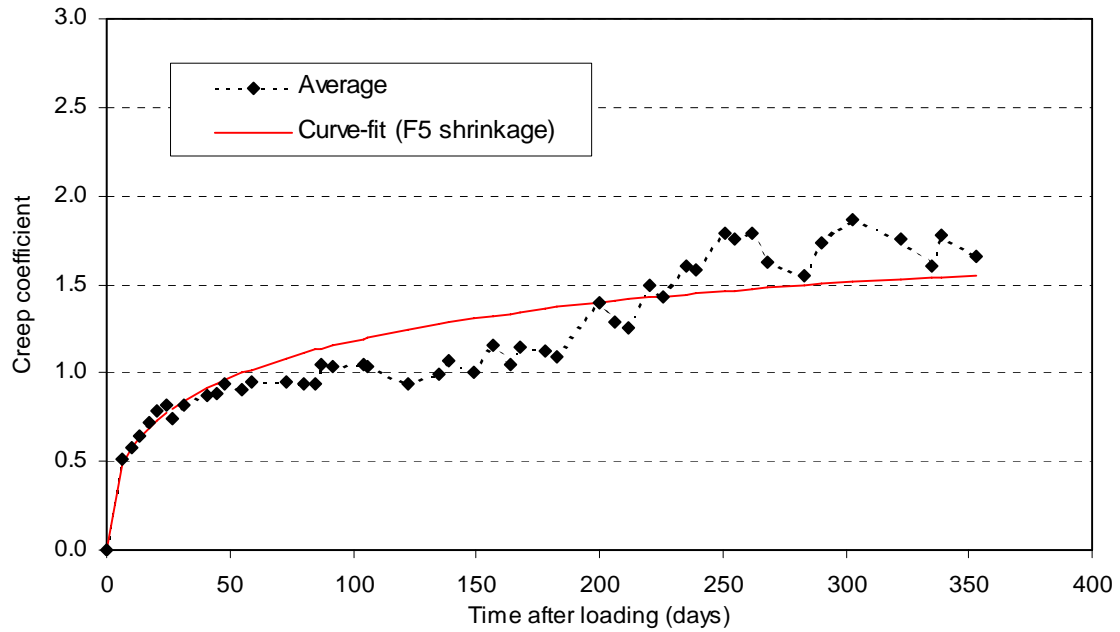


Figure 3.58: Average creep coefficient from the November batch concrete (F5 shrinkage) from first loading (prestressing).

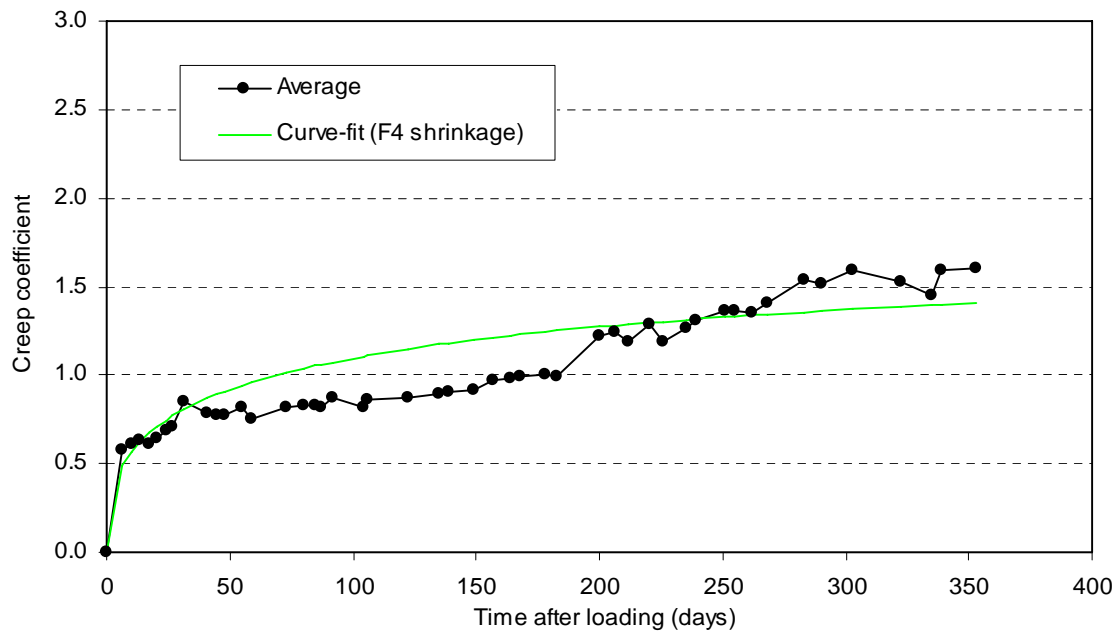


Figure 3.59: Average creep coefficient from the March batch concrete (measured shrinkage) from first loading (prestressing).

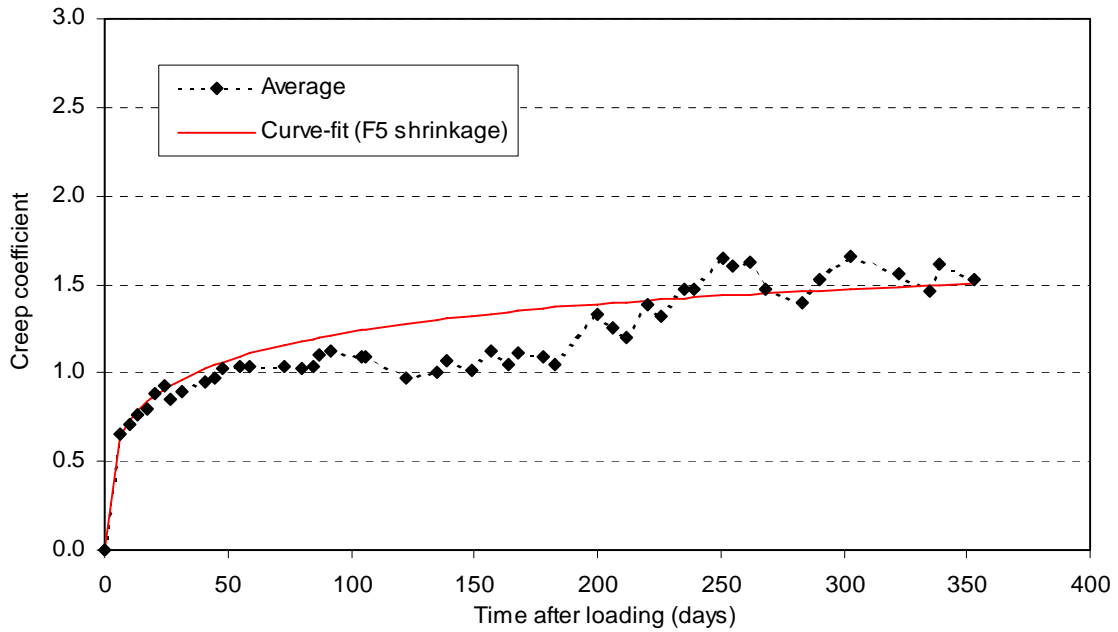


Figure 3.60: Average creep coefficient from the March batch concrete (F5 shrinkage) from first loading (prestressing).

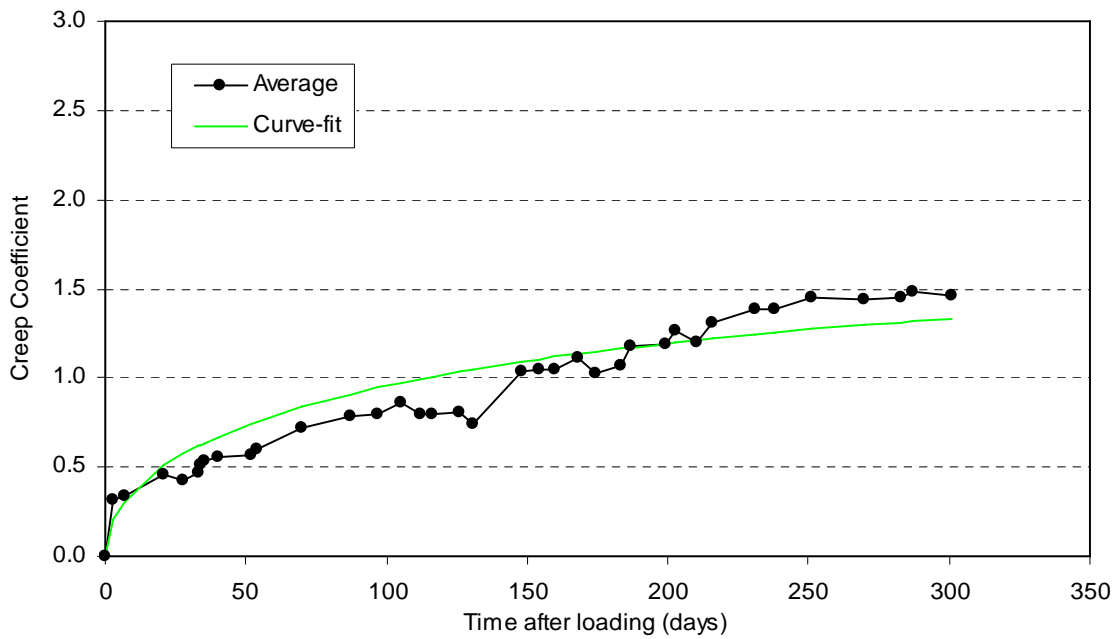


Figure 3.61: Average creep coefficient from the April batch concrete (measured shrinkage) from first loading (prestressing).

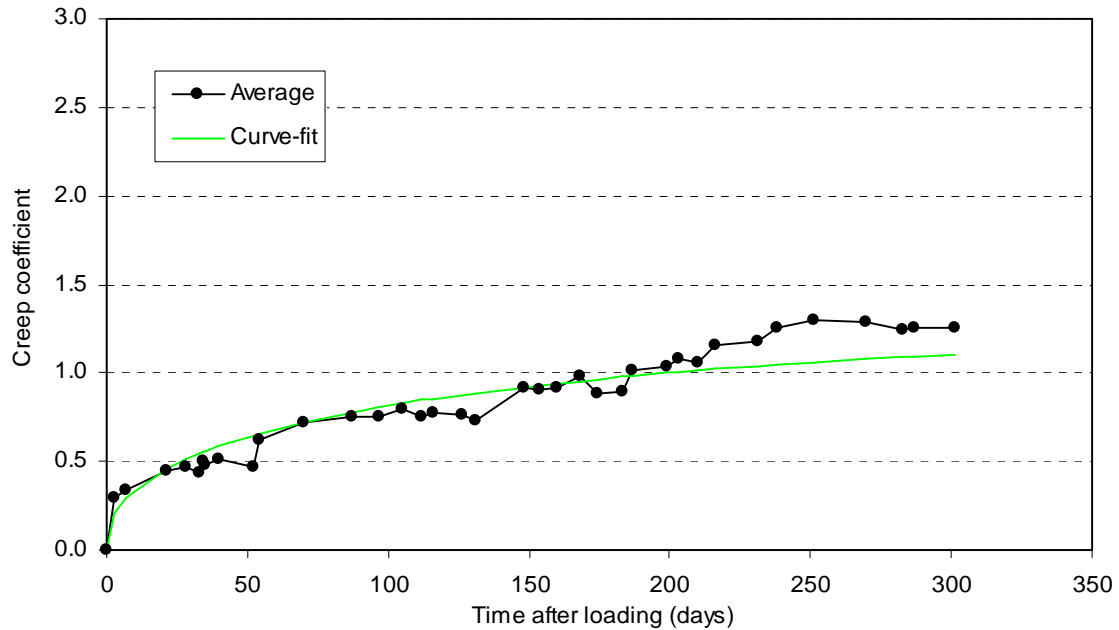


Figure 3.62: Average creep coefficient from the May batch concrete (measured shrinkage) from first loading (prestressing).

3.6.3. Curve-fit for Creep at Second Loading

As mentioned previously, the experimental shrinkage from the F4 concrete batches was not reliable. The values of shrinkage from F4 were significantly in excess of predictions, as will be shown in Section 3.7. For this reason, the experimental shrinkage from the F4 concrete batches and the experimental F5 shrinkage were removed from the experimental creep in the F4 concrete batches. This was shown to make a considerable difference to the experimental creep for the first loading creep tests. This results as the shrinkage that was removed differed considerably between the experimental cases and the shrinkage from F5 used for F4, as presented in Figure 3.46 and Figure 3.49. For the second loading (removal of falsework) creep tests, the rate of increase in shrinkage significantly diminished. Thus, both the experimental F4 shrinkage used outright and the F5 shrinkage that was used in combination with the F4 creep strain do not create significant changes in the creep coefficient.

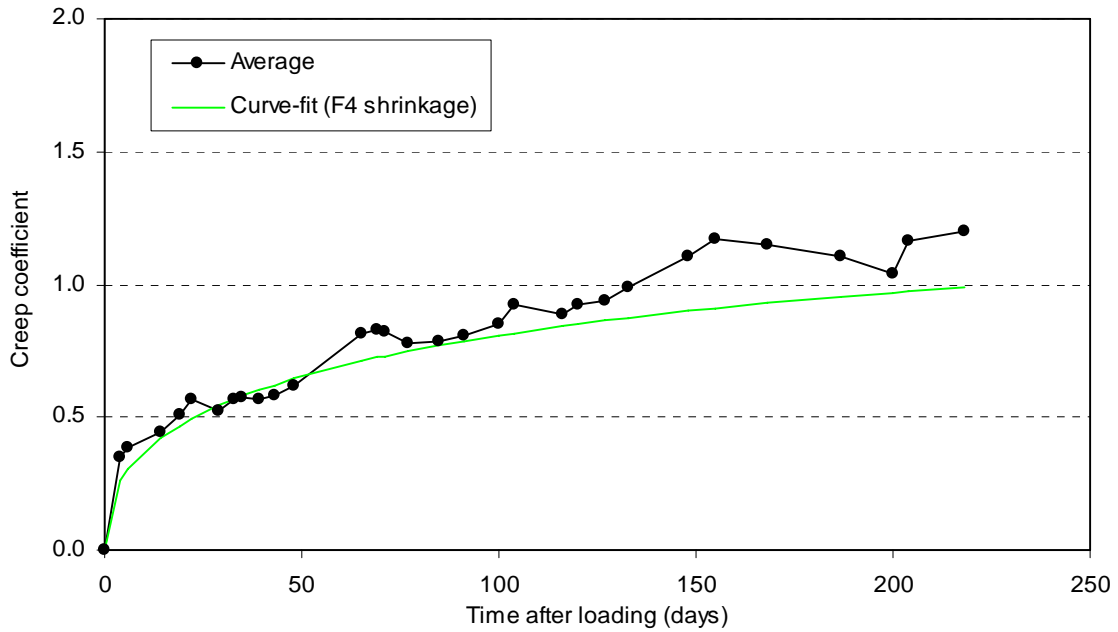


Figure 3.63: Average creep coefficient from the October batch concrete (measured shrinkage) from second loading (removal of falsework).

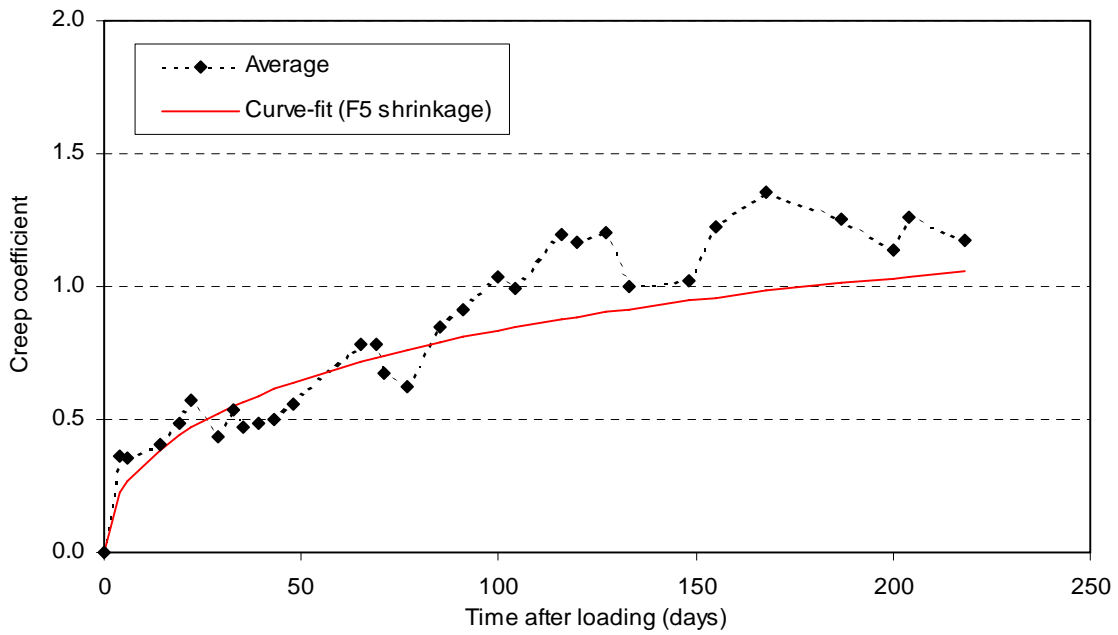


Figure 3.64: Average creep coefficient from the October batch concrete (F5 shrinkage) from second loading (removal of falsework).

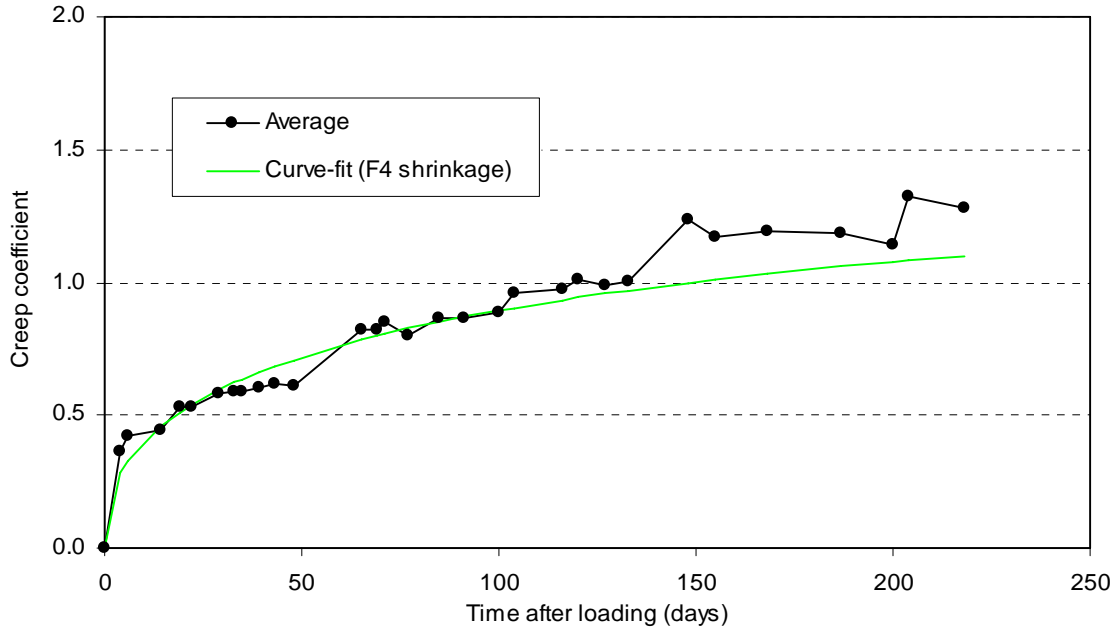


Figure 3.65: Average creep coefficient from the November batch concrete (measured shrinkage) from second loading (removal of falsework).

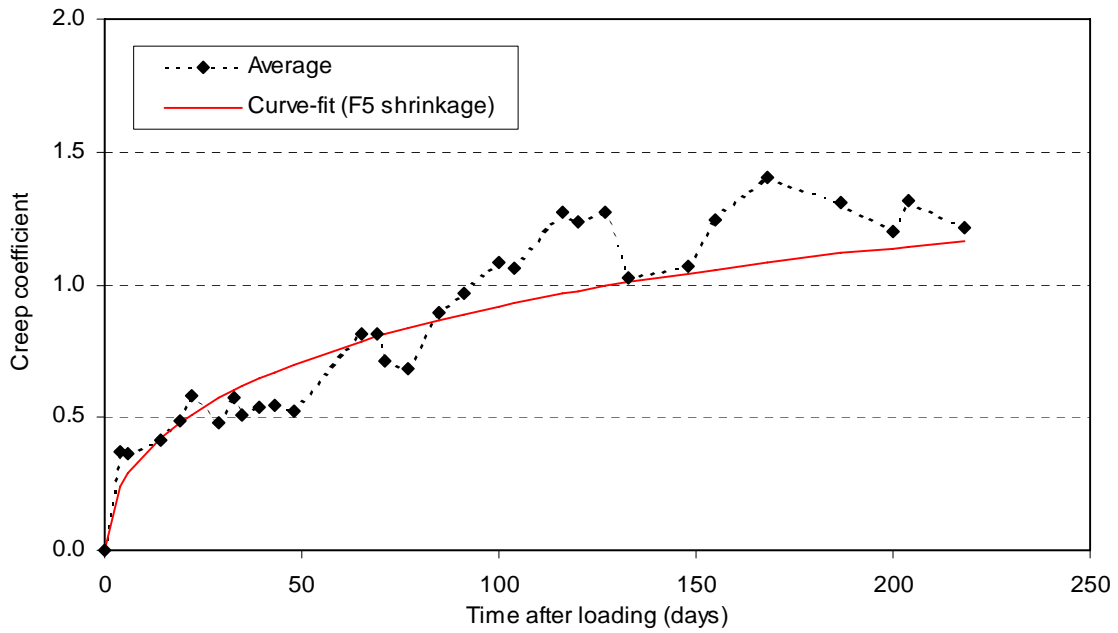


Figure 3.66: Average creep coefficient from the November batch concrete (F5 shrinkage) from second loading (removal of falsework).

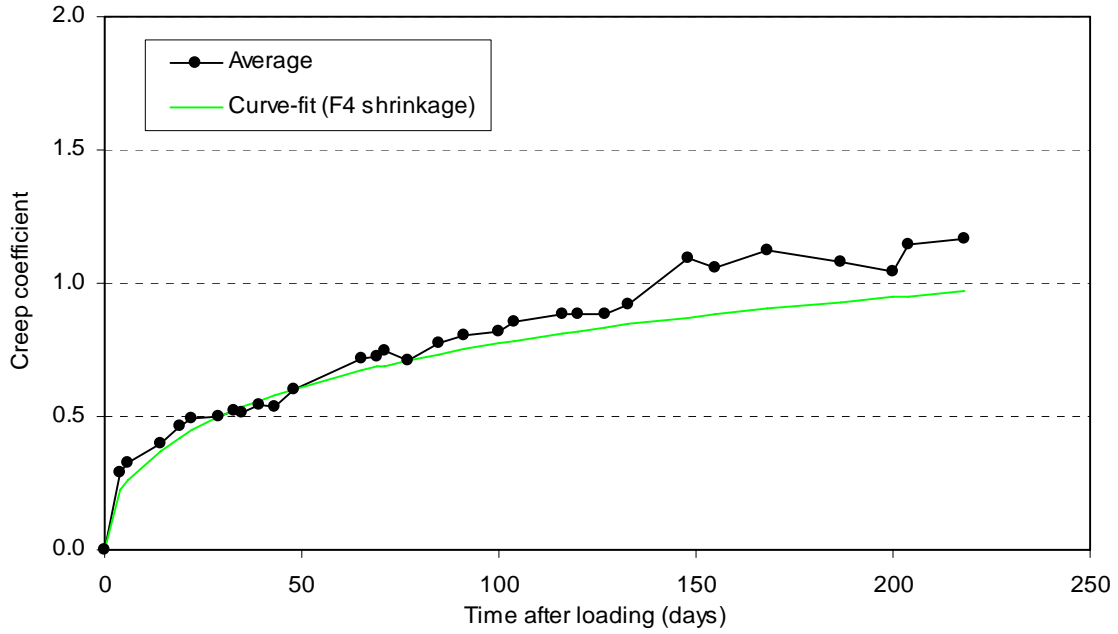


Figure 3.67: Average creep coefficient from the March batch concrete (measured shrinkage) from second loading (removal of falsework).

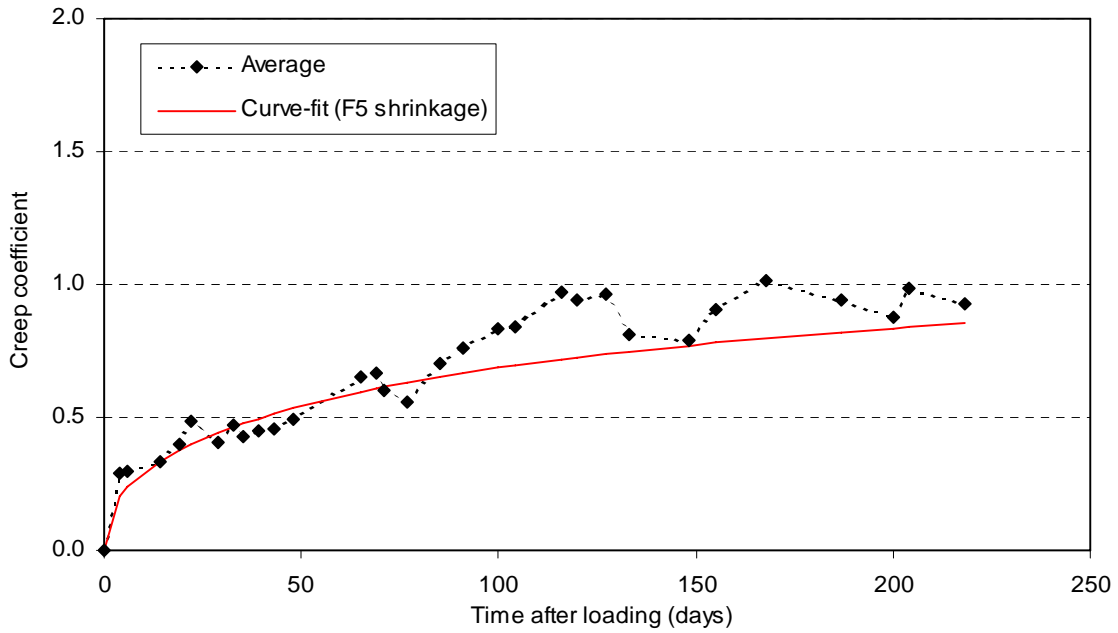


Figure 3.68: Average creep coefficient from the March batch concrete (F5 shrinkage) from second loading (removal of falsework).

3.6.4. Curve-fit for Creep at Third Loading

The best-fit curves for the creep coefficients at the third loading are presented here for the experimental data.

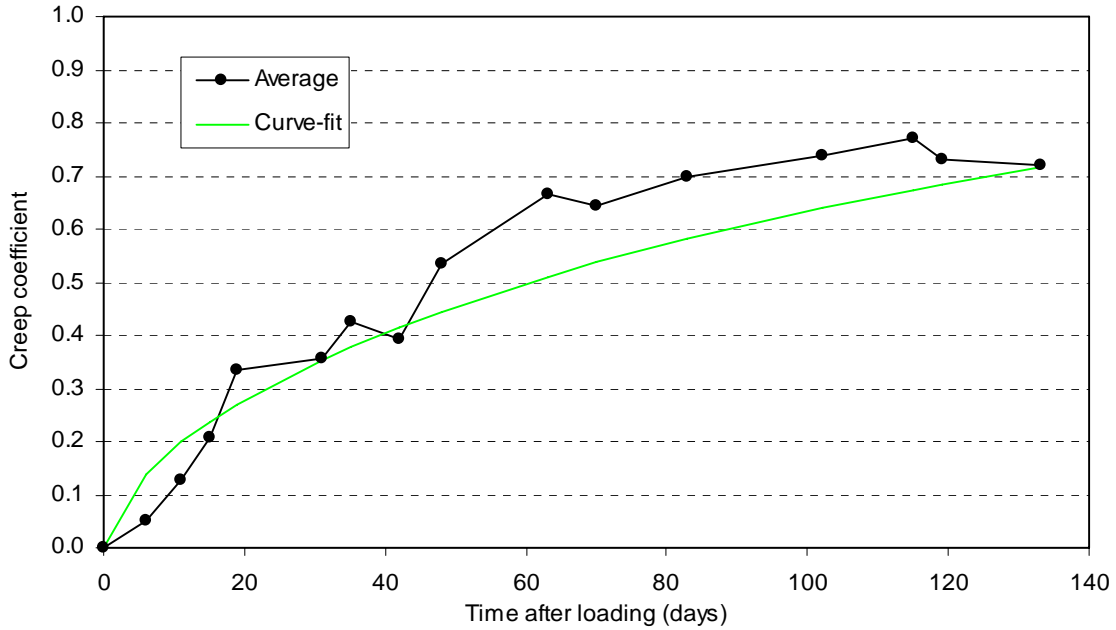


Figure 3.69: Average creep coefficient from the April batch concrete (measured shrinkage) from second loading (removal of hinge supporting falsework).

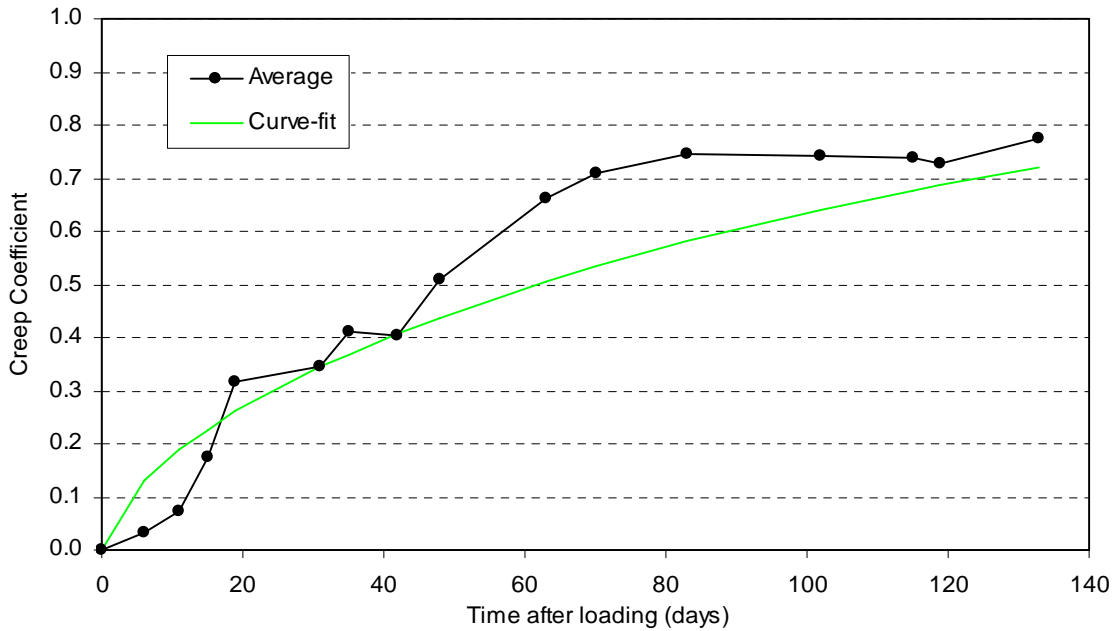


Figure 3.70: Average creep coefficient from the May batch concrete (measured shrinkage) from second loading (removal of hinge supporting falsework).

3.7. Specifications Predictions of Creep and Shrinkage: Test Specimen

The specifications presented in Section 2.2 were used to produce predictions of the creep and shrinkage for the test specimens. The amount of creep and shrinkage that occur in the concrete is dependent on the size of the element, accommodated using V/S (as outlined in Section 2.2.1), among other factors. The predictions of creep and shrinkage for the bridge are different from the predictions of the creep and shrinkage for the test specimens since the V/S ratio is different for both. The specifications predictions of creep and shrinkage for the bridge are included in Section 3.8. Not only are the specifications predictions of creep and shrinkage different because of the difference in size of the elements, but the experimental creep and shrinkage obtained through testing cannot be used outright as input into the computer analyses that are described in Chapter 4. The specifications predictions of creep and shrinkage will be useful in proportioning the experimental creep and shrinkage to appropriate values that are suitable for the bridge.

The creep and shrinkage were calculated for each concrete using the method of processing the measured data presented in Section 3.4 and illustrated in Section 3.5. A method of curve fitting, developed by Ghali et al [15], was adopted using calibration of the CEB-FIP [10] equations for the collected data to provide a smooth progression of creep and shrinkage over the monitoring period as well as to project ultimate values.

The specifications predictions for creep and shrinkage for each concrete type was generated using the methods presented in Chapter 2. The inputs that were utilized in producing the predictions are presented in Table 3.5 for all concrete types.

Table 3.5: Inputs as used in specifications for prediction of creep and shrinkage for the test specimens and bridge.

		Input Value					Units
		October	November	March	April	May	
Concrete type							
Input Parameter	V/S Test Specimen	38 (1.5)	38 (1.5)	38 (1.5)	38 (1.5)	38 (1.5)	mm (in.)
	V/S Bridge	114 (4.49)	114 (4.49)	114 (4.49)	110 (4.33)	110 (4.33)	mm (in.)
	Relative Humidity	66	66	66	67	67	%
	28-day Mean Concrete Compressive Strength	41 (5.9)	43 (6.2)	31 (4.6)	39 (5.6)	28 (4.0)	MPa (ksi)
	Concrete age at end of curing	7	7	7	7	10	days
	Concrete age from casting at post-tensioning; first loading	169	141	20	45	17	days
	Concrete age from casting at hinge loading; second loading	290	262	141	202	174	days

The V/S ratio of the bridge was calculated from the known dimensions of the cross section and provided in Table 3.5. Since the length of the bridge is considerable, the area at the ends of the span is negligible compared to the total surface area of the bridge. For this reason, the V/S ratio may be calculated from Eq. 3.20.

$$\frac{V}{S} = \frac{A_c l}{P l} = \frac{A_c}{P} \quad (3.20)$$

A_c = area of the bridge cross-section

P = the total – internal and external – perimeter of the cross-section

l = span length of the bridge

The time and loading sequence of the material tests correspond to important casting and loading instants of the bridge construction. The creep test specimens were loaded within a few days from the actual bridge loading. The figures in the following sections compare the measured creep and shrinkage with the predicted values from specifications.

The measured 28-day concrete strength varied from the characteristic concrete strength by -0.07 to 1.5 ksi, as is normally the case in construction practice. Though the -0.07 ksi is alarming since it is a lower value than the specified strength, this is not a significant variation and the difference is less than 2%.

The data collected for shrinkage from the October, November, and March concretes, the concrete taken from F4, is not reliable. Monitoring of the shrinkage strains in the F4 concrete specimens began at the onset of loading – 175, 147, and 26 days after casting – for the October, November and March concrete, respectively. The October and November concretes exhibited nearly 200 microstrain of shrinkage after 15 days after monitoring began. Such shrinkage can be expected for concrete within a few days after the end of curing [2, 22]. The October and November concretes, having several months of drying before loading, do not behave as would be expected and the match to the predicted behavior is extremely poor. The March concrete demonstrates similar behavior to that of the October and November concrete, experiencing considerably more shrinkage than predicted. The shrinkage of March concrete, while considerably larger than predictions, maintains a closer relation to the predictions than the October and November concrete types. These discrepancies can be seen in Figure 3.71, Figure 3.73, and Figure 3.75. A few possibilities for these discrepancies exist. The initial measurements of the shrinkage strain may not have been taken correctly. Examination of the figures for the strains in these three concrete types displays considerable increase in the strain within the first few days after measurements were taken. Additionally, these three concrete types may not have been cured in the manner described. The concrete may have been removed from the forms shortly after the concrete hardened and not moist cured with burlap.

The experimental creep for the October, November, and March concrete, appear to demonstrate likely and predictable behavior. All experimental creep and shrinkage measurements obtained for the F5 concrete show correlation to predictions with an average error of about 30%.

At critical points during the construction sequence of the bridge, the concrete cast dates, stressing ages, removal of falsework, and hinge loading were noted, as will be explained in a later chapter. The predictions of creep and shrinkage are based on the ages of the concrete at which these occurrences took place in the bridge.

3.7.1. Shrinkage Strain

The experimental shrinkage strain is presented in Figure 3.71 to Figure 3.78 for the five concrete types used in F4 and F5 and compared to the predicted shrinkage strains. The shrinkage that is of importance here is that which occurs within the interval after load has been applied. Shrinkage that occurs before the application of load does not influence prestress loss, as the tendons have not yet been placed into the prestressing ducts. The shrinkage occurring within the interval prior to stressing may be subtracted from the total strain to yield the amount of shrinkage that has occurred after stressing. The shrinkage for the F4 batches of concrete was not measured until loading occurred. The figures presented in this section for the shrinkage in F4 display the experimental shrinkage compared to the specifications predictions of shrinkage beginning at loading. The shrinkage in the F5 concrete batches was measured beginning from curing and is thus compared to the specifications predictions over the same period.

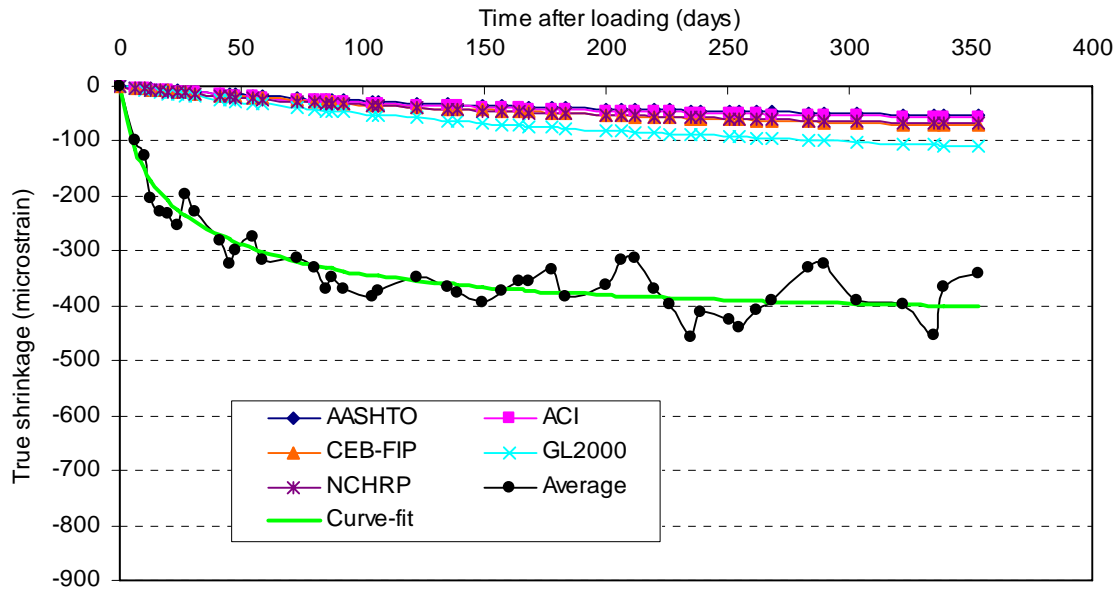


Figure 3.71: Experimental and predicted test specimen shrinkage for the F4 October concrete at first loading (prestressing) using measured shrinkage.

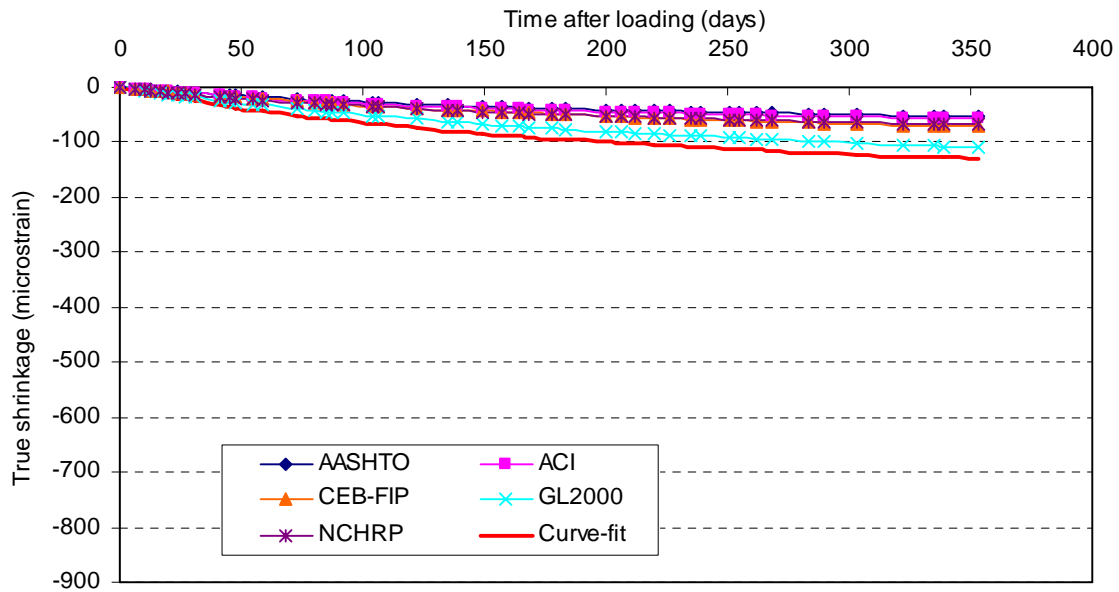


Figure 3.72: Experimental and predicted test specimen shrinkage for the F4 October concrete at first loading (prestressing) using F5 shrinkage.

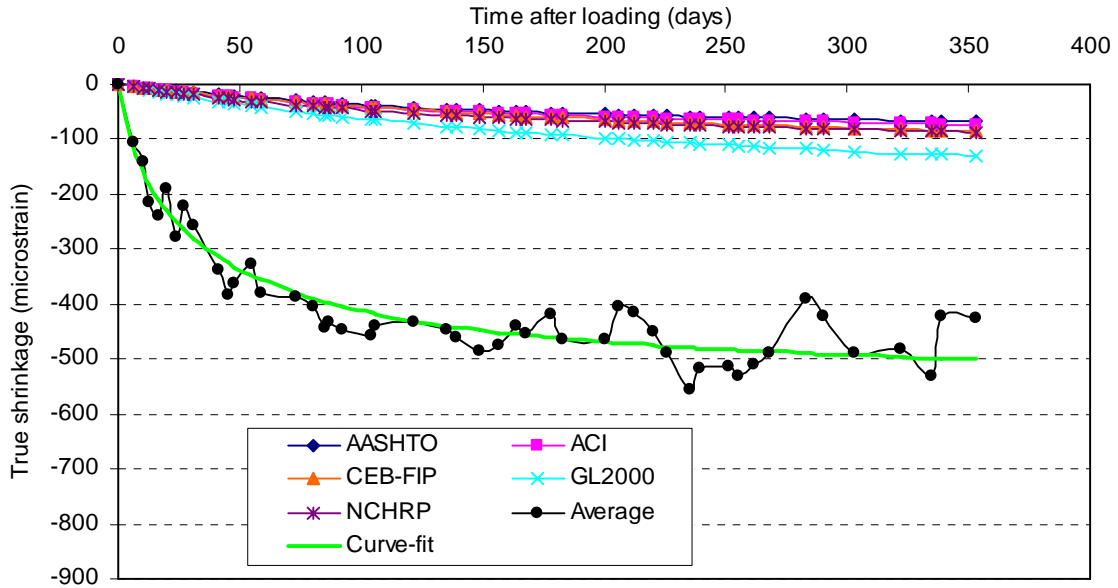


Figure 3.73: Experimental and predicted test specimen shrinkage for the F4 November concrete at first loading (prestressing) using measured shrinkage.

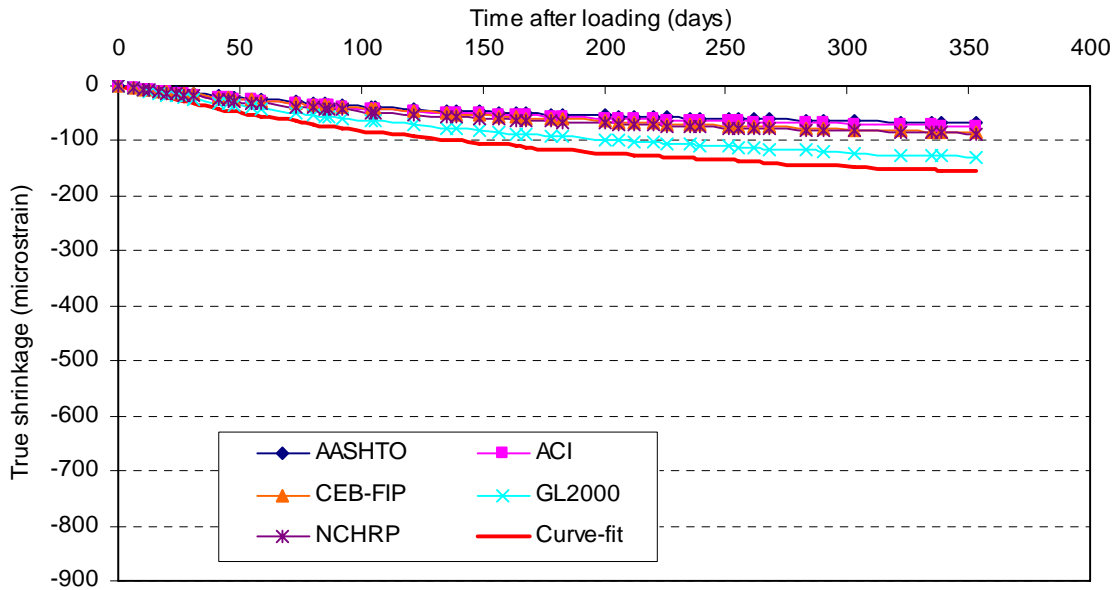


Figure 3.74: Experimental and predicted test specimen shrinkage for the F4 November concrete at first loading (prestressing) using F5 shrinkage.

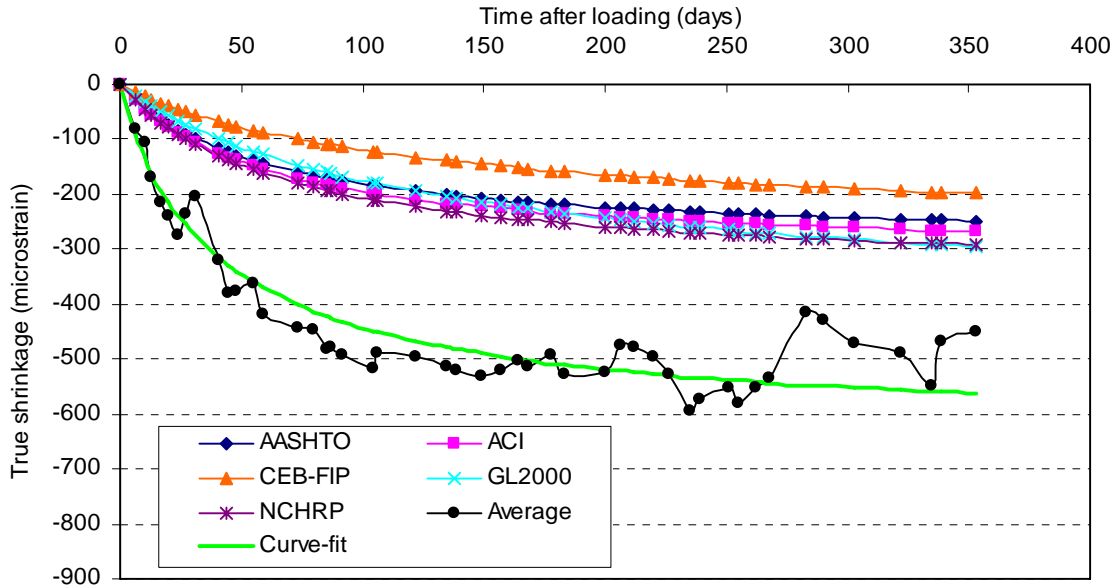


Figure 3.75: Experimental and predicted test specimen shrinkage for the F4 March concrete at first loading (prestressing) using measured shrinkage.

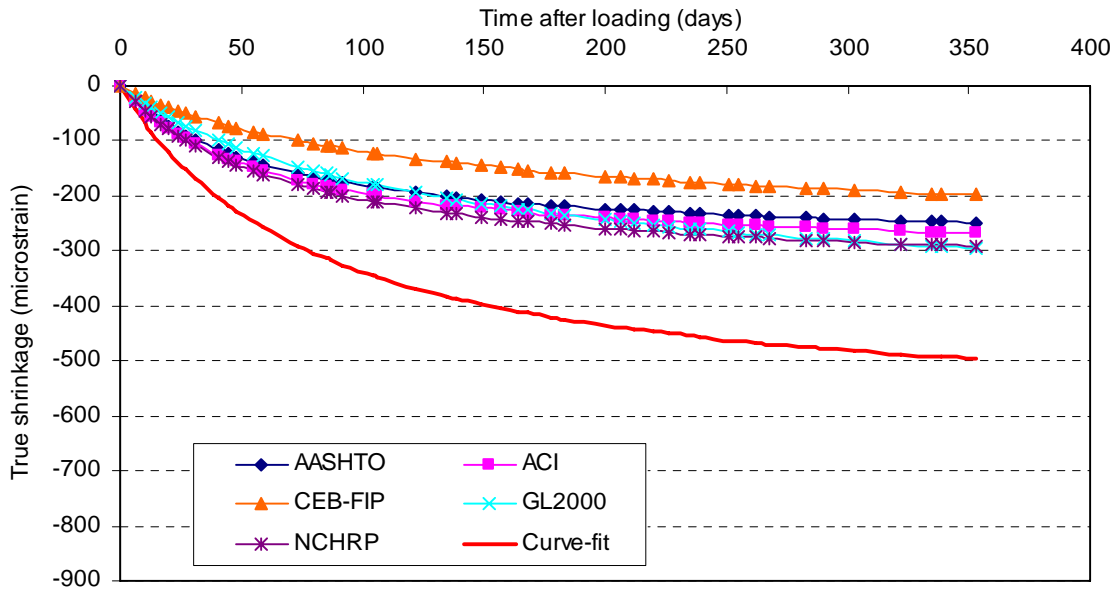


Figure 3.76: Experimental and predicted test specimen shrinkage for the F4 March concrete at first loading (prestressing) using F5 shrinkage.

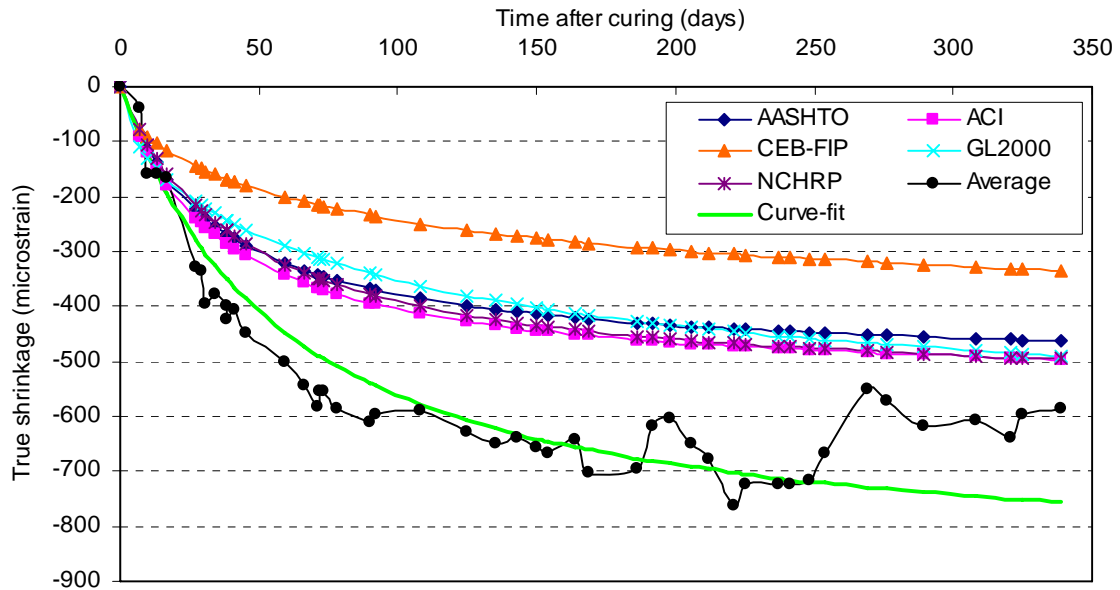


Figure 3.77: Experimental and predicted test specimen shrinkage for the F5 April concrete at first loading (prestressing).

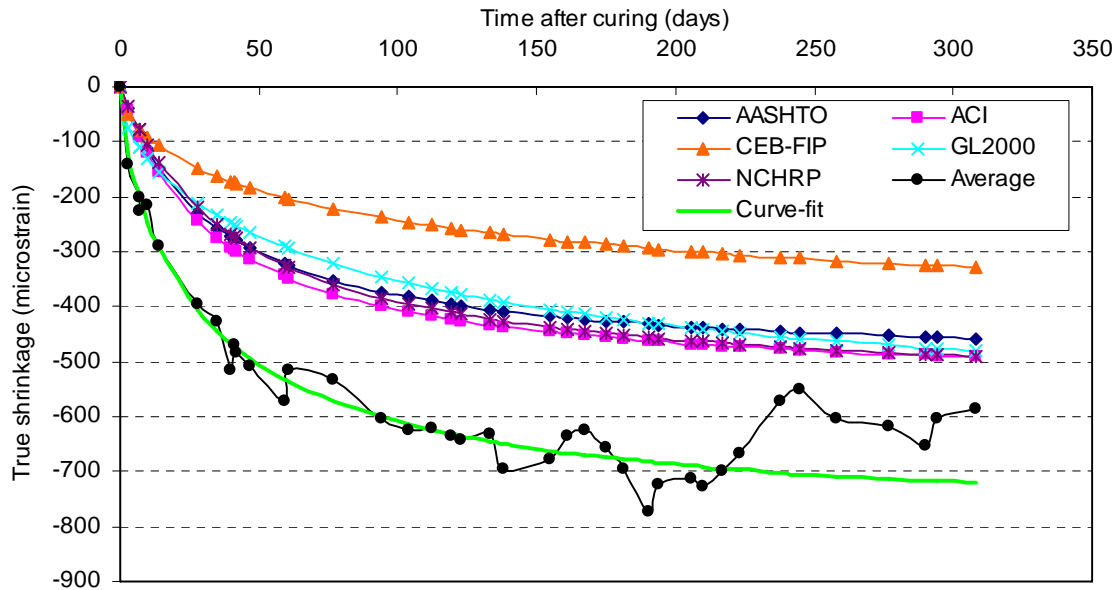


Figure 3.78: Experimental and predicted test specimen shrinkage for the F5 May concrete at first loading (prestressing).

3.7.2. Creep from First Loading

Figure 3.79 to Figure 3.86 display the creep coefficient for the first series of loading for each of the five concretes. In these figures, the measured creep coefficient is compared to the predicted creep coefficient for the same period.

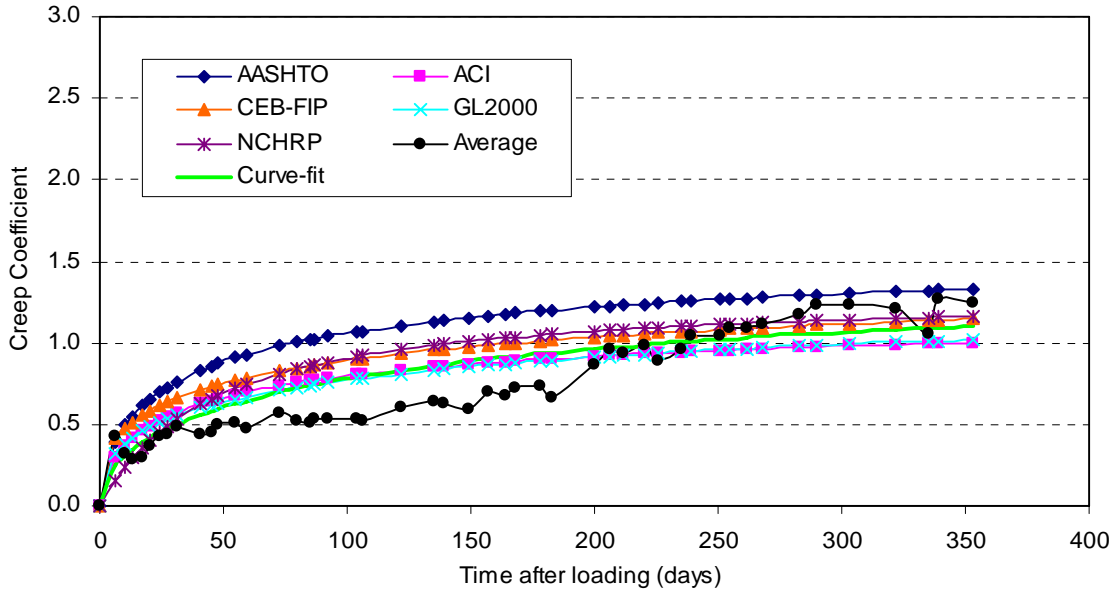


Figure 3.79: Experimental and predicted test specimen creep coefficient (using measured shrinkage) for the F4 October concrete at first loading (prestressing).

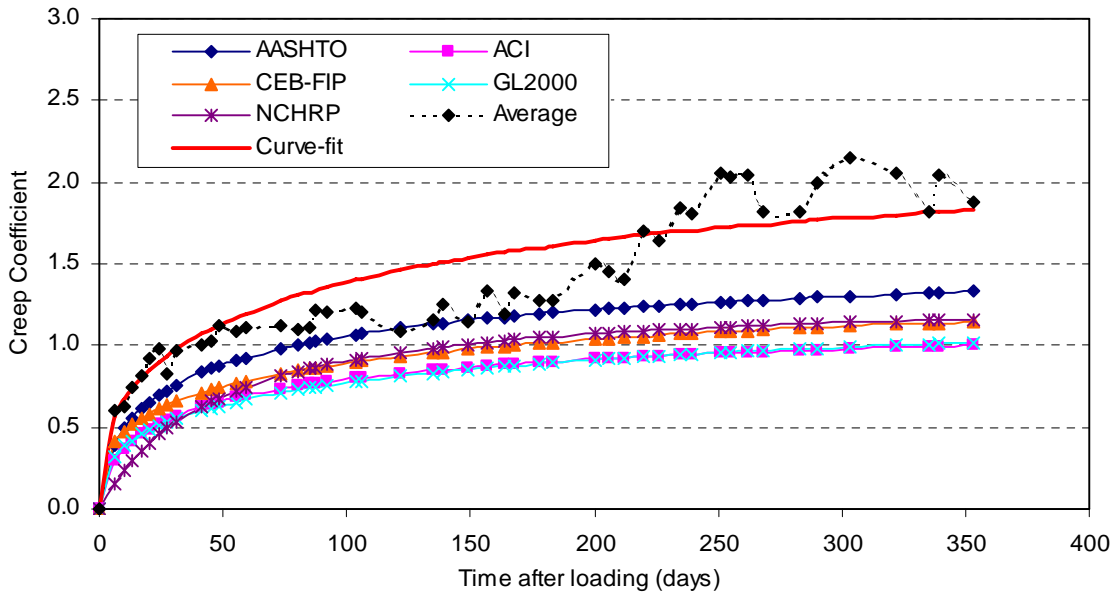


Figure 3.80: Experimental and predicted test specimen creep coefficient (using F5 shrinkage) for the F4 October concrete at first loading (prestressing).

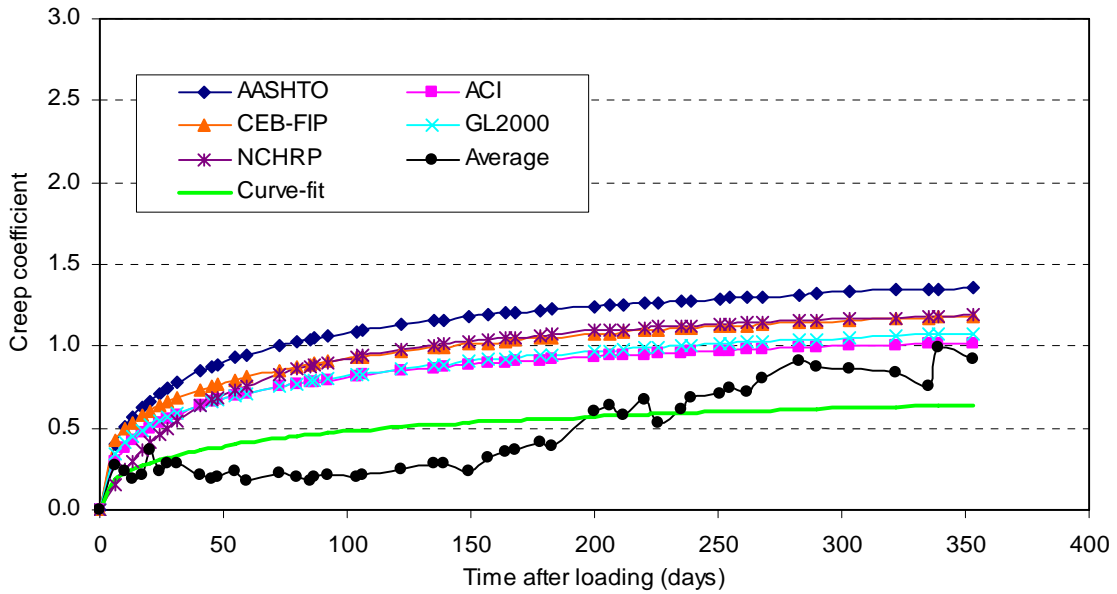


Figure 3.81: Experimental and predicted test specimen creep coefficient (using measured shrinkage) for the F4 November concrete at first loading (prestressing).

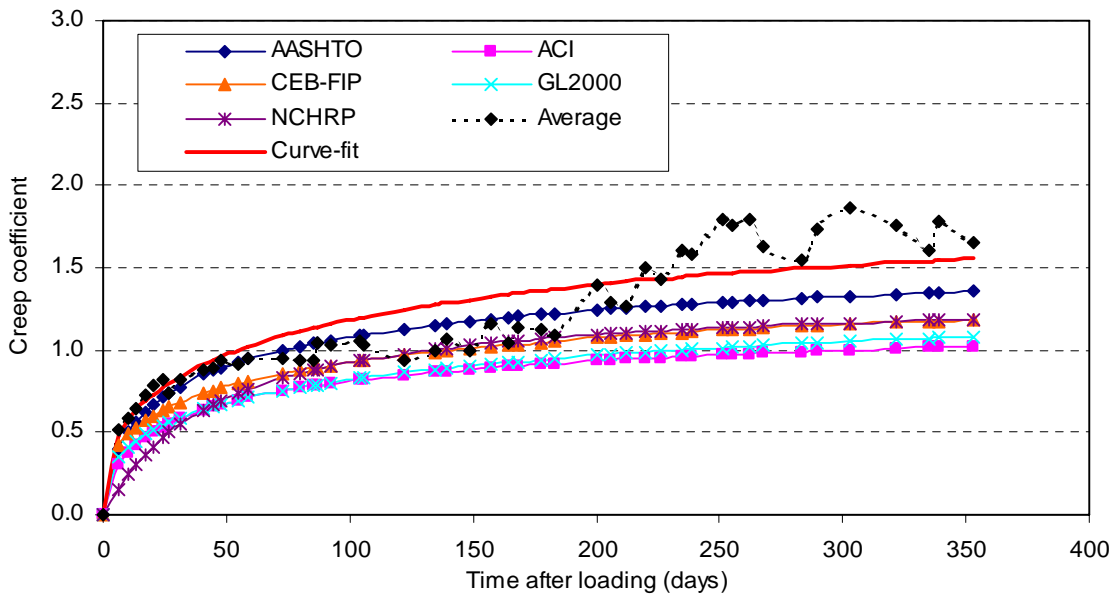


Figure 3.82: Experimental and predicted test specimen creep coefficient (using F5 shrinkage) for the F4 November concrete at first loading (prestressing).

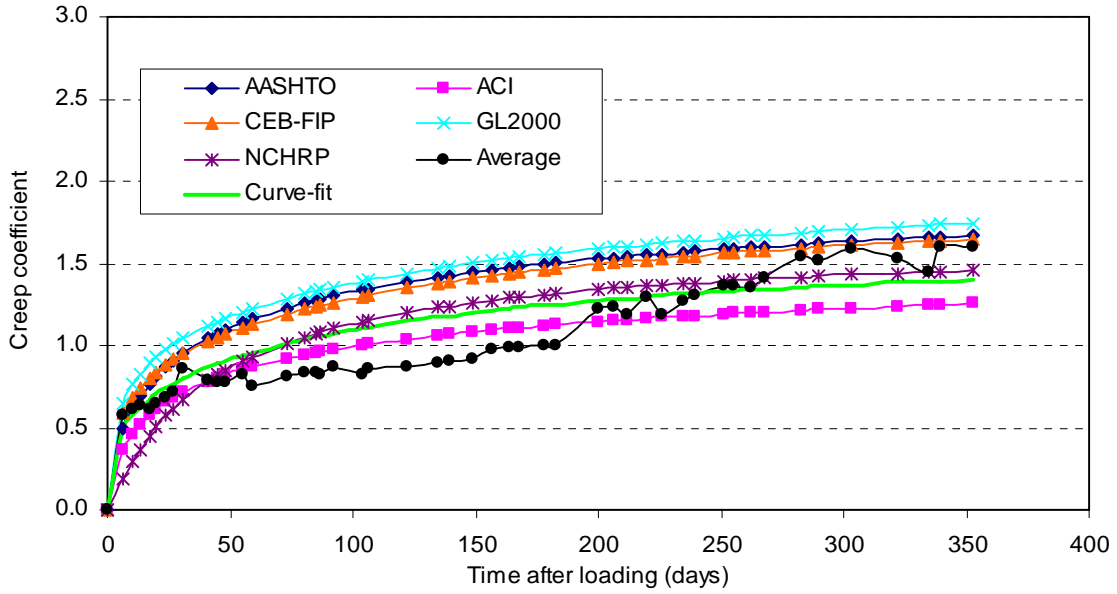


Figure 3.83: Experimental and predicted test specimen creep coefficient (using measured shrinkage) for the F4 March concrete at first loading (prestressing).

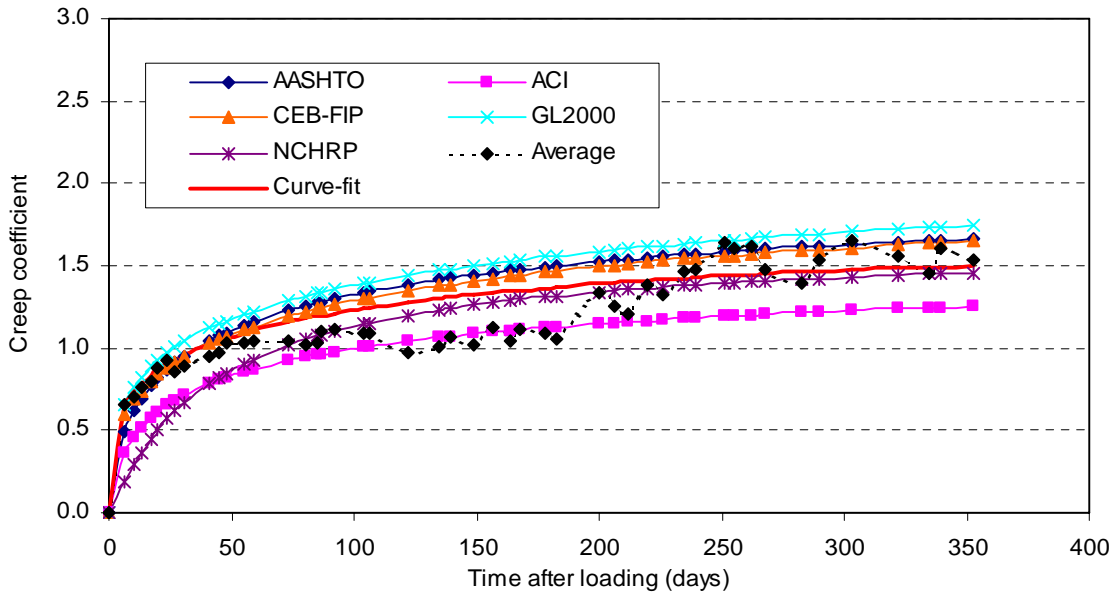


Figure 3.84: Experimental and predicted test specimen creep coefficient (using F5 shrinkage) for the F4 March concrete at first loading (prestressing).

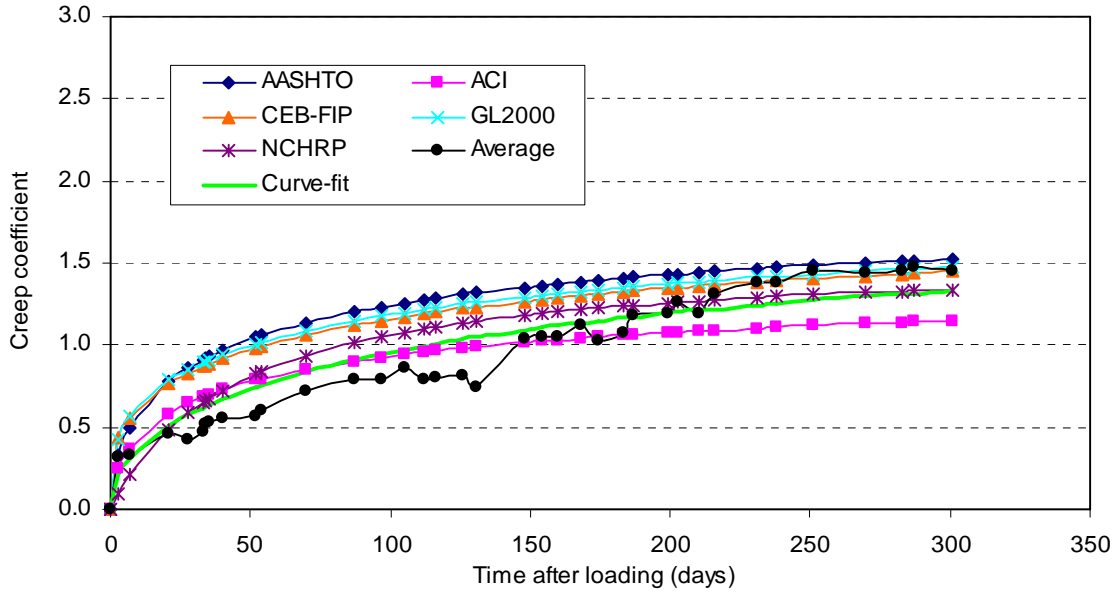


Figure 3.85: Experimental and predicted test specimen creep coefficient (using measured shrinkage) for the F5 April concrete at first loading (prestressing).

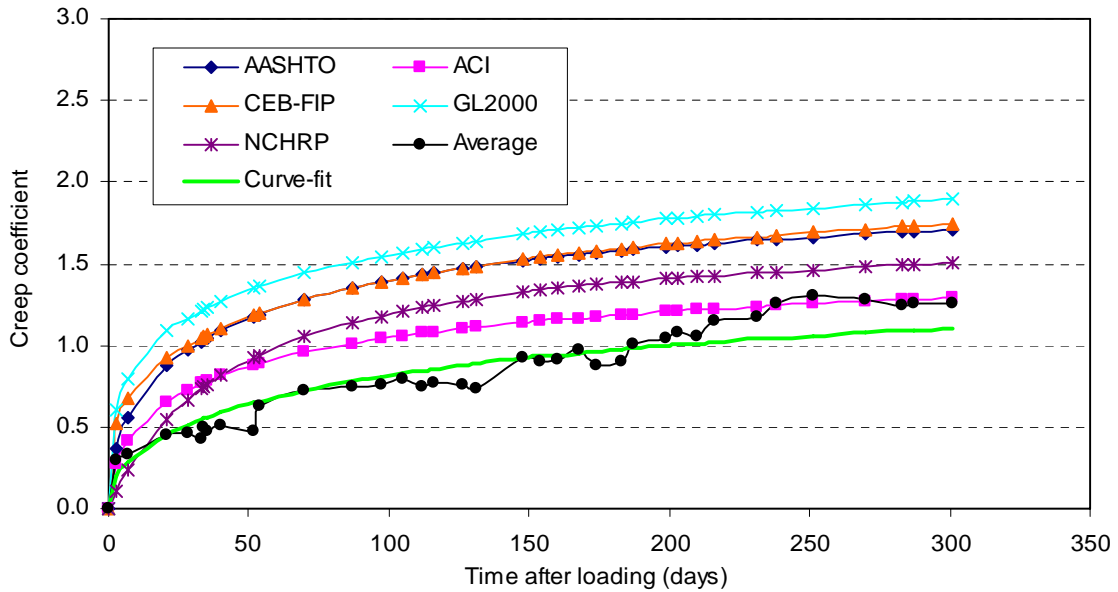


Figure 3.86: Experimental and predicted test specimen creep coefficient (using measured shrinkage) for the F5 May concrete at first loading (prestressing).

3.7.3. Creep from Second Loading

The creep coefficient for the second stage of loading for the concrete in F4 is presented in Figure 3.87 to Figure 3.94. This application of load corresponds to the instant at which the falsework was removed, thus subjecting removing all artificial restraints on the structure and subjecting the structure to its full self-weight. The material tests for second loading (removal of falsework) were not performed for the F5 concrete, thus only the specifications predictions are presented. The experimental creep coefficient in these figures is shown compared to the predicted creep values.

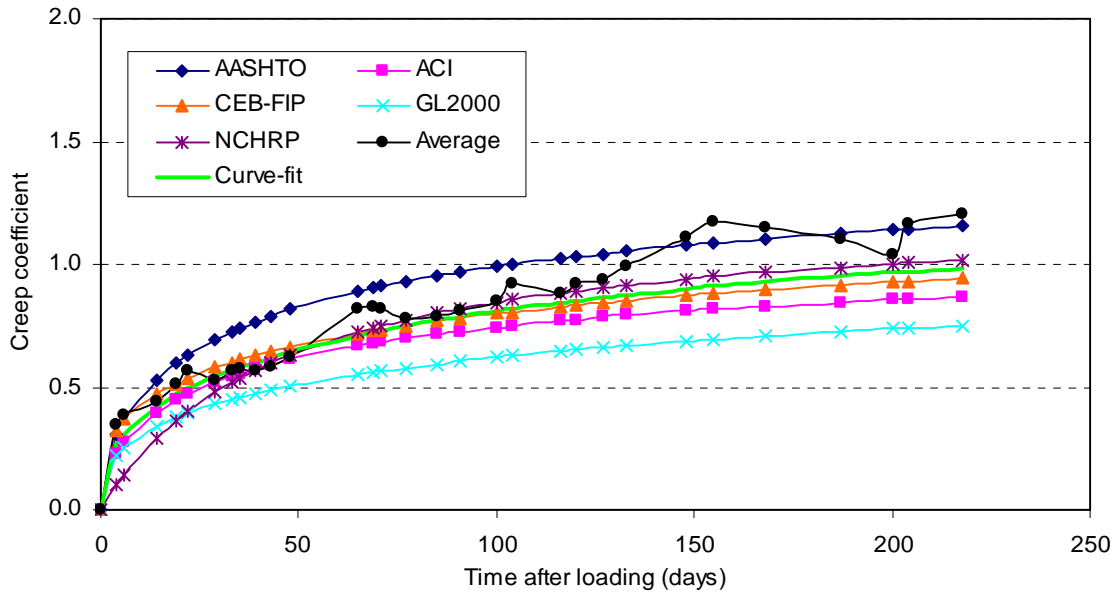


Figure 3.87: Experimental and predicted test specimen creep coefficient (using measured shrinkage) for the F4 October concrete at second loading (removal of falsework).

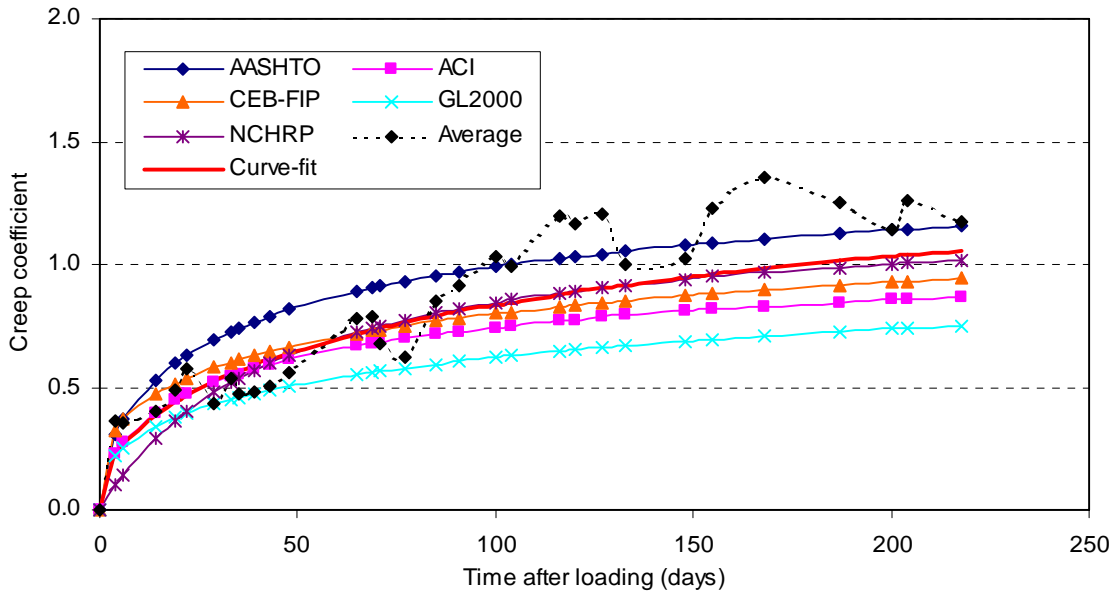


Figure 3.88: Experimental and predicted test specimen creep coefficient (using F5 shrinkage) for the F4 October concrete at second loading (removal of falsework).

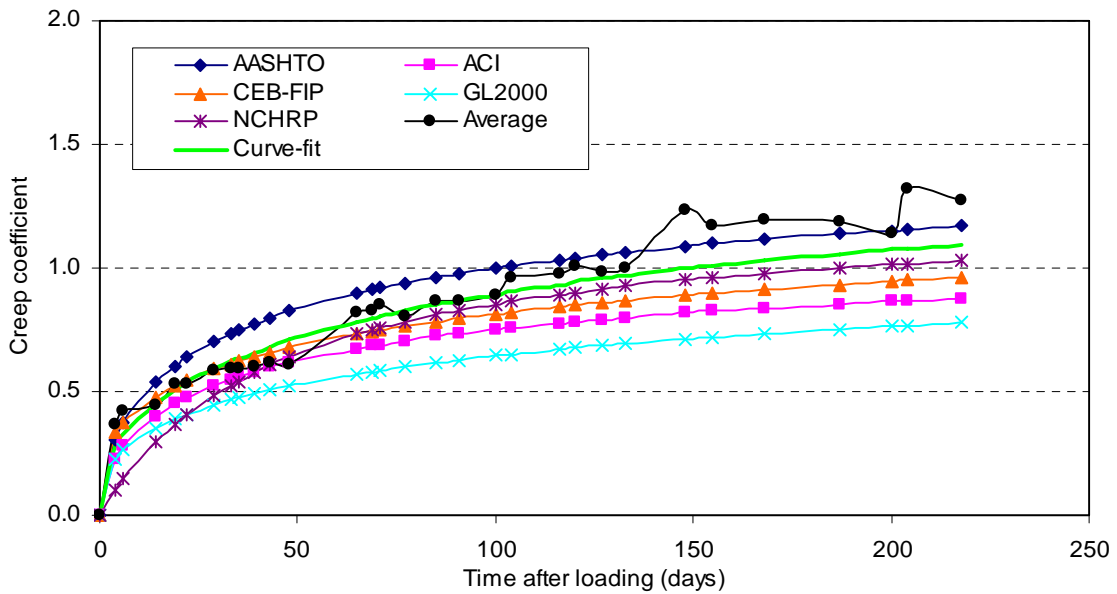


Figure 3.89: Experimental and predicted test specimen creep coefficient (using measured shrinkage) for the F4 November concrete at second loading (removal of falsework).

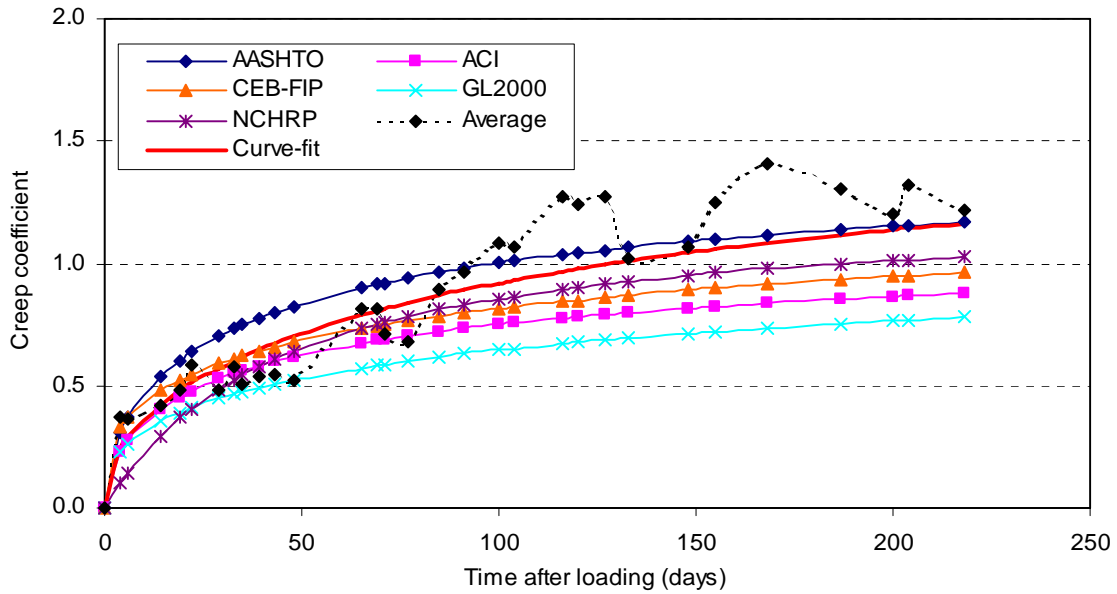


Figure 3.90: Experimental and predicted test specimen creep coefficient (using F5 shrinkage) for the F4 November concrete at second loading (removal of falsework).

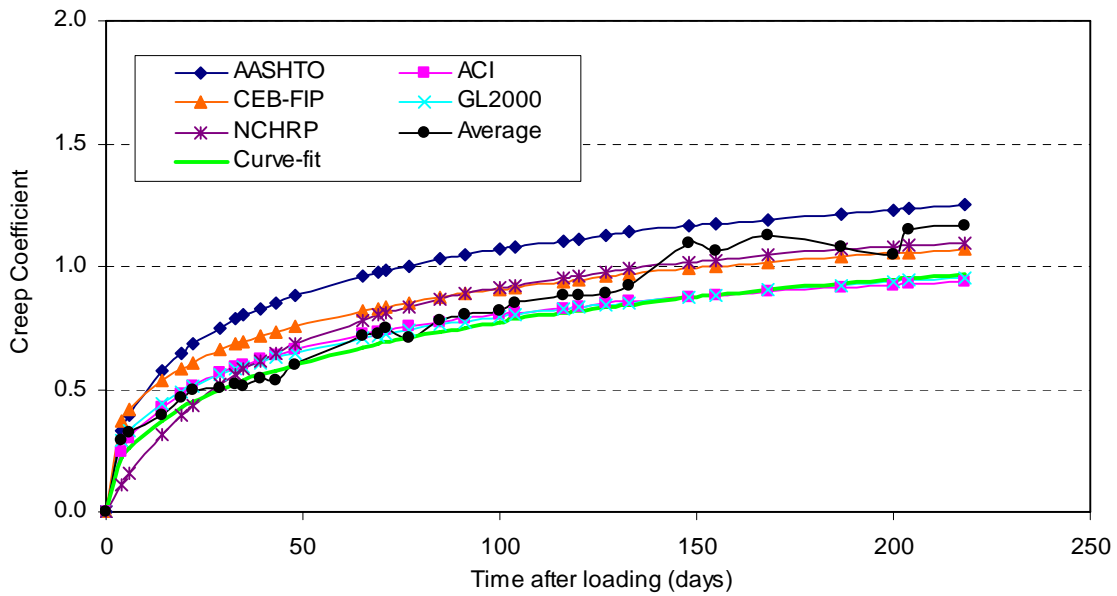


Figure 3.91: Experimental and predicted test specimen creep coefficient (using measured shrinkage) for the F4 March concrete at second loading (removal of falsework).

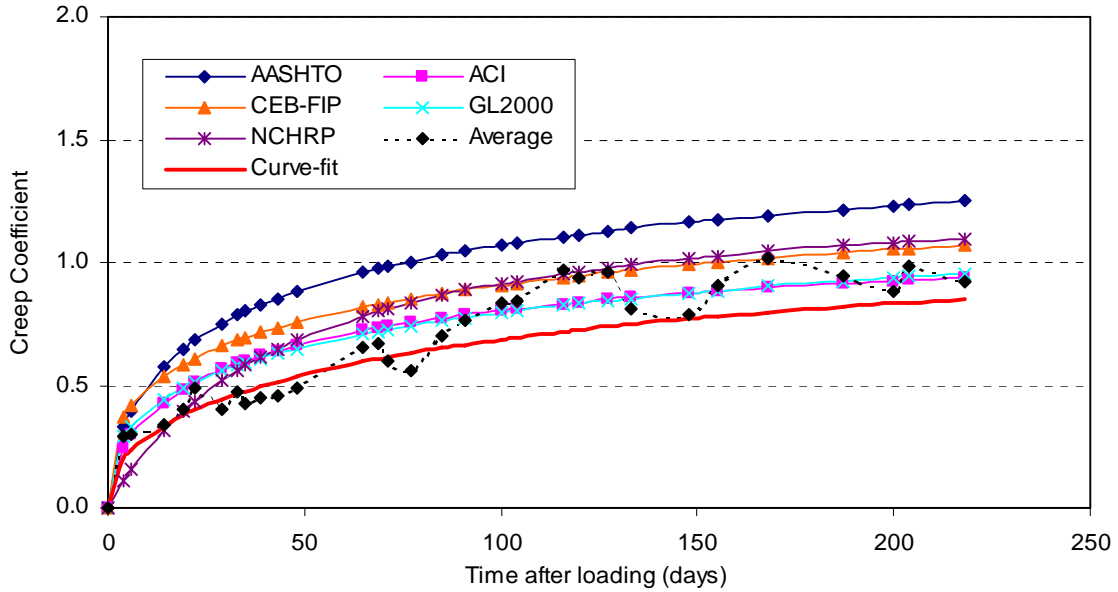


Figure 3.92: Experimental and predicted test specimen creep coefficient (using F5 shrinkage) for the F4 March concrete at second loading (removal of falsework).

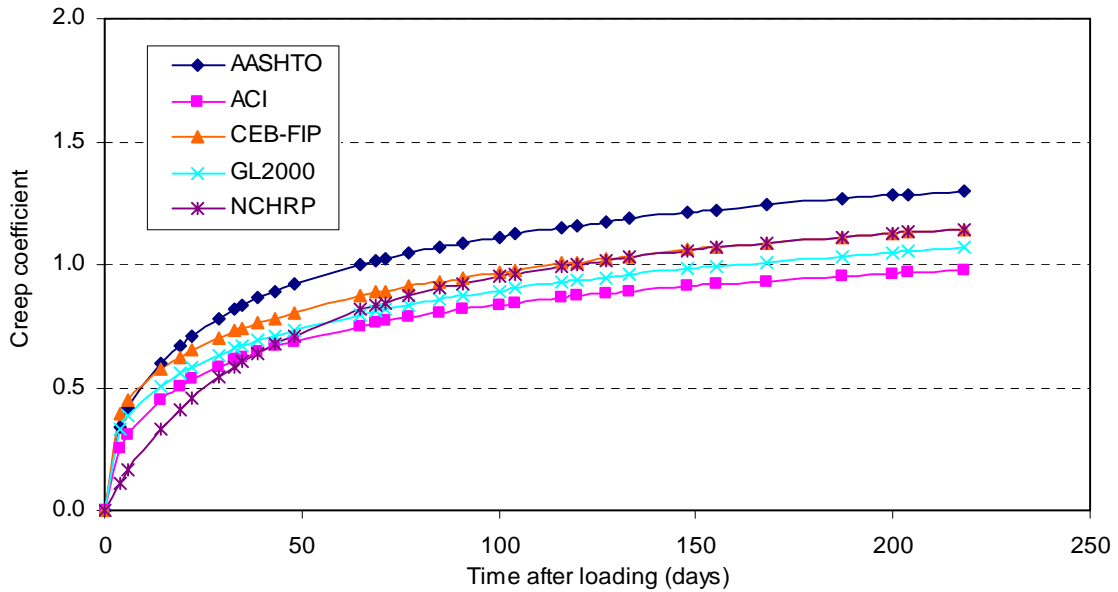


Figure 3.93: Predicted test specimen creep coefficient for the F5 April concrete at second loading (removal of falsework).

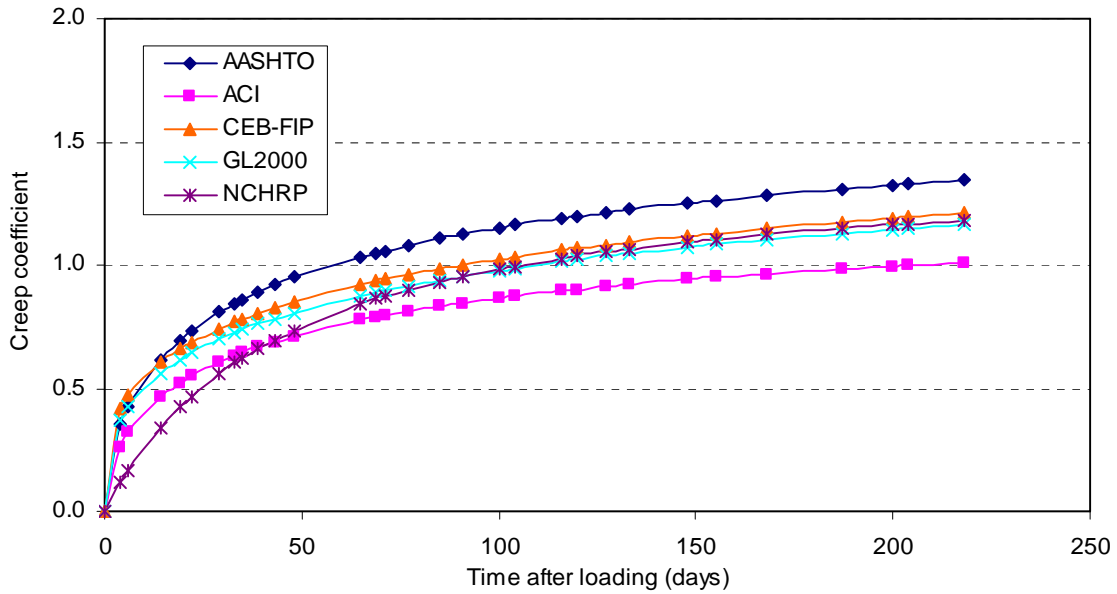


Figure 3.94: Predicted test specimen creep coefficient for the F5 May concrete at second loading (removal of falsework).

3.7.4. Creep from Third Loading

The creep coefficients for the test specimens are presented in Figure 3.95 and Figure 3.96 for the point corresponding to the removal of hinge supporting falsework in F5.

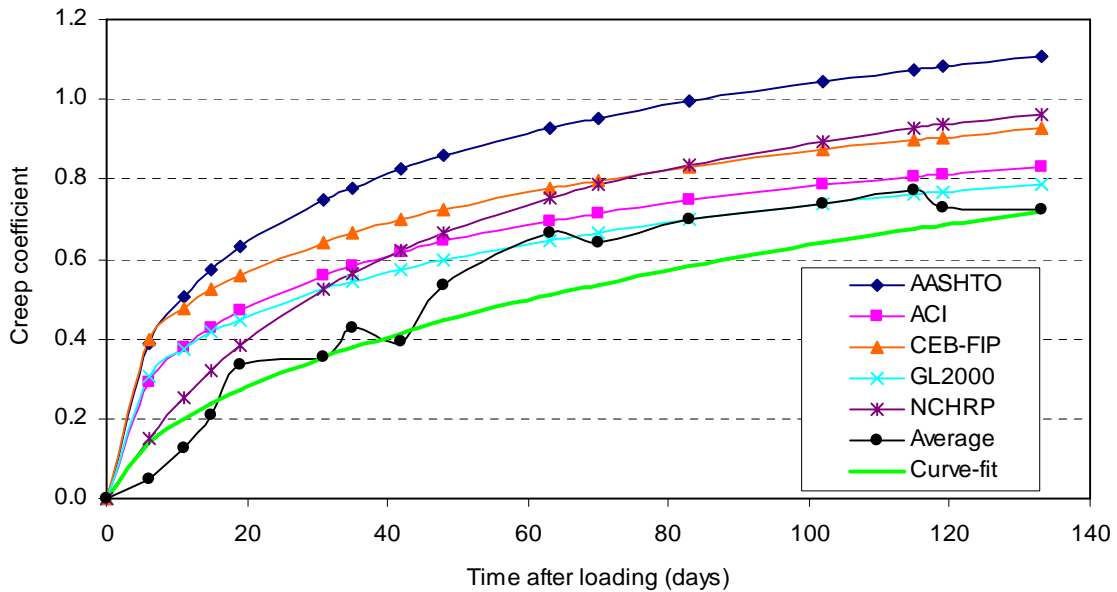


Figure 3.95: Experimental and predicted test specimen creep coefficient for the F5 April concrete at second loading (removal of hinge supporting falsework).

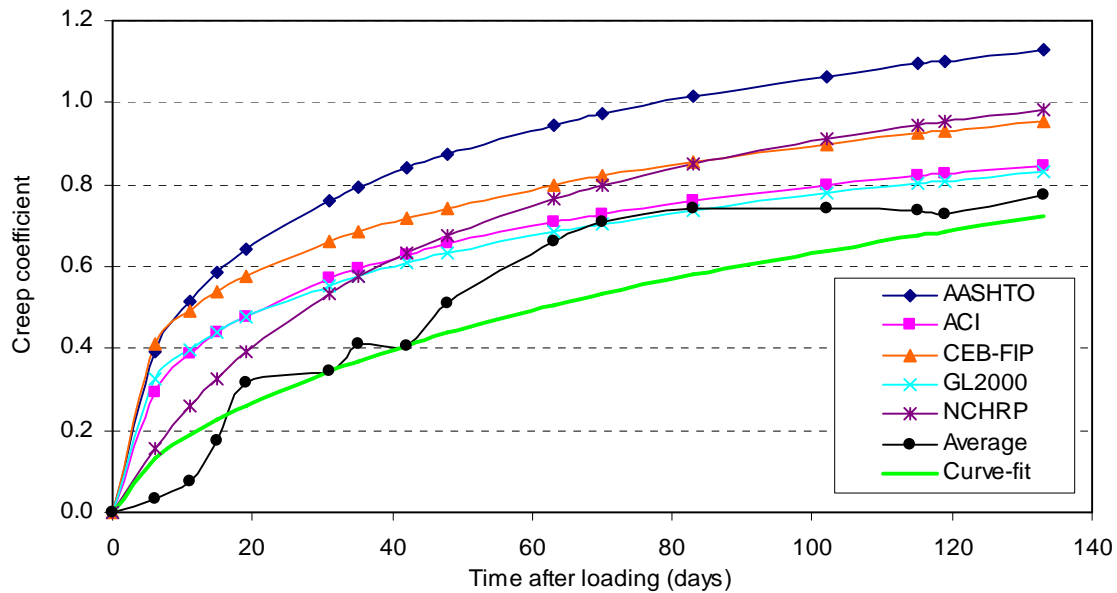


Figure 3.96: Experimental and predicted test specimen creep coefficient for the F5 May concrete at second loading (removal of hinge supporting falsework).

3.8. Specifications Predictions of Creep and Shrinkage: Bridge

In Section 3.7, the methods presented in Section 2.2 were used to predict the creep and shrinkage for the test specimens. The specifications predictions were compared to the experimental values obtained through testing. As was mentioned previously, the creep and shrinkage compared adequately with the specifications predictions for all concretes except for shrinkage in the F4 concrete batches. For this reason, both the measured shrinkage and the shrinkage obtained from the F5 concrete were used to obtain the true creep in F4. In this section, the comparison of experimental shrinkage with the specifications predictions will identify the lack of correlation between of the F4 shrinkage to the predictions.

In this section, the same methods from Section 2.2 to predict the creep and shrinkage for the test specimens are used to predict the creep and shrinkage for the bridge. It was mentioned in Section 2.2, that the creep and shrinkage are

dependent on the V/S ratio of the concrete elements. The creep and shrinkage in the bridge is different from that of the test specimens. Although this is directly accommodated by inputs of V/S in the specifications (or h_0) to accommodate different size elements, no tests of creep and shrinkage were performed for specimens with V/S ratios comparable to that of the bridge. Conducting experiments on specimens with V/S ratios comparable to that of the bridge is unfeasible due to size constraints of testing. For this reason, the experimental creep and shrinkage were proportioned to reflect creep and shrinkage values that are realistic for the bridge. The V/S ratio for the test specimens is 1.5 in. while that of the bridge is 4.5 in., used in this research. Though the V/S ratio of the bridge is three times that of the test specimens, the creep and shrinkage are not three times different from one another. The inputs used for producing creep and shrinkage predictions using the specifications are provided in Table 3.5.

The method of curve fitting [15] applied to the measured material properties from the tests to generate a smooth progression of the creep and shrinkage over time is discussed in Section 3.6. The equations produced by this method were used to produce values of creep and shrinkage beyond the point in time for which the measured creep and shrinkage were included in this Report, at the theoretical end of service life of the bridge, selected as 20,000 days, as will be described in Section 5.4. In general, the predictions of creep and shrinkage produced by the CEB-FIP [10] specification were closest to the values obtained through material testing. Additionally, the curve-fitting [15] method makes use of the CEB-FIP [10] specification equations to produce the curve for the measured data. The measured material test values were adjusted for the appropriate V/S ratio of the bridge by multiplying the measured value by the ratio of values produced by the CEB-FIP [10] specification for points in time at which measurements were made. For shrinkage, Eq. 3.21 accommodates the adjustment in measured shrinkage.

$$\varepsilon_{sh}(t_i, t_0)_{bridge, measured} = \varepsilon_{sh}(t_i, t_0)_{specimen, measured} \left(\frac{\varepsilon_{sh}(t_i, t_0)_{bridge, CEB-FIP}}{\varepsilon_{sh}(t_i, t_0)_{specimen, CEB-FIP}} \right) \quad (3.21)$$

Eq. 3.22 adjusts the measured creep for the bridge.

$$\phi(t_i, t_0)_{bridge, measured} = \phi(t_i, t_0)_{specimen, measured} \left(\frac{\phi(t_i, t_0)_{bridge, CEB-FIP}}{\phi(t_i, t_0)_{specimen, CEB-FIP}} \right) \quad (3.22)$$

An example calculation is performed here using the calculated creep and shrinkage using the experimental data from testing to illustrate the method of producing creep coefficients that are suitable for the bridge.

For shrinkage a procedure that used the CEB-FIP [10] equations was adopted for producing shrinkage values from the material tests that could be expected for the bridge concrete. The April batch concrete will be used to demonstrate the calculation of shrinkage for the bridge from the material test values. Table 3.6 displays the CEB-FIP [10] predicted values of shrinkage for the test specimen and bridge in columns 2 and 3, respectively. The predicted shrinkage for the test specimen (column 2, Table 3.6) is displayed in Figure 3.77 while that of the bridge (column 3, Table 3.6) is displayed in Figure 3.102. The ratio of the predicted shrinkage values is presented in column 4. The values of the best-fit curve to the experimental data from material testing for the April batch concrete in column 17 in Table 3.2 is located in column 5 of Table 3.6. Using Eq. 3.21, the expected shrinkage for the bridge is calculated for the point in time 339 days after the end of curing.

$$\varepsilon_{sh}(t_{339i}, t_0)_{bridge, measured} = -756 \left(\frac{-167}{-334} \right) = -756(0.50) = -378$$

The shrinkage strain value of -378 microstrain is located in column 6 of Table 3.6 and corresponds to the point at 339 days in Figure 3.102.

The shrinkage for the bridge from the other concrete batches was determined using the same method presented here and is included in Section 3.8.1.

Table 3.6: Values associated with the calculation of experimental shrinkage for the bridge.

Time (days)	$\epsilon_{sh}(t_i, t_0)_{specimen, CEB-FIP}$ ($\mu m/m$)	$\epsilon_{sh}(t_i, t_0)_{bridge, CEB-FIP}$ ($\mu m/m$)	$\epsilon_{sh}(t_i, t_0)_{specimen, CEB-FIP} /$ $\epsilon_{sh}(t_i, t_0)_{bridge, CEB-FIP}$	$\epsilon_{sh}(t_i, t_0)_{specimen, measured}$ ($\mu m/m$)	$\epsilon_{sh}(t_i, t_0)_{bridge, measured}$ ($\mu m/m$)
1	2	3	4	5	6
0	0	0	0	0	0
7	-77	-26	0.34	-88	-30
10	-91	-31	0.34	-123	-42
13	-104	-35	0.34	-155	-53
17	-117	-41	0.35	-195	-67
27	-145	-51	0.35	-278	-98
29	-149	-53	0.35	-292	-103
31	-154	-55	0.35	-306	-108
34	-160	-57	0.36	-325	-116
38	-168	-60	0.36	-349	-125
38	-168	-60	0.36	-349	-125
41	-173	-63	0.36	-366	-132
45	-180	-65	0.36	-386	-141
59	-200	-75	0.37	-447	-167
66	-209	-79	0.38	-473	-178
71	-215	-82	0.38	-489	-186
72	-216	-82	0.38	-492	-187
73	-217	-83	0.38	-495	-189
78	-222	-85	0.38	-510	-196
90	-234	-91	0.39	-541	-211
92	-236	-92	0.39	-545	-214
108	-249	-100	0.40	-578	-232
125	-261	-107	0.41	-607	-249
135	-267	-111	0.41	-622	-258
143	-272	-114	0.42	-632	-265
150	-275	-116	0.42	-641	-271
154	-277	-118	0.42	-645	-274
164	-282	-121	0.43	-656	-282
169	-285	-123	0.43	-661	-285
186	-292	-128	0.44	-677	-297
192	-294	-130	0.44	-682	-301
198	-297	-132	0.44	-686	-305
206	-300	-134	0.45	-692	-310
212	-302	-136	0.45	-697	-314
221	-305	-139	0.45	-703	-320
225	-306	-140	0.46	-705	-322
237	-310	-143	0.46	-712	-329
241	-311	-144	0.46	-715	-331
248	-313	-146	0.47	-719	-335
254	-315	-148	0.47	-722	-338
269	-319	-151	0.47	-729	-346
276	-321	-153	0.48	-732	-349
289	-324	-156	0.48	-738	-356
308	-328	-160	0.49	-745	-365
321	-331	-163	0.49	-750	-370
325	-331	-164	0.50	-751	-372
339	-334	-167	0.50	-756	-378

For each concrete batch, a range of shrinkage values for the period beyond that for which shrinkage was measured is presented. This period begins at T363 for F4 and T303 for F5. T363 and T303 represent the ages after which prestressing was applied beyond which no additional data is considered in this Report, as explained in more detail in Section 4.3. This range is bounded by the extrapolated values of shrinkage determined using the best-fit [15] equations on the upper bound (maximum). The lower bound (minimum) is formed by a

constant and is equal to the shrinkage that was obtained from the measured data. The range of possible shrinkage values is depicted in Figure 3.97; this range is also noted in each of the figures in Section 3.8.1.

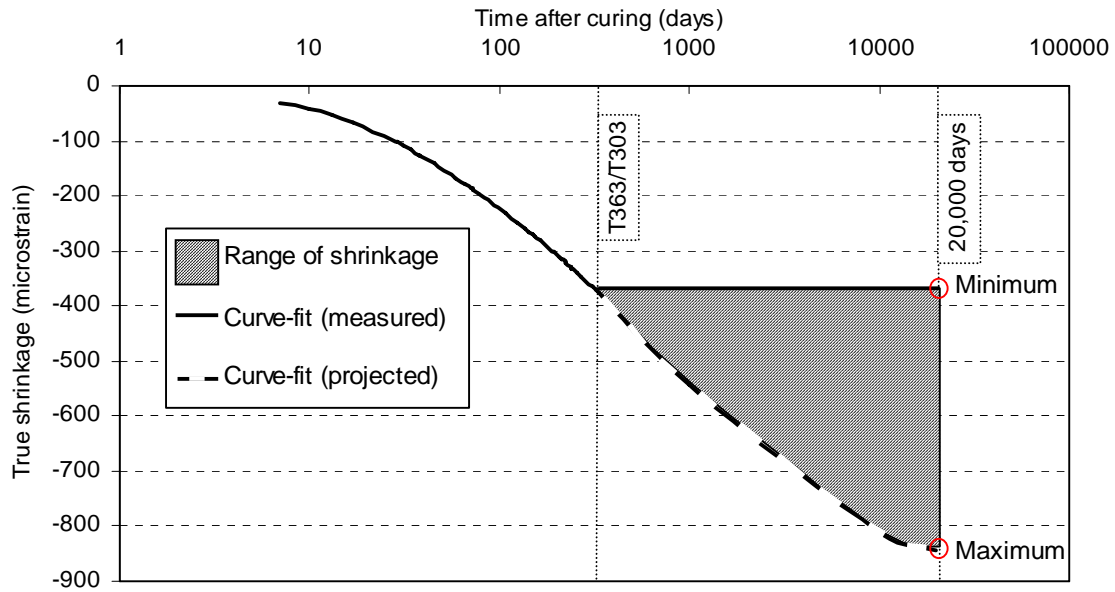


Figure 3.97: Example representative range of shrinkage for the concrete used in the material tests.

Table 3.7 displays the calculated predictions of creep using the CEB-FIP [10] equations in Section 2.2.4 for V/S ratios corresponding to the bridge and test specimens.

Table 3.7: Values associated with the calculation of experimental creep for the bridge.

Time (days)	$\phi(t_i, t_0)_{\text{bridge, CEB-FIP}}$	$\phi(t_i, t_0)_{\text{specimen, CEB-FIP}}$	$\frac{\phi(t_i, t_0)_{\text{bridge, CEB-FIP}}}{\phi(t_i, t_0)_{\text{specimen, CEB-FIP}}}$	$\phi(t_i, t_0)_{\text{specimen, measured}}$	$\phi(t_i, t_0)_{\text{bridge, measured}}$
1	2	3	4	5	6
0	0.00	0.00	0.00	0.00	0.00
3	0.43	0.33	0.75	0.21	0.16
7	0.56	0.42	0.75	0.31	0.23
21	0.77	0.58	0.75	0.51	0.38
28	0.83	0.63	0.76	0.58	0.43
33	0.87	0.66	0.76	0.62	0.47
34	0.88	0.66	0.76	0.63	0.47
35	0.88	0.67	0.76	0.63	0.48
40	0.92	0.70	0.76	0.67	0.51
52	0.98	0.75	0.76	0.75	0.57
54	0.99	0.76	0.76	0.76	0.58
70	1.06	0.81	0.76	0.84	0.64
87	1.12	0.86	0.77	0.91	0.70
97	1.15	0.88	0.77	0.95	0.73
105	1.17	0.90	0.77	0.97	0.75
112	1.19	0.92	0.77	0.99	0.77
116	1.20	0.93	0.77	1.01	0.78
126	1.22	0.94	0.77	1.04	0.80
131	1.23	0.95	0.77	1.05	0.81
148	1.27	0.98	0.78	1.09	0.85
154	1.28	0.99	0.78	1.11	0.86
160	1.29	1.00	0.78	1.12	0.87
168	1.30	1.01	0.78	1.14	0.88
174	1.31	1.02	0.78	1.15	0.89
183	1.32	1.03	0.78	1.16	0.91
187	1.33	1.04	0.78	1.17	0.92
199	1.35	1.05	0.78	1.19	0.93
203	1.35	1.06	0.78	1.20	0.94
210	1.36	1.07	0.78	1.21	0.95
216	1.37	1.07	0.78	1.22	0.96
231	1.38	1.09	0.79	1.24	0.98
238	1.39	1.10	0.79	1.25	0.99
251	1.40	1.11	0.79	1.27	1.00
270	1.42	1.13	0.79	1.30	1.02
283	1.43	1.14	0.79	1.31	1.04
287	1.44	1.14	0.79	1.32	1.04
301	1.45	1.15	0.79	1.33	1.06

For this example, the time of 301 days will be used. In columns 2 and 3 of Table 3.7, the values of 1.45 and 1.15 were calculated from the CEB-FIP [10] specification equations presented in Section 2.2.4. A graphical representation of the progression of predicted creep values for the test specimens (column 2, Table 3.7) is located in Figure 3.85 while the predicted creep for the bridge (column 3, Table 3.7) is represented in Figure 3.107. The ratio of these values 0.79 is listed in column 4 (Table 3.7). The curve-fit of the experimental creep coefficient is provided in column 5 (Table 3.7) and is the best-fit of the data presented in column 33 of Table 3.3. Eq. 3.22 is used to produce the value of the measured creep coefficient that can be expected, determined using the method described previously in this section. For the point in time 301 days after loading

(prestressing) the creep coefficient for the bridge is calculated from Eq. 3.22 as follows.

$$\phi(t_{301}, t_0)_{bridge, measured} = 1.33 \left(\frac{1.15}{1.45} \right) = 1.33(0.79) = 1.06$$

The expected bridge creep coefficient of 1.06 calculated in the above equation occurs at the point in time corresponding to 301 days after prestressing and is located in Figure 3.107.

The creep coefficients for the other concrete batches are calculated similarly. Since the specifications predictions of creep can be made for any point in time and the curve-fit to the experimental data can project values beyond those that were measured, this method can be used to predict ultimate values of creep from the material tests. These ultimate values are provided in the figures in Sections 3.8.2, 3.8.3, and 3.8.4.

Like that of shrinkage, the ultimate values of creep determined from the best-fit [15] equations represent the maximum shrinkage that is expected to occur. The lower bound (minimum) was taken as that which was measured at T363 or T303 for F4 and F5, respectively. Between the minimum and maximum bounds of creep for each concrete the actual creep is expected to occur. The range of possible creep values is represented in each of the creep figures in the following sections (Sections 3.8.2, 3.8.3, and 3.8.4) as well as represented in Figure 3.98.

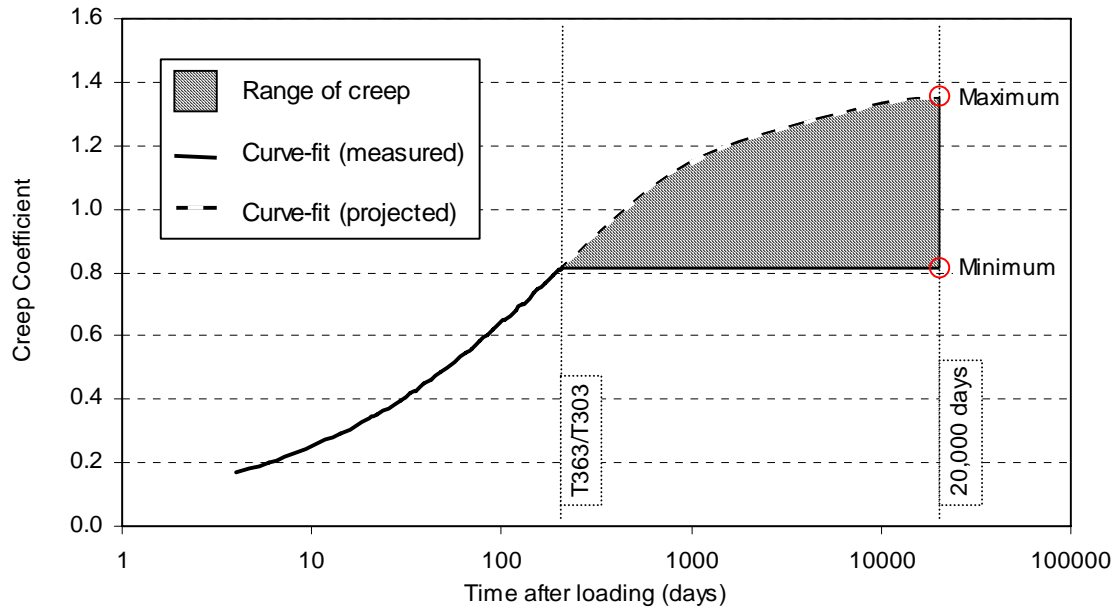


Figure 3.98: Example representative range of creep for the concrete used in the material tests.

3.8.1. Shrinkage Strain

This section presents the shrinkage strains for the five concrete batches from F4 and F5. As has been mentioned previously, the shrinkage for F4 was taken as the experimental shrinkage as well as that from F5, since the experimental F4 shrinkage was not reliable.

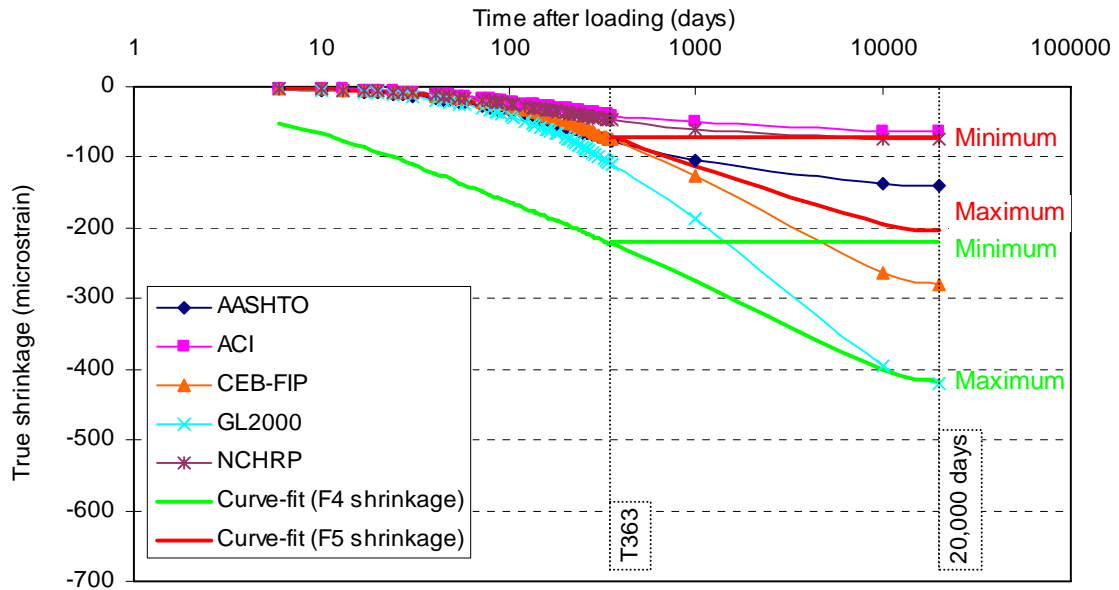


Figure 3.99: Experimental and predicted bridge shrinkage strain for the F4 October concrete.

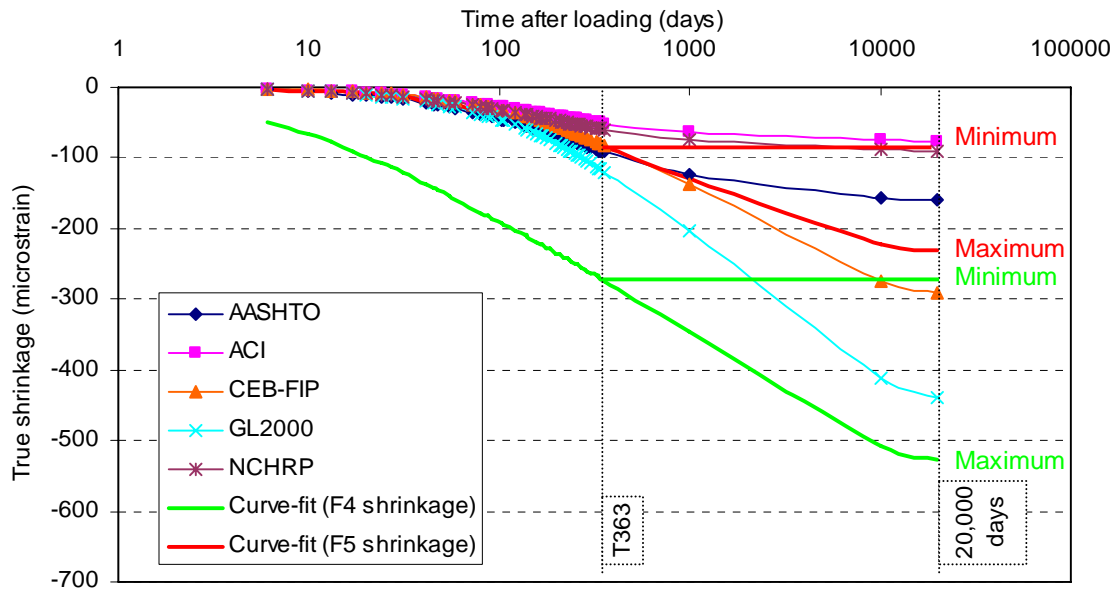


Figure 3.100: Experimental and predicted bridge shrinkage strain for the F4 November concrete.

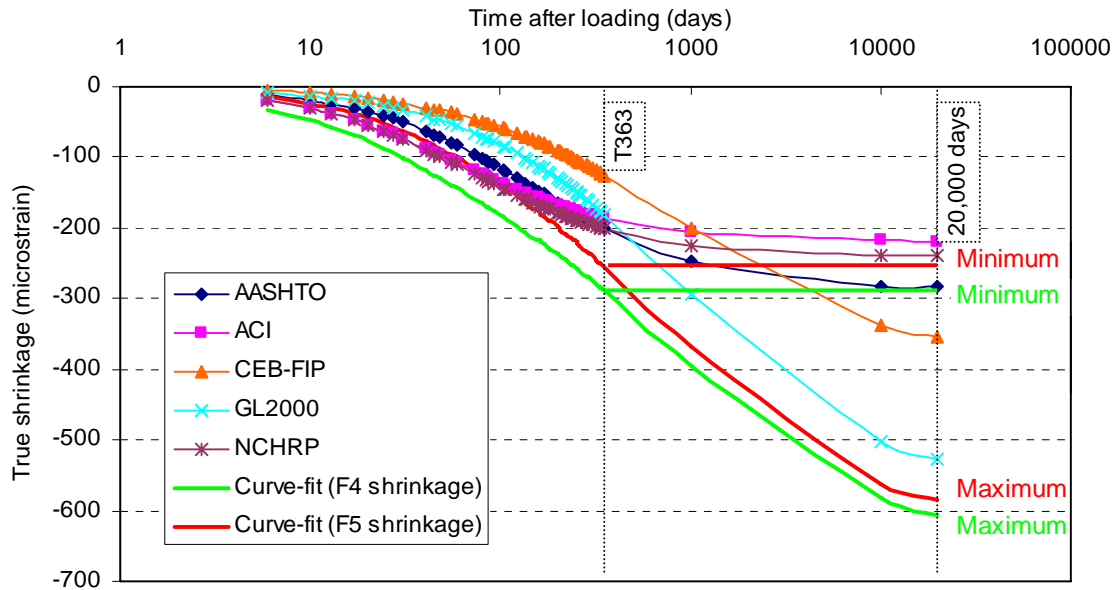


Figure 3.101: Experimental and predicted bridge shrinkage strain for the F4 March concrete.

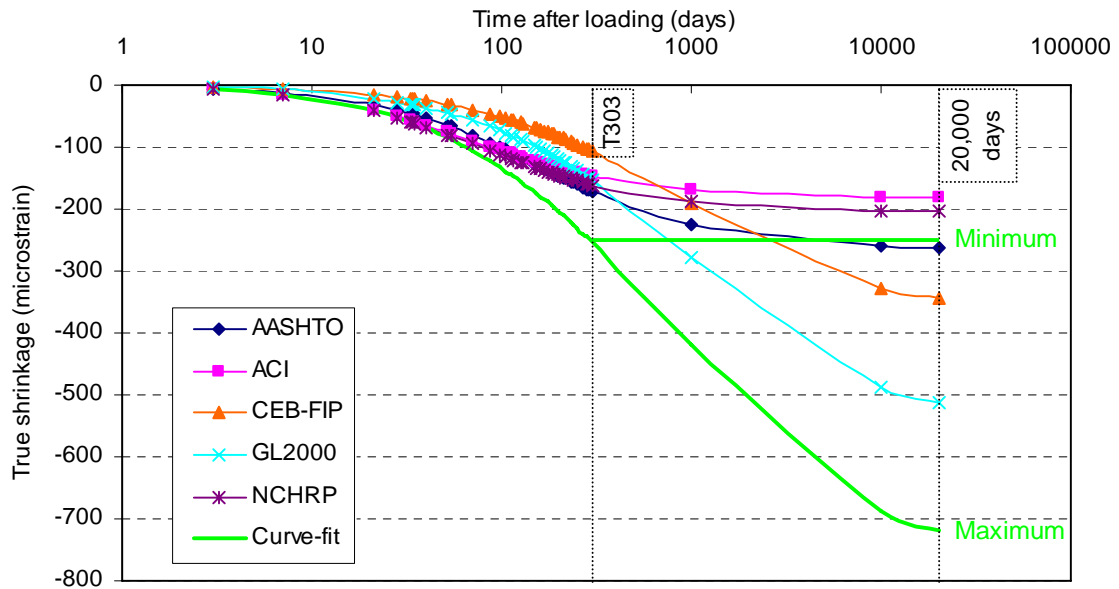


Figure 3.102: Experimental and predicted bridge shrinkage strain for the F5 April concrete.

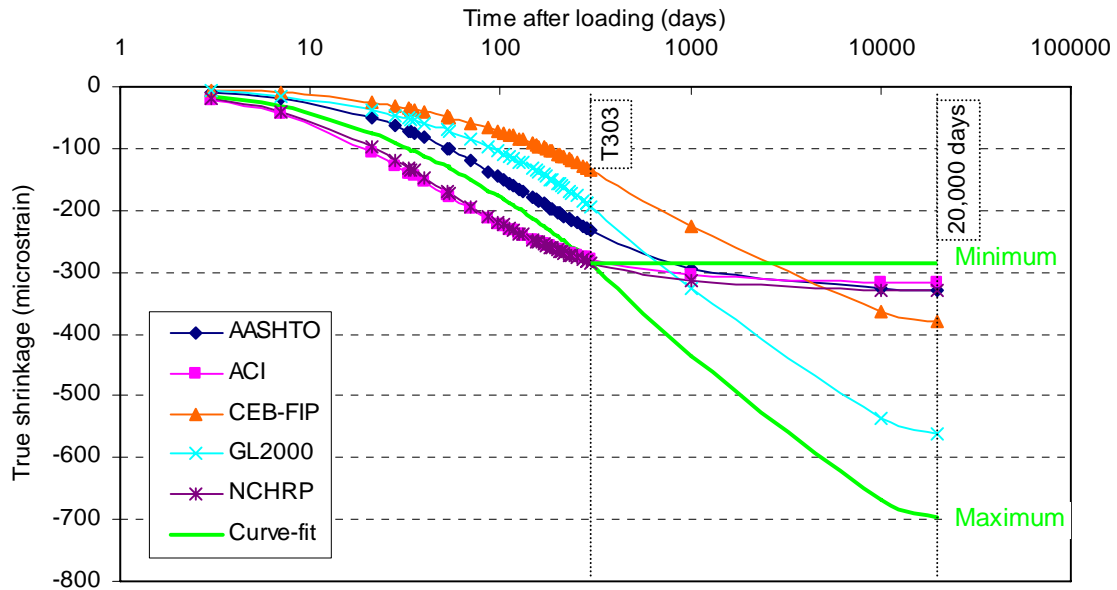


Figure 3.103: Experimental and predicted bridge shrinkage strain for the F5 May concrete.

3.8.2. Creep at First Loading

The figures in this section display the creep coefficients that were predicted using the specifications in Section 2.2.4 and from the experimental values from testing. The first loading instant corresponds to the application of prestressing in both frames.

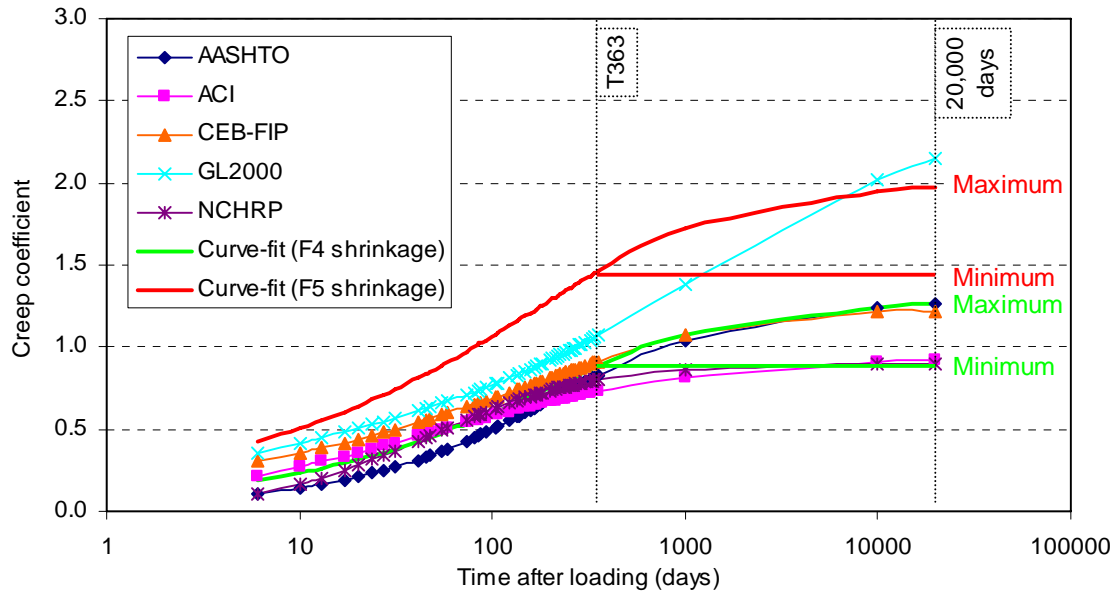


Figure 3.104: Experimental and predicted bridge creep coefficient for the F4 October concrete at first loading (prestressing).

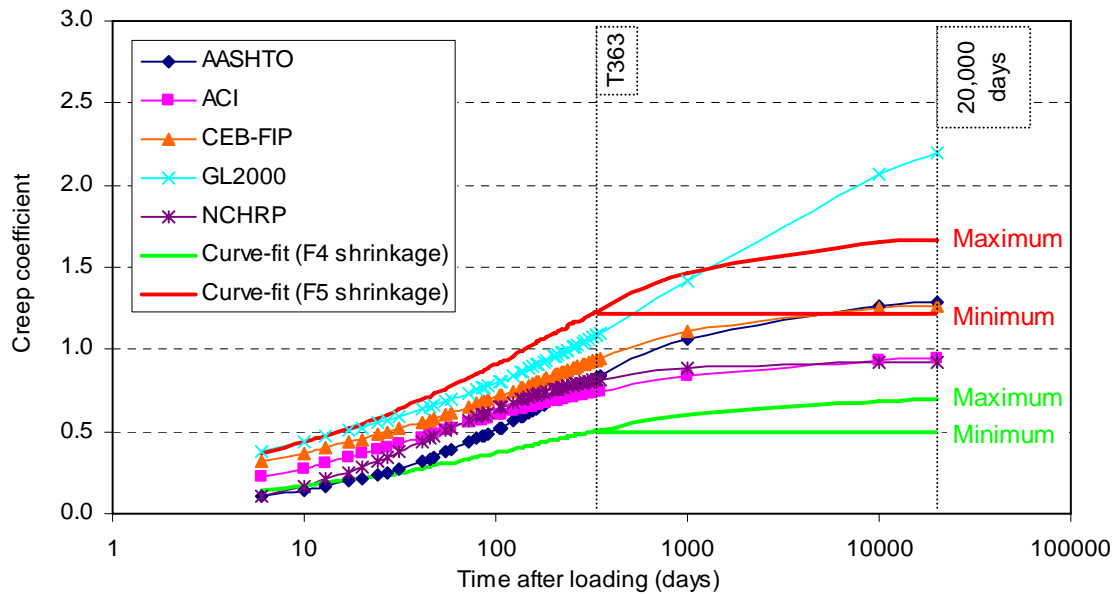


Figure 3.105: Experimental and predicted bridge creep coefficient for the F4 November concrete at first loading (prestressing).

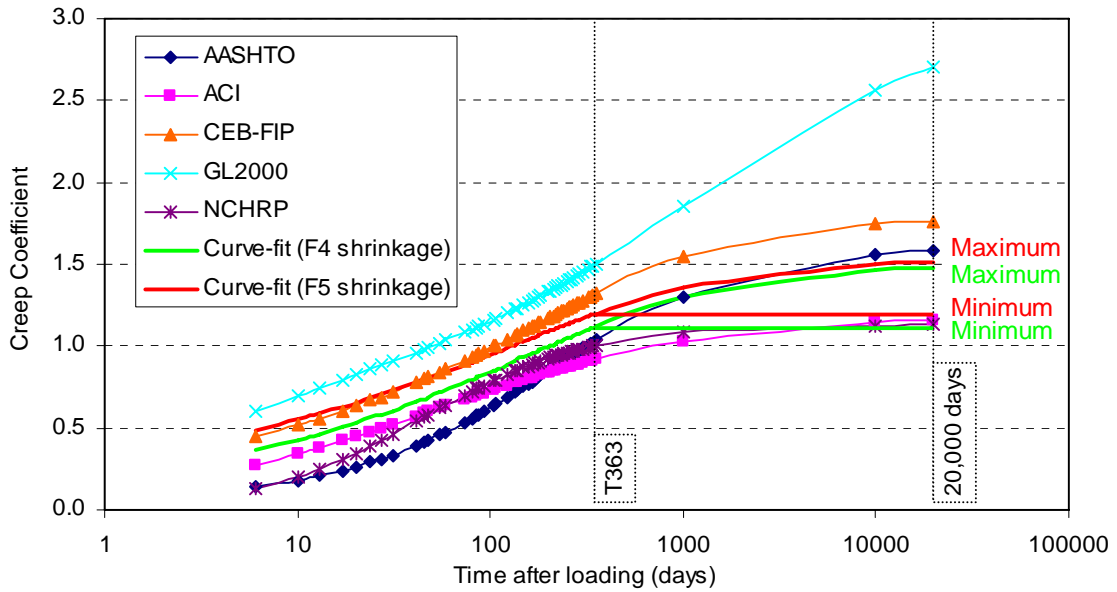


Figure 3.106: Experimental and predicted bridge creep coefficient for the F4 March concrete at first loading (prestressing).

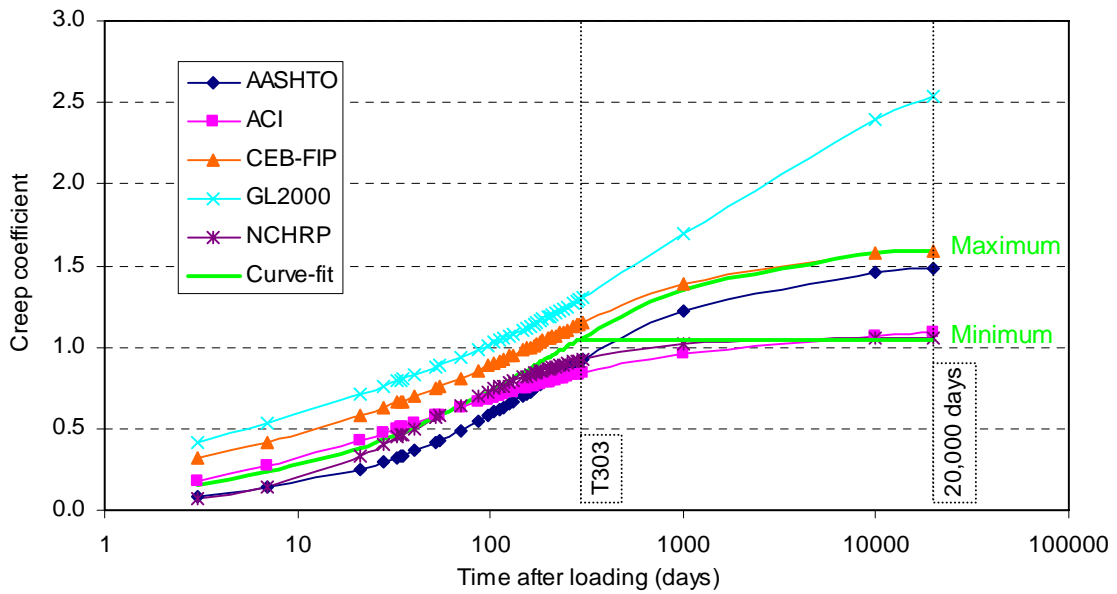


Figure 3.107: Experimental and predicted bridge creep coefficient for the F5 April concrete at first loading (prestressing).

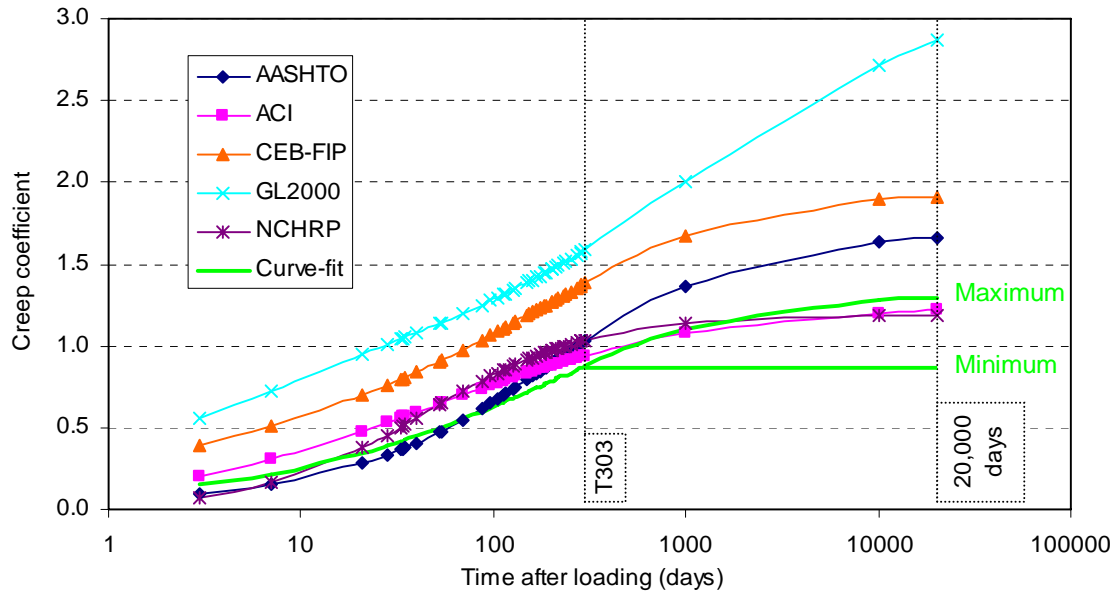


Figure 3.108: Experimental and predicted bridge creep coefficient for the F5 May concrete at first loading (prestressing).

3.8.3. Creep at Second Loading

The additional load induced from the removal of falsework produces the creep at second loading. Since the falsework restricts true deformation, the removal of the falsework activates the remaining structural self-weight applying additional load to the structure.

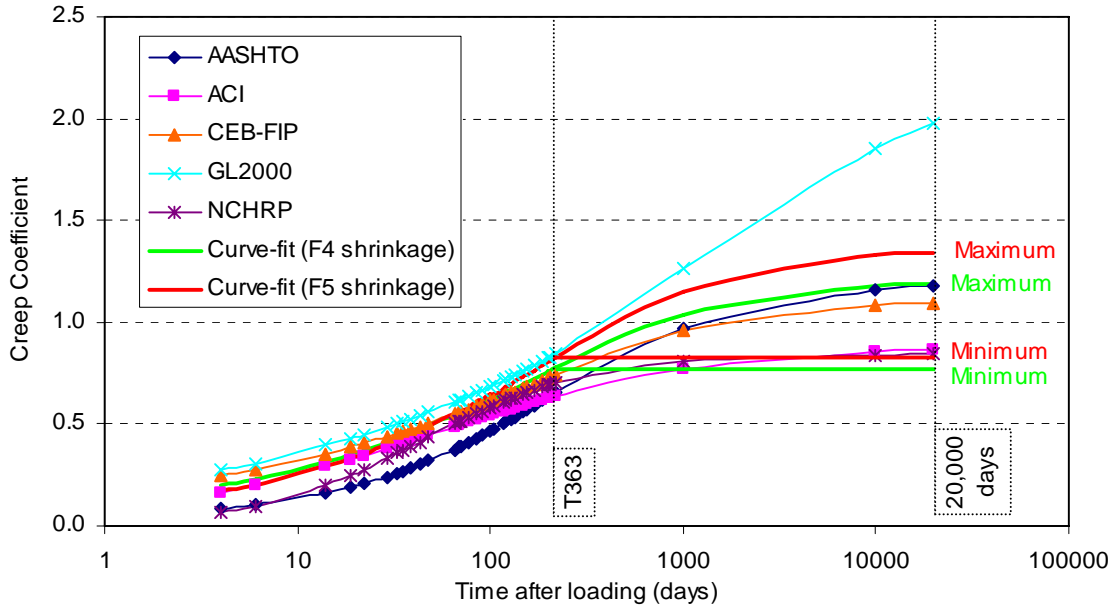


Figure 3.109: Experimental and predicted bridge creep coefficient for the F4 October concrete at second loading (removal of falsework).

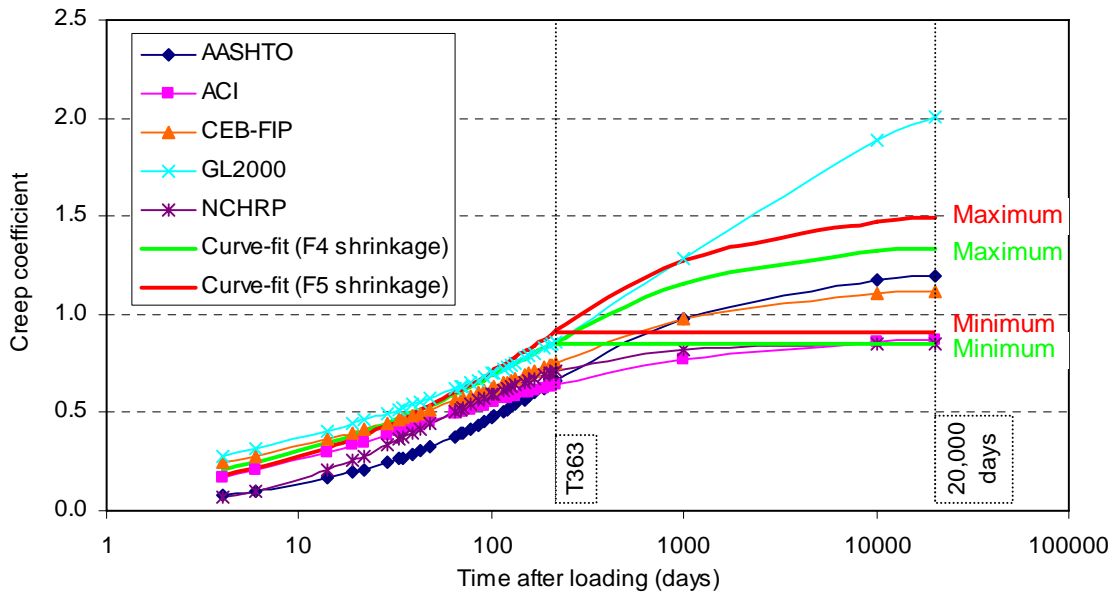


Figure 3.110: Experimental and predicted bridge creep coefficient for the F4 November concrete at second loading (removal of falsework).

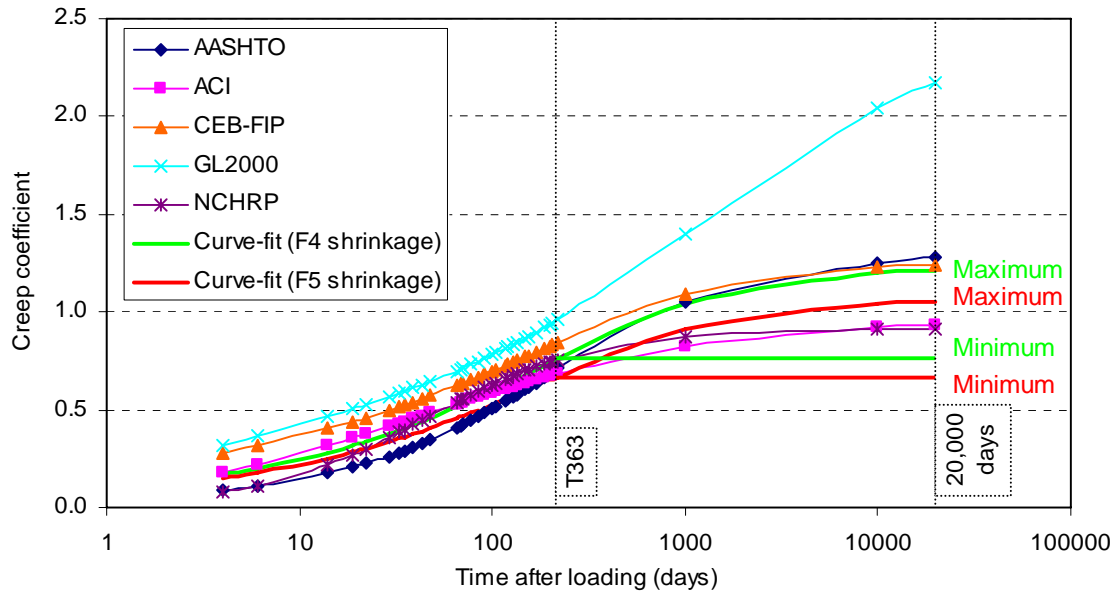


Figure 3.111: Experimental and predicted bridge creep coefficient for the F4 March concrete at second loading (removal of falsework).

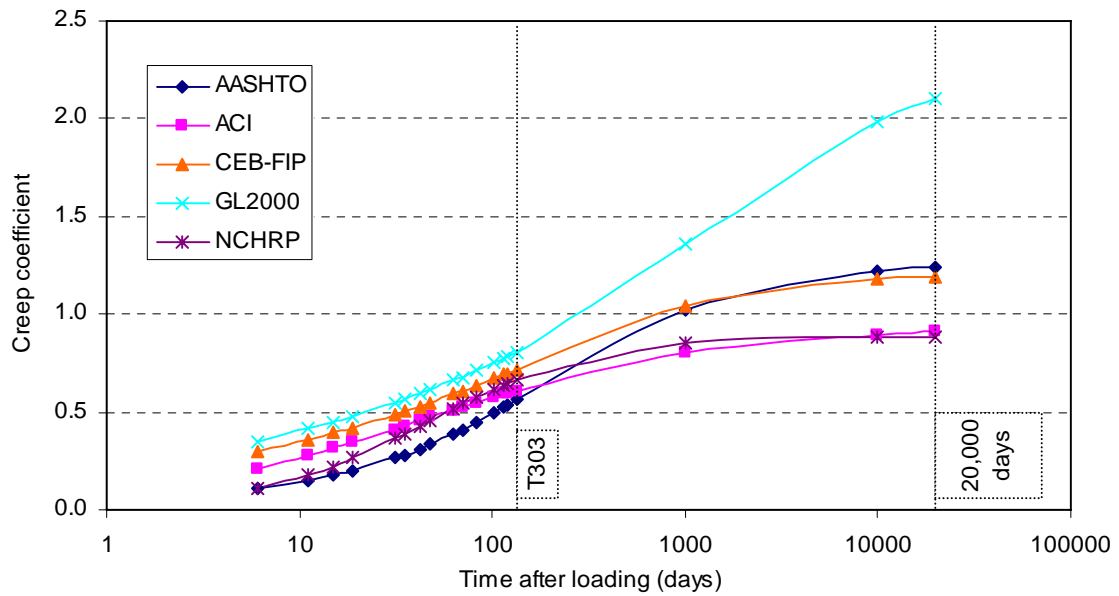


Figure 3.112: Experimental and predicted bridge creep coefficient for the F5 April concrete at second loading (removal of falsework).

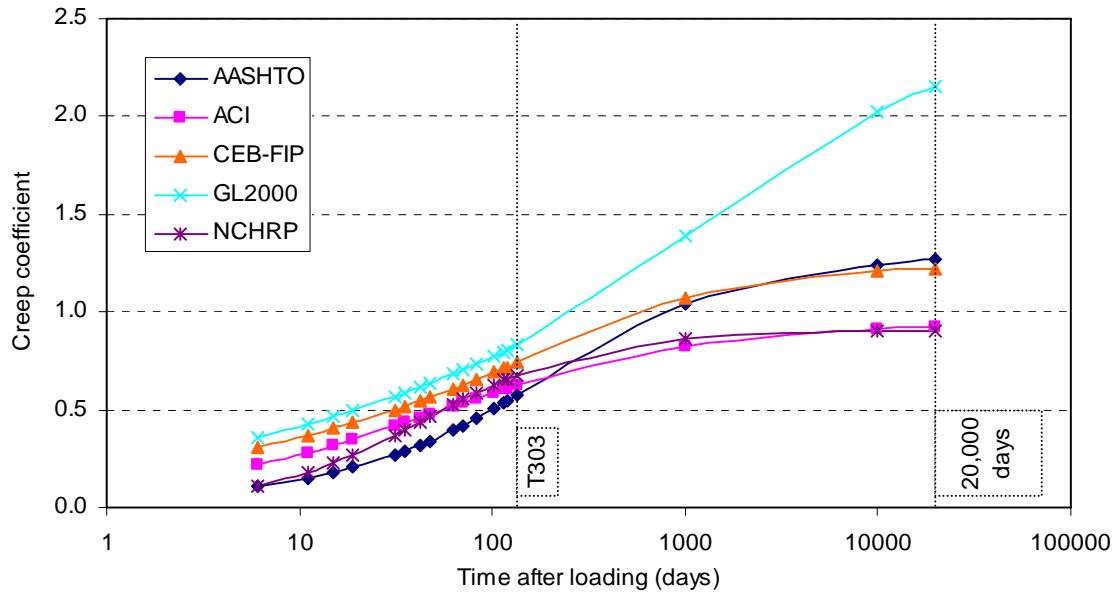


Figure 3.113: Experimental and predicted bridge creep coefficient for the F5 May concrete at second loading (removal of falsework).

3.8.4. Creep at Third Loading

The additional load from adjacent frames at the hinges causes the creep at third loading. The third loading only exists in F5, since the removal of falsework in F4 encompassed the adjacent frame loads.

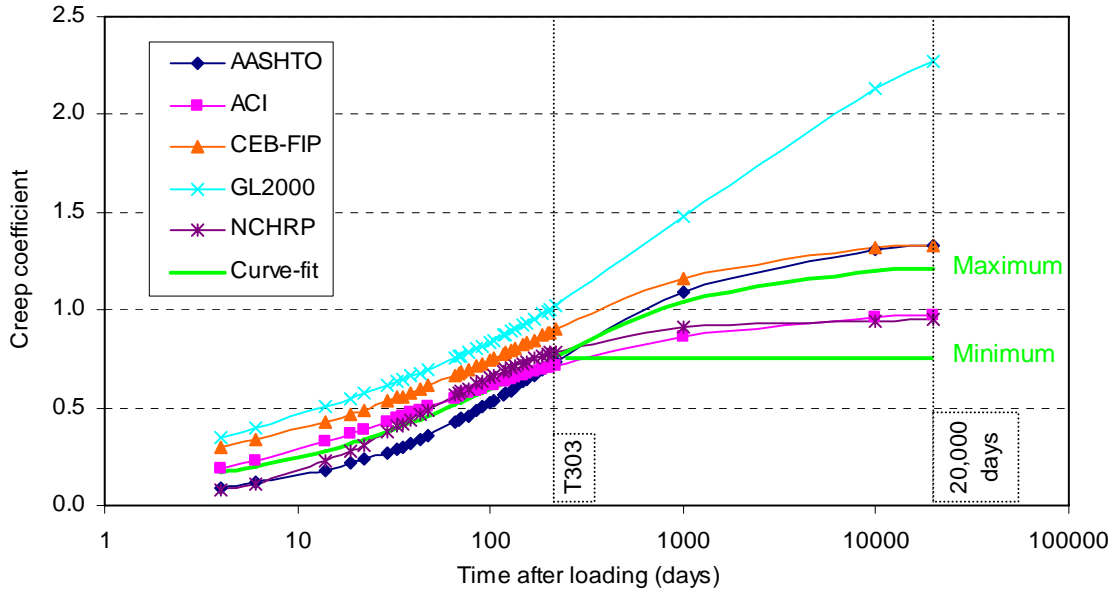


Figure 3.114: Experimental and predicted bridge creep coefficient for the F5 April concrete at third loading (removal of hinge supporting falsework).

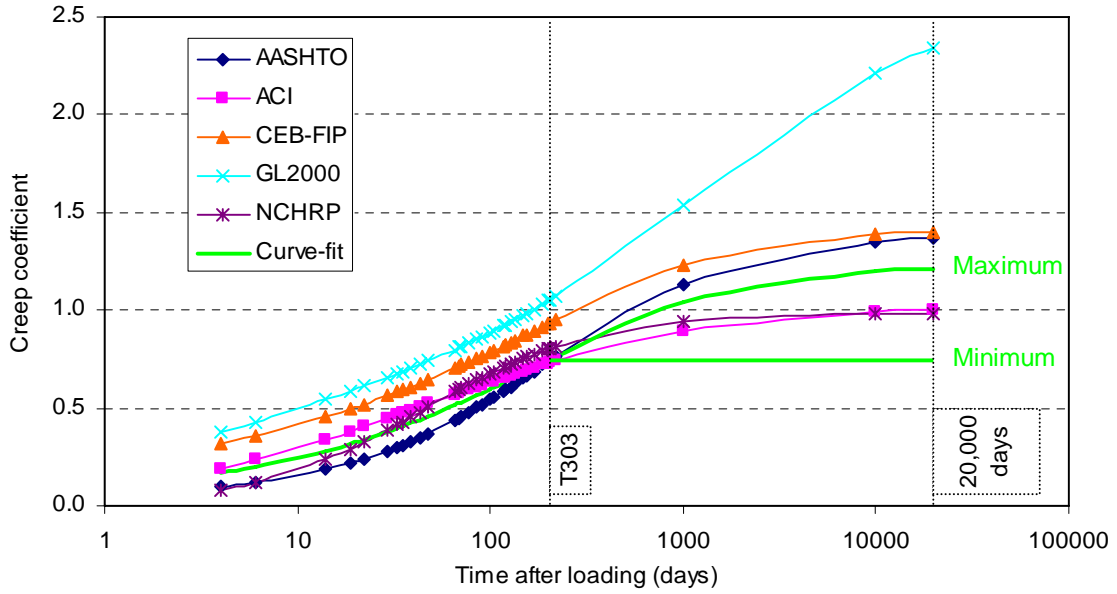


Figure 3.115: Experimental and predicted bridge creep coefficient for the F5 May concrete at third loading (removal of hinge supporting falsework).

3.9. Commentary on Creep and Shrinkage

Examination of the creep and shrinkage predictions compared to the experimentally determined values shows that the fit of the data does not consistently match predictions in all cases. In general, the predictions for shrinkage for the concrete in F4 have the poorest correlation with the experimental data (Figure 3.99, Figure 3.100, and Figure 3.101). The use of the F5 concrete shrinkage to produce expected values of shrinkage for F4 is acceptable and produced values that correlated well with the specifications predictions.

For creep in F4, two methods of producing the creep coefficients were used. The experimental shrinkage from F4 and the expected shrinkage from the F5 concrete were removed from the creep strain to produce creep coefficients for the F4 concrete batches. Though the experimental shrinkage from F4 used with the creep strain produced creep coefficients that correlated better with the specifications predictions than the expected shrinkage from the F5 concrete, an important consideration must be made. The creep and shrinkage both influence the prestress loss. Though the experimental shrinkage from F4 was much larger than expected, the creep was well correlated with the predictions. For the other case, the shrinkage from F5 that could be expected for F4 was well correlated with the specifications predictions of shrinkage; however, the creep coefficient was larger than predictions. All predictions of creep for F5 correlated well with the specifications predictions. The predictions of shrinkage for F5 correlated acceptably with the specifications for the specimens; however, when used to produce shrinkage for the bridge, largely exceeded predictions at 20,000 days after casting (55 years). Though some predictions of creep and shrinkage were exceeded by the upper bound values, the range of creep and shrinkage values reasonably encompassed the specifications predictions. The upper bound values of creep and shrinkage at 20,000 days were extrapolated based on the first years deformation. Additional measurements will alter the best-fit curves and produce a new range of values. It is not expected that the actual creep and shrinkage, as it

progresses, will fall outside of the range of values presented here. The range of creep and shrinkage is used in subsequent chapters to present the range of strains, prestress loss, and concrete stresses that are possible with range of creep and shrinkage that are available at the present time.

From the above considerations, the shrinkage from F5 that was used for F4 (since the F4 shrinkage was not reliable) produced creep and shrinkage values that are more reasonable than the other methods. These values will be used in the analyses presented in later chapters.

A discussion regarding possible improvements to the material tests is provided in Appendix H.

4. Analysis of I5/805 Truck Connector

4.1. Introduction

This chapter outlines the analysis of Frame 4 (F4) and Frame 5 (F5) in the I5/805 Bridge. Analysis of F4 and F5 was performed using the advanced computer program Cracked Plane Frame (CPF) [16] using inputs representative of the actual bridge frames selected for this research. CPF [16] is an advanced structural analysis computer program that performs calculations on time-dependent stresses and deformations on concrete plane frames, which can be either prestressed or non-prestressed. The program calculates the displacements of the structure during service. The effect of concrete creep and shrinkage and relaxation of prestressed steel are accommodated. The program considers cracking and the resulting deflections, reactions, and internal forces in statically indeterminate structures. Members can be composed of multiple concrete parts, each with different properties representing different ages at loading or introduction within the structure. An example input file for CPF [16] is provided in Appendix G.

4.2. Description of I5/805 Truck Connector

The I5/805 Truck Connector is a six-frame continuous highway bridge recently constructed in San Diego, California. The intended purpose of the bridge is to provide several lanes for trucks traveling from Southbound Interstate 5 to Southbound Interstate 805. The bridge is a post-tensioned three-cell box girder, with multiple layers of prestressing tendons. This bridge was selected for monitoring because it is representative of the typical highway bridge constructed in California and its proximity to the UCSD campus.

The I5/805 Bridge is constructed in a valley over existing freeways. The span lengths and column heights vary considerably between frames. The length of the bridge dictated its division into six frames. Intermediate hinges that join adjacent frames separate the frames. For this research, the two selected frames, F4 and

F5, are shown in Figure 4.1, which also shows the position of the bridge with respect to existing highways.



Figure 4.1: Layout of I5/805 Bridge and surrounding highways.

4.2.1. Frame 4

F4 is of particular interest for the reason that Span 13, at 80.62 m, exceeds AASHTO [2] specifications limits for predicting the prestress loss. Though not depicted in Figure 4.2 – as the capability of CPF does not extend to out-of-plane (3-D) analysis – F4 is curved in both the horizontal and vertical directions and has a 2% transverse slope downward towards the centroid of horizontal curvature. The large concrete volume of F4 dictated pouring the concrete of the frame in three stages. The contractor opted to pour the soffit and girders in two stages and the deck in a third stage. This choice resulted in a construction joint near the inflection point (16.6 m from the centerline of bent 14) in the instrumented span of F4 between the monitored sections. The concrete comprising the soffit and webs was poured on October 5 and November 2, 2004. The deck for F4 was poured on March 3, 2005 (t_0). Prestressing began on March 18, 2005, but problems with the prestressing equipment postponed completion of prestressing the tendons until five days later on March 23, 2005. Grouting of the ducts occurred on March 25, 2005. Falsework was removed on July 22, 2005 (t_1).

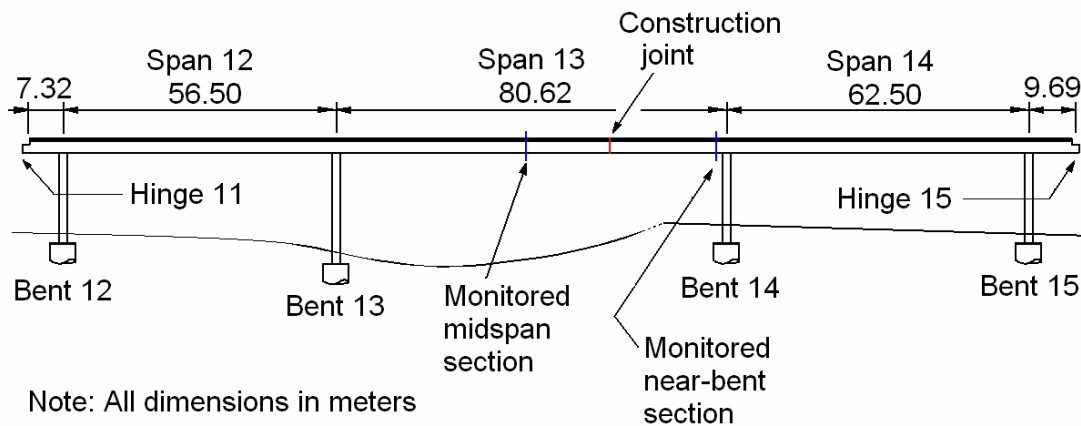


Figure 4.2: Layout of F4.

4.2.2. Frame 5

F5 falls within the dimensional limits for the prestress to be calculated by the specifications. The instrumented span of F5 (Span 16) is 52.82 m in length as

shown in Figure 4.3. Unlike F4, F5 is not curved horizontally. The superstructure of F5 was constructed in two stages. The soffit and webs were cast on April 5, 2005 while the deck was cast on May 3 the same year. Prestressing was completed in one day on May 20, 2005 (t_0) with grouting occurring three days later. The falsework was removed on July 29, 2005 (t_1), while the hinges were loaded on October 26, 2005 (t_2).

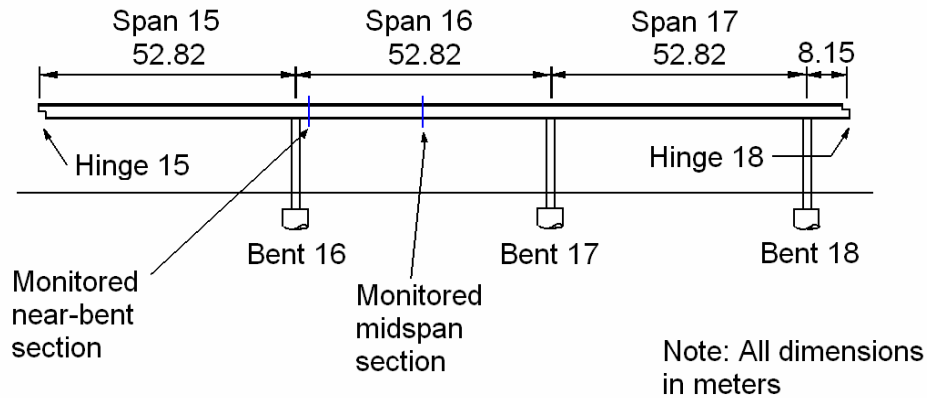


Figure 4.3: Layout of F5.

F4 and F5 were analyzed using CPF incorporating the measured material properties, which are believed to most closely resemble the material properties of the concrete in the bridge. The dates, or more appropriately, the ages of the concrete within the bridge, at significant construction events, are very important. The dates and ages of such events are indicated in Table 4.1 and Table 4.2 for F4 and F5, respectively. The material properties used in the analyses were taken from the figures in Section 3.8 corresponding to the ages of the concrete at significant events.

Table 4.1: Dates and ages of significant construction events of F4.

Concrete Casting Date	Concrete Reference Name	Concrete age at event, in days:		
		Stressing (March 23, 2005)	Grouting (March 25, 2005)	Falsework Removal (July 22, 2005)
October 5, 2004	October	169	171	290
November 2, 2004	November	141	143	262
March 3, 2005	March	20	22	141

Table 4.2: Dates and ages of significant construction events of F5.

Concrete Casting Date	Concrete Reference Name	Concrete age at event, in days:			
		Stressing (May 20, 2005)	Grouting (May 23, 2005)	Falsework Removal (July 29, 2005)	Hinge Loading (October 26, 2005)
April 5, 2005	April	45	48	115	202
May 3, 2005	May	17	20	87	174

4.3. Capabilities of CPF

As addressed in Chapter 1, the main problems with existing methods of determining the prestress loss are that 1.) the actual material properties are inaccurately used or represented and 2.) the methods are not accurate.

The experimentally determined creep coefficient, shrinkage, and prestressing steel relaxation are used as input data to the program. CPF is capable of performing the analysis for differing material properties that may exist for various components of the bridge, such as in the soffit and webs and the deck, respectively.

The time-dependent analysis of the frames was discretized into intervals. The bounds of each interval correspond to a significant construction or loading event of the frame under consideration. The corresponding creep coefficient, shrinkage, and relaxation for each interval are listed in Table 4.3 and Table 4.4 for F4 and F5, respectively. The measured creep and shrinkage for the bridge were calculated using the experimental creep and shrinkage, adjusted for the appropriate V/S of the bridge. Additionally, the creep and shrinkage for the bridge were calculated using the ACI [3] and CEB-FIP [10] specifications. These specifications were selected as they represent two commonly used methods used in design. No prestressed steel relaxation tests were conducted; the prestressed steel relaxation $\Delta\bar{\sigma}_{pr}$ was calculated using Eq. 2.2 and is included in Table 4.3 and Table 4.4. The aging coefficient χ , calculated from Ghali et al [18], is also given in Table 4.3 and Table 4.4 since it slightly varies with time.

Though designated as an event in Table 4.3 and Table 4.4, the T363 and T303 entries, for F4 and F5, respectively, do not indicate instances at which load was applied, like the other events in these tables. There existed a timeframe for this research, from April 2005 to May 2006. No data beyond March 20, 2006 was included in the analysis. T363 and T303 designate the number of days after the concrete was prestressed, in the respective frames, on March 20, 2006. The material tests and bridge monitoring program are intended to continue beyond

this date; however, for practicality, this time was selected and represents a point at which all construction had been completed and the frames were free to deform under their own weight. In F4, T363 (t_2) occurred 241 days after the last instant in which self-load was applied to the structure. In F5, T303 (t_3) represents a point in time 147 days after the last application of structural load. Inspection of the monitored strains presented in Section 5.3 will reveal that the monitored strain had reached a reasonably asymptotic value within an average of about 3% of the strain at the last instant load was applied. The theoretical end of service life was selected at 20,000 days (55 years). This is represented as t_3 for F4 and t_4 for F5.

The material properties – creep and shrinkage – obtained through material testing of the specimens were used to produce the creep and shrinkage that could be expected from the bridge, as discussed in Section 3.8. The measured material properties from the tests were adjusted for the appropriate V/S of the bridge. As was mentioned in Section 3.5, the shrinkage data from F4 were not reliable. The measured material test values of the shrinkage in F4 (Table 4.3) were determined based on the amount of shrinkage that had occurred in F5.

To make predictions of the strains, prestress loss, and concrete stress at the theoretical end of service life of the bridge (20,000 days after loading), it was necessary to extrapolate values of creep and shrinkage for this point in time. This procedure was mentioned in Section 3.8. In Table 4.3 and Table 4.4, the creep and shrinkage occurring between prestressing and T363 or T303 for F4 and F5, respectively, was taken directly from the line that represents the measured creep or shrinkage for each concrete batch. For points beyond T363 or T303, a projected (extrapolated) value was used as a maximum (calculated from the best-fit equations). The minimum creep and shrinkage were taken as the values that occurred at T363 or T303. The range of creep and shrinkage represent the extremes of possible material behavior that can be expected over a period of 20,000 days. This is illustrated in Figure 4.4 for shrinkage and Figure 4.5 for creep.

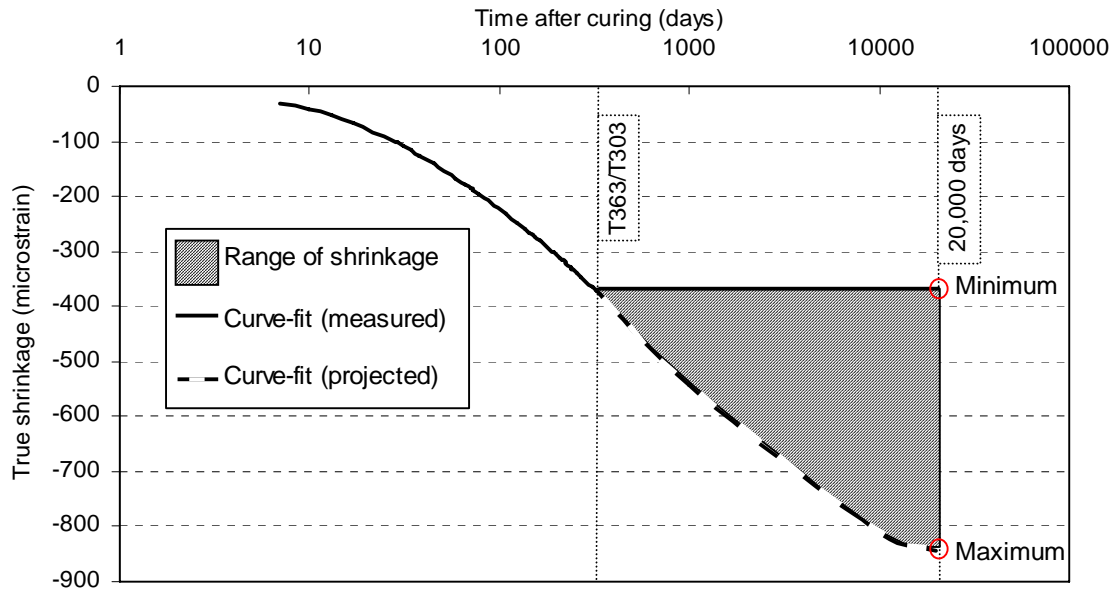


Figure 4.4: Example representative range of shrinkage for the concrete used in the material tests.

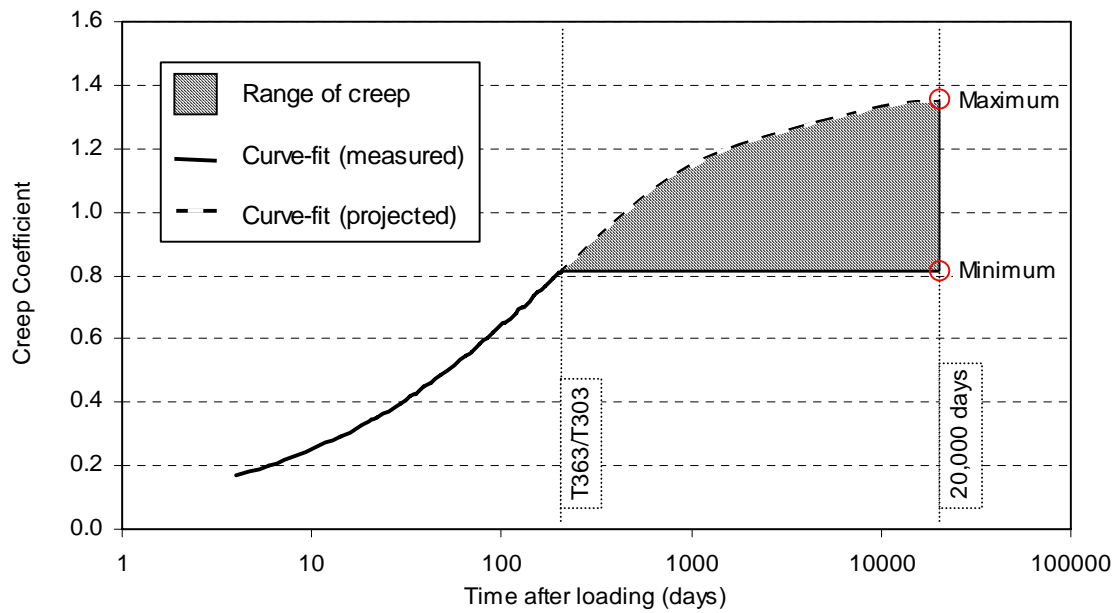


Figure 4.5: Example representative range of creep for the concrete used in the material tests.

Table 4.3: Material properties used in the analysis of F4 at significant construction events.

Concrete		October				November				March				$\Delta\bar{\sigma}_{pr}$ (MPa)
Material Properties	Date of event	$\phi(t_i, t_0)$	$\phi(t_i, t_1)$	$\varepsilon_{sh}(t_i, t_0)$ ($\mu\text{m}/\text{m}$)	$\chi(t_i, t_0)$	$\phi(t_i, t_0)$	$\phi(t_i, t_1)$	$\varepsilon_{sh}(t_i, t_0)$ ($\mu\text{m}/\text{m}$)	$\chi(t_i, t_0)$	$\phi(t_i, t_0)$	$\phi(t_i, t_1)$	$\varepsilon_{sh}(t_i, t_0)$ ($\mu\text{m}/\text{m}$)	$\chi(t_i, t_0)$	
Stressing $t_0 = 0$ days	March 23, 2005	ACI	0	-	0	-	0	-	0	-	0	-	0	0
		CEB-FIP	0	-	0	-	0	-	0	-	0	-	0	-
		Measured	0	-	0	-	0	-	0	-	0	-	0	-
Falsework removal $t_1 = 121$ days	July 22, 2005	ACI	0.61	0	-23	0.94	0.62	0	-31	0.93	0.76	0	-146	0.89
		CEB-FIP	0.72	0	-33	0.94	0.75	0	-37	0.93	1.04	0	-66	0.89
		Measured	1.13	0	-36	0.94	0.96	0	-43	0.93	0.99	0	-155	0.89
T363 $t_2 = 363$ days	March 20, 2006	ACI	0.73	0.64	-40	0.95	0.75	0.64	-51	0.93	0.92	0.69	-187	0.89
		CEB-FIP	0.91	0.74	-75	0.95	0.95	0.75	-82	0.93	1.32	0.84	-125	0.89
		Measured	1.46	0.83	-72	0.95	1.24	0.91	-85	0.93	1.20	0.67	-255	0.89
Theoretical end of service $t_3 = 20000$ days		ACI	0.92	0.86	-63	0.95	0.94	0.87	-76	0.93	1.16	0.93	-218	0.88
		CEB-FIP	1.22	1.09	-280	0.95	1.26	1.11	-292	0.93	1.76	1.24	-354	0.88
		Minimum Extrapolated	1.46	0.83	-72	0.95	1.24	0.91	-85	0.93	1.20	0.67	-255	0.88
Maximum Extrapolated	1.97	1.34	-203	0.95	1.67	1.49	-232	0.93	1.52	1.06	-585	0.88		

Table 4.4: Material properties used in the analysis of F5 at significant construction events.

Concrete Material Properties	Date of event	April						May						$\Delta\bar{\sigma}_{pr}$ (MPa)			
		$\phi(t_i, t_0)$	$\phi(t_i, t_1)$	$\phi(t_i, t_2)$	$\varepsilon_{sh}(t_i, t_0)$ ($\mu\text{m}/\text{m}$)	$\chi(t_i, t_0)$	$\phi(t_i, t_0)$	$\phi(t_i, t_1)$	$\phi(t_i, t_2)$	$\varepsilon_{sh}(t_i, t_0)$ ($\mu\text{m}/\text{m}$)	$\chi(t_i, t_0)$	$\phi(t_i, t_0)$	$\phi(t_i, t_1)$		$\phi(t_i, t_2)$	$\varepsilon_{sh}(t_i, t_0)$ ($\mu\text{m}/\text{m}$)	$\chi(t_i, t_0)$
Stressing $t_0 = 0$ days	May 20, 2005	ACI	0	-	-	0	-	-	-	0	-	0	-	-	0	-	0
		CEB-FIP	0	-	-	0	-	-	-	0	-	0	-	-	0	-	0
		Measured	0	-	-	0	-	-	-	0	-	0	-	-	0	-	0
Falsework removal $t_1 = 69$ days	July 29, 2005	ACI	0.63	0	-	-90	-	0.70	0	-	-199	-	0.98	0	-	-59	0.90
		CEB-FIP	0.81	0	-	-39	-	0.98	0	-	-151	-	0.55	0	-	-151	-
		Measured	0.64	0	-	-106	-	0.85	0.59	0	-252	-	1.20	0.74	0	-96	0.89
Hinge loading $t_2 = 156$ days	October 26, 2005	ACI	0.75	0.57	0	-126	-	0.73	0.54	0	-220	-	0.94	0.74	0.62	-279	-
		CEB-FIP	1.00	0.70	0	-72	-	0.94	0.74	0.74	-134	-	1.38	0.95	0.74	-134	-
		Measured	0.87	0.54	0	-180	-	0.88	0.76	0.56	-284	-	1.22	1.01	0.93	-318	-
T303 $t_3 = 303$ days	March 20, 2006	ACI	0.84	0.72	0.61	-147	-	1.22	1.01	0.93	-318	-	1.91	1.40	1.22	-378	-
		CEB-FIP	1.15	0.90	0.72	-107	-	0.88	0.76	0.56	-284	-	0.88	0.76	0.56	-284	-
		Measured	1.06	0.76	0.55	-253	-	1.29	1.21	1.30	-697	-	1.29	1.21	1.30	-697	-
Theoretical end of service $t_4 = 20000$ days		ACI	1.09	0.97	0.91	-182	-	0.88	0.88	0.88	-	-	-	-	-	-	-
		CEB-FIP	1.59	1.33	1.19	-344	-	1.29	1.21	1.30	-697	-	1.29	1.21	1.30	-697	-
		Minimum Extrapolated	1.06	0.76	0.55	-253	-	0.88	0.88	0.88	-	-	0.88	0.88	0.88	-284	0.85
Maximum Extrapolated	1.59	1.21	1.25	-719	-	1.29	1.21	1.30	-697	-	1.29	1.21	1.30	-697	-	-28.83	

4.4. Analysis Assumptions and Approximations

In preparing the CPF [16] analysis, several assumptions were required. Some of the assumptions were made simply to lessen the required time to run the computer program. In each of these cases, the results of analysis for the actual bridge arrangement or conditions were compared to those including the assumptions and found to differ within acceptable tolerance less than 1%. Other assumptions were made because of some limitations in the computer analysis program. The following sections include the assumptions as classified within the material or structural level.

4.4.1. Structural and Geometrical Assumptions

- Since the bridge has only a slight horizontal curvature, plane analysis is assumed. The elimination of bridge curvature only influences the initial elastic deformation of the bridge. Creep and shrinkage are time-dependent influences that do not change their influence due to curvature. Idealization of curved bridges as plane in analysis is acceptable if the horizontal eccentricity of the tendons is less than 2% of the span length and if the central angle is less than 35° [2]. The bridge studied here meets both of these requirements, as shown in Appendix B.
- The moments of inertia for girder webs are grouped. In plane frame analysis only the moment of inertia about the primary axis of bending is considered. The moment of inertia is the same for the grouped case as it is in the actual configuration, regardless of the spacing between girder webs. Though grouping the webs significantly reduces the moment of inertia of the section about its transverse axis, this does not affect the analysis since out-of-plane bending is ignored. Additionally, the tapered overhangs of the cross section are idealized as a solid slab with equivalent thickness to that of the deck. Calculations performed indicate

that this assumption creates a difference of about 0.5% in the moment of inertia. Accompanying calculations are provided in Appendix B.

- Prestress ducts are grouped from the four webs to combine area at each level of tendon. Each of the four girders contains several levels of prestressing tendons; each level of tendon is at the same height in each girder. Idealizing the four tendons as a single tendon at each level is possible because the moment of inertia about the primary axis of bending is unaffected by taking the gross area of ducts at each level.
- Prestress tendons are grouped for each level. Again, the prestressing strands are lumped to represent a single tendon at each level of prestress. Therefore, the amount of prestress loss for all tendons at the same level of a particular cross section is assumed to be the same.
- Prestress ducts follow exactly the prestress tendon profiles; the centroid of the ducts is assumed to coincide with the centroid of the tendons. In the actual bridge, the prestress ducts are two to three times larger in area than the area of the prestress tendon. When stressed, the strands will naturally rest on the inside curve of the duct. For such a reason, the duct is eccentric to the centroid of the prestressing tendons; however, this eccentricity is small and the change in the moment of inertia is small as compared to the gross section.
- The two non-prestressed steel layers in the soffit and deck are lumped into one layer at mid-height of the soffit and deck, respectively.
- Contribution of longitudinal non-prestressed steel through the webs and bent-cap, at the same levels as that in the webs, is negligible. For analysis purposes, the steel in these locations is removed to hasten the rate of calculation. Several analyses were performed with this steel either included or excluded. Comparing the results at critical sections from these analyses reveal that the exclusion of this steel is acceptable and results in no considerable differences. Calculations are performed in Appendix B.

- Outrigger columns are grouped into a single column element. The outrigger at B15 of F4 consists of two identical columns formed into a bent cap. With the assumption that the bridge can be analyzed as a plane frame, the moment of inertia and area of each column is summed to form a member with equivalent area properties.
- Bents are assumed fixed at their respective bases. Below ground level, the bents form into Cast In Drilled Hole (CIDH) piles. The CIDH pile, pile cap, and surrounding soil are considerably stiffer than bridge columns. For such a reason, the columns are assumed to connect to a rigid base that terminates at the top of the CIDH pile. Ghali et al [17] showed that this assumption yielded realistic results in analyzing the Confederation Bridge with CPF.
- The bent and superstructure elements are treated as rigidly connected at the nodes. Analysis is performed using straight one-dimensional elements for all bridge members.
- Weight of barrier is ignored. For the bridge under study, the barrier has been placed long enough after stressing and its weight, compared to the bridge self-weight, can be assumed to have a negligible influence on the analysis results.
- In the F5 analysis, the cantilever in F4 supporting the F5 span at hinge 15 (H15) is an elastic support. The displacement of H15 is dependent on the reaction from the prestress and dead load. The prestress reaction changes over time as a result of creep, shrinkage and applied loads while the dead load reaction changes as the loads are increased at each interval within the analysis.
- Shear deformations are neglected in the analysis given the large span to depth ratio of the bridge girders.

- Prestress loading in the transverse direction is applied at the B15 outrigger; however, the stress induced from this load acts independently as the load applied along the longitudinal direction of the structure.
- Load at hinges from adjacent frames analyzed as concentrated load located at a single point in the plane idealization, imposed on the structure in full at the appropriate instant for which it occurred in the actual bridge.
- Horizontal and vertical curvature of the actual bridge is ignored in analysis. Additionally, the degree of slope is low compared to the span of the bridge.
- All falsework is assumed to be removed in a single instant
- Corner chamfers are not included

4.4.2. Input Material Parameter Assumptions

- Prestress relaxation calculated per ACI [3] equation for low relaxation strands
- Average relative humidity over monitoring period used for creep and shrinkage predictions
- The prestressing ducts were grouted soon after tensioning of the tendons. Though grouting was not immediate after tensioning, the period was short enough to allow the assumption that the tendons and girders are compatible immediately upon stressing.
- Creep and shrinkage do not occur in the columns or hinges. The columns are cast far in advance of the superstructure, thus significant shrinkage has already taken place. In general practice, cross sectional areas of columns in bridges are much larger than what is required to resist gravity loads, thus axial stresses in columns are very small compared to those in the bridge superstructure. The relatively low axial stresses in columns combined with the fact that they are loaded at a late age would result in

small creep strains and in turn very small axial displacements, which can be neglected in the analysis of the superstructure.

4.5. Frame Idealization

Both F4 and F5 were analyzed to closely resemble the as-built I5/805 Bridge frames as represented in the Caltrans Contract Drawings. The bridge cross sections, as depicted in these drawings, are represented in Figure 4.6. This figure displays the general layout of the monitored sections of the bridge and the locations of prestressed and non-prestressed reinforcement. The depths and thickness of the girders and locations of prestressed and non-prestressed steel differ between F4 and F5 at the monitored sections.

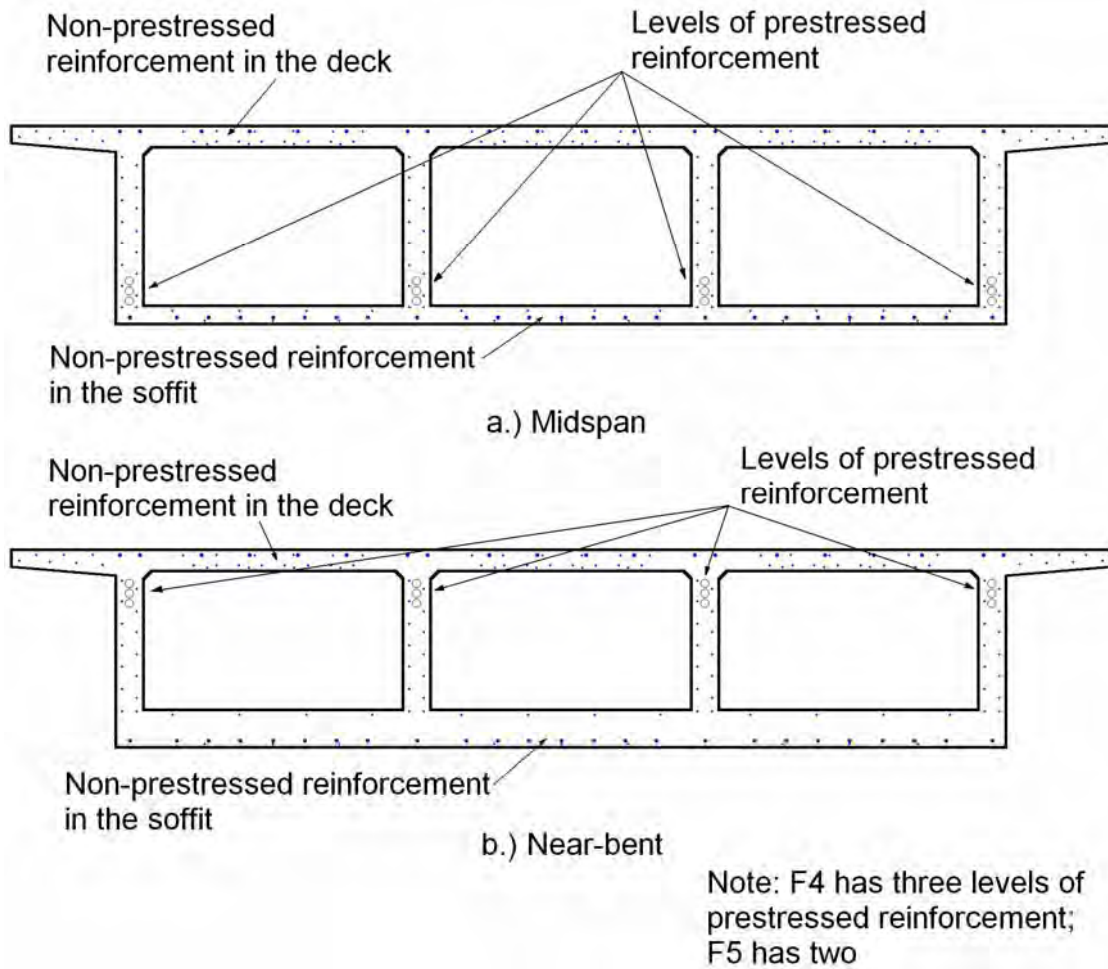


Figure 4.6: Layout of actual bridge cross sections.

As depicted in Figure 4.7, the bridge cross section was idealized such that it could be represented in the CPF [16] analysis. The methods perform calculations in a plane and a reference axis was selected at a depth near the centroidal axis of the section. The thickness of the webs was varied according to the width of the flare at the section near the supports. Non-prestressed reinforcement is represented as the area of the actual reinforcement at the levels in the concrete that it actually occurs.

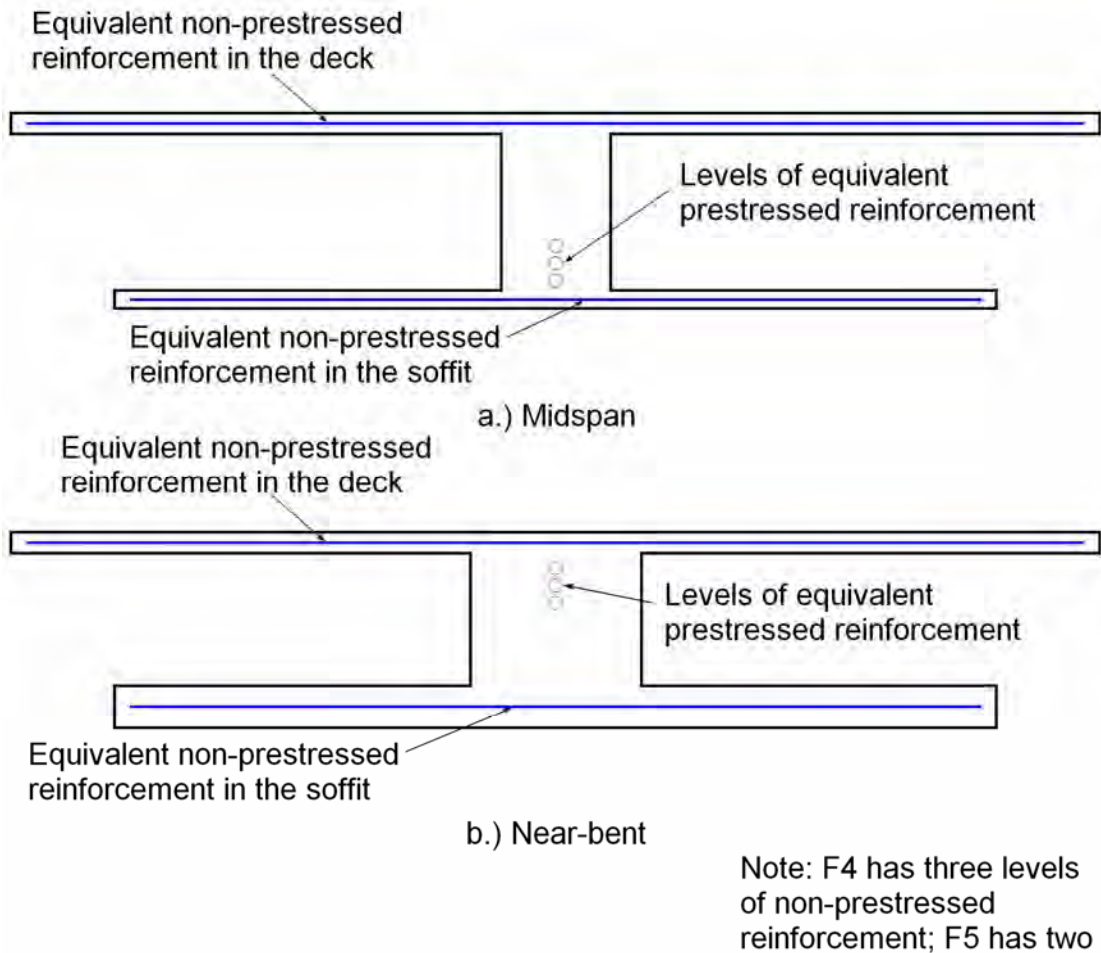


Figure 4.7: Layout of idealized bridge cross sections.

4.5.1. Frame 4

CPF calculates the deformation of the bridge with respect to a user defined reference axis, which does not have to coincide with the centroidal axis of the given cross section. CPF uses an idealized structure to perform structural

analysis to obtain the deformation of the frame, as depicted in Figure 4.8 for F4. The depths of the reference axes were selected to coincide closely with the centroidal axis of the superstructure for F4 and F5. For the superstructure of F4, the reference axis was selected at 1.5 m below the top surface of the deck; for the columns, was selected at the centroid of each member.

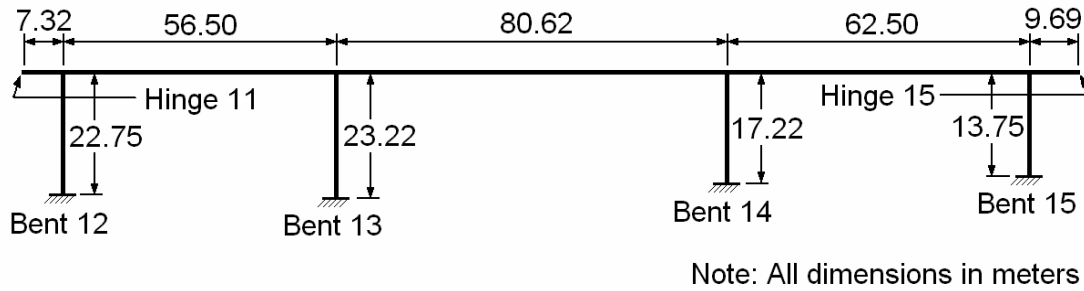
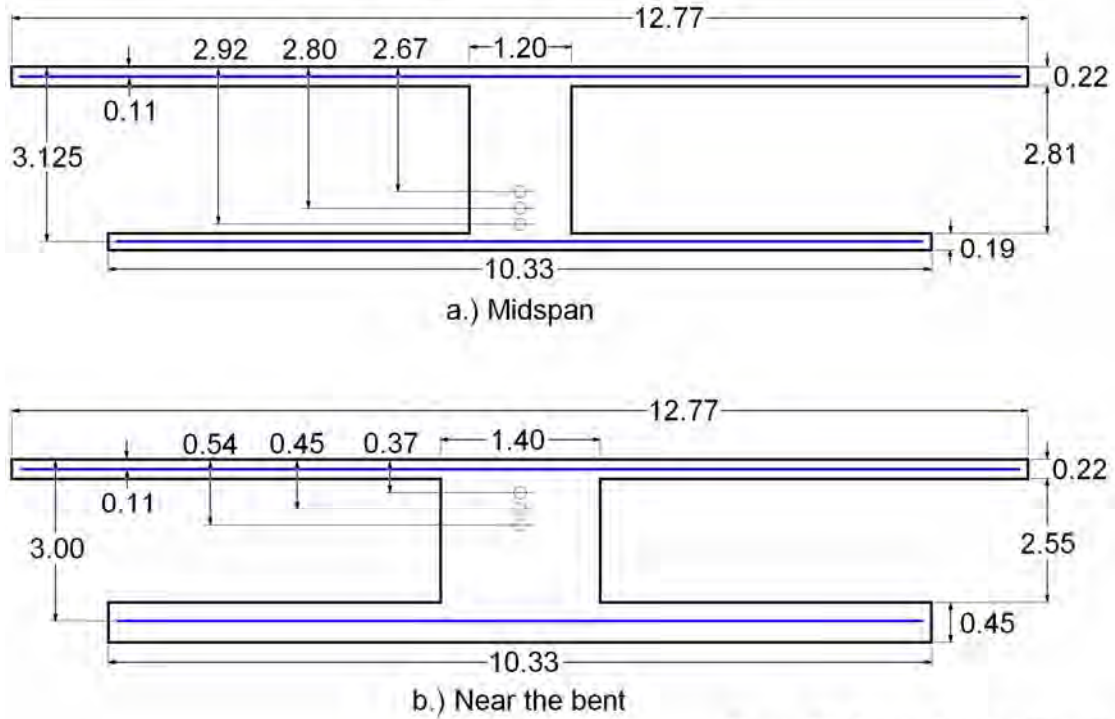


Figure 4.8: Idealization of F4.

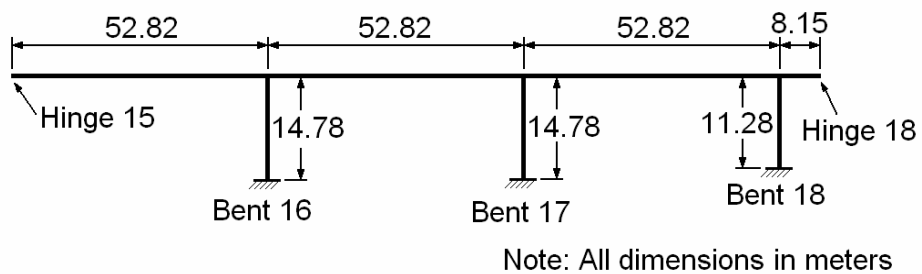
The idealized midspan and near-bent cross sections of F4, at the monitored locations, are represented in Figure 4.9 included with the dimensions used as input to the CPF [16] analysis.



Note: All dimensions in meters
 Figure 4.9: Idealized cross sections of F4 at midspan and near the bent.

4.5.2. Frame 5

F5 was idealized in the same manner as F4, as shown in Figure 4.10. The reference axis was selected at 1.1 m below the surface of the deck while that of the columns was selected at the centroid of each member.



Note: All dimensions in meters
 Figure 4.10: Idealization of F5.

The idealized midspan and near-bent cross sections of F5 are represented in Figure 4.11, which includes the dimensions used as input to the CPF [16] analysis.

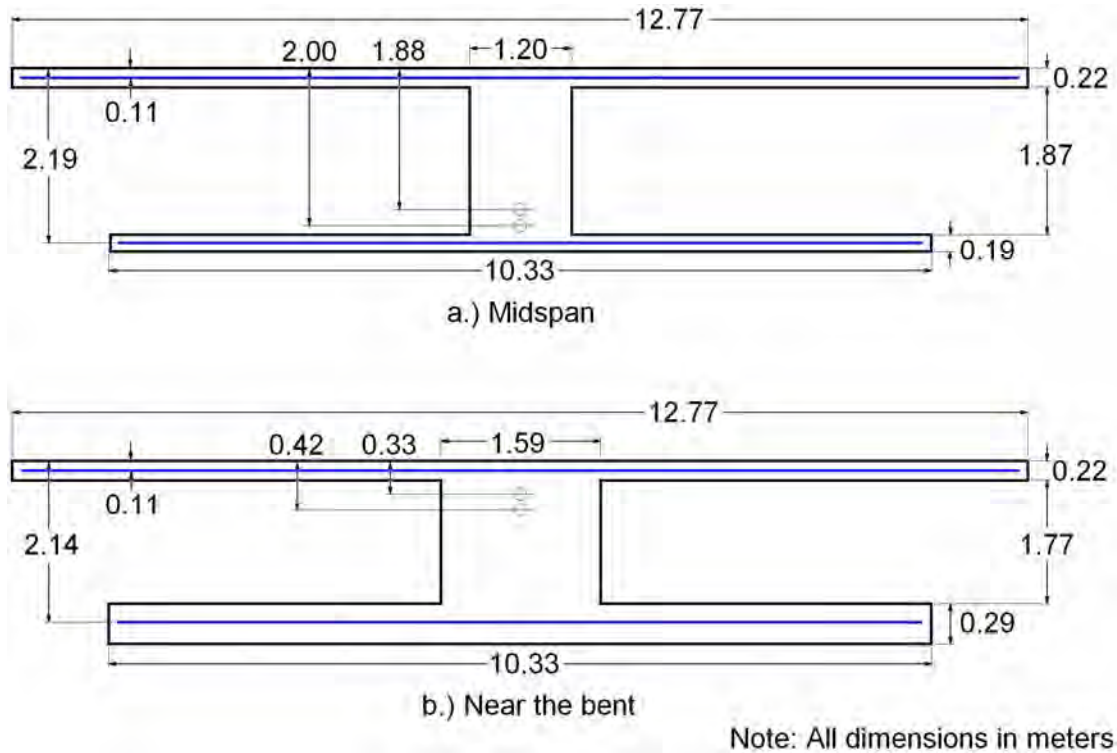


Figure 4.11: Idealized cross sections of F5 at midspan and near the bent.

4.6. Loading Events

There are several loading cases that are possible for the monitored frames used in this research. When prestressing is applied, the structure cambers and lifts off the falsework near midspan. The presence of falsework restrained deformations at some locations that would have been possible in the absence of the falsework. If the falsework were removed instantaneously after the prestressing had been applied then the structure would deform naturally, since the full self-weight of the structure would be applied at once. The falsework was not removed immediately after prestressing was applied and led to the adoption of a loading case that imposed 50% of the structural self-weight when prestressing was applied and the remaining 50% of the self-weight at the point in

time at which the falsework was removed. This loading case will be referred to as Loading Case 50/50 (LC50/50) and will be described in detail in Section 4.6.1. In Section 5.3 the appropriateness of this load case in accurately accommodating the true loading of the bridge will be revealed. Though CPF [16] is capable of accommodating multiple load cases, other methods utilized in this Report are not. These methods require the use of inputs representing all loads that are applied in full in one instant. This load case will be referred to as Loading Case 100/0 (LC100/0) and is described in Section 4.6.2.

To accurately accommodate the application of load as well as the support conditions imposed by the falsework, the support conditions were

4.6.1. Loading Case 50/50

When prestress was applied, the structure cambered and lifted off the falsework near midspan. The presence of falsework, though, forced deformation to occur that would not be present in the absence of falsework if the full structure self weight were imposed at once. For this reason, 50% of the structure weight was imposed in analysis at the same time as prestressing occurred, as indicated in Figure 4.12 and for F4 and F5, respectively. The assumption that 50% of the self-weight is imposed at prestressing and the remaining 50% is imposed with the removal of falsework will be justified in Section 5.3.

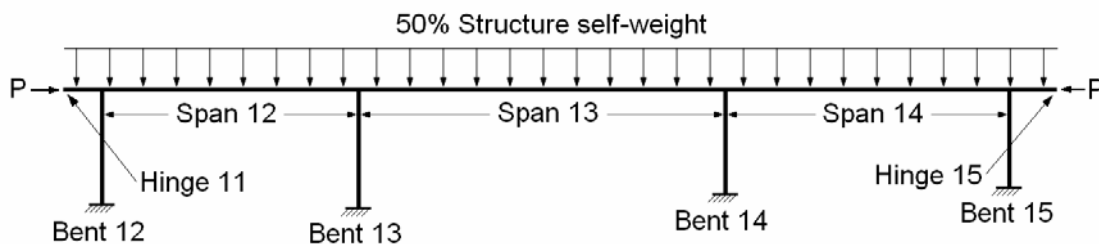


Figure 4.12: Loads applied on F4 initially at prestressing for the LC50/50 load case..

About 121 days after prestressing F4, its falsework was removed. The vertical displacement restraint imposed by the falsework was removed at this time, thus the remaining self-weight was applied in analysis, as shown in Figure 4.13. At

this time, the reactions from the adjacent frames (Frame 3 and Frame 5) were imposed at hinges 11 and 15, and designated as V11 and V15, respectively.

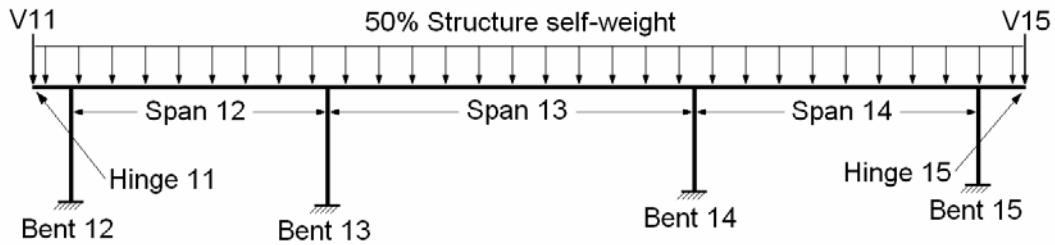


Figure 4.13: Loads applied on F4 at the removal of falsework for the LC50/50 load case..

The analysis for F5 was performed using 50% of the structural self-weight applied simultaneously with prestressing, similar to that in F4, as shown in Figure 4.14.

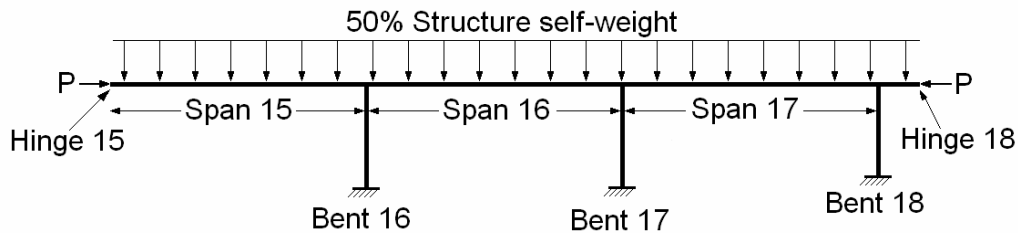


Figure 4.14: Loads applied on F5 initially at prestressing for the LC50/50 load case..

The falsework was removed 69 days after prestressing; at this time, the remaining 50% of the structural self-weight was applied to the structure, as shown in Figure 4.15. At this time, though, the falsework still remained supporting the cantilever at hinge 18.

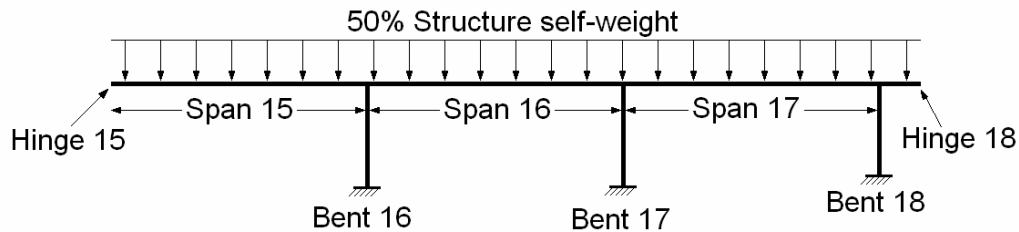


Figure 4.15: Loads applied on F5 at the removal of falsework for the LC50/50 load case..

At a time 156 days after prestressing, the falsework supporting the hinge was removed. When this falsework was removed, the reaction from span 18 (at hinge 18) was imposed, designated as V18 in Figure 4.16.

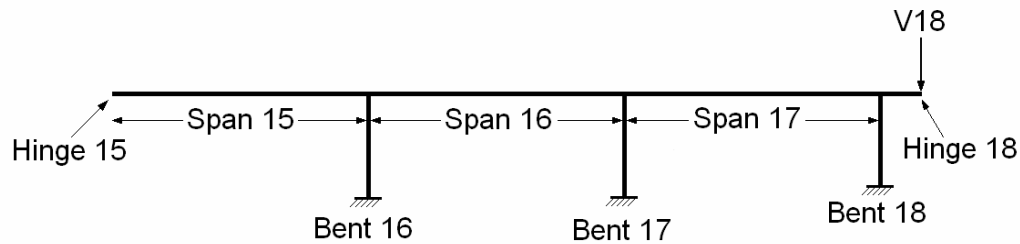


Figure 4.16: Loads applied on F5 at the removal of falsework supporting the hinge (hinge loading) for the LC50/50 load case.

4.6.2. Loading Case 100/0

Analysis using CPF [16] is capable of accommodating multiple instants of loading, thus uses the LC50/50 load case. Another method, Prediction of Long-Term Prestress Losses (Proposed Method) [29] (Section 6.3) is capable of accommodating only one instant of loading. Since several of the methods are not capable of accommodating multiple load cases, the LC100/0 load case was investigated since it is what a design engineer would typically use in practice. It is not appropriate to use the input stress and strain profiles from LC50/50 to the specifications or Proposed Method [29] since the loads applied later are not accommodated.

For the LC100/0 load case, the full structural self-weight is applied at the same time as prestressing. Any loads at the hinges induced by adjacent frame loads are applied at this time as well. The loads applied in F4 and F5 using the LC100/0 load case are represented in Figure 4.17 and Figure 4.18, respectively.

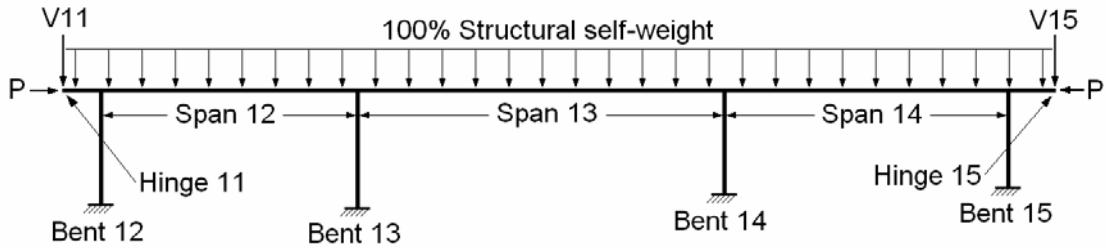


Figure 4.17: Loads applied on F4 at prestressing for the LC100/0 load case.

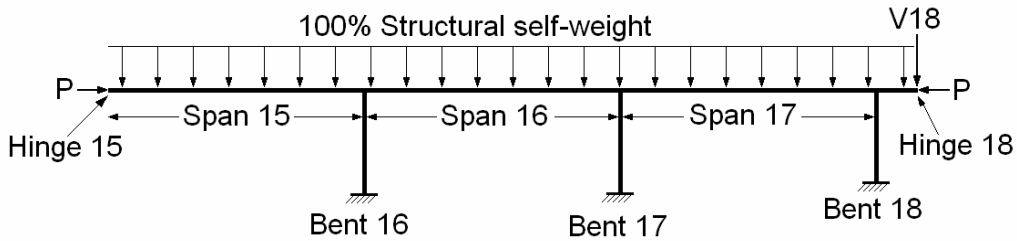


Figure 4.18: Loads applied on F5 at prestressing for the LC100/0 load case.

The change in the prestress over time, as a result of all time-dependent influences, is incorporated in the analysis and presented for all intervals in the CPF [16] output. The strain profiles and prestress losses occurring within F4 and F5 over the monitoring period at significant intervals are presented in Chapter 5. Long-term predictions of the prestress loss are then presented.

5. Field Measurements

5.1. Introduction

Coordination with Caltrans engineers and the contractor facilitated placement of vibrating-wire (VW) strain gages within the bridge superstructure. VW strain gages embedded in the concrete were selected for their long-term reliability, as monitoring is planned to continue over many years.

The bridge was instrumented with several VW strain gages in each girder stem at critical sections, as indicated in Figure 4.2 and Figure 4.3. A data-logger system [11] was used to collect the strain readings at routine intervals. The strain gages provided data for the determination of the strain profile of specific sections of the bridge girders over the monitoring period. The change in strain in the concrete over time can be directly related to the change in stress in the prestressing tendons, which is presented in that chapter. The monitored strains are compared with the analysis results using the computer program CPF [16] in Section 5.4.

Comparing the results of monitoring with computer analysis only on the basis of long-term prestress loss is not adequate to verify the accuracy of the analyses. Similarities in prestress loss may be coincidental and based on entirely different strain profiles for the sections under consideration. To assure the accuracy of the analyses, the monitored data was used twice, first at prestressing and then at a later time after construction had been completed. The strains predicted by the model were compared with both sets of monitored data to validate the accuracy of analysis at prestressing and T363 or T303. T363 and T303 represent the time in days after loading (post-tensioning) of Frame 4 (F4) and Frame 5 (F5), respectively. The times T363 and T303 also correspond to points in time 241 and 147 days after the last instant permanent load was applied (reactions from adjacent frames), respectively, for F4 and F5. The strains can be used to determine the change in concrete stress over time to be checked at these critical sections and indicate whether cracking might occur.

5.2. Instrumentation

Both F4 and F5 were instrumented with a number of embedment type VW strain gages manufactured by Slope Indicator [28], which also measure temperature. These gages were located at positions of maximum stress: one section at midspan and the other near the bent, in both frames, as depicted in Figure 4.2 for F4 and Figure 4.3 for F5.

The VW gages near the bent-caps were placed 305 mm (12 in.) from the outside face of the bent-cap. This was done to exclude any confinement effect from the adjacent bent-caps.

The gages were affixed to the longitudinal non-prestressed reinforcement before the concrete was cast, as shown in Figure 5.1. The gages are 140 mm long; the movable parts of each gage are the disks (end circular flanges) that translate with adjacent concrete deformation. Styrofoam standoffs were used to hold the gage about 25 mm away from the longitudinal reinforcement so that it would not impede the free movement of the disks. Nylon tie-wraps were used to secure the gages to the standoffs and longitudinal reinforcement.

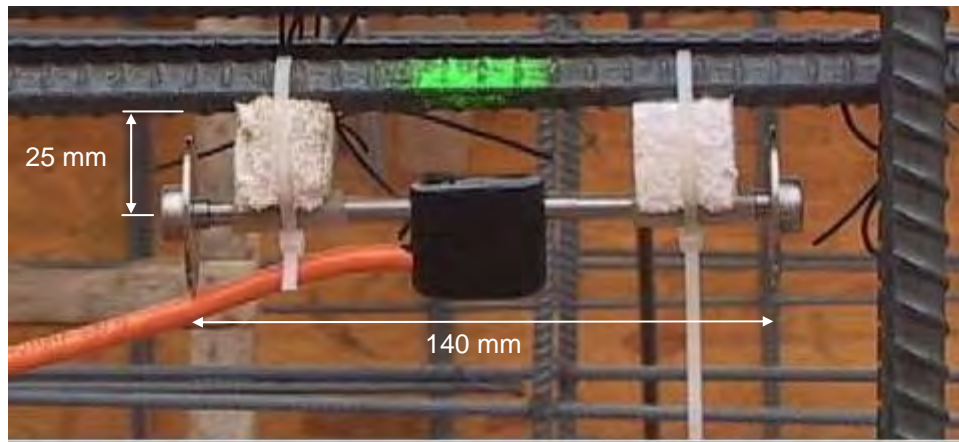


Figure 5.1: Elevation view of typical placement of VW strain gages affixed to longitudinal reinforcement.

The locations of the gages as they are placed in both frames, at midspan and near the bent, are indicated in Figure 5.2. Reinforcement is not shown for clarity. The actual depths of the gages were measured prior to the placement of the

concrete and are indicated in Table 5.1 and Table 5.2. A minimum of three gages was installed through the depth of each stem at all selected locations. Gages were placed near the mid-depth of both the deck and soffit and near the centroid of the gross section in the web portion of each stem. At each section, one of the stems was equipped with two additional gages, in the upper half of the concrete, to enable improved recording of temperature distribution, which was expected to be highly nonlinear at this location [17, 20, 27]. The recorded temperatures were used to determine the thermal strain influence, as will be described later.

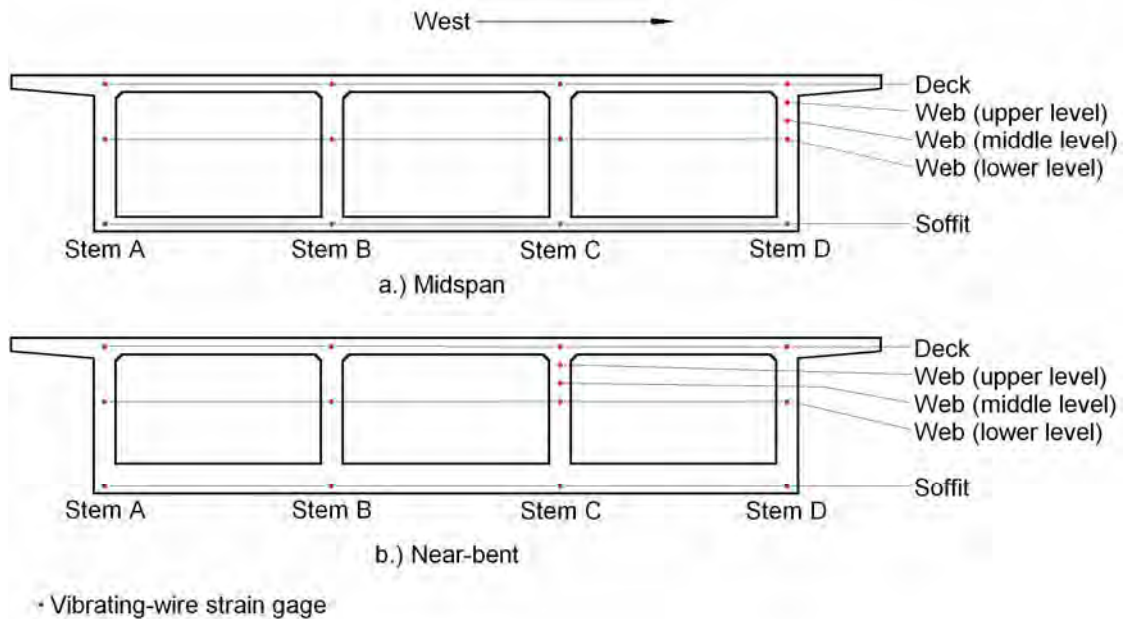


Figure 5.2: Typical locations of strain gages as mounted through the superstructure cross-section for both F4 and F5 and cardinal orientation.

Table 5.1: Gage depths for F4.

Gage level	Distance from top fiber (m)							
	Midspan				Near the bent			
	Stem A	Stem B	Stem C	Stem D	Stem A	Stem B	Stem C	Stem D
Deck	0.09	0.09	0.09	0.09	0.09	0.09	0.09	0.09
Web (upper level)	-	-	-	0.48	-	-	0.50	-
Web (middle level)	-	-	-	0.68	-	-	0.68	-
Web (lower level)	1.54	1.57	1.56	1.57	1.57	1.56	1.57	1.55
Soffit	3.10	3.10	3.10	3.09	3.10	3.10	3.09	3.09

Table 5.2: Gage depths for F5.

Gage level	Distance from top fiber (m)							
	Midspan				Near the bent			
	Stem A	Stem B	Stem C	Stem D	Stem A	Stem B	Stem C	Stem D
Deck	0.09	0.09	0.09	0.09	0.09	0.09	0.09	0.09
Web (upper level)	-	-	-	0.34	-	-	0.34	-
Web (middle level)	-	-	-	0.48	-	-	0.48	-
Web (lower level)	1.10	1.10	1.10	1.10	1.10	1.10	1.10	1.10
Soffit	2.15	2.15	2.15	2.15	2.15	2.15	2.15	2.15

Each of the strain gages is connected to a data-logging system, manufactured by Campbell Scientific [11], located at the bridge site. This system was programmed to collect the strain data from the gages at specified intervals, which the system stored until manually downloaded onto a portable computer.

5.3. Data Monitoring

To exclude the effect of any initial strains that might have been present in the VW gages, the data-loggers for F4 and F5 were operational several days before prestressing occurred. Deformations due to creep effects occur rapidly during the initial three months after stressing [25]. These deformations were captured beginning immediately with the application of load (prestress). The effects of shrinkage occur immediately upon the end of curing, so the influence of shrinkage on the prestress loss depends on the elapsed time between the end of curing and loading, thus varies considerably between F4 and F5. For these reasons, in the first two months after prestressing, F4 was monitored every hour; this frequency was later reduced to 12 hours through T363 or about one year after prestressing. F5 was monitored every hour for the period of time research was conducted and included in this Report through the point in time T303, approximately 10 months after prestressing. Examination of the data reveal that it would have been beneficial to monitor F4 at a frequency of one hour for a longer period of time, as additional comparisons of strain and temperature between the two frames could have been made. Examination of the strains indicated that monitoring at a frequency of one hour resulted in large variation in strain

throughout the day caused by thermal gradients through the monitored sections, which will be indicated later in this section.

The placement of VW strain gages through the depth of the girders enabled the determination of the strain profile through the superstructure at points in time over the monitoring period. The strain profiles were used to determine the changes in stress in the concrete (at critical locations) and prestressing steel which were verified against the analytical results, presented earlier. The majority of gages provided readings that indicated a linear strain profile through the depth of the section, verifying that plane sections remained plane in the monitored sections. A few of the gages provided unrealistic strain readings – values that varied unpredictably, indicated zero, or values that greatly exceeded the values from other gages at respective locations. The readings from these gages were discarded, as will be discussed later in this section.

Strain readings that are indicative of the actual bridge deformation are dependent on the correct orientation of the VW gages in the longitudinal direction of the bridge. It was determined that some of the VW gages were either damaged or became dislodged from their intended positions and thus indicated unreliable levels of strain. The gages also indicate temperature, which, unlike the strain readings, is not dependent on the orientation of the gage; to a major extent, the temperature does not fluctuate significantly in the longitudinal direction. For this reason, although the strain reading from some gages was determined to be unrealistic, all temperature readings followed consistent trends, even at the locations of unrealistic or incorrect strain. The temperatures from the gages that provided no usable strain were used solely to observe the temperature variation through the sections.

Some small deviation from a linear path was expected for all gages. Creating a straight-line strain profile was accomplished by a least-squares regression of the data, as will be explained in the present section 5.3.

Accidents due to personnel working around the locations of the instrumentation boxes at the bridge site resulted in the disconnection of the

power to the data-loggers on a few occasions. None of the incidents occurred during or immediately after major construction events – the points in time where the most significant changes in strain were expected.

5.3.1. Data Analysis

The strains and temperatures in the bridge were monitored at known intervals. In F4, readings from the gages were monitored once every hour for the first 60 days after prestressing was applied. After 60 days, the frequency of monitoring in F4 was reduced to twice per day (once every 12 hours). Measurements were then taken at 3:00 am and 3:00 pm and remained at this frequency through T363, i.e., 363 days after prestressing. In F5, data was collected every hour through T303, i.e., 303 days after prestressing.

Examination of the data showed that at 3:00 am, the measured data were generally the closest to the average daily values of strain and temperature. In Section 5.3.2, the strains presented for the deformation of the bridge were taken using the strain at 3:00 am as a reference. Taking the strains at 3:00 am serves as a suitable baseline since the strains are at a common point in time as well as very close to the daily average, thus the thermal influence was not at an extreme. It is more appropriate to use the strains at a common point in time (3:00 am) than at a daily average since an average does not represent the state at a single point in time, but throughout the day. A temperature of 17 °C was used as a baseline in F4 and 25 °C was used for F5. The thermal baselines for the two frames are different because of the time of year at which the concrete was prestressed. To remove the thermal influence, a temperature at the reference point in time after prestressing (3:00 am) was used as the baseline.

The thermal expansion coefficient was calculated from the monitored data. The gages provided both strain and the associated temperature at points in time throughout the day, and, as such, allowed correlation of the change in strain with the change in temperature. Examination of the data showed that at all four monitored locations, the strain varied minimally beginning about 200 days after

prestressing. After 200 days, the influence of creep and shrinkage were minimal, as shown in Section 5.3.2. The primary deformation (90% of the deformation at T363 and T303) of the bridge resulting from creep and shrinkage occurred within this period of time. After this period of time, short-term changes in strain were almost entirely the result of change in temperature. For this research, a period of one day was considered short-term and used to correlate the change in strain with the change in temperature. A period of one day allows any influences resulting from time lag on the change in strain with change in temperature to be minimal. The ratio between the daily variation of minimum and maximum strain and that of the minimum and maximum temperature were used to determine the thermal expansion coefficients.

The thermal expansion coefficient was calculated by taking the slope of the line describing the relationship between strain and associated temperature, as shown in Figure 5.4, for all gage locations. In F4, the thermal expansion coefficient was calculated as 8.93 microstrain/°C. In F5, the thermal expansion coefficient was calculated as 8.58 microstrain/°C. The thermal expansion coefficients were calculated from the average of all thermal expansion coefficients from all gage locations. In Figure 5.3 a range of thermal expansion coefficients from two gages in F5 is presented as well as the average thermal expansion coefficient for all concrete in F5.

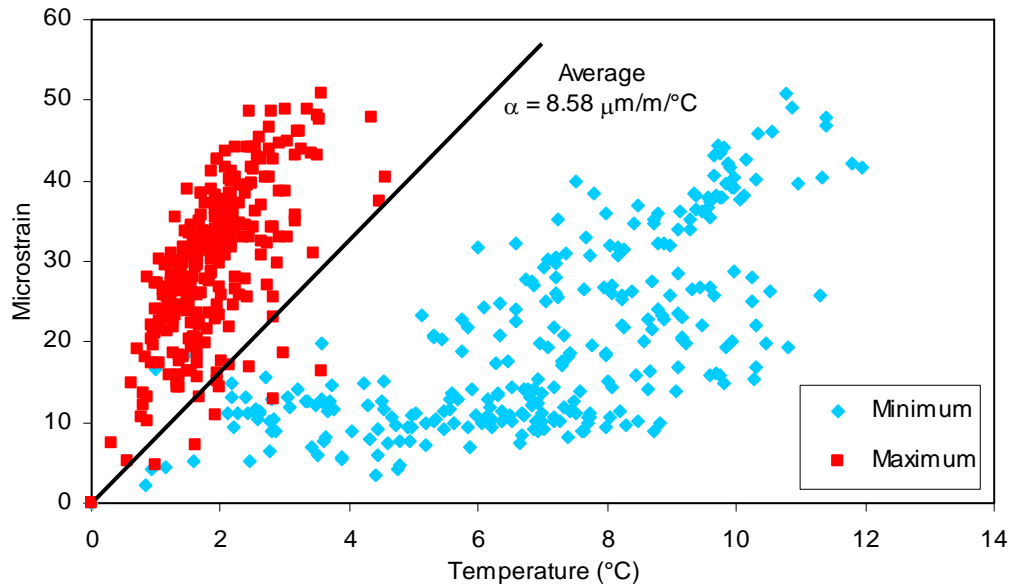


Figure 5.3: Correlation between change in temperature and change in strain.

The calculated thermal expansion coefficients are in good accordance with the accepted range for concrete of 6 to 13 microstrain/°C [19]. These values are presented in Table 5.3. The similarity between the F4 and F5 coefficients and their correlation to the accepted norm provide support for the accuracy of the data and calculation method.

Table 5.3: Thermal expansion coefficients for all gage locations.

Gage location	Thermal expansion coefficient: $\mu\text{m}/\text{m}/^\circ\text{C}$	
	Frame 4	Frame 5
Stem A Soffit	11.29	5.77
Stem A Web	11.12	4.53
Stem A Deck	19.94	-
Stem B Deck	3.63	6.54
Stem C Deck	4.10	5.41
Stem D Soffit	5.71	3.90
Stem D Web	-	14.35
Stem D Web	-	16.48
Stem D Web	-	14.17
Stem D Deck	5.83	5.03
Stem A Soffit	14.81	7.62
Stem A Web	6.53	16.61
Stem A Deck	14.19	4.68
Stem B Deck	6.98	10.00
Stem C Web	-	15.94
Stem C Deck	5.64	8.27
Stem D Soffit	6.34	6.34
Stem D Web	-	5.86
Stem D Deck	-	2.99
Average	8.93	8.58

It was determined from the monitored temperature data from both frames that increased temperatures resulting from hydration were not an influence in either frame once prestressing had been applied. Though it would have been useful to monitor the temperatures in the concrete beginning with the placement of concrete, the gages were not activated for purposes of monitoring at regular intervals until only a few days before the concrete was prestressed. In both frames, prestressing occurred long after the increased temperatures resulting from heat of hydration had dissipated.

5.3.1.1. Thermal Influences

Figure 5.4 and Figure 5.5 display the average temperatures experienced in the concrete at the three primary levels at which the gages were located for F4 and F5, respectively. Additionally, the average concrete temperatures are compared to the average ambient air temperature that existed at the time. It can be seen in

Figure 5.4 and Figure 5.5 that the fluctuation of concrete temperature varies almost consistently with the change in ambient air temperature for daily variation in temperature of more than 3 °C. Additionally, there existed a time-lag of the concrete temperature that occurred slightly behind the change in ambient air temperature.

It can be seen that the concrete temperature exceeded the air temperature by about 5 °C in both F4 and F5 for a period that ended about 260 days after prestressing in F4 and about 200 days after prestressing in F5. F4 was prestressed 60 days prior to F5, thus the point in time at which the ambient temperature and the concrete temperature reached equilibrium in both frames was approximately the same point in time. This occurred in November 2005. After this point in time, the concrete temperature varied consistently with the air temperature within about 1 °C.

It should be noted that the gages were calibrated at a temperature that was 5 °C higher than the actual temperature. It is for this reason that the concrete temperature appears to exceed the ambient air temperature for most points in time. It is not expected that the concrete temperature would exceed the ambient air temperature; however, this was not discovered until all data had been processed. Note must be taken that, although the presented concrete temperatures are in excess of 5 °C, all calculations were based on relative temperature changes, thus the difference between temperatures at all points in time is the same.

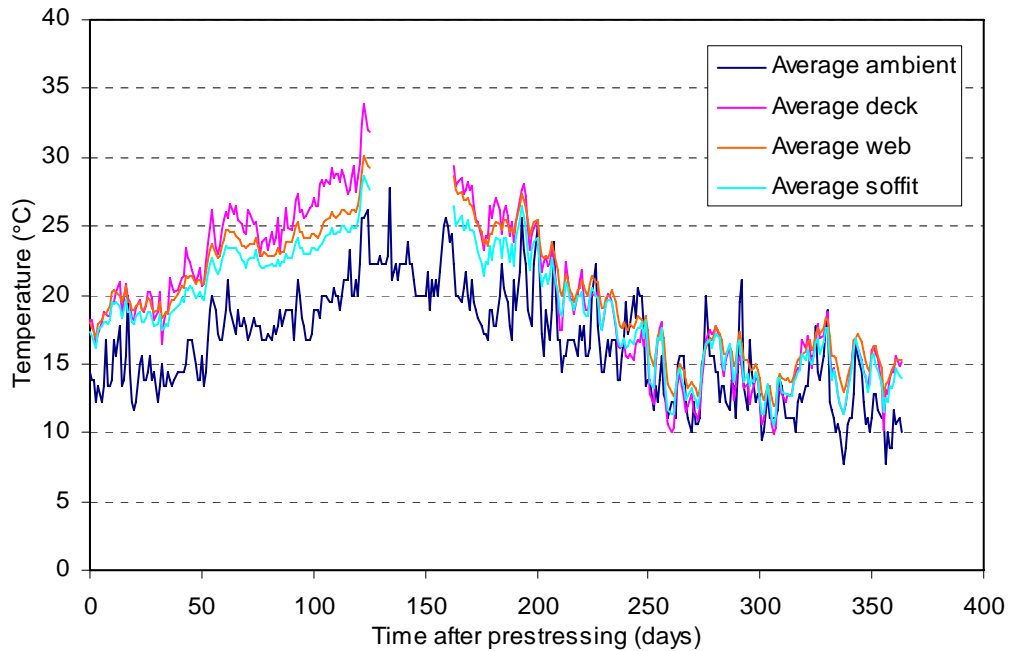


Figure 5.4: Average temperature in F4 and ambient air temperature during the monitoring period.

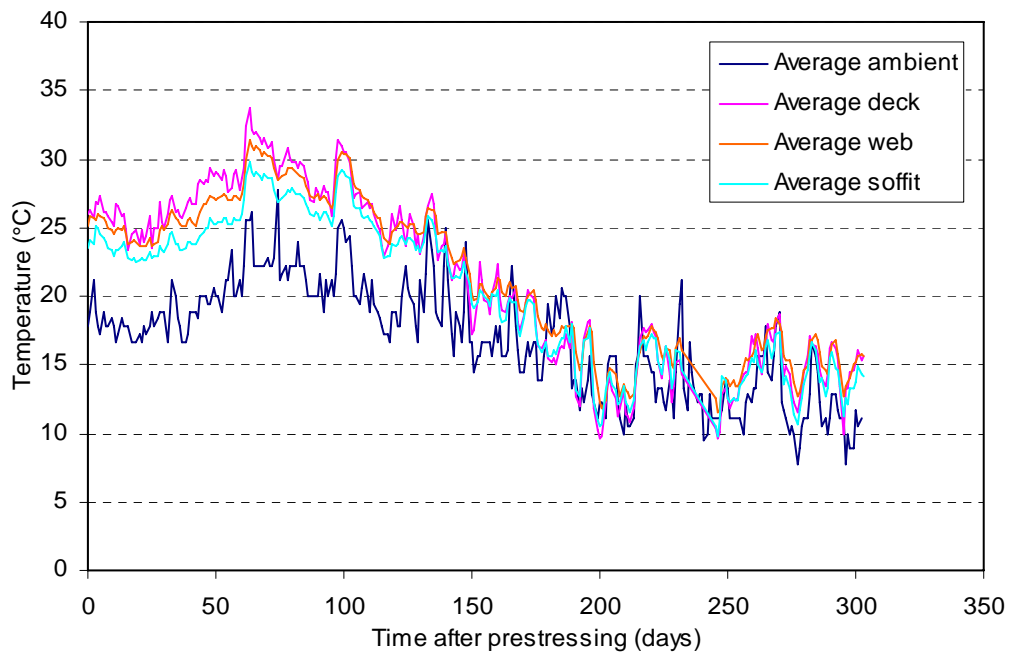


Figure 5.5: Average temperature in F5 and ambient air temperature during the monitoring period.

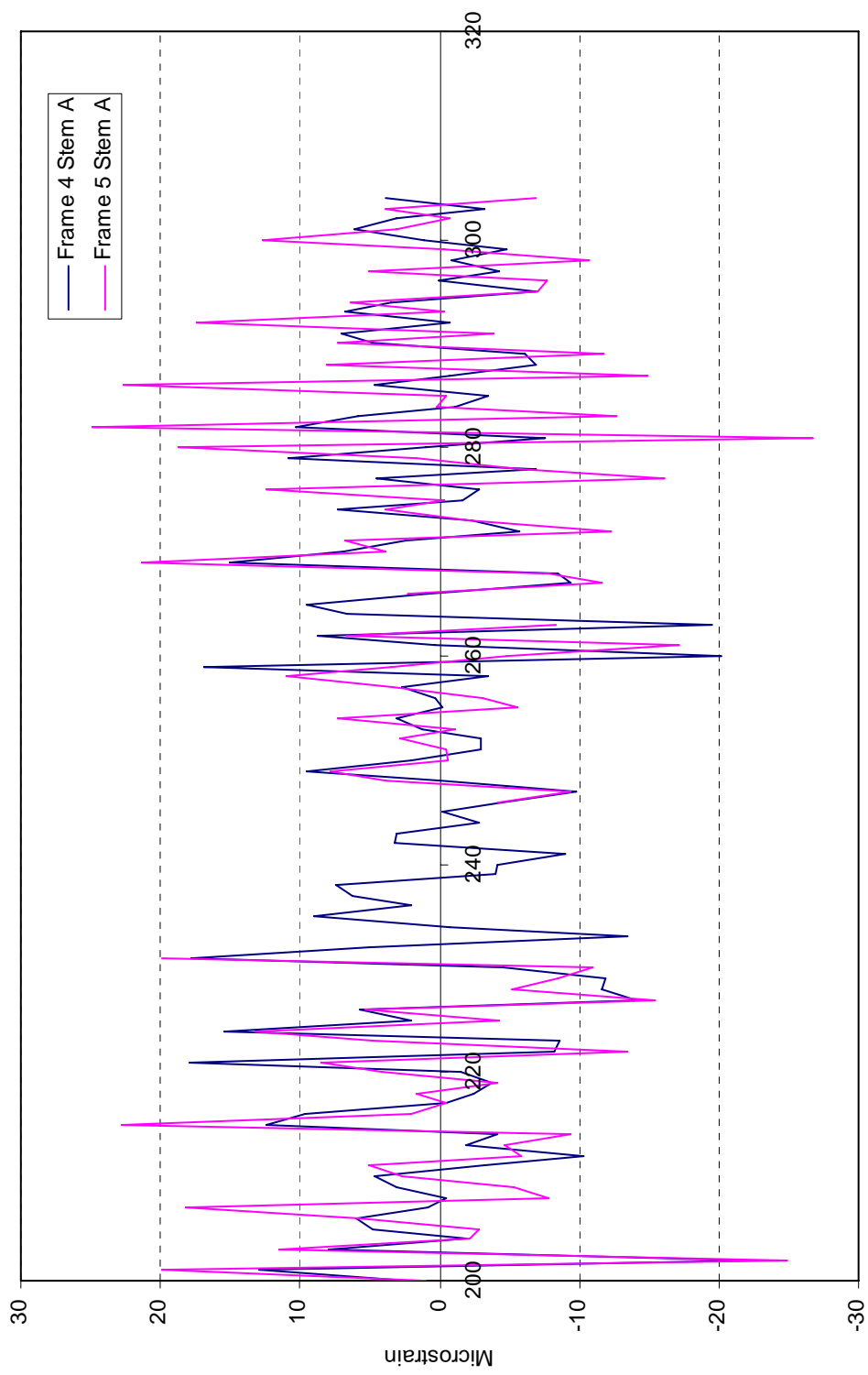
The stems at each of the four monitored locations exhibited similar behavior in terms of daily variation in strain and temperature. This is the result of the orientation of the stems with respect to each other. At all four monitored sections,

Stem A represents an exterior web and is oriented facing east, Stem B and C are interior girders, and Stem D is an exterior girder that faces west. The respective positions of the gages are shown in Figure 5.2. The trends discussed in this section apply to all stems and the respective positions; however, the observed behavior of only selected representative sections will be included herein. The additional figures representing monitored strains and temperatures at other sections can be found in the Appendix C.

It should be noted for clarity, that the strains for each of the respective sections are not the same. The illustration here is that the absolute temperature, change in temperature, and corresponding change in strain are similar in terms of trend at corresponding gage locations, and thus allows the presentation of only one representative section.

Figure 5.6 displays the daily variation in strain in Stem A of F4 and F5. It can be seen in this figure that the strain fluctuates between the different sections consistently for the majority of the time. It must be noted that the strain is presented for a period beginning 200 days after prestressing of F5. This was done for several reasons. The change in strain was observed to decrease substantially beginning about 200 days after prestressing because the majority of creep and shrinkage influences had already occurred.

The monitoring frequency of F4 was decreased 60 days after prestressing to twice per day, while F5 was monitored every hour. For this reason, the fluctuation in strain shown in Figure 5.6 is not consistent for every point in time. It must be noted; however, that the variation between strain in the two sections in F4 and F5 does not exceed 19 microstrain, corresponding to a difference in temperature of about 3 °C. This difference in temperature was shown (from the data from F5) to exist during the times that data was not collected in F4, since the monitoring times did not capture the full daily variation in temperature and strain.



Time after prestressing Frame 5

Figure 5.6: Maximum daily variation in strain in Stem A of F4 and F5.

Figure 5.7 displays the daily variation in concrete temperature in Stem A of F4 and F5 at the reference point in time of 3:00 am and shows that the temperature fluctuates consistently between locations. The trends in Figure 5.7 are consistent for all other gage locations in other stems.

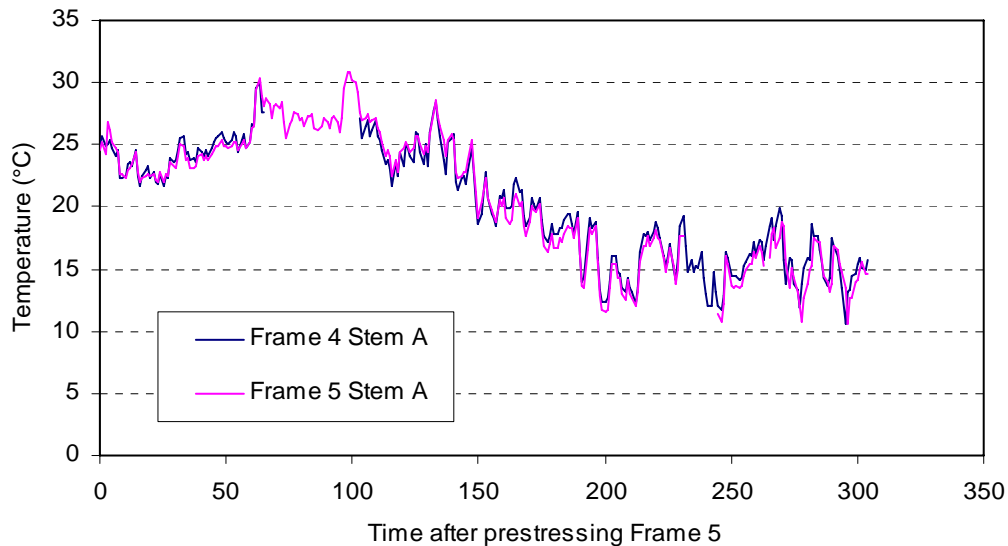


Figure 5.7: Daily variation in concrete temperature in Stem A of F4 and F5 at 3:00 am.

For each gage location, the minimum, maximum, and average temperature and strain are presented. Additionally, the strain and temperature are presented as measured at 3:00 am. Examination of the data indicated the time of 3:00 am coincided consistently at most locations with the average strain and temperature that were measured throughout the day. The 3:00 am strain was used in generating the strain profiles presented later in this section for each of the four monitored sections.

As was explained previously in this section, it is expected that the daily variation in strain would correlate with variations in temperature at respective gage locations through the depth of the sections as well as at the respective locations of the gages at the four monitored sections. The frequency of monitoring was reduced in F4 at 60 days after prestressing was applied from once every hour to twice per day at 3:00 am and 3:00 pm. The reduction in monitoring frequency also reduced the range of strains and temperatures that

were collected. For this reason, the collected data are presented for F5, as the monitoring frequency remained hourly for the duration of monitoring used for this research. The changes in strain and temperature that occurred in F4 are evident and similar to the trends identified from the monitored data in F5. The representative figures for the monitored data in F4 are presented in Appendix C.

5.3.1.1.1. Exterior Stem

The following figures (Figure 5.8 to Figure 5.13) examine the temperatures that were developed in Stem A of F5 at midspan. The minimum and maximum temperatures as well as the average and values at 3:00 am are presented. As mentioned previously, the behavior of stems in respective positions was very similar. The variation in strains and temperatures presented are representative of each stem with corresponding designations; the reason for this is that the orientation of respective stems is the same at each of the four monitored sections, as shown in Figure 5.2.

The strain and corresponding temperature that are experienced in the soffit (Stem A of F5 at midspan) are displayed in Figure 5.8 and Figure 5.9, respectively. As expected for a soffit location, the temperature of the concrete at this location was lower than the temperature of the concrete in the deck by about 5 °C. The temperature and strain at this location varied more than in the deck and web, displaying an average variation between minimum and maximum strain and temperature of about 100 microstrain and 8 °C, respectively.

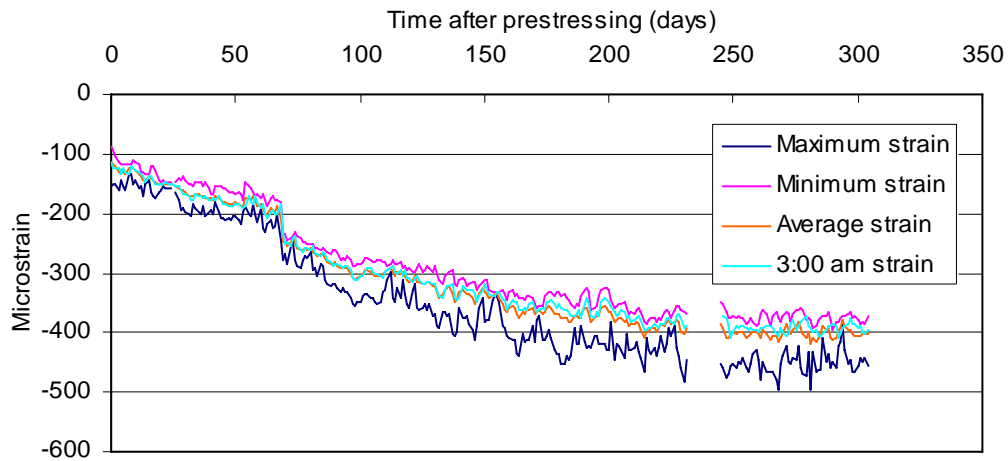


Figure 5.8: Strain in Stem A of F5 in the soffit.

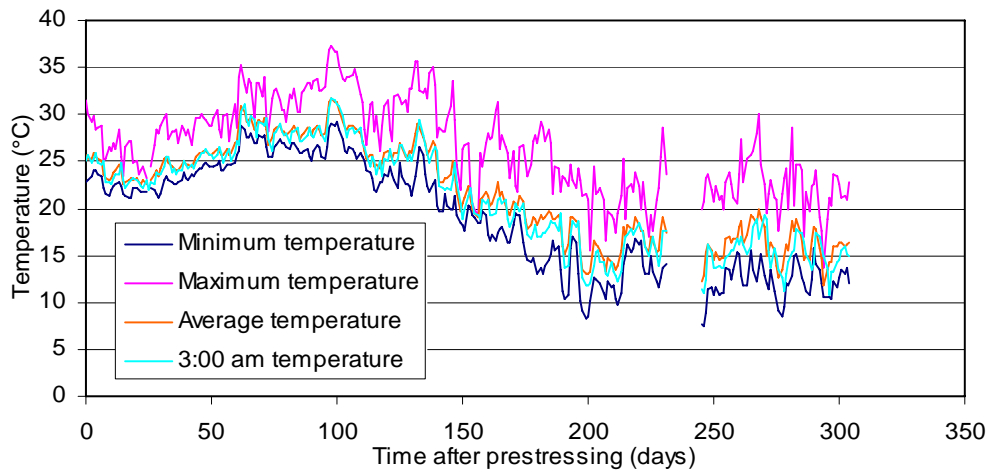


Figure 5.9: Temperature in Stem A of F5 in the soffit.

Both the deck and web gages indicated daily variation in strain of about 35 microstrain, as shown in Figure 5.10 and Figure 5.12. The change in temperature was similarly consistent between the deck and web (Figure 5.11 and Figure 5.13), with a daily variation of about 6 °C.

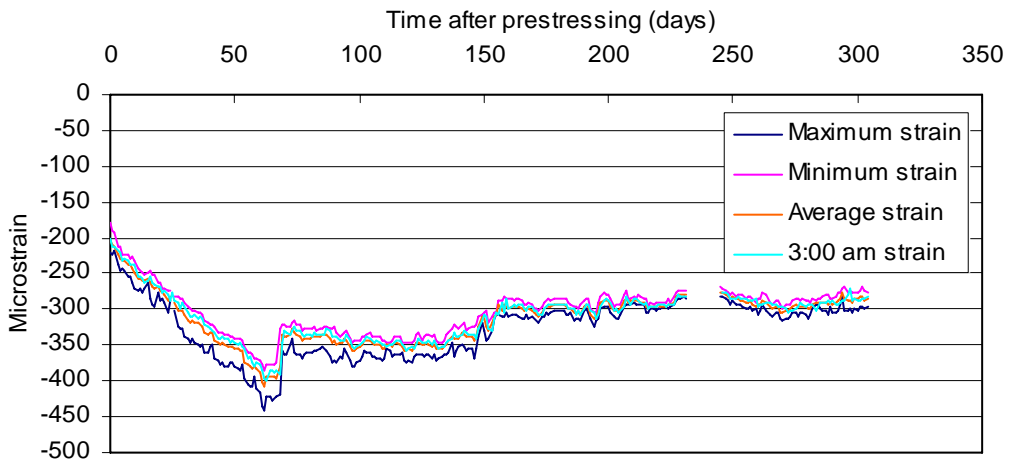


Figure 5.10: Strain in Stem A of F5 in the deck.

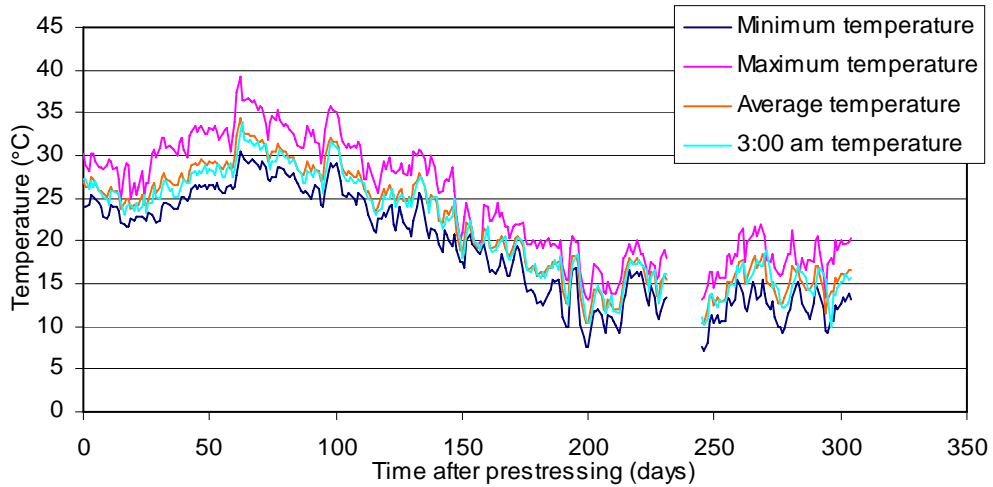


Figure 5.11: Temperature in Stem A of F5 in the deck.

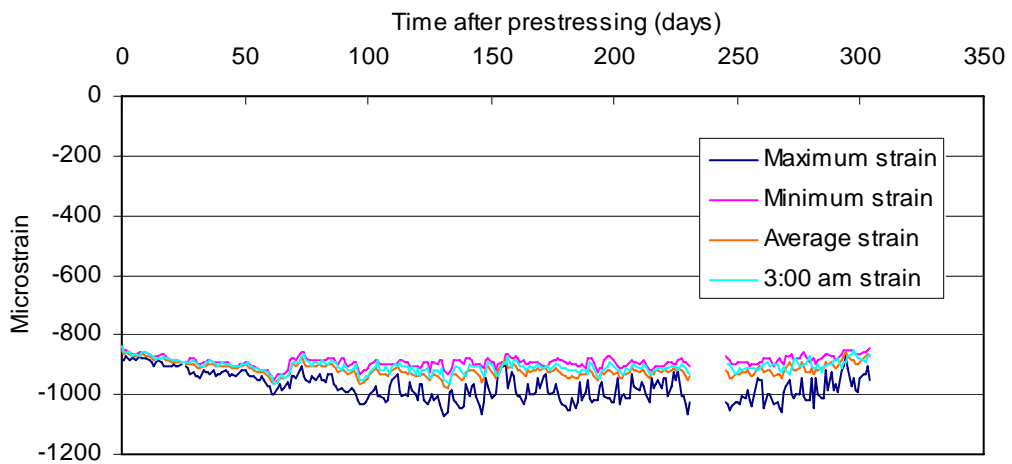


Figure 5.12: Strain in Stem A of F5 in the web.

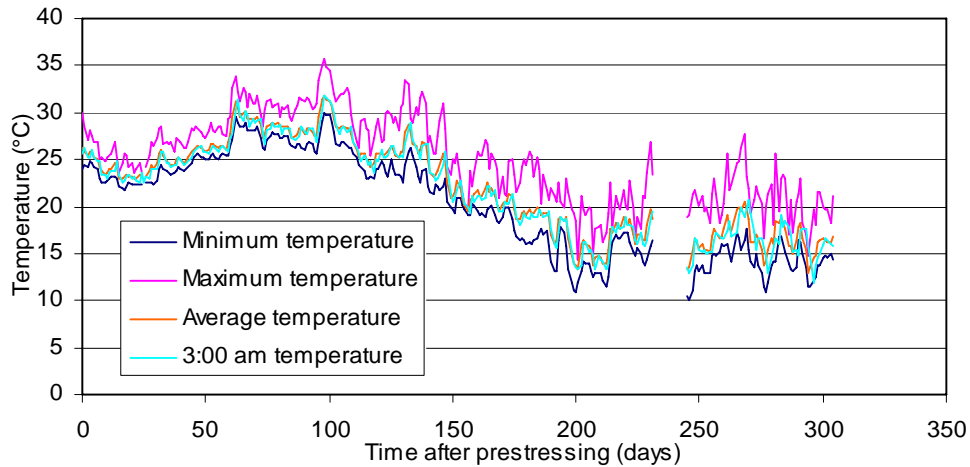


Figure 5.13: Temperature in Stem A of F5 in the web.

5.3.1.1.2. Interior Stem

Figure 5.8 to Figure 5.13 (in the previous section) examined the behavior of the strain and variation of temperature through the depth of an exterior girder, Stem A in F5 at midspan. In this section (Section 5.3.1.1.2), the strains and temperatures for an interior girder (Stem C in F5 at midspan) are presented to illustrate major differences in the daily variations that were experienced. As was mentioned previously, interior stems B and C at the levels of the gages in the web and in the soffit were never subject to direct solar radiation; however, the deck was subject to similar solar exposure throughout the day monitored by all gages. It is for this reason that the web and soffit in the interior girders experienced not only a decreased variation of temperature but a decreased range of thermal strains, as will be shown in the following figures in this section. It was chosen to display the temperatures and strains from F5 (as opposed to F4) for the same reason as that of the exterior stem (in Section 5.3.1.1.1). F4 was not monitored hourly beginning 60 days after prestressing, thus the daily extremes in temperature and strain are only extremes at two points in time and are not appropriate for describing the daily behavior. It was shown in Figure 5.6 and Figure 5.7 that the strains and temperatures in F4 and F5 were similar at corresponding points in time, thus the presentation of the F5 strains and

temperatures are appropriate for describing the behavior of respective stems. The strains and temperatures from F5 at midspan in Stem C are presented in Figure 5.14 to Figure 5.19.

In Figure 5.14, the strain progression with time in the deck of F5 at midspan is presented. It can be seen that the daily variation is about 50 microstrain; while in Figure 5.15 the daily variation in temperature is about 7 °C.

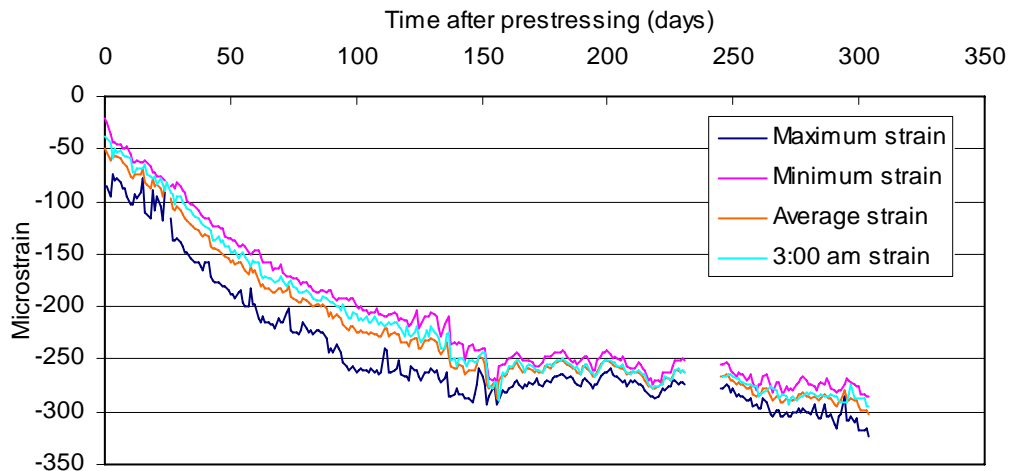


Figure 5.14: Strain in Stem C of F5 in the deck.

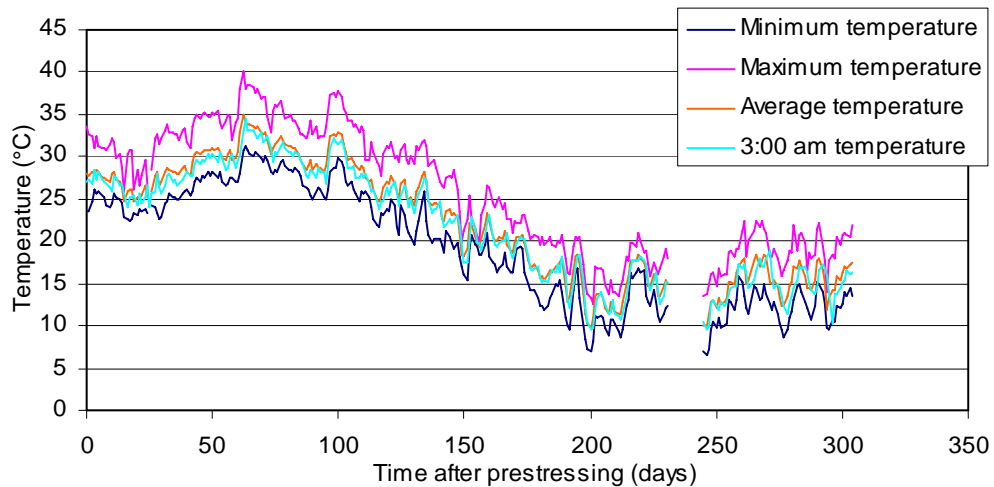


Figure 5.15: Temperature in Stem C of F5 in the deck.

Compared to the deck, the web and soffit experienced a small range of daily temperatures and strains, as indicated in Figure 5.16 and Figure 5.17, respectively. In the web of Stem C, the daily variation of strain did not exceed 25

microstrain while the variation in temperature never exceeded 1 °C throughout the duration of monitored data used in this Report.

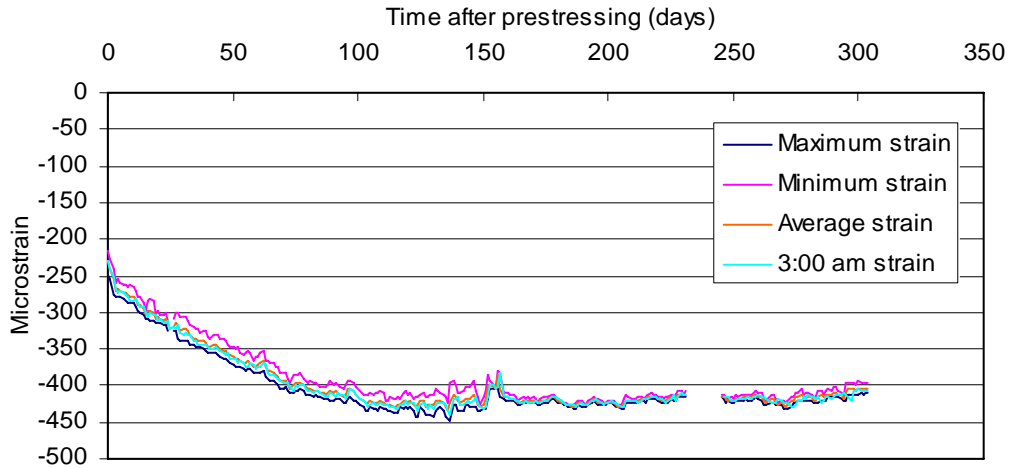


Figure 5.16: Strain in Stem C of F5 in the web.

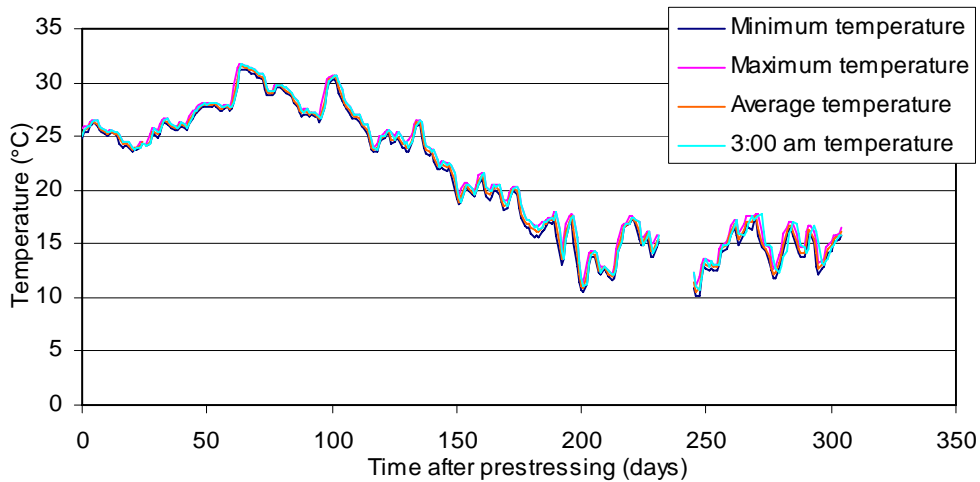


Figure 5.17: Temperature in Stem C of F5 in the web.

The soffit experienced a range of variation of about 30 microstrain for the first 150 days after prestressing, a range that increased to about 50 microstrain for the next 150 days, as shown in Figure 5.18. The range of temperature followed similar trends with the strain, indicated in Figure 5.19. This is not the result of the presence of falsework, as the falsework was removed 69 days after prestressing. For 150 days after prestressing, the temperature varied no more than 1 °C, but after about 150 days, the range of temperature variation increased to about 3 °C.

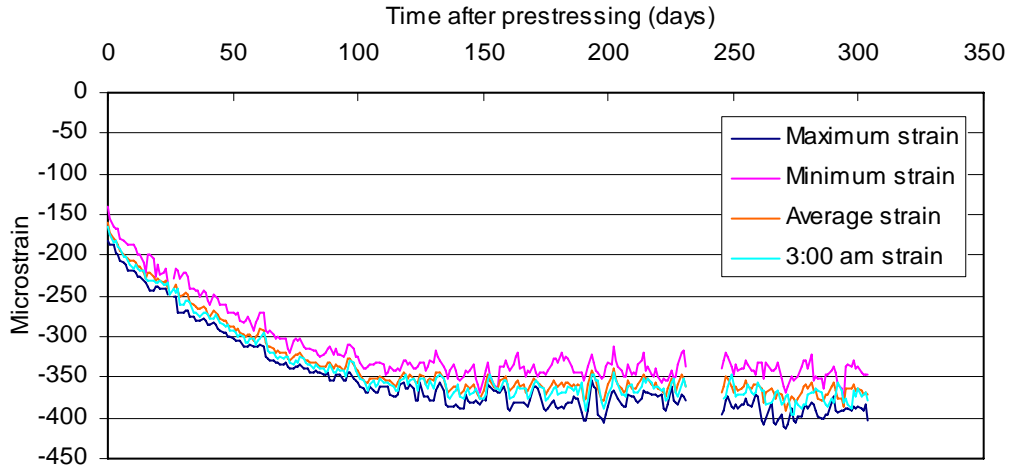


Figure 5.18: Strain in Stem C of F5 in the soffit.

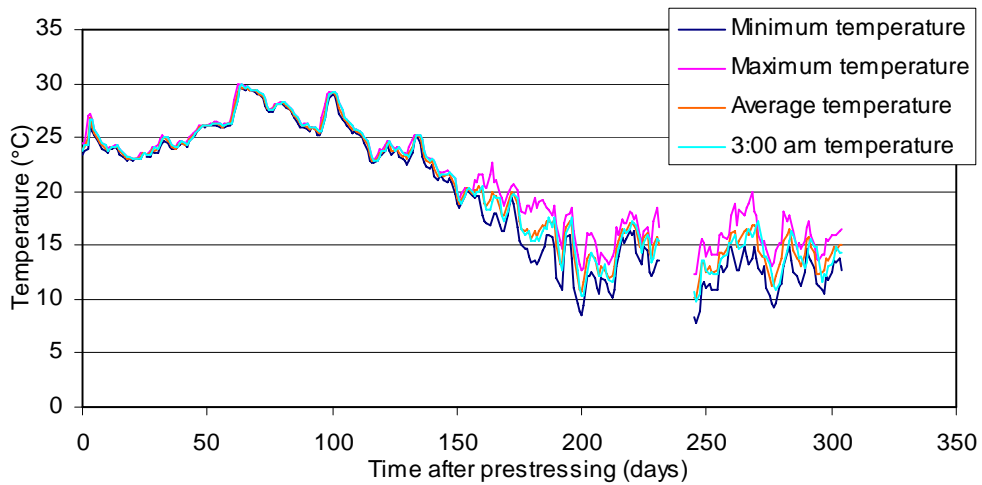


Figure 5.19: Temperature in Stem C of F5 in the soffit.

Of important note is the fact that the temperatures and strains presented in Figure 5.8 to Figure 5.13 through the depth of Stem A in F5 at midspan are representative of the behavior of Stem A at all four monitored sections. Similarly, in Figure 5.14 to Figure 5.19, the strains and temperatures presented for Stem C in F5 are representative of the monitored behavior of Stem C at the other monitored sections in F4 and F5 corresponding to Stem C. Although the strain and temperature data are presented here for the Stem A and Stem C locations only in F5 only, these locations are representative of the behavior of interior and exterior stems in general. The remaining data are presented for the other stems at monitored sections in both F4 and F5 in Appendix C.

It can be seen that the change in temperature correlates directly with a change in strain. As expected for concrete and in justification of the calculated thermal expansion coefficient, the maximum and minimum temperatures correlate with the minimum and maximum strain, respectively. Since the strains presented here indicate compression, increases in temperature reduce the compression and displays a reduction in the monitored strain.

It was apparent upon inspecting the temperature variations that existed during monitoring, that the presence of falsework was not a significant influence on the temperature in the concrete. The falsework materials create a barrier between the concrete and the ambient air and from direct solar radiation while it is in place. It can be seen, though, from Figure 5.4 and Figure 5.5, that after the falsework was removed (121 and 69 days after prestressing in F4 and F5, respectively), no significant changes in temperature were observed. The presence of falsework did not appear to alter the minimum and maximum temperatures that were experienced in the concrete. Rather, the falsework only shifted the time of day at which the extreme temperatures were observed.

5.3.1.1.3. Daily Temperature Variation

Figure 5.20 to Figure 5.23 demonstrate some of the behaviors identified in the previous sections. It is important to note that these figures only demonstrate the behavior over a single day in the two stems described, Stem A and C, from Sections 5.3.1.1.1 and 5.3.1.1.2.

In Stem A (Figure 5.20), the temperatures varied considerably throughout the day (100 days after prestressing), a range in excess of 10 °C in the deck. The temperature varied about 4 °C in the soffit and web. The temperature in the soffit did not vary within the period from 9:00 am to 3:00 pm, which is notable given that the solar radiation occurred on exterior Stem A during this time. The trend can also be observed that the temperature in the soffit exceeded the temperature in the web for the majority of the day by about 1 °C. Over the 24-hour period presented in Figure 5.20, the temperature profile through the section at the

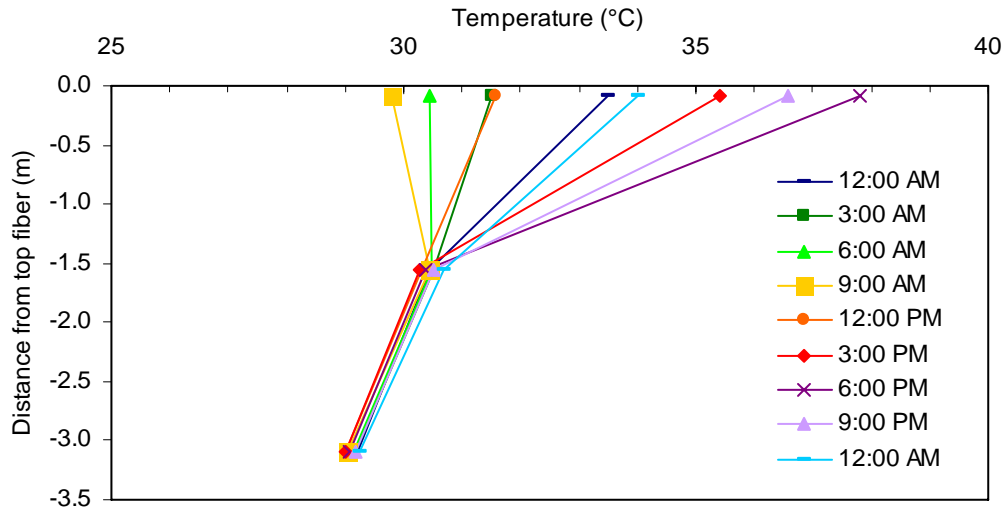


Figure 5.21: Temperature profile over a 24-hour period 100 days after prestressing in Stem C of F5 at midspan.

Figure 5.22 presents the temperature distribution through the depth of Stem A 150 days after prestressing over a period of 24 hours. It can be seen that the high temperature was experienced around 6:00 pm, similar to the other sections. Also, the low temperature was experienced around 9:00 am. The range of temperature variation is also similar to the Stem A section at 100 days after prestressing (Figure 5.20). The difference occurs in that the high temperature was not experienced in the deck, but the high temperature occurred in the web, with the deck temperature even lower than in the soffit. This is not behavior that is expected unless direct solar radiation is prevented throughout the day and only emerges later in the day to provide radiation to the vertical surfaces. It is not known, though, if this actually occurred, but serves as a reasonable explanation. Regardless of the reason for the occurrence, the treatment of thermal strain is the same.

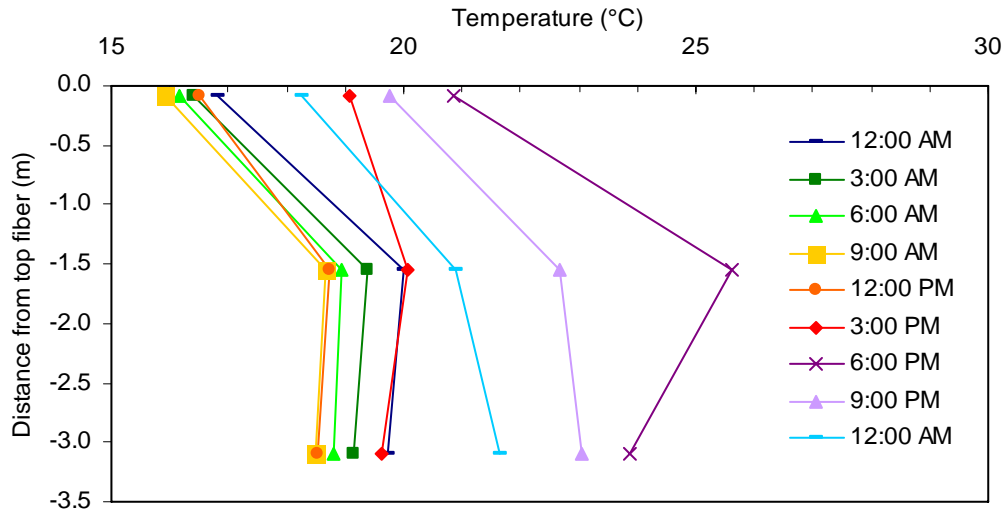


Figure 5.22: Temperature profile over a 24-hour period 150 days after prestressing in Stem A of F5 at midspan.

Figure 5.23 presents the temperature distribution through Stem C 150 days after prestressing. The temperatures in the soffit and web are reasonably consistent with the temperatures in the web and soffit in Stem A from 3:00 am to 12:00 pm. Similarly to the other presented temperature profiles the maximum temperature was experienced around 6:00 pm. The temperature in the deck at this time was almost the same as in Stem A at 21 °C.

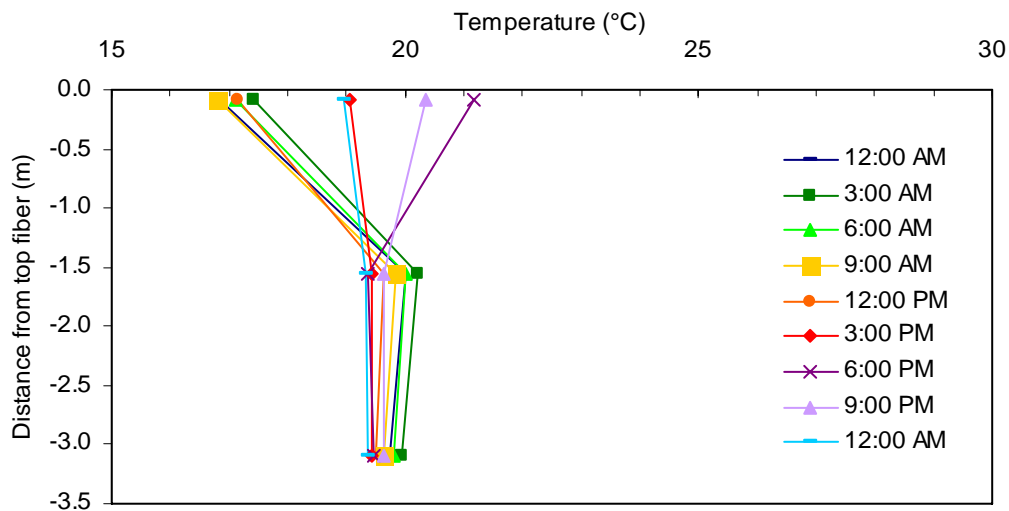


Figure 5.23: Temperature profile over a 24-hour period 150 days after prestressing in Stem C of F5 at midspan.

beginning of the day (12:00 am, 100 days after prestressing) is almost equivalent to the temperature profile through the section one day later (12:00 am, 101 days after prestressing).

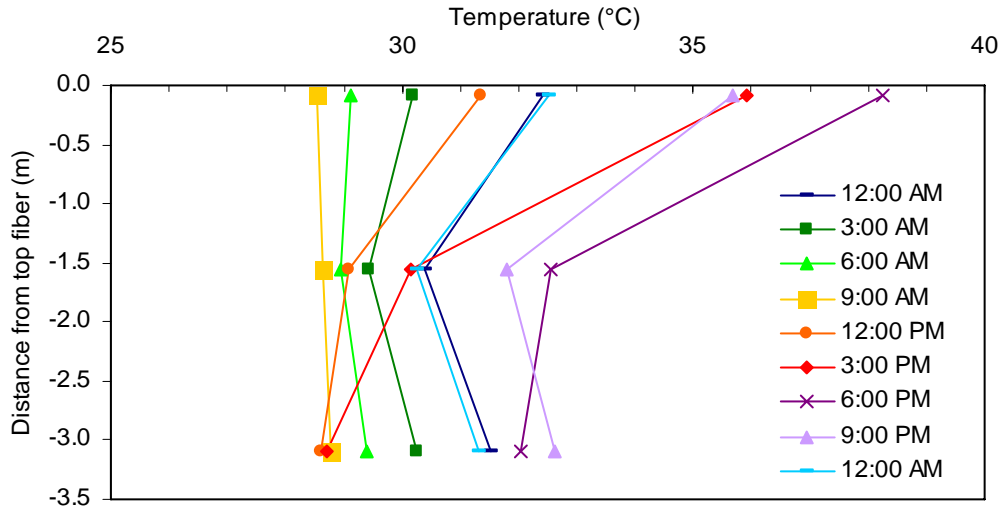


Figure 5.20: Temperature profile over a 24-hour period 100 days after prestressing in Stem A of F5 at midspan.

Figure 5.21 presents the temperature profile through the depth of Stem C at 100 days after prestressing, the same period of time presented for Stem A in Figure 5.20. It can be seen that a temperature variation only exists in the deck. In the web and soffit, the variation is minimal and less than 1 °C over the day. Similar to Stem A over the same time period, the range of temperature experienced over the day was about 8 °C.

The lowest temperature experienced in the soffit in Stem A was about the lowest temperature experienced in the soffit in Stem C; in Stem C, though, the lowest temperature was almost constant throughout the day. The daily high temperature was experienced at 6:00 pm in both Stem A and C in the deck.

From the previously presented figures, it is apparent that the behavior due to temperature is not consistently predictable. As it would be assumed, that the temperature in the deck would always exceed that in the soffit and web, it was shown that this does not always happen to be the case. The thermal influence is a significant factor in the deformation of the bridge and must be included in the analysis of structural strain. Consideration of thermal influence is complicated by the restraints provided through the columns and continuity of the structure.

5.3.1.2. Verification of Load Cases

The loading cases used for analysis were discussed in Section 4.6. The cases used in analysis were selected based on limitations of computer program CPF [16]. It was assumed (as mentioned in Section 4.6.1) that 50% of the structural self-weight was applied simultaneously with prestressing. The remaining 50% of the structural self-weight was activated with the removal of falsework. In F4, the removal of falsework was accompanied by the addition of load at the hinges from adjacent frames (Frame 3 and Frame 5). In F5, the additional load from the adjacent frame (Frame 6) was applied in a third instant of loading. The LC50/50 load case was used for the comparison of strains in Section 5.4 as this load case most accurately captures the actual loads in the bridge. The LC100/0 load case in Section 4.6.2 is used in Section 6.5 to demonstrate the use of a simplified load case to predict prestress loss and still retain accuracy.

Using the strain data obtained from monitoring it was possible to verify the load case assumptions for both frames. The method used was verified by comparing the change in value of bending moments when the falsework was removed. At this time, the full structural self-weight was applied. This can also be captured through analysis. By comparing the change in moments for the same instant during construction, it was possible to verify that the correct loads were applied at appropriate times in the analyses.

When the falsework is removed, the concrete undergoes an instantaneous change in strain, as depicted in Figure 5.24. Depending on the location (at

midspan or near the bent) the change in strain in the deck and the soffit are in opposing directions.

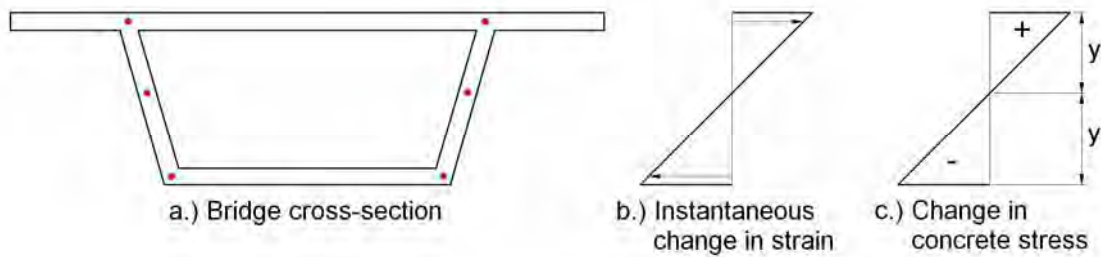


Figure 5.24: Determination of the change in moment from monitored data.

As expressed in Eq. 5.1, the change in strain can be used to determine the change in concrete stress by utilizing the modulus of elasticity of concrete.

$$\Delta\sigma = E_c\Delta\varepsilon \quad (5.1)$$

The change in concrete stress can be used to determine the change in moment.

$$\Delta M = \frac{I\Delta\sigma}{y} \quad (5.2)$$

Where the moment of inertia I and the depth of the centroidal axis y are based on the dimensions of the cross section and are easily determined.

In Section 5.3.2, the change in moment for each monitored location in F4 and F5 is compared to the change in moment that was obtained through structural analysis. Since the change occurs instantaneously, time-dependent properties do not influence the results.

5.3.2. Strain Results from Monitoring

This section presents the strains that were monitored in the bridge at all locations in F4 and F5 for the selected point in time (3:00 am).

5.3.2.1. Frame 4 Midspan

Gages were located in each stem in the deck, web, and soffit at each of the four monitored sections in F4 and F5. In Figure 5.26 to Figure 5.28 the strains at each gage depth for F4 at midspan are compared to illustrate trends between gages at corresponding depths through the transverse direction of each section. This is also done for the other monitored locations in F4 and F5 in Sections 5.3.2.2, 5.3.2.3, and 5.3.2.4. This comparison assures the accuracy of the strain existing at each gage depth of the sections. The strains presented in Figure 5.29 to Figure 5.32 will aid in assuring the validity of the gage readings in providing a realistic strain profile for each section. The strain profiles are presented for each stem, through the depth of the section, to illustrate the change in strain with respect to depth. Additionally, the upper and middle web level gages (see Figure 5.2) are only located in one stem at each location; the figures displaying the strain through the depth of the section make use of the additional web location gages in providing the strain profiles.

At prestressing, each of the four girders in F4 at midspan experienced about 85 microstrain in the deck, as shown in Figure 5.26. The monitored strain in the deck displayed a maximum variation of about 50 microstrain for the duration of monitoring. The strain in the deck increased nearly linearly to about 250 microstrain at 121 days after prestressing, immediately before the falsework was removed. When the falsework was removed, the concrete experienced an immediate increase in strain of 100 microstrain. The activation of additional self-weight resulted in a change in moment of 28.60 MN-m, determined using Eq. 5.2. The change in moment calculated from the monitored strain is consistent with the analytical change in moment of 29.90 MN-m, which is 4.5% greater than the actual change in moment. The changes in moment are presented graphically in Figure 5.25.

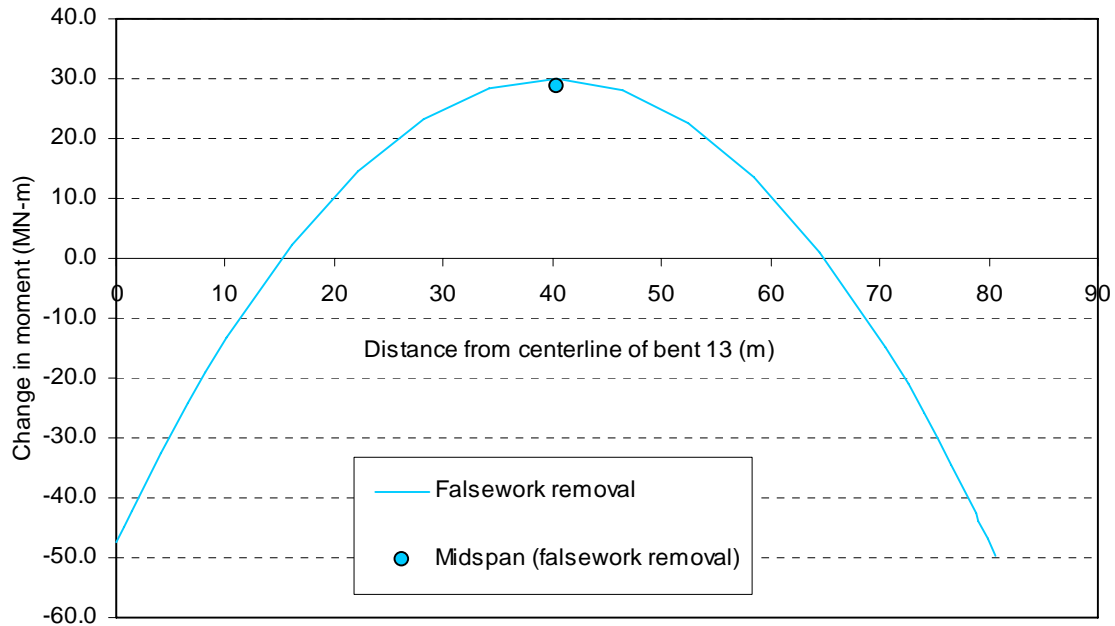


Figure 5.25: Change in moment for F4 at midspan.

The strain continued to increase after the removal of falsework (1.1 microstrain per day) at a similar rate that occurred before the falsework was removed, nearly linearly until about 200 days after prestressing. Beginning at 200 days, the change in strain dramatically decreased. Between 200 days and T363 (a period of about 163 days) the strain increased about 25 microstrain and appeared to be approaching an asymptotic value between 400 and 500 microstrain.

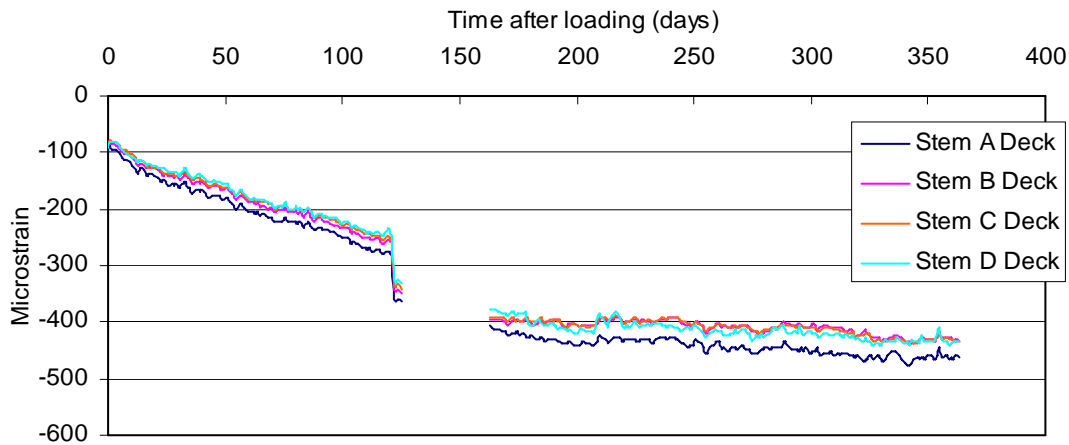


Figure 5.26: Monitored strain in the deck at 3:00 am in F4 at the midspan section.

In the web of F4 at midspan, the strain increased immediately upon prestressing to about 170 microstrain, as shown in Figure 5.27. Over the next 15 days, the strain increased by about 50 microstrain. After this time the rate of change decreased to a nearly linear rate of 1.1 microstrain per day to a point in time about 200 days after prestressing. When the falsework was removed, neither the rate of change of strain or the absolute strain changed. The reason for this is that the web gages were placed near the centroid of the section for which only change in strain from the added moment occurs at the extreme fibers; no change occurs in the strain near the centroid of the section.

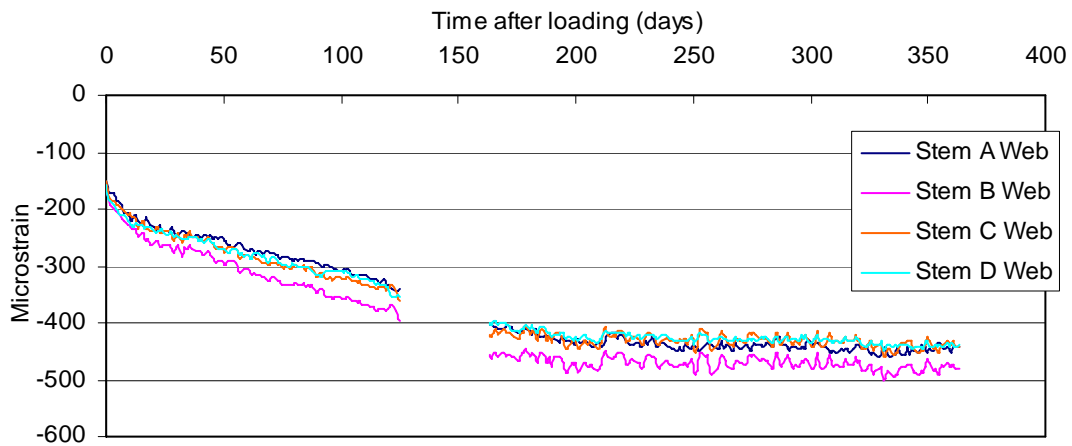


Figure 5.27: Monitored strain in the web at 3:00 am in F4 at the midspan section.

In the soffit (F4 midspan), the girders underwent about 240 microstrain of shortening when prestress was applied, as shown in Figure 5.28. In each stem, the strain progressed nearly linearly for a period of 121 days to the point at which the falsework was removed. At this time, the removal of falsework activated the remaining structural self-weight, which applied tension to the soffit and a decrease in strain of about 100 microstrain, characteristic of a change in moment of 28.60 MN-m from the monitored strain. After this time, the strain progressed at a similar rate as that before the removal of falsework until about 200 days after prestressing. Between the period 200 days after prestressing to T363, the concrete only experienced daily fluctuations in strain and appeared to have

reached an asymptotic value of 370 to 470 microstrain that varied between stems.

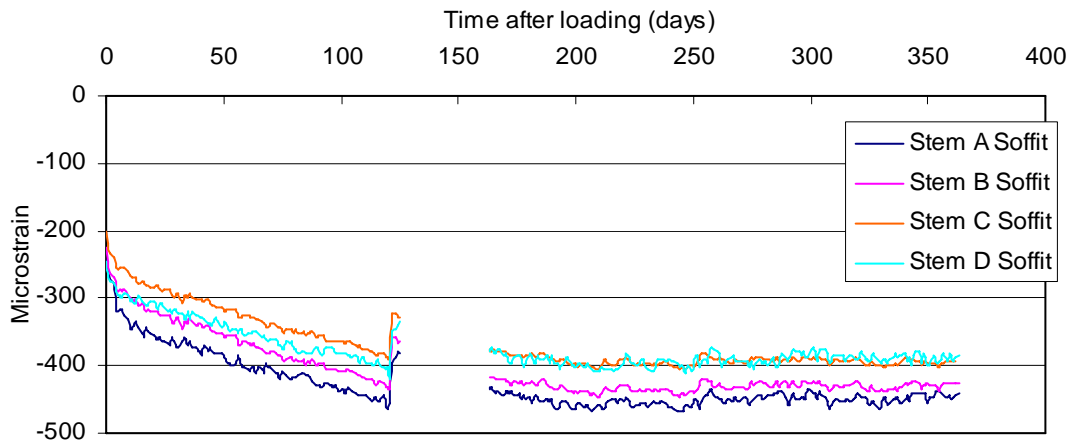


Figure 5.28: Monitored strain in the soffit at 3:00 am in F4 at the midspan section.

In Figure 5.29 to Figure 5.32 the strains in the individual stems are presented to illustrate the general progression of strain in each stem. In Figure 5.26 to Figure 5.28, it can be seen that the strains in the deck, web, and soffit progressed similarly at each respective gage level over the course of monitoring from prestressing to T363. Figure 5.29 to Figure 5.32 show the monitored strains through the depths of each stem in F4 at midspan. Aside from the upper and middle level gage readings in Stem D (Figure 5.32), the strains are the same as those presented in Figure 5.26 to Figure 5.28, thus the same reason for changes in strain exist as before. In Figure 5.29 to Figure 5.32, the representations illustrate more effectively the change in curvature with the added moment occurring when the falsework was removed. Additional implications that can be seen from these figures are that the curvature (and hence the strain profile) change substantially during monitoring. This will be shown in Figure 5.44 for specific points in time, but can be seen in Figure 5.29 to Figure 5.32 for the duration of monitoring.

It can be seen that immediately preceding prestressing, the strain in the deck and soffit varied by about 200 microstrain, a difference that was upheld until the removal of falsework 121 days after prestressing. After the falsework was

removed, the difference in strain between the deck and soffit decreased dramatically to about 50 microstrain in each stem. The progression of strain from this point on varied almost negligibly in Stem A (Figure 5.29) to about 100 microstrain in Stem D (Figure 5.32), a spread that appeared to increase slowly with time. Stems B and C experienced a range of variation between the deck and soffit locations of about 60 microstrain after the falsework was removed. Given that F4 is curved and, at midspan, the most significant influence of the prestress in the transverse direction takes place, it is expected that some differences between stems would occur in the long-term strain, which appears to be the occurrence here; however, plane frame analysis cannot verify this due to the horizontal curvature of the bridge.

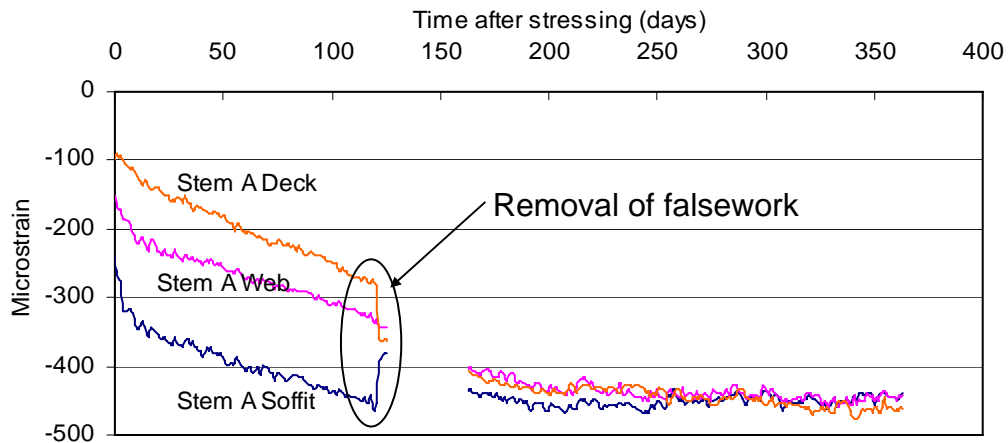


Figure 5.29: Monitored strains in Stem A in F4 at midspan.

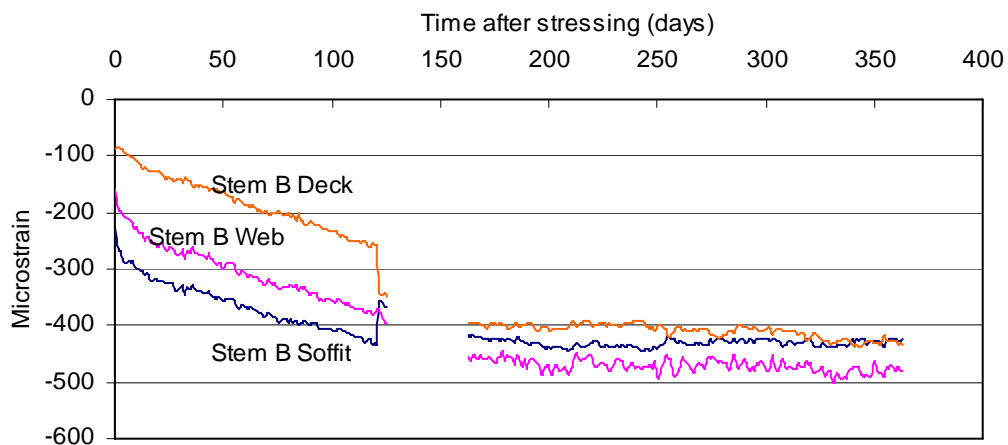


Figure 5.30: Monitored strains in Stem B in F4 at midspan.

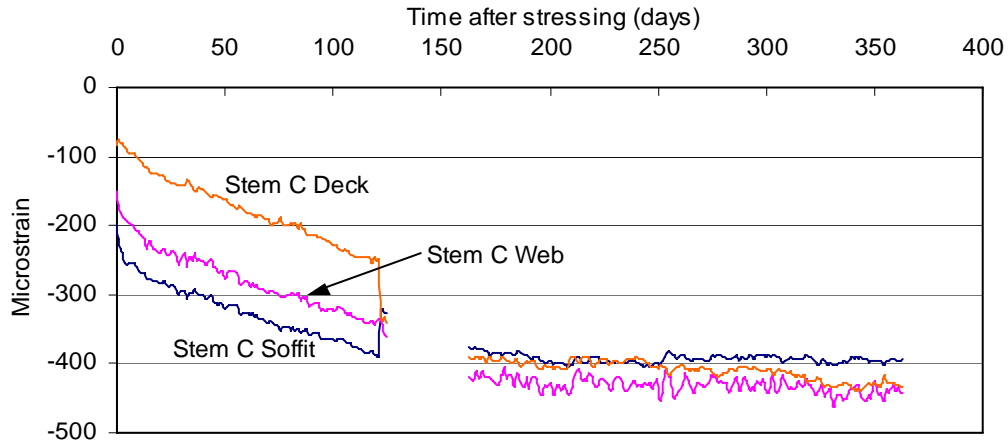


Figure 5.31: Monitored strains in Stem C in F4 at midspan.

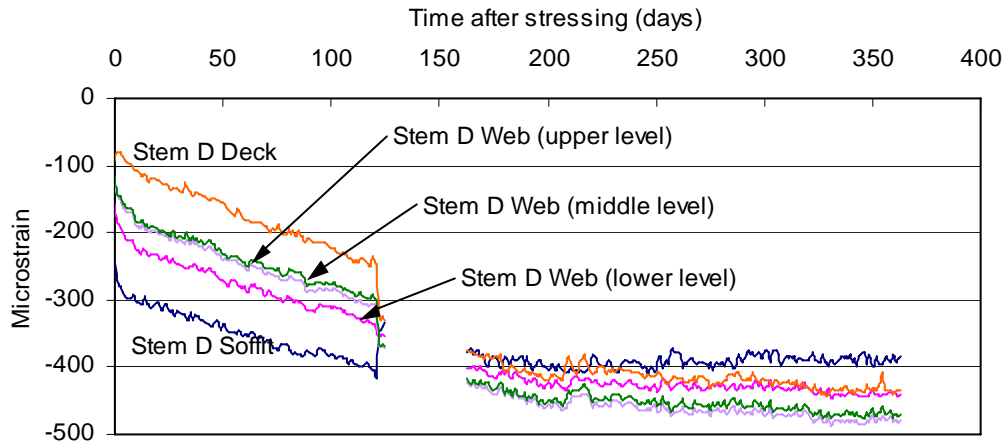


Figure 5.32: Monitored strains in Stem D in F4 at midspan.

It was apparent upon visual inspection of the data which gages followed a linear strain profile and those with likely malfunctions. Several different methods were used to assess the validity of the gage readings, as will be explained for each instance in which unreasonable readings were likely. Stem A, in which the tendons were stressed 5 days prior to the tendons in the other stems, exhibited similar deformation to the other stems, despite the different times of prestressing.

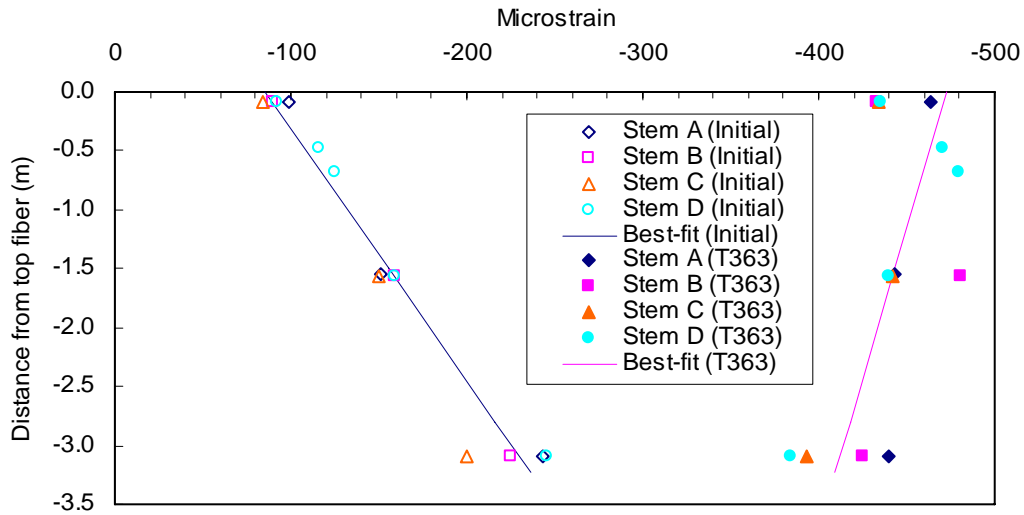


Figure 5.33: Monitored strain profile at prestressing and at T363 in F4 at midspan without faulty gage readings at 3:00 am.

It can be seen in Figure 5.33 that the initial strain readings follow a linear profile, as illustrated with the best-fit line, determined using a least-squares linear regression of the data. Gage readings that varied significantly and did not support a linear profile were discarded for all points in time. The strain readings for T363 follow reasonably a linear profile, which is similarly indicated by a best-fit line. It is important to note that the curvature changes from the initial profile to T363. A reversal of curvature, as indicated by the monitored data, signifies that the bridge has undergone displacement from upward camber to downward deflection.

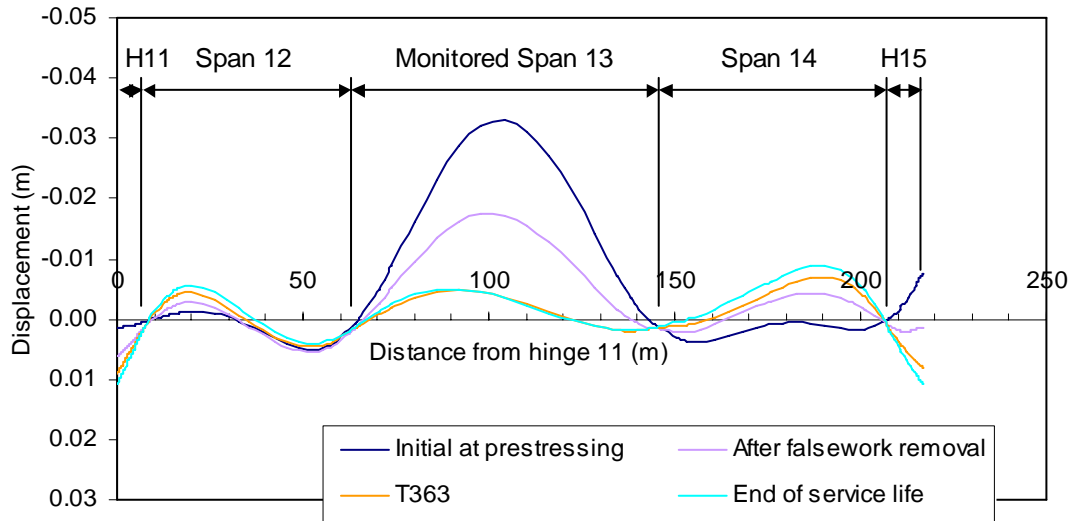


Figure 5.34: Vertical displacement of F4 at midspan.

The displacement results are provided through analysis and are not actual measured displacement (as this was not measured as part of the research). It will be shown in Section 5.4 that the strains indicated through computer analysis of F4 and F5 correlate with the monitored strain over the period for which monitored data exist. Since the strains and curvatures are directly influenced by the deformation of the entire structure, it is appropriate to use the analytical results to demonstrate the deformation of the actual bridge. Figure 5.34 displays the computed displacements for F4 at various points during the life of the structure.

5.3.2.2. Frame 4 Near the Bent

Only one of three tendons (of 12 total in F4) in Stem A was prestressed before the prestressing equipment malfunctioned, as mentioned in Section 0. In Figure 5.39 the difference in strain in Stem A can be seen compared to the strains recorded in Stems B, C and D (Figure 5.40 to Figure 5.42). The strain in the soffit indicated by the Stem A gage (Figure 5.37) does not indicate strain that suggests different behavior occurring from the other stems. The reason for this is that the soffit is the furthest section from the prestressing tendons at the near-bent location. Thus, the prestress has the least influence on the soffit, as can be seen in the data. Since only one strain profile can exist for a section that is to be

compared to a plane frame analysis, the strains that showed most variation from the other gages required elimination in order to generate strain profiles that were most representative.

When the prestress was fully applied to all stems, the concrete exhibited a shortening of about 200 microstrain in the deck in each of the four stems, as shown in Figure 5.35. Starting immediately after the application of prestress, the strain in the deck progressed nearly linearly at a rate of about 1.4 to 2.4 microstrain per day until immediately before the falsework was removed. Stem A displayed the least amount of strain compared to the other three stems. This occurrence was brought about by the fact that one tendon in Stem A was prestressed five days before the tendons in the other girders. The application of prestress to the tendons initiates creep, with the maximum creep rate occurring immediately after the application of the prestress load (2.4 microstrain per day). Since Stem A was allowed to creep for a few days before the remaining tendons were stressed, the strain that occurred in Stem A was less compared to that in the other stems because creep strain had already commenced.

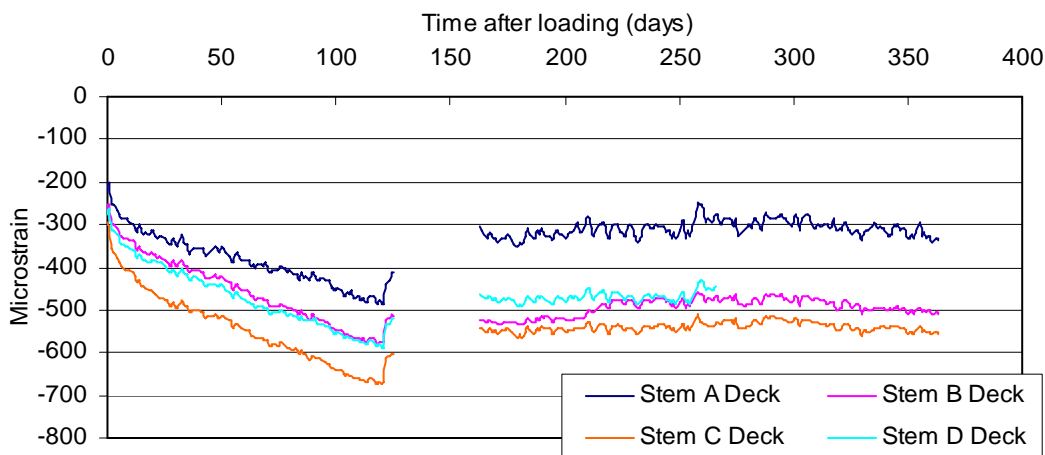


Figure 5.35: Monitored strain in the deck at 3:00 am in F4 at the near-bent section.

In Figure 5.36 the strains in the web are presented. The strains indicated through monitoring by the gages in Stems B, C, and D follow very consistent trends with a maximum variation of about 35 microstrain between the three gages at any time. The gages in Stems B, C, and D indicate initial strain at

prestressing of about 80 microstrain. The strain increased in each of these three stems to a value of about 180 microstrain at T363 at which time the strain appeared to have reached an approximately asymptotic value. In Stem A, the initial strain in Stem A at prestressing was 135 microstrain. The strain in Stem A progressed to 330 microstrain at T363, a value about 100% larger than that indicated by the other gages in the stems at the same gage level.

Considering the grouping of the Stem B, C, and D gages and the range of variation of about 35 microstrain, it would appear that only the Stem A gage indicated a faulty value. In the absence of strain data from the deck and soffit, this explanation could hold reasonable credibility. This is not the case, though. As shown in Figure 5.40, Figure 5.41, and Figure 5.42 the strains in the web did not maintain a linear relationship with the gages in the deck and soffit. This behavior could be explained if the section was cracked or if a considerable temperature gradient existed through the section that demonstrated significant non-linearity beyond what would normally be expected. Neither of these two situations existed for the bridge and thus must be eliminated as possible explanations. Since the strain profile can reasonably be expressed to be linear and consistent through all stems for a plane frame, the Stem B, C, and D gage readings were not used in creating a strain profile for F4 near the bent. Figure 5.44 displays the strain, in the web of Stem A, remained linear with the strains indicated by the gages in the deck and soffit.

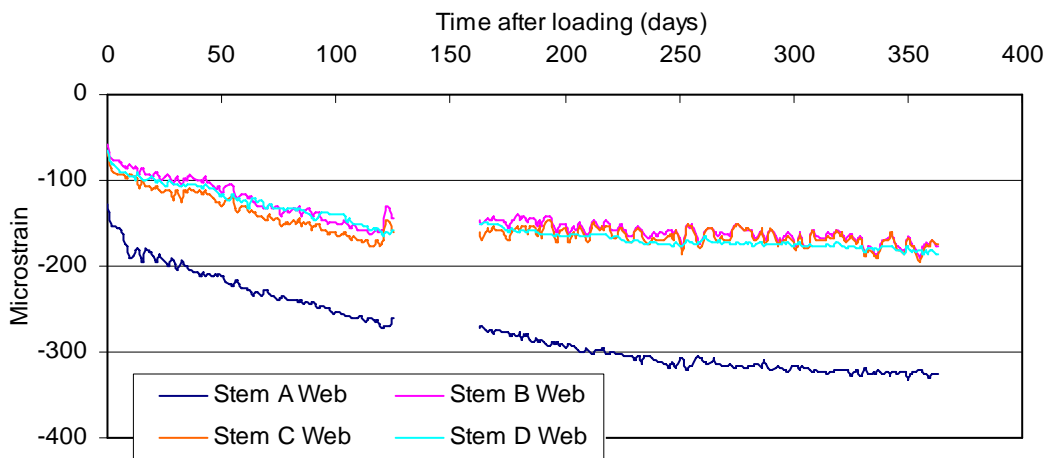


Figure 5.36: Monitored strain in the web at 3:00 am in F4 at the near-bent section.

Figure 5.37 displays the behavior of the monitored strain in the soffit. When the prestress was fully applied, the strain in the four stems immediately increased to about 70 microstrain. The progression of strain in each of the stems occurred at approximately the same rate during monitoring with a maximum variation of about 55 microstrain between the highest and lowest monitored strain values at any point in time. When the falsework was removed at 121 days after prestressing, the strain increased uniformly by about 70 microstrain, though the total strain value after the removal of falsework varied between 190 and 240 microstrain. After the falsework was removed, the strain increased rapidly during the period that power was lost to the data-logging equipment. Though there is no data for the 38 days that power was lost, it is apparent upon visual inspection that the strain demonstrated further increase for about 50 days after the falsework was removed. Beginning around 200 days after prestressing, the strain increased at a low rate of about 0.2 microstrain per day compared to the initial progression after prestressing was applied.

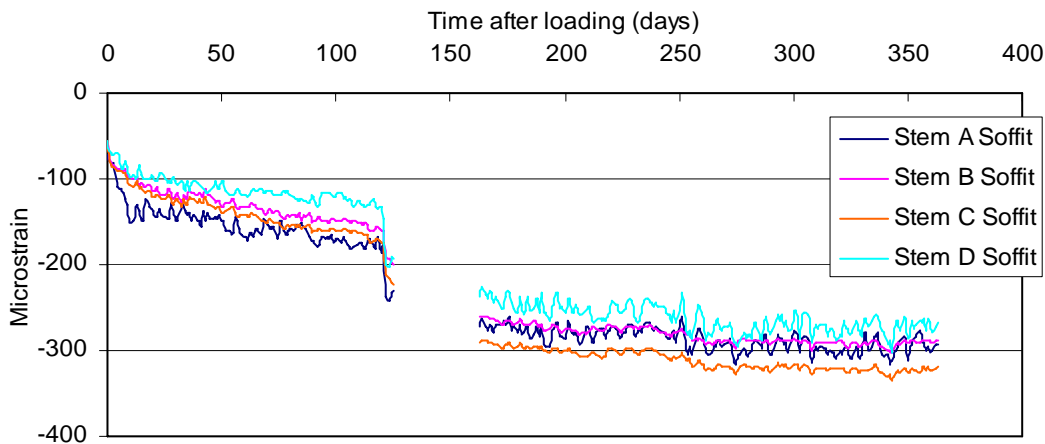


Figure 5.37: Monitored strain in the soffit at 3:00 am in F4 at the near-bent section.

The initial strain in the deck was not as consistent as in the soffit when prestress was fully applied. The fact that the strain increased from Stem A to Stem C by about 50 microstrain per stem, but decreased by about 50 microstrain in Stem D indicates some configuration influences. Stem A is on the inside of

horizontal curvature, which places more stress on the outside curve of the superstructure. The influence of the bent cap is different between stem locations as well as the influence of the bent in providing bending and torsional restraints on the section. Because plane frame analysis was performed, these influences cannot be verified.

The initial elastic deformation among the four stems was similar immediately following prestressing, but a difference in behavior can be seen with the development of strain that occurs over time between Stem A and Stems B, C, and D. Stems B, C, and D deform approximately the same over the monitoring period, as evidenced in Figure 5.40 to Figure 5.42. In Stems B, C, and D, after the initial 85 microstrain occurred at prestressing, the strain increased to about 150 microstrain at both the soffit and web gage levels up to a point immediately before the removal of falsework, at 121 days after prestressing.

The removal of falsework created considerable change in the strains. As mentioned previously, the removal of falsework activates the remaining self-weight of the structure adding moment to the near-bent location. The additional moment at this location causes an immediate change in strain at the extreme fibers of the section. Opposite to that at midspan, the additional moment causes tension in the top fiber and compression in the bottom fiber. With the removal of falsework, the strain in the deck and soffit exhibited significantly different behavior. Unfortunately, since power to the data logger for F4 was lost four days after the falsework was removed (125 days after prestressing) for a period of 38 days, the exact progression of strain cannot be seen. After power was restored to the data logger, the strains in Stems B, C, and D progressed to a value around 300 microstrain in the soffit. In the deck, the strain varied from about 400 to 500 microstrain at T363.

When the falsework was removed, the added self-weight was activated inducing a change in moment of -34.47 MN-m at the bent, calculated from Eq. 5.2. The additional load creates tension in the deck and compression in the soffit. A change in moment of -42.58 MN-m was determined analytically and is 23.5%

greater than the change in moment obtained from the monitored strain. The changes in moment determined using the monitored strain data and from analysis are presented in Figure 5.38.

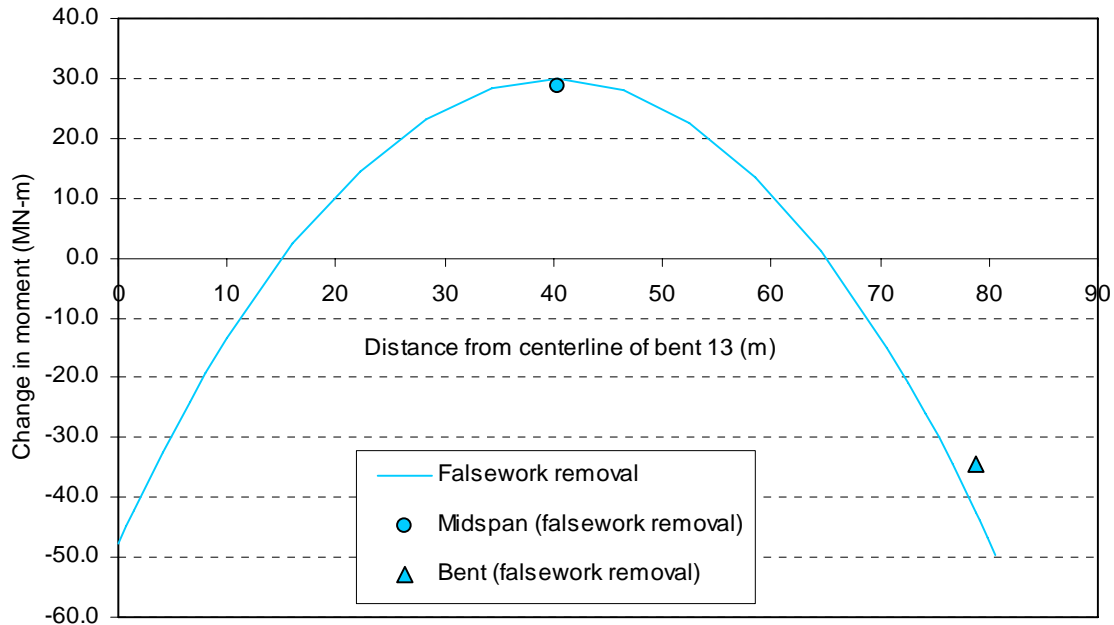


Figure 5.38: Change in moment for F4 at midspan and near the bent.

In Figure 5.39 it is clear that the operation of prestressing the tendons in the four girders at different times significantly altered the behavior of the bridge. Compared to the monitored strains in Stems B, C, and D (displayed in Figure 5.40 to Figure 5.42), the Stem A strain (Figure 5.39) follows a very different development. As discussed previously in this section, the strain in the web did not remain linearly correlated with the strains in the deck and soffit in Stems B, C, and D. Comparatively, the strains in the webs at the monitored locations in F5 follow more closely a linear profile as shown in Sections 5.3.2.3 and 5.3.2.4. The more routine procedure of prestressing in F5 results in the improved linearity of the strain profiles.

In the web, little to no change in strain is measured since the gages in the web are located near the centroid of the section. The change in curvature occurred about the centroid of the section and no change in strain occurred at this depth of the section as indicated by the gages. Stem A is the only location in F4 near the

bent that displays, for all points during monitoring, a strain profile that is linear. In all stems at the F4 near-bent location, the strain in the soffit displayed an increase of 90 microstrain when the falsework was removed, characteristic of compression resulting from the added self-weight and change in moment of -34.47 MN-m. In the deck, the strain decreased by 90 microstrain when the falsework was removed, characteristic of resulting tension induced by the added moment from self-weight. In Stems B, C, and D (Figure 5.40 to Figure 5.42), the strain in the web displayed no change when the falsework was removed, which is expected for strain near the centroid of the section. Despite this, the gages in the webs of these three stems increased at the same rate as that in the soffit to the point at which the falsework was removed. This behavior is not expected for the reasons mentioned previously and is grounds for discounting the readings of these gages.

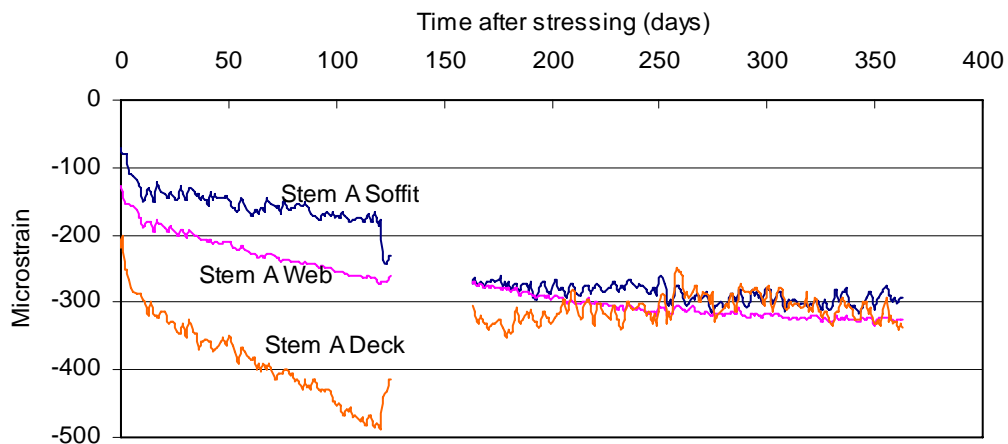


Figure 5.39: Monitored strains in Stem A in F4 near the bent.

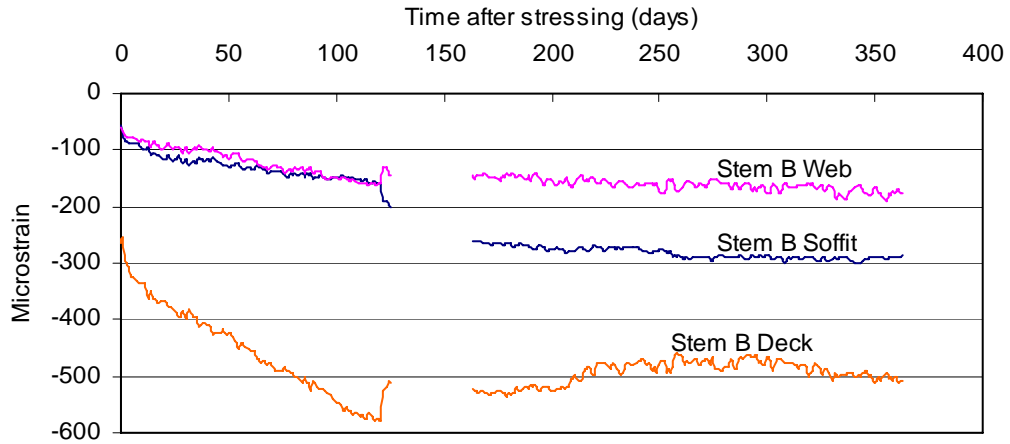


Figure 5.40: Monitored strains in Stem B in F4 near the bent.

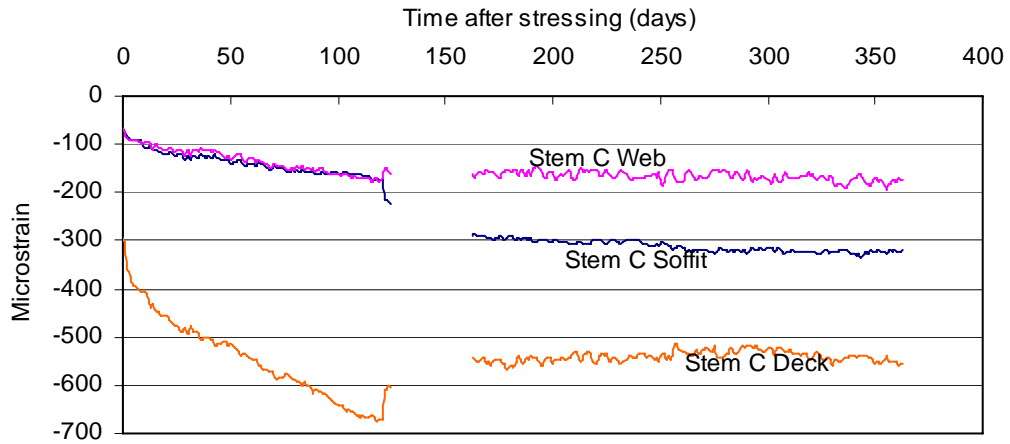


Figure 5.41: Monitored strains in Stem C in F4 near the bent.

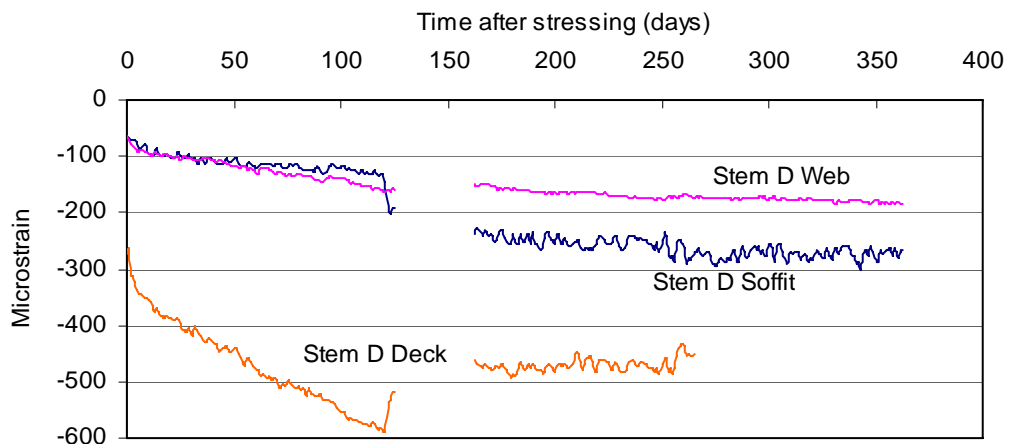


Figure 5.42: Monitored strains in Stem D in F4 near the bent.

Examining Figure 5.43 puts the aforementioned trends into perspective. As mentioned, the strain in the soffit and web was nearly the same in Stems B, C, and D at the application of prestressing to the point at which the falsework was removed. This is evidenced in Figure 5.43 showing almost the same strain values for the three web level gages in the initial strain profile as indicated in the figure. The strain in the deck far exceeded the strain in the webs and soffit. At T363, the differences in strain are further pronounced. The strain at the web level changes the least compared to the strains from the other gages in the deck and soffit, from prestressing to T363. Both the upper and middle web level gages indicated strains that were not realistic for the duration of monitoring. One gage indicated zero strain. The other gage indicated strains that varied by several thousand microstrain in both the tensile and compressive regions between consecutive days. All four of the gage readings at the soffit level are tightly grouped with a maximum spread of about 20 microstrain at all instances during monitoring and are very likely valid. The strain in the deck at prestressing was tightly grouped. At T363, the grouping of strain in the deck had spread; however, signify that the curvature had not changed over this period of time. One of the deck level gages malfunctioned partially through the monitoring period, as indicated in Figure 5.42; however, it remained capable of providing indications of temperatures for the location.

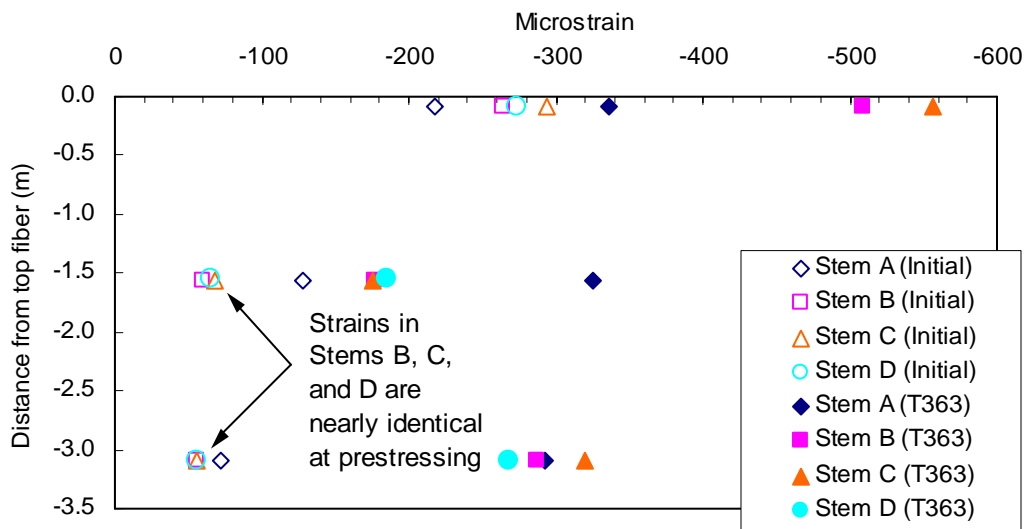


Figure 5.43: Monitored strains at prestressing and T363 in F4 near the bent at 3:00 am.

In selecting the gages that were not indicative of the actual strain, several scenarios were considered. If the deck level gages were disregarded, as well as the Stem A gage reading at the web level, a best-fit line through the soffit and deck level gages would appear to be nearly vertical. This is not behavior that can be expected since the prestress and self-weight create large moments at the bent. These moments typically counteract one another; however, since the falsework was in place when prestress was applied, the full self-weight was not able to fully balance the prestress moment. For moments from prestressing and self-weight that balance, a vertical strain profile is possible, but in this case, the falsework restraints would not allow this behavior to occur. From the previous discussion, the strain profile in F4 near the bent appears in Figure 5.44.

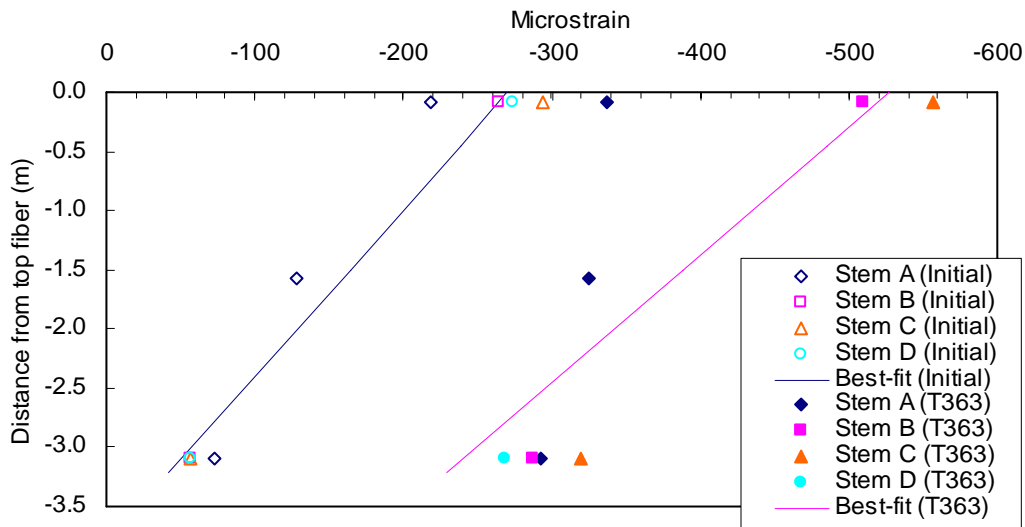


Figure 5.44: Monitored strain profile at prestressing and T363 in F4 near the bent without faulty gage readings at 3:00 am.

5.3.2.3. Frame 5 Midspan

When prestress was applied to F5, the shortening in the deck was about 60 microstrain, which is consistently indicated in Stems B, C, and D, as shown in Figure 5.46. The gage in the deck portion of Stem A was identified as a malfunctioned gage by the fact that the strain readings varied by several thousand microstrain in both tensile and compressive directions. However, the

gage remained capable of indicating temperature. One area of particular note in the monitored data for both sections in F4 and F5 at midspan, at all gage levels, is the difference in the rate of increase in strain. In F4, after prestressing, the strain increased linearly until a point around 200 days after prestressing. In F5, the strain did not increase at a linear rate, but followed a curved progression. A further difference is that when the falsework was removed in F5, the strain at midspan did not change noticeably and the progression of strain continued at about the same rate as before the falsework was removed.

Unlike the instant when the falsework was removed in F4 at midspan, (Figure 5.26 to Figure 5.28), in F5 at midspan, the falsework removal is almost unobservable in the strain profiles, as shown in Figure 5.46 to Figure 5.48 (69 days after prestressing). When the falsework was removed, the change in strain of 45 microstrain was used to determine the change in moment using Eq. 5.2. The change in moment was calculated as 7.92 MN-m. Performing analysis yields a change in moment 7.49 MN-m, which is 5.4% less than the change in moment obtained using the monitored strain. It must be noted that the change in strain used to calculate the change in moment was essentially the same as the daily change in monitored strain from thermal influences and additional construction loads. If the change in strain used to determine the 7.92 MN-m change in moment were considered noise, a change in moment of 0 MN-m would be obtained. Regardless of the change in strain used, the change in moment is small, which is supported by analysis.

A significant, but temporary, change occurred in the strain when the hinge was loaded at 156 days after prestressing. The load applied at the hinge is 3.82 MN and creates an additional moment of 1.23 MN-m at the midspan location determined from the monitored data using Eq. 5.2. This compares to the 0.99 MN-m change in analytical moment, which is 19.5% less than the change obtained from the monitored data. The changes in moment determined from the monitored data and from analysis are shown in Figure 5.45.

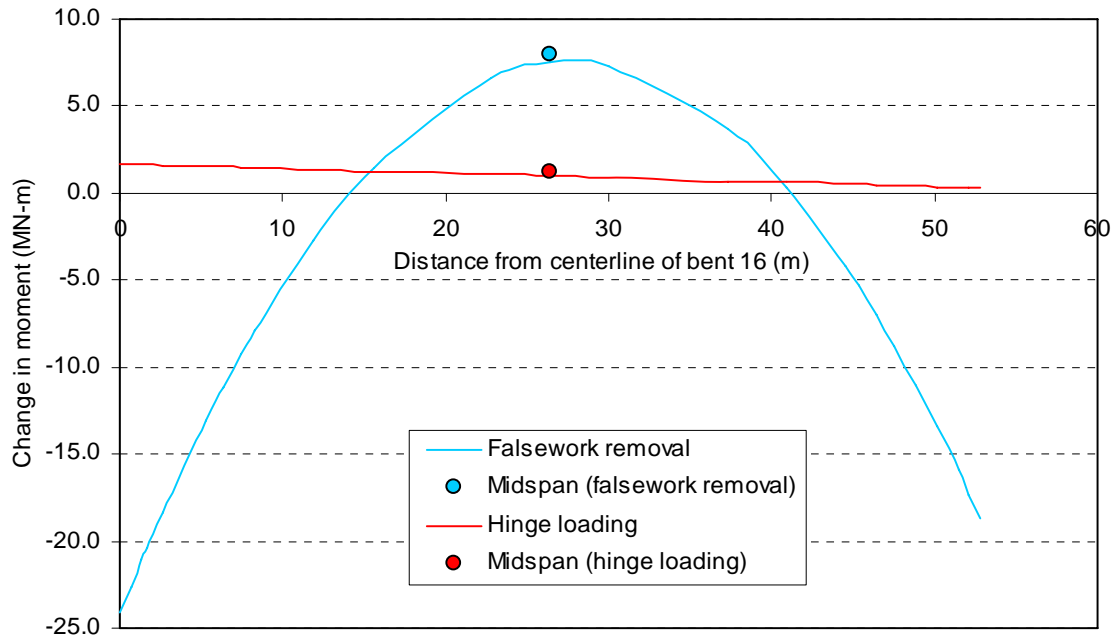


Figure 5.45: Change in moment for F5 at midspan.

As indicated through analysis presented later (Section 5.4), the change in moment mentioned above creates almost no change in curvature through the section, which is demonstrated by the monitored data beginning about 10 days after the hinge was loaded. The monitored data, though, within about 10 days after the hinge was loaded, indicate that a small change in curvature occurred during this time. This change occurs since the falsework supporting the hinge could not be removed at once. Portions of the hinge retained external support during this process and other areas were not supported, the strain adjusted according to the restraints imposed on the section. After the hinge supporting falsework was completely removed, the structure was free to deform and did not display permanent change in strain. Beginning soon after the hinge was loaded, the rate of change in the strain dramatically reduced. At T303, the strain had increased about 40 microstrain in about 150 days, which compared to the initial change in strain in the first 150 days after prestressing, 200 to 250 microstrain, is distinctly lower.

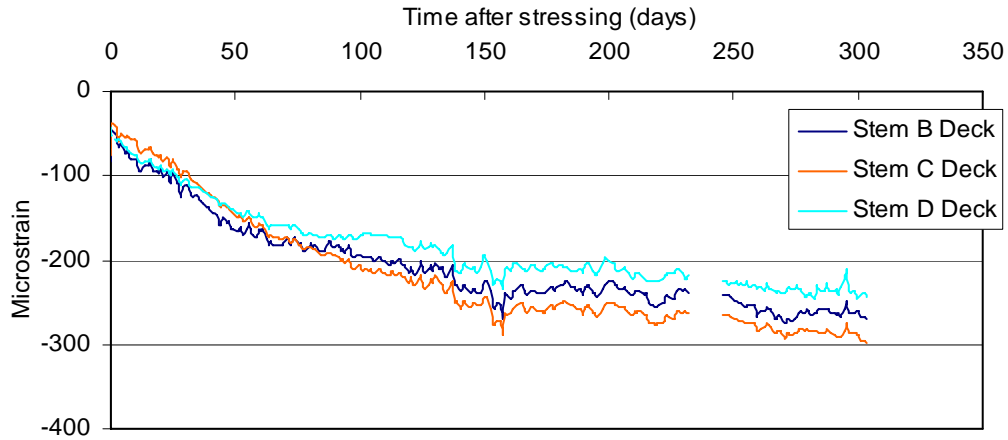


Figure 5.46: Monitored strain in the deck at 3:00 am in F5 at the midspan section.

In the web of F5 at midspan, the strain increased immediately when prestressing was applied to about 160 microstrain, as shown in Figure 5.47. Throughout monitoring, the gages in the web indicated a spread of data about 50 microstrain. When the hinge load was applied, no change in strain occurred as identified by gages located near the centroid of the section. Beginning about 150 days after prestressing, the change in strain was minimal and appeared to have approached an asymptotic value between 330 and 380 microstrain, with all fluctuations in strain occurring between consecutive days.

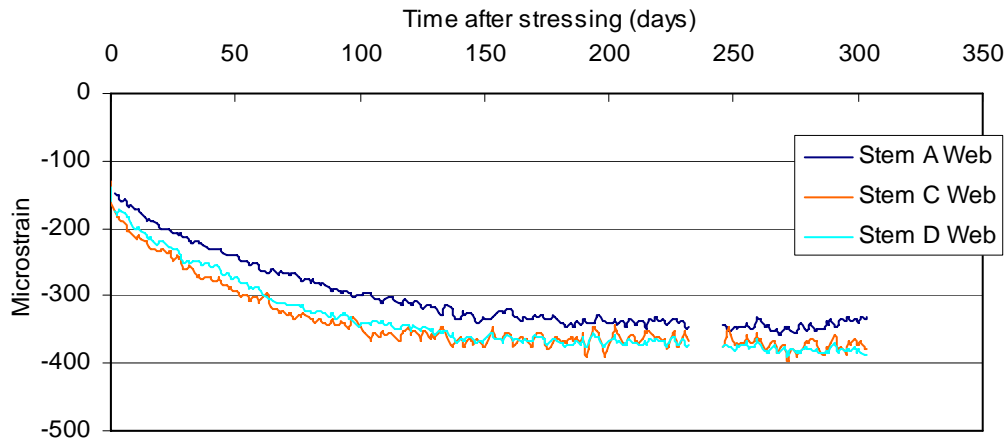


Figure 5.47: Monitored strain in the web at 3:00 am in F5 at the midspan section.

In the soffit, each of the gages indicated about 240 microstrain of shortening when prestressing was applied, as shown in Figure 5.48. For the duration of

monitoring, the gages displayed a maximum variation of strain within 40 microstrain. As similarly observed at the deck and web gage locations in F5 at midspan (Figure 5.46 and Figure 5.47), the additional load induced by the hinge created insignificant change in strain and did not alter the development rate of strain. In contrast to the behavior in the deck, the additional load from the hinge caused tension in the soffit and decreased the strain by about 60 microstrain. As mentioned previously, the additional moment induced by loading the hinge was not large enough to cause major changes in the deformation, which is indicated by the monitored data about 10 days after the hinge was loaded. The reason for the change is that the falsework supporting the hinge was not removed all at once, but over a period of several days, allowing temporary deformation, but, provided the comparatively small additional moment (compared to the existing moment before hinge loading), the change did not persist.

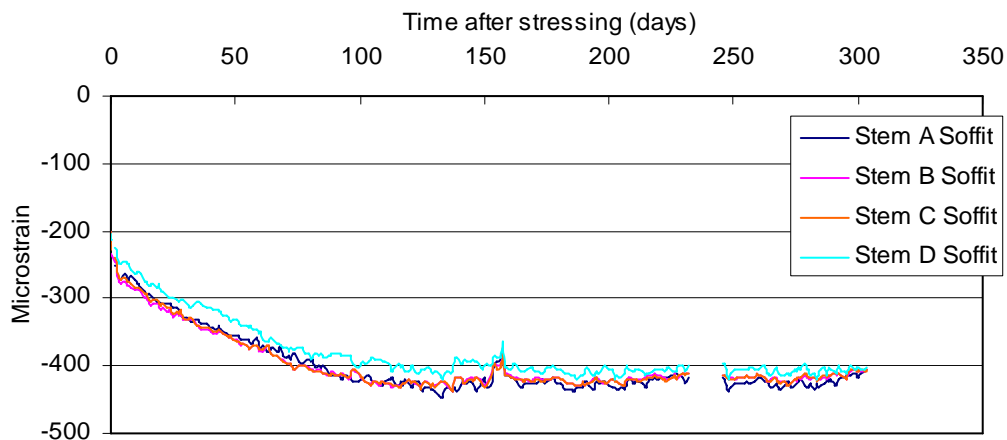


Figure 5.48: Monitored strain in the soffit at 3:00 am in F5 at the midspan section.

In Figure 5.46 to Figure 5.48, the strains were compared at specific levels (deck, web, and soffit; Figure 5.2) within the superstructure. Figure 5.49 to Figure 5.52 present the strains in each stem through the section depth. This aids in illustrating several of the previously mentioned points. Since the strains at specific gage levels are the same for each corresponding position in both sets of figures, the explanations for the observed trends are the same. It is evident in Figure 5.49 to Figure 5.52 that the additional self-weight from the hinge loading

adjusted the strain temporarily when the supporting falsework was removed at 156 days after prestressing.

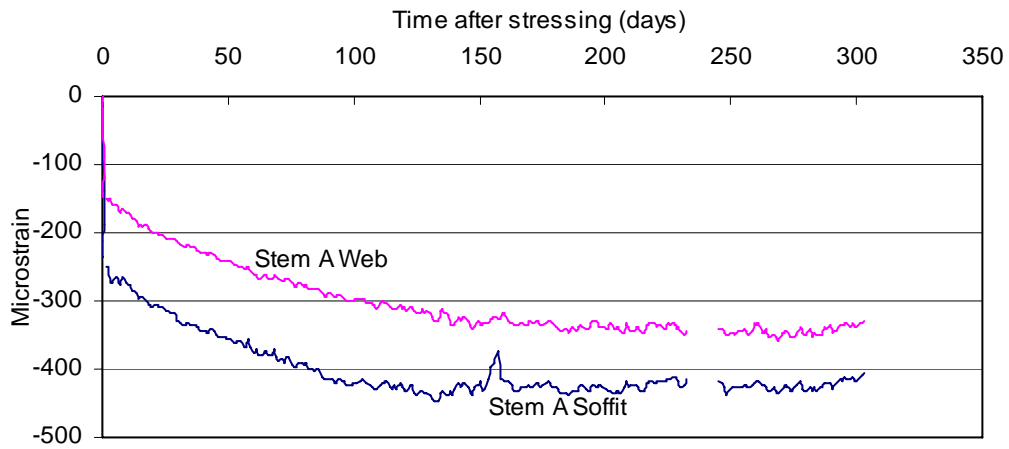


Figure 5.49: Monitored strains in Stem A in F5 at midspan.

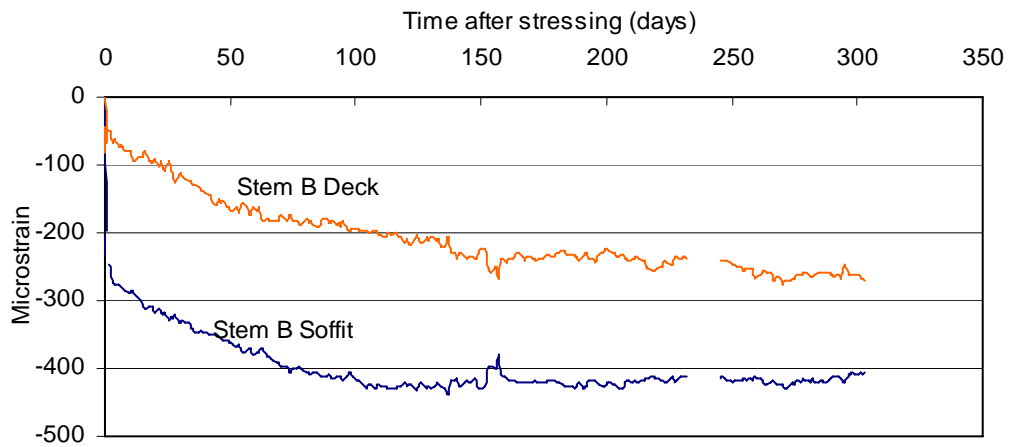


Figure 5.50: Monitored strains in Stem B in F5 at midspan.

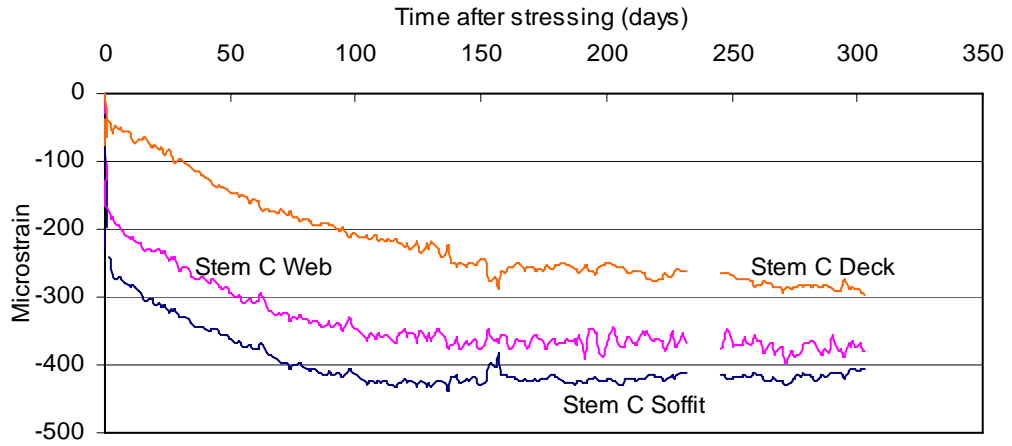


Figure 5.51: Monitored strains in Stem C in F5 at midspan.

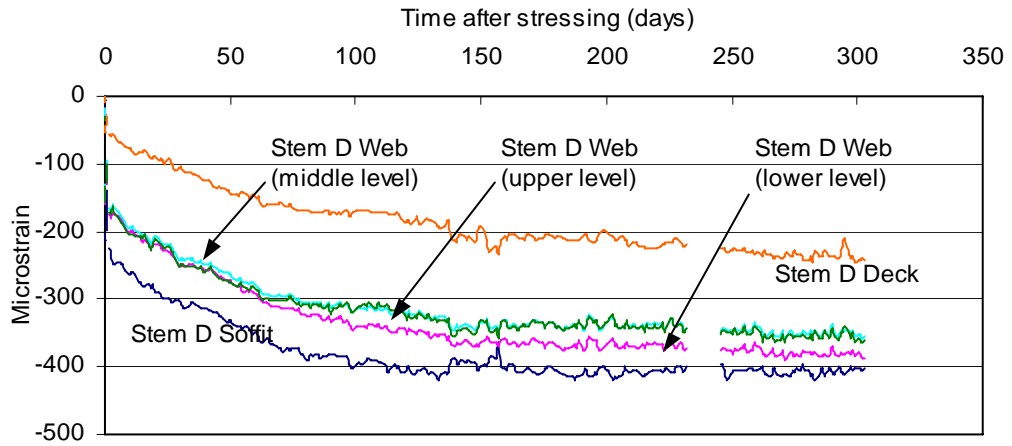


Figure 5.52: Monitored strains in Stem D in F5 at midspan.

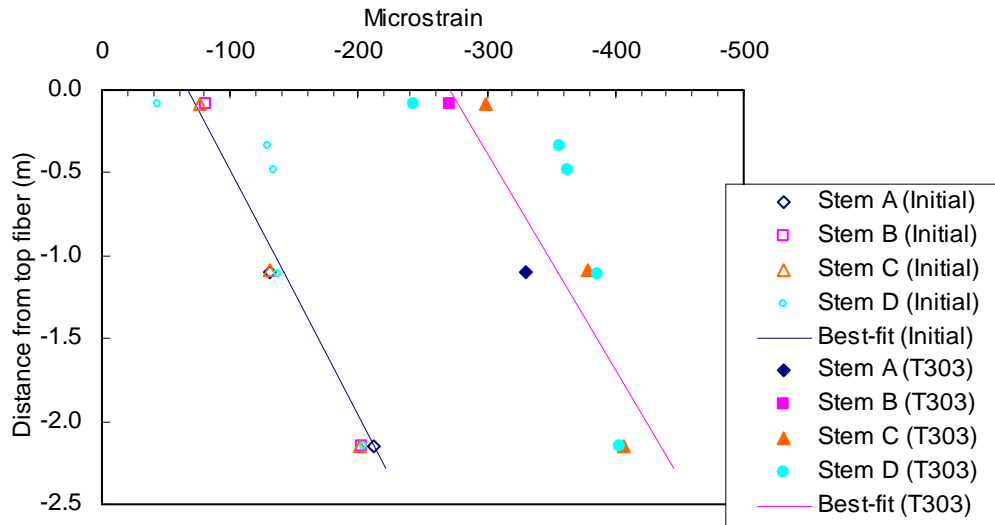


Figure 5.53: Monitored strain profile at prestressing and T303 in F5 at midspan without faulty gage readings at 3:00 am.

It is shown in Figure 5.53 that constant curvature is maintained in F5 at midspan throughout the monitoring period. Since all major changes in strain occurred during the monitoring period, it is not expected that the curvature will change directions (from negative to positive) over the life of the structure as additional monitoring is conducted. The reason that the curvature does not change direction is illustrated in Figure 5.54. When prestressing was applied, the monitored span (span 16) cambered upward resulting in an initial strain profile similar to that in Figure 5.53. After the falsework is removed, span 15 deflects downward as the restraint provided at hinge 15 is minimal. The continuity of the structure and the self-weight of span 15 maintain an upward deflection of span 16 through the end of service life. Though the displacements produced in Figure 5.54 were determined through analysis, it will be shown in Section 5.4 that the monitored strains correlate very closely with the analysis results, thus allows the use of the analytical strain diagram to produce long-term predictions of the structural displacements for this frame.

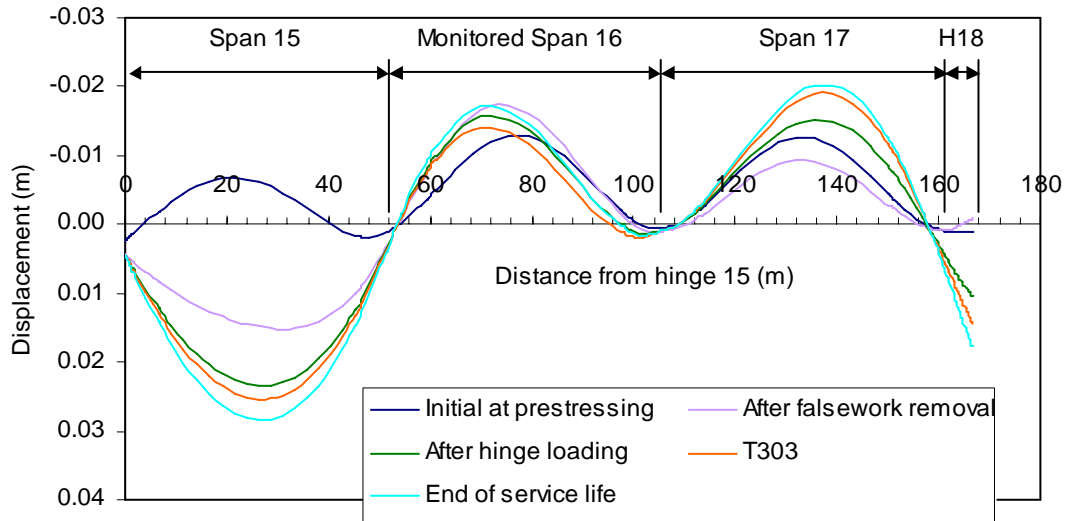


Figure 5.54: Vertical displacement of F5 at significant intervals during monitoring.

5.3.2.4. Frame 5 Near the Bent

When prestressing was applied to F5, the monitored section near the bent underwent a shortening between 150 and 200 microstrain in the deck, as indicated by the gages. After the falsework was removed, the strain generally showed a progression that ultimately reversed the curvature at the monitored location, which will be described further in this section. A large contribution of the change in strain that ultimately reversed the curvature (around 130 days after prestressing was applied) was experienced immediately upon the falsework removal. In the deck, the strain decreased about 80 microstrain instantly when the falsework was removed, to a value of ranging from 220 to 320 microstrain among the gages in the deck, as shown in Figure 5.55.

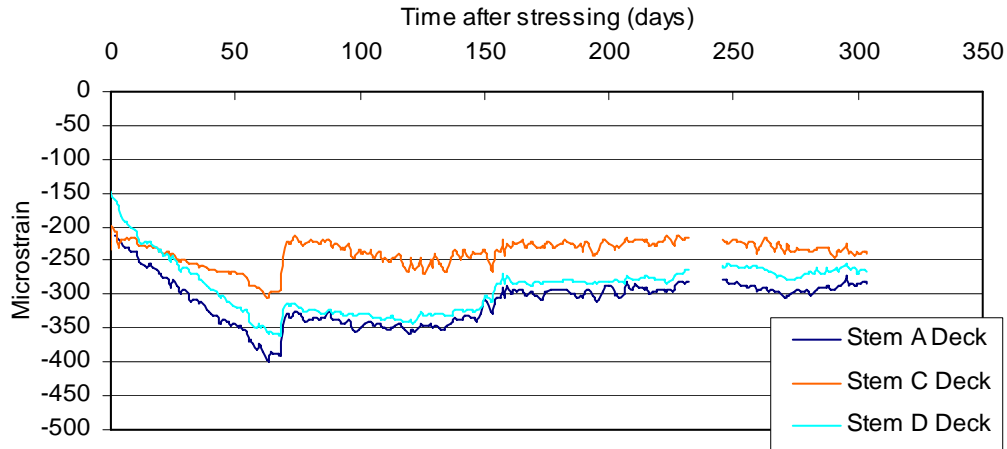


Figure 5.55: Monitored strain in the deck at 3:00 am in F5 at the near-bent section.

In the web, the initial strain at the application of prestress varied between 155 and 850 microstrain between the four gages, as indicated in Figure 5.56. This large difference between strains is not reasonable and indicates some faulty gages. Strain of 850 microstrain would indicate cracking in the superstructure, which was not present. Though all of the gages display similar daily changes in strain, the initial strain after prestressing varies widely between each of the stems. Forcing an adjustment to the data in an attempt to correct for the initial variation in strain is not appropriate, since this would not necessarily be the correct adjustment. For this reason, only the Stem D strain was used in generating the strain profiles at this section.

When the falsework was removed, the strain in the web increased by about 40 microstrain, shown in Figure 5.56, indicating gage placement slightly above the centroidal axis of the section. After the falsework removal, the strain displayed behavior that approached an asymptotic value around 330 microstrain.

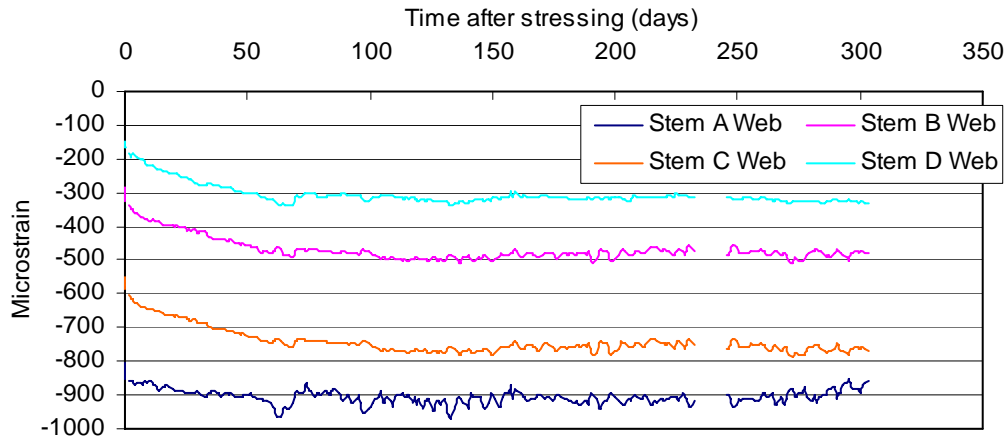


Figure 5.56: Monitored strain in the web at 3:00 am in F5 at the near-bent section.

When prestressing was applied, the strain increased in each of the four stems to about 100 microstrain in the soffit of F5 at the near-bent section. The strain increased immediately after the falsework was removed by about 70 microstrain, shown in Figure 5.58 and varied between 240 and 270 microstrain. The changes in strain in the deck and soffit are caused by the additional moment from the activation of remaining structural self-weight, causing tension in the deck and compression in the soffit. Using Eq. 5.2 and the change in strain of 85 microstrain, the added self-weight created a change in moment of -15.98 MN-m. From structural analysis of the frame, the removal of falsework resulted in a change in moment of -20.41 MN-m, 27.7% greater than the change in moment from monitoring. The loading of the hinge created a change in moment of 1.88 MN-m calculated from the change in strain of 10 microstrain using Eq. 5.2. From analysis, the change in moment at this instant was 1.64 MN-m, 12.8% different from the change in moment from monitoring. The moments determined from the monitored strain data and from analysis are presented in Figure 5.57 for the F5 midspan and near-bent locations.

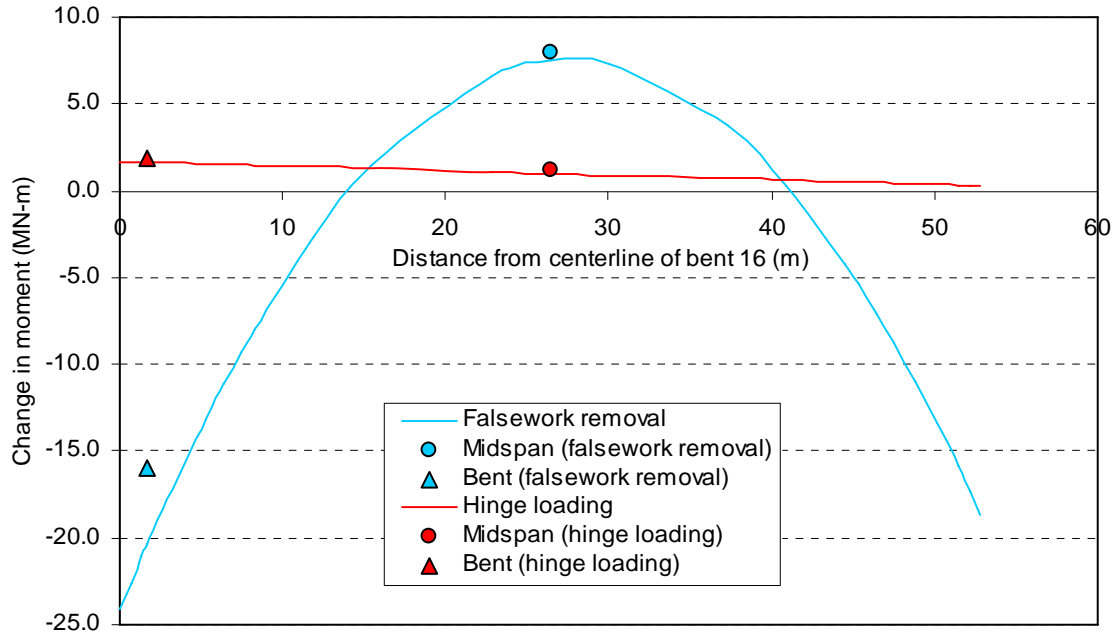


Figure 5.57: Changes in moment for F5 at midspan and near the near-bent.

The correlation between analytical and monitored changes in moment is acceptable for all four monitored sections based on the low error percentages associated with the changes in moment. Though there exist some differences between the monitored and analytical results, since only two locations were monitored and are available for comparison to analytical results, it is only possible to speculate the behavior at other locations. Although possible to make informed judgment regarding the possible moment at non-monitored locations, there exist some variations in the methods used in bridge construction that allow the differences in actual and assumed loading conditions. Some of the moments calculated using Eq. 5.2 were greater than analytical results while some were less. Selecting variable weights for the structure could result in user specific bias. The selected loads used in analysis for producing stresses, strains and, moments for comparison to the monitored data are suitable for this research.

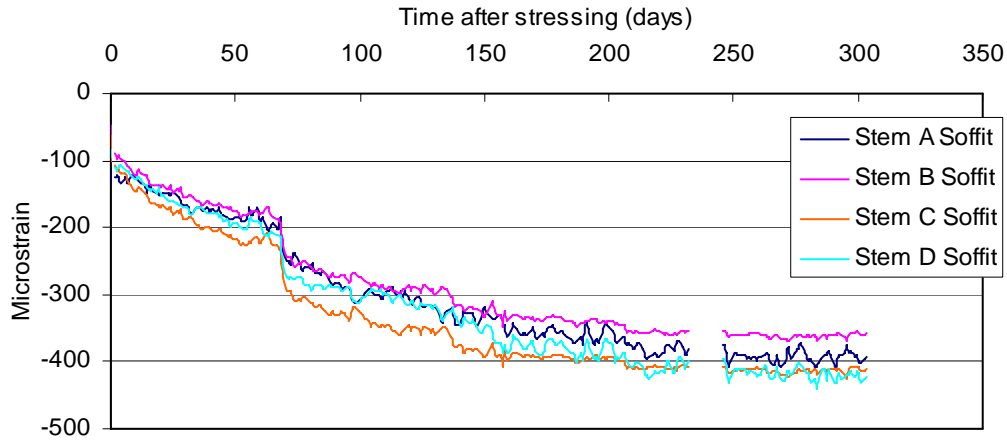


Figure 5.58: Monitored strain in the soffit at 3:00 am in F5 at the near-bent section.

The theoretical response of the bridge in terms of long-term displacements were determined using CPF [16]. Since the strains produced through analysis with CPF [16] correlate well with the monitored strain results, it is acceptable to assert future deformation with the results of analysis. This is shown in Section 5.4. It was shown in Figure 5.54 that the continuity of the structure has a strong influence on the reversal in curvature that occurred at about 130 days after prestressing. Figure 5.59 shows the same displacement of F5 as that depicted in Figure 5.54; only the displacement of the monitored portion of F5 is included to illustrate the change in curvature. In Figure 5.54 it can be seen that both span 16 and span 17 camber upwards through the end of service life. Span 15 is hinged at the inflection point near B15 (see Figure 4.3). Hinge 15 provided no rotational restraint for span 15 and allowed for the deformation that occurred in this span over time. When prestressing was applied, span 15 cambered upward as the falsework was still in place and the full dead load was not imposed. It can be seen that the deformation of this span directed the reversal of curvature at the bent location between prestressing and the point in time before the hinge was loaded.

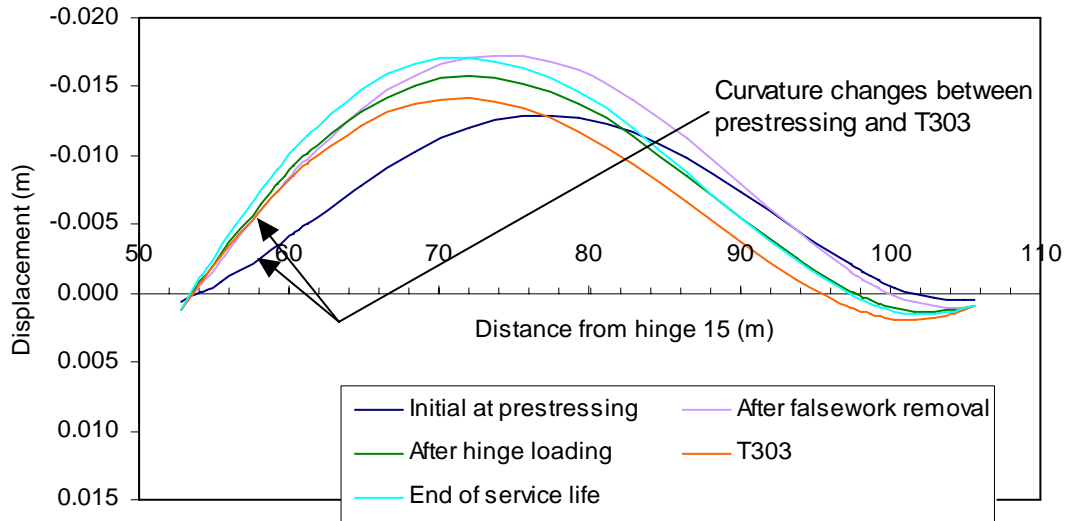


Figure 5.59: Vertical displacement of span 16 in F5.

The additional load (3.82 MN) from the adjacent frame was applied at hinge 18. The load from the adjacent span on the hinge influenced the deformation at hinge 18, as evidenced in Figure 5.54. This deformation negligibly altered the strain readings at midspan. This resulted from the fact that the restraint from hinge 15 is minimal and span 16 cambered upwards for the life of the structure, as extrapolated from the CPF [16] analysis results, verified in Section 5.4. At the bent, the influence of the additional hinge load is more profound but does not result in further changes in curvature, the reasons for which were discussed in Section 5.3.2.3.

In Figure 5.60, Figure 5.62, and Figure 5.63 the change in curvature is visible at about 130 days after prestressing. The strains in the concrete at all gage depths were nearly equivalent and the strain profile was progressing from a negative slope at prestressing to a positive slope at T303. This change did not occur instantaneously as the material properties involved – creep and shrinkage – influenced the deformation of the frame over time. Since the superstructure is continuous across the frame, the deformation of span 15 created the curvature reversal that developed with time, as shown in Figure 5.54.

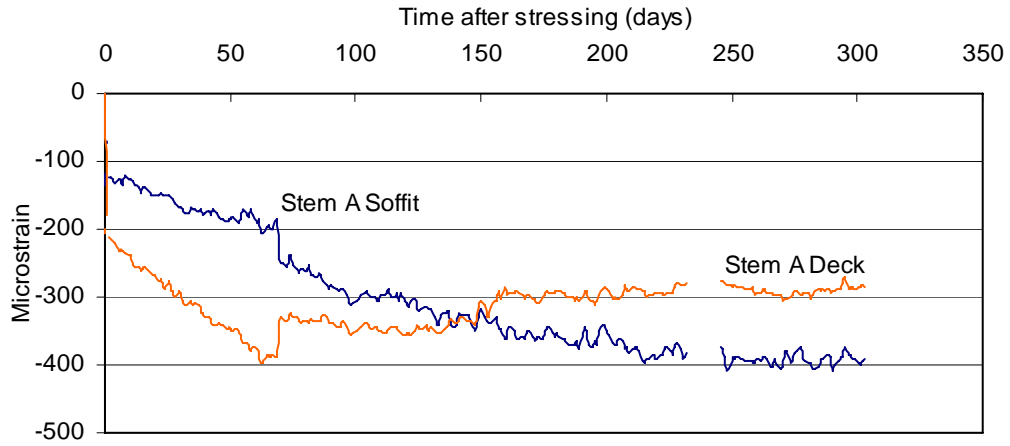


Figure 5.60: Monitored strains in Stem A in F5 near the bent.

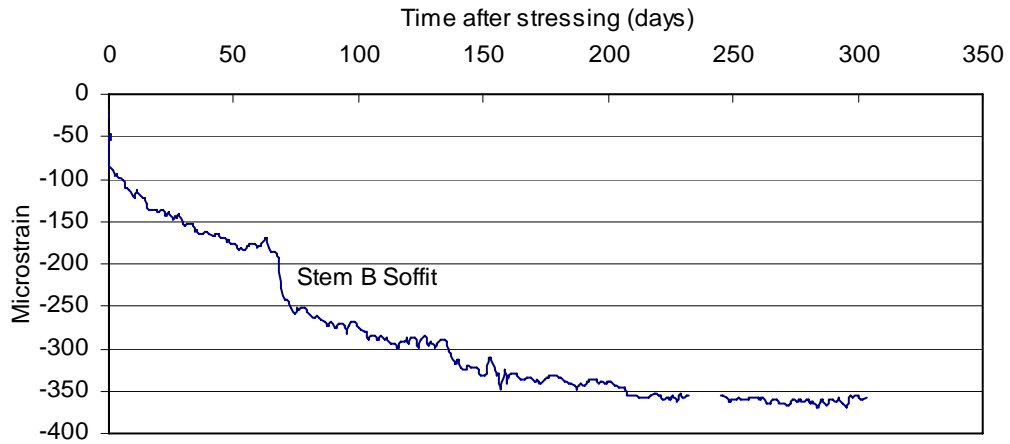


Figure 5.61: Monitored strains in Stem B in F5 near the bent.

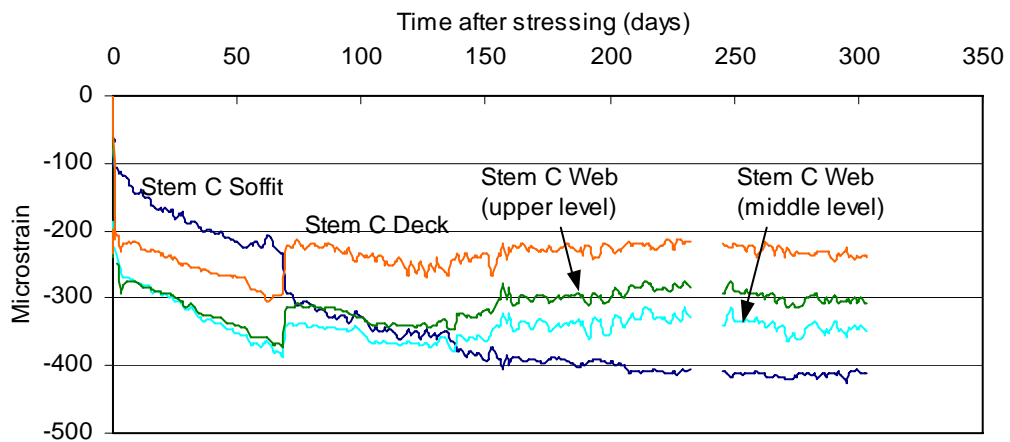


Figure 5.62: Monitored strains in Stem C in F5 near the bent.

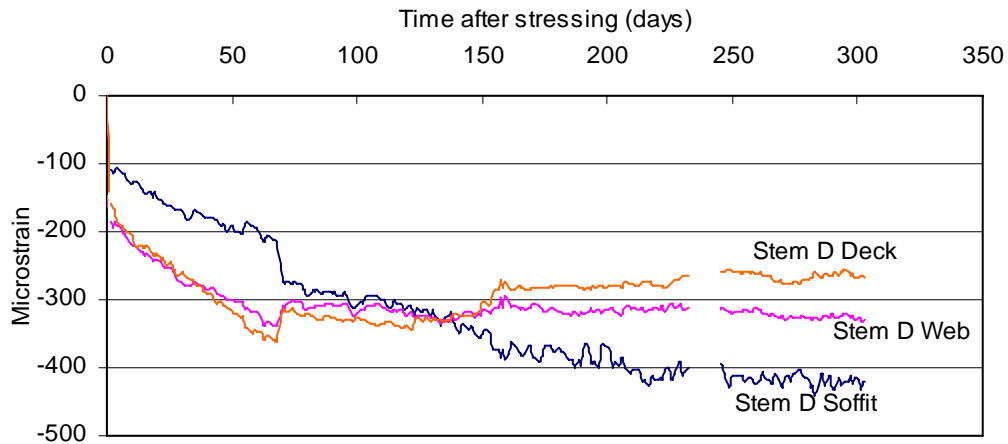


Figure 5.63: Monitored strains in Stem D in F5 near the bent.

Unexpected strain was monitored in the web. Only one of the four gages in the web indicated a strain that consistently followed the trends of the gages in the deck and soffit. Examination of Figure 5.64 displays the variation of the measured strain at the web level. Aside from the Stem D gage that provided reasonable strain values, the Stem A, B, and C gages indicated strains that did not maintain linearity throughout monitoring. At the final monitored instant (T303), each of these three gages indicated further increase in strain. Though the strain increased through the section in all stems and gage levels, the Stem A, B, and C gages strain increased much more than expected and do not follow the other gages.

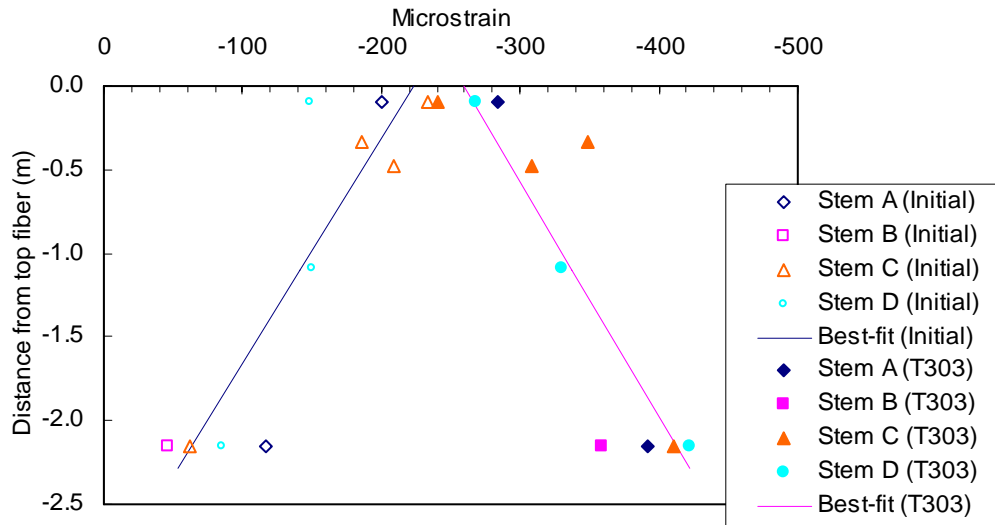


Figure 5.64: Monitored strain profile at prestressing and T303 in F5 near the bent from gage readings at 3:00 am.

5.3.3. Discussion on Strains

It is not particularly appropriate to compare the strains in F4 and F5, as the forces and moments are very different at corresponding midspan and near-bent locations. However, general observations of behavior can be made.

The differences between the strains at midspan and near-bent locations in F4 and F5 are distinct. When the falsework is removed in F4, a large instantaneous change in strain is evident at midspan. For the same event in F5 at midspan, the change in strain is almost indistinguishable. A much more pronounced change is apparent when the hinge is loaded in F5. However, this change lasts only temporarily, after which the strain continues to progress as it had before hinge loading, resulting from the comparatively small moments to those existing in the section before hinge loading.

In F4 at midspan, the strains are grouped between 400 and 450 microstrain for gages in all levels, indicating a strain profile with little curvature. The strains at midspan in F5 are more varied from the deck to the soffit and suggest more curvature than that in F4. The strain in the deck is about 250 microstrain while 420 microstrain is indicated at the soffit level. In F4 near the bent, the strain in

the soffit was about 300 microstrain and 500 microstrain in the deck at T363. At T303 in F5 near the bent, the soffit strain was 300 microstrain, while the deck strain was around 200 microstrain.

5.4. Strains from Analysis and Field Monitoring

The analytical strain profiles were obtained using CPF [16]. All input data and assumptions used in developing the CPF [16] inputs were discussed previously in Sections 4.3, 4.4, 4.5, and 4.6. The comparison of monitored and analytical strain will be useful in justifying the analysis inputs used in CPF [16] and the ability of the analysis to predict the long-term prestress loss.

The presented analytical strains correspond to several instances of particular interest. These instances are 1.) the initial strain immediately after post-tensioning, 2.) the strain in the sections at the last point in time the collected data was used for this research (T363 for F4 and T303 for F5, discussed in Section 4.3), and 3.) a projected strain at the end of service life, 20,000 days after stressing. An age of 20,000 days (55 years) was selected for the theoretical end of service life because a common design lifespan for similar bridges is on the order of 50 years [19]. For ease of displaying the long-term predictions of material properties, an end of service life of 20,000 days was selected. This time is approximately 5 years longer than the end of service life specified in [19]. Though this theoretically extends the life of the bridge by 10% over that of typical a lifespan, the material properties creep and shrinkage increase over this time period less than 1% from the values at 50 years. For this reason, the changes to the analysis results based on the differences in material properties are insignificant. The strain profiles obtained with analysis are compared to the monitored strain at prestressing and at T363 and T303 for F4 and F5, respectively. Accompanying the monitored strain profiles, later in this section, are projected strain profiles determined from analysis at a theoretical end of service life, which are useful in verifying that no unexpected behavior (such as cracking) might occur.

As mentioned in earlier, the material properties obtained through testing were projected for the theoretical end of service life using a best fit to the available data [15]. It was described that the projection of creep and shrinkage would not exceed the extrapolated value at the end of service life. Also, it was mentioned that the projected ultimate values might be larger than the actual material properties at the actual point in time. The minimum material properties at the end of service life were taken as the same values that were obtained at T363 or T303. The minimum and maximum material properties produced a range over which creep and shrinkage are expected to actually occur in 20,000 days as described in Sections 3.8 and 4.3. Since the larger the creep and shrinkage the larger the strain, and hence the prestress loss, the strain in the concrete corresponding to the maximum projected material properties is presented in this section.

Throughout the monitoring period reported in this study, the bridge was closed to traffic. This created ideal conditions for monitoring the change in strain since only permanent loads were present during this period.

The instances in time at which significant construction events occurred are represented by the material properties and loading and support conditions that are input into the analyses. CPF [16] has the capability of using time as an input if the user desires the material properties to be calculated by the program. The other option using CPF [16] is to represent the instances at which construction events occurred by the value of the material properties existing at the time of the event. Since the material properties under consideration here – concrete creep and shrinkage and prestressed steel relaxation – are all time-dependent, the values of these material properties input into CPF [16] reflect the time at which the event occurred, thus explicit time inputs are not necessary. The material properties input to analysis were taken at times corresponding to the age of the structure at which the event occurred, which are presented in Table 5.4 and Table 5.5 for F4 and F5, respectively. The values in these tables are taken from those in Table 4.3 and Table 4.4 for F5; however, since the analyses are based

on time intervals to define the events that occur during construction, the values in Table 5.4 and Table 5.5 are presented.

Intermediate intervals – removal of falsework and hinge loading – are not presented in the strain diagrams for several reasons. Primarily, the monitored strain does not change instantaneously and therefore may not correlate with the results of CPF [16] analysis. Additionally, this period is subject to considerable fluctuation in strain due to construction loads, which causes deformation that is not easily captured through analysis. The two instances selected to compare the monitored data to the strains produced through analysis existed at times when the deformation of the bridge was reasonably unchanging. Examination of the monitored data indicated that the strain rate of change was not significant at the points in time that it was used for comparison to analytical strains. The first instant, at prestressing, is not influenced by time dependent properties. At prestressing, the strain that exists in the section is the result of elastic shortening. Since this occurs instantaneously after prestress is applied, the influence of concrete creep and shrinkage are negligible. At T363 and T303, these instances occurred 241 and 147 days after the last instant at which structural load was applied in F4 and F5, respectively. The figures in Section 5.3 show that the strains at the monitored bridge sections had approached an asymptotic value at each level of the gages, indicating that no substantial changes had occurred in the concrete since the last instant load was applied. For this reason, it is appropriate to compare the strains obtained through monitoring with those of analysis at prestressing and T363 and T303. The monitored strains at instances of major construction events, such as when the falsework was removed and the hinge was loaded, display substantial change in strain within a short period of time. The abrupt changes that occurred at loading events do not only cause instantaneous change, but also alter the long-term progression of strain.

5.4.1. Frame Analysis

Each analysis performed for F4 and F5 utilized derived material properties from ACI [3], CEB-FIP [10], or the material tests and were performed using the

different load cases described in Section 4.6. The ACI [3] and CEB-FIP [10] specifications were selected, as these are two of the more frequently used methods used in design (commonly used by design engineers). Material tests, though available here, would not readily be at the disposal of an engineer. Inputs representing the construction sequence, structure geometry, and loading scenario were used to accommodate each frame, covered in Sections 4.3, 4.5, and 4.6, respectively. The structural geometry and loading scenario remains the same for the three F4 analyses and the same among the three F5 analyses. The derived material property inputs used in this analysis for F4 are presented in Table 5.4 for F4 and Table 5.5 for F5.

Material Property Inputs from ACI

The ACI [3] specification was used for producing the material properties of creep and shrinkage for this analysis, which is covered in Section 2.2.3.

Material Property Inputs from CEB-FIP

The CEB-FIP [10] specification was used for deriving the material property inputs for this analysis, which is covered in Section 2.2.4.

Material Property Inputs from Testing (Measured)

The measured material properties presented in an earlier chapter were used to generate the material property inputs to these analyses. The measured material properties were not used outright as input, as the V/S ratio of the test specimens and the bridge is not equivalent. The measured material properties were proportioned for the V/S of the bridge in Section 3.8.

Table 5.4: Material property inputs used for analysis of F4.

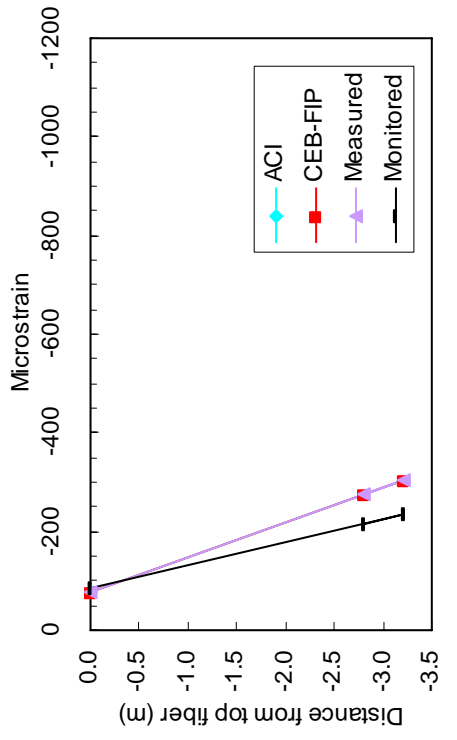
Concrete		October				November				March				$\Delta\bar{\sigma}_{pr}$ (MPa)	
Material Properties	Date of event	$\phi(t_i, t_0)$	$\phi(t_i, t_1)$	$\varepsilon_{sh}(t_i, t_{i+1})$ ($\mu\text{m/m}$)	$\chi(t_i, t_0)$	$\phi(t_i, t_0)$	$\phi(t_i, t_1)$	$\varepsilon_{sh}(t_i, t_{i+1})$ ($\mu\text{m/m}$)	$\chi(t_i, t_0)$	$\phi(t_i, t_0)$	$\phi(t_i, t_1)$	$\varepsilon_{sh}(t_i, t_{i+1})$ ($\mu\text{m/m}$)	$\chi(t_i, t_0)$		
Stressing $t_0 = 0$ days	March 23, 2005	ACI	0	-	0	0	-	0	-	0	-	0	-	0	
		CEB-FIP	0	-	0	-	-	-	0	-	-	-	0	-	0
		Measured	0	-	0	-	-	-	0	-	-	-	0	-	0
Falsework removal $t_1 = 121$ days	July 22, 2005	ACI	0.61	0	-23	0.62	0	-31	0.93	0.76	0	-146	0.89	-17.89	
		CEB-FIP	0.72	0	-33	0.75	0	-37	0.93	1.04	0	-66	0.89	-17.89	
		Measured	1.13	0	-36	0.96	0	-43	0.93	0.99	0	-155	0.89	-17.89	
T363 $t_2 = 363$ days	March 20, 2006	ACI	0.73	0.64	-17	0.75	0.64	-20	0.93	0.92	0.69	-41	0.89	-2.46	
		CEB-FIP	0.91	0.74	-42	0.95	0.75	-45	0.93	1.32	0.84	-59	0.89	-2.46	
		Measured	1.46	0.83	-36	1.24	0.91	-42	0.93	1.20	0.67	-100	0.89	-2.46	
Theoretical end of service $t_3 = 20000$ days		ACI	0.92	0.86	-23	0.94	0.87	-25	0.93	1.16	0.93	-32	0.88	-8.99	
		CEB-FIP	1.22	1.09	-204	1.26	1.11	-210	0.93	1.76	1.24	-229	0.88	-8.99	
		Minimum Extrapolated	1.46	0.83	0	0.95	0.91	0	0.93	1.20	0.67	0	0.88	-8.99	
Maximum Extrapolated		1.97	1.34	-131		1.67	1.49	-147		1.52	1.06	-329			

Table 5.5: Material property inputs used for analysis of F5.

Concrete		April						May					
Material Properties	Date of event	$\phi(t_i, t_0)$	$\phi(t_i, t_1)$	$\phi(t_i, t_2)$	$\varepsilon_{sh}(t_i, t_{i+1})$ ($\mu\text{m}/\text{m}$)	$\chi(t_i, t_0)$	$\phi(t_i, t_0)$	$\phi(t_i, t_1)$	$\phi(t_i, t_2)$	$\varepsilon_{sh}(t_i, t_{i+1})$ ($\mu\text{m}/\text{m}$)	$\chi(t_i, t_0)$	$\Delta\sigma_{pr}$ (MPa)	
Stressing $t_0 = 0$ days	May 20, 2005	ACI	0	-	-	0	0	-	-	0	-	0	
		CEB-FIP	0	-	-	0	-	-	-	0	-	-	
		Measured	0	-	-	0	-	-	-	0	-	-	
Falsework removal $t_1 = 69$ days	July 29, 2005	ACI	0.63	0	-	-90	0.70	0	-	-199	0.90	-16.34	
		CEB-FIP	0.81	0	-	-39	0.98	0	-	-59	0.90	-16.34	
		Measured	0.64	0	-	-106	0.55	0	-	-151	0.90	-16.34	
Hinge loading $t_2 = 156$ days	October 26, 2005	ACI	0.75	0.57	0	-36	0.85	0.59	0	-53	0.89	-1.80	
		CEB-FIP	1.00	0.70	0	-32	1.20	0.74	0	-37	0.89	-1.80	
		Measured	0.87	0.54	0	-74	0.73	0.54	0	-69	0.89	-1.80	
T303 $t_3 = 303$ days	March 20, 2006	ACI	0.84	0.72	0.61	-22	0.94	0.74	0.62	-27	0.89	-1.46	
		CEB-FIP	1.15	0.90	0.72	-35	1.38	0.95	0.74	-38	0.89	-1.46	
		Measured	1.06	0.76	0.55	-73	0.88	0.76	0.56	-64	0.89	-1.46	
Theoretical end of service $t_4 = 20000$ days		ACI	1.09	0.97	0.91	-35	1.22	1.01	0.93	-38	0.85	-9.23	
		CEB-FIP	1.59	1.33	1.19	-237	1.91	1.40	1.22	-244	0.85	-9.23	
		Minimum Extrapolated	1.06	0.76	0.55	0	0.88	0.76	0.56	0	0.85	-9.23	
Maximum Extrapolated	1.59	1.21	1.25	-467	1.29	1.21	1.30	1.30	-412	0.85	-9.23		

5.4.2. Analysis Results of Frame 4

The material property inputs used in the three analyses for F4 are presented in Table 4.3. The inputs representing the construction sequence, structure geometry, and loading are presented in Sections 4.3, 4.5, and 4.6, respectively. Results are presented here for the midspan and near-bent sections of F4 corresponding to the locations of the VW gages.



● Vibrating-wire strain gage

Figure 5.65: Cross-section of F4 at midspan.

Figure 5.66: Strain profile in F4 at midspan immediately after prestressing.

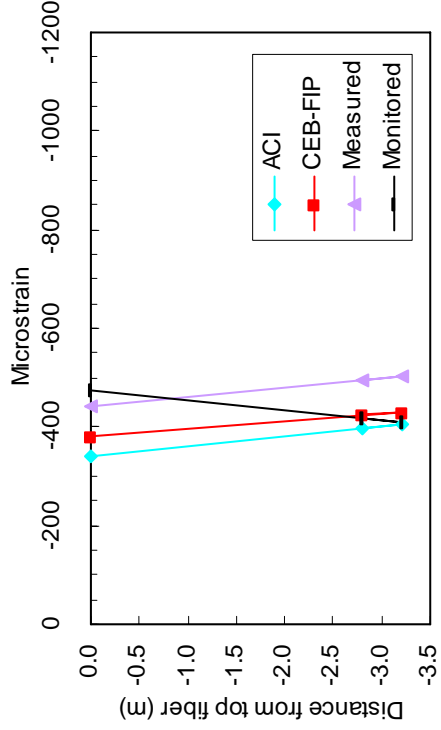


Figure 5.67: Strain profile in F4 at midspan at T363.

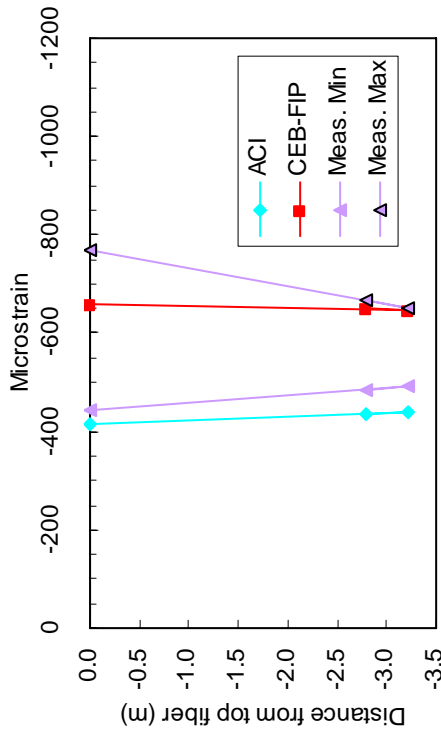


Figure 5.68: Strain profile in F4 at midspan at a theoretical end of service life

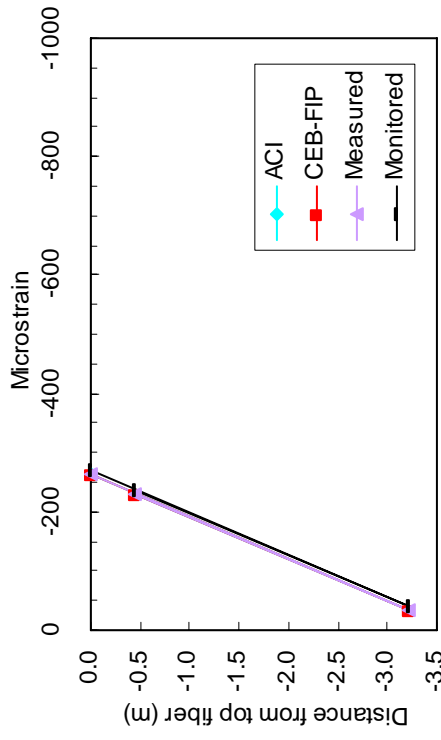


Figure 5.69: Cross-section of F4 near the bent.

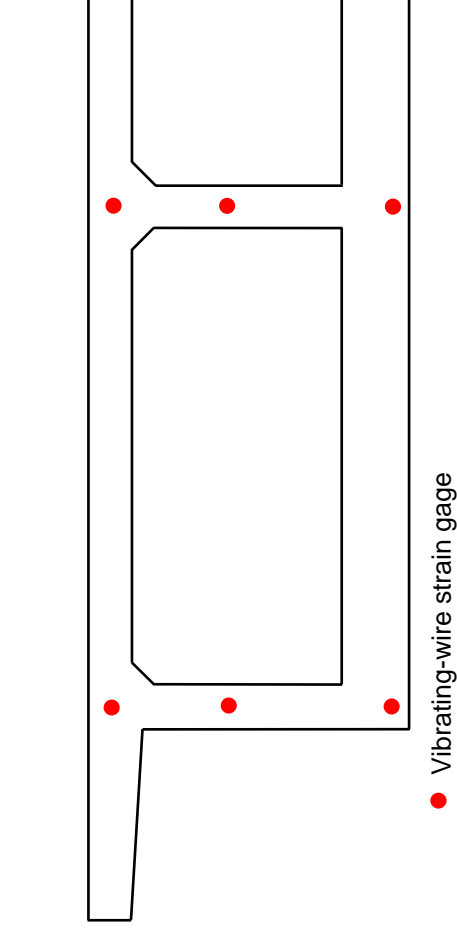


Figure 5.70: Strain profile of F4 near the bent immediately after prestressing.

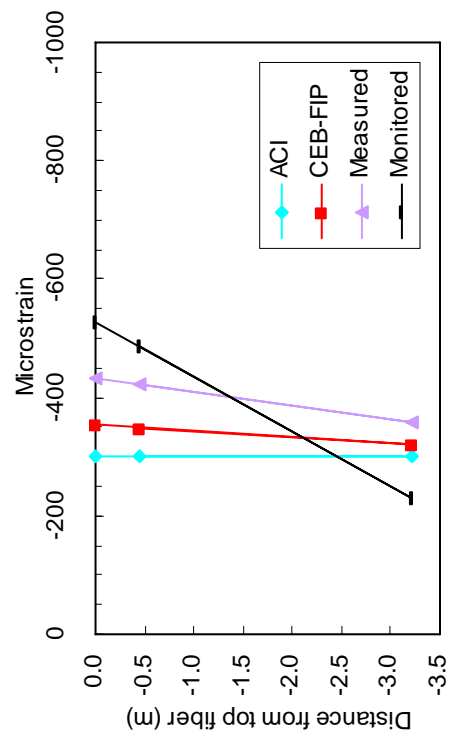


Figure 5.71: Strain profile of F4 near the bent at T363.

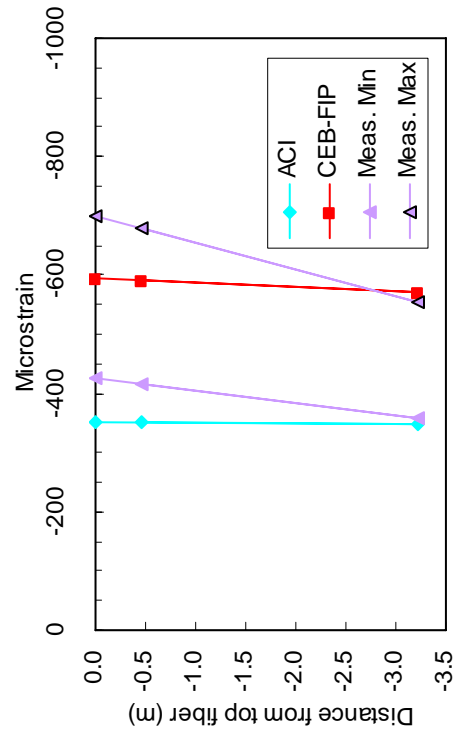


Figure 5.72: Strain profile of F4 near the bent at theoretical end service life.

5.4.2.1. Frame 4 Midspan

The initial strain profile of F4 at midspan in Figure 5.66 displays a strain that is 27.3% larger than the monitored strain at the level of the centroid of the prestressing tendons, 2.795 m below the top fiber of the section. The initial strain profile occurs due to prestressing and self-weight only and is not influenced by time-dependent properties. For this reason, the initial analytical strain profile for each of the three analyses is equivalent. The differences between monitored and analytical strains are presented in Table 5.6.

The strain at midspan from analysis with ACI [3] derived material property inputs, in Figure 5.67, at T363 is 4.7% less than the monitored strain at the level of the prestressing tendons. The analysis using the derived CEB-FIP [10] material properties is 1.6% larger than the monitored strain at the level of the prestressing tendons for T363. These two analyses display much better correlation with the monitored strain than that of the analysis using the measured material properties as input, which generated a strain at the level of the prestressing tendons that is 18% larger than the monitored strain at T363.

The three analyses produced varied predictions of the strain at the theoretical end of service life, as seen in Figure 5.68. The strains produced utilizing the derived ACI [3] and CEB-FIP [10] material properties do not increase at similar rates. This results from the progression of creep and shrinkage that was determined from each specification. At T363, the derived ACI [3] and CEB-FIP [10] material properties are similar, as can be seen in Table 4.3. Within the period between T363 and the theoretical end of service, the derived ACI [3] material properties increase only slightly while the derived CEB-FIP [10] material properties continue to increase more rapidly. This behavior can be seen in Figure 5.73 and Figure 5.74 for typical development of creep and shrinkage, respectively. Predominantly, the CEB-FIP [10] specification produced material properties that demonstrated larger increases in material property values beginning about 100 days after prestressing was applied compared to the

development of material properties produced by ACI [3]. This is evident in the predictions of shrinkage, Figure 5.74. For this reason the analytical strains produced using the derived material properties from ACI [3] do not change substantially between T363 and the theoretical end of service as the change produced by CEB-FIP [10] derived material properties.

While the best-fit [15] follows the progression of creep and shrinkage up to the points in time at T363 and T303, it is also influenced by environmental factors. These influenced could be present in the monitored data and hence the best-fit. As more creep and shrinkage values become available over time, improved long-term predictions can be made. The extrapolated data, though, serve as an acceptable maximum for the data available at the time of conducting the analysis. As time continues, an expected extrapolated value of the measured data will be lower than the maximum presented herein, as indicated in Figure 5.73 and Figure 5.74.

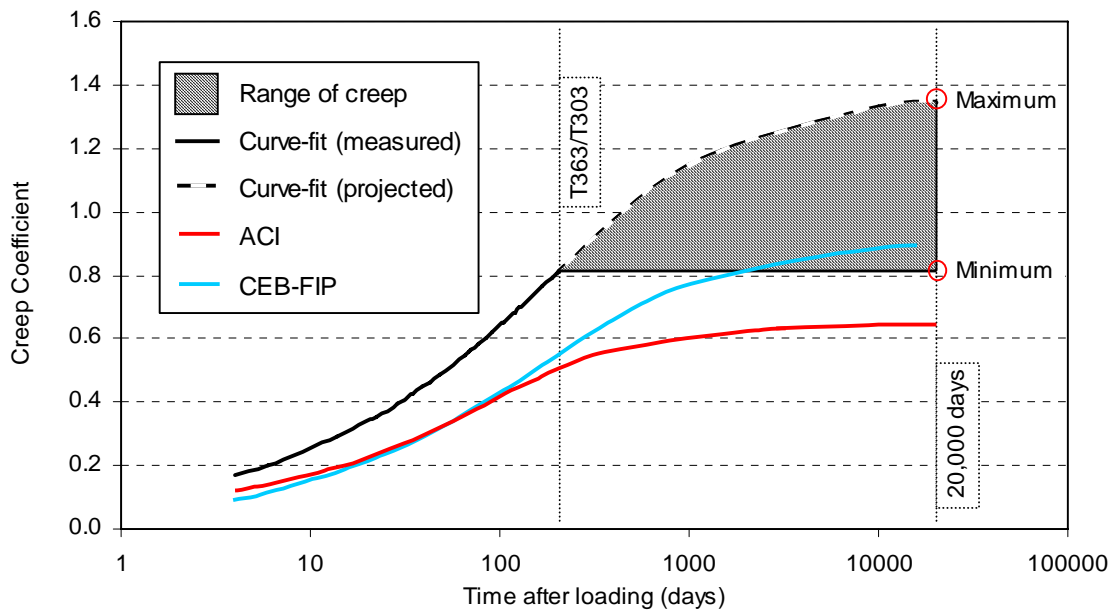


Figure 5.73: Typical development of long-term creep of concrete in F4 and F5.

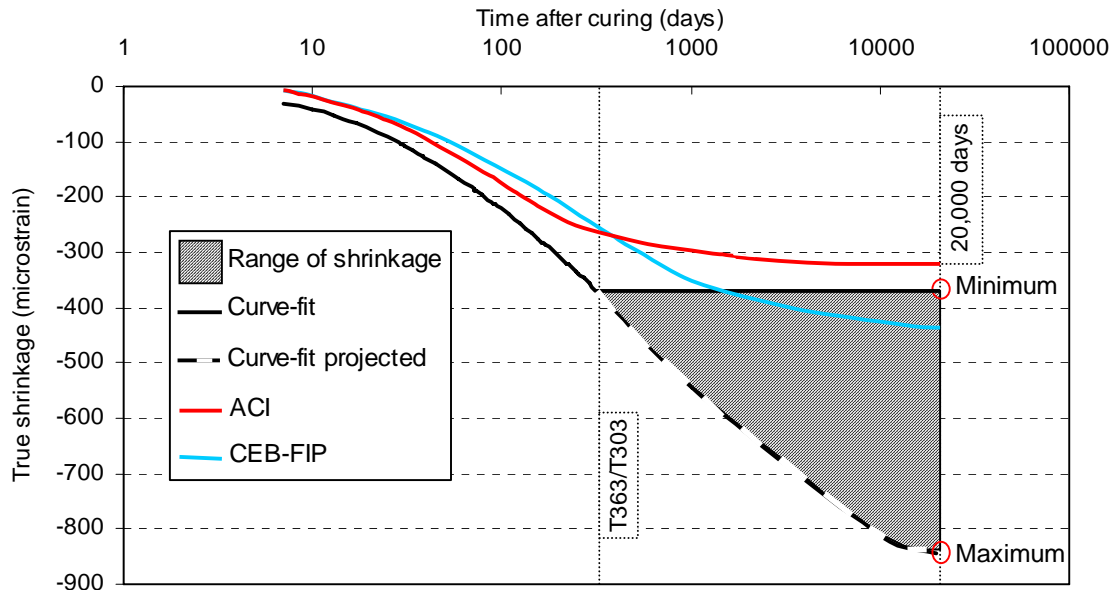


Figure 5.74: Typical development of long-term shrinkage of concrete in F4 and F5

5.4.2.2. Frame 4 Bent

The initial strain profile when prestressing was applied in F4 near the bent, shown in Figure 5.70, produced through the three analyses is 3.3% less than the monitored strain at the level of the prestressing tendons, 0.454 m below the top fiber. Table 5.6 presents the differences between the monitored and analytical strains. The change in strain occurring between prestressing and T363 exhibits similar behavior to that observed in F4 at midspan, displayed in Figure 5.71. The strains produced using the derived ACI [3] and CEB-FIP [10] material property inputs through analysis are 38.2% and 28.0% lower than the monitored strain at this time at the level of the prestressing tendons. The analysis using measured properties results in a strain at the level of the prestressing tendons that is 12.8% larger than the monitored strain. Examination of Figure 5.71 displays the correlation of monitored to analytical strains. Though the measured material property inputs result in strain that is 3.2% larger than the monitored strain, it is apparent in Figure 5.71 that the slope of the analytical strain diagrams do not correlate well to the monitored strain and the correlation at the level of the prestressing tendons is coincidental.

Table 5.6: Monitored and analytical strains at the level of the centroid of the prestressing tendons in F4.

	Depth of prestress from top fiber (m)	Occasion	Bridge Monitoring	ACI		CEB-FIP		Measured (material tests)					
				ϵ_c ($\mu\text{m}/\text{m}$)	% difference from monitored	ϵ_c ($\mu\text{m}/\text{m}$)	% difference from monitored	Minimum material properties	Maximum material properties	ϵ_c ($\mu\text{m}/\text{m}$)	% difference from monitored	ϵ_c ($\mu\text{m}/\text{m}$)	% difference from monitored
Midspan	2.795	Initial (prestressing)	-216	-275	27.3	-275	27.3	-275	27.3	-275	27.3	-275	27.3
		T363	-418	-398	4.7	-425	1.6	-493	18.0	-493	18.0	-493	18.0
		Theoretical end of service	-	-434	-	-650	-	-484	-	-667	-	-667	-
Near the Bent	0.454	Initial (prestressing)	-238	-230	3.3	-230	3.3	-230	3.3	-230	3.3	-230	3.3
		T363	-485	-300	38.2	-349	28.0	-423	12.8	-423	12.8	-423	12.8
		Theoretical end of service	-	-351	-	-592	-	-415	-	-678	-	-678	-

5.4.2.3. General Comments for Frame 4 Strain Results

There are several reasons that the results of analysis for F4 do not show better correlation with the monitored data at prestressing and at T363. These instances can be noted in the strain diagrams presented in Section 5.3. The occurrences described below are related to the monitored data for the points in time that the discrepancies were noted to exist.

- The falsework remained in place for a period of time longer than would normally occur. The bridge contractor usually prefers to remove the falsework at the earliest possible time to allow the material to be used in other projects. At prestressing, the concrete has already been in the forms for six months since casting. After prestressing was applied, the falsework remained for another four months. The falsework was removed slowly, over the course of about three weeks allowing for changes in strain to occur that would not be expected had the falsework been removed at a faster pace. The falsework restricted both the longitudinal and vertical displacement of the structure, as shown in Figure 5.34. In the longitudinal direction, the falsework provided frictional resistance. Motion in the vertical direction was constrained by the falsework that would not be experienced if removed shortly after stressing, which can be evidenced in Figure 5.67 and Figure 5.71 comparing the monitored and analytical strains.
- When prestressing was initially applied, the prestress jack suffered some malfunctions after the first tendon was stressed. Though F4 contains 12 tendons, the force from a single tendon that is not distributed evenly in all girders can result in significantly different behavior than tendons stressed at the same time. About five days elapsed before the jack was repaired and brought back into service to stress the remaining tendons. The behavior of the strains resulting from this occurrence can be observed in Figure 5.39 to Figure 5.42.

- The hinges at the ends of F4 (H11 and H15) did not align correctly with the adjacent frames. To correct the misalignment, a jacking procedure was employed to adjust the superstructure to the appropriate elevation. The individuals responsible for jacking the structure did not take note of the applied jacking force merely applying a level sufficient to correct the misalignment.
- The analysis of F4 was performed for a plane frame, as discussed with the assumptions in Chapter 4. The actual F4 is curved in the horizontal direction, which plane frame analysis does not take into account. In a horizontally curved structure, such as F4, the prestress applies a greater stress on the outer girders compared to the inner girders. A least-squares linear regression was fit to the monitored strain data.

5.4.3. Analysis Results of Frame 5

The three F5 analyses utilized derived material property inputs from ACI [3], CEB-FIP [10], and the material tests, which are presented in Table 4.4. The structure geometry inputs are presented in Chapter 4. Results corresponding to the midspan and near-bent locations of VW gages are presented in this section.

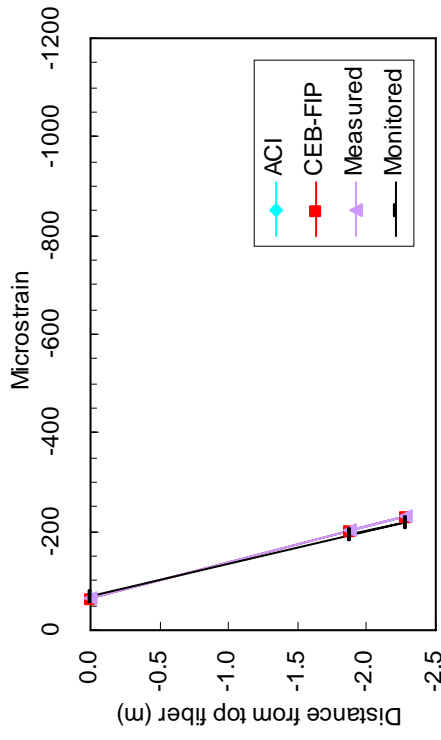


Figure 5.75: Cross-section of F5 at midspan.

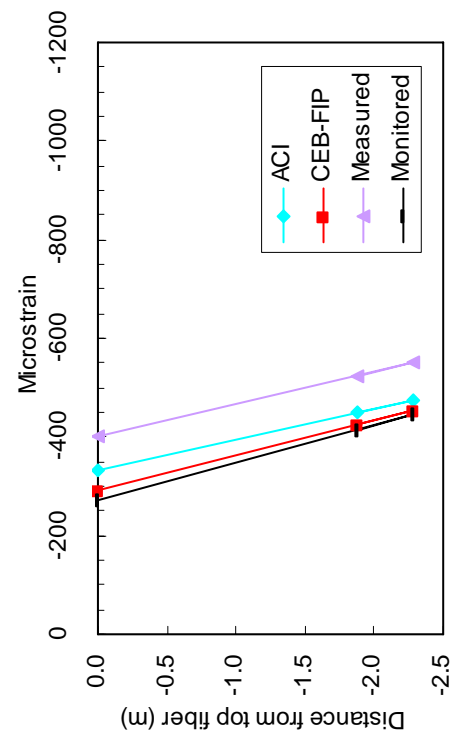


Figure 5.77: Strain profile of F5 at midspan at T303.

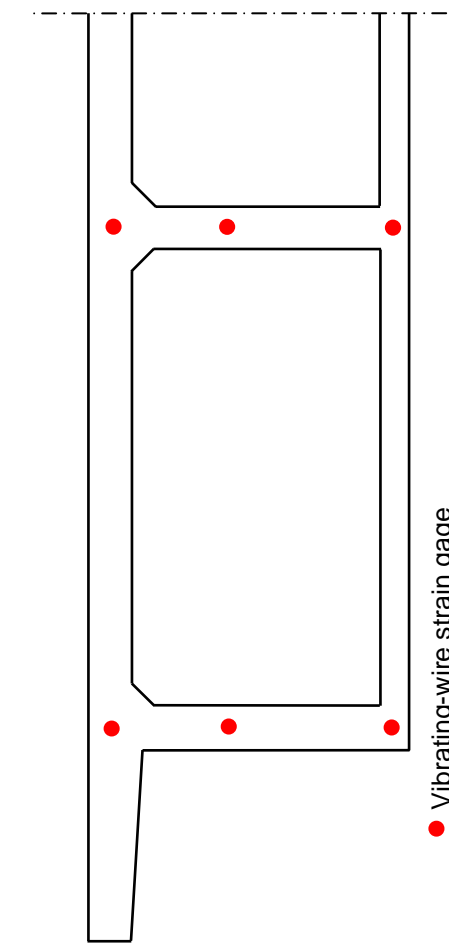


Figure 5.76: Strain profile of F5 at midspan immediately after prestressing.

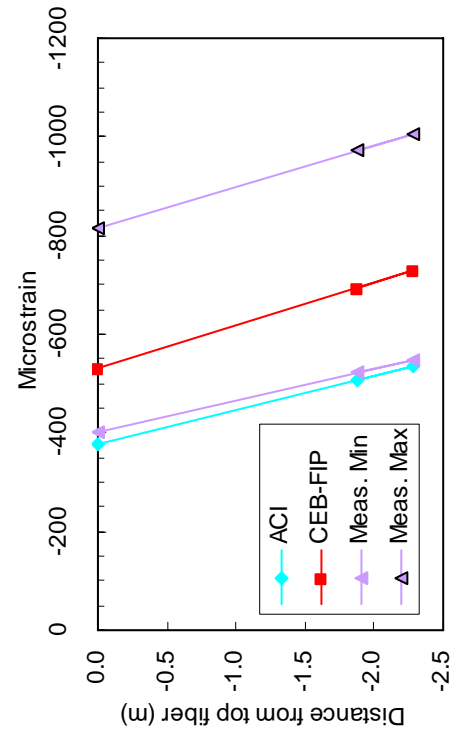
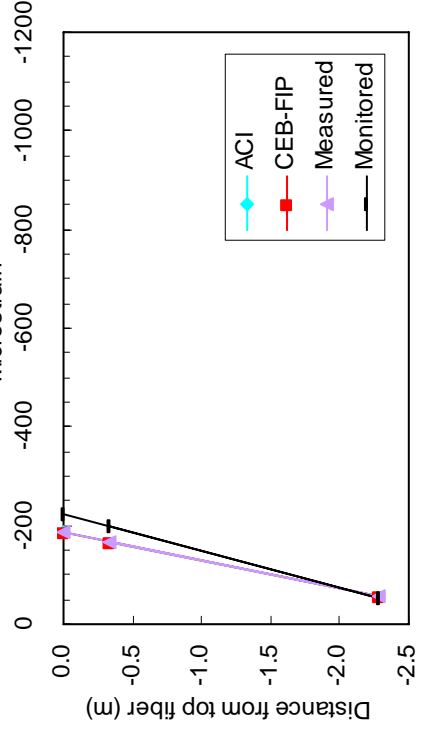


Figure 5.78: Strain profile of F5 at midspan at a theoretical end of service life.



● Vibrating-wire strain gage

Figure 5.79: Cross-section of F5 near the bent.

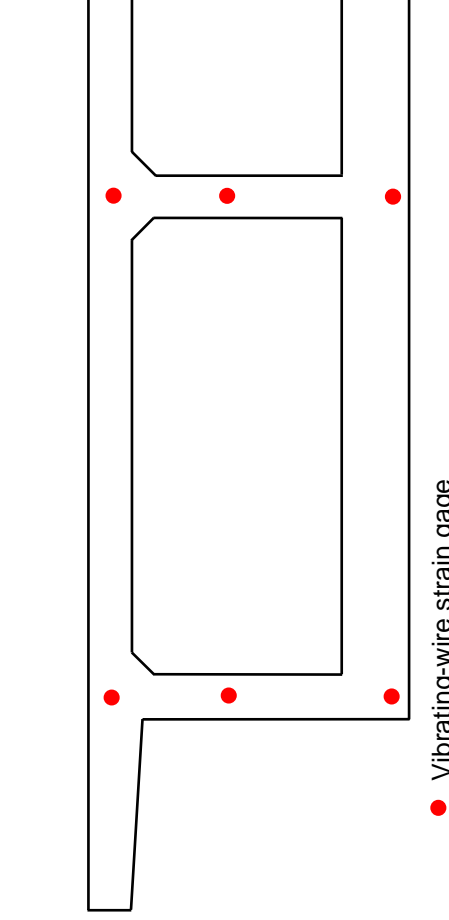


Figure 5.80: Strain profile of F5 near the bent immediately after prestressing.

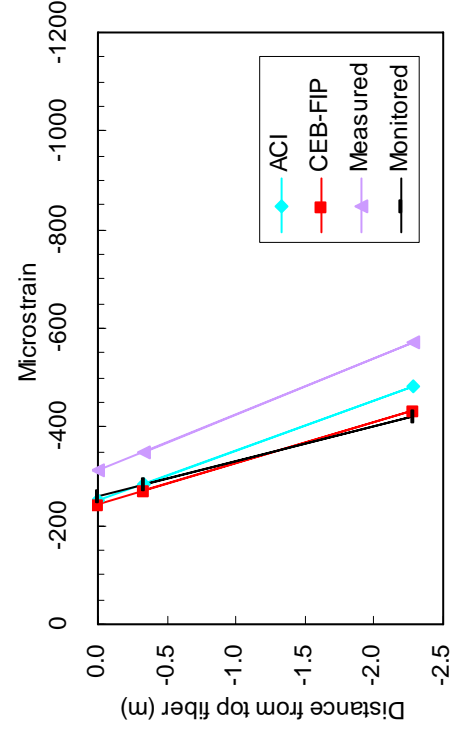


Figure 5.81: Strain profile of F5 near the bent at T303.

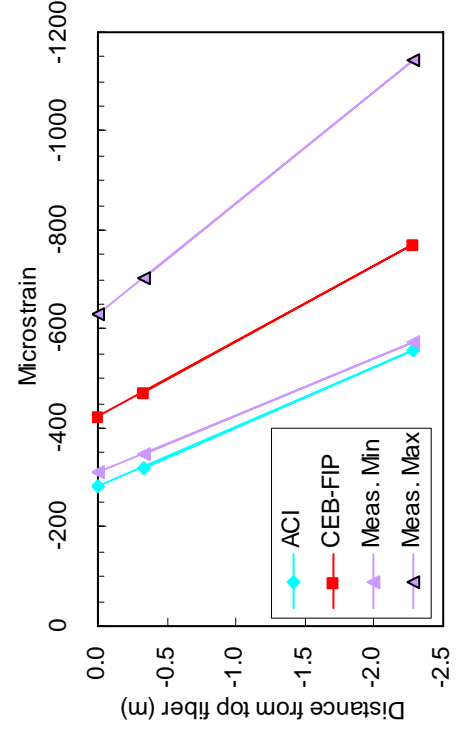


Figure 5.82: Strain profile of F5 near the bent at a theoretical end of service life.

5.4.3.1. Frame 5 Midspan

The results of F5 analysis appear significantly improved as compared to the results of F4. This is largely a result of the less complicated construction sequence of F5. The prestress was applied in full over the course of one day. The falsework did not remain in place for such a lengthy period as that of F4. As F5 is not curved in the horizontal direction, it is more appropriate for comparison to plane frame analysis.

When the prestress is applied in F5 at midspan, the analytical strains are 4.6% greater than the monitored strain at the level of the prestressing tendons, 1.88 m below the top fiber of the prestressing tendons, as shown in Figure 5.76. Differences between the monitored and analytical strains are presented in Table 5.7.

At T303, the ACI [3] derived material property inputs generated predictions of strain that are 8.2% larger than the monitored strain at the level of the prestressing tendons (Figure 5.77). The CEB-FIP [10] derived material property inputs resulted in a strain profile 2.5% larger than the monitored strain at the same point in time and section depth. The strain profile generated using the measured material properties was 26.3% larger than the monitored strain at the level of the prestressing tendons. The reason behind the acute differences in analysis results between the derived ACI [3] and CEB-FIP [10] material property inputs and the measured material properties is the development rate of the material properties, as illuminated in Figure 5.73 and Figure 5.74.

At T303, the derived ACI [3] and CEB-FIP [10] creep and shrinkage material properties complement one another and produce analysis results that are similar. The measured material properties exceed the ACI [3] and CEB-FIP [10] properties at all points in time and consequently produce analytical strains that exceed those of ACI [3] and CEB-FIP [10].

5.4.3.2. Frame 5 Bent

For F5 near the bent, the initial strain at prestressing is 15.7% lower than that obtained through monitoring at the level of the prestressing tendons 0.34 m below the top fiber of the section, as shown in Figure 5.80. Differences in strain between the monitored and analytical strains appear in Table 5.7.

At T303, the strains produced using the derived ACI [3] and CEB-FIP [10] material property inputs demonstrated correlation to the monitored strain 0.9% greater and 3.7% lower than the monitored strain at the level of the prestressing tendons (Figure 5.81). The strain profile generated through analysis using the measured material property inputs is 23.8% larger than the monitored strain at the level of the prestressing tendons. This is expected based on the correlation of previous strain profiles for other sections in F4 and F5.

At the theoretical end of service life Figure 5.80, the ACI [3], CEB-FIP [10], and measured strain display progressively larger strains for the same reasons as discussed previously for the other sections.

Table 5.7: Monitored and analytical strains at the level of the centroid of the prestressing tendons in F5.

	Depth of prestress from top fiber (m)	Occasion	Bridge Monitoring	ACI		CEB-FIP		Measured (material tests)					
				ϵ_c ($\mu\text{m/m}$)	% difference from monitored	ϵ_c ($\mu\text{m/m}$)	% difference from monitored	Minimum material properties	Maximum material properties	ϵ_c ($\mu\text{m/m}$)	% difference from monitored	ϵ_c ($\mu\text{m/m}$)	% difference from monitored
Midspan	1.877	Initial (prestressing)	-194	-203	4.6	-203	4.6	-203	-203	-203	4.6	-203	4.6
		T303	-415	-449	8.2	-425	2.5	-524	-524	-524	26.3	-524	26.3
		Theoretical end of service	-	-508	-	-693	-	-522	-522	-972	-	-972	-
Near the Bent	0.343	Initial (prestressing)	-199	-168	15.7	-168	15.7	-168	-168	-168	15.7	-168	15.7
		T303	-282	-285	0.9	-272	3.7	-349	-349	-349	23.8	-349	23.8
		Theoretical end of service	-	-321	-	-474	-	-348	-348	-703	-	-703	-

5.5. Commentary for Frame 4 and Frame 5

The results of all analysis, both F4 and F5, indicate similar trends of the strain progression with time for the cases examined. The material properties used in analysis displayed in Table 4.3 and Table 4.4 indicate the differences in development trends of the material properties. Considerable change in both creep and shrinkage occurred within the first 200 days after prestressing was applied, which is reflected in the analytical strain profiles.

The calculated CEB-FIP [10] material properties existing at T363 for F4 and T303 for F5 are similar to those of ACI [3]. However, the development of these material properties with time occurred at a different rate than that of ACI [3]. The similarities in material properties produced from ACI [3] and CEB-FIP [10] at T363 and T303 is coincidental. The predicted ACI [3] and CEB-FIP [10] material properties increasingly differ with time. The analysis results using the derived ACI [3] material property inputs shows very little change in strain between T363 in F4 and T303 in F5 and the theoretical end of service life in both frames. The CEB-FIP [10] material properties increase much more than the ACI [3] material properties between T363 or T303 and the theoretical end of service life leading to differences in strain at the end of service life.

The ACI [3], CEB-FIP [10], and measured material property inputs each produced unique strain profiles for F4 and F5 which varied substantially. This is not an unexpected result. The derived ACI [3] and CEB-FIP [10] material property inputs were generated using the specifications with the specific V/S input for the bridge. The measured material properties were taken from the tests, with a small V/S, and adjusted for the V/S of the bridge, which is larger. The development rate of the material properties for the test specimens and the bridge are different. The method of proportioning the material test values for the bridge is based on the development rate for the test specimens and not the bridge, resulting in substantially different strain profiles at all points in time, and most notably, at the end of service life. The strain profiles produced using the measured material properties from testing were similar to the strains produced

using the CEB-FIP [10] material properties for analysis of F4. This results as the CEB-FIP [10] specification was used in adjusting the measured material properties. Also, in F4, the concrete was not prestressed until several months after it was cast. Although the shrinkage was found to be excessive for both F4 and F5, the shrinkage after many months was not large, using the shrinkage from F5 for that of F4. For F5, the shrinkage was larger than predictions, since the concrete was prestressed at a young age. Much shrinkage occurred after prestressing, thus leading to predictions of strain for F5 using the measured material properties that greatly exceed those of ACI [3] and CEB-FIP [10] at the end of service life.

The strain profiles predicted with CPF [16] showed acceptable correlation with the measured strains in F4, while showing excellent correlation with the monitored strains in F5 at prestressing and T363 or T303. Table 5.6 and Table 5.7 display the error differences between the monitored and analytical results from these two frames. Although many of the strain profiles of the CPF [16] analysis were shown to have good correlation with the monitored strains, some of the CPF [16] analyses were not able to adequately capture the behavior of the bridge. The strains are an intermediate step in the determination of prestress loss from the monitored data. The variation in correlation of the analytical and monitored strains on the influence of prestress loss is not direct, as the monitoring program does not account for intrinsic relaxation. In some instances the curvatures of the strain profiles of CPF [16] and monitoring have slopes with opposite directions. None of the strains displayed unexpected behavior. Although some of the strain profiles showed considerable mismatch, determination and use of the strains are only an intermediate step in the achievement of the end goal. The influence of the variations in strain are discussed earlier.

The results of analysis are compared to the monitored strains at the level of the prestressing tendons in Table 5.6 and Table 5.7. These two tables present the difference percentages of the analytical strains from the monitored strains. These differences will be useful for comparison to the prestress loss values and differences between the monitored and analytical results in an earlier chapter.

As mentioned previously in an earlier chapter as well as in Section 5.4, the measured material properties were taken at minimum and maximum values. These extremes were used as they represent the expected range of creep and shrinkage that can be expected for the bridge. Used as input to analysis in CPF [16], upper and lower bound (maximum and minimum) strains are obtained for the monitored sections. The minimum and maximum material properties produce corresponding minimum and maximum strain predictions for the monitored sections. It can be expected that the range of strain in the concrete at the theoretical end of service life will occur somewhere between the range of strain predictions from the minimum and maximum material properties. This range of concrete strain is presented in Table 5.6 and Table 5.7 to illustrate the range of strain that can be expected for each bridge frame at the theoretical end of service life.

It can be seen in Table 5.6 and Table 5.7 that the use of the minimum measured material properties as input into the CPF [16] analysis results in identical strains at T363 or T303 and the theoretical end of service life for F4 and F5, respectively. The reason that this occurs is because the minimum material properties were taken as those that occurred at T363 or T303. Since the material properties are the same the concrete strains are the same as well. The strains are not identical at T363 or T303 and the theoretical end of service life because intrinsic relaxation of the prestressing steel occurs regardless of the behavior of the concrete and is a change in stress without associated strain. The stresses in the concrete adjust due to this loss in prestress and results in small differences in the strain at these points in time.

The strains are a direct link to the prestress loss that occurs in the bridge. It has been shown that the strain profiles for the three analyses of F4 and F5 at the theoretical end of service life are quite varied. Certainly, the amount of prestress loss that is indicated by the three analyses will follow the trends of the strains, with the largest prestress loss resulting from the analysis with the measured material properties and lowest amount in the analysis with the ACI [3] properties. The CEB-FIP [10] material properties should result in a prestress loss that is

between the values of the other two analyses. The important question will be the magnitude of prestress loss that occurs and whether the differences in strain are indicative of the differences in long-term loss. Intrinsic relaxation is not indicated by a change in strain; relaxation must be added to the stress determined from monitoring, as will be described in the next chapter.

The material property values obtained through the tests should create analysis results that follow the results of monitoring. It has been shown that the measured material properties, when used as input to the computer analyses, produced results that exceed those obtained through monitoring. The measured material properties, if accurately characterized through testing (which is not implied by the shrinkage tests for the F4 and F5 concrete), used as input into the analysis should produce results that match very well the monitored data. As shown in this chapter, the calculated material properties from the ACI [3] and CEB-FIP [10] specifications, used as input in analysis, compared more closely with the monitored strains than the strain profiles produced using the maximum material property inputs from testing. Use of the F5 shrinkage for F4 produced good results. This occurred because the amount of shrinkage that occurred in F4 was very small beginning after the application of prestressing. The minimum material properties from testing produced considerably lowered predictions of strain and were much closer to the analyses using the specifications predictions. The actual strain is expected to occur within the range of values produced using the measured material properties; the fact that the analysis results using the minimum material properties are similar to the specifications results, this is acceptable.

Examining the figures for bridge shrinkage in Section 3.8 it can be seen that the shrinkage produced from the curves fit to the measured data exceeds the predictions of ACI [3] and CEB-FIP [10]. This trend results in the predictions of strain at the end of service life that are larger using the measured material properties as input, especially for F5. It must be noted that the creep and shrinkage values for the theoretical end of service life are predictions only and are based on the available data at the present time of writing this Report. It is

expected that the predictions of strain using the measured material properties represent the largest extreme. Several of the measured data points for creep and shrinkage do not follow trends in a particularly predictable fashion. For this reason, the curve-fit produces end of service life predictions that are larger than the predictions of ACI [3] and CEB-FIP [10]. With additional measuring of creep and shrinkage from the material test specimens, an improved data series will be obtained. This is shown schematically in Figure 5.73 and Figure 5.74.

In Section 3.7, the results of material testing were compared to the material properties predicted using the specifications. In most cases the specification based predictions of creep and shrinkage did not produce a wide range of results. The measured material properties were not as well correlated to the specifications as the specifications predictions were to one another. This is especially true for shrinkage, which far exceeded predictions. Creep was adequately correlated to the specifications predictions, especially as the age of the concrete at loading increased. The tight clustering of material property predictions confirms the validity of the specifications methods. This does not prove that the material tests are incorrect; however, it strongly implies that perhaps more considerations are required in controlling the development of the tested properties. In the development of the specifications methods, material tests were conducted similar to those performed as part of this research and discussed in an earlier chapter. Unlike the tests for this research in which three specimens were used for each creep test and two specimens for each shrinkage test, in the development of the equations for the specifications, several hundred specimens were tested under strict control [3, 5, 12, 17, 21]. The temperature and humidity were maintained at nearly constant levels. The tests conducted as part of this research were not controlled in the same manner. The test specimens were subject to the exact environmental influences and due to the substantial differences in size, do not behave in the same manner as a larger structure.

6. Long-Term Prestress Loss

6.1. Introduction

The prestress losses presented in this chapter are those determined for specific sections in Frame 4 (F4) and Frame 5 (F5), over the monitoring period considered in this research. Analysis results are presented in this chapter corresponding to the strains in Chapter 5 at T363 and T303 for F4 and F5, respectively. Additionally, the losses were estimated through analysis at an assumed theoretical end of service life for the bridge at 20,000 days, or approximately 55 years. Regardless of whether 55 years is the actual end of service life for the I5/805 Bridge, the time-dependent material properties increase less than 2% between 20,000 days and 100,000 days (274 years), a period of time of 219 years. From analysis, the prestress loss within this period of time would increase no more than 2%, depending on the magnitude of the initial material properties used to predict the final deformation at 274 years.

The strain profiles obtained from monitoring and analysis were shown to be closely correlated in Chapter 5. With this in mind, it is appropriate to compare the prestress loss determined from monitoring and analysis at the theoretical end of service life. Since predictions made by the specifications cannot be made at intermediate time periods comparison of the prestress loss at T363 and T303 is not appropriate. For this reason, the predicted prestress loss from analysis is also presented. A simplified method referred to as the Proposed Method [29], to be described later in Section 6.3, is used to predict prestress loss levels at T363 and T303 as well as at the end of service life.

6.2. Prestress Loss obtained from Monitored Data

The prestressing steel tendons were grouted soon after post-tensioning and are assumed to be fully bonded to the concrete for and therefore the change in strain in the concrete, at the same level of the prestressing steel, equals the change in strain in the prestressing steel. The change in stress cannot be

measured explicitly from the bridge, as the tendons themselves were not instrumented. Electrical resistance strain gages were considered to be unreliable for long-term monitoring and could further be damaged during post-tensioning, and hence were not used.

The change in prestress $\Delta\sigma_{ps}$, indicated through monitoring, was calculated using Eq. 6.1.

$$\Delta\sigma_{ps} = \Delta\varepsilon_c E_p + \overline{\Delta\sigma_{pr}} \quad (6.1)$$

The loss in prestress caused by creep and shrinkage in the concrete was determined from the change in monitored strain $\Delta\varepsilon_c$ at the level of the prestressing tendons, between the time of prestressing and T363 or T303, multiplied by the modulus of elasticity of the prestressing steel E_p . The monitored change in strain was influenced by thermal strain and hence thermal strain was subtracted from the quantity $\Delta\varepsilon_c$ as explained in Section 5.3.1. The reduced relaxation $\overline{\Delta\sigma_{pr}}$ is a measure of the change in stress without associated change in strain and cannot be measured with the VW gages. The values of $\overline{\Delta\sigma_{pr}}$ were determined with Eqs. 2.2 and 2.3.

The prestress loss obtained using the monitored data in the upcoming sections is presented and compared to the loss indicated through analysis for both F4 and F5. Although the strain profiles in Chapter 5 show the influence of time-dependent changes in material properties on the strain, the strain profiles are an intermediate step in the determination of loss since the reduced relaxation quantity has to be added to the product of $\Delta\varepsilon_c$ and E_p .

The monitored prestress losses are presented corresponding to daily averages of the prestress loss for the duration of monitoring. It is emphasized that bridge monitoring should continue for a longer period of time to collect enough data to provide a more accurate estimate of the prestress loss at the theoretical end of service life. In the current case, the use of a shorter time period of monitoring results in the use of a range of possible values.

Unless otherwise noted, all prestress loss values presented exclude the immediate losses that occurred at transfer. At the end of the chapter, the losses due to time-dependent influences will be shown in their calculated or measured states in addition to the immediate prestress loss to give the total prestress loss.

6.2.1. Frame 4 Midspan

The strains obtained from monitoring, were previously discussed in Section 5.3. The gages at different levels within each of the monitored stems provided data to create a strain profile through the section at all points in time. In Eq. 6.1, the term $\Delta\varepsilon_c$ relates to the change in strain at the level of the prestressing tendons between prestressing and T363 for F4. The change in strain between any point in time and the initial strain at prestressing was used to obtain $\Delta\varepsilon_c$ for all points in time between prestressing and T363. The change in monitored strain, at the level of the centroid of the prestressing tendons, resulting from creep and shrinkage in F4 at midspan, between prestressing and T363, is displayed in Figure 6.1.

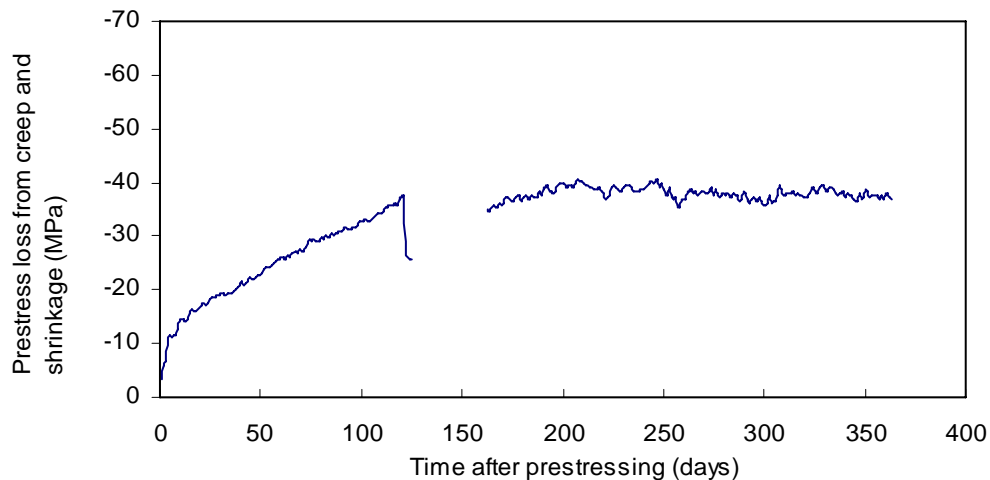


Figure 6.1: Prestress losses resulting from creep and shrinkage in F4 at midspan between prestressing and T363.

The intrinsic relaxation of the tendons in F4 at midspan that has occurred over time between prestressing and T363 is presented in Figure 6.2. The intrinsic

relaxation was calculated with an initial stress σ_{p0} of 1.246 GPa and a yield stress σ_{py} of 1.586 GPa.

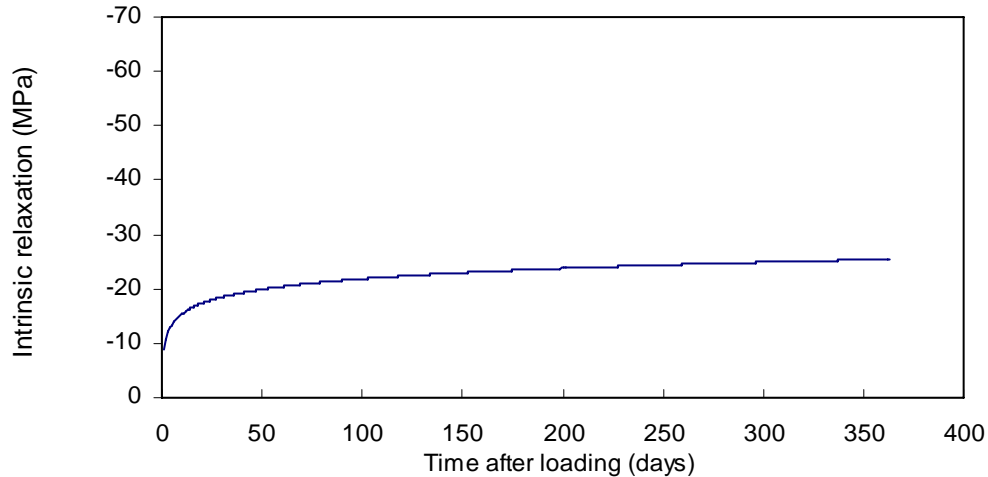


Figure 6.2: Intrinsic relaxation of tendons used in F4 between prestressing and T363.

Prestressing tendons that are stressed between two fixed points are subject to losses in stress due to intrinsic relaxation, as discussed in the preceding paragraph. In the monitored bridge spans considered in this research, the tendons are anchored at the ends of the superstructure. The concrete in the bridge creeps from the applied prestress axial load and shrinkage occurs in the concrete as water is lost through hydration. As creep and shrinkage occur, the ends of the member move towards one another and result in changes in strain. The change in strain over time decreases the stress in the tendons as well as creep in the concrete, which allows the reduction of intrinsic relaxation. The intrinsic relaxation is reduced by χ_r to produce the reduced relaxation, presented in Figure 6.3.

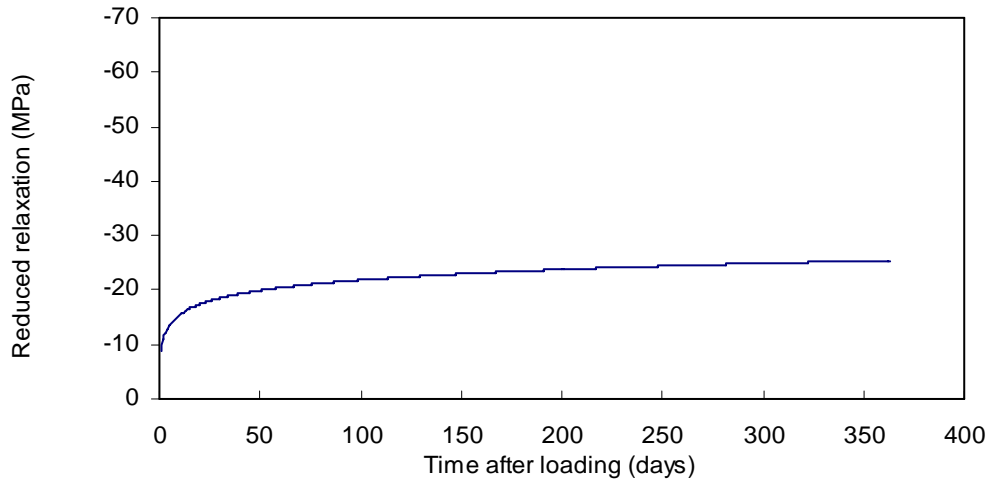


Figure 6.3: Reduced relaxation of tendons used in F4 between prestressing and T363.

The prestress loss that occurred over the monitoring period, from prestressing to T363 (Figure 6.4), is the sum of the loss values resulting from creep and shrinkage (Figure 6.1) and reduced relaxation (Figure 6.3).

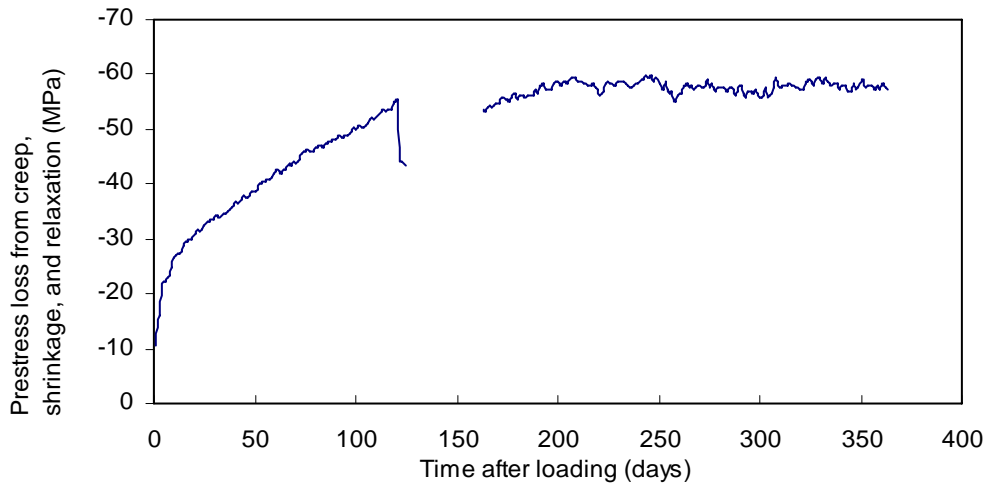


Figure 6.4: Prestress losses resulting from creep, shrinkage, and relaxation in F4 at midspan between prestressing and T363.

At midspan, the prestressing tendons are nearest the soffit. For this reason, the progression of prestress loss at this location (Figure 6.4) is reasonably reflected by the shape of the strain progression in the soffit Figure 5.28.

It can be seen in Figure 6.4 that the prestress increased by 10 MPa when the falsework was removed, 121 days after prestressing. About 200 days after prestressing, the prestress does not vary substantially (not more than 3 MPa) and appears to have reached an asymptotic value of about 60 MPa.

6.2.2. Frame 4 Near the Bent

The loss in prestress resulting from creep and shrinkage obtained from the monitored data is presented in Figure 6.5. As the prestressing tendons at the location near the bent are located near the deck, the prestress loss progresses similar to the strain in the deck of F4 near the bent, as shown in Figure 5.35.

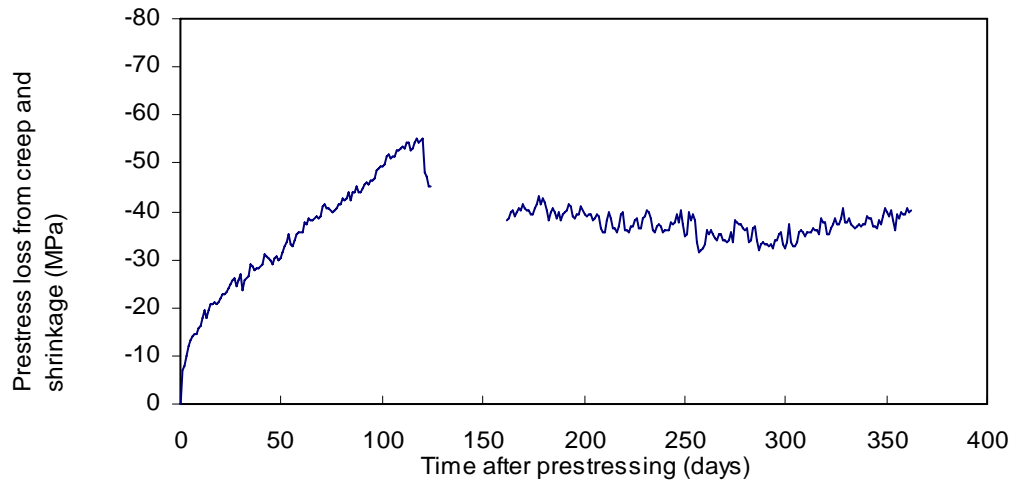


Figure 6.5: Prestress losses resulting from creep and shrinkage in F4 near the bent between prestressing and T363.

Adding the loss due to creep and shrinkage (Figure 6.5) with that of relaxation (Figure 6.3) results in the combined prestress losses from time-dependent influences (Figure 6.6).

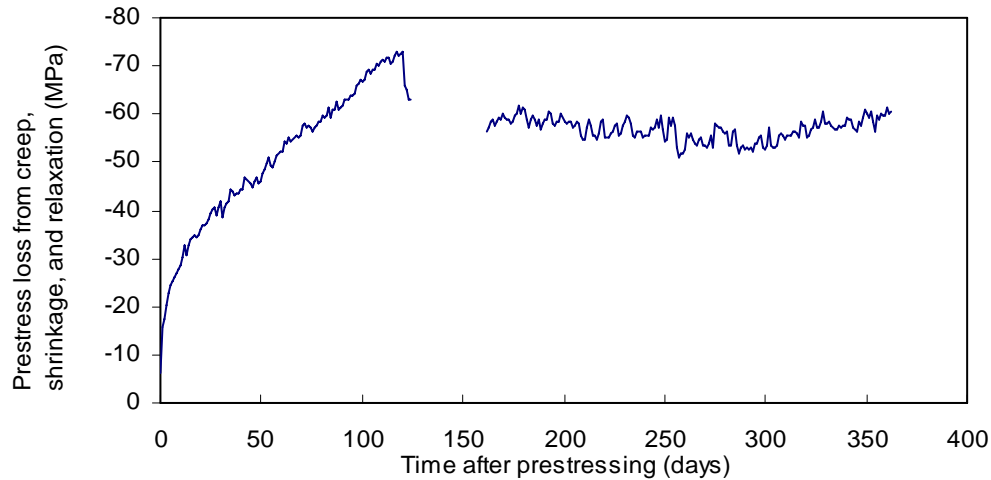


Figure 6.6: Prestress losses resulting from creep, shrinkage, and relaxation in F4 near the bent between prestressing and T363.

When the falsework was removed, a prestress gain of 10 MPa occurred. This resulted from the added load imposed on the structure, which created additional tension in the tendons. It is apparent that the prestress gained another 5 MPa during the next 40 days. Starting about 200 days after prestressing, the prestress loss fluctuated within 5 MPa of an approximately asymptotic value of 60 MPa.

6.2.3. Frame 5 Midspan

The prestress loss obtained from the monitored data resulting from creep and shrinkage is presented in Figure 6.7 for the section at midspan in F5. As discussed in Section 5.3.2.3, the point in time at which the falsework was removed is not visually apparent; this event occurred 69 days after prestressing. The instant at which the hinge was loaded is identifiable, through a sharp decrease in prestress loss, 156 days after prestressing. The prestress loss appears to have reached an asymptotic value of about 40 MPa after the hinge was loaded. A short-term change in prestress was observed immediately after the falsework was removed, noting that the falsework supporting the hinge was not removed in one instant. Due to the restraints of the hinge supporting falsework, the strain, and hence the stress, adjusted during the period of

removal, but reached a constant state after the falsework was fully removed, fluctuating within 4 MPa.

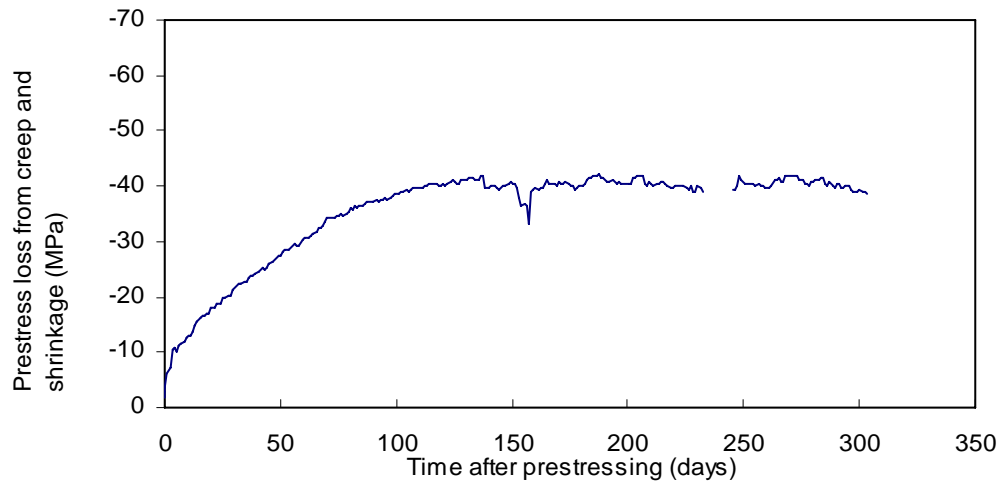


Figure 6.7: Prestress losses resulting from creep and shrinkage in F5 at midspan between prestressing and T303.

The intrinsic relaxation of the tendons was calculated from Eq. 2.2 and is presented in Figure 6.8. The initial stress in the tendons at prestressing was taken as 1.277 GPa. The prestressing steel yield stress was taken as 1.586 GPa.

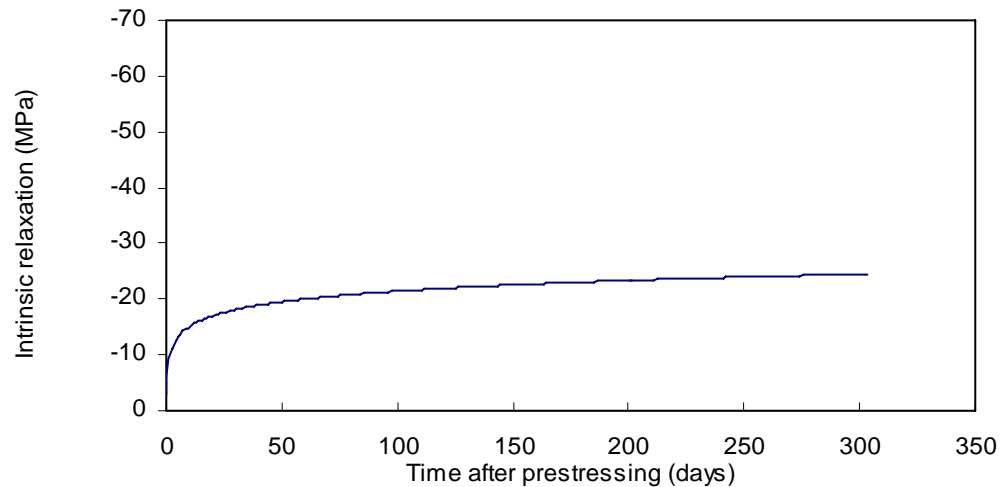


Figure 6.8: Intrinsic relaxation of tendons used in F5 between prestressing and T303.

The intrinsic relaxation (Figure 6.8) is reduced by 20% to yield the reduced relaxation, as discussed in Section 2.1.3, presented in Figure 6.9.

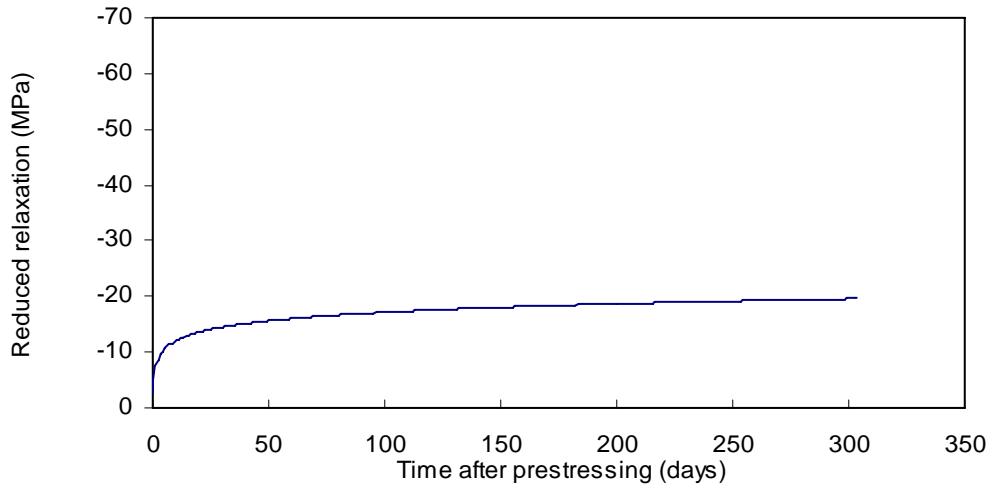


Figure 6.9: Reduced relaxation of tendons for F5 between prestressing and T303.

The sum of the influences of creep, shrinkage, and relaxation, for the period during monitoring, on prestress losses is shown in Figure 6.10. It can be seen that after the hinge was loaded, the prestress loss fluctuated within 4 MPa about an asymptotic value of 60 MPa.

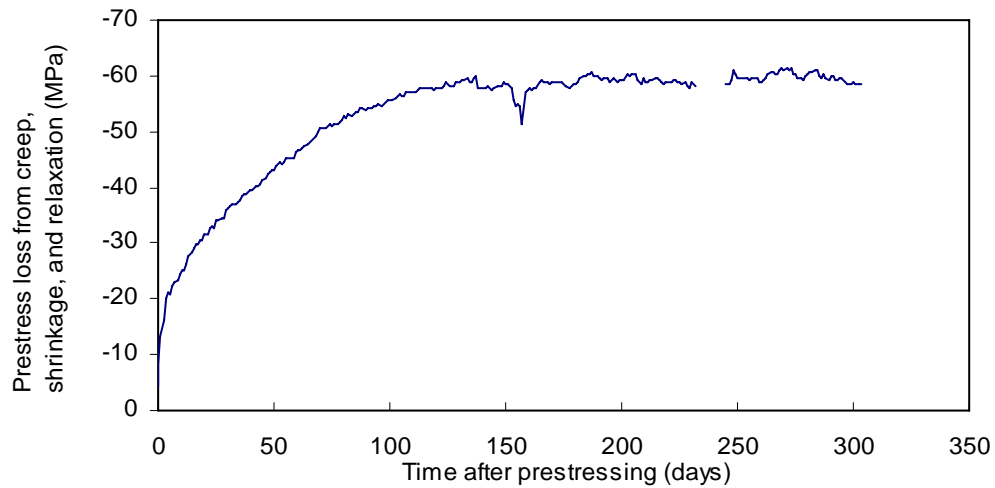


Figure 6.10: Prestress losses resulting from creep, shrinkage, and relaxation in F5 at midspan between prestressing and T303.

6.2.4. Frame 5 Near the Bent

The prestress loss resulting from creep and shrinkage, as obtained from the monitored data in F5 near the bent, is presented in Figure 6.11. The initial increase in prestress loss resulting from creep and shrinkage occurred rapidly until reaching a maximum at 69 days after prestressing, when the falsework was removed. The stress in the tendons decreased by 8 MPa when the falsework was removed. The added tension on the tendons from the additional self-weight increases the prestress. After the immediate gain in prestress when the falsework was removed, the prestress loss continued to increase by about 7 MPa to a point immediately prior to the loading of the hinge.

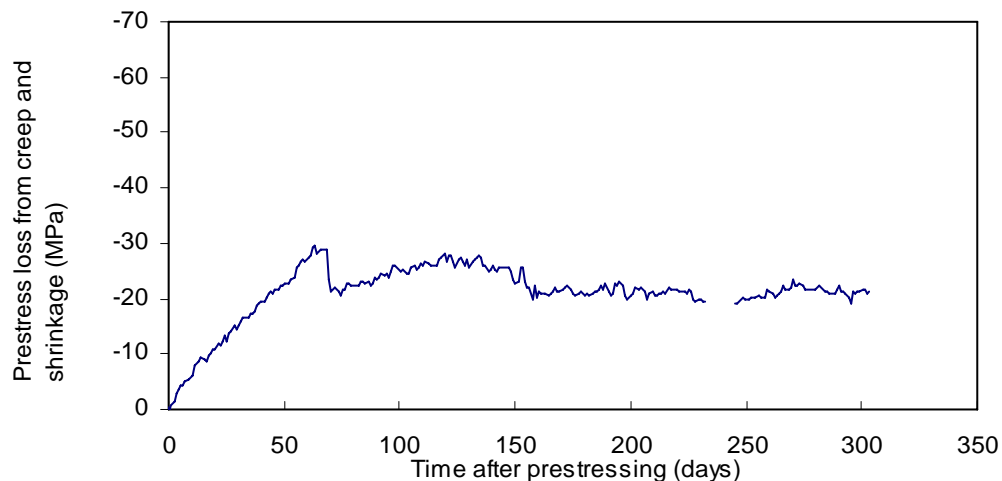


Figure 6.11: Prestress losses resulting from creep and shrinkage in F5 near the bent between prestressing and T303.

The prestress loss that occurred in F5 near the bent between prestressing and T303 is included in Figure 6.12, reflecting the sum of the influences of creep, shrinkage, and relaxation. The losses resulting from relaxation are the same as those for the midspan location in F5, presented in Figure 6.9. The strain at the level of the prestressing tendons is most similar to the concrete strain in the deck near the bent (Figure 5.55). The prestress loss maintained an approximately asymptotic value of about 40 MPa, which varied about 3 MPa for 150 days after the hinge was loaded to T303.

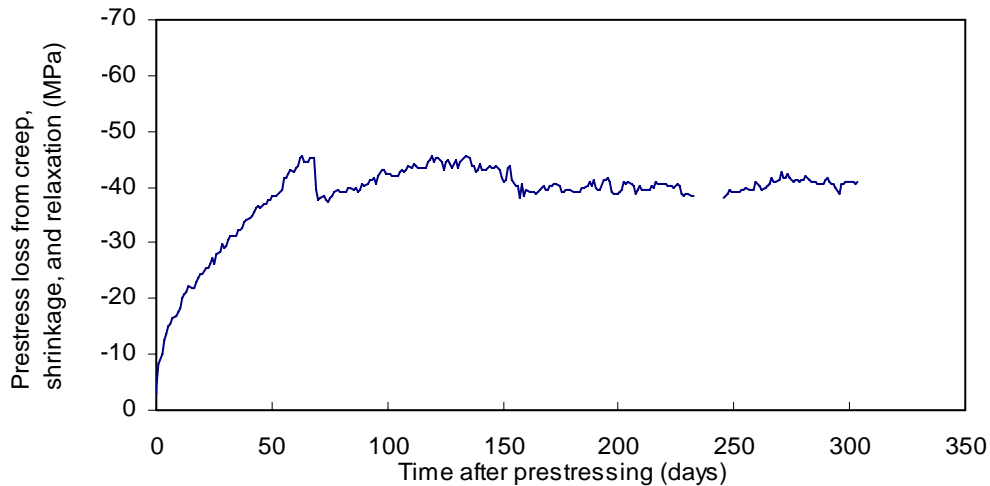


Figure 6.12: Prestress losses resulting from creep, shrinkage, and relaxation in F5 near the bent between prestressing and T303.

6.3. Prestress Loss: Proposed Method

As mentioned previously, the use of a simplified analytical method, denoted as the “Proposed Method” [29], was used in this research for producing estimates of the prestress loss at T363 and T303 as well as at the theoretical end of service life. The steps used to determine prestress loss predictions with the Proposed Method are included in Appendix D.

In using the Proposed Method all loads must be imposed in full at the same time prestress is applied. Determination of prestress loss at any instant in time during the life of the structure is accommodated through the inputs of creep and shrinkage. The creep and shrinkage were taken from ACI [3], CEB-FIP [10], and as measured from testing. The Proposed Method [29] can currently only accommodate a single type of concrete and as such, only one creep and shrinkage value. For this reason, the values of creep and shrinkage provided in Table 4.3 and Table 4.4 were used to formulate a weighted average of creep and shrinkage based on the concrete areas experiencing particular creep and shrinkage, as presented in Table 6.1. The section geometries are represented in Figure 4.9 and Figure 4.11. The inputs for time-dependent material properties,

prestressed and non-prestressed reinforcement, and modulus of elasticity are presented in Table 6.1.

Table 6.1: Inputs used in the Proposed Method [29].

Input Parameter	Symbol	Units	Frame 4		Frame 5		
			T363	End of service	T303	End of service	
Prestressed steel relaxation	$\Delta\sigma_{pr}$	MPa	-29.3		-28.8		
Prestressing steel modulus of elasticity	E_p	GPa	193		193		
Concrete modulus of elasticity	E_c	GPa	33		32		
Prestressed steel area	A_{ps}	mm ²	42280		27440		
Non-prestressed steel area, deck	$A_{s,top}$	mm ²	35000		35000		
Non-prestressed steel area, soffit	$A_{s,bot}$	mm ²	31000		31000		
ACI	Shrinkage strain	ϵ_{sh}	$\mu\text{m}/\text{m}$	88	114	195	231
	Creep coefficient	$\phi(t,t_0)$		0.80	1.06	0.88	1.14
CEB-FIP	Shrinkage strain	ϵ_{sh}	$\mu\text{m}/\text{m}$	89	306	106	356
	Creep coefficient	$\phi(t,t_0)$		1.03	1.53	1.22	1.71
Measured	Shrinkage strain	ϵ_{sh}	$\mu\text{m}/\text{m}$	131	327	264	711
	Creep coefficient	$\phi(t,t_0)$		1.31	1.63	0.99	1.48
Aging coefficient	χ		0.93		0.87		
Relative humidity	RH	%	66		67		

6.3.1. Strain Profiles Determined Using the Proposed Method

To generate predictions of prestress loss, the Proposed Method [29] requires that the initial strain profile through the section at the time of prestressing be used as input. The initial strain profiles (at prestressing) were determined using CPF [16]. The strain profiles at T363 and T303 as well as at the theoretical end of service life were calculated using the Proposed Method [29] and CPF [16] to be used for comparison. The prestress loss calculated using the Proposed Method [29] is presented in Section 6.5 and is compared to the predictions of other methods.

It was necessary to use the full self-weight of the structure applied simultaneously with prestressing (LC100/0), as the Proposed Method [29] makes no accommodation for the application of load at other instants. The strain profiles of the Proposed Method [29] are not being compared to the monitored results because the monitored results are for a loading case similar to that of LC50/50.

In Figure 6.13, the initial strain profile (at prestressing) used as input to the Proposed Method [29] for analysis of F4 at midspan is shown. The initial strain profiles for each of the monitored sections were taken from CPF [16], as indicated in Figure 6.13 through Figure 6.16.

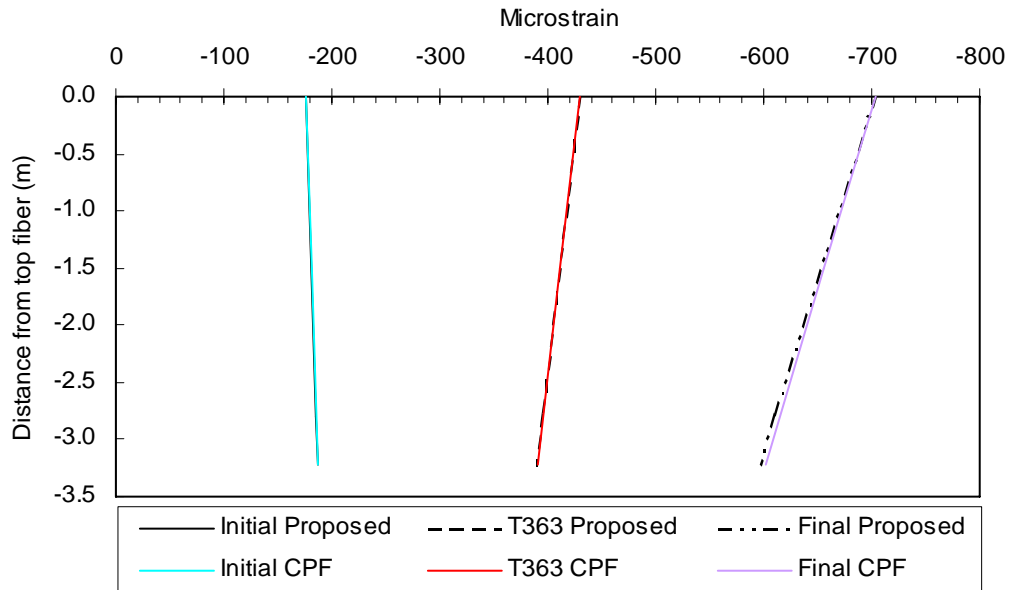


Figure 6.13: Strain profiles for the monitored midspan section in F4 at prestressing, T363, and the theoretical end of service life using CEB-FIP material property inputs.

Similar to the strain profiles in F4 at midspan, the strain profiles at the other monitored sections produced by the Proposed Method [29] are nearly identical to those determined through analysis using CPF [16]. Figure 6.14 through Figure 6.16 present the strain profiles at prestressing (initial), at T363 or T303, and at the theoretical end of service life for F4 and F5.

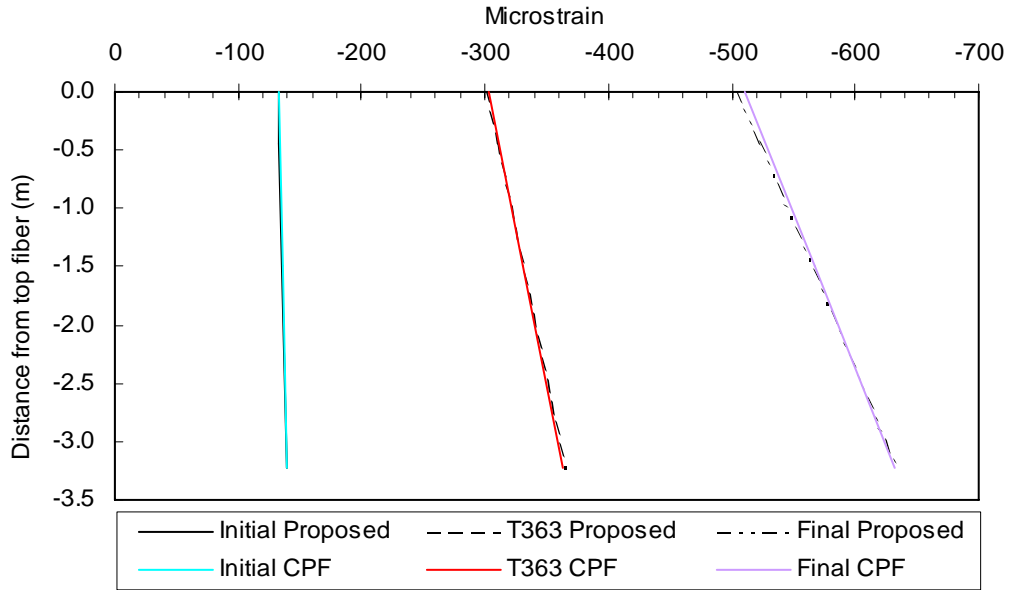


Figure 6.14: Strain profiles for the monitored section near the bent in F4 at prestressing, T363, and the theoretical end of service life using CEB-FIP material property inputs.

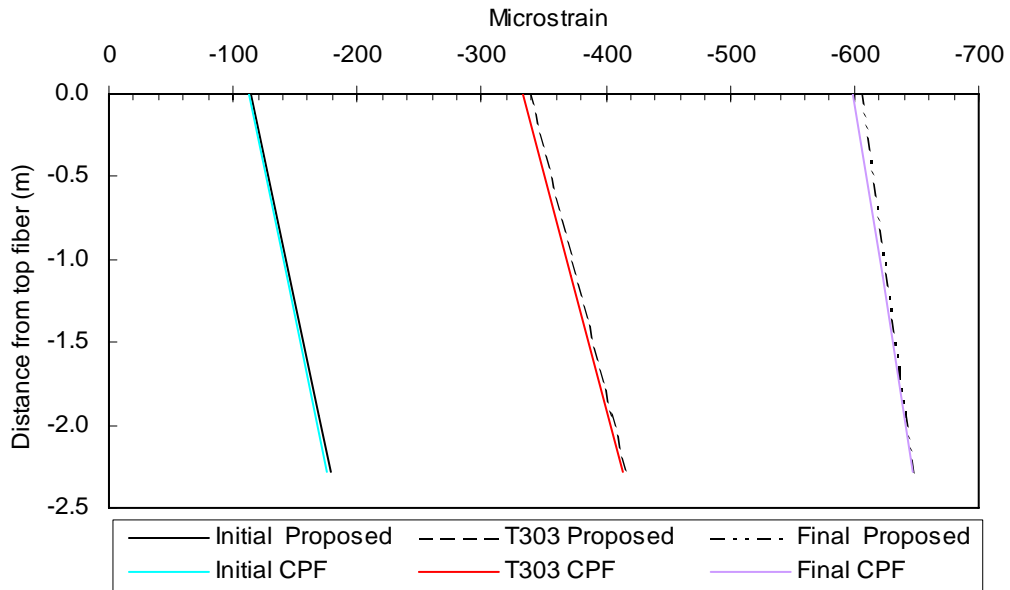


Figure 6.15: Strain profiles for the monitored midspan section in F5 at prestressing, T303, and the theoretical end of service life using CEB-FIP material property inputs.

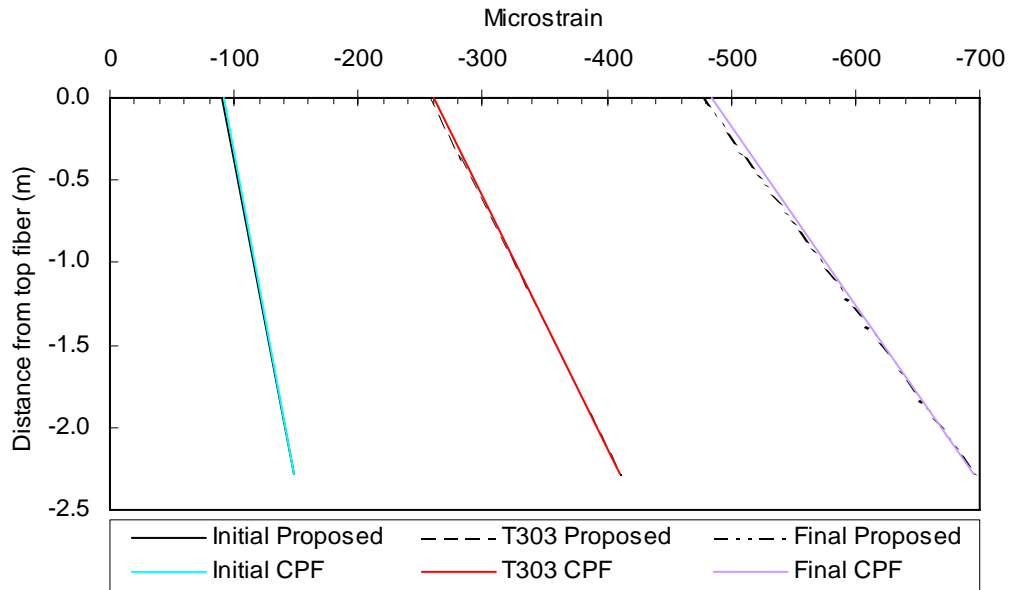


Figure 6.16: Strain profiles for the monitored section near the bent in F5 at prestressing, T303, and the theoretical end of service life using CEB-FIP material property inputs.

It can be seen that at T363 or T303 and at the theoretical end of service life, the strain profiles calculated using the Proposed Method [29] and CPF [16] are essentially the same. The figures presented in this section (Section 6.3.1) verify that the Proposed Method [29] produces essentially identical results as that of CPF [16]. This is significant in that the Proposed Method [29] is a considerably simpler method than CPF [16]. The strain profiles produced through analysis using the ACI [3] and measured material properties are included in Appendix E. Associated prestress losses for all sets of material properties are included in Section 6.5.

6.3.2. Proposed Method Prestress Loss

In this section, the prestress losses determined using the Proposed Method [29] are examined. The prestress loss values determined from the Proposed Method [29] using the inputs discussed in the previous section are presented for F4 and F5 in

Table 6.2. It can be seen that the prestress loss values calculated with these two methods are very similar for corresponding points in time. Like the similarities

in strain profiles, the calculated prestress loss values further emphasize that the simpler Proposed Method [29] can calculate prestress losses comparable to the more complicated CPF [16].

Table 6.2: Comparison of prestress loss values determined using the Proposed Method and CPF at significant instances during the life of the structure (LC100/0).

Point in time	Material property inputs	Analysis method	Prestress loss (MPa)			
			Frame 4		Frame 5	
			Midspan	Bent	Midspan	Bent
T363 (363 days after prestressing)	ACI	CPF	-53	-47	-	-
		Proposed Method	-55	-51	-	-
	CEB-FIP	CPF	-59	-51	-	-
		Proposed Method	-62	-56	-	-
	Min. Measured (tests)	CPF	-71	-63	-	-
		Proposed Method	-74	-67	-	-
	Max. Measured (tests)	CPF	-71	-63	-	-
		Proposed Method	-74	-67	-	-
T303 (303 days after prestressing)	ACI	CPF	-	-	-72	-56
		Proposed Method	-	-	-73	-66
	CEB-FIP	CPF	-	-	-65	-48
		Proposed Method	-	-	-66	-59
	Min. Measured (tests)	CPF	-	-	-86	-67
		Proposed Method	-	-	-86	-82
	Max. Measured (tests)	CPF	-	-	-85	-66
		Proposed Method	-	-	-86	-82
End of service life (20,000 days after prestressing)	ACI	CPF	-73	-66	-92	-72
		Proposed Method	-74	-69	-92	-89
	CEB-FIP	CPF	-115	-108	-128	-99
		Proposed Method	-113	-106	-122	-115
	Min. Measured (tests)	CPF	-79	-72	-93	-77
		Proposed Method	-82	-76	-95	-92
	Max. Measured (tests)	CPF	-119	-112	-180	-142
		Proposed Method	-118	-111	-171	-169

6.4. Long-Term Prestress Loss: Specifications Predictions

The prestress loss was predicted with the specifications for F4 and F5 at the locations of the monitored sections. The input data used in the specifications were obtained from the geometry, material properties, and loads; these inputs are presented in Table 6.3. The results of the different methods and use of different inputs will be shown in Section 6.5.

The AASHTO Refined [2] and CHBDC [9] methods allow the structural self-weight to be applied in one or two instances, corresponding to LC100/0 or LC50/50, respectively. These methods were developed to allow additional loading at a future instant. Here, it was useful to use the future-loading instant to accommodate the removal of falsework. In the AASHTO Refined [2] method, Eq. 2.57 includes two concrete stress terms. The first term, f_{cgp} , represents the stress in the concrete at the level of the centroid of the prestressing tendons imposed by all permanent loads simultaneously with prestressing. The term Δf_{cdp} represents the change in concrete stress at the level of the centroid of the prestressing tendons due to additional loads applied after prestressing. Similar to the AASHTO Refined [2] method, the CHBDC [9] specification (Eq. 2.62) requires input of the initial stress f_{cgp} (representing stress due to loads applied with prestressing) and change in stress Δf_{cdp} to represent additional load applied after prestressing. As mentioned in Section 4.6, LC100/0 and LC50/50 accommodate the two loading instances used with these specifications.

Table 6.3: Input parameters used in the specifications for predicting prestress loss in F4 and F5.

Input Parameter	Symbol	Units	Frame 4		Frame 5	
			Midspan	Bent	Midspan	Bent
Initial concrete stress at prestress centroid imposed by prestressing and 100% self-weight	f_{cgp}	MPa	-6.39	-4.19	-5.46	-2.97
Change in concrete stress at prestress centroid from permanent loads applied after transfer	Δf_{cdp}	MPa	0.00	0.00	0.00	0.00
Initial concrete stress at prestress centroid imposed by prestressing and 50% self-weight	f_{cgp}	MPa	-9.10	-7.55	-6.37	-5.27
Change in concrete stress at prestress centroid from permanent loads applied after transfer, 50% self-weight	Δf_{cdp}	MPa	3.00	3.22	1.16	2.35
Prestressed steel relaxation	$\Delta\sigma_{pr}$	MPa	-29.3	-29.3	-28.8	-28.8
Prestressing steel ultimate stress	f_{pu}	MPa	1862	1862	1862	1862
Prestressing steel initial stress	f_{p0}	MPa	1391	1391	1391	1391
Yield stress of prestressed steel	f_{py}	MPa	1675	1675	1675	1675
Yield stress of non-prestressed steel	f_y	MPa	414	414	414	414
Prestressing steel modulus of elasticity	E_p	GPa	193	193	193	193
Concrete modulus of elasticity	E_c	GPa	33	33	32	32
Prestressed steel area	A_{ps}	mm ²	42280	42280	27440	27440
Non-prestressed steel area, deck	$A_{s,top}$	mm ²	35000	35000	35000	35000
Non-prestressed steel area, soffit	$A_{s,bot}$	mm ²	31000	31000	31000	31000
Net concrete area	A_c	m ²	7.96	10.80	6.87	8.62
Concrete moment of inertia	I_c	m ⁴	12.53	16.62	5.57	6.68
Depth of prestress from centroid of concrete section (positive downward)	y_p	m	1.257	-1.240	0.874	-0.742
Shrinkage strain	ϵ_{sh}	$\mu\text{m}/\text{m}$	306	306	356	356
Creep coefficient	$\phi(t,t_0)$		1.53	1.53	1.71	1.71
Aging coefficient	χ		0.93	0.93	0.87	0.87
Relative humidity	RH	%	66	66	67	67

The values of prestress loss calculated with the specifications are presented in Table 6.4 and Table 6.5 for F4 and F5, respectively. It should be noted that the AASHTO Approximate [2] method presents the same result for both the LC50/50 and LC100/0 load cases, because the AASHTO Approximate [2] method calculates the prestress loss independent of applied stress, as evidenced in Eq. 2.55. The CEB-FIP [10] specification does not account for stresses applied after the initial transfer of prestress so was used for only LC100/0.

Table 6.4: Prestress loss values for F4 at the end of service life determined using the specifications.

Location	Load Case	Prestress Loss (MPa)			
		Specification			
		AASHTO Approximate	AASHTO Refined	CEB-FIP	CHBDC
Midspan	LC50/50	-	-198	-	-206
	LC100/0	-123	-148	-133	-148
Near-bent	LC50/50	-	-182	-	-193
	LC100/0	-123	-123	-120	-126

Table 6.5: Prestress loss values for F5 at the end of service life determined using the specifications.

Location	Load Case	Prestress Loss (MPa)			
		Specification			
		AASHTO Approximate	AASHTO Refined	CEB-FIP	CHBDC
Midspan	LC50/50	-	-155	-	-160
	LC100/0	-121	-137	-145	-139
Near-bent	LC50/50	-	-150	-	-161
	LC100/0	-121	-109	-126	-113

6.5. Prestress Loss from Analysis

Using the material properties derived from ACI [3], CEB-FIP [10], and the long-term projected measured properties from testing as input, the analyses present prestress loss values for the theoretical end of service life in F4 and F5.

It should be noted that the monitored strains appeared to reach asymptotic values at T363 and T303 for both F4 and F5. Though it is intended that monitoring will continue for many years, the implications from the monitored strain is that the final value will be within the range predicted by the analyses using the derived material properties from ACI [3], CEB-FIP [10], and measured from testing as input. The inputs for the analyses are presented in Table 5.4 and Table 5.5. The prestress losses from analysis are presented for the points in time at T363 and T303 (for F4 and F5, respectively) and the theoretical end of service life. These analytical results are compared to the results of monitoring. Monitoring must continue for an extended period of time to collect strains that can be compared to the theoretical end of service life predictions and prestress loss.

Through monitoring, it was only possible to determine the change in concrete strain, and hence the change of stress in the prestressing tendons. For these reasons, the results of analysis was used to determine the initial prestress at the jacking end of the tendons as well as the initial tendon stresses at the monitored sections. Analytical results can be used for the initial prestress at the ends of the member and at the monitored sections because initial stresses are not influenced by time-dependent variation in material properties and the initial deformation obtained through analysis reflected that of monitoring. The correlation of the initial monitored strain profiles at the four monitored sections with the analytical results was shown in Section 5.4.

6.5.1. Initial Prestress Losses at Transfer

The jack used to stress the tendons during prestressing inserts wedges around each of the tendon strands to retain the initial stress placed in the tendon. To be effective, the tendons must relax in order to fully anchor the wedges against the bearing surface at the ends of the members. This initial relaxation is a substantial portion of the prestress that is lost over the life of the structure. The initial prestress after transfer is the maximum prestress that the structure will

experience since immediate losses prevent the full jacking stress from being transferred.

In both F4 and F5, the prestress was applied to both ends of the superstructure. After being placed through the ducts, the tendons at the first end of the structure were stressed at 80% of the jacking stress. The second end was then prestressed at the remaining 20% of the jacking stress. This operation significantly improves the distribution of prestress along the length of the member since frictional losses are kept to a minimum. In the bridge, because sequential prestressing was performed, elastic shortening losses occur. In analysis, all tendons are assumed to be stressed at the same time, thus elastic shortening losses are not considered. These losses were taken into account by reducing the initial tendon stress at transfer; however, these losses are usually small compared to those of friction and anchor set. Anchor-set losses are not a significant influence at the monitored sections since friction in the ducts through the member limit the distribution of anchor-set losses though the length of the member and at the monitored sections.

6.5.1.1. Frame 4

In F4, the specified jacking prestress force was 58.85 MN, which translates to an initial tendon stress of 1.39 GPa. To accommodate the elastic shortening, an initial prestress of 1.38 GPa was used in analysis. After complete jacking at the second end of the member, losses due to anchor-set and elastic shortening losses result in an initial prestress of 1.25 GPa in the tendons. This loss caused an immediate reduction of the jacking stress by 9.4%.

Since the tendons are grouped at similar levels, the influence of creep and shrinkage is similar, and the relaxation of the tendons is essentially the same, the stress at the centroid of the three tendons will be used throughout. The immediate losses at transfer at the monitored locations and at the jacking ends of the member are presented in Table 6.6.

6.5.1.2. Frame 5

The jacking force applied to F5 is 37.95 MN creating an initial stress in the tendons of 1.38 GPa. The jacking stress, after elastic shortening losses, was taken as 1.37 GPa. The immediate losses after transfer lead to an initial prestress at the end of the member of 1.28 GPa, a 6.6% decrease from the jacking stress. The immediate losses at transfer at the monitored locations and at the jacking ends of the member are presented in Table 6.7.

6.5.1.3. Comparison of Prestress at Jacking

In Table 6.6 and Table 6.7, the stresses associated with the jacking operation are provided. In F5, the initial prestress at the jacked end immediately after transfer is higher than in F4. It can be seen that at the midspan sections in F4 and F5, the initial prestress was between 10 to 11% lower than the jacking stress. The loss of stress at the near-bent location was lower than loss in stress at midspan in both spans. This results as the self-weight of the superstructure maintains higher tension on the tendons at the near-bent location, thus the initial prestress does not decrease as substantially as it does at midspan.

Table 6.6: Prestress losses before and after stress transfer in F4.

Location	Jacking stress at location	Initial stress at location	Reduction from jacking stress at location	Reduction from initial stress at location
	GPa	GPa	%	%
Jacked end	1.375	1.246	9.4	-
Midspan	-	1.226	10.8	1.6
Bent	-	1.233	10.3	1.0

Table 6.7: Prestress losses before and after stress transfer in F5.

Location	Jacking stress at location	Initial stress at location	Reduction from jacking stress at location	Reduction from initial stress at location
	GPa	GPa	%	%
Jacked end	1.369	1.278	6.6	-
Midspan	-	1.226	10.4	4.1
Bent	-	1.277	6.7	0.1

6.5.2. Frame 4 Midspan

It is appropriate to expect the trends of the prestress losses to be reflected in the strain profiles that were observed in Chapter 5. In each of the three analysis cases using the material property inputs of ACI [3], CEB-FIP [10] and the measured values from material testing, the strains were observed to become progressively larger, in the order presented, at the theoretical end of service life as can be seen in Figure 6.17. This trend is evident in all the figures for strains occurring after prestressing in Section 5.4.

The results of analysis using ACI [3] and CEB-FIP [10] specification derived material property inputs reveal almost the same prestress loss value at T363. This is expected given the similarity in material property inputs, represented in Figure 5.73 and Figure 5.74 at this time. These values are 25.4 and 16.9% lower than the prestress loss obtained through monitoring. As shown in Figure 5.66, the initial analysis strain at this location exceeded the monitored strain by 27.3% at the level of the prestressing tendons immediately after prestressing, so supports the correlation of strain and associated prestress loss. This also suggests that, since the reduced relaxation is added separately, that the differences in strain reflect smaller differences in prestress loss. At T363, the analytical strain, using the measured material properties as input, exceeds the monitored strain by 18%.

It is notable that using the CEB-FIP [10] specifications equation for the prediction of prestress loss (Eq. 2.60) generates almost the same value of loss as the analytical method that utilizes the CEB-FIP [10] derived material

properties as input (Figure 6.17). These different methods produce essentially the same results.

At the theoretical end of service life, the specifications predictions for LC100/0 encompass a range of prestress loss from 123 to 148 MPa representing loss of 10.0 to 12.1% from the initial prestress value. Analysis (LC50/50) produces a range of variation from 60 to 105 MPa corresponding to losses of 4.9 to 8.6% from the initial prestress value. Using the specifications for LC50/50, a range of prestress loss from 198 to 206 MPa was calculated, representing loss of 16.2 to 16.8% of the initial prestress. It can be seen here that the specifications use of LC50/50 significantly overestimates prestress loss at the end of service compared to CPF [16].

It is noteworthy that the range produced by analysis is considerably wider than that of the specifications. The range of variation of specification based prestress loss predictions is 25 MPa while that of CPF [16] analysis varies by 45 MPa. Most specifications calculate internally the time-dependent material properties based on inputs of relative humidity and initial stress. This indicates that the specifications make a reasonably adequate account for material properties for conditions similar to those, which the bridge is exposed., leading to acceptable long-term prestress loss predictions.

At T363, the predictions from the LC100/0 and LC50/50 analysis results differ by about 1.4%. At the end of service life, the difference between the LC100/0 and LC50/50 analysis results decreases to about 1.0%. This results because at the end of service life the structure has had a very long time to deform. Since all structural loads are eventually applied to the structure in either load case, at a point in time very distant from the instant the loads were applied, the prestress loss is similar since the creep, shrinkage, and relaxation ultimate values are equivalent.

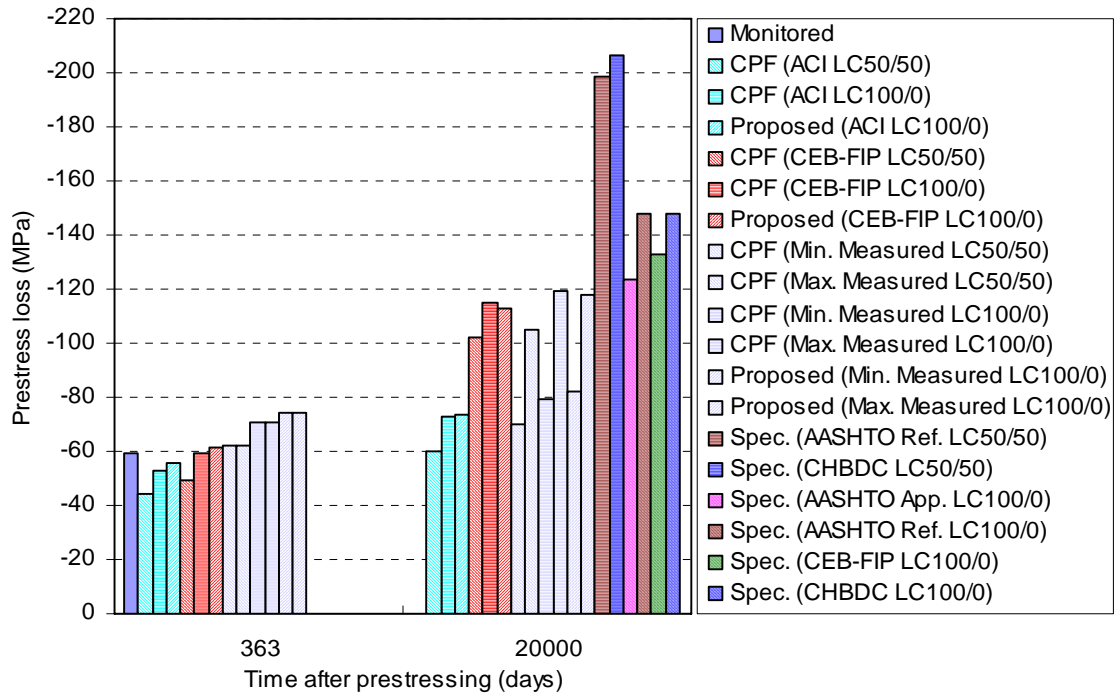


Figure 6.17: Prestress loss in F4 at midspan.

Table 6.8 presents the prestress loss values calculated using the different methods discussed within this Report. The points in time T363 and the theoretical end of service life are presented, as these points represent instances best suited for comparing the calculated values to the monitored data and specifications predictions, respectively. Figure 6.17 displays graphically the information displayed in Table 6.8, which is useful for understanding the respective magnitudes of prestress loss. Table 6.8 indicates the amount of loss that has occurred with reference to the initial prestress existing in the section immediately after the transfer of prestress.

Table 6.8: Prestress loss values calculated for F4 at midspan for points in time at T363 and the theoretical end of service life.

			Midspan					
			T363			Theoretical end of service life		
Prestress			Loss (MPa)	Loss (ksi)	% Remaining	Loss (MPa)	Loss (ksi)	% Remaining
Monitored			-59	-8.6	95.2	-	-	-
CPF	LC50/50	ACI	-44	-6.4	96.4	-60	-8.7	95.1
		CEB-FIP	-49	-7.1	96.0	-102	-14.8	91.7
		Min. Measured (tests)	-62	-9.0	95.0	-70	-10.2	94.3
		Max. Measured (tests)	-62	-9.0	95.0	-105	-15.2	91.4
	LC100/0	ACI	-53	-7.7	95.7	-73	-10.6	94.1
		CEB-FIP	-59	-8.6	95.2	-115	-16.7	90.6
		Min. Measured (tests)	-71	-10.3	94.2	-79	-11.5	93.6
		Max. Measured (tests)	-71	-10.3	94.2	-119	-17.3	90.3
Proposed Method	LC100/0	ACI	-55	-8.0	95.5	-74	-10.7	94.0
		CEB-FIP	-62	-8.9	95.0	-113	-16.4	90.8
		Min. Measured (tests)	-74	-10.8	93.9	-82	-11.9	93.3
		Max. Measured (tests)	-74	-10.8	93.9	-118	-17.1	90.4
Specifications	LC50/50	AASHTO Refined	-	-	-	-198	-28.8	83.8
		CHBDC	-	-	-	-206	-29.9	83.2
	LC100/0	AASHTO Approximate	-	-	-	-123	-17.9	90.0
		AASHTO Refined	-	-	-	-148	-21.5	87.9
		CEB-FIP	-	-	-	-133	-19.3	89.2
		CHBDC	-	-	-	-148	-21.5	87.9

6.5.3. Frame 4 Near the Bent

The prestress losses for the monitored section in F4 near the bent at T363 and the theoretical end of service life are presented in Figure 6.18. The prestress loss obtained from LC50/50 analysis with CPF [16] using the measured material properties from the tests correlates better with the monitored stress than the analyses using the ACI [3] and CEB-FIP [10] material properties. The prestress loss predictions using CPF [16] at the end of service life and LC100/0 are only slightly larger than the corresponding predictions using LC50/50. This occurs for the same reasons as described for F4 at midspan in Section 6.5.2.

The loss values produced using the specifications for LC100/0 form a range of loss of 9.7 to 10.1% from the initial prestress initially existing at the section from 120 to 126 MPa. The specifications predictions for LC50/50 are 182 and 193 MPa, representing losses 14.9 to 15.7% of the initial prestress. The prestress loss value determined using the Proposed Method [29] are a maximum of 5 MPa lower than the CPF [16] predictions using LC100/0 at the end of service life, which corresponds to 0.4% of the initial prestress.

The specifications predictions are most similar to the results of analysis using the CEB-FIP [10] and measured material properties. The CEB-FIP [10] specification and measured material properties analysis differ by 1.3% of the initial prestress. Comparatively, the ACI [3] analysis result of prestress loss is 47 MPa lower than that of the CEB-FIP [10] prediction, representing 3.9% of the initial prestress.

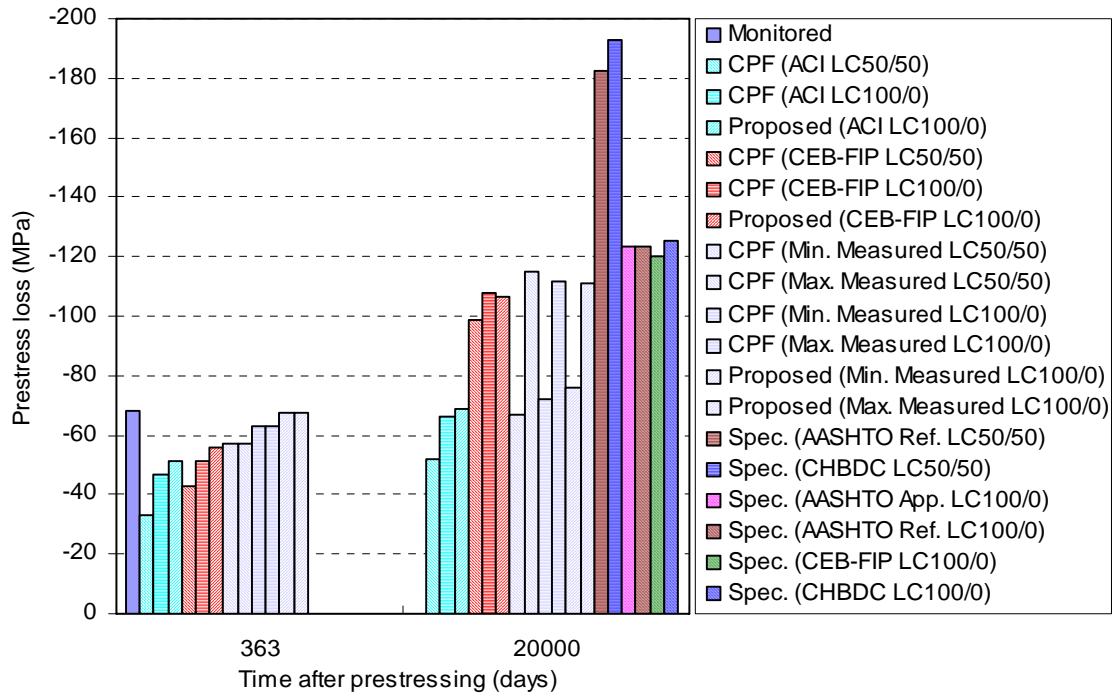


Figure 6.18: Prestress loss in F4 near the bent.

Table 6.9 presents a summary of prestress losses calculated at T363 and the theoretical end of service life using the methods described herein. The prestress loss calculated from the monitored data is presented for T363 for comparison to analysis using the Proposed Method [29] and CPF [16].

Table 6.9: Prestress loss values calculated for F4 near the bent for points in time at T363 and the theoretical end of service life.

			Near the Bent					
			T363			Theoretical end of service life		
Prestress			Loss (MPa)	Loss (ksi)	% Remaining	Loss (MPa)	Loss (ksi)	% Remaining
Monitored			-68	-9.9	94.5	-	-	-
CPF	LC50/50	ACI	-33	-4.8	97.3	-52	-7.5	95.8
		CEB-FIP	-43	-6.2	96.5	-99	-14.4	91.9
		Min. Measured (tests)	-57	-8.3	95.4	-67	-9.7	94.5
		Max. Measured (tests)	-57	-8.3	95.4	-115	-16.7	90.6
	LC100/0	ACI	-47	-6.8	96.2	-66	-9.6	94.6
		CEB-FIP	-51	-7.4	95.8	-108	-15.7	91.2
		Min. Measured (tests)	-63	-9.1	94.9	-72	-10.4	94.1
		Max. Measured (tests)	-63	-9.1	94.9	-112	-16.2	90.9
Proposed Method	LC100/0	ACI	-51	-7.4	95.8	-69	-9.9	94.4
		CEB-FIP	-56	-8.1	95.5	-106	-15.4	91.3
		Min. Measured (tests)	-67	-9.8	94.5	-76	-11.0	93.8
		Max. Measured (tests)	-67	-9.8	94.5	-111	-16.1	90.9
Specifications	LC50/50	AASHTO Refined	-	-	-	-182	-26.5	85.1
		CHBDC	-	-	-	-193	-27.9	84.3
	LC100/0	AASHTO Approximate	-	-	-	-123	-17.9	90.0
		AASHTO Refined	-	-	-	-123	-17.9	90.0
		CEB-FIP	-	-	-	-120	-17.4	90.2
		CHBDC	-	-	-	-126	-18.2	89.8

6.5.4. Frame 5 Midspan

The result of analysis using the ACI [3] and CEB-FIP [10] material property inputs for F5 at midspan are essentially the same at T303. These two loss values are within 5 MPa of the loss obtained through monitoring, or 8.1% different from the monitored stress. A difference of 5 MPa represents a difference from the initial prestress of 0.4%. The prestress loss obtained from analysis using the measured material properties from testing is 20 MPa (32.2%) higher than the monitored stress. The loss obtained from analysis using the measured material properties represents a decrease from the initial prestress existing initially within the section of 6.7%.

The specifications predictions of prestress loss for the theoretical end of service life with LC100/0 in F5 near the bent are similar to the analysis predictions using CEB-FIP [10] material property inputs. Most specifications predict prestress losses almost the same as that of the CEB-FIP [10] analysis, as shown in Figure 6.19, the maximum difference from the CEB-FIP [10] analysis result is 23 MPa, a loss corresponding to a difference of 1.9% of the initial prestress in the section between the methods.

The specifications loss predictions at the theoretical end of service life for F5 at midspan indicate a spread of loss from 121 to 145 MPa for LC100/0. This range of loss represents a decrease in the initial stress from 9.8 to 11.8%. Comparatively, the results of analysis (LC100/0) indicate a range of loss values from 88 to 178 MPa. The analytical results signify loss from 7.2 to 14.5% from the initial prestress. The specifications predictions of prestress loss for LC50/50 do not exceed the LC100/0 loss predictions by as large a margin as in F4. In F5, the difference between the two load cases does not exceed 20 MPa. The specifications (LC100/0) produce a range of loss values from the initial prestress of 2.0% while the analysis (LC50/50) results varies within 7.3%. This is quite significant since it indicates that the specifications equations are not diverse enough in accommodating actual differences in material properties.

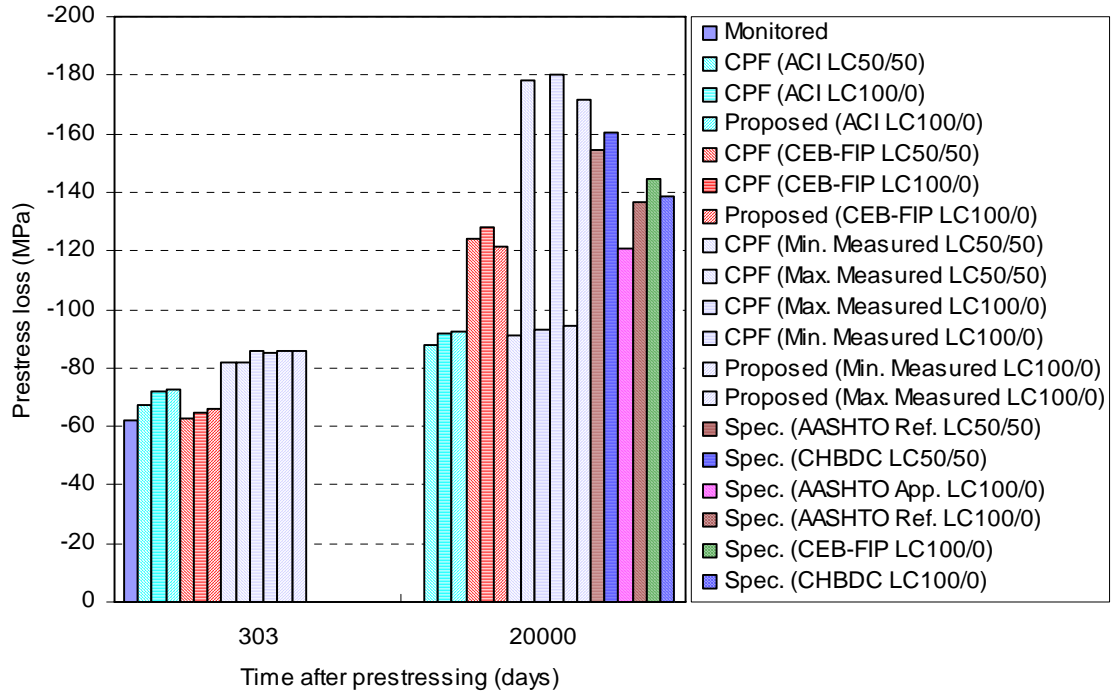


Figure 6.19: Prestress loss in F5 at midspan.

Similar to the tables presented previously for F4, Table 6.10 displays the values of prestress loss calculated with the methods discussed herein, the same values in tabular form as those in Figure 6.19.

Table 6.10: Prestress loss values calculated for F5 at midspan for points in time at T303 and the theoretical end of service life.

			Midspan					
			T303			Theoretical end of service life		
Prestress			Loss (MPa)	Loss (ksi)	% Remaining	Loss (MPa)	Loss (ksi)	% Remaining
Monitored			-62	-9.0	94.9	-	-	-
CPF	LC50/50	ACI	-67	-9.7	94.5	-88	-12.8	92.8
		CEB-FIP	-63	-9.1	94.9	-124	-18.0	89.9
		Min. Measured (tests)	-82	-11.9	93.3	-91	-13.2	92.6
		Max. Measured (tests)	-82	-11.9	93.3	-178	-25.8	85.5
	LC100/0	ACI	-72	-10.4	94.1	-92	-13.3	92.5
		CEB-FIP	-65	-9.4	94.7	-128	-18.6	89.6
		Min. Measured (tests)	-86	-12.5	93.0	-93	-13.5	92.4
		Max. Measured (tests)	-85	-12.3	93.1	-180	-26.1	85.3
Proposed Method	LC100/0	ACI	-73	-10.5	94.1	-92	-13.4	92.5
		CEB-FIP	-66	-9.6	94.6	-122	-17.6	90.1
		Min. Measured (tests)	-86	-12.5	93.0	-95	-13.7	92.3
		Max. Measured (tests)	-86	-12.5	93.0	-171	-24.8	86.0
Specifications	LC50/50	AASHTO Refined	-	-	-	-155	-22.4	87.4
		CHBDC	-	-	-	-160	-23.3	86.9
	LC100/0	AASHTO Approximate	-	-	-	-121	-17.5	90.2
		AASHTO Refined	-	-	-	-137	-19.8	88.8
		CEB-FIP	-	-	-	-145	-21.0	88.2
		CHBDC	-	-	-	-139	-20.1	88.7

6.5.5. Frame 5 Near the Bent

At T303, the prestress loss values produced through analysis (LC50/50) using the material property inputs from ACI [3], CEB-FIP [10], and the material tests varied within 12 MPa. The monitored loss value was 22 MPa lower than the values produced through analysis. This corresponds to a difference from the initial prestress of 1.7%.

At T303 the analysis results using the LC100/0 load case resulted in prestress losses very similar to the prestress losses from the LC50/50 load case with a maximum difference of 8 MPa (0.63% of the initial prestress). At the theoretical end of service life, the two analysis load cases resulted in small differences in prestress losses as well, with a maximum difference of prestress loss between methods of 10 MPa (0.78% of the initial prestress). This reinforces the appropriateness of the simplified load case (LC100/0) used in analysis, as shown for the other sections as well.

The values of prestress loss calculated using the specifications vary between 109 and 126 MPa (8.5 to 9.8% reduction from the initial prestress). The specifications predictions for LC50/50 are similar to the analysis predictions using the measured material properties; however, are significantly higher than the specifications predictions for LC100/0. This reinforces the possibility that the specifications use of multiple loading instances is not appropriate for capturing the actual bridge behavior. The experimental shrinkage for F5 was determined to drastically exceed the specifications predictions of shrinkage. It cannot be ascertained that the specifications use of LC50/50 is appropriate, even though the predictions correlate reasonably well with the analysis prediction with the measured material properties.

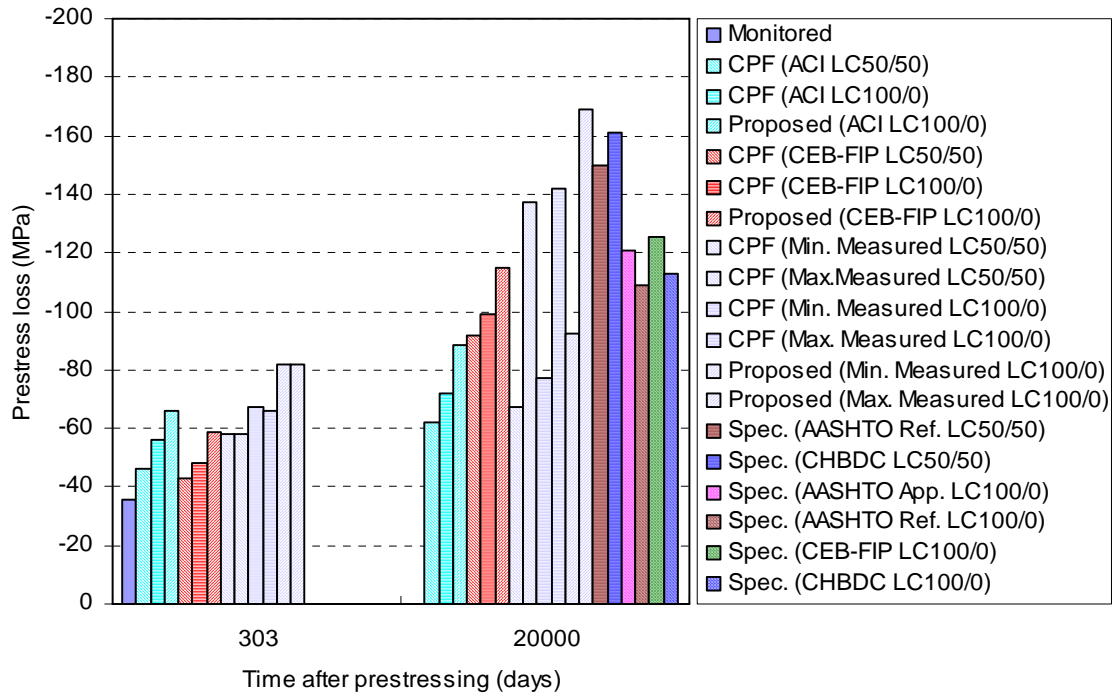


Figure 6.20: Prestress loss in F5 near the bent.

Values of calculated prestress losses at T303 and the theoretical end of service life are presented in Table 6.11.

Table 6.11: Prestress loss values calculated for F5 near the bent for points in time at T303 and the theoretical end of service life.

			Near the Bent					
			T303			Theoretical end of service life		
Prestress			Loss (MPa)	Loss (ksi)	% Remaining	Loss (MPa)	Loss (ksi)	% Remaining
Monitored			-36	-5.2	97.2	-	-	-
CPF	LC50/50	ACI	-46	-6.7	96.4	-62	-9.0	95.1
		CEB-FIP	-43	-6.2	96.6	-92	-13.3	92.8
		Min. Measured (tests)	-58	-8.4	95.5	-67	-9.7	94.8
		Max. Measured (tests)	-58	-8.4	95.5	-137	-19.9	89.3
	LC100/0	ACI	-56	-8.1	95.6	-72	-10.4	94.4
		CEB-FIP	-48	-7.0	96.2	-99	-14.4	92.2
		Min. Measured (tests)	-67	-9.7	94.8	-77	-11.2	94.0
		Max. Measured (tests)	-66	-9.6	94.8	-142	-20.6	88.9
Proposed Method	LC100/0	ACI	-66	-9.6	94.8	-89	-12.8	93.1
		CEB-FIP	-59	-8.5	95.4	-115	-16.6	91.0
		Min. Measured (tests)	-82	-11.9	93.6	-92	-13.4	92.8
		Max. Measured (tests)	-82	-11.9	93.6	-169	-24.5	86.8
Specifications	LC50/50	AASHTO Refined	-	-	-	-150	-21.8	88.2
		CHBDC	-	-	-	-161	-23.4	87.4
	LC100/0	AASHTO Approximate	-	-	-	-121	-17.5	90.5
		AASHTO Refined	-	-	-	-109	-15.8	91.5
		CEB-FIP	-	-	-	-126	-18.2	90.2
		CHBDC	-	-	-	-113	-16.4	91.2

6.5.6. Commentary on Predicted Long-Term Prestress Loss

It can be observed that for both F4 and F5 at midspan and near the bent, the specification based predictions of prestress loss are clustered around the results of analysis using the material property inputs from CEB-FIP [10]. As mentioned in Chapter 5, the analytical strains produced using the material property inputs from CEB-FIP [10] were similar to those obtained through monitoring at T363 or T303 for F4 and F5, respectively.

The ACI [3] specification derived material properties do not exhibit much change from T363 or T303 to the theoretical end of service life. The CEB-FIP [10] material properties show more increase (about 36%) between T363 and T303 to the end of service life than ACI [3] (about 27%). The range of creep and shrinkage produced through testing is approximately bounded by the ACI [3] and CEB-FIP [10] material properties.

Though more drastic differences in the predicted prestress loss at the end of service life were expected, the most considerable differences were experienced between the different results of analysis. Most of the specifications predictions were clustered around the predicted values of prestress loss indicated through analysis using the CEB-FIP [10] material properties as input. The ACI [3] material properties used as input into analysis produced consistently the lowest value of long-term loss while the measured material properties used as input predicted consistently the greatest loss, though for F4, this was similar to the CEB-FIP [10] prediction. The results of the three analyses produced a maximum range of values between 84 and 93% of the initial prestress. For comparison, the specifications predictions (for LC100/0) of the long-term prestress loss are all similar, with values that range from about 88 to 92% of the initial prestress at the end of service life.

The Proposed Method [29], which is far simpler to use than the analytical program CPF [16], was shown to produce nearly equivalent results to that of analysis with CPF [16] for corresponding sets of material property inputs. Further, the Proposed Method [29] analysis uses only one type of concrete. CPF [16]

allows multiple concrete parts in the structure. This was shown to have minimal impact on the prestress loss predictions. The differences in material properties between multiple concrete parts were captured by inputs representing the average material properties, as used in the Proposed Method [29], for a single equivalent concrete part.

One point of notice is that the AASHTO Approximate [2] method results in predominantly better predictions of the prestress loss than that produced by the AASHTO Refined [2] method for the bridge frames studied. As was indicated in Chapter 2, the AASHTO Approximate [2] method takes few input parameters, none of which specifically represent the concrete or the environmental conditions. Thus for all bridges, regardless of location or concrete material properties, the same loss value will be presented. The observance of improved prestress loss prediction with the simpler AASHTO Approximate [2] method over that of the AASHTO Refined [2] method is unexpected. The AASHTO Refined [2] method takes as input relative humidity and the initial concrete stress at the level of the prestressing tendons with the purpose of generating improved estimates. Here, the implication can be made that the AASHTO Approximate [2] method is appropriate for producing prestress loss predictions for the conditions of the I5/805 Bridge. Other locations may not compare as well as the predictions presented here.

The difference in treatment of the dead load between the analytical methods (CPF [16] and Proposed Method [29]) and the specifications results in some of the variation in indicated prestress loss at the end of service life. Analysis with CPF [16] used a loading scenario that was intended to most accurately capture the actual behavior of the bridge (LC50/50). The specifications use the input value of initial stress existing within the concrete to formulate the prediction of long-term prestress loss. The specifications were used with the applied stress from the structural self-weight applied in full at prestressing (LC100/0). Several of the considered specifications can accommodate one instance of load applied after prestressing is applied. This instance was used to capture the prestress

loss with 50% of the self-weight applied at prestressing and the remaining self-weight applied after prestressing.

For each of the monitored sections, at the end of service life the analysis predictions of LC50/50 and LC100/0 load cases differed by no more than 14 MPa at the end of service life. The analytical values of loss are presented in Table 6.8 to Table 6.11, but a 14 MPa difference is practically insignificant, as it represents 1.1% of the initial prestress. This indicates that loading sequence plays a minimal role in the prestress loss at the end of service life. Provided that in analysis, all loads have been imposed, regardless of whether loads simulate LC50/50, LC100/0, or other load case combination, the prestress loss at the end of service life is dependent primarily on the ultimate values of creep and shrinkage. Though correct predictions of prestress loss are dependent on correct material property inputs, it is beneficial for designers to know that the loading during construction will not have profound influences on the deformation at the end of service life.

At the theoretical end of service life, the results of all calculated prestress values occurs within a range of 9% of the initial prestress. This is the result of using material property inputs that are widely varied, thus the results of analysis create the extremes for all calculated values. As mentioned previously in this section, it is important to note that the theoretical end of service life predictions of prestress loss utilize values of creep and shrinkage that were projected based on the available data at the time this Report was written. Certainly the development of creep and shrinkage will differ with the advent of additional data from the material tests, thus altering the prestress loss at the end of service life. Already, at the writing of this Report, considerably creep and shrinkage had already taken place, thus less amounts of creep and shrinkage are expected to occur between T363 or T303 and the end of service life.

If the range of strain produced through analysis using the range of extrapolated material properties is considered the range over which the actual strains occur, then the bounds set by the minimum and maximum analytical strain provides a range over which the prestress loss would be expected to

occur. A change in strain of 5.2 microstrain correlates to a change in prestress of 1 MPa. The results of analysis predict a maximum difference in strain of about 260 microstrain in F4 and 450 microstrain in F5, at the level of the prestressing tendons. This range of difference correlates with a range of change in prestress of 51 MPa in F4, a value representing a change from the initial prestress of 4.1%. In F5, the change in strain correlates with a change in prestress of 87 MPa, relating to a change from the initial prestress of 6.8%. Neither of these changes in prestress would have profound influence on the long-term performance of the bridge. The variation is primarily the result of large predictions of creep and shrinkage from the material tests used as input to the CPF [16] analysis. As discussed previously in this section, reduction of ultimate material properties (creep and shrinkage) would reduce the long-term prestress losses, accommodated by the best-fit equations.

6.5.7. Total Long-Term Prestress Losses from all Influences

In an effort to understand the influence of time-dependent material properties, the prestress losses presented thus far throughout this Report have been presented with reference to the initial prestress through each of the monitored sections. Losses existing between jacking and immediately after transfer are not time-dependent, and thus are not appropriate for inclusion in comparison to the influences of time-dependent material behavior. In Section 6.5.1 the prestress losses resulting from friction and anchor-set losses were discussed. The initial losses are supplemented by the time-dependent losses to present the total losses that can be expected over the life of the structure. The remaining prestress at the end of service life is presented in terms of total stress as well as percentage of the jacking stress remaining in the tendons at the end of service life.

The total prestress loss determined for F4 at midspan at the theoretical end of service life for combined influences is presented in Table 6.12. The remaining prestress calculated through analysis varies between 80 and 84% of the jacking stress. CPF [16] and the Proposed Method [29] produce essentially the same

prestress loss at the end of service life. The specifications (LC100/0) produced total prestress loss estimates that result in about 79 to 80% of the initial prestress remaining at the end of service life. Using the specifications with LC50/50 indicated losses about 3 to 4% lower than the corresponding specifications using LC100/0, with totals of about 75% of the jacking stress.

Table 6.12: Total prestress losses from all influences in F4 at midspan at the end of service life.

			Stresses prior to time-dependent influences (MPa)	Prestress loss (MPa)	Remaining prestress at end of service life (MPa)	Remaining prestress at end of service life (%)
Jacking stress (MPa)			1375	-	-	-
Initial stress (MPa)			1228	-	-	-
CPF	LC50/50	ACI	-	-60	1168	84.9
		CEB-FIP	-	-102	1126	81.9
		Min. Measured (tests)	-	-70	1158	84.2
		Max. Measured (tests)	-	-105	1123	81.7
	LC100/0	ACI	-	-73	1155	84.0
		CEB-FIP	-	-115	1113	80.9
		Min. Measured (tests)	-	-79	1149	83.6
		Max. Measured (tests)	-	-119	1109	80.7
Proposed Method	LC100/0	ACI	-	-74	1154	83.9
		CEB-FIP	-	-113	1115	81.1
		Min. Measured (tests)	-	-82	1146	83.3
		Max. Measured (tests)	-	-118	1110	80.7
Specifications	LC50/50	AASHTO Refined	-	-198	1030	74.9
		CHBDC	-	-206	1022	74.3
	LC100/0	AASHTO Approximate	-	-123	1105	80.3
		AASHTO Refined	-	-148	1080	78.5
		CEB-FIP	-	-133	1095	79.6
		CHBDC	-	-148	1080	78.5

The total prestress losses at the end of service life for the section near the bent in F4 are presented in Table 6.13. The range of remaining prestress at the

end of service life (from analysis) is slightly higher at the bent location than at midspan, 80 to 85% of the jacking stress. The larger remaining prestress at the bent location is typical, since the moment, and hence the tension, in the tendons is higher at this location, maintaining a higher stress. Similarly, higher remaining prestress is calculated using LC100/0 with the specifications, around 81% of the jacking stress. LC50/50 resulted in remaining prestress of about 77% of the jacking stress at the end of service life.

Table 6.13: Total prestress losses from all influences in F4 near the bent at the end of service life.

			Stresses prior to time-dependent influences (MPa)	Prestress loss (MPa)	Remaining prestress at end of service life (MPa)	Remaining prestress at end of service life (%)
Jacking stress (MPa)			1375	-	-	-
Initial stress (MPa)			1233	-	-	-
CPF	LC50/50	ACI	-	-52	1181	85.9
		CEB-FIP	-	-99	1134	82.5
		Min. Measured (tests)	-	-67	1166	84.8
		Max. Measured (tests)	-	-115	1118	81.3
	LC100/0	ACI	-	-66	1167	84.9
		CEB-FIP	-	-108	1125	81.8
		Min. Measured (tests)	-	-72	1161	84.4
		Max. Measured (tests)	-	-112	1121	81.5
Proposed Method	LC100/0	ACI	-	-69	1164	84.7
		CEB-FIP	-	-106	1127	81.9
		Min. Measured (tests)	-	-76	1157	84.2
		Max. Measured (tests)	-	-111	1122	81.6
Specifications	LC50/50	AASHTO Refined	-	-182	1051	76.4
		CHBDC	-	-193	1040	75.7
	LC100/0	AASHTO Approximate	-	-123	1110	80.7
		AASHTO Refined	-	-123	1110	80.7
		CEB-FIP	-	-120	1113	80.9
		CHBDC	-	-126	1107	80.5

Table 6.14 displays the total prestress losses for F5 at midspan at the theoretical end of service life. The analytical predictions of prestress loss ranges from 75 to 82% of the jacking stress. The analytical results using CPF [16] indicates about the same remaining stress at the end of service life as the Proposed Method [29]. Almost identical to the analytical prediction using the CEB-FIP [10] material property inputs are the specifications predictions from LC100/0, around 80% of the jacking stress. LC50/50 provides estimates of the prestress loss at the end of service life of about 78%.

Table 6.14: Total prestress losses from all influences in F5 at midspan at the end of service life.

			Stresses prior to time-dependent influences (MPa)	Prestress loss (MPa)	Remaining prestress at end of service life (MPa)	Remaining prestress at end of service life (%)
Jacking stress (MPa)			1369	-	-	-
Initial stress (MPa)			1226	-	-	-
CPF	LC50/50	ACI	-	-88	1138	83.1
		CEB-FIP	-	-124	1102	80.5
		Min. Measured (tests)	-	-91	1135	82.9
		Max. Measured (tests)	-	-178	1048	76.6
	LC100/0	ACI	-	-92	1134	82.8
		CEB-FIP	-	-128	1098	80.2
		Min. Measured (tests)	-	-93	1133	82.8
		Max. Measured (tests)	-	-180	1046	76.4
Proposed Method	LC100/0	ACI	-	-92	1134	82.8
		CEB-FIP	-	-122	1104	80.7
		Min. Measured (tests)	-	-95	1131	82.6
		Max. Measured (tests)	-	-171	1055	77.0
Specifications	LC50/50	AASHTO Refined	-	-155	1071	78.3
		CHBDC	-	-160	1066	77.8
	LC100/0	AASHTO Approximate	-	-121	1105	80.7
		AASHTO Refined	-	-137	1089	79.6
		CEB-FIP	-	-145	1081	79.0
		CHBDC	-	-139	1087	79.4

The remaining prestress predicted for the F5 near-bent location is indicated in Table 6.15. The minimum analytical prediction of prestress loss using the measured material properties as input, predicting 82% of the jacking stress will remain at the end of service life. The minimum remaining prestress calculated for this section is 76% produced though analysis using the maximum extrapolated material properties from testing.

Table 6.15: Total prestress losses from all influences in F5 near the bent at the end of service life.

			Stresses prior to time-dependent influences (MPa)	Prestress loss (MPa)	Remaining prestress at end of service life (MPa)	Remaining prestress at end of service life (%)
Jacking stress (MPa)			1369	-	-	-
Initial stress (MPa)			1277	-	-	-
CPF	LC50/50	ACI	-	-62	1215	88.8
		CEB-FIP	-	-92	1185	86.6
		Min. Measured (tests)	-	-67	1210	88.4
		Max. Measured (tests)	-	-137	1140	83.3
	LC100/0	ACI	-	-72	1205	88.0
		CEB-FIP	-	-99	1178	86.0
		Min. Measured (tests)	-	-77	1200	87.7
		Max. Measured (tests)	-	-142	1135	82.9
Proposed Method	LC100/0	ACI	-	-89	1188	86.8
		CEB-FIP	-	-115	1162	84.9
		Min. Measured (tests)	-	-92	1185	86.5
		Max. Measured (tests)	-	-169	1108	80.9
Specifications	LC50/50	AASHTO Refined	-	-150	1127	82.3
		CHBDC	-	-161	1116	81.5
	LC100/0	AASHTO Approximate	-	-121	1156	84.5
		AASHTO Refined	-	-109	1168	85.3
		CEB-FIP	-	-126	1151	84.1
		CHBDC	-	-113	1164	85.0

Using the LC50/50 load case predicts about 3 to 4% lower remaining prestress than the use of LC100/0 in the specifications. The remaining prestress predicted by the specifications using LC100/0 are most similar to the results of the CEB-FIP [10] analysis than the other analytical predictions.

The methods considered have generally predicted remaining prestress values at the end of service life between about 80 to 85% of the jacking stress. Some of the specifications using the LC50/50 load case predicted prestress loss values

about 3 to 4% lower than the corresponding specification predictions using LC100/0. A reasonably consistent value of loss was experienced at transfer, when the jacking stress decreased immediately by about 10%. The remaining 5 to 10% of the initial prestress was lost due to time-dependent influences; location also plays a significant role in the prestress loss. The locations near the bents experienced less loss than at midspan.

This research has indicated that the specifications accommodation for load applied after prestressing may not be appropriate. The overestimation of prestress loss using this method is not drastic, showing a difference of about 3 to 4% of the remaining prestress using complementary methods with the full self-weight applied simultaneously with prestressing.

6.6. Concrete Stresses

Overestimation and underestimation of the prestress loss can create severe serviceability problems as well as being economically unfeasible for the long-term in terms of service and material costs. Problems that can result from inaccurate loss predictions are cracking and excessive camber or deflection, to name some of the more prominent issues.

The change in strain in the concrete is directly related to the change in stress, as captured through monitoring. These stresses are proportional to the strains presented in Chapter 5, thus the correlation of monitored to analytical strains were used to assert the future correlation performance of the bridge without the monitored data at the end of service life. A method is presented to calculate the change in stress in the concrete from the loss values determined from the specifications, as the specifications do not provide better means of calculating the change. These stresses are calculated for each of the specifications using Eqs. 6.2 and 6.3.

$$\Delta\sigma_{top} = -A_{ps}\Delta\sigma_{ps}\left(\frac{1}{A_1} - \frac{d_1(d_{ps} - d_1)}{I_1}\right) \quad (6.2)$$

$$\Delta\sigma_{bottom} = -A_{ps}\Delta\sigma_{ps}\left(\frac{1}{A_1} - \frac{(h-d_1)(d_{ps}-d_1)}{I_1}\right) \quad (6.3)$$

The initial stress is usually not an involved computation and it is expected that when using this method, the initial stress could be easily obtained. The actual initial stress is provided through monitoring as well as through the analysis using CPF [16] for verification of the analysis procedures. The initial stress profiles are not those obtained through monitoring, the reasons for which will be described later in this section. The initial stress profile must correlate to the prestress loss associated with the initial stress. Thus, the calculated change in stress for the LC50/50 load case must be taken from the LC50/50 load case initial stress profile. Similarly, for the LC100/0 load case, the calculated change in stress must be taken from the initial stress profile of the LC100/0 load case.

It is expected that changes in prestress would lead to proportional changes in concrete stress. This does not hold true because the specifications predictions of prestress loss do not account for compatibility between the concrete and prestressing tendons, thus the changes are not proportional.

Possibly, the most significant influence on the change in stress indicated by Eqs. 6.2 and 6.3 compared to the results of analysis is that non-prestressed steel is neglected. The stress profiles are significantly different depending on the method used to calculate the values. Though the implication has been made that the specifications are acceptable for producing predictions of prestress loss, the specifications do not make accurate account of the stress profile thus the change in stress over time is not accurate. The initial stress and strain profiles are relatively straightforward to obtain, as the initial state is not influenced by any time-dependent changes in the concrete or steel. The general practice in design is to apply the change in prestress in the opposite direction and subtract this stress from the initial stress in the tendons. This method does not account for the non-prestressed reinforcement and eliminates the correct distribution of stress through the section, resulting in the redistribution of the stress over time, as will be shown.

Several specifications predictions of prestress loss are not suited for accommodating intermediate instances during the life of the structure at which additional load may be applied to the structure. For this reason, the assumptions made for CPF [16] analysis cannot be used here. To generate the initial stress profile, a situation in which all of the structural self-weight is added simultaneously with prestressing is examined. The initial analytical stress profile for each monitored location corresponding to the application all the self-weight in total in one instant (LC100/0 load case) are provided in this section.

The stress profiles presented for the end of service life in the following sections from analysis using the material property inputs from testing represent the minimum stresses (least compressive) that can be expected in the concrete. Concrete compressive stress decreases with increase in prestress loss. For both bridge frames, the extrapolated material properties from testing exceeded the predictions for material properties of both ACI [3] and CEB-FIP [10]. For this reason, the prestress loss produced using the measured material properties is larger than that of the analyses using the ACI [3] and CEB-FIP [10] material properties. Hence, the concrete stresses produced using the measured material properties are the lowest (least compressive). The comparisons of CPF [16] and the Proposed Method [29] using the ACI [3] and measured material properties are located in Appendix F.

6.6.1. Frame 4 Midspan

In Figure 6.21 the stress is presented for F4 at midspan. The initial stress profile determined from the monitored data is included and compared to the initial stress profile obtained through analysis with CPF [16] using the LC50/50 load case. In Figure 6.21 the stress profiles produced with the three analysis cases using the ACI [3], CEB-FIP [10], and measured material properties from the material tests are included.

The analysis results using the measured material properties as input results in the most conservative estimate of the long-term stress in the concrete. Provided

that the results of analysis indicated the highest strains and the largest prestress losses when the measured material properties were used as input, the lowest concrete compressive stress as produced from this analysis is expected.

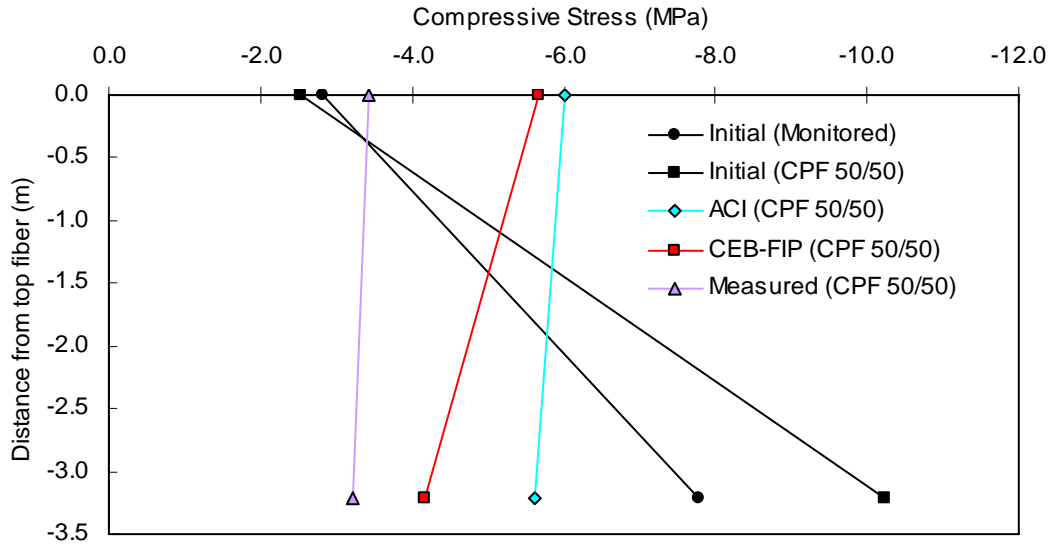


Figure 6.21: Stress profiles at prestressing and the theoretical end of service life obtained using CPF; 50% self-weight applied at prestressing and remaining 50% applied with the removal of falsework in F4 at midspan.

The stress profile calculated with the Proposed Method [29] is presented in Figure 6.22 initially, when prestressing is applied, and long-term, at the theoretical end of service life. The initial and long-term stress values are nearly identical between both methods.

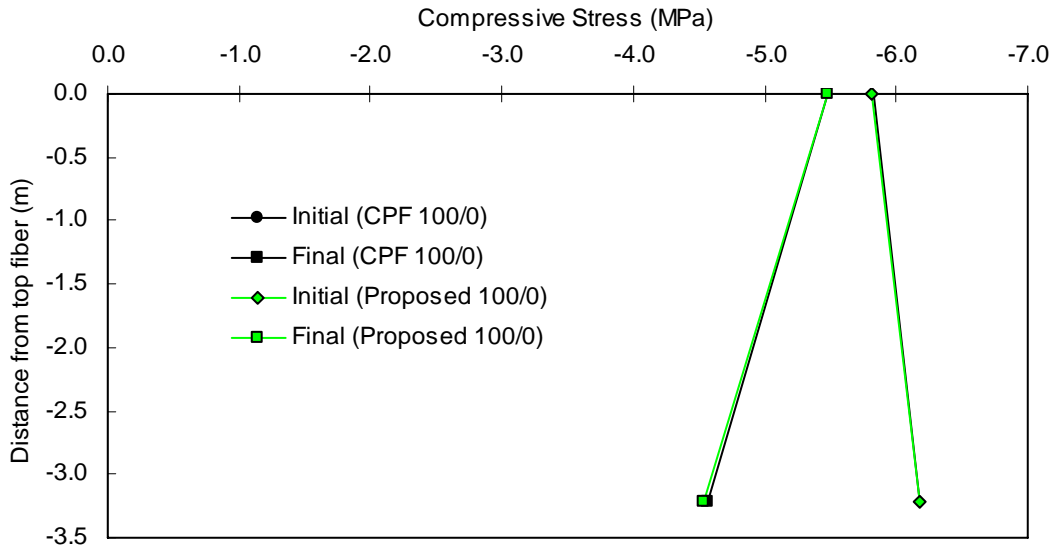


Figure 6.22: Stress profiles at prestressing and the theoretical end of service life obtained using CPF and the Proposed Method; 100% self-weight applied at prestressing in F4 at midspan.

The initial stress profile in Figure 6.23 was determined using CPF [16] (LC100/0) since Eqs. 6.2 and 6.3 require an initial stress value from which the change in concrete stress may be calculated. The four specifications predictions of the change in stress between prestressing and the theoretical end of service life indicate a decrease from the initial stress by 22.5 to 30.0% at the critical fiber in the soffit nearest the prestressing tendons. In the deck, the concrete stress is predicted to decrease by 5.2% from the initial stress in the concrete.

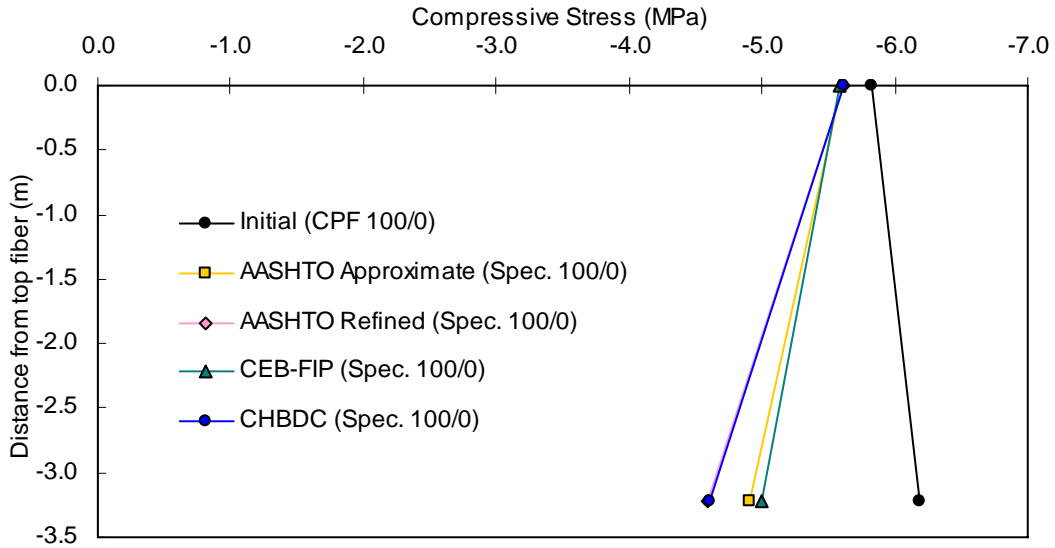


Figure 6.23: Stress profiles determined with the specifications using the full self-weight at prestressing in F4 at midspan.

CPF [16] was used to generate the stress profile in Figure 6.24 for LC50/50. The stress decreased by 14.4 to 23.8% between the four specifications in the bottom fiber of the section. In the top fiber of the section, the prestress displayed an increase by 4.3%, representing a change in stress of 0.13 MPa.

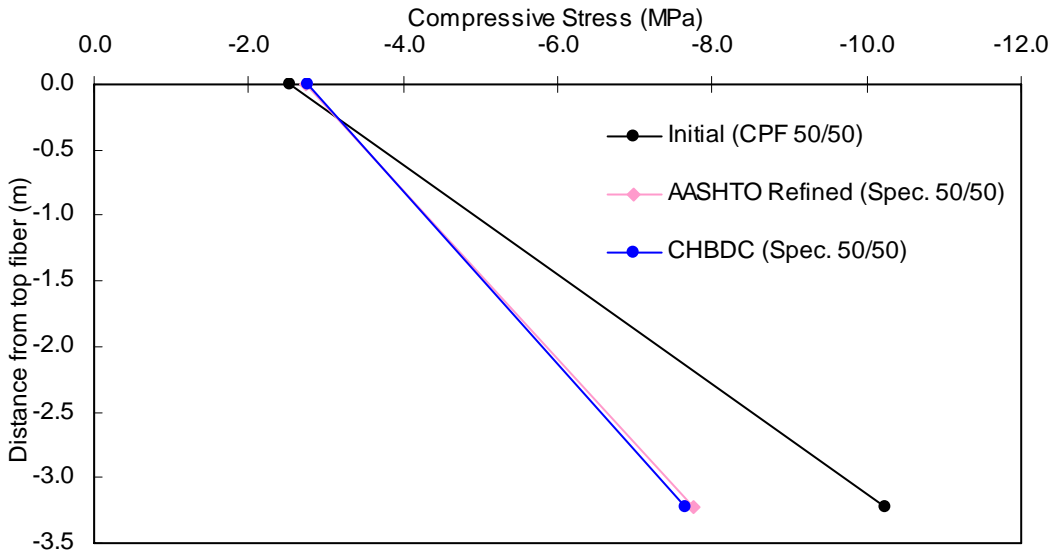


Figure 6.24: Stress profiles determined with the specifications using 50% of the self-weight at prestressing in F4 at midspan.

Table 6.16 puts the long-term concrete stress values from each of the utilized method into perspective. Initial stress profiles are not shown, since depending on the load case, the initial stress profiles vary substantially. The long-term stress values are appropriate for comparison because for either load case the full structural self-weight is imposed on the structure.

It can be seen that the specifications predictions of long-term concrete stress using the LC50/50 load case does not result in acceptable predictions of concrete stress. The specifications do not make account for the presence of reinforcement in the structure, thus the distribution of stress though the section does not occur as it would if the reinforcement were accounted. For this reason, the change in stress from the initial stress profile at the critical fibers, in both the LC100/0 and LC50/50 load cases, is small compared to the change calculated with CPF [16] and the Proposed Method [29]. It is also for this reason that the use of the LC50/50 load case in obtaining the initial stress profile does not account for the change in stress with the remaining 50% self-weight applied after prestressing. Though a larger prestress loss is calculated using the LC50/50 load case, this increase does not accommodate the full change in stress with the additional 50% of the structural self-weight.

Table 6.16: Stresses from all considered methods at the theoretical end of service life in F4 at midspan.

Method	Load Case	Event	Inputs		Stress (MPa)		
					Top	Bottom	
Monitored					-2.82	-7.78	
Analysis	LC50/50	Initial		CPF	-2.53	-10.24	
		Final	ACI		-6.01	-5.63	
			CEB-FIP		-5.68	-4.18	
			Measured		-3.44	-3.21	
	LC100/0	Initial		CPF	-5.83	-6.18	
				Proposed	-5.81	-6.17	
		Final	ACI		CPF	-5.48	-4.56
					Proposed	-5.49	-4.53
			CEB-FIP		CPF	-5.15	-3.70
					Proposed	-5.15	-3.63
		Measured		CPF	-5.09	-3.59	
				Proposed	-5.10	-3.52	
Specifications	LC100/0	Initial		CPF	-5.83	-6.18	
		Final	AASHTO Appr.		-5.60	-4.91	
			AASHTO Ref.		-5.62	-4.60	
			CEB-FIP		-5.59	-4.99	
	CHBDC		-5.62	-4.60			
	LC50/50	Initial		CPF	-2.53	-10.24	
		Final	AASHTO Ref.		-2.75	-7.75	
			CHBDC		-2.76	-7.65	

6.6.2. Frame 4 Near the Bent

Figure 6.25 displays the initial stress profile that was obtained using the monitored data. The analytical initial stress profile obtained through use of CPF [16] is 2% lower than the initial stress profile from monitoring at the critical section, top fiber of the deck. The three analysis predictions of concrete stress follow reasonably the trends identified for the prestress loss in which the lowest remaining prestress loss correlates to the least concrete compressive stress at the end of service life.

The initial stress in the concrete when prestressing was performed was 9.0 MPa at the critical fiber in the deck; the initial prestress obtained from CPF [16] analysis was 8.9 MPa. The concrete stress decreased by 51% to 4.4 MPa, indicated by the analysis using the ACI [3] derived material property inputs. The

analysis using the CEB-FIP [10] material properties as input indicated a concrete stress at the theoretical end of service life of 3.9 MPa corresponding to a decrease of 56% from the initial stress at the critical fiber. The measured material properties from testing indicated a decrease in stress at the critical fiber at the theoretical end of service life by 87% to 1.2 MPa. Though the measured material properties are very conservative compared to the specifications predictions, the stress at the critical fiber at the end of service life is near the tensile region. A situation of overloading could force the stress in the concrete to further diminish and place the concrete in tension in the deck fibers of the section.

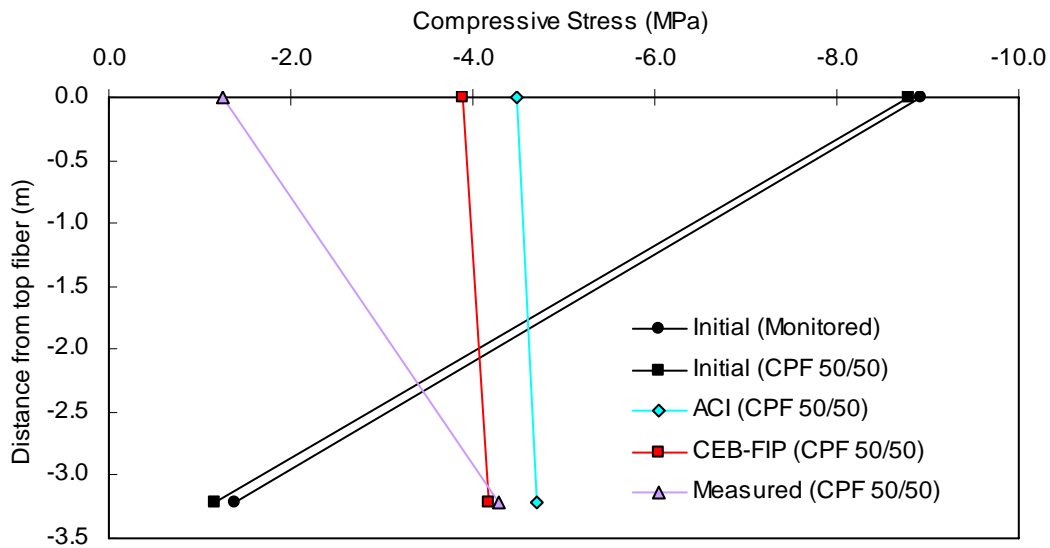


Figure 6.25: Stress profiles at prestressing and the theoretical end of service life obtained using CPF; 50% self-weight applied at prestressing and remaining 50% applied with the removal of falsework in F4 near the bent.

Figure 6.26 displays the calculated stress profiles using the Proposed Method [29] at prestressing and the theoretical end of service life using the material properties from CEB-FIP [10]. These stress profiles are shown compared to the stresses obtained through analysis in CPF [16] using a LC100/0 load distribution case.

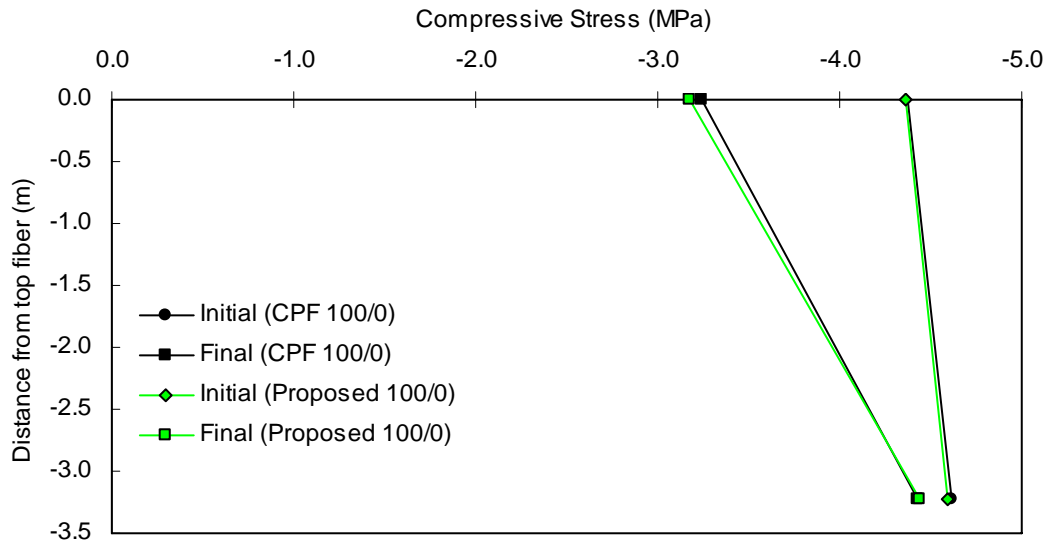


Figure 6.26: Stress profiles at prestressing and the theoretical end of service life obtained using CPF and the Proposed Method; 100% self-weight applied at prestressing in F4 near the bent.

The stress profiles calculated using the specifications are presented in Figure 6.27 for LC100/0. The initial stress in the deck (critical fiber) at prestressing is 4.0 MPa. The specifications indicate a decrease in concrete stress over the life of the structure between 1.0 and 1.3 MPa, representing a change in stress of 25 to 33% from the initial stress. Similar to the calculated concrete stress at midspan, at the near-bent section, the concrete stress increased a by 0.2 MPa between prestressing and the theoretical end of service life. This change though occurs opposite the extreme fiber and has no influence on the concrete stress at the critical section.

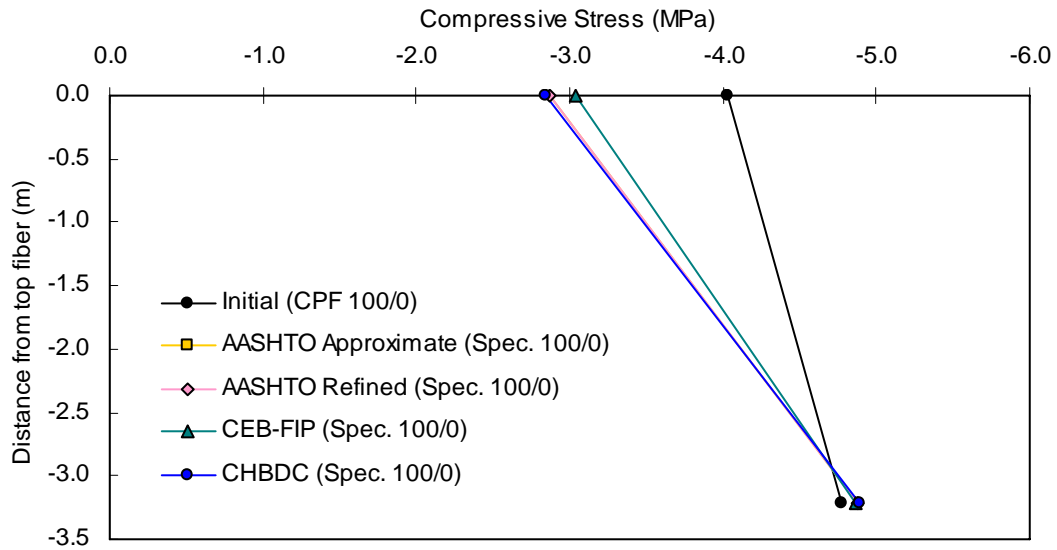


Figure 6.27: Stress profiles determined with the specifications using the full self-weight at prestressing in F4 near the bent.

The LC50/50 load case was used to calculate the initial stress profile indicated in Figure 6.28. The specifications change in concrete stress between prestressing and the theoretical end of service life are shown. As non-prestressed reinforcement is not accounted in the method used with the specifications, the change in concrete stress is a maximum of 20% from the initial stress at the critical fiber, a change representing a 1.3 MPa decrease in compressive stress, while that of LC50/50, though not as appropriate as analysis, is better correlated with the results of analysis.

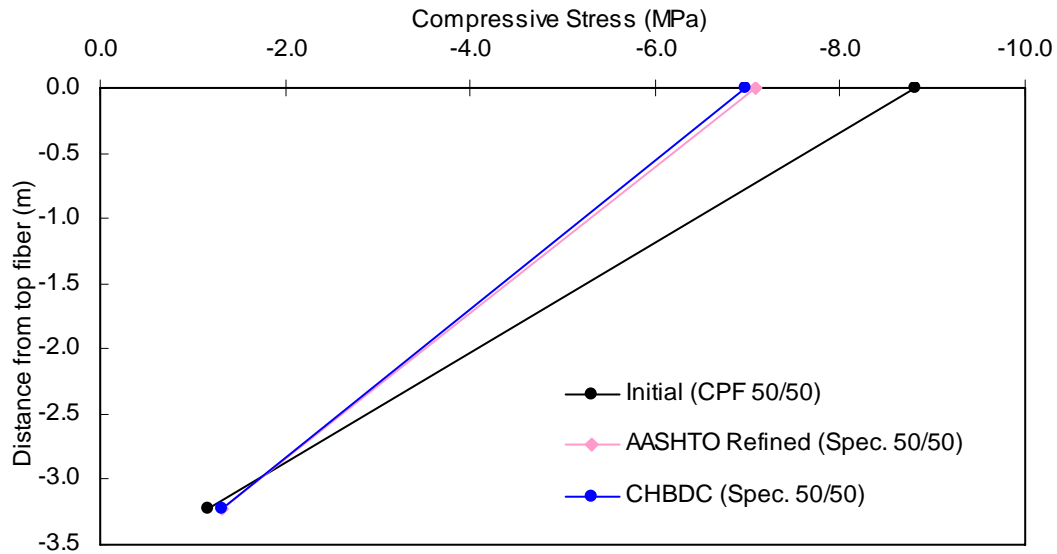


Figure 6.28: Stress profiles determined with the specifications using 50% of the self-weight at prestressing in F4 near the bent.

The observed behavior of all methods used for calculating concrete stress at the theoretical end of service life is presented in Table 6.17. The use of the LC50/50 load case for calculating the initial stress profile in the concrete to be used with the specifications is again seen here as an inappropriate method for producing the long-term concrete stress.

Table 6.17: Stresses from all considered methods at the theoretical end of service life in F4 near the bent.

Method	Load Case	Event	Inputs	Stress (MPa)			
				Top	Bottom		
Monitored				-8.92	-1.38		
Analysis	LC50/50	Initial		CPF	-8.80	-1.16	
		Final	ACI		-4.48	-4.71	
			CEB-FIP		-3.89	-4.18	
			Measured		-1.24	-4.28	
	LC100/0	Initial		CPF	-4.37	-4.61	
				Proposed	-4.36	-4.59	
		Final	ACI		CPF	-3.24	-4.43
					Proposed	-3.17	-4.44
			CEB-FIP		CPF	-2.57	-4.23
					Proposed	-2.45	-4.25
			Measured		CPF	-2.48	-4.20
					Proposed	-2.37	-4.23
Specifications	LC100/0	Initial		CPF	-2.40	-4.45	
		Final	AASHTO Appr.		-2.86	-4.88	
			AASHTO Ref.		-2.86	-4.88	
			CEB-FIP		-3.04	-4.87	
	CHBDC		-2.84	-4.89			
	LC50/50	Initial		CPF	-8.80	-1.16	
		Final	AASHTO Ref.		-7.08	-1.31	
			CHBDC		-6.98	-1.32	

For the same reasons mentioned for F4 at midspan, the LC50/50 case used with the specifications does not produce acceptable long-term concrete stress predictions. Though the LC50/50 initial stress profile was used (this stress profile is the most accurate for comparison to the monitored data) the change in concrete stress over time using LC50/50 with the specifications is incorrect. The specifications long-term predictions of concrete stress using LC100/0 correlate better with the analysis predictions than the specifications use of LC50/50.

The stress in the concrete in F4 near the bent at the theoretical end of service life is predicted with the measured material properties as the most conservative compressive stress value. The stress varies from 1.24 to 4.28 MPa in the deck and soffit, respectively; the deck is the critical fiber at this section. The remaining methods used to predict the long-term stress all exceed the analysis results utilizing the measured material property inputs. Each of the methods used

produced a soffit level prediction of the remaining compressive stress varied from 4.12 to 4.88 MPa, a range of 0.76 MPa. This range is not large compared to the top fiber of the section. The reason for this is that the bottom fiber is not the critical fiber of the section.

The Proposed Method [29] produces a prediction of the long-term concrete stress that trails the specifications predictions consistently by about 0.6 MPa and is the nearest in terms of absolute stress to the specifications predictions. Though the stress prediction from analysis using the measured material properties as input produces the most conservative end of service life prediction of the concrete stress, it is likely that this stress is overly conservative. This occurs because the maximum extrapolated material properties appear to exceed predictions, resulting in reduced concrete stresses at the end of service life. The concrete strains and prestress loss values determined from analysis using the ACI [3] and CEB-FIP [10] material properties as input matched closely the monitored strains and determined prestress loss at T363. The analysis using the measured material properties greatly exceeded the predictions using the ACI [3] and CEB-FIP [10] material properties. Projecting the future trends, the measured material properties are likely overly conservative. The Proposed Method [29] predicts prestress loss that is more conservative than the analyses using ACI [3] and CEB-FIP [10] material properties.

6.6.3. Frame 5 Midspan

The initial stress profile immediately after prestressing, obtained from the monitored data, is indicated in Figure 6.29. The result of analysis of the initial stress profile using the LC50/50 load case for F5 is indicated in Figure 6.29. The correlation between the stress obtained from the monitored data and that indicated through analysis is 1.9% different at the critical fiber (soffit). The long-term concrete stress profiles determined using the material property inputs using the ACI [3], CEB-FIP [10], and measured from the material tests produce stress results that vary as expected based on the material property inputs used in the analyses.

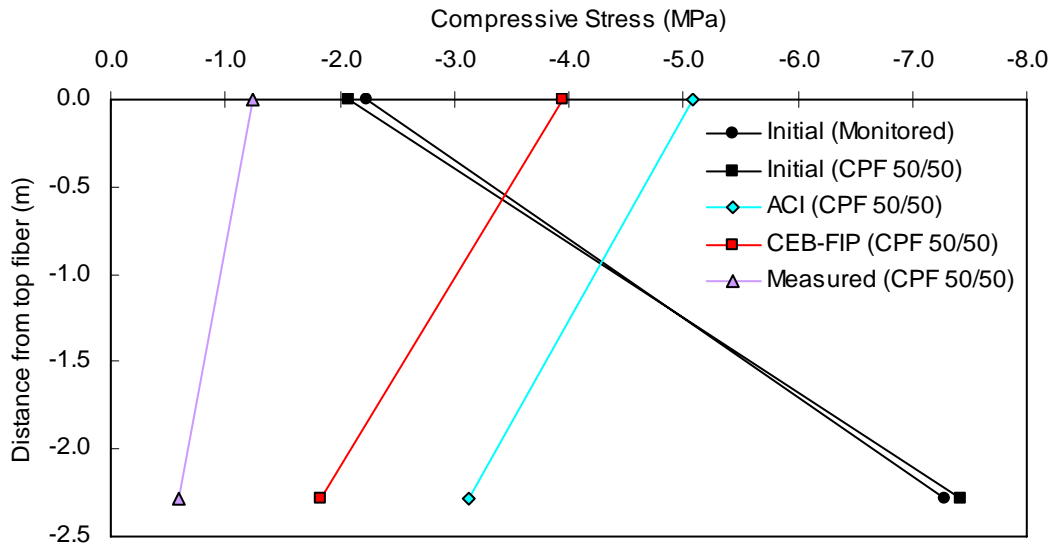


Figure 6.29: Stress profiles at prestressing and the theoretical end of service life obtained using CPF; 50% self-weight applied at prestressing and remaining 50% applied with the removal of falsework in F5 at midspan.

The stress profiles obtained from analysis using the LC100/0 load case and weighted material properties of CEB-FIP [10] from CPF [16] and the Proposed Method [29] are presented in Figure 6.30. It can be seen that the both the initial (prestressing) and final (theoretical end of service life) stress profiles correlate well between the methods. Differences of 0.9% and 0.3% at prestressing and at the theoretical end of service life exist between the two methods, respectively.

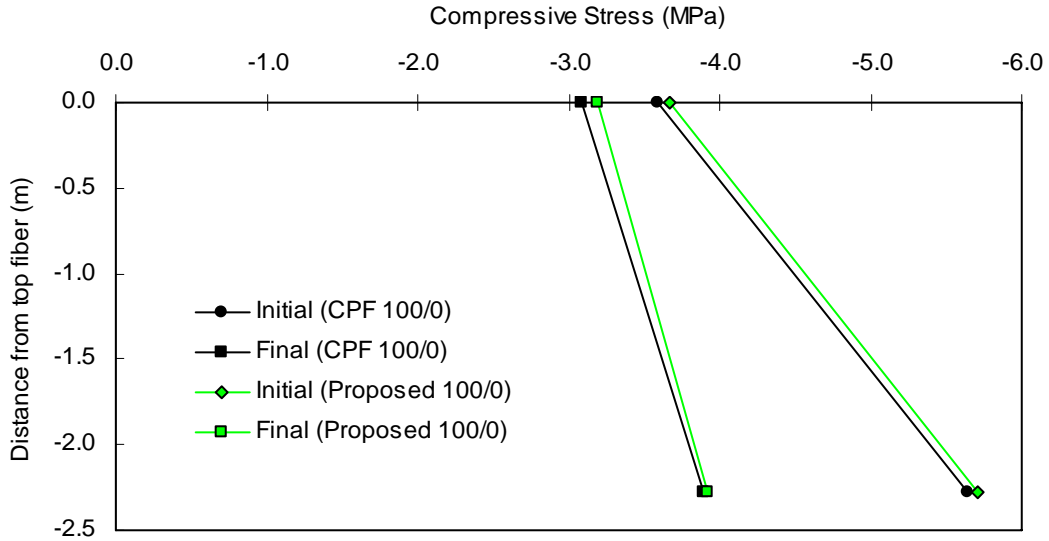


Figure 6.30: Stress profiles at prestressing and the theoretical end of service life obtained using CPF and the Proposed Method; 100% self-weight applied at prestressing in F5 at midspan.

Figure 6.31 displays the concrete stresses that were determined with use of the specifications and the LC100/0 load case. The initial stress profile is the same as that in Figure 6.30. The concrete stress at the end of service life for the critical fiber in the soffit, predicted by the specifications, varies from 4.4 to 4.6 MPa. This change is about 1.2 MPa, or 21% less than the initial stress at the critical fiber of 5.7 MPa. The stress in the deck is predicted to change negligibly over the life of the structure.

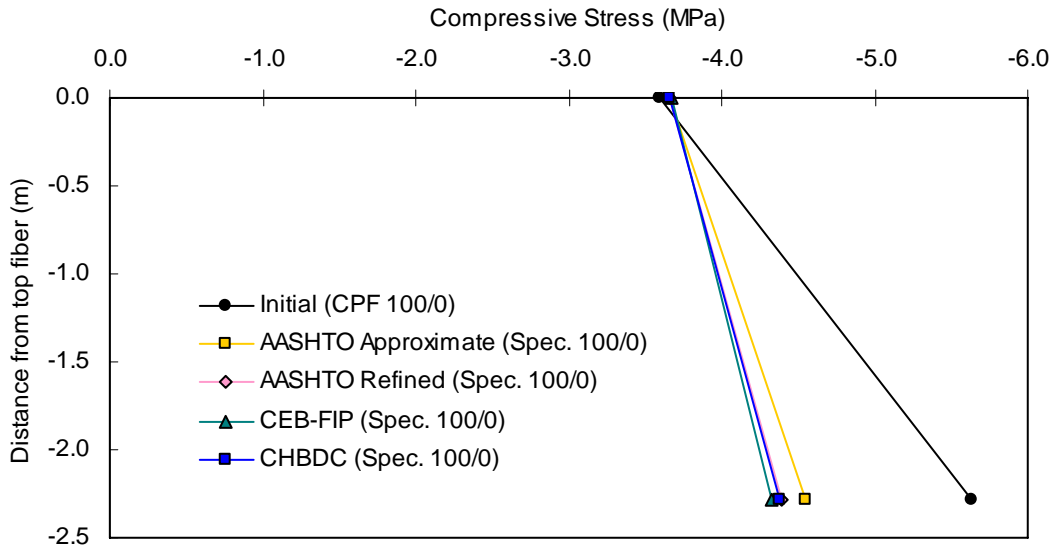


Figure 6.31: Stress profiles determined with the specifications using the full self-weight at prestressing in F5 at midspan.

Using the LC50/50 load case to determine the concrete stress at the end of service life produces predictions that are similar between the two methods. The initial stress profile is the same as the initial stress profile in Figure 6.29. The change in stress at the critical fiber over the life of the structure is 1.4 MPa, representing a change from the initial stress of 19%.

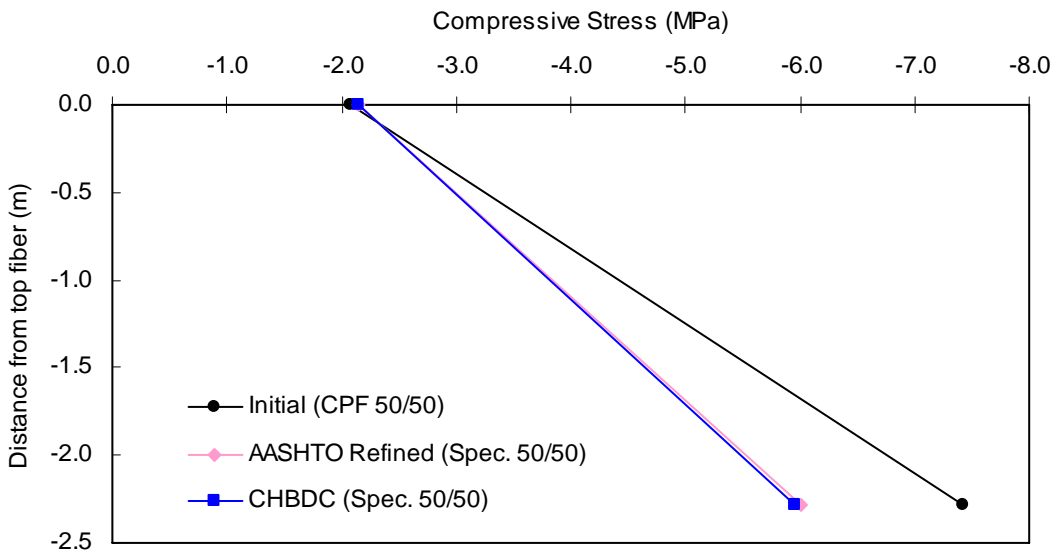


Figure 6.32: Stress profiles determined with the specifications using 50% of the self-weight at prestressing in F5 at midspan.

The final stress values at the theoretical end of service life are presented in Table 6.18. Comparing all of the predictions of concrete stress, the range of stresses in the concrete at the critical fiber is between 3.4 and 6.3 MPa. The range of stresses in the deck fiber of the section ranges between 2.2 and 3.9 MPa. Both the ranges, for the deck and soffit, indicate values in which the maximum compressive stress is nearly 100% larger than the lowest stress. It may be noted, though, that this range includes values that are not particularly representative of states predicted by other methods.

Table 6.18: Stresses from all considered methods at the theoretical end of service life in F5 at midspan.

Method	Load Case	Event	Inputs	Stress (MPa)			
				Top	Bottom		
Monitored				-2.23	-7.28		
Analysis	LC50/50	Initial		CPF	-2.07	-7.42	
		Final	ACI		-5.09	-3.12	
			CEB-FIP		-3.94	-1.83	
			Measured		-1.24	-0.60	
	LC100/0	Initial		CPF	-3.59	-5.64	
				Proposed	-3.67	-5.71	
		Final	ACI	CPF	-3.08	-3.89	
					Proposed	-3.19	-3.92
			CEB-FIP	CPF	-2.83	-3.29	
					Proposed	-2.93	-3.31
		Measured		CPF	-2.31	-2.28	
				Proposed	-2.43	-2.23	
Specifications	LC100/0	Initial		CPF	-3.59	-5.64	
		Final	AASHTO Appr.		-3.65	-4.54	
			AASHTO Ref.		-3.66	-4.40	
			CEB-FIP		-3.67	-4.33	
	CHBDC		-3.66	-4.38			
	LC50/50	Initial		CPF	-2.07	-7.42	
		Final	AASHTO Ref.		-2.15	-6.02	
			CHBDC		-2.16	-5.96	

In Table 6.18 it can be seen that the calculated stress using the specifications LC100/0 load case results in stresses at the critical fiber within 0.6 MPa of the analytical predictions. Comparatively, the specifications predictions of stress using the LC50/50 load case exceed the analytical predictions by as much as 2 MPa at the critical fiber. As was seen for the monitored locations in F4, the initial

stress profile for use with the specifications LC50/50 case correlates well with the initial monitored stress profile. This does not indicate that the LC50/50 case, when used with the specifications, is appropriate, since the change in stress over time disregards the presence of non-prestressed steel. The specifications use of LC100/0 results in stresses that correlate better with the analytical results of CPF [16].

6.6.4. Frame 5 Near the Bent

The initial stress profile determined from the monitored data is presented for the monitored section in F5 near the bent in Figure 6.33. The initial stress profile produced from analysis using CPF [16] and the LC50/50 load case is 1.4 MPa (19%) lower than the stress from monitoring. At prestressing, the tendons place a higher stress in the upper portion of the section near the critical fiber in the deck. At the theoretical end of service life, the stress profile reverses direction, placing more stress on the bottom fibers, occurring because the self-weight of the structure is imposed for a long period placing the lower portion of the section (near the soffit) in a state with higher compressive stress. It can be seen that all three of the analyses calculate a reversal of the stress profile. The analysis using the measured material properties produces a stress of nearly zero. Though this is alarming, it should be mentioned that the measured material properties for F5, especially shrinkage, greatly exceeded the material property predictions of ACI [3] and CEB-FIP [10]. It is not expected that the concrete stresses would reach such a state so near the tensile region.

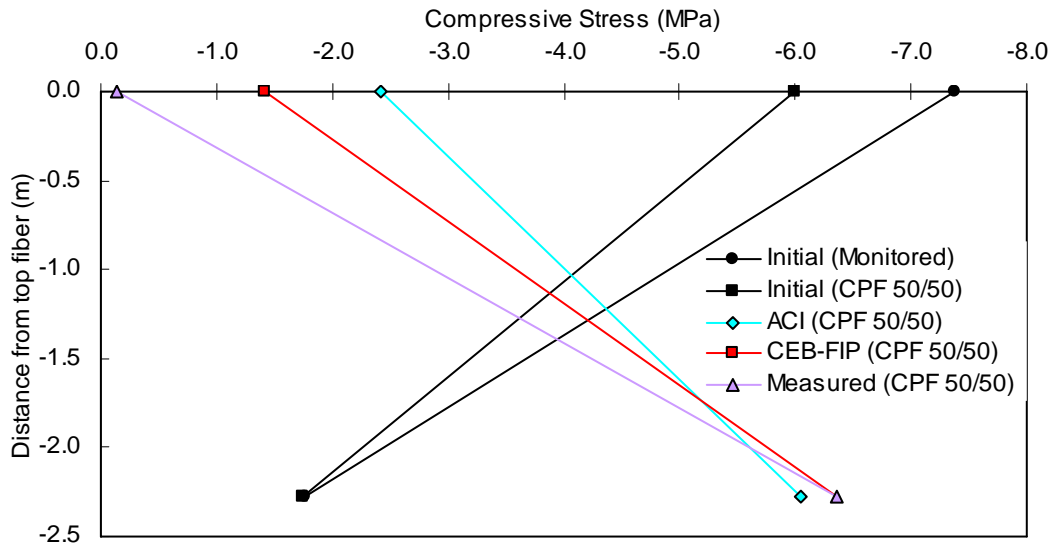


Figure 6.33: Stress profiles at prestressing and the theoretical end of service life obtained using CPF; 50% self-weight applied at prestressing and remaining 50% applied with the removal of falsework in F5 near the bent.

The stress profiles calculated from using the Proposed Method [29] and CPF [16] using the LC100/0 load case with CEB-FIP [10] material properties are presented in Figure 6.34. The correlation of stress profiles at prestressing and the theoretical end of service life are similar at both points in time. In the critical fiber (deck), the difference between the Proposed Method [29] and CPF [16] at prestressing is 2.0%; at the theoretical end of service life, the difference between compressive stresses is 12%, representing a difference of 0.14 MPa.

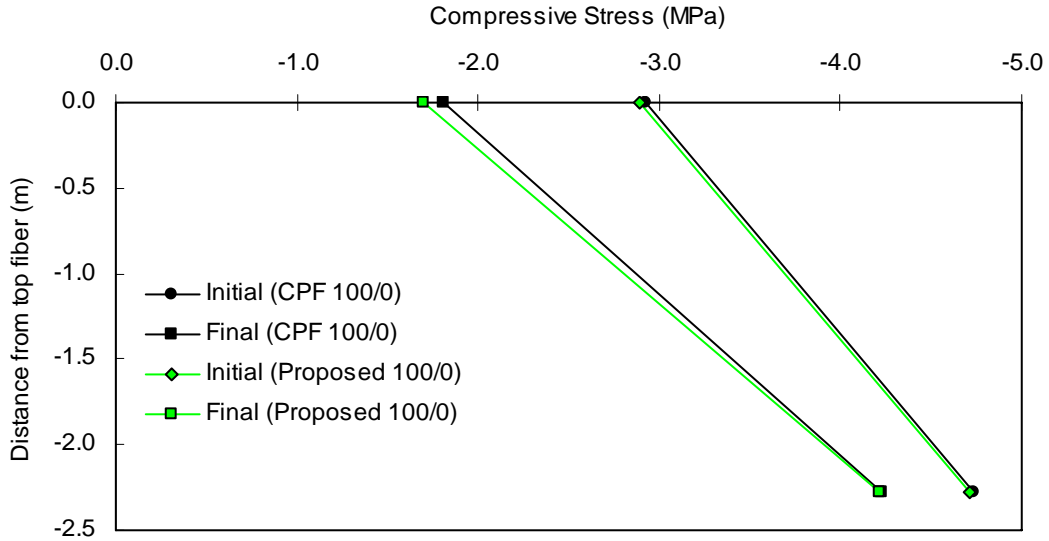


Figure 6.34: Stress profiles at prestressing and the theoretical end of service life obtained using CPF and the Proposed Method; 100% self-weight applied at prestressing in F4 near the bent.

The long-term compressive stresses determined using the specifications predictions of prestress loss for F5 near the bent are shown in Figure 6.35. This figure shows that the stress in the critical fiber (deck) at the end of service life is about 0.76 MPa lower than the initial stress at prestressing, representing a decrease of 20%.

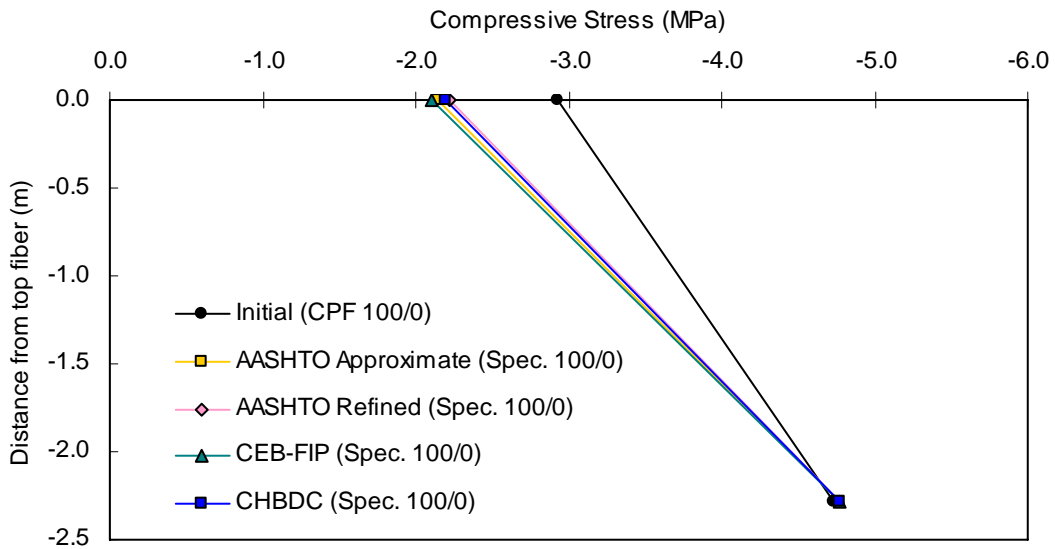


Figure 6.35: Stress profiles determined with the specifications using the full self-weight at prestressing in F5 near the bent.

Figure 6.36 displays the long-term concrete stresses determined from the LC50/50 load case. Compared to Figure 6.35, it can be seen that the long-term change in stress does not capture the reversal of the slope of the stress through the section. As mentioned previously for other monitored locations, this occurs because the method used for calculating the change in stress does not accommodate the non-prestressed reinforcement and, as such, does not account for accurate changes in stress over the life of the structure. At the critical fiber (deck), the stress changes about 1 MPa between prestressing and the theoretical end of service life, a decrease in compressive stress by 17%.

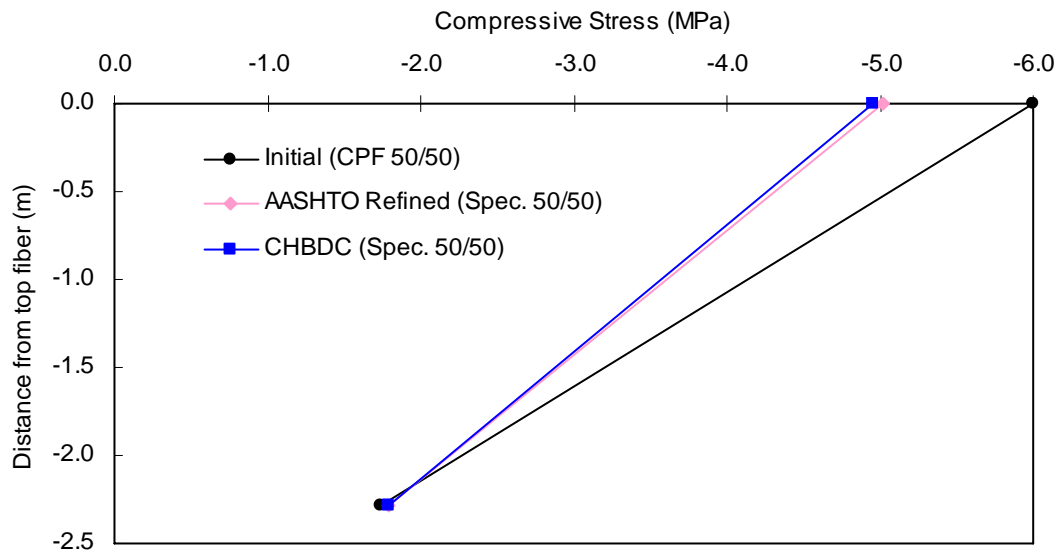


Figure 6.36: Stress profiles determined with the specifications using 50% of the self-weight at prestressing in F5 near the bent.

The stress profiles in the monitored section at the theoretical end of service life near the bent in F5 are presented in Table 6.19. It was mentioned that the analysis using the measured material properties as input resulted in the lowest compressive stress and the most conservative value at the end of service life. When compared to the other stress values, it is apparent that the prediction of the concrete stress calculated using the Proposed Method [29] results in a slightly more conservative stress profile than the CPF [16] analysis using ACI [3] material properties.

In Table 6.19 it is shown that the stresses calculated using the LC50/50 load case with the specifications does not produce stress profiles that are indicative of the stress at the end of service life. As mentioned previously for the other monitored locations in this section, the change in stress over time is not adequately accommodated by the specifications methods. The initial stress profile for the LC50/50 load case is shown in Figure 6.33. It is clear that the slope of the stress profile changes directions over time, as indicated by the analysis of CPF [16] and the Proposed Method [29]. The specifications predictions of concrete stress at the end of service life are better predicted using the LC100/0 load case. The reason for this exists because the LC100/0 load case initiates with the stress profile in the same direction as the stress at the end of service life. Though not as conservative estimate as the CPF [16] analyses and the Proposed Method [29], the specifications predictions for the LC100/0 load case are much improved compared to those of the LC50/50 load case.

Table 6.19: Stresses from all considered methods at the theoretical end of service life in F5 near the bent.

Method	Load Case	Event	Inputs	Stress (MPa)			
				Top	Bottom		
Monitored				-7.38	-1.77		
Analysis	LC50/50	Initial		CPF	-6.00	-1.74	
		Final	ACI	CPF	-2.42	-6.05	
			CEB-FIP	CPF	-1.41	-6.36	
			Measured	CPF	-0.14	-6.35	
	LC100/0	Initial		CPF	-2.93	-4.73	
				Proposed	-2.89	-4.71	
		Final	ACI	CPF	-1.81	-4.23	
					Proposed	-1.70	-4.21
			CEB-FIP	CPF	-1.41	-3.97	
					Proposed	-1.29	-3.96
		Measured		CPF	-0.57	-3.57	
				Proposed	-0.38	-3.58	
Specifications	LC100/0	Initial		CPF	-2.93	-4.73	
		Final	AASHTO Appr.		-2.14	-4.77	
			AASHTO Ref.		-2.22	-4.77	
			CEB-FIP		-2.11	-4.77	
	CHBDC			-2.19	-4.77		
	LC50/50	Initial		CPF	-6.00	-1.74	
		Final	AASHTO Ref.		-5.02	-1.79	
			CHBDC			-4.95	-1.79

6.6.5. Commentary on Long-Term Concrete Stress Predictions

Using Eqs. 6.2 and 6.3, the concrete stress was calculated using the prestress loss values determined from the specifications. It can be seen that using either load case to calculate the change in concrete stress results in small variation between the four specifications considered. The specifications loss values relate to a decrease in the initial stress at the end of service life of a maximum of 10% at the critical fiber of each of the four monitored locations, obtained using LC100/0. Compared to the predictions through analysis with CPF [16] and the Proposed Method [29], it is clear that the specifications discount for the inclusion of non-prestressed reinforcement significantly alters the long-term change in stress.

In each of the figures, the stress results from the CPF [16] analysis are included, using the same material property inputs and full self-weight loading scenario as those used with the Proposed Method [29]. The results of analysis from the Proposed Method [29] and CPF [16] analysis are nearly identical, with a maximum difference between the two method's concrete stress resultants at the end of service life of 7.1%. This outcome indicates that the Proposed Method [29] is capable of producing predictions of the long-term concrete stress and other associated deformation as adequately as the predictions of the CPF [16] computer analysis. This is very significant since this finding suggests that the Proposed Method [29] can be used in place of the CPF [16] analysis. The Proposed Method [29] is accurate for all cases since equilibrium and compatibility are upheld.

The Proposed Method [29] is well suited to generate accurate predictions of the prestress loss and concrete stress points during the life of the structure. Although this method does not have the ability to accommodate more than one concrete type or loading instance, this does not have a drastic influence on the outcome at the theoretical end of service life. It was shown that differences in loading might create differences in the deformation early in the life of the structure between the monitored spans and the analytical results. Variations in

deformation between methods at the end of service life appear to diminish and are dependent primarily on the ultimate values of creep and shrinkage.

The specifications should not be used for a LC50/50 load case to determine the long-term concrete stress. Though satisfactory results are produced using the prestress loss for the LC50/50 load case, use of the initial stress profile with the change in stress from the corresponding prestress loss is not acceptable. This occurs because the specifications predictions do not accommodate the correct distribution of stress resulting from the presence of non-prestressed reinforcement, thus the change is not accurate. Prestress losses calculated from the LC50/50 load case using the specifications were about 6% larger than the predictions calculated with the LC100/0 load case with corresponding methods.

The occurrences stated previously, with regard to the prestress and strain, are notable, but it is premature to make definitive judgments about the long-term state of the bridge knowing only the prestress loss and strain profiles. Although it was certainly useful to compare the strains and prestress loss during monitoring to the analysis, as this serves as the basis for acknowledging the appropriateness of the predicted long-term values, strains and prestress losses do not directly indicate the performance of the concrete over the long-term.

It can be seen in the figures that the long-term concrete stresses are further into the compressive region than several of the analysis results. This research was begun with the premonition that the specifications predictions overestimate the remaining concrete compressive stress. This is reinforced by the results in the figures; however, the influence is not particularly severe.

7. Conclusions

7.1. Project Summary

This Report has addressed two significant issues that influence the long-term materials related deformation of post-tensioned bridges. The first of these aspects relates to testing and characterization of the material properties. Material characterization was performed to determine the creep and shrinkage in the concrete used within two monitored bridge spans. The second aspect studies the effects of creep and shrinkage on the long-term deformations and prestress losses in the class of bridges under consideration.

At the materials level, test specimens were mounted in specially designed fixtures, which applied a nearly constant compressive load to the specimens. The creep coefficient was measured from these tests. Additional unloaded specimens were used to determine shrinkage. These tests were performed with the intent of capturing and characterizing the material properties for the concrete used in the bridge to eliminate error when the results of analysis were compared to monitoring. The experimental creep and shrinkage were compared to values predicted using available specifications.

Two recently constructed spans of the I5/805 Bridge in San Diego, California were instrumented with vibrating wire strain gages and monitored for the first year after the application of prestress. The bridge is representative of a current design of California highway bridges. The collected strains from the spans provided the time-dependent deformation of the structure. These strains were used for determining the loss in prestress that occurred over the monitoring period. This prestress loss was compared to the loss predicted by available specifications and through the use of a computer analysis program “CPF” [16] as well as a new Proposed Method [29]. These methods were used to predict the end of service life values of prestress loss and change in concrete stress.

7.2. Significant Findings

This research has resulted in the following findings of significance:

- The shrinkage obtained through material testing is highly dependent on environmental influences and this needs to be considered to a greater extent in design.
- The measured values of creep showed improved correlation with the predicted values as the age at loading increased.
- The commonly used best-fit equations developed by Ghali et al [15] for creep and shrinkage do not accommodate changes in the measured values at later ages as those early in the life of the concrete.
- The use of a load case that balanced 50% of the structural self-weight with prestressing and the remaining 50% with the removal of falsework (LC50/50) showed better correlation with the monitored data than the case with 100% of the structural self-weight applied with prestressing (LC100/0). The first load case was able to provide excellent predictions of initial strain profiles compared to the monitored strain.
- In Frame 4, the results of analysis at an intermediate point in time (T363) were within 11 MPa of the loss obtained through monitoring, i.e., 16%.
- In Frame 5, the results of analysis at an intermediate point in time (T303) were within 22 MPa of the loss obtained through monitoring, i.e., 61%.

The following findings relate to behavior based on extrapolated data and future projections of bridge deformation at a theoretical end of service life.

- The minimum bound ultimate shrinkage values determined by direct use of data at T363 and T303 (as shown in Figure 5.74) compared well with the specifications predictions.

- The minimum bound ultimate creep values determined by direct use of data at T363 and T303 (as shown in Figure 5.73) were slightly less than the specifications predictions in most cases.
- The measured creep and shrinkage appeared to reach asymptotes faster than was indicated by the best-fit equations, thus ultimate values may be closer to the minimum extrapolated values.
- In Frame 4, all predictions of prestress loss using ACI [3], CEB-FIP [10], and the measured material properties as input to analysis were lower than the specifications predictions using LC100/0 and substantially lower than the use of LC50/50 with the specifications.
- In Frame 5, the ACI and minimum measured material properties used as input to analysis resulted in lower prestress loss than the specifications using LC100/0. The maximum measured material properties used as input to analysis produced prestress losses that considerably exceeded (by about 100%) the minimum prestress loss predictions (using the minimum measured material properties as input to analysis) and were larger than most of the specifications predictions using both load cases.
- Since the specifications primarily provided larger predictions of prestress loss than what was indicated through analysis, the specifications predictions of loss are acceptable only in providing initial estimates and should not be taken as accurate for purposes of final design.
- The specifications do not adequately account for instants of multiple loading; the use of LC50/50 with the specifications equations significantly overestimates prestress loss at the end of service compared to CPF [16].
- The specifications predictions of concrete stress do not accommodate the presence of non-prestressed steel. The changes in concrete stress

over time are not accurately reflected in the predictions in the same way as the analytical predictions of stress.

- The presence of falsework is not as significant to the bridge deformation at the end of service life as it is early on in the life of the structure. Despite the differences in modeled configurations, the most significant influence on the long-term prestress loss is accurate characterization (and hence, input) of material properties (creep, shrinkage, and relaxation). As long as the analysis includes all permanent loads, the time or sequence at which the loads are applied (other than prestressing) has diminished influence on the bridge deformation with time.
- The Proposed Method [29] was shown to be capable of capturing the bridge behavior as compared to the predictions of CPF [16].

7.3. Research Discussion

As the measured material properties were used for determining the creep and shrinkage for the bridge, the influence of exposure is reflected in the creep and shrinkage produced for the bridge. This indicates that size effects and environmental influences need to be considered more closely.

Several of the specifications used within this research for producing prestress loss predictions are not entirely applicable for the bridge frames analyzed. Namely, the AASHTO Approximate [2] specification states that the method is applicable for bridges up to 48.8 m in length. Additionally, this method can be used to determine the loss for bridges prestressed between 10 and 30 days after concrete casting with relative humidity between 40 and 100%. The AASHTO Refined [2] method is appropriate for bridges up to 76.2 m in length. The monitored span in F4 is 80.62 (exceeding both methods allowable length) and F5 is 52.85 m (exceeding the AASHTO Approximate [2] allowable length). Furthermore, F4 was prestressed several months after concrete casting. It should also be noted that the range of relative humidity (40 to 100%) is a very

large range that encompasses significantly different environments. Material behavior varies considerably as exposed to different relative humidity and it is not possible for such a large range to be appropriate for all areas. The CEB-FIP [10] specification does not account for non-prestressed steel in its formulation of prestress loss prediction. These issues signal that the specifications may not be appropriate for the bridge used in this research. While this is true, the accommodation of some load cases produced some prestress loss predictions that correlated well with analytical results. It was found that the specifications that accommodate two instances of loading produce much larger long-term prestress loss predictions than with the load applied all at once.

To verify that the analyses were correct, the analytical results were compared to the results of monitoring. A comparison of strain and prestress loss was done to show the correlation of monitored to analytical behavior. Since the monitored data could only be compared to the analytical results to the point in time T363 or T303, comparisons beyond these points in time were based on extrapolated data. In general, the monitored data compared well to the analytical results, as summarized in the previous section. The projected future behavior at an assumed theoretical end of service life, 55 years after prestressing, showed lower loss predictions than available specifications for predicting prestress loss.

The analytical predictions of prestress loss at the theoretical end of service life are taken to reflect actual losses that can be expected in the bridge. Though it is not possible to predict for certain what the prestress loss will be when 55 years is reached, the values presented were determined using methods that determine displacements based on material behavior. To accommodate the possibility of a range of material property variation, maximum and minimum prestress losses were determined. From analysis using the material property inputs from ACI [3], CEB-FIP [10], and from testing, a range of prestress loss values was obtained, which varied between 3 to 6% of the jacking stress at the end of service life. Primarily the analytical predictions showed variation with remaining prestress of about 80 to 85% of the jacking stress.

7.4. Recommendations for Future Research

The following recommendations are made to broaden the understanding of the effect of time-dependent materials characteristics on response of prestressed bridges.

- Deflections of the bridge superstructure should be measured during loading and during other significant events during construction
- Deformations should be monitored from the instant concrete is placed
- Monitoring should be conducted at a larger number of sections and locations along a span and through more frequent data collection over longer periods of time
- Effect of environmental conditions different from those in San Diego should be considered to assess flexibility of the model
- Effects of falsework, and the time of its removal, on the development of creep and shrinkage should be studied
- Effects of construction sequence, especially the time between concrete pours, time between casting and prestressing, removal of formwork and other loading need to be considered as these are likely to have significant effects on the overall response. Since specifications usually assume “ideal” construction conditions and sequences in operation, variations as seen regularly on construction sites may cause substantial deviation from predicted response. The use of a scale laboratory test is recommended to enable development of a base-line.

In addition effects such as span length, number of cells and the effect of hinges should also be studied in greater depth. Further the extension of this work to determination of prestress losses in unbonded post-tensioned bridges, precast segmental bridges, and bridges using FRP reinforcement and tendons are recommended. *It is noted that this is an interim report and recommendations for implementation will be given in the final report for this project.*

Appendix A

Measured Data from Material Testing: Creep

First Loading

For this research, two bridge frames were monitored: Frame 4 (F4) and Frame 5 (F5). The concrete in F4 was poured on three separate days, October 5, 2004; November 2, 2004; and March 3, 2005. The concrete in F5 was poured on two separate days, April 5, 2005 and May 3, 2005. The concrete poured on each separate day in F4 and F5 is labeled by the name of the month in which it was cast, as no month contains more than a single concrete pour. The casting dates and reference names of the concretes are listed in the following Table A1. More information regarding the placement of each concrete batch can be found in previous sections.

Table A1: Concrete casting dates and reference names.

Concrete Casting Date	Concrete Reference Name
October 5, 2004	October
November 2, 2004	November
March 3, 2005	March
April 5, 2005	April
May 3, 2005	May

October creep using F4 shrinkage (Part 1 of Table)

Time (days)	DEMEC Reading (DR)						Measured creep strain ($\mu\text{m/m}$) $\epsilon_{\text{CST},i}$						Thermal/ Shrinkage strain ($\mu\text{m/m}$)
	1A	1B	2A	2B	3A	3B	1A	1B	2A	2B	3A	3B	
initial	0.010	0.006	0.016	0.022	0.006	0.004	0	0	0	0	0	0	-
0	-0.066	-0.076	-0.080	-0.028	-0.135	-0.028	-380	-410	-480	-250	-705	-160	0
6	-0.125	-0.120	-0.139	-0.066	-0.215	-0.043	-675	-630	-775	-440	-1105	-235	-91
10	-0.122	-0.124	-0.132	-0.070	-0.209	-0.051	-660	-650	-740	-460	-1075	-275	-129
13	-0.127	-0.128	-0.139	-0.082	-0.217	-0.060	-685	-670	-775	-520	-1115	-320	-181
17	-0.133	-0.134	-0.146	-0.084	-0.225	-0.064	-715	-700	-810	-530	-1155	-340	-204
20	-0.150	-0.139	-0.163	-0.087	-0.240	-0.065	-800	-725	-895	-545	-1230	-345	-222
24	-0.153	-0.146	-0.166	-0.094	-0.248	-0.069	-815	-760	-910	-580	-1270	-365	-229
27	-0.143	-0.140	-0.152	-0.087	-0.233	-0.060	-765	-730	-840	-545	-1195	-320	-179
31	-0.155	-0.147	-0.164	-0.097	-0.245	-0.067	-825	-765	-900	-595	-1255	-355	-210
41	-0.158	-0.153	-0.166	-0.098	-0.246	-0.073	-840	-795	-910	-600	-1260	-385	-240
45	-0.163	-0.155	-0.164	-0.102	-0.255	-0.073	-865	-805	-900	-620	-1305	-385	-254
48	-0.168	-0.161	-0.175	-0.106	-0.265	-0.078	-890	-835	-955	-640	-1355	-410	-267
55	-0.167	-0.159	-0.174	-0.105	-0.266	-0.077	-885	-825	-950	-635	-1360	-405	-256
59	-0.171	-0.161	-0.178	-0.106	-0.269	-0.077	-905	-835	-970	-640	-1375	-405	-282
73	-0.172	-0.163	-0.178	-0.113	-0.273	-0.078	-910	-845	-970	-675	-1395	-410	-264
80	-0.173	-0.159	-0.176	-0.108	-0.280	-0.078	-915	-825	-960	-650	-1430	-410	-275
85	-0.174	-0.160	-0.182	-0.109	-0.282	-0.079	-920	-830	-990	-655	-1440	-415	-290
87	-0.182	-0.170	-0.188	-0.114	-0.287	-0.086	-960	-880	-1020	-680	-1465	-450	-314
92	-0.183	-0.169	-0.187	-0.116	-0.286	-0.084	-965	-875	-1015	-690	-1460	-440	-314
104	-0.187	-0.171	-0.194	-0.117	-0.298	-0.085	-985	-885	-1050	-695	-1520	-445	-334
106	-0.185	-0.171	-0.194	-0.115	-0.290	-0.083	-975	-885	-1050	-685	-1480	-435	-331
122	-0.179	-0.165	-0.183	-0.110	-0.291	-0.076	-945	-855	-995	-660	-1485	-400	-270
135	-0.186	-0.172	-0.189	-0.114	-0.300	-0.082	-980	-890	-1025	-680	-1530	-430	-286
139	-0.191	-0.177	-0.196	-0.121	-0.306	-0.088	-1005	-915	-1060	-715	-1560	-460	-319
149	-0.186	-0.170	-0.191	-0.115	-0.302	-0.082	-980	-880	-1035	-685	-1540	-430	-304
157	-0.200	-0.181	-0.204	-0.126	-0.315	-0.095	-1050	-935	-1100	-740	-1605	-495	-325
164	-0.191	-0.175	-0.193	-0.118	-0.307	-0.085	-1005	-905	-1045	-700	-1565	-445	-290
168	-0.197	-0.184	-0.199	-0.126	-0.313	-0.096	-1035	-950	-1075	-740	-1595	-500	-311
178	-0.194	-0.182	-0.199	-0.124	-0.319	-0.090	-1020	-940	-1075	-730	-1625	-470	-300
183	-0.192	-0.182	-0.180	-0.129	-0.300	-0.101	-1010	-940	-980	-755	-1530	-525	-306
200	-0.215	-0.204	-0.229	-0.114	-0.354	-0.108	-1125	-1050	-1225	-680	-1800	-560	-321
206	-0.208	-0.195	-0.218	-0.134	-0.344	-0.101	-1090	-1005	-1170	-780	-1750	-525	-284
212	-0.204	-0.194	-0.212	-0.134	-0.339	-0.098	-1070	-1000	-1140	-780	-1725	-510	-281
220	-0.223	-0.210	-0.237	-0.153	-0.363	-0.116	-1165	-1080	-1265	-875	-1845	-600	-361
226	-0.220	-0.208	-0.232	-0.149	-0.361	-0.111	-1150	-1070	-1240	-855	-1835	-575	-380
235	-0.228	-0.225	-0.239	-0.162	-0.372	-0.128	-1190	-1155	-1275	-920	-1890	-660	-409
239	-0.230	-0.221	-0.241	-0.158	-0.373	-0.124	-1200	-1135	-1285	-900	-1895	-640	-370
251	-0.253	-0.234	-0.262	-0.173	-0.392	-0.137	-1315	-1200	-1390	-975	-1990	-705	-460
255	-0.250	-0.235	-0.258	-0.175	-0.388	-0.136	-1300	-1205	-1370	-985	-1970	-700	-435
262	-0.257	-0.235	-0.261	-0.173	-0.394	-0.135	-1335	-1205	-1385	-975	-2000	-695	-446
268	-0.233	-0.224	-0.247	-0.160	-0.372	-0.124	-1215	-1150	-1315	-910	-1890	-640	-355
283	-0.226	-0.229	-0.226	-0.173	-0.353	-0.130	-1180	-1175	-1210	-975	-1795	-670	-324
290	-0.250	-0.242	-0.253	-0.174	-0.380	-0.135	-1300	-1240	-1345	-980	-1930	-696	-376
303	-0.263	-0.245	-0.270	-0.181	-0.403	-0.142	-1365	-1255	-1430	-1015	-2045	-730	-431
322	-0.255	-0.239	-0.265	-0.178	-0.398	-0.138	-1325	-1225	-1405	-1000	-2020	-710	-415
335	-0.240	-0.226	-0.251	-0.160	-0.389	-0.122	-1250	-1160	-1335	-910	-1975	-630	-401
339	-0.255	-0.238	-0.269	-0.177	-0.406	-0.135	-1325	-1220	-1425	-995	-2060	-695	-399
353	-0.245	-0.231	-0.257	-0.165	-0.397	-0.125	-1275	-1185	-1365	-935	-2015	-645	-355

October creep using F4 shrinkage (Part 2 of Table)

Time (days)	Measured creep strain less shrinkage and thermal strain ($\mu\text{m/m}$) $\epsilon_{cre,i}$						True creep strain ($\mu\text{m/m}$) $\epsilon_{cr,i}$						Creep coefficient $\phi(t,t_0)$						
	1A	1B	2A	2B	3A	3B	1A	1B	2A	2B	3A	3B	1A	1B	2A	2B	3A	Average	
0	-380	-410	-480	-250	-705	-160	0	0	0	0	0	0	0	0	0	0	0	0	0
6	-584	-539	-684	-349	-1014	-144	-204	-129	-204	-99	-309	16	0.54	0.31	0.42	0.39	0.44	0.42	0.42
10	-531	-521	-611	-331	-946	-146	-151	-111	-131	-81	-241	14	0.40	0.27	0.27	0.32	0.34	0.32	0.32
13	-504	-489	-594	-339	-934	-139	-124	-79	-114	-89	-229	21	0.33	0.19	0.24	0.35	0.32	0.29	0.29
17	-511	-496	-606	-326	-951	-136	-131	-86	-126	-76	-246	24	0.35	0.21	0.26	0.30	0.35	0.29	0.29
20	-577	-502	-672	-322	-1007	-123	-197	-93	-192	-72	-303	37	0.52	0.23	0.40	0.29	0.43	0.37	0.37
24	-586	-531	-681	-351	-1041	-136	-206	-121	-201	-101	-336	24	0.54	0.30	0.42	0.40	0.48	0.43	0.43
27	-586	-551	-661	-366	-1016	-141	-206	-141	-181	-116	-311	19	0.54	0.34	0.38	0.46	0.44	0.43	0.43
31	-615	-555	-690	-385	-1045	-145	-235	-145	-210	-135	-340	15	0.62	0.35	0.44	0.54	0.48	0.49	0.49
41	-600	-555	-670	-360	-1020	-145	-220	-145	-190	-110	-315	15	0.58	0.35	0.40	0.44	0.45	0.44	0.44
45	-611	-551	-646	-366	-1051	-131	-231	-141	-166	-116	-346	29	0.61	0.34	0.35	0.46	0.49	0.45	0.45
48	-622	-567	-687	-372	-1087	-143	-242	-158	-207	-122	-383	17	0.64	0.38	0.43	0.49	0.54	0.50	0.50
55	-629	-569	-694	-379	-1104	-149	-249	-159	-214	-129	-399	11	0.65	0.39	0.45	0.51	0.57	0.51	0.51
59	-622	-552	-687	-357	-1092	-123	-242	-143	-207	-107	-388	37	0.64	0.35	0.43	0.43	0.55	0.48	0.48
73	-646	-581	-706	-411	-1131	-146	-266	-171	-226	-161	-426	14	0.70	0.42	0.47	0.64	0.60	0.57	0.57
80	-640	-550	-685	-375	-1155	-135	-260	-140	-205	-125	-450	25	0.68	0.34	0.43	0.50	0.64	0.52	0.52
85	-630	-540	-700	-365	-1150	-125	-250	-130	-220	-115	-445	35	0.66	0.32	0.46	0.46	0.63	0.50	0.50
87	-646	-566	-706	-366	-1151	-136	-266	-156	-226	-116	-446	24	0.70	0.38	0.47	0.46	0.63	0.53	0.53
92	-651	-561	-701	-376	-1146	-126	-271	-151	-221	-126	-441	34	0.71	0.37	0.46	0.50	0.63	0.53	0.53
104	-651	-551	-716	-361	-1186	-111	-271	-141	-236	-111	-481	49	0.71	0.34	0.49	0.44	0.68	0.54	0.54
106	-644	-554	-719	-354	-1149	-104	-264	-144	-239	-104	-444	56	0.69	0.35	0.50	0.41	0.63	0.52	0.52
122	-675	-585	-725	-390	-1215	-130	-295	-175	-245	-140	-510	30	0.78	0.43	0.51	0.56	0.72	0.60	0.60
135	-694	-604	-739	-394	-1244	-144	-314	-194	-259	-144	-539	16	0.83	0.47	0.54	0.57	0.76	0.64	0.64
139	-686	-596	-741	-396	-1241	-141	-306	-186	-261	-146	-536	19	0.81	0.45	0.54	0.58	0.76	0.63	0.63
149	-676	-576	-731	-381	-1236	-126	-296	-166	-251	-131	-531	34	0.78	0.41	0.52	0.52	0.75	0.60	0.60
157	-725	-610	-775	-415	-1280	-170	-345	-200	-295	-165	-575	-10	0.91	0.49	0.61	0.66	0.82	0.70	0.70
164	-715	-615	-755	-410	-1275	-155	-335	-205	-275	-160	-570	5	0.88	0.50	0.57	0.64	0.81	0.68	0.68
168	-724	-639	-764	-429	-1284	-189	-344	-229	-284	-179	-579	-29	0.90	0.56	0.59	0.71	0.82	0.72	0.72
178	-720	-640	-775	-430	-1325	-170	-340	-230	-295	-180	-620	-10	0.89	0.56	0.61	0.72	0.88	0.73	0.73
183	-704	-634	-674	-449	-1224	-219	-324	-224	-194	-199	-519	-59	0.85	0.55	0.40	0.79	0.74	0.67	0.67
200	-804	-729	-904	-359	-1479	-239	-424	-319	-424	-109	-774	-79	1.12	0.78	0.88	0.43	1.10	0.86	0.86
206	-806	-721	-886	-496	-1466	-241	-426	-311	-406	-246	-761	-81	1.12	0.76	0.85	0.98	1.08	0.96	0.96
212	-789	-719	-859	-499	-1444	-229	-409	-309	-379	-249	-739	-69	1.08	0.75	0.79	0.99	1.05	0.93	0.93
220	-804	-719	-904	-514	-1484	-239	-424	-309	-424	-264	-779	-79	1.12	0.75	0.88	1.05	1.10	0.98	0.98
226	-770	-690	-860	-475	-1455	-195	-390	-280	-380	-225	-750	-35	1.03	0.68	0.79	0.90	1.06	0.89	0.89
235	-781	-746	-866	-511	-1481	-251	-401	-336	-386	-261	-776	-91	1.06	0.82	0.80	1.04	1.10	0.97	0.97
239	-830	-765	-915	-530	-1525	-270	-450	-355	-435	-280	-820	-110	1.18	0.87	0.91	1.12	1.16	1.05	1.05
251	-855	-740	-930	-515	-1530	-245	-475	-330	-450	-265	-825	-85	1.25	0.80	0.94	1.06	1.17	1.04	1.04
255	-865	-770	-935	-550	-1535	-265	-485	-360	-455	-300	-830	-105	1.28	0.88	0.95	1.20	1.18	1.10	1.10
262	-889	-759	-939	-529	-1554	-249	-509	-349	-459	-279	-849	-89	1.34	0.85	0.96	1.11	1.20	1.09	1.09
268	-860	-795	-960	-555	-1535	-285	-480	-385	-480	-305	-830	-125	1.26	0.94	1.00	1.22	1.18	1.12	1.12
283	-856	-851	-886	-651	-1471	-346	-476	-441	-406	-401	-766	-186	1.25	1.08	0.85	1.60	1.09	1.17	1.17
290	-924	-864	-969	-604	-1554	-320	-544	-454	-489	-354	-849	-160	1.43	1.11	1.02	1.41	1.20	1.23	1.23
303	-934	-824	-999	-584	-1614	-299	-554	-414	-519	-334	-909	-139	1.46	1.01	1.08	1.33	1.29	1.23	1.23
322	-910	-810	-990	-585	-1605	-295	-530	-400	-510	-335	-900	-135	1.39	0.98	1.06	1.34	1.28	1.21	1.21
335	-849	-759	-934	-509	-1574	-229	-469	-349	-454	-259	-869	-69	1.23	0.85	0.95	1.03	1.23	1.06	1.06
339	-926	-821	-1026	-596	-1661	-296	-546	-411	-546	-346	-956	-136	1.44	1.00	1.14	1.38	1.36	1.26	1.26
353	-920	-830	-1010	-580	-1660	-290	-540	-420	-530	-330	-955	-130	1.42	1.02	1.10	1.32	1.35	1.24	1.24

October creep using F5 shrinkage (Part 1 of Table)

Time (days)	DEMEC Reading (DR)						Measured creep strain ($\mu\text{m/m}$) $\epsilon_{\text{CST},i}$						Thermal/ Shrinkage strain ($\mu\text{m/m}$)
	1A	1B	2A	2B	3A	3B	1A	1B	2A	2B	3A	3B	
initial	0.010	0.006	0.016	0.022	0.006	0.004	0	0	0	0	0	0	-
0	-0.066	-0.076	-0.080	-0.028	-0.135	-0.028	-380	-410	-480	-250	-705	-160	0
6	-0.125	-0.120	-0.139	-0.066	-0.215	-0.043	-675	-630	-775	-440	-1105	-235	-5
10	-0.122	-0.124	-0.132	-0.070	-0.209	-0.051	-660	-650	-740	-460	-1075	-275	-9
13	-0.127	-0.128	-0.139	-0.082	-0.217	-0.060	-685	-670	-775	-520	-1115	-320	-11
17	-0.133	-0.134	-0.146	-0.084	-0.225	-0.064	-715	-700	-810	-530	-1155	-340	-15
20	-0.150	-0.139	-0.163	-0.087	-0.240	-0.065	-800	-725	-895	-545	-1230	-345	-17
24	-0.153	-0.146	-0.166	-0.094	-0.248	-0.069	-815	-760	-910	-580	-1270	-365	-20
27	-0.143	-0.140	-0.152	-0.087	-0.233	-0.060	-765	-730	-840	-545	-1195	-320	-23
31	-0.155	-0.147	-0.164	-0.097	-0.245	-0.067	-825	-765	-900	-595	-1255	-355	-26
41	-0.158	-0.153	-0.166	-0.098	-0.246	-0.073	-840	-795	-910	-600	-1260	-385	-32
45	-0.163	-0.155	-0.164	-0.102	-0.255	-0.073	-865	-805	-900	-620	-1305	-385	-35
48	-0.168	-0.161	-0.175	-0.106	-0.265	-0.078	-890	-835	-955	-640	-1355	-410	-37
55	-0.167	-0.159	-0.174	-0.105	-0.266	-0.077	-885	-825	-950	-635	-1360	-405	-41
59	-0.171	-0.161	-0.178	-0.106	-0.269	-0.077	-905	-835	-970	-640	-1375	-405	-44
73	-0.172	-0.163	-0.178	-0.113	-0.273	-0.078	-910	-845	-970	-675	-1395	-410	-52
80	-0.173	-0.159	-0.176	-0.108	-0.280	-0.078	-915	-825	-960	-650	-1430	-410	-55
85	-0.174	-0.160	-0.182	-0.109	-0.282	-0.079	-920	-830	-990	-655	-1440	-415	-58
87	-0.182	-0.170	-0.188	-0.114	-0.287	-0.086	-960	-880	-1020	-680	-1465	-450	-59
92	-0.183	-0.169	-0.187	-0.116	-0.286	-0.084	-965	-875	-1015	-690	-1460	-440	-61
104	-0.187	-0.171	-0.194	-0.117	-0.298	-0.085	-985	-885	-1050	-695	-1520	-445	-67
106	-0.185	-0.171	-0.194	-0.115	-0.290	-0.083	-975	-885	-1050	-685	-1480	-435	-68
122	-0.179	-0.165	-0.183	-0.110	-0.291	-0.076	-945	-855	-995	-660	-1485	-400	-74
135	-0.186	-0.172	-0.189	-0.114	-0.300	-0.082	-980	-890	-1025	-680	-1530	-430	-79
139	-0.191	-0.177	-0.196	-0.121	-0.306	-0.088	-1005	-915	-1060	-715	-1560	-460	-81
149	-0.186	-0.170	-0.191	-0.115	-0.302	-0.082	-980	-880	-1035	-685	-1540	-430	-84
157	-0.200	-0.181	-0.204	-0.126	-0.315	-0.095	-1050	-935	-1100	-740	-1605	-495	-87
164	-0.191	-0.175	-0.193	-0.118	-0.307	-0.085	-1005	-905	-1045	-700	-1565	-445	-89
168	-0.197	-0.184	-0.199	-0.126	-0.313	-0.096	-1035	-950	-1075	-740	-1595	-500	-91
178	-0.194	-0.182	-0.199	-0.124	-0.319	-0.090	-1020	-940	-1075	-730	-1625	-470	-94
183	-0.192	-0.182	-0.180	-0.129	-0.300	-0.101	-1010	-940	-980	-755	-1530	-525	-95
200	-0.215	-0.204	-0.229	-0.114	-0.354	-0.108	-1125	-1050	-1225	-680	-1800	-560	-100
206	-0.208	-0.195	-0.218	-0.134	-0.344	-0.101	-1090	-1005	-1170	-780	-1750	-525	-101
212	-0.204	-0.194	-0.212	-0.134	-0.339	-0.098	-1070	-1000	-1140	-780	-1725	-510	-103
220	-0.223	-0.210	-0.237	-0.153	-0.363	-0.116	-1165	-1080	-1265	-875	-1845	-600	-105
226	-0.220	-0.208	-0.232	-0.149	-0.361	-0.111	-1150	-1070	-1240	-855	-1835	-575	-106
235	-0.228	-0.225	-0.239	-0.162	-0.372	-0.128	-1190	-1155	-1275	-920	-1890	-660	-108
239	-0.230	-0.221	-0.241	-0.158	-0.373	-0.124	-1200	-1135	-1285	-900	-1895	-640	-109
251	-0.253	-0.234	-0.262	-0.173	-0.392	-0.137	-1315	-1200	-1390	-975	-1990	-705	-112
255	-0.250	-0.235	-0.258	-0.175	-0.388	-0.136	-1300	-1205	-1370	-985	-1970	-700	-113
262	-0.257	-0.235	-0.261	-0.173	-0.394	-0.135	-1335	-1205	-1385	-975	-2000	-695	-114
268	-0.233	-0.224	-0.247	-0.160	-0.372	-0.124	-1215	-1150	-1315	-910	-1890	-640	-115
283	-0.226	-0.229	-0.226	-0.173	-0.353	-0.130	-1180	-1175	-1210	-975	-1795	-670	-118
290	-0.250	-0.242	-0.253	-0.174	-0.380	-0.135	-1300	-1240	-1345	-980	-1930	-696	-119
303	-0.263	-0.245	-0.270	-0.181	-0.403	-0.142	-1365	-1255	-1430	-1015	-2045	-730	-122
322	-0.255	-0.239	-0.265	-0.178	-0.398	-0.138	-1325	-1225	-1405	-1000	-2020	-710	-125
335	-0.240	-0.226	-0.251	-0.160	-0.389	-0.122	-1250	-1160	-1335	-910	-1975	-630	-127
339	-0.255	-0.238	-0.269	-0.177	-0.406	-0.135	-1325	-1220	-1425	-995	-2060	-695	-128
353	-0.245	-0.231	-0.257	-0.165	-0.397	-0.125	-1275	-1185	-1365	-935	-2015	-645	-130

October creep using F5 shrinkage (Part 2 of Table)

Time (days)	Measured creep strain less shrinkage and thermal strain ($\mu\text{m/m}$) $\epsilon_{cre,i}$						True creep strain ($\mu\text{m/m}$) $\epsilon_{cr,i}$						Creep coefficient $\phi(t, t_0)$						
	1A	1B	2A	2B	3A	3B	1A	1B	2A	2B	3A	3B	1A	1B	2A	2B	3A	3B	Average
0	-380	-410	-480	-250	-705	-160	0	0	0	0	0	0	0	0	0	0	0	0	0
6	-670	-625	-769	-434	-1100	-230	-290	-215	-290	-185	-395	-70	0.76	0.52	0.60	0.74	0.56	0.43	0.60
10	-651	-641	-731	-451	-1066	-266	-271	-231	-251	-201	-361	-106	0.71	0.56	0.52	0.80	0.51	0.66	0.63
13	-673	-658	-763	-508	-1103	-308	-293	-248	-283	-258	-398	-149	0.77	0.61	0.59	1.03	0.57	0.93	0.75
17	-700	-685	-795	-515	-1140	-325	-320	-275	-315	-265	-435	-165	0.84	0.67	0.66	1.06	0.62	1.03	0.81
20	-783	-708	-878	-528	-1213	-328	-403	-298	-398	-278	-508	-168	1.06	0.73	0.83	1.11	0.72	1.05	0.92
24	-795	-740	-890	-560	-1250	-345	-415	-330	-410	-310	-545	-185	1.09	0.80	0.85	1.24	0.77	1.15	0.99
27	-742	-707	-817	-522	-1172	-297	-362	-297	-337	-272	-467	-137	0.95	0.73	0.70	1.09	0.66	0.86	0.83
31	-799	-739	-874	-569	-1229	-329	-419	-329	-394	-319	-524	-169	1.10	0.80	0.82	1.28	0.74	1.06	0.97
41	-807	-762	-877	-567	-1227	-353	-427	-352	-397	-317	-522	-193	1.13	0.86	0.83	1.27	0.74	1.20	1.00
45	-830	-770	-865	-585	-1270	-350	-450	-360	-385	-335	-565	-190	1.18	0.88	0.80	1.34	0.80	1.19	1.03
48	-853	-798	-918	-603	-1318	-373	-473	-388	-438	-353	-613	-213	1.24	0.95	0.91	1.41	0.87	1.33	1.12
55	-844	-784	-908	-593	-1319	-364	-464	-374	-429	-344	-614	-204	1.22	0.91	0.89	1.37	0.87	1.27	1.09
59	-861	-791	-926	-596	-1331	-361	-481	-381	-446	-346	-626	-201	1.27	0.93	0.93	1.38	0.89	1.26	1.11
73	-858	-793	-918	-623	-1343	-358	-478	-383	-438	-373	-638	-198	1.26	0.93	0.91	1.49	0.91	1.24	1.12
80	-860	-770	-905	-595	-1375	-355	-480	-360	-425	-345	-670	-195	1.26	0.88	0.88	1.38	0.95	1.22	1.09
85	-862	-772	-932	-597	-1382	-357	-482	-362	-452	-347	-677	-197	1.27	0.88	0.94	1.39	0.96	1.23	1.11
87	-901	-821	-961	-621	-1406	-391	-521	-411	-481	-371	-701	-231	1.37	1.00	1.00	1.48	0.99	1.44	1.22
92	-904	-814	-954	-629	-1399	-379	-524	-404	-474	-379	-694	-219	1.38	0.98	0.99	1.51	0.98	1.37	1.20
104	-918	-818	-983	-628	-1453	-378	-538	-408	-503	-378	-748	-218	1.42	1.00	1.05	1.51	1.06	1.36	1.23
106	-907	-817	-982	-617	-1412	-367	-527	-407	-502	-367	-707	-207	1.39	0.99	1.05	1.47	1.00	1.30	1.20
122	-871	-781	-921	-586	-1411	-326	-491	-371	-441	-336	-706	-166	1.29	0.90	0.92	1.34	1.00	1.04	1.08
135	-901	-811	-946	-601	-1451	-351	-521	-401	-466	-351	-746	-191	1.37	0.98	0.97	1.40	1.06	1.19	1.16
139	-924	-834	-979	-634	-1479	-379	-544	-424	-499	-384	-774	-219	1.43	1.03	1.04	1.54	1.10	1.37	1.25
149	-896	-796	-951	-601	-1456	-346	-516	-386	-471	-351	-751	-186	1.36	0.94	0.98	1.40	1.06	1.16	1.15
157	-963	-848	-1013	-653	-1518	-408	-583	-438	-533	-403	-813	-248	1.53	1.07	1.11	1.61	1.15	1.55	1.34
164	-916	-816	-956	-611	-1476	-356	-536	-406	-476	-361	-771	-196	1.41	0.99	0.99	1.44	1.09	1.22	1.19
168	-944	-859	-984	-649	-1504	-409	-564	-449	-504	-399	-799	-249	1.49	1.10	1.05	1.60	1.13	1.56	1.32
178	-926	-846	-981	-636	-1531	-376	-546	-436	-501	-386	-826	-216	1.44	1.06	1.04	1.55	1.17	1.35	1.27
183	-915	-845	-885	-660	-1435	-430	-535	-435	-405	-410	-730	-270	1.41	1.06	0.84	1.64	1.04	1.69	1.28
200	-1025	-950	-1125	-580	-1700	-460	-645	-540	-645	-330	-995	-300	1.70	1.32	1.34	1.32	1.41	1.88	1.50
206	-989	-904	-1069	-679	-1649	-424	-609	-494	-589	-429	-944	-264	1.60	1.20	1.23	1.71	1.34	1.65	1.46
212	-967	-897	-1037	-677	-1622	-407	-587	-487	-557	-427	-917	-247	1.55	1.19	1.16	1.71	1.30	1.54	1.41
220	-1060	-975	-1160	-770	-1740	-495	-680	-565	-680	-520	-1035	-335	1.79	1.38	1.42	2.08	1.47	2.10	1.71
226	-1044	-964	-1134	-749	-1729	-469	-664	-554	-654	-499	-1024	-309	1.75	1.35	1.36	2.00	1.45	1.93	1.64
235	-1082	-1047	-1167	-812	-1782	-552	-702	-637	-687	-562	-1077	-392	1.85	1.55	1.43	2.25	1.53	2.45	1.84
239	-1091	-1026	-1176	-791	-1786	-531	-711	-616	-696	-541	-1081	-371	1.87	1.50	1.45	2.16	1.53	2.32	1.81
251	-1203	-1088	-1278	-863	-1878	-593	-823	-678	-798	-613	-1173	-433	2.17	1.65	1.66	2.45	1.66	2.71	2.05
255	-1187	-1092	-1257	-872	-1857	-587	-807	-682	-777	-622	-1152	-427	2.12	1.66	1.62	2.49	1.63	2.67	2.03
262	-1221	-1091	-1271	-861	-1886	-581	-841	-681	-791	-611	-1181	-421	2.21	1.66	1.65	2.44	1.68	2.63	2.05
268	-1100	-1035	-1200	-795	-1775	-525	-720	-625	-720	-545	-1070	-365	1.89	1.52	1.50	2.18	1.52	2.28	1.82
283	-1062	-1057	-1092	-857	-1677	-552	-682	-647	-612	-607	-972	-392	1.79	1.58	1.27	2.43	1.38	2.45	1.82
290	-1180	-1120	-1225	-860	-1810	-577	-800	-711	-745	-610	-1105	-417	2.11	1.73	1.55	2.44	1.57	2.61	2.00
303	-1243	-1133	-1308	-893	-1923	-608	-863	-723	-828	-643	-1218	-448	2.27	1.76	1.73	2.57	1.73	2.80	2.14
322	-1200	-1100	-1280	-875	-1895	-585	-820	-690	-800	-625	-1190	-425	2.16	1.68	1.67	2.50	1.69	2.66	2.06
335	-1123	-1033	-1208	-783	-1848	-503	-743	-623	-728	-533	-1143	-343	1.96	1.52	1.52	2.13	1.62	2.14	1.81
339	-1197	-1092	-1297	-867	-1932	-567	-817	-682	-817	-617	-1227	-407	2.15	1.66	1.70	2.47	1.74	2.55	2.05
353	-1145	-1055	-1235	-805	-1885	-515	-765	-645	-755	-555	-1180	-355	2.01	1.57	1.57	2.22	1.67	2.22	1.88

November creep using F4 shrinkage (Part 1 of Table)

Time (days)	DEMEC Reading (DR)						Measured creep strain ($\mu\text{m/m}$) $\epsilon_{\text{CST},i}$						Thermal/ Shrinkage strain ($\mu\text{m/m}$)
	1A	1B	2A	2B	3A	3B	1A	1B	2A	2B	3A	3B	
initial	0.014	0.015	0.012	-0.015	0.013	0.023	0	0	0	0	0	0	-
0	-0.091	-0.043	-0.089	-0.077	-0.092	-0.039	-526	-290	-505	-310	-525	-310	0
6	-0.132	-0.083	-0.138	-0.118	-0.143	-0.068	-731	-490	-750	-515	-780	-455	-100
10	-0.138	-0.085	-0.144	-0.117	-0.147	-0.088	-761	-500	-780	-510	-800	-555	-142
13	-0.139	-0.091	-0.148	-0.124	-0.155	-0.093	-766	-530	-800	-545	-840	-580	-190
17	-0.145	-0.099	-0.153	-0.131	-0.163	-0.100	-796	-570	-825	-580	-880	-615	-214
20	-0.151	-0.102	-0.163	-0.134	-0.173	-0.106	-826	-585	-875	-595	-930	-645	-182
24	-0.156	-0.104	-0.167	-0.137	-0.175	-0.110	-851	-595	-895	-610	-940	-665	-252
27	-0.150	-0.100	-0.159	-0.136	-0.166	-0.102	-821	-575	-855	-605	-895	-625	-202
31	-0.157	-0.104	-0.168	-0.139	-0.177	-0.110	-856	-595	-900	-620	-950	-665	-237
41	-0.162	-0.109	-0.173	-0.144	-0.181	-0.122	-881	-620	-925	-645	-970	-725	-296
45	-0.166	-0.111	-0.178	-0.146	-0.180	-0.120	-901	-630	-950	-655	-965	-715	-311
48	-0.170	-0.116	-0.182	-0.152	-0.183	-0.124	-921	-655	-970	-685	-980	-735	-329
55	-0.169	-0.116	-0.180	-0.150	-0.181	-0.123	-916	-655	-960	-675	-970	-730	-309
59	-0.173	-0.120	-0.185	-0.153	-0.184	-0.124	-936	-675	-985	-690	-985	-735	-349
73	-0.177	-0.119	-0.185	-0.158	-0.183	-0.128	-956	-670	-985	-715	-980	-755	-339
80	-0.175	-0.119	-0.186	-0.156	-0.189	-0.127	-946	-670	-990	-705	-1010	-750	-351
85	-0.176	-0.120	-0.185	-0.157	-0.190	-0.131	-951	-675	-985	-710	-1015	-770	-364
87	-0.185	-0.128	-0.194	-0.168	-0.196	-0.136	-996	-715	-1030	-765	-1045	-795	-397
92	-0.186	-0.127	-0.194	-0.167	-0.195	-0.136	-1001	-710	-1030	-760	-1040	-795	-391
104	-0.189	-0.130	-0.198	-0.167	-0.200	-0.140	-1016	-725	-1050	-760	-1065	-815	-407
106	-0.189	-0.128	-0.196	-0.168	-0.201	-0.135	-1016	-715	-1040	-765	-1070	-790	-396
122	-0.183	-0.122	-0.192	-0.160	-0.194	-0.131	-986	-685	-1020	-725	-1035	-770	-354
135	-0.185	-0.126	-0.197	-0.168	-0.201	-0.137	-996	-705	-1045	-765	-1070	-800	-366
139	-0.195	-0.132	-0.204	-0.172	-0.210	-0.142	-1046	-735	-1080	-785	-1115	-825	-401
149	-0.190	-0.128	-0.199	-0.167	-0.205	-0.138	-1021	-715	-1055	-760	-1090	-805	-395
157	-0.203	-0.139	-0.212	-0.183	-0.215	-0.151	-1086	-770	-1120	-840	-1140	-870	-426
164	-0.194	-0.130	-0.205	-0.173	-0.211	-0.143	-1041	-725	-1085	-790	-1120	-830	-372
168	-0.201	-0.139	-0.211	-0.180	-0.217	-0.152	-1076	-770	-1115	-825	-1150	-875	-407
178	-0.200	-0.138	-0.212	-0.177	-0.221	-0.150	-1071	-765	-1120	-810	-1170	-865	-387
183	-0.198	-0.140	-0.196	-0.181	-0.211	-0.152	-1061	-775	-1040	-830	-1120	-875	-386
200	-0.221	-0.156	-0.240	-0.195	-0.251	-0.173	-1176	-855	-1260	-900	-1320	-980	-424
206	-0.214	-0.149	-0.233	-0.190	-0.241	-0.164	-1141	-820	-1225	-875	-1270	-935	-374
212	-0.210	-0.148	-0.230	-0.190	-0.235	-0.163	-1121	-815	-1210	-875	-1240	-930	-384
220	-0.229	-0.163	-0.255	-0.206	-0.257	-0.182	-1216	-890	-1335	-955	-1350	-1025	-442
226	-0.225	-0.158	-0.252	-0.198	-0.250	-0.180	-1196	-865	-1320	-915	-1315	-1015	-471
235	-0.237	-0.173	-0.256	-0.217	-0.263	-0.194	-1256	-940	-1340	-1010	-1380	-1085	-509
239	-0.239	-0.171	-0.259	-0.212	-0.262	-0.191	-1266	-930	-1355	-985	-1375	-1070	-474
251	-0.260	-0.186	-0.279	-0.227	-0.283	-0.205	-1371	-1005	-1455	-1060	-1480	-1140	-550
255	-0.257	-0.184	-0.274	-0.225	-0.279	-0.205	-1356	-995	-1430	-1050	-1460	-1140	-526
262	-0.268	-0.186	-0.277	-0.228	-0.279	-0.206	-1411	-1005	-1445	-1065	-1460	-1145	-547
268	-0.244	-0.172	-0.261	-0.215	-0.270	-0.202	-1291	-935	-1365	-1000	-1415	-1125	-451
283	-0.238	-0.173	-0.244	-0.220	-0.244	-0.200	-1261	-940	-1280	-1025	-1285	-1115	-385
290	-0.258	-0.188	-0.267	-0.231	-0.265	-0.206	-1361	-1015	-1395	-1080	-1390	-1145	-475
303	-0.271	-0.195	-0.284	-0.235	-0.282	-0.216	-1426	-1050	-1480	-1100	-1475	-1195	-530
322	-0.265	-0.188	-0.275	-0.230	-0.277	-0.204	-1396	-1015	-1435	-1075	-1450	-1135	-500
335	-0.249	-0.178	-0.268	-0.212	-0.273	-0.196	-1316	-965	-1400	-985	-1430	-1095	-479
339	-0.263	-0.189	-0.286	-0.226	-0.289	-0.206	-1386	-1020	-1490	-1055	-1510	-1145	-456
353	-0.254	-0.180	-0.274	-0.217	-0.280	-0.198	-1341	-975	-1430	-1010	-1465	-1105	-437

November creep using F4 shrinkage (Part 2 of Table)

Time (days)	Measured creep strain less shrinkage and thermal strain ($\mu\text{m/m}$) $\epsilon_{cre,i}$						True creep strain ($\mu\text{m/m}$) $\epsilon_{cr,i}$						Creep coefficient $\phi(t,t_0)$						
	1A	1B	2A	2B	3A	3B	1A	1B	2A	2B	3A	3B	1A	1B	2A	2B	3A	3B	Average
0	-526	-290	-505	-310	-525	-310	0	0	0	0	0	0	0	0	0	0	0	0	0
6	-631	-390	-650	-415	-680	-355	-105	-100	-145	-105	-155	-45	0.20	0.34	0.29	0.34	0.30	0.15	0.27
10	-619	-357	-637	-368	-657	-412	-92	-67	-132	-58	-132	-102	0.18	0.23	0.26	0.19	0.25	0.33	0.24
13	-576	-340	-610	-355	-650	-390	-50	-50	-105	-45	-125	-80	0.09	0.17	0.21	0.15	0.24	0.26	0.19
17	-583	-356	-611	-366	-666	-401	-56	-66	-106	-56	-141	-91	0.11	0.23	0.21	0.18	0.27	0.29	0.22
20	-644	-402	-692	-413	-747	-462	-117	-112	-187	-103	-222	-152	0.22	0.39	0.37	0.33	0.42	0.49	0.37
24	-599	-342	-642	-358	-687	-412	-72	-52	-137	-48	-162	-102	0.14	0.18	0.27	0.15	0.31	0.33	0.23
27	-619	-372	-652	-403	-692	-422	-92	-82	-147	-93	-167	-112	0.18	0.28	0.29	0.30	0.32	0.36	0.29
31	-619	-357	-662	-383	-712	-427	-92	-67	-157	-73	-187	-117	0.18	0.23	0.31	0.23	0.36	0.38	0.28
41	-585	-324	-629	-349	-674	-429	-59	-34	-124	-39	-149	-119	0.11	0.12	0.25	0.13	0.28	0.38	0.21
45	-590	-319	-639	-344	-654	-404	-64	-29	-134	-34	-129	-94	0.12	0.10	0.26	0.11	0.25	0.30	0.19
48	-593	-326	-641	-356	-651	-406	-66	-36	-136	-46	-126	-96	0.13	0.12	0.27	0.15	0.24	0.31	0.20
55	-608	-346	-651	-366	-661	-421	-81	-56	-146	-56	-136	-111	0.15	0.19	0.29	0.18	0.26	0.36	0.24
59	-588	-326	-636	-341	-636	-386	-61	-36	-131	-31	-111	-76	0.12	0.12	0.26	0.10	0.21	0.25	0.18
73	-618	-331	-646	-376	-641	-416	-91	-41	-141	-66	-116	-106	0.17	0.14	0.28	0.21	0.22	0.34	0.23
80	-595	-319	-639	-354	-659	-399	-69	-29	-134	-44	-134	-89	0.13	0.10	0.26	0.14	0.25	0.29	0.20
85	-588	-311	-621	-346	-651	-406	-61	-21	-116	-36	-126	-96	0.12	0.07	0.23	0.12	0.24	0.31	0.18
87	-599	-317	-632	-368	-647	-397	-72	-27	-127	-58	-122	-87	0.14	0.09	0.25	0.19	0.23	0.28	0.20
92	-610	-319	-639	-369	-649	-404	-84	-29	-134	-59	-124	-94	0.16	0.10	0.26	0.19	0.24	0.30	0.21
104	-609	-317	-642	-353	-657	-407	-82	-27	-137	-43	-132	-97	0.16	0.09	0.27	0.14	0.25	0.31	0.20
106	-620	-319	-644	-369	-674	-394	-94	-29	-139	-59	-149	-84	0.18	0.10	0.27	0.19	0.28	0.27	0.22
122	-633	-331	-666	-371	-681	-416	-106	-41	-161	-61	-156	-106	0.20	0.14	0.32	0.20	0.30	0.34	0.25
135	-630	-339	-679	-399	-704	-434	-104	-49	-174	-89	-179	-124	0.20	0.17	0.34	0.29	0.34	0.40	0.29
139	-645	-334	-679	-384	-714	-424	-119	-44	-174	-74	-189	-114	0.23	0.15	0.34	0.24	0.36	0.37	0.28
149	-626	-320	-660	-365	-695	-410	-100	-30	-155	-55	-170	-100	0.19	0.10	0.31	0.18	0.32	0.32	0.24
157	-660	-344	-694	-414	-714	-444	-134	-54	-189	-104	-189	-134	0.25	0.19	0.37	0.33	0.36	0.43	0.32
164	-669	-352	-712	-418	-747	-457	-142	-62	-207	-108	-222	-147	0.27	0.22	0.41	0.35	0.42	0.48	0.36
168	-669	-362	-707	-418	-742	-467	-142	-72	-202	-108	-217	-157	0.27	0.25	0.40	0.35	0.41	0.51	0.37
178	-684	-377	-732	-423	-782	-477	-157	-87	-227	-113	-257	-167	0.30	0.30	0.45	0.36	0.49	0.54	0.41
183	-675	-389	-654	-444	-734	-489	-149	-99	-149	-134	-209	-179	0.28	0.34	0.29	0.43	0.40	0.58	0.39
200	-753	-431	-836	-476	-896	-556	-226	-141	-331	-166	-371	-246	0.43	0.49	0.66	0.54	0.71	0.79	0.60
206	-768	-446	-851	-501	-896	-561	-241	-156	-346	-191	-371	-251	0.46	0.54	0.69	0.62	0.71	0.81	0.64
212	-738	-431	-826	-491	-856	-546	-211	-141	-321	-181	-331	-236	0.40	0.49	0.64	0.58	0.63	0.76	0.58
220	-774	-447	-892	-513	-907	-582	-247	-157	-387	-203	-382	-272	0.47	0.54	0.77	0.65	0.73	0.88	0.67
226	-725	-394	-849	-444	-844	-544	-199	-104	-344	-134	-319	-234	0.38	0.36	0.68	0.43	0.61	0.75	0.53
235	-748	-431	-831	-501	-871	-576	-221	-141	-326	-191	-346	-266	0.42	0.49	0.65	0.62	0.66	0.86	0.61
239	-793	-456	-881	-511	-901	-596	-266	-166	-376	-201	-376	-286	0.51	0.57	0.75	0.65	0.72	0.92	0.69
251	-821	-455	-905	-510	-930	-590	-295	-165	-400	-200	-405	-280	0.56	0.57	0.79	0.65	0.77	0.90	0.71
255	-830	-469	-904	-524	-934	-614	-304	-179	-399	-214	-409	-304	0.58	0.62	0.79	0.69	0.78	0.98	0.74
262	-864	-457	-897	-518	-912	-597	-337	-167	-392	-208	-387	-287	0.64	0.58	0.78	0.67	0.74	0.93	0.72
268	-840	-484	-914	-549	-964	-674	-314	-194	-409	-239	-439	-364	0.60	0.67	0.81	0.77	0.84	1.17	0.81
283	-876	-555	-895	-640	-900	-730	-350	-265	-390	-330	-375	-420	0.66	0.91	0.77	1.06	0.71	1.35	0.91
290	-886	-540	-920	-605	-915	-670	-360	-250	-415	-295	-390	-360	0.68	0.86	0.82	0.95	0.74	1.16	0.87
303	-896	-520	-950	-570	-945	-665	-370	-230	-445	-260	-420	-355	0.70	0.79	0.88	0.84	0.80	1.15	0.86
322	-896	-515	-935	-575	-950	-635	-370	-225	-430	-265	-425	-325	0.70	0.78	0.85	0.86	0.81	1.05	0.84
335	-838	-486	-921	-506	-951	-616	-311	-196	-416	-196	-426	-306	0.59	0.68	0.82	0.63	0.81	0.99	0.75
339	-930	-564	-1034	-599	-1054	-689	-404	-274	-529	-289	-529	-379	0.77	0.94	1.05	0.93	1.01	1.22	0.99
353	-904	-537	-992	-573	-1027	-667	-377	-247	-487	-263	-502	-357	0.72	0.85	0.97	0.85	0.96	1.15	0.92

November creep using F5 shrinkage (Part 1 of Table)

Time (days)	DEMEC Reading (DR)						Measured creep strain ($\mu\text{m/m}$) $\epsilon_{\text{CST},i}$						Thermal/ Shrinkage strain ($\mu\text{m/m}$)
	1A	1B	2A	2B	3A	3B	1A	1B	2A	2B	3A	3B	
initial	0.014	0.015	0.012	-0.015	0.013	0.023	0	0	0	0	0	0	-
0	-0.091	-0.043	-0.089	-0.077	-0.092	-0.039	-526	-290	-505	-310	-525	-310	0
6	-0.132	-0.083	-0.138	-0.118	-0.143	-0.068	-731	-490	-750	-515	-780	-455	-7
10	-0.138	-0.085	-0.144	-0.117	-0.147	-0.088	-761	-500	-780	-510	-800	-555	-12
13	-0.139	-0.091	-0.148	-0.124	-0.155	-0.093	-766	-530	-800	-545	-840	-580	-15
17	-0.145	-0.099	-0.153	-0.131	-0.163	-0.100	-796	-570	-825	-580	-880	-615	-19
20	-0.151	-0.102	-0.163	-0.134	-0.173	-0.106	-826	-585	-875	-595	-930	-645	-22
24	-0.156	-0.104	-0.167	-0.137	-0.175	-0.110	-851	-595	-895	-610	-940	-665	-26
27	-0.150	-0.100	-0.159	-0.136	-0.166	-0.102	-821	-575	-855	-605	-895	-625	-29
31	-0.157	-0.104	-0.168	-0.139	-0.177	-0.110	-856	-595	-900	-620	-950	-665	-33
41	-0.162	-0.109	-0.173	-0.144	-0.181	-0.122	-881	-620	-925	-645	-970	-725	-41
45	-0.166	-0.111	-0.178	-0.146	-0.180	-0.120	-901	-630	-950	-655	-965	-715	-45
48	-0.170	-0.116	-0.182	-0.152	-0.183	-0.124	-921	-655	-970	-685	-980	-735	-47
55	-0.169	-0.116	-0.180	-0.150	-0.181	-0.123	-916	-655	-960	-675	-970	-730	-52
59	-0.173	-0.120	-0.185	-0.153	-0.184	-0.124	-936	-675	-985	-690	-985	-735	-55
73	-0.177	-0.119	-0.185	-0.158	-0.183	-0.128	-956	-670	-985	-715	-980	-755	-65
80	-0.175	-0.119	-0.186	-0.156	-0.189	-0.127	-946	-670	-990	-705	-1010	-750	-69
85	-0.176	-0.120	-0.185	-0.157	-0.190	-0.131	-951	-675	-985	-710	-1015	-770	-72
87	-0.185	-0.128	-0.194	-0.168	-0.196	-0.136	-996	-715	-1030	-765	-1045	-795	-74
92	-0.186	-0.127	-0.194	-0.167	-0.195	-0.136	-1001	-710	-1030	-760	-1040	-795	-77
104	-0.189	-0.130	-0.198	-0.167	-0.200	-0.140	-1016	-725	-1050	-760	-1065	-815	-83
106	-0.189	-0.128	-0.196	-0.168	-0.201	-0.135	-1016	-715	-1040	-765	-1070	-790	-84
122	-0.183	-0.122	-0.192	-0.160	-0.194	-0.131	-986	-685	-1020	-725	-1035	-770	-92
135	-0.185	-0.126	-0.197	-0.168	-0.201	-0.137	-996	-705	-1045	-765	-1070	-800	-98
139	-0.195	-0.132	-0.204	-0.172	-0.210	-0.142	-1046	-735	-1080	-785	-1115	-825	-100
149	-0.190	-0.128	-0.199	-0.167	-0.205	-0.138	-1021	-715	-1055	-760	-1090	-805	-104
157	-0.203	-0.139	-0.212	-0.183	-0.215	-0.151	-1086	-770	-1120	-840	-1140	-870	-107
164	-0.194	-0.130	-0.205	-0.173	-0.211	-0.143	-1041	-725	-1085	-790	-1120	-830	-110
168	-0.201	-0.139	-0.211	-0.180	-0.217	-0.152	-1076	-770	-1115	-825	-1150	-875	-111
178	-0.200	-0.138	-0.212	-0.177	-0.221	-0.150	-1071	-765	-1120	-810	-1170	-865	-114
183	-0.198	-0.140	-0.196	-0.181	-0.211	-0.152	-1061	-775	-1040	-830	-1120	-875	-116
200	-0.221	-0.156	-0.240	-0.195	-0.251	-0.173	-1176	-855	-1260	-900	-1320	-980	-122
206	-0.214	-0.149	-0.233	-0.190	-0.241	-0.164	-1141	-820	-1225	-875	-1270	-935	-123
212	-0.210	-0.148	-0.230	-0.190	-0.235	-0.163	-1121	-815	-1210	-875	-1240	-930	-125
220	-0.229	-0.163	-0.255	-0.206	-0.257	-0.182	-1216	-890	-1335	-955	-1350	-1025	-127
226	-0.225	-0.158	-0.252	-0.198	-0.250	-0.180	-1196	-865	-1320	-915	-1315	-1015	-129
235	-0.237	-0.173	-0.256	-0.217	-0.263	-0.194	-1256	-940	-1340	-1010	-1380	-1085	-131
239	-0.239	-0.171	-0.259	-0.212	-0.262	-0.191	-1266	-930	-1355	-985	-1375	-1070	-132
251	-0.260	-0.186	-0.279	-0.227	-0.283	-0.205	-1371	-1005	-1455	-1060	-1480	-1140	-135
255	-0.257	-0.184	-0.274	-0.225	-0.279	-0.205	-1356	-995	-1430	-1050	-1460	-1140	-136
262	-0.268	-0.186	-0.277	-0.228	-0.279	-0.206	-1411	-1005	-1445	-1065	-1460	-1145	-138
268	-0.244	-0.172	-0.261	-0.215	-0.270	-0.202	-1291	-935	-1365	-1000	-1415	-1125	-139
283	-0.238	-0.173	-0.244	-0.220	-0.244	-0.200	-1261	-940	-1280	-1025	-1285	-1115	-142
290	-0.258	-0.188	-0.267	-0.231	-0.265	-0.206	-1361	-1015	-1395	-1080	-1390	-1145	-144
303	-0.271	-0.195	-0.284	-0.235	-0.282	-0.216	-1426	-1050	-1480	-1100	-1475	-1195	-146
322	-0.265	-0.188	-0.275	-0.230	-0.277	-0.204	-1396	-1015	-1435	-1075	-1450	-1135	-150
335	-0.249	-0.178	-0.268	-0.212	-0.273	-0.196	-1316	-965	-1400	-985	-1430	-1095	-152
339	-0.263	-0.189	-0.286	-0.226	-0.289	-0.206	-1386	-1020	-1490	-1055	-1510	-1145	-153
353	-0.254	-0.180	-0.274	-0.217	-0.280	-0.198	-1341	-975	-1430	-1010	-1465	-1105	-155

November creep using F5 shrinkage (Part 2 of Table)

Time (days)	Measured creep strain less shrinkage and thermal strain ($\mu\text{m/m}$) $\epsilon_{cre,i}$						True creep strain ($\mu\text{m/m}$) $\epsilon_{cr,i}$						Creep coefficient $\phi(t,t_0)$						
	1A	1B	2A	2B	3A	3B	1A	1B	2A	2B	3A	3B	1A	1B	2A	2B	3A	3B	Average
0	-526	-290	-505	-310	-525	-310	0	0	0	0	0	0	0	0	0	0	0	0	0
6	-724	-483	-743	-508	-773	-448	-198	-193	-238	-198	-248	-138	0.38	0.67	0.47	0.64	0.47	0.44	0.51
10	-750	-488	-768	-498	-788	-543	-223	-198	-263	-188	-263	-233	0.42	0.68	0.52	0.61	0.50	0.75	0.58
13	-752	-515	-785	-530	-825	-565	-225	-225	-280	-220	-300	-255	0.43	0.78	0.55	0.71	0.57	0.82	0.64
17	-777	-551	-806	-561	-861	-596	-251	-261	-301	-251	-336	-286	0.48	0.90	0.60	0.81	0.64	0.92	0.72
20	-804	-563	-853	-573	-908	-623	-278	-273	-348	-263	-383	-313	0.53	0.94	0.69	0.85	0.73	1.01	0.79
24	-825	-569	-869	-584	-914	-639	-299	-279	-364	-274	-389	-329	0.57	0.96	0.72	0.88	0.74	1.06	0.82
27	-793	-546	-826	-576	-866	-596	-266	-256	-321	-266	-341	-286	0.51	0.88	0.64	0.86	0.65	0.92	0.74
31	-824	-562	-867	-587	-917	-632	-297	-272	-362	-277	-392	-322	0.56	0.94	0.72	0.89	0.75	1.04	0.82
41	-840	-579	-884	-604	-929	-684	-314	-289	-379	-294	-404	-374	0.60	1.00	0.75	0.95	0.77	1.21	0.88
45	-857	-585	-905	-610	-920	-670	-330	-295	-400	-300	-395	-360	0.63	1.02	0.79	0.97	0.75	1.16	0.89
48	-874	-608	-923	-638	-933	-688	-348	-318	-418	-328	-408	-378	0.66	1.10	0.83	1.06	0.78	1.22	0.94
55	-864	-603	-908	-623	-918	-678	-338	-313	-403	-313	-393	-368	0.64	1.08	0.80	1.01	0.75	1.19	0.91
59	-881	-620	-930	-635	-930	-680	-355	-330	-425	-325	-405	-370	0.67	1.14	0.84	1.05	0.77	1.19	0.94
73	-891	-605	-920	-650	-915	-690	-365	-315	-415	-340	-390	-380	0.69	1.09	0.82	1.10	0.74	1.23	0.94
80	-877	-601	-921	-636	-941	-681	-351	-311	-416	-326	-416	-371	0.67	1.07	0.82	1.05	0.79	1.20	0.93
85	-879	-602	-912	-638	-942	-697	-353	-313	-408	-328	-418	-387	0.67	1.08	0.81	1.06	0.80	1.25	0.94
87	-923	-641	-956	-691	-971	-721	-396	-351	-451	-381	-446	-411	0.75	1.21	0.89	1.23	0.85	1.33	1.04
92	-925	-633	-953	-684	-963	-718	-398	-343	-448	-373	-438	-408	0.76	1.18	0.89	1.20	0.84	1.32	1.03
104	-933	-642	-967	-677	-982	-732	-407	-352	-462	-367	-457	-422	0.77	1.21	0.91	1.18	0.87	1.36	1.05
106	-932	-631	-956	-681	-986	-706	-406	-341	-451	-371	-461	-396	0.77	1.18	0.89	1.20	0.88	1.28	1.03
122	-894	-593	-928	-633	-943	-678	-368	-303	-423	-323	-418	-368	0.70	1.04	0.84	1.04	0.80	1.19	0.93
135	-898	-607	-947	-667	-972	-702	-372	-317	-442	-357	-447	-392	0.71	1.09	0.88	1.15	0.85	1.26	0.99
139	-947	-635	-980	-685	-1015	-725	-420	-345	-475	-375	-490	-415	0.80	1.19	0.94	1.21	0.93	1.34	1.07
149	-918	-611	-951	-656	-986	-701	-391	-321	-446	-346	-461	-391	0.74	1.11	0.88	1.12	0.88	1.26	1.00
157	-980	-663	-1013	-733	-1033	-763	-453	-373	-508	-423	-508	-453	0.86	1.29	1.01	1.36	0.97	1.46	1.16
164	-932	-615	-975	-681	-1010	-720	-405	-325	-470	-371	-485	-410	0.77	1.12	0.93	1.20	0.92	1.32	1.04
168	-965	-659	-1004	-714	-1039	-764	-439	-369	-499	-404	-514	-454	0.83	1.27	0.99	1.30	0.98	1.46	1.14
178	-957	-650	-1005	-696	-1055	-750	-430	-360	-500	-386	-530	-440	0.82	1.24	0.99	1.24	1.01	1.42	1.12
183	-945	-659	-924	-714	-1004	-759	-419	-369	-419	-404	-479	-449	0.80	1.27	0.83	1.30	0.91	1.45	1.09
200	-1055	-733	-1138	-779	-1198	-858	-528	-443	-633	-468	-673	-548	1.00	1.53	1.25	1.51	1.28	1.77	1.39
206	-1018	-697	-1102	-752	-1147	-812	-492	-407	-597	-442	-622	-502	0.93	1.40	1.18	1.42	1.18	1.62	1.29
212	-996	-690	-1085	-750	-1115	-805	-470	-400	-580	-440	-590	-495	0.89	1.38	1.15	1.42	1.12	1.60	1.26
220	-1089	-763	-1208	-828	-1223	-898	-563	-473	-703	-518	-698	-588	1.07	1.63	1.39	1.67	1.33	1.90	1.50
226	-1067	-736	-1191	-786	-1186	-886	-541	-446	-686	-476	-661	-576	1.03	1.54	1.36	1.54	1.26	1.86	1.43
235	-1125	-809	-1209	-879	-1249	-954	-599	-519	-704	-569	-724	-644	1.14	1.79	1.39	1.83	1.38	2.08	1.60
239	-1134	-798	-1223	-853	-1243	-938	-608	-508	-718	-543	-718	-628	1.15	1.75	1.42	1.75	1.37	2.02	1.58
251	-1236	-870	-1320	-925	-1345	-1005	-710	-580	-815	-615	-820	-695	1.35	2.00	1.61	1.98	1.56	2.24	1.79
255	-1220	-859	-1294	-914	-1324	-1004	-694	-569	-789	-604	-799	-694	1.32	1.96	1.56	1.95	1.52	2.24	1.76
262	-1274	-867	-1307	-927	-1322	-1007	-747	-577	-802	-617	-797	-697	1.42	1.99	1.59	1.99	1.52	2.25	1.79
268	-1152	-796	-1226	-861	-1276	-986	-626	-506	-721	-551	-751	-676	1.19	1.74	1.43	1.78	1.43	2.18	1.62
283	-1119	-797	-1137	-883	-1142	-972	-592	-507	-632	-573	-617	-662	1.13	1.75	1.25	1.85	1.18	2.14	1.55
290	-1217	-871	-1251	-936	-1246	-1001	-691	-581	-746	-626	-721	-691	1.31	2.00	1.48	2.02	1.37	2.23	1.74
303	-1280	-903	-1333	-954	-1328	-1048	-753	-613	-828	-644	-803	-738	1.43	2.12	1.64	2.08	1.53	2.38	1.86
322	-1246	-865	-1285	-925	-1300	-985	-720	-575	-780	-615	-775	-675	1.37	1.98	1.54	1.98	1.48	2.18	1.76
335	-1164	-813	-1248	-833	-1278	-943	-638	-523	-743	-523	-753	-633	1.21	1.80	1.47	1.69	1.43	2.04	1.61
339	-1233	-867	-1337	-902	-1357	-992	-707	-577	-832	-592	-832	-682	1.34	1.99	1.65	1.91	1.58	2.20	1.78
353	-1186	-820	-1275	-855	-1310	-950	-660	-530	-770	-545	-785	-640	1.25	1.83	1.52	1.76	1.49	2.06	1.65

March creep using F4 shrinkage (Part 1 of Table)

Time (days)	DEMEC Reading (DR)						Measured creep strain ($\mu\text{m/m}$) $\epsilon_{\text{CST},i}$						Thermal/ Shrinkage strain ($\mu\text{m/m}$)
	1A	1B	2A	2B	3A	3B	1A	1B	2A	2B	3A	3B	
initial	0.009	-0.097	0.010	-0.202	0.020	-0.004	0	0	0	0	0	0	-
0	-0.088	-0.181	-0.116	-0.267	-0.103	-0.064	-485	-420	-630	-325	-615	-300	0
6	-0.154	-0.250	-0.197	-0.308	-0.184	-0.120	-815	-765	-1035	-531	-1020	-580	-76
10	-0.163	-0.264	-0.210	-0.311	-0.191	-0.127	-860	-835	-1100	-546	-1055	-615	-108
13	-0.172	-0.271	-0.219	-0.318	-0.202	-0.135	-905	-870	-1145	-581	-1110	-655	-143
17	-0.183	-0.278	-0.228	-0.325	-0.211	-0.140	-960	-905	-1190	-616	-1155	-680	-191
20	-0.191	-0.287	-0.236	-0.334	-0.223	-0.153	-1000	-950	-1230	-661	-1215	-745	-230
24	-0.199	-0.294	-0.247	-0.338	-0.232	-0.159	-1040	-985	-1285	-681	-1260	-775	-250
27	-0.195	-0.292	-0.242	-0.335	-0.226	-0.155	-1020	-975	-1260	-666	-1230	-755	-216
31	-0.206	-0.299	-0.247	-0.347	-0.226	-0.164	-1075	-1010	-1285	-726	-1230	-800	-187
41	-0.217	-0.308	-0.263	-0.354	-0.246	-0.173	-1130	-1056	-1365	-761	-1330	-845	-278
45	-0.225	-0.313	-0.271	-0.357	-0.251	-0.175	-1170	-1081	-1405	-776	-1355	-855	-308
48	-0.233	-0.317	-0.276	-0.361	-0.257	-0.184	-1210	-1101	-1430	-796	-1385	-900	-343
55	-0.238	-0.322	-0.285	-0.362	-0.265	-0.185	-1235	-1126	-1475	-801	-1425	-905	-345
59	-0.242	-0.329	-0.289	-0.365	-0.269	-0.182	-1255	-1161	-1495	-816	-1445	-890	-387
73	-0.250	-0.336	-0.292	-0.371	-0.277	-0.188	-1295	-1196	-1510	-846	-1485	-920	-393
80	-0.247	-0.341	-0.292	-0.372	-0.278	-0.190	-1280	-1221	-1510	-851	-1490	-930	-392
85	-0.251	-0.339	-0.294	-0.374	-0.281	-0.195	-1300	-1211	-1520	-861	-1505	-955	-403
87	-0.261	-0.347	-0.302	-0.381	-0.287	-0.200	-1350	-1251	-1560	-896	-1535	-980	-445
92	-0.261	-0.349	-0.304	-0.382	-0.291	-0.206	-1350	-1261	-1570	-901	-1555	-1010	-440
104	-0.267	-0.353	-0.304	-0.388	-0.295	-0.201	-1380	-1281	-1570	-931	-1575	-985	-466
106	-0.266	-0.349	-0.311	-0.386	-0.297	-0.201	-1375	-1261	-1605	-921	-1585	-985	-448
122	-0.262	-0.342	-0.306	-0.380	-0.294	-0.193	-1355	-1226	-1580	-891	-1570	-945	-416
135	-0.267	-0.346	-0.311	-0.385	-0.303	-0.198	-1380	-1246	-1605	-916	-1615	-970	-432
139	-0.274	-0.354	-0.319	-0.390	-0.309	-0.204	-1415	-1286	-1645	-941	-1645	-1000	-462
149	-0.272	-0.352	-0.318	-0.387	-0.305	-0.200	-1405	-1276	-1640	-926	-1625	-980	-442
157	-0.286	-0.361	-0.329	-0.396	-0.318	-0.211	-1475	-1321	-1695	-971	-1690	-1035	-475
164	-0.280	-0.355	-0.321	-0.390	-0.314	-0.205	-1445	-1291	-1655	-941	-1670	-1005	-438
168	-0.284	-0.362	-0.328	-0.395	-0.316	-0.214	-1465	-1326	-1690	-966	-1680	-1050	-467
178	-0.285	-0.359	-0.328	-0.395	-0.322	-0.212	-1470	-1311	-1690	-966	-1710	-1040	-460
183	-0.285	-0.363	-0.316	-0.391	-0.311	-0.210	-1470	-1331	-1630	-946	-1655	-1030	-448
200	-0.309	-0.382	-0.360	-0.411	-0.355	-0.232	-1590	-1426	-1850	-1046	-1875	-1140	-485
206	-0.302	-0.375	-0.353	-0.406	-0.350	-0.225	-1555	-1391	-1815	-1021	-1850	-1105	-445
212	-0.298	-0.372	-0.350	-0.402	-0.343	-0.222	-1535	-1376	-1800	-1001	-1815	-1090	-447
220	-0.317	-0.388	-0.367	-0.417	-0.360	-0.239	-1630	-1456	-1885	-1076	-1900	-1175	-490
226	-0.311	-0.381	-0.364	-0.414	-0.354	-0.237	-1600	-1421	-1870	-1061	-1870	-1165	-511
235	-0.322	-0.397	-0.376	-0.429	-0.369	-0.252	-1655	-1501	-1930	-1136	-1945	-1240	-546
239	-0.327	-0.399	-0.378	-0.424	-0.370	-0.249	-1680	-1511	-1940	-1111	-1950	-1225	-532
251	-0.348	-0.413	-0.396	-0.443	-0.387	-0.264	-1785	-1581	-2030	-1206	-2035	-1300	-588
255	-0.344	-0.412	-0.393	-0.437	-0.384	-0.259	-1765	-1576	-2015	-1176	-2020	-1275	-575
262	-0.347	-0.413	-0.397	-0.440	-0.386	-0.261	-1780	-1581	-2035	-1191	-2030	-1285	-588
268	-0.329	-0.400	-0.379	-0.428	-0.376	-0.251	-1690	-1516	-1945	-1131	-1980	-1235	-497
283	-0.318	-0.405	-0.358	-0.435	-0.345	-0.261	-1635	-1541	-1840	-1166	-1825	-1285	-410
290	-0.339	-0.415	-0.379	-0.443	-0.364	-0.263	-1740	-1591	-1945	-1206	-1920	-1295	-485
303	-0.355	-0.421	-0.397	-0.448	-0.385	-0.270	-1820	-1621	-2035	-1231	-2025	-1330	-512
322	-0.350	-0.409	-0.396	-0.437	-0.383	-0.260	-1795	-1561	-2030	-1176	-2015	-1280	-506
335	-0.338	-0.403	-0.392	-0.425	-0.384	-0.244	-1735	-1531	-2010	-1116	-2020	-1200	-495
339	-0.351	-0.415	-0.407	-0.439	-0.400	-0.259	-1800	-1591	-2085	-1186	-2100	-1275	-500
353	-0.345	-0.410	-0.397	-0.445	-0.389	-0.255	-1770	-1566	-2035	-1216	-2045	-1255	-463

March creep using F4 shrinkage (Part 2 of Table)

Time (days)	Measured creep strain less shrinkage and thermal strain ($\mu\text{m/m}$) $\epsilon_{cre,i}$						True creep strain ($\mu\text{m/m}$) $\epsilon_{cr,i}$						Creep coefficient $\phi(t,t_0)$						
	1A	1B	2A	2B	3A	3B	1A	1B	2A	2B	3A	3B	1A	1B	2A	3A	3B	Average	
0	-485	-420	-630	-325	-615	-300	0	0	0	0	0	0	0	0	0	0	0	0	0
6	-739	-689	-959	-455	-944	-504	-254	-269	-329	-129	-329	-204	0.52	0.64	0.52	0.54	0.68	0.58	
10	-752	-727	-992	-437	-947	-507	-267	-307	-362	-112	-332	-207	0.55	0.73	0.57	0.54	0.69	0.62	
13	-762	-727	-1002	-437	-967	-512	-277	-307	-372	-112	-352	-212	0.57	0.73	0.59	0.57	0.71	0.63	
17	-769	-715	-999	-425	-964	-489	-284	-294	-369	-99	-349	-189	0.59	0.70	0.59	0.57	0.63	0.61	
20	-770	-721	-1000	-431	-985	-515	-285	-301	-370	-106	-370	-215	0.59	0.72	0.59	0.60	0.72	0.64	
24	-790	-736	-1035	-431	-1010	-525	-305	-316	-405	-106	-395	-225	0.63	0.75	0.64	0.64	0.75	0.68	
27	-804	-760	-1044	-450	-1014	-539	-319	-339	-414	-124	-399	-239	0.66	0.81	0.66	0.65	0.80	0.71	
31	-888	-823	-1098	-539	-1043	-613	-403	-403	-468	-213	-428	-313	0.83	0.96	0.74	0.70	1.04	0.85	
41	-852	-777	-1087	-482	-1051	-567	-367	-357	-457	-157	-437	-267	0.76	0.85	0.72	0.71	0.89	0.79	
45	-862	-772	-1097	-467	-1046	-547	-377	-352	-467	-142	-432	-247	0.78	0.84	0.74	0.70	0.82	0.78	
48	-867	-757	-1087	-452	-1041	-557	-382	-337	-457	-127	-427	-257	0.79	0.80	0.72	0.69	0.86	0.77	
55	-890	-781	-1130	-456	-1080	-560	-405	-361	-500	-131	-465	-260	0.84	0.86	0.79	0.76	0.87	0.82	
59	-868	-773	-1108	-429	-1058	-503	-383	-353	-478	-103	-443	-203	0.79	0.84	0.76	0.72	0.68	0.76	
73	-902	-802	-1117	-452	-1091	-527	-417	-382	-487	-127	-477	-227	0.86	0.91	0.77	0.77	0.76	0.81	
80	-888	-828	-1118	-459	-1098	-538	-403	-408	-488	-133	-483	-238	0.83	0.97	0.77	0.79	0.79	0.83	
85	-897	-807	-1117	-457	-1101	-552	-412	-387	-487	-132	-487	-252	0.85	0.92	0.77	0.79	0.84	0.83	
87	-905	-806	-1115	-451	-1090	-535	-420	-386	-485	-126	-475	-235	0.87	0.92	0.77	0.77	0.78	0.82	
92	-910	-821	-1130	-461	-1115	-570	-425	-401	-500	-136	-500	-270	0.88	0.95	0.79	0.81	0.90	0.87	
104	-914	-815	-1104	-465	-1109	-519	-429	-395	-474	-140	-494	-219	0.88	0.94	0.75	0.80	0.73	0.82	
106	-927	-812	-1157	-473	-1136	-537	-442	-392	-527	-147	-521	-237	0.91	0.93	0.84	0.85	0.79	0.86	
122	-939	-810	-1164	-475	-1154	-529	-454	-389	-534	-150	-539	-229	0.94	0.93	0.85	0.88	0.76	0.87	
135	-948	-813	-1173	-484	-1183	-538	-463	-393	-543	-158	-568	-238	0.95	0.94	0.86	0.92	0.79	0.89	
139	-953	-823	-1183	-479	-1183	-538	-468	-403	-553	-153	-568	-238	0.96	0.96	0.88	0.92	0.79	0.90	
149	-963	-833	-1198	-484	-1183	-538	-478	-413	-568	-158	-568	-238	0.99	0.98	0.90	0.92	0.79	0.92	
157	-1000	-846	-1220	-496	-1215	-560	-515	-426	-590	-171	-600	-260	1.06	1.01	0.94	0.98	0.87	0.97	
164	-1007	-852	-1217	-503	-1231	-567	-522	-432	-587	-177	-616	-267	1.08	1.03	0.93	1.00	0.89	0.99	
168	-998	-858	-1223	-499	-1213	-583	-513	-438	-593	-173	-598	-283	1.06	1.04	0.94	0.97	0.94	0.99	
178	-1010	-851	-1230	-506	-1250	-580	-525	-431	-600	-181	-635	-280	1.08	1.03	0.95	1.03	0.93	1.01	
183	-1022	-882	-1182	-498	-1206	-582	-537	-462	-552	-172	-591	-282	1.11	1.10	0.88	0.96	0.94	1.00	
200	-1105	-941	-1365	-561	-1390	-655	-620	-521	-735	-236	-775	-355	1.28	1.24	1.17	1.26	1.18	1.23	
206	-1110	-946	-1370	-576	-1405	-660	-625	-526	-740	-251	-790	-360	1.29	1.25	1.18	1.29	1.20	1.24	
212	-1088	-929	-1353	-554	-1368	-643	-603	-508	-723	-229	-753	-343	1.24	1.21	1.15	1.22	1.14	1.19	
220	-1140	-966	-1395	-586	-1410	-685	-655	-546	-765	-261	-795	-385	1.35	1.30	1.21	1.29	1.28	1.29	
226	-1089	-910	-1359	-550	-1359	-654	-604	-490	-729	-225	-744	-354	1.25	1.17	1.16	1.21	1.18	1.19	
235	-1109	-955	-1384	-590	-1399	-694	-624	-535	-754	-265	-784	-394	1.29	1.27	1.20	1.27	1.31	1.27	
239	-1148	-979	-1408	-579	-1418	-693	-663	-558	-778	-254	-803	-393	1.37	1.33	1.23	1.31	1.31	1.31	
251	-1197	-992	-1441	-618	-1446	-712	-712	-572	-812	-292	-831	-412	1.47	1.36	1.29	1.35	1.37	1.37	
255	-1190	-1001	-1440	-602	-1445	-700	-705	-581	-810	-276	-830	-400	1.45	1.38	1.29	1.35	1.33	1.36	
262	-1192	-992	-1446	-603	-1441	-697	-707	-572	-817	-277	-826	-397	1.46	1.36	1.30	1.34	1.32	1.36	
268	-1193	-1019	-1448	-634	-1483	-738	-708	-598	-818	-309	-868	-438	1.46	1.42	1.30	1.41	1.46	1.41	
283	-1225	-1131	-1430	-757	-1415	-875	-740	-711	-800	-431	-800	-575	1.53	1.69	1.27	1.30	1.92	1.54	
290	-1255	-1106	-1460	-722	-1435	-810	-770	-686	-830	-396	-820	-510	1.59	1.63	1.32	1.33	1.70	1.51	
303	-1308	-1109	-1523	-719	-1513	-818	-823	-688	-893	-394	-898	-518	1.70	1.64	1.42	1.46	1.73	1.59	
322	-1289	-1055	-1524	-670	-1509	-774	-804	-635	-894	-345	-894	-474	1.66	1.51	1.42	1.45	1.58	1.52	
335	-1240	-1036	-1515	-621	-1525	-705	-755	-616	-885	-296	-910	-405	1.56	1.47	1.41	1.48	1.35	1.45	
339	-1300	-1091	-1585	-687	-1600	-775	-815	-671	-955	-361	-985	-475	1.68	1.60	1.52	1.60	1.58	1.60	
353	-1307	-1102	-1571	-753	-1581	-792	-822	-682	-942	-427	-966	-492	1.69	1.62	1.49	1.57	1.64	1.60	

March creep using F5 shrinkage (Part 1 of Table)

Time (days)	DEMEC Reading (DR)						Measured creep strain ($\mu\text{m/m}$) $\epsilon_{\text{CST},i}$						Thermal/ Shrinkage strain ($\mu\text{m/m}$)
	1A	1B	2A	2B	3A	3B	1A	1B	2A	2B	3A	3B	
initial	0.009	-0.097	0.010	-0.202	0.020	-0.004	0	0	0	0	0	0	-
0	-0.088	-0.181	-0.116	-0.267	-0.103	-0.064	-485	-420	-630	-325	-615	-300	0
6	-0.154	-0.250	-0.197	-0.308	-0.184	-0.120	-815	-765	-1035	-531	-1020	-580	-42
10	-0.163	-0.264	-0.210	-0.311	-0.191	-0.127	-860	-835	-1100	-546	-1055	-615	-67
13	-0.172	-0.271	-0.219	-0.318	-0.202	-0.135	-905	-870	-1145	-581	-1110	-655	-84
17	-0.183	-0.278	-0.228	-0.325	-0.211	-0.140	-960	-905	-1190	-616	-1155	-680	-106
20	-0.191	-0.287	-0.236	-0.334	-0.223	-0.153	-1000	-950	-1230	-661	-1215	-745	-121
24	-0.199	-0.294	-0.247	-0.338	-0.232	-0.159	-1040	-985	-1285	-681	-1260	-775	-140
27	-0.195	-0.292	-0.242	-0.335	-0.226	-0.155	-1020	-975	-1260	-666	-1230	-755	-153
31	-0.206	-0.299	-0.247	-0.347	-0.226	-0.164	-1075	-1010	-1285	-726	-1230	-800	-169
41	-0.217	-0.308	-0.263	-0.354	-0.246	-0.173	-1130	-1056	-1365	-761	-1330	-845	-206
45	-0.225	-0.313	-0.271	-0.357	-0.251	-0.175	-1170	-1081	-1405	-776	-1355	-855	-219
48	-0.233	-0.317	-0.276	-0.361	-0.257	-0.184	-1210	-1101	-1430	-796	-1385	-900	-228
55	-0.238	-0.322	-0.285	-0.362	-0.265	-0.185	-1235	-1126	-1475	-801	-1425	-905	-247
59	-0.242	-0.329	-0.289	-0.365	-0.269	-0.182	-1255	-1161	-1495	-816	-1445	-890	-258
73	-0.250	-0.336	-0.292	-0.371	-0.277	-0.188	-1295	-1196	-1510	-846	-1485	-920	-290
80	-0.247	-0.341	-0.292	-0.372	-0.278	-0.190	-1280	-1221	-1510	-851	-1490	-930	-304
85	-0.251	-0.339	-0.294	-0.374	-0.281	-0.195	-1300	-1211	-1520	-861	-1505	-955	-313
87	-0.261	-0.347	-0.302	-0.381	-0.287	-0.200	-1350	-1251	-1560	-896	-1535	-980	-317
92	-0.261	-0.349	-0.304	-0.382	-0.291	-0.206	-1350	-1261	-1570	-901	-1555	-1010	-326
104	-0.267	-0.353	-0.304	-0.388	-0.295	-0.201	-1380	-1281	-1570	-931	-1575	-985	-344
106	-0.266	-0.349	-0.311	-0.386	-0.297	-0.201	-1375	-1261	-1605	-921	-1585	-985	-347
122	-0.262	-0.342	-0.306	-0.380	-0.294	-0.193	-1355	-1226	-1580	-891	-1570	-945	-368
135	-0.267	-0.346	-0.311	-0.385	-0.303	-0.198	-1380	-1246	-1605	-916	-1615	-970	-383
139	-0.274	-0.354	-0.319	-0.390	-0.309	-0.204	-1415	-1286	-1645	-941	-1645	-1000	-387
149	-0.272	-0.352	-0.318	-0.387	-0.305	-0.200	-1405	-1276	-1640	-926	-1625	-980	-396
157	-0.286	-0.361	-0.329	-0.396	-0.318	-0.211	-1475	-1321	-1695	-971	-1690	-1035	-404
164	-0.280	-0.355	-0.321	-0.390	-0.314	-0.205	-1445	-1291	-1655	-941	-1670	-1005	-410
168	-0.284	-0.362	-0.328	-0.395	-0.316	-0.214	-1465	-1326	-1690	-966	-1680	-1050	-413
178	-0.285	-0.359	-0.328	-0.395	-0.322	-0.212	-1470	-1311	-1690	-966	-1710	-1040	-421
183	-0.285	-0.363	-0.316	-0.391	-0.311	-0.210	-1470	-1331	-1630	-946	-1655	-1030	-424
200	-0.309	-0.382	-0.360	-0.411	-0.355	-0.232	-1590	-1426	-1850	-1046	-1875	-1140	-435
206	-0.302	-0.375	-0.353	-0.406	-0.350	-0.225	-1555	-1391	-1815	-1021	-1850	-1105	-439
212	-0.298	-0.372	-0.350	-0.402	-0.343	-0.222	-1535	-1376	-1800	-1001	-1815	-1090	-443
220	-0.317	-0.388	-0.367	-0.417	-0.360	-0.239	-1630	-1456	-1885	-1076	-1900	-1175	-447
226	-0.311	-0.381	-0.364	-0.414	-0.354	-0.237	-1600	-1421	-1870	-1061	-1870	-1165	-450
235	-0.322	-0.397	-0.376	-0.429	-0.369	-0.252	-1655	-1501	-1930	-1136	-1945	-1240	-455
239	-0.327	-0.399	-0.378	-0.424	-0.370	-0.249	-1680	-1511	-1940	-1111	-1950	-1225	-457
251	-0.348	-0.413	-0.396	-0.443	-0.387	-0.264	-1785	-1581	-2030	-1206	-2035	-1300	-462
255	-0.344	-0.412	-0.393	-0.437	-0.384	-0.259	-1765	-1576	-2015	-1176	-2020	-1275	-464
262	-0.347	-0.413	-0.397	-0.440	-0.386	-0.261	-1780	-1581	-2035	-1191	-2030	-1285	-467
268	-0.329	-0.400	-0.379	-0.428	-0.376	-0.251	-1690	-1516	-1945	-1131	-1980	-1235	-470
283	-0.318	-0.405	-0.358	-0.435	-0.345	-0.261	-1635	-1541	-1840	-1166	-1825	-1285	-475
290	-0.339	-0.415	-0.379	-0.443	-0.364	-0.263	-1740	-1591	-1945	-1206	-1920	-1295	-478
303	-0.355	-0.421	-0.397	-0.448	-0.385	-0.270	-1820	-1621	-2035	-1231	-2025	-1330	-482
322	-0.350	-0.409	-0.396	-0.437	-0.383	-0.260	-1795	-1561	-2030	-1176	-2015	-1280	-489
335	-0.338	-0.403	-0.392	-0.425	-0.384	-0.244	-1735	-1531	-2010	-1116	-2020	-1200	-492
339	-0.351	-0.415	-0.407	-0.439	-0.400	-0.259	-1800	-1591	-2085	-1186	-2100	-1275	-493
353	-0.345	-0.410	-0.397	-0.445	-0.389	-0.255	-1770	-1566	-2035	-1216	-2045	-1255	-497

March creep using F5 shrinkage (Part 2 of Table)

Time (days)	Measured creep strain less shrinkage and thermal strain ($\mu\text{m/m}$) $\epsilon_{cre,i}$						True creep strain ($\mu\text{m/m}$) $\epsilon_{cr,i}$						Creep coefficient $\phi(t,t_0)$						
	1A	1B	2A	2B	3A	3B	1A	1B	2A	2B	3A	3B	1A	1B	2A	3A	3B	Average	
0	-485	-420	-630	-325	-615	-300	0	0	0	0	0	0	0	0	0	0	0	0	0
6	-773	-723	-993	-489	-978	-538	-288	-303	-363	-163	-363	-238	0.59	0.72	0.58	0.59	0.79	0.66	
10	-793	-768	-1033	-479	-988	-548	-308	-348	-403	-153	-373	-248	0.64	0.83	0.64	0.61	0.83	0.71	
13	-821	-786	-1061	-496	-1026	-571	-336	-366	-431	-171	-411	-271	0.69	0.87	0.68	0.67	0.90	0.76	
17	-854	-800	-1084	-510	-1049	-574	-369	-379	-454	-184	-434	-274	0.76	0.90	0.72	0.71	0.91	0.80	
20	-879	-830	-1109	-540	-1094	-624	-394	-409	-479	-214	-479	-324	0.81	0.97	0.76	0.78	1.08	0.88	
24	-900	-846	-1145	-541	-1120	-635	-415	-426	-515	-216	-505	-335	0.86	1.01	0.82	0.82	1.12	0.93	
27	-867	-823	-1107	-513	-1077	-602	-382	-402	-477	-188	-462	-302	0.79	0.96	0.76	0.75	1.01	0.85	
31	-906	-841	-1116	-557	-1061	-631	-421	-421	-486	-231	-446	-331	0.87	1.00	0.77	0.72	1.10	0.89	
41	-924	-850	-1159	-555	-1124	-639	-439	-430	-529	-230	-509	-339	0.91	1.02	0.84	0.83	1.13	0.95	
45	-951	-862	-1186	-557	-1136	-637	-466	-442	-556	-232	-521	-337	0.96	1.05	0.88	0.85	1.12	0.97	
48	-982	-873	-1202	-568	-1157	-672	-497	-453	-572	-243	-542	-372	1.03	1.08	0.91	0.88	1.24	1.03	
55	-987	-878	-1227	-553	-1177	-658	-502	-458	-597	-228	-562	-358	1.04	1.09	0.95	0.91	1.19	1.04	
59	-997	-903	-1237	-558	-1187	-632	-512	-482	-607	-233	-572	-332	1.06	1.15	0.96	0.93	1.11	1.04	
73	-1005	-905	-1220	-556	-1195	-630	-520	-485	-590	-230	-580	-330	1.07	1.15	0.94	0.94	1.10	1.04	
80	-976	-916	-1206	-547	-1186	-626	-491	-496	-576	-221	-571	-326	1.01	1.18	0.91	0.93	1.09	1.02	
85	-986	-897	-1206	-547	-1191	-642	-501	-477	-576	-222	-576	-342	1.03	1.13	0.92	0.94	1.14	1.03	
87	-1033	-934	-1243	-579	-1218	-663	-548	-513	-613	-254	-603	-363	1.13	1.22	0.97	0.98	1.21	1.10	
92	-1024	-935	-1244	-575	-1229	-684	-539	-515	-614	-250	-614	-384	1.11	1.23	0.98	1.00	1.28	1.12	
104	-1036	-936	-1226	-587	-1231	-641	-551	-516	-596	-261	-616	-341	1.14	1.23	0.95	1.00	1.14	1.09	
106	-1028	-914	-1258	-574	-1238	-638	-543	-493	-628	-249	-623	-338	1.12	1.17	1.00	1.01	1.13	1.09	
122	-987	-858	-1212	-523	-1202	-577	-502	-438	-582	-198	-587	-277	1.04	1.04	0.92	0.95	0.92	0.98	
135	-997	-863	-1222	-533	-1232	-587	-512	-443	-592	-208	-617	-287	1.06	1.05	0.94	1.00	0.96	1.00	
139	-1028	-899	-1258	-554	-1258	-613	-543	-479	-628	-229	-643	-313	1.12	1.14	1.00	1.05	1.04	1.07	
149	-1008	-879	-1243	-529	-1228	-584	-523	-459	-613	-204	-613	-284	1.08	1.09	0.97	1.00	0.95	1.02	
157	-1071	-917	-1291	-567	-1286	-631	-586	-497	-661	-242	-671	-331	1.21	1.18	1.05	1.09	1.10	1.13	
164	-1035	-881	-1245	-531	-1260	-595	-550	-461	-615	-206	-645	-295	1.13	1.10	0.98	1.05	0.98	1.05	
168	-1052	-913	-1277	-553	-1267	-637	-567	-493	-647	-228	-652	-337	1.17	1.17	1.03	1.06	1.12	1.11	
178	-1049	-890	-1269	-545	-1289	-619	-564	-470	-639	-220	-674	-319	1.16	1.12	1.01	1.10	1.06	1.09	
183	-1046	-906	-1206	-522	-1231	-606	-561	-486	-576	-196	-616	-306	1.16	1.16	0.91	1.00	1.02	1.05	
200	-1154	-990	-1414	-611	-1439	-705	-669	-570	-784	-285	-824	-405	1.38	1.36	1.25	1.34	1.35	1.33	
206	-1116	-952	-1376	-582	-1411	-666	-631	-531	-746	-257	-796	-366	1.30	1.26	1.18	1.29	1.22	1.25	
212	-1092	-933	-1357	-558	-1372	-647	-607	-513	-727	-233	-757	-347	1.25	1.22	1.15	1.23	1.16	1.20	
220	-1183	-1009	-1438	-629	-1453	-728	-698	-588	-808	-304	-838	-428	1.44	1.40	1.28	1.36	1.43	1.38	
226	-1150	-970	-1420	-611	-1419	-715	-665	-550	-790	-285	-805	-415	1.37	1.31	1.25	1.31	1.38	1.32	
235	-1200	-1046	-1475	-681	-1490	-785	-715	-626	-845	-356	-875	-485	1.47	1.49	1.34	1.42	1.62	1.47	
239	-1223	-1054	-1483	-654	-1493	-768	-738	-634	-853	-329	-878	-468	1.52	1.51	1.35	1.43	1.56	1.47	
251	-1323	-1118	-1567	-744	-1572	-838	-838	-698	-938	-418	-957	-538	1.73	1.66	1.49	1.56	1.79	1.65	
255	-1301	-1112	-1551	-712	-1556	-811	-816	-691	-921	-387	-941	-511	1.68	1.65	1.46	1.53	1.70	1.60	
262	-1313	-1114	-1568	-724	-1563	-818	-828	-693	-938	-399	-948	-518	1.71	1.65	1.49	1.54	1.73	1.62	
268	-1220	-1046	-1475	-662	-1510	-765	-735	-626	-845	-336	-895	-465	1.52	1.49	1.34	1.46	1.55	1.47	
283	-1159	-1065	-1364	-691	-1349	-810	-674	-645	-734	-365	-734	-510	1.39	1.54	1.17	1.19	1.70	1.40	
290	-1262	-1113	-1467	-728	-1442	-817	-777	-693	-837	-403	-827	-517	1.60	1.65	1.33	1.34	1.72	1.53	
303	-1337	-1138	-1552	-749	-1542	-848	-852	-718	-922	-423	-927	-548	1.76	1.71	1.46	1.51	1.83	1.65	
322	-1306	-1072	-1541	-688	-1526	-791	-821	-652	-911	-362	-911	-491	1.69	1.55	1.45	1.48	1.64	1.56	
335	-1243	-1038	-1518	-624	-1527	-708	-758	-618	-888	-298	-913	-408	1.56	1.47	1.41	1.48	1.36	1.46	
339	-1306	-1097	-1591	-693	-1606	-782	-821	-677	-961	-367	-991	-482	1.69	1.61	1.53	1.61	1.61	1.61	
353	-1273	-1069	-1538	-719	-1548	-758	-788	-648	-908	-394	-933	-458	1.62	1.54	1.44	1.52	1.53	1.53	

April creep (Part 1 of Table)

Time (days)	DEMEC Reading (DR)						Measured creep strain ($\mu\text{m/m}$) $\epsilon_{\text{CST},i}$						Thermal/ Shrinkage strain ($\mu\text{m/m}$)
	1A	1B	2A	2B	3A	3B	1A	1B	2A	2B	3A	3B	
initial	-0.111	-0.091	-0.100	-0.041	-0.040	-0.107	0	0	0	0	0	0	-
0	-0.208	-0.184	-0.207	-0.117	-0.154	-0.182	-485	-465	-535	-380	-570	-375	0
3	-0.253	-0.217	-0.252	-0.150	-0.199	-0.218	-710	-630	-760	-545	-795	-555	-50
7	-0.264	-0.223	-0.263	-0.155	-0.208	-0.223	-765	-660	-815	-570	-840	-580	-79
21	-0.287	-0.240	-0.284	-0.168	-0.231	-0.240	-880	-745	-920	-635	-955	-665	-116
28	-0.291	-0.247	-0.292	-0.171	-0.237	-0.243	-900	-780	-960	-650	-985	-680	-154
33	-0.297	-0.251	-0.299	-0.173	-0.244	-0.257	-931	-800	-995	-660	-1020	-750	-168
34	-0.305	-0.258	-0.306	-0.180	-0.251	-0.257	-971	-835	-1031	-695	-1055	-750	-176
35	-0.305	-0.261	-0.306	-0.186	-0.253	-0.262	-971	-850	-1031	-725	-1065	-775	-181
40	-0.311	-0.264	-0.312	-0.191	-0.258	-0.264	-1001	-865	-1061	-750	-1090	-785	-195
52	-0.320	-0.272	-0.319	-0.197	-0.267	-0.272	-1046	-905	-1096	-780	-1135	-825	-225
54	-0.325	-0.271	-0.324	-0.195	-0.272	-0.271	-1071	-900	-1121	-770	-1160	-820	-218
70	-0.324	-0.271	-0.331	-0.194	-0.277	-0.274	-1066	-900	-1156	-765	-1185	-835	-175
87	-0.345	-0.289	-0.351	-0.209	-0.298	-0.290	-1171	-990	-1256	-840	-1290	-915	-234
97	-0.342	-0.286	-0.351	-0.207	-0.298	-0.287	-1156	-975	-1256	-830	-1290	-900	-221
105	-0.358	-0.300	-0.365	-0.221	-0.310	-0.298	-1236	-1045	-1326	-900	-1350	-956	-255
112	-0.353	-0.292	-0.357	-0.212	-0.303	-0.292	-1211	-1005	-1286	-855	-1315	-925	-253
116	-0.361	-0.301	-0.363	-0.220	-0.308	-0.297	-1251	-1050	-1316	-895	-1340	-951	-284
126	-0.357	-0.299	-0.363	-0.217	-0.316	-0.296	-1231	-1040	-1316	-880	-1380	-946	-275
131	-0.354	-0.300	-0.350	-0.217	-0.307	-0.296	-1216	-1045	-1251	-880	-1335	-946	-289
148	-0.389	-0.325	-0.399	-0.240	-0.352	-0.321	-1391	-1171	-1496	-995	-1560	-1071	-318
154	-0.377	-0.316	-0.392	-0.231	-0.350	-0.290	-1331	-1126	-1461	-950	-1550	-915	-249
160	-0.371	-0.314	-0.388	-0.231	-0.341	-0.296	-1301	-1116	-1441	-950	-1505	-946	-239
168	-0.396	-0.330	-0.412	-0.246	-0.360	-0.317	-1426	-1196	-1561	-1025	-1600	-1051	-307
174	-0.393	-0.324	-0.408	-0.241	-0.357	-0.310	-1411	-1166	-1541	-1000	-1585	-1016	-324
183	-0.405	-0.342	-0.421	-0.258	-0.367	-0.327	-1471	-1256	-1606	-1085	-1635	-1101	-377
187	-0.420	-0.341	-0.425	-0.256	-0.368	-0.333	-1546	-1251	-1626	-1075	-1640	-1131	-347
199	-0.437	-0.354	-0.445	-0.269	-0.385	-0.350	-1631	-1316	-1726	-1140	-1725	-1216	-423
203	-0.435	-0.354	-0.441	-0.268	-0.383	-0.350	-1621	-1316	-1706	-1135	-1715	-1216	-383
210	-0.438	-0.353	-0.445	-0.268	-0.386	-0.351	-1636	-1311	-1726	-1135	-1730	-1221	-419
216	-0.416	-0.342	-0.428	-0.255	-0.371	-0.340	-1526	-1256	-1641	-1070	-1655	-1166	-294
231	-0.406	-0.346	-0.400	-0.264	-0.342	-0.324	-1476	-1276	-1501	-1115	-1510	-1086	-209
238	-0.431	-0.355	-0.427	-0.270	-0.361	-0.336	-1601	-1321	-1636	-1145	-1605	-1146	-289
251	-0.454	-0.363	-0.448	-0.275	-0.381	-0.346	-1716	-1361	-1741	-1170	-1705	-1196	-324
270	-0.444	-0.354	-0.446	-0.262	-0.380	-0.337	-1666	-1316	-1731	-1105	-1700	-1151	-289
283	-0.432	-0.347	-0.449	-0.254	-0.389	-0.318	-1606	-1281	-1746	-1065	-1745	-1056	-250
287	-0.445	-0.357	-0.460	-0.266	-0.406	-0.324	-1671	-1331	-1801	-1125	-1830	-1086	-293
301	-0.434	-0.349	-0.447	-0.259	-0.389	-0.326	-1616	-1291	-1736	-1090	-1745	-1096	-263

April creep (Part 2 of Table)

Time (days)	Measured creep strain less shrinkage and thermal strain ($\mu\text{m/m}$) $\epsilon_{cre,i}$						True creep strain ($\mu\text{m/m}$) $\epsilon_{cr,i}$						Creep coefficient $\phi(t, t_0)$							
	1A	1B	2A	2B	3A	3B	1A	1B	2A	2B	3A	3B	1A	1B	2A	2B	3A	3B	Average	
0	-485	-465	-535	-380	-570	-375	0	0	0	0	0	0	0	0	0	0	0	0	0	0
3	-660	-580	-710	-495	-745	-505	-175	-115	-175	-115	-175	-130	0.36	0.25	0.33	0.30	0.31	0.35	0.32	
7	-687	-581	-737	-491	-761	-501	-201	-116	-201	-111	-191	-126	0.41	0.25	0.38	0.29	0.34	0.34	0.33	
21	-764	-629	-804	-519	-839	-549	-279	-164	-269	-139	-269	-174	0.57	0.35	0.50	0.36	0.47	0.46	0.45	
28	-747	-626	-807	-496	-831	-526	-261	-161	-271	-116	-261	-151	0.54	0.35	0.51	0.31	0.46	0.40	0.43	
33	-763	-633	-828	-492	-853	-583	-278	-167	-293	-112	-282	-208	0.57	0.36	0.55	0.30	0.50	0.55	0.47	
34	-794	-659	-854	-519	-879	-574	-309	-194	-319	-139	-309	-199	0.64	0.42	0.60	0.36	0.54	0.53	0.51	
35	-789	-669	-849	-544	-884	-594	-304	-204	-314	-164	-314	-219	0.63	0.44	0.59	0.43	0.55	0.58	0.54	
40	-805	-670	-865	-555	-895	-590	-320	-205	-330	-175	-325	-215	0.66	0.44	0.62	0.46	0.57	0.57	0.55	
52	-820	-680	-870	-555	-910	-600	-335	-215	-335	-175	-340	-225	0.69	0.46	0.63	0.46	0.60	0.60	0.57	
54	-853	-683	-903	-552	-943	-603	-368	-217	-368	-172	-372	-228	0.76	0.47	0.69	0.45	0.65	0.61	0.60	
70	-890	-725	-980	-590	-1010	-660	-405	-260	-445	-210	-440	-285	0.83	0.56	0.83	0.55	0.77	0.76	0.72	
87	-937	-756	-1022	-606	-1056	-682	-451	-291	-486	-226	-486	-306	0.93	0.63	0.91	0.59	0.85	0.82	0.79	
97	-934	-754	-1034	-609	-1069	-679	-449	-289	-499	-229	-499	-304	0.93	0.62	0.93	0.60	0.87	0.81	0.79	
105	-980	-790	-1070	-645	-1095	-700	-495	-325	-535	-265	-525	-325	1.02	0.70	1.00	0.70	0.92	0.87	0.87	
112	-958	-753	-1033	-602	-1063	-673	-473	-287	-498	-222	-492	-298	0.97	0.62	0.93	0.58	0.86	0.79	0.79	
116	-967	-766	-1032	-611	-1056	-666	-481	-301	-496	-231	-486	-291	0.99	0.65	0.93	0.61	0.85	0.78	0.80	
126	-955	-765	-1040	-605	-1105	-670	-470	-300	-505	-225	-535	-295	0.97	0.64	0.94	0.59	0.94	0.79	0.81	
131	-927	-756	-962	-591	-1046	-656	-441	-291	-426	-211	-476	-281	0.91	0.63	0.80	0.56	0.84	0.75	0.75	
148	-1073	-853	-1178	-677	-1242	-753	-588	-387	-643	-297	-672	-378	1.21	0.83	1.20	0.78	1.18	1.01	1.04	
154	-1082	-877	-1212	-701	-1301	-666	-596	-411	-676	-321	-731	-291	1.23	0.88	1.26	0.84	1.28	0.78	1.05	
160	-1062	-877	-1202	-711	-1266	-707	-576	-411	-666	-331	-696	-331	1.19	0.88	1.25	0.87	1.22	0.88	1.05	
168	-1119	-889	-1254	-719	-1294	-744	-634	-424	-719	-339	-724	-369	1.31	0.91	1.34	0.89	1.27	0.98	1.12	
174	-1087	-841	-1217	-676	-1261	-691	-601	-376	-681	-296	-691	-316	1.24	0.81	1.27	0.78	1.21	0.84	1.03	
183	-1094	-879	-1229	-709	-1259	-724	-609	-414	-694	-328	-689	-349	1.25	0.89	1.30	0.86	1.21	0.93	1.07	
187	-1199	-904	-1279	-729	-1294	-784	-714	-439	-744	-349	-724	-409	1.47	0.94	1.39	0.92	1.27	1.09	1.18	
199	-1208	-893	-1303	-717	-1302	-793	-723	-427	-768	-337	-732	-417	1.49	0.92	1.43	0.89	1.28	1.11	1.19	
203	-1238	-933	-1323	-752	-1332	-833	-753	-467	-788	-372	-762	-458	1.55	1.00	1.47	0.98	1.34	1.22	1.26	
210	-1217	-891	-1307	-716	-1311	-801	-731	-426	-771	-336	-741	-426	1.51	0.92	1.44	0.88	1.30	1.14	1.20	
216	-1232	-962	-1347	-776	-1361	-872	-747	-496	-811	-396	-791	-496	1.54	1.07	1.52	1.04	1.39	1.32	1.31	
231	-1267	-1067	-1292	-906	-1301	-877	-782	-601	-757	-526	-731	-501	1.61	1.29	1.41	1.38	1.28	1.34	1.39	
238	-1312	-1032	-1347	-856	-1316	-857	-827	-566	-811	-476	-746	-481	1.70	1.22	1.52	1.25	1.31	1.28	1.38	
251	-1392	-1037	-1417	-846	-1381	-872	-907	-571	-882	-466	-811	-496	1.87	1.23	1.65	1.23	1.42	1.32	1.45	
270	-1377	-1027	-1442	-816	-1411	-862	-892	-561	-907	-436	-841	-486	1.84	1.21	1.69	1.15	1.48	1.30	1.44	
283	-1356	-1030	-1496	-815	-1495	-805	-870	-565	-960	-435	-925	-430	1.79	1.21	1.79	1.14	1.62	1.15	1.45	
287	-1378	-1038	-1508	-832	-1538	-793	-893	-573	-973	-452	-967	-418	1.84	1.23	1.82	1.19	1.70	1.11	1.48	
301	-1353	-1028	-1473	-827	-1483	-833	-868	-563	-938	-447	-912	-458	1.79	1.21	1.75	1.18	1.60	1.22	1.46	

May creep (Part 1 of Table)

Time (days)	DEMEC Reading (DR)						Measured creep strain ($\mu\text{m/m}$) $\epsilon_{\text{CST},i}$						Thermal/ Shrinkage strain ($\mu\text{m/m}$)
	1A	1B	2A	2B	3A	3B	1A	1B	2A	2B	3A	3B	
initial	0.017	0.035	0.029	0.050	0.018	0.047	0	0	0	0	0	0	-
0	-0.088	-0.067	-0.096	-0.021	-0.125	-0.010	-525	-510	-625	-355	-715	-285	0
3	-0.127	-0.112	-0.139	-0.062	-0.168	-0.055	-720	-735	-840	-560	-930	-510	-59
7	-0.144	-0.127	-0.157	-0.075	-0.187	-0.069	-805	-810	-930	-625	-1025	-580	-118
21	-0.171	-0.161	-0.185	-0.105	-0.217	-0.100	-940	-980	-1070	-775	-1175	-735	-209
28	-0.177	-0.173	-0.194	-0.110	-0.225	-0.106	-970	-1040	-1115	-800	-1215	-765	-236
33	-0.185	-0.187	-0.200	-0.120	-0.233	-0.116	-1010	-1110	-1145	-850	-1255	-815	-301
34	-0.188	-0.189	-0.205	-0.126	-0.239	-0.119	-1025	-1120	-1170	-880	-1285	-830	-290
35	-0.190	-0.190	-0.208	-0.128	-0.242	-0.123	-1035	-1125	-1185	-890	-1300	-850	-310
40	-0.194	-0.191	-0.211	-0.136	-0.247	-0.130	-1055	-1130	-1200	-930	-1325	-885	-318
52	-0.202	-0.203	-0.224	-0.143	-0.259	-0.140	-1095	-1190	-1265	-965	-1385	-935	-385
54	-0.208	-0.211	-0.228	-0.148	-0.264	-0.140	-1125	-1230	-1285	-990	-1410	-935	-336
70	-0.214	-0.217	-0.235	-0.153	-0.273	-0.147	-1155	-1260	-1320	-1015	-1455	-970	-318
87	-0.233	-0.242	-0.256	-0.172	-0.297	-0.164	-1250	-1385	-1425	-1110	-1575	-1055	-408
97	-0.230	-0.238	-0.255	-0.173	-0.294	-0.164	-1235	-1365	-1420	-1115	-1560	-1055	-396
105	-0.247	-0.249	-0.270	-0.182	-0.305	-0.175	-1320	-1420	-1495	-1160	-1615	-1110	-438
112	-0.242	-0.243	-0.264	-0.176	-0.298	-0.169	-1295	-1390	-1465	-1130	-1580	-1080	-430
116	-0.249	-0.253	-0.271	-0.184	-0.307	-0.172	-1330	-1440	-1500	-1170	-1625	-1095	-459
126	-0.247	-0.254	-0.270	-0.181	-0.310	-0.175	-1320	-1445	-1495	-1155	-1640	-1110	-461
131	-0.247	-0.252	-0.265	-0.184	-0.314	-0.178	-1320	-1435	-1470	-1170	-1660	-1125	-480
148	-0.267	-0.279	-0.299	-0.203	-0.338	-0.200	-1420	-1570	-1640	-1265	-1780	-1235	-502
154	-0.261	-0.266	-0.291	-0.194	-0.329	-0.188	-1390	-1505	-1600	-1220	-1735	-1175	-465
160	-0.261	-0.269	-0.290	-0.194	-0.324	-0.187	-1390	-1520	-1595	-1220	-1710	-1170	-459
168	-0.276	-0.282	-0.309	-0.212	-0.345	-0.203	-1465	-1585	-1690	-1310	-1815	-1250	-510
174	-0.270	-0.279	-0.305	-0.207	-0.342	-0.199	-1435	-1570	-1670	-1285	-1800	-1230	-539
183	-0.280	-0.293	-0.315	-0.222	-0.347	-0.216	-1485	-1640	-1720	-1360	-1825	-1315	-587
187	-0.287	-0.297	-0.318	-0.221	-0.351	-0.217	-1520	-1660	-1735	-1355	-1845	-1320	-544
199	-0.307	-0.310	-0.338	-0.235	-0.370	-0.232	-1620	-1725	-1835	-1425	-1940	-1395	-613
203	-0.304	-0.310	-0.335	-0.234	-0.368	-0.230	-1605	-1725	-1820	-1420	-1930	-1385	-585
210	-0.307	-0.310	-0.337	-0.234	-0.367	-0.232	-1620	-1725	-1830	-1420	-1925	-1395	-599
216	-0.288	-0.300	-0.319	-0.228	-0.360	-0.224	-1525	-1675	-1740	-1390	-1890	-1355	-493
231	-0.283	-0.303	-0.290	-0.230	-0.319	-0.224	-1500	-1690	-1595	-1400	-1685	-1355	-428
238	-0.304	-0.315	-0.315	-0.239	-0.339	-0.247	-1605	-1750	-1720	-1445	-1785	-1470	-467
251	-0.317	-0.330	-0.333	-0.245	-0.358	-0.243	-1670	-1825	-1810	-1475	-1880	-1450	-509
270	-0.311	-0.327	-0.334	-0.238	-0.356	-0.225	-1640	-1810	-1815	-1440	-1870	-1360	-498
283	-0.301	-0.299	-0.331	-0.226	-0.359	-0.217	-1590	-1670	-1800	-1380	-1885	-1320	-464
287	-0.313	-0.307	-0.333	-0.235	-0.368	-0.224	-1650	-1710	-1810	-1425	-1930	-1355	-500
301	-0.304	-0.303	-0.326	-0.226	-0.361	-0.218	-1605	-1690	-1775	-1380	-1895	-1325	-463

May creep (Part 2 of Table)

Time (days)	Measured creep strain less shrinkage and thermal strain ($\mu\text{m/m}$) $\epsilon_{cre,i}$						True creep strain ($\mu\text{m/m}$) $\epsilon_{cr,i}$						Creep coefficient $\phi(t,t_0)$					
	1A	1B	2A	2B	3A	3B	1A	1B	2A	2B	3A	3B	1A	1B	2A	2B	3A	Average
0	-525	-510	-625	-355	-715	-285	0	0	0	0	0	0	0	0	0	0	0	0
3	-661	-676	-781	-501	-871	-451	-136	-166	-156	-146	-156	-166	0.26	0.33	0.25	0.41	0.22	0.29
7	-687	-692	-812	-507	-907	-462	-162	-182	-187	-152	-192	-177	0.31	0.36	0.30	0.43	0.27	0.33
21	-731	-771	-861	-566	-966	-526	-206	-261	-236	-211	-251	-241	0.39	0.51	0.38	0.59	0.35	0.45
28	-734	-803	-879	-563	-979	-528	-209	-294	-254	-209	-264	-244	0.40	0.58	0.41	0.59	0.37	0.47
33	-709	-808	-843	-548	-954	-513	-184	-299	-219	-194	-239	-229	0.35	0.59	0.35	0.55	0.33	0.43
34	-735	-830	-880	-590	-995	-540	-210	-320	-255	-235	-280	-255	0.40	0.63	0.41	0.66	0.39	0.50
35	-725	-815	-875	-580	-990	-540	-200	-305	-250	-225	-275	-255	0.38	0.60	0.40	0.63	0.38	0.48
40	-737	-812	-882	-612	-1007	-567	-212	-302	-257	-257	-292	-282	0.40	0.59	0.41	0.72	0.41	0.51
52	-710	-805	-880	-580	-1000	-550	-185	-295	-255	-225	-285	-265	0.35	0.58	0.41	0.63	0.40	0.47
54	-789	-893	-948	-653	-1073	-598	-264	-383	-324	-298	-359	-313	0.50	0.75	0.52	0.84	0.50	0.62
70	-837	-942	-1002	-697	-1137	-652	-312	-432	-377	-342	-422	-367	0.59	0.85	0.60	0.96	0.59	0.72
87	-842	-977	-1017	-702	-1167	-647	-317	-467	-392	-347	-452	-362	0.60	0.92	0.63	0.98	0.63	0.75
97	-838	-968	-1023	-718	-1163	-658	-314	-458	-398	-363	-448	-373	0.60	0.90	0.64	1.02	0.63	0.76
105	-882	-982	-1057	-722	-1177	-672	-357	-472	-432	-367	-462	-387	0.68	0.93	0.69	1.03	0.65	0.80
112	-865	-960	-1035	-700	-1150	-650	-340	-450	-410	-345	-435	-365	0.65	0.88	0.66	0.97	0.61	0.75
116	-871	-981	-1041	-711	-1166	-636	-346	-471	-416	-356	-451	-351	0.66	0.92	0.67	1.00	0.63	0.78
126	-858	-983	-1033	-693	-1178	-648	-333	-473	-408	-338	-463	-363	0.64	0.93	0.65	0.95	0.65	0.76
131	-840	-954	-990	-689	-1180	-644	-315	-445	-365	-335	-465	-360	0.60	0.87	0.58	0.94	0.65	0.73
148	-918	-1068	-1138	-763	-1278	-733	-393	-558	-513	-408	-563	-448	0.75	1.09	0.82	1.15	0.79	0.92
154	-925	-1039	-1135	-754	-1270	-709	-400	-530	-510	-400	-555	-425	0.76	1.04	0.82	1.13	0.78	0.90
160	-931	-1061	-1136	-761	-1251	-711	-406	-551	-511	-406	-536	-426	0.77	1.08	0.82	1.14	0.75	0.91
168	-955	-1074	-1179	-799	-1305	-739	-430	-565	-555	-444	-590	-454	0.82	1.11	0.89	1.25	0.82	0.98
174	-896	-1031	-1131	-746	-1261	-691	-371	-521	-506	-391	-546	-406	0.71	1.02	0.81	1.10	0.76	0.88
183	-898	-1053	-1133	-773	-1238	-728	-373	-543	-508	-418	-523	-443	0.71	1.07	0.81	1.18	0.73	0.90
187	-976	-1116	-1191	-811	-1301	-776	-451	-606	-566	-456	-586	-491	0.86	1.19	0.91	1.28	0.82	1.01
199	-1007	-1112	-1222	-812	-1327	-782	-482	-602	-597	-457	-612	-497	0.92	1.18	0.96	1.29	0.86	1.04
203	-1019	-1139	-1234	-834	-1344	-799	-495	-629	-609	-479	-630	-514	0.94	1.23	0.98	1.35	0.88	1.08
210	-1021	-1126	-1231	-820	-1326	-796	-496	-616	-606	-466	-611	-511	0.94	1.21	0.97	1.31	0.85	1.06
216	-1032	-1182	-1247	-897	-1397	-862	-507	-672	-622	-542	-682	-577	0.97	1.32	1.00	1.53	0.95	1.15
231	-1072	-1262	-1167	-972	-1257	-927	-547	-752	-542	-617	-542	-642	1.04	1.47	0.87	1.74	0.76	1.18
238	-1138	-1283	-1253	-978	-1318	-1003	-613	-773	-628	-623	-603	-718	1.17	1.52	1.01	1.76	0.84	1.26
251	-1161	-1316	-1301	-966	-1371	-941	-636	-806	-676	-611	-656	-656	1.21	1.58	1.08	1.72	0.92	1.30
270	-1142	-1312	-1317	-942	-1372	-862	-617	-802	-692	-587	-657	-577	1.18	1.57	1.11	1.65	0.92	1.29
283	-1126	-1206	-1336	-916	-1421	-856	-601	-696	-711	-561	-706	-571	1.14	1.36	1.14	1.58	0.99	1.24
287	-1150	-1209	-1309	-924	-1430	-854	-625	-699	-685	-569	-715	-569	1.19	1.37	1.10	1.60	1.00	1.25
301	-1142	-1227	-1312	-917	-1432	-862	-617	-717	-687	-562	-717	-577	1.18	1.41	1.10	1.58	1.00	1.25

Second Loading

The second loading event corresponds to the removal of falsework. When the falsework is removed, additional load is applied on the structure initiating creep. The second loading event occurs for all concrete batches, but is presented only for the concrete in F4 (October, November, and March) because the F5 concrete (April and May) creep at second loading was not measured.

October creep using F4 shrinkage (Part 1 of Table)

Time (days)	DEMEC Reading (DR)						Measured creep strain ($\mu\text{m/m}$) $\epsilon_{\text{CST},i}$						Thermal/Shrinkage strain ($\mu\text{m/m}$)
	1A	1B	2A	2B	3A	3B	1A	1B	2A	2B	3A	3B	
initial	0.039	0.041	0.034	0.034	0.038	0.042	0	0	0	0	0	0	-
0	-0.056	-0.013	-0.060	-0.014	-0.057	-0.023	-475	-270	-470	-240	-475	-325	0
4	-0.082	-0.035	-0.090	-0.041	-0.086	-0.051	-605	-380	-620	-375	-620	-465	-6
6	-0.081	-0.035	-0.089	-0.041	-0.089	-0.049	-600	-380	-615	-375	-635	-455	9
14	-0.085	-0.036	-0.096	-0.044	-0.094	-0.054	-620	-385	-650	-390	-660	-480	9
19	-0.090	-0.042	-0.103	-0.049	-0.103	-0.059	-645	-415	-685	-415	-705	-505	1
22	-0.101	-0.048	-0.110	-0.058	-0.108	-0.067	-700	-445	-720	-460	-730	-545	-12
29	-0.093	-0.038	-0.102	-0.049	-0.098	-0.056	-660	-395	-680	-415	-680	-490	22
33	-0.101	-0.046	-0.109	-0.056	-0.106	-0.063	-700	-435	-715	-448	-720	-525	1
35	-0.095	-0.042	-0.105	-0.050	-0.102	-0.058	-670	-415	-695	-420	-700	-500	24
39	-0.096	-0.043	-0.107	-0.052	-0.102	-0.059	-675	-420	-705	-430	-700	-505	16
43	-0.097	-0.044	-0.108	-0.054	-0.104	-0.062	-680	-425	-710	-440	-710	-520	12
48	-0.100	-0.047	-0.114	-0.062	-0.107	-0.067	-695	-440	-740	-480	-725	-545	6
65	-0.120	-0.062	-0.133	-0.071	-0.129	-0.083	-795	-515	-835	-525	-835	-625	-9
69	-0.123	-0.065	-0.136	-0.072	-0.122	-0.084	-810	-530	-850	-530	-800	-630	-7
71	-0.112	-0.058	-0.126	-0.067	-0.114	-0.077	-755	-495	-800	-505	-760	-595	29
77	-0.109	-0.055	-0.123	-0.064	-0.113	-0.071	-740	-480	-785	-490	-755	-565	31
85	-0.125	-0.067	-0.140	-0.078	-0.135	-0.089	-820	-540	-870	-560	-865	-655	-49
91	-0.131	-0.073	-0.144	-0.085	-0.139	-0.095	-850	-570	-890	-595	-885	-685	-67
100	-0.139	-0.079	-0.157	-0.092	-0.154	-0.101	-890	-600	-955	-630	-960	-715	-96
104	-0.138	-0.078	-0.153	-0.087	-0.151	-0.097	-885	-595	-935	-605	-945	-695	-57
116	-0.152	-0.089	-0.170	-0.103	-0.168	-0.115	-955	-650	-1020	-685	-1030	-785	-147
120	-0.148	-0.087	-0.168	-0.100	-0.167	-0.112	-935	-640	-1010	-670	-1025	-770	-122
127	-0.153	-0.090	-0.173	-0.102	-0.171	-0.114	-960	-655	-1035	-680	-1045	-780	-134
133	-0.137	-0.075	-0.157	-0.089	-0.156	-0.102	-880	-580	-955	-615	-970	-720	-42
148	-0.137	-0.079	-0.160	-0.090	-0.160	-0.100	-880	-600	-970	-620	-990	-710	-11
155	-0.151	-0.094	-0.174	-0.103	-0.175	-0.116	-950	-675	-1040	-685	-1065	-790	-64
168	-0.161	-0.099	-0.185	-0.114	-0.188	-0.128	-1000	-700	-1095	-740	-1130	-850	-119
187	-0.155	-0.091	-0.177	-0.108	-0.180	-0.124	-970	-660	-1055	-710	-1090	-830	-102
200	-0.147	-0.087	-0.169	-0.100	-0.169	-0.115	-930	-640	-1015	-670	-1035	-785	-89
204	-0.157	-0.094	-0.182	-0.116	-0.180	-0.122	-980	-675	-1080	-750	-1090	-820	-86
218	-0.149	-0.088	-0.172	-0.107	-0.173	-0.119	-940	-645	-1030	-705	-1055	-805	-42

October creep using F4 shrinkage (Part 2 of Table)

Time (days)	Measured creep strain less shrinkage and thermal strain ($\mu\text{m/m}$) $\epsilon_{\text{Cre},i}$						True creep strain ($\mu\text{m/m}$) $\epsilon_{\text{Cr},i}$						Creep coefficient $\phi(t, t_0)$					
	1A	1B	2A	2B	3A	3B	1A	1B	2A	2B	3A	3B	1B	2A	3A	3B	Average	
0	-	-	-	-	-	-	0	0	0	0	0	0	0	0	0	0	0	0
4	-599	-374	-614	-369	-614	-459	-124	-104	-144	-129	-139	-134	0.38	0.31	0.29	0.41	0.35	
6	-609	-389	-624	-384	-644	-464	-134	-119	-154	-144	-169	-139	0.44	0.33	0.36	0.43	0.39	
14	-629	-394	-659	-399	-669	-489	-154	-124	-189	-159	-194	-164	0.46	0.40	0.41	0.50	0.44	
19	-646	-416	-686	-416	-706	-506	-171	-146	-216	-176	-231	-181	0.54	0.46	0.49	0.56	0.51	
22	-687	-432	-707	-447	-717	-532	-212	-162	-237	-207	-242	-207	0.60	0.51	0.51	0.64	0.56	
29	-682	-417	-702	-437	-702	-512	-207	-147	-232	-197	-227	-187	0.55	0.49	0.48	0.58	0.52	
33	-701	-436	-716	-449	-721	-526	-226	-166	-246	-209	-246	-201	0.62	0.52	0.52	0.62	0.57	
35	-694	-439	-719	-444	-724	-524	-219	-169	-249	-204	-249	-199	0.63	0.53	0.52	0.61	0.57	
39	-691	-436	-721	-446	-716	-521	-216	-166	-251	-206	-241	-196	0.62	0.53	0.51	0.60	0.57	
43	-692	-437	-722	-452	-722	-532	-217	-167	-252	-212	-247	-207	0.62	0.54	0.52	0.64	0.58	
48	-701	-446	-746	-486	-731	-551	-226	-176	-276	-246	-256	-226	0.65	0.59	0.54	0.70	0.62	
65	-786	-506	-826	-516	-826	-616	-311	-236	-356	-276	-351	-291	0.87	0.76	0.74	0.90	0.82	
69	-802	-522	-842	-522	-792	-622	-327	-252	-372	-282	-317	-297	0.94	0.79	0.67	0.92	0.83	
71	-784	-524	-829	-534	-789	-624	-309	-254	-359	-294	-314	-299	0.94	0.76	0.66	0.92	0.82	
77	-771	-511	-816	-521	-786	-596	-296	-241	-346	-281	-311	-271	0.89	0.74	0.66	0.83	0.78	
85	-771	-491	-821	-511	-816	-606	-296	-221	-351	-271	-341	-281	0.82	0.75	0.72	0.87	0.79	
91	-782	-502	-822	-527	-817	-617	-307	-232	-352	-287	-342	-292	0.86	0.75	0.72	0.90	0.81	
100	-794	-504	-859	-534	-864	-619	-319	-234	-389	-294	-389	-294	0.87	0.83	0.82	0.90	0.85	
104	-827	-537	-877	-547	-887	-637	-352	-267	-407	-307	-412	-312	0.99	0.87	0.87	0.96	0.92	
116	-807	-502	-872	-537	-882	-637	-332	-232	-402	-297	-407	-312	0.86	0.86	0.86	0.96	0.88	
120	-812	-517	-887	-547	-902	-647	-337	-247	-417	-307	-427	-322	0.92	0.89	0.90	0.99	0.92	
127	-826	-521	-901	-546	-911	-646	-351	-251	-431	-306	-436	-321	0.93	0.92	0.92	0.99	0.94	
133	-837	-537	-912	-572	-927	-677	-362	-267	-442	-332	-452	-352	0.99	0.94	0.95	1.08	0.99	
148	-869	-589	-959	-609	-979	-699	-394	-319	-489	-369	-504	-374	1.18	1.04	1.06	1.15	1.11	
155	-886	-611	-976	-621	-1001	-726	-411	-341	-506	-381	-526	-401	1.26	1.08	1.11	1.23	1.17	
168	-881	-581	-976	-621	-1011	-731	-406	-311	-506	-381	-536	-406	1.15	1.08	1.13	1.25	1.15	
187	-867	-557	-952	-607	-987	-727	-392	-287	-482	-367	-512	-402	1.06	1.03	1.08	1.24	1.10	
200	-841	-551	-926	-581	-946	-696	-366	-281	-456	-341	-471	-371	1.04	0.97	0.99	1.14	1.04	
204	-894	-589	-994	-664	-1004	-734	-419	-319	-524	-424	-529	-409	1.18	1.11	1.11	1.26	1.17	
218	-897	-602	-987	-662	-1012	-762	-422	-332	-517	-422	-537	-437	1.23	1.10	1.13	1.35	1.20	

October creep using F5 shrinkage (Part 1 of Table)

Time (days)	DEMEC Reading (DR)						Measured creep strain ($\mu\text{m/m}$) $\epsilon_{\text{CST},i}$						Thermal/Shrinkage strain ($\mu\text{m/m}$)
	1A	1B	2A	2B	3A	3B	1A	1B	2A	2B	3A	3B	
initial	0.039	0.041	0.034	0.034	0.038	0.042	0	0	0	0	0	0	-
0	-0.056	-0.013	-0.060	-0.014	-0.057	-0.023	-475	-270	-470	-240	-475	-325	0
4	-0.082	-0.035	-0.090	-0.041	-0.086	-0.051	-605	-380	-620	-375	-620	-465	-2
6	-0.081	-0.035	-0.089	-0.041	-0.089	-0.049	-600	-380	-615	-375	-635	-455	-2
14	-0.085	-0.036	-0.096	-0.044	-0.094	-0.054	-620	-385	-650	-390	-660	-480	-5
19	-0.090	-0.042	-0.103	-0.049	-0.103	-0.059	-645	-415	-685	-415	-705	-505	-7
22	-0.101	-0.048	-0.110	-0.058	-0.108	-0.067	-700	-445	-720	-460	-730	-545	-8
29	-0.093	-0.038	-0.102	-0.049	-0.098	-0.056	-660	-395	-680	-415	-680	-490	-11
33	-0.101	-0.046	-0.109	-0.056	-0.106	-0.063	-700	-435	-715	-448	-720	-525	-12
35	-0.095	-0.042	-0.105	-0.050	-0.102	-0.058	-670	-415	-695	-420	-700	-500	-13
39	-0.096	-0.043	-0.107	-0.052	-0.102	-0.059	-675	-420	-705	-430	-700	-505	-14
43	-0.097	-0.044	-0.108	-0.054	-0.104	-0.062	-680	-425	-710	-440	-710	-520	-15
48	-0.100	-0.047	-0.114	-0.062	-0.107	-0.067	-695	-440	-740	-480	-725	-545	-17
65	-0.120	-0.062	-0.133	-0.071	-0.129	-0.083	-795	-515	-835	-525	-835	-625	-22
69	-0.123	-0.065	-0.136	-0.072	-0.122	-0.084	-810	-530	-850	-530	-800	-630	-23
71	-0.112	-0.058	-0.126	-0.067	-0.114	-0.077	-755	-495	-800	-505	-760	-595	-24
77	-0.109	-0.055	-0.123	-0.064	-0.113	-0.071	-740	-480	-785	-490	-755	-565	-25
85	-0.125	-0.067	-0.140	-0.078	-0.135	-0.089	-820	-540	-870	-560	-865	-655	-27
91	-0.131	-0.073	-0.144	-0.085	-0.139	-0.095	-850	-570	-890	-595	-885	-685	-29
100	-0.139	-0.079	-0.157	-0.092	-0.154	-0.101	-890	-600	-955	-630	-960	-715	-31
104	-0.138	-0.078	-0.153	-0.087	-0.151	-0.097	-885	-595	-935	-605	-945	-695	-32
116	-0.152	-0.089	-0.170	-0.103	-0.168	-0.115	-955	-650	-1020	-685	-1030	-785	-35
120	-0.148	-0.087	-0.168	-0.100	-0.167	-0.112	-935	-640	-1010	-670	-1025	-770	-36
127	-0.153	-0.090	-0.173	-0.102	-0.171	-0.114	-960	-655	-1035	-680	-1045	-780	-37
133	-0.137	-0.075	-0.157	-0.089	-0.156	-0.102	-880	-580	-955	-615	-970	-720	-38
148	-0.137	-0.079	-0.160	-0.090	-0.160	-0.100	-880	-600	-970	-620	-990	-710	-42
155	-0.151	-0.094	-0.174	-0.103	-0.175	-0.116	-950	-675	-1040	-685	-1065	-790	-43
168	-0.161	-0.099	-0.185	-0.114	-0.188	-0.128	-1000	-700	-1095	-740	-1130	-850	-45
187	-0.155	-0.091	-0.177	-0.108	-0.180	-0.124	-970	-660	-1055	-710	-1090	-830	-49
200	-0.147	-0.087	-0.169	-0.100	-0.169	-0.115	-930	-640	-1015	-670	-1035	-785	-51
204	-0.157	-0.094	-0.182	-0.116	-0.180	-0.122	-980	-675	-1080	-750	-1090	-820	-51
218	-0.149	-0.088	-0.172	-0.107	-0.173	-0.119	-940	-645	-1030	-705	-1055	-805	-54

October creep using F5 shrinkage (Part 2 of Table)

Time (days)	Measured creep strain less shrinkage and thermal strain ($\mu\text{m/m}$) $\epsilon_{\text{cre},i}$						True creep strain ($\mu\text{m/m}$) $\epsilon_{\text{cr},i}$						Creep coefficient $\phi(t, t_0)$					
	1A	1B	2A	2B	3A	3B	1A	1B	2A	2B	3A	3B	1B	2A	3A	3B	Average	
0	-475	-270	-470	-240	-475	-325	0	0	0	0	0	0	0	0	0	0	0	0
4	-603	-378	-618	-373	-618	-463	-128	-108	-148	-133	-143	-138	0.40	0.32	0.30	0.43	0.36	
6	-598	-378	-613	-373	-633	-453	-123	-108	-143	-133	-158	-128	0.40	0.30	0.33	0.39	0.36	
14	-614	-380	-645	-385	-654	-475	-140	-110	-175	-145	-180	-150	0.41	0.37	0.38	0.46	0.40	
19	-638	-408	-678	-408	-698	-498	-163	-138	-208	-168	-223	-173	0.51	0.44	0.47	0.53	0.49	
22	-692	-437	-712	-452	-722	-537	-217	-167	-242	-212	-247	-212	0.62	0.51	0.52	0.65	0.58	
29	-649	-384	-669	-404	-669	-479	-174	-114	-199	-164	-194	-154	0.42	0.42	0.41	0.47	0.43	
33	-688	-423	-703	-436	-708	-513	-213	-153	-233	-196	-233	-188	0.57	0.50	0.49	0.58	0.53	
35	-657	-402	-682	-407	-687	-487	-182	-132	-212	-167	-212	-162	0.49	0.45	0.45	0.50	0.47	
39	-661	-406	-691	-416	-686	-491	-186	-136	-221	-176	-211	-166	0.50	0.47	0.44	0.51	0.48	
43	-665	-410	-695	-425	-695	-505	-190	-140	-225	-185	-220	-180	0.52	0.48	0.46	0.55	0.50	
48	-678	-423	-723	-463	-708	-528	-203	-153	-253	-223	-233	-203	0.57	0.54	0.49	0.63	0.56	
65	-773	-493	-813	-503	-813	-603	-298	-223	-343	-263	-338	-278	0.83	0.73	0.71	0.86	0.78	
69	-787	-507	-827	-507	-777	-607	-312	-237	-357	-267	-302	-282	0.88	0.76	0.64	0.87	0.79	
71	-731	-471	-776	-481	-736	-571	-256	-201	-306	-241	-261	-246	0.75	0.65	0.55	0.76	0.68	
77	-715	-455	-760	-465	-730	-540	-240	-185	-290	-225	-255	-215	0.68	0.62	0.54	0.66	0.62	
85	-793	-513	-843	-533	-838	-628	-318	-243	-373	-293	-363	-303	0.90	0.79	0.76	0.93	0.85	
91	-821	-541	-861	-566	-856	-656	-346	-271	-391	-326	-381	-331	1.00	0.83	0.80	1.02	0.91	
100	-859	-569	-924	-599	-929	-684	-384	-299	-454	-359	-454	-359	1.11	0.97	0.96	1.10	1.03	
104	-853	-563	-903	-573	-913	-663	-378	-293	-433	-333	-438	-338	1.09	0.92	0.92	1.04	0.99	
116	-920	-615	-985	-650	-995	-750	-445	-345	-515	-410	-520	-425	1.28	1.10	1.10	1.31	1.19	
120	-899	-604	-974	-634	-989	-734	-424	-334	-504	-394	-514	-409	1.24	1.07	1.08	1.26	1.16	
127	-923	-618	-998	-643	-1008	-743	-448	-348	-528	-403	-533	-418	1.29	1.12	1.12	1.29	1.20	
133	-841	-541	-916	-576	-931	-681	-366	-271	-446	-336	-456	-356	1.01	0.95	0.96	1.10	1.00	
148	-838	-558	-928	-578	-948	-668	-363	-288	-458	-338	-473	-343	1.07	0.98	1.00	1.06	1.02	
155	-907	-632	-997	-642	-1022	-747	-432	-362	-527	-402	-547	-422	1.34	1.12	1.15	1.30	1.23	
168	-954	-655	-1049	-695	-1084	-804	-480	-385	-580	-455	-610	-480	1.42	1.23	1.28	1.48	1.35	
187	-921	-611	-1006	-661	-1041	-781	-446	-341	-536	-421	-566	-456	1.26	1.14	1.19	1.40	1.25	
200	-879	-589	-964	-619	-984	-734	-404	-319	-494	-379	-509	-409	1.18	1.05	1.07	1.26	1.14	
204	-928	-623	-1028	-698	-1038	-768	-453	-353	-558	-458	-563	-443	1.31	1.19	1.19	1.36	1.26	
218	-886	-591	-976	-651	-1001	-751	-411	-321	-506	-411	-526	-426	1.19	1.08	1.11	1.31	1.17	

November creep using F4 shrinkage (Part 1 of Table)

Time (days)	DEMEC Reading (DR)						Measured creep strain ($\mu\text{m/m}$) $\epsilon_{\text{CST},i}$						Thermal/ Shrinkage strain ($\mu\text{m/m}$)
	1A	1B	2A	2B	3A	3B	1A	1B	2A	2B	3A	3B	
initial	0.040	0.044	0.044	0.040	0.038	0.039	0	0	0	0	0	0	-
0	-0.028	-0.037	-0.027	-0.041	-0.029	-0.047	-340	-405	-355	-405	-335	-430	0
4	-0.053	-0.065	-0.053	-0.071	-0.056	-0.080	-465	-545	-485	-555	-470	-595	-2
6	-0.053	-0.066	-0.051	-0.073	-0.056	-0.079	-465	-550	-475	-565	-470	-590	17
14	-0.058	-0.067	-0.057	-0.076	-0.061	-0.086	-490	-555	-505	-580	-495	-625	4
19	-0.061	-0.071	-0.062	-0.083	-0.068	-0.094	-505	-575	-530	-615	-530	-665	9
22	-0.068	-0.081	-0.070	-0.091	-0.074	-0.100	-540	-625	-570	-655	-560	-695	-27
29	-0.061	-0.074	-0.063	-0.085	-0.067	-0.092	-505	-590	-535	-625	-525	-655	26
33	-0.070	-0.083	-0.069	-0.093	-0.073	-0.099	-550	-635	-565	-665	-555	-690	-9
35	-0.064	-0.077	-0.065	-0.087	-0.069	-0.095	-520	-605	-545	-635	-535	-670	16
39	-0.070	-0.079	-0.066	-0.090	-0.070	-0.097	-550	-615	-550	-650	-540	-680	9
43	-0.069	-0.081	-0.066	-0.089	-0.073	-0.098	-545	-625	-550	-645	-555	-685	11
48	-0.065	-0.082	-0.065	-0.084	-0.070	-0.105	-525	-630	-545	-620	-540	-720	12
65	-0.091	-0.104	-0.089	-0.114	-0.094	-0.117	-655	-740	-665	-770	-660	-780	-25
69	-0.093	-0.103	-0.090	-0.115	-0.096	-0.112	-665	-735	-670	-775	-670	-755	-24
71	-0.088	-0.095	-0.082	-0.106	-0.090	-0.101	-640	-695	-630	-730	-640	-700	25
77	-0.083	-0.092	-0.081	-0.104	-0.087	-0.105	-615	-680	-625	-720	-625	-720	15
85	-0.100	-0.108	-0.097	-0.122	-0.104	-0.120	-700	-760	-705	-810	-710	-795	-44
91	-0.106	-0.111	-0.104	-0.129	-0.108	-0.127	-730	-775	-740	-845	-730	-830	-72
100	-0.112	-0.125	-0.111	-0.140	-0.115	-0.140	-760	-845	-775	-900	-765	-895	-110
104	-0.109	-0.122	-0.109	-0.137	-0.115	-0.143	-745	-830	-765	-885	-765	-910	-75
116	-0.123	-0.135	-0.126	-0.159	-0.129	-0.160	-815	-895	-850	-995	-835	-995	-151
120	-0.122	-0.134	-0.122	-0.155	-0.130	-0.156	-810	-890	-830	-975	-840	-975	-127
127	-0.126	-0.137	-0.124	-0.157	-0.129	-0.162	-830	-905	-840	-985	-835	-1005	-149
133	-0.104	-0.128	-0.102	-0.144	-0.108	-0.142	-720	-860	-730	-920	-730	-905	-52
148	-0.109	-0.122	-0.115	-0.141	-0.122	-0.140	-745	-830	-795	-905	-800	-895	14
155	-0.125	-0.134	-0.125	-0.160	-0.128	-0.160	-825	-890	-845	-1000	-830	-995	-76
168	-0.137	-0.146	-0.137	-0.170	-0.140	-0.177	-885	-950	-905	-1050	-890	-1080	-131
187	-0.130	-0.142	-0.131	-0.161	-0.135	-0.169	-850	-930	-875	-1005	-865	-1040	-101
200	-0.120	-0.132	-0.120	-0.155	-0.131	-0.165	-800	-880	-820	-975	-845	-1020	-80
204	-0.130	-0.144	-0.135	-0.166	-0.132	-0.170	-850	-940	-895	-1030	-850	-1045	-57
218	-0.125	-0.140	-0.124	-0.159	-0.125	-0.161	-825	-920	-840	-995	-815	-1000	-39

November creep using F4 shrinkage (Part 2 of Table)

Time (days)	Measured creep strain less shrinkage and thermal strain ($\mu\text{m/m}$) $\epsilon_{\text{cre},i}$						True creep strain ($\mu\text{m/m}$) $\epsilon_{\text{cr},i}$						Creep coefficient $\phi(t, t_0)$						
	1A	1B	2A	2B	3A	3B	1A	1B	2A	2B	3A	3B	1A	1B	2A	2B	3A	3B	Average
0	-	-	-	-	-	-	0	0	0	0	0	0	0	0	0	0	0	0	0
4	-462	-542	-482	-552	-467	-592	-122	-137	-127	-147	-132	-162	0.36	0.34	0.36	0.36	0.40	0.38	0.37
6	-482	-567	-492	-582	-487	-607	-142	-162	-137	-177	-152	-177	0.42	0.40	0.39	0.44	0.46	0.41	0.42
14	-494	-559	-509	-584	-499	-629	-154	-154	-154	-179	-164	-199	0.45	0.38	0.43	0.44	0.49	0.46	0.44
19	-514	-584	-539	-624	-539	-674	-174	-179	-184	-219	-204	-244	0.51	0.44	0.52	0.54	0.61	0.57	0.53
22	-512	-597	-542	-627	-532	-667	-172	-192	-187	-222	-197	-237	0.51	0.48	0.53	0.55	0.59	0.55	0.53
29	-531	-616	-561	-651	-551	-681	-191	-211	-206	-246	-216	-251	0.56	0.52	0.58	0.61	0.65	0.58	0.58
33	-541	-626	-556	-656	-546	-681	-201	-221	-201	-251	-211	-251	0.59	0.55	0.57	0.62	0.63	0.58	0.59
35	-536	-621	-561	-651	-551	-686	-196	-216	-206	-246	-216	-256	0.58	0.53	0.58	0.61	0.65	0.60	0.59
39	-559	-624	-559	-659	-549	-689	-219	-219	-204	-254	-214	-259	0.64	0.54	0.57	0.63	0.64	0.60	0.60
43	-556	-636	-561	-656	-566	-696	-216	-231	-206	-251	-231	-266	0.64	0.57	0.58	0.62	0.69	0.62	0.62
48	-537	-642	-557	-632	-552	-732	-197	-237	-202	-227	-217	-302	0.58	0.59	0.57	0.56	0.65	0.70	0.61
65	-630	-715	-640	-745	-635	-755	-290	-310	-285	-340	-300	-325	0.85	0.77	0.80	0.84	0.90	0.76	0.82
69	-641	-711	-646	-751	-646	-731	-301	-306	-291	-346	-311	-301	0.89	0.76	0.82	0.85	0.93	0.70	0.82
71	-665	-720	-655	-755	-665	-725	-325	-315	-300	-350	-330	-295	0.96	0.78	0.85	0.86	0.99	0.69	0.85
77	-630	-695	-640	-735	-640	-735	-290	-290	-285	-330	-305	-305	0.85	0.72	0.80	0.81	0.91	0.71	0.80
85	-656	-716	-661	-766	-666	-751	-316	-311	-306	-361	-331	-321	0.93	0.77	0.86	0.89	0.99	0.75	0.86
91	-657	-702	-667	-772	-657	-757	-317	-297	-312	-367	-322	-327	0.93	0.73	0.88	0.91	0.96	0.76	0.86
100	-650	-735	-665	-790	-655	-785	-310	-330	-310	-385	-320	-355	0.91	0.81	0.87	0.95	0.96	0.83	0.89
104	-670	-755	-690	-810	-690	-835	-330	-350	-335	-405	-355	-405	0.97	0.86	0.94	1.00	1.06	0.94	0.96
116	-664	-744	-699	-844	-684	-844	-324	-339	-344	-439	-349	-414	0.95	0.84	0.97	1.08	1.04	0.96	0.97
120	-682	-762	-702	-847	-712	-847	-342	-357	-347	-442	-377	-417	1.01	0.88	0.98	1.09	1.13	0.97	1.01
127	-681	-756	-691	-836	-686	-856	-341	-351	-336	-431	-351	-426	1.00	0.87	0.95	1.06	1.05	0.99	0.99
133	-667	-807	-677	-867	-677	-852	-327	-402	-322	-462	-342	-422	0.96	0.99	0.91	1.14	1.02	0.98	1.00
148	-759	-844	-809	-919	-814	-909	-419	-439	-454	-514	-479	-479	1.23	1.08	1.28	1.27	1.43	1.11	1.23
155	-749	-814	-769	-924	-754	-919	-409	-409	-414	-519	-419	-489	1.20	1.01	1.17	1.28	1.25	1.14	1.17
168	-754	-819	-774	-919	-759	-949	-414	-414	-419	-514	-424	-519	1.22	1.02	1.18	1.27	1.26	1.21	1.19
187	-749	-829	-774	-904	-764	-939	-409	-424	-419	-499	-429	-509	1.20	1.05	1.18	1.23	1.28	1.18	1.19
200	-720	-800	-740	-895	-765	-940	-380	-395	-385	-490	-430	-510	1.12	0.98	1.08	1.21	1.28	1.19	1.14
204	-792	-882	-837	-972	-792	-987	-452	-477	-482	-567	-457	-557	1.33	1.18	1.36	1.40	1.37	1.30	1.32
218	-786	-881	-801	-956	-776	-961	-446	-476	-446	-551	-441	-531	1.31	1.18	1.26	1.36	1.32	1.24	1.28

November creep using F5 shrinkage (Part 1 of Table)

Time (days)	DEMEC Reading (DR)						Measured creep strain ($\mu\text{m/m}$) $\epsilon_{\text{CST},i}$						Thermal/ Shrinkage strain ($\mu\text{m/m}$)
	1A	1B	2A	2B	3A	3B	1A	1B	2A	2B	3A	3B	
initial	0.040	0.044	0.044	0.040	0.038	0.039	0	0	0	0	0	0	-
0	-0.028	-0.037	-0.027	-0.041	-0.029	-0.047	-340	-405	-355	-405	-335	-430	0
4	-0.053	-0.065	-0.053	-0.071	-0.056	-0.080	-465	-545	-485	-555	-470	-595	-2
6	-0.053	-0.066	-0.051	-0.073	-0.056	-0.079	-465	-550	-475	-565	-470	-590	-3
14	-0.058	-0.067	-0.057	-0.076	-0.061	-0.086	-490	-555	-505	-580	-495	-625	-6
19	-0.061	-0.071	-0.062	-0.083	-0.068	-0.094	-505	-575	-530	-615	-530	-665	-8
22	-0.068	-0.081	-0.070	-0.091	-0.074	-0.100	-540	-625	-570	-655	-560	-695	-10
29	-0.061	-0.074	-0.063	-0.085	-0.067	-0.092	-505	-590	-535	-625	-525	-655	-13
33	-0.070	-0.083	-0.069	-0.093	-0.073	-0.099	-550	-635	-565	-665	-555	-690	-14
35	-0.064	-0.077	-0.065	-0.087	-0.069	-0.095	-520	-605	-545	-635	-535	-670	-15
39	-0.070	-0.079	-0.066	-0.090	-0.070	-0.097	-550	-615	-550	-650	-540	-680	-16
43	-0.069	-0.081	-0.066	-0.089	-0.073	-0.098	-545	-625	-550	-645	-555	-685	-18
48	-0.065	-0.082	-0.065	-0.084	-0.070	-0.105	-525	-630	-545	-620	-540	-720	-20
65	-0.091	-0.104	-0.089	-0.114	-0.094	-0.117	-655	-740	-665	-770	-660	-780	-26
69	-0.093	-0.103	-0.090	-0.115	-0.096	-0.112	-665	-735	-670	-775	-670	-755	-27
71	-0.088	-0.095	-0.082	-0.106	-0.090	-0.101	-640	-695	-630	-730	-640	-700	-27
77	-0.083	-0.092	-0.081	-0.104	-0.087	-0.105	-615	-680	-625	-720	-625	-720	-29
85	-0.100	-0.108	-0.097	-0.122	-0.104	-0.120	-700	-760	-705	-810	-710	-795	-32
91	-0.106	-0.111	-0.104	-0.129	-0.108	-0.127	-730	-775	-740	-845	-730	-830	-33
100	-0.112	-0.125	-0.111	-0.140	-0.115	-0.140	-760	-845	-775	-900	-765	-895	-36
104	-0.109	-0.122	-0.109	-0.137	-0.115	-0.143	-745	-830	-765	-885	-765	-910	-37
116	-0.123	-0.135	-0.126	-0.159	-0.129	-0.160	-815	-895	-850	-995	-835	-995	-40
120	-0.122	-0.134	-0.122	-0.155	-0.130	-0.156	-810	-890	-830	-975	-840	-975	-41
127	-0.126	-0.137	-0.124	-0.157	-0.129	-0.162	-830	-905	-840	-985	-835	-1005	-43
133	-0.104	-0.128	-0.102	-0.144	-0.108	-0.142	-720	-860	-730	-920	-730	-905	-44
148	-0.109	-0.122	-0.115	-0.141	-0.122	-0.140	-745	-830	-795	-905	-800	-895	-48
155	-0.125	-0.134	-0.125	-0.160	-0.128	-0.160	-825	-890	-845	-1000	-830	-995	-49
168	-0.137	-0.146	-0.137	-0.170	-0.140	-0.177	-885	-950	-905	-1050	-890	-1080	-52
187	-0.130	-0.142	-0.131	-0.161	-0.135	-0.169	-850	-930	-875	-1005	-865	-1040	-56
200	-0.120	-0.132	-0.120	-0.155	-0.131	-0.165	-800	-880	-820	-975	-845	-1020	-58
204	-0.130	-0.144	-0.135	-0.166	-0.132	-0.170	-850	-940	-895	-1030	-850	-1045	-59
218	-0.125	-0.140	-0.124	-0.159	-0.125	-0.161	-825	-920	-840	-995	-815	-1000	-61

November creep using F5 shrinkage (Part 2 of Table)

Time (days)	Measured creep strain less shrinkage and thermal strain ($\mu\text{m/m}$) $\epsilon_{\text{cre},i}$						True creep strain ($\mu\text{m/m}$) $\epsilon_{\text{cr},i}$						Creep coefficient $\phi(t, t_0)$							
	1A	1B	2A	2B	3A	3B	1A	1B	2A	2B	3A	3B	1A	1B	2A	2B	3A	3B	Average	
0	-	-	-	-	-	-	0	0	0	0	0	0	0	0	0	0	0	0	0	0
4	-463	-543	-483	-553	-468	-593	-123	-138	-128	-148	-133	-163	0.36	0.34	0.36	0.37	0.40	0.38	0.37	
6	-462	-547	-472	-562	-467	-587	-122	-142	-117	-157	-132	-157	0.36	0.35	0.33	0.39	0.39	0.37	0.36	
14	-484	-549	-499	-574	-489	-619	-144	-144	-144	-169	-154	-189	0.42	0.35	0.40	0.42	0.46	0.44	0.42	
19	-496	-566	-521	-606	-521	-656	-156	-161	-166	-201	-186	-226	0.46	0.40	0.47	0.50	0.56	0.53	0.48	
22	-530	-615	-560	-645	-550	-685	-190	-210	-205	-240	-215	-255	0.56	0.52	0.58	0.59	0.64	0.59	0.58	
29	-492	-577	-522	-612	-512	-642	-152	-172	-167	-207	-177	-212	0.45	0.43	0.47	0.51	0.53	0.49	0.48	
33	-536	-621	-551	-651	-541	-676	-196	-216	-196	-246	-206	-246	0.58	0.53	0.55	0.61	0.61	0.57	0.58	
35	-505	-590	-530	-620	-520	-655	-165	-185	-175	-215	-185	-225	0.49	0.46	0.49	0.53	0.55	0.52	0.51	
39	-533	-598	-533	-633	-523	-663	-194	-194	-179	-229	-189	-234	0.57	0.48	0.50	0.56	0.56	0.54	0.54	
43	-527	-607	-532	-627	-537	-667	-187	-202	-177	-222	-202	-237	0.55	0.50	0.50	0.55	0.60	0.55	0.54	
48	-505	-610	-525	-600	-520	-700	-165	-205	-170	-195	-185	-270	0.49	0.51	0.48	0.48	0.55	0.63	0.52	
65	-629	-714	-639	-744	-634	-754	-289	-309	-284	-339	-299	-324	0.85	0.76	0.80	0.84	0.89	0.75	0.82	
69	-638	-708	-643	-748	-643	-728	-298	-303	-288	-343	-308	-298	0.88	0.75	0.81	0.85	0.92	0.69	0.82	
71	-612	-667	-602	-702	-612	-672	-272	-262	-247	-297	-277	-242	0.80	0.65	0.70	0.73	0.83	0.56	0.71	
77	-586	-651	-596	-691	-596	-691	-246	-246	-241	-286	-261	-261	0.72	0.61	0.68	0.71	0.78	0.61	0.68	
85	-668	-728	-673	-778	-678	-763	-328	-323	-318	-373	-343	-333	0.97	0.80	0.90	0.92	1.02	0.77	0.90	
91	-696	-741	-706	-811	-696	-796	-356	-336	-351	-406	-361	-366	1.05	0.83	0.99	1.00	1.08	0.85	0.97	
100	-724	-809	-739	-864	-729	-859	-384	-404	-384	-459	-394	-429	1.13	1.00	1.08	1.13	1.18	1.00	1.09	
104	-708	-793	-728	-848	-728	-873	-368	-388	-373	-443	-393	-443	1.08	0.96	1.05	1.09	1.17	1.03	1.06	
116	-775	-855	-810	-955	-795	-955	-435	-450	-455	-550	-460	-525	1.28	1.11	1.28	1.36	1.37	1.22	1.27	
120	-769	-849	-789	-934	-799	-934	-429	-444	-434	-529	-464	-504	1.26	1.10	1.22	1.31	1.38	1.17	1.24	
127	-787	-862	-797	-942	-792	-962	-447	-457	-442	-537	-457	-532	1.31	1.13	1.25	1.33	1.36	1.24	1.27	
133	-675	-815	-685	-875	-685	-860	-335	-410	-330	-470	-350	-430	0.99	1.01	0.93	1.16	1.05	1.00	1.02	
148	-697	-782	-747	-857	-752	-847	-357	-377	-392	-452	-417	-417	1.05	0.93	1.10	1.12	1.25	0.97	1.07	
155	-775	-840	-795	-950	-780	-945	-436	-436	-441	-545	-446	-516	1.28	1.08	1.24	1.35	1.33	1.20	1.25	
168	-833	-898	-853	-998	-838	-1028	-493	-493	-498	-593	-503	-598	1.45	1.22	1.40	1.46	1.50	1.39	1.40	
187	-794	-874	-819	-949	-809	-984	-454	-469	-464	-544	-474	-554	1.34	1.16	1.31	1.34	1.42	1.29	1.31	
200	-742	-822	-762	-917	-787	-962	-402	-417	-407	-512	-452	-532	1.18	1.03	1.15	1.26	1.35	1.24	1.20	
204	-791	-881	-836	-971	-791	-986	-451	-476	-481	-566	-456	-556	1.33	1.18	1.36	1.40	1.36	1.29	1.32	
218	-763	-858	-778	-933	-753	-938	-424	-454	-424	-529	-419	-509	1.25	1.12	1.19	1.31	1.25	1.18	1.22	

March creep using F4 shrinkage (Part 1 of Table)

Time (days)	DEMEC Reading (DR)						Measured creep strain ($\mu\text{m/m}$) $\epsilon_{\text{CST},i}$						Thermal/ Shrinkage strain ($\mu\text{m/m}$)
	1A	1B	2A	2B	3A	3B	1A	1B	2A	2B	3A	3B	
initial	0.043	0.041	0.035	0.034	0.039	0.032	0	0	0	0	0	0	-
0	-0.062	-0.042	-0.070	-0.037	-0.068	-0.046	-525	-415	-525	-355	-535	-390	0
4	-0.091	-0.067	-0.102	-0.067	-0.103	-0.081	-670	-540	-685	-505	-710	-565	-6
6	-0.092	-0.068	-0.104	-0.072	-0.102	-0.082	-675	-545	-695	-530	-705	-570	8
14	-0.097	-0.070	-0.111	-0.071	-0.112	-0.089	-700	-555	-730	-525	-755	-605	14
19	-0.105	-0.075	-0.122	-0.078	-0.119	-0.099	-740	-580	-785	-560	-790	-655	9
22	-0.113	-0.085	-0.129	-0.088	-0.129	-0.102	-780	-630	-820	-610	-840	-670	-19
29	-0.108	-0.078	-0.123	-0.077	-0.120	-0.094	-755	-595	-790	-555	-795	-630	17
33	-0.116	-0.086	-0.130	-0.086	-0.128	-0.102	-795	-635	-825	-600	-835	-670	-11
35	-0.110	-0.083	-0.126	-0.081	-0.123	-0.097	-765	-620	-805	-575	-810	-645	6
39	-0.113	-0.084	-0.128	-0.084	-0.128	-0.099	-780	-625	-815	-590	-835	-655	9
43	-0.116	-0.086	-0.130	-0.086	-0.127	-0.102	-795	-635	-825	-600	-830	-670	-4
48	-0.118	-0.095	-0.132	-0.095	-0.130	-0.108	-805	-680	-835	-645	-845	-700	8
65	-0.140	-0.108	-0.153	-0.108	-0.150	-0.126	-915	-745	-940	-710	-945	-790	-29
69	-0.140	-0.111	-0.155	-0.110	-0.152	-0.123	-915	-760	-950	-720	-955	-775	-35
71	-0.134	-0.105	-0.147	-0.104	-0.146	-0.117	-885	-730	-910	-690	-925	-745	11
77	-0.131	-0.102	-0.144	-0.099	-0.142	-0.122	-870	-715	-895	-665	-905	-770	9
85	-0.145	-0.115	-0.161	-0.115	-0.159	-0.136	-940	-780	-980	-745	-990	-840	-34
91	-0.152	-0.122	-0.168	-0.124	-0.166	-0.144	-975	-815	-1015	-790	-1025	-880	-55
100	-0.161	-0.129	-0.179	-0.133	-0.172	-0.159	-1020	-850	-1070	-835	-1055	-955	-90
104	-0.160	-0.129	-0.180	-0.133	-0.175	-0.159	-1015	-850	-1075	-835	-1070	-955	-76
116	-0.173	-0.143	-0.196	-0.151	-0.189	-0.179	-1080	-920	-1155	-925	-1140	-1055	-133
120	-0.171	-0.139	-0.192	-0.150	-0.189	-0.174	-1070	-900	-1135	-920	-1140	-1030	-119
127	-0.175	-0.142	-0.196	-0.151	-0.190	-0.176	-1090	-915	-1155	-925	-1145	-1040	-133
133	-0.150	-0.128	-0.183	-0.142	-0.183	-0.168	-965	-845	-1090	-880	-1110	-1000	-41
148	-0.162	-0.127	-0.187	-0.131	-0.165	-0.149	-1025	-840	-1110	-825	-1020	-905	46
155	-0.172	-0.142	-0.197	-0.151	-0.176	-0.168	-1075	-915	-1160	-925	-1075	-1000	-29
168	-0.185	-0.150	-0.208	-0.165	-0.193	-0.184	-1140	-955	-1215	-995	-1160	-1080	-56
187	-0.182	-0.143	-0.199	-0.156	-0.189	-0.177	-1125	-920	-1170	-950	-1140	-1045	-50
200	-0.172	-0.138	-0.194	-0.150	-0.187	-0.174	-1075	-895	-1145	-920	-1130	-1030	-39
204	-0.181	-0.151	-0.204	-0.160	-0.198	-0.170	-1120	-960	-1195	-970	-1185	-1010	-44
218	-0.179	-0.146	-0.194	-0.150	-0.194	-0.167	-1110	-935	-1145	-920	-1165	-995	-8

March creep using F4 shrinkage (Part 2 of Table)

Time (days)	Measured creep strain less shrinkage and thermal strain ($\mu\text{m/m}$) $\epsilon_{\text{Cre},i}$						True creep strain ($\mu\text{m/m}$) $\epsilon_{\text{Cr},i}$						Creep coefficient $\phi(t, t_0)$					
	1A	1B	2A	2B	3A	3B	1A	1B	2A	2B	3A	3B	1A	1B	2A	3A	Average	
0	-	-	-	-	-	-	0	0	0	0	0	0	0	0	0	0	0	0
4	-664	-534	-679	-499	-704	-559	-139	-119	-154	-144	-169	-169	0.26	0.29	0.29	0.32	0.29	
6	-682	-552	-702	-537	-712	-577	-157	-137	-177	-182	-177	-187	0.30	0.33	0.34	0.33	0.33	
14	-714	-569	-744	-539	-769	-619	-189	-154	-219	-184	-234	-229	0.36	0.37	0.42	0.44	0.40	
19	-749	-589	-794	-569	-799	-664	-224	-174	-269	-214	-264	-274	0.43	0.42	0.51	0.49	0.46	
22	-761	-611	-801	-591	-821	-651	-236	-196	-276	-236	-286	-261	0.45	0.47	0.53	0.54	0.50	
29	-772	-612	-807	-572	-812	-647	-247	-197	-282	-217	-277	-257	0.47	0.48	0.54	0.52	0.50	
33	-784	-624	-814	-589	-824	-659	-259	-209	-289	-234	-289	-269	0.49	0.50	0.55	0.54	0.52	
35	-771	-626	-811	-581	-816	-651	-246	-211	-286	-226	-281	-261	0.47	0.51	0.55	0.53	0.51	
39	-789	-634	-824	-599	-844	-664	-264	-219	-299	-244	-309	-274	0.50	0.53	0.57	0.58	0.54	
43	-791	-631	-821	-596	-826	-666	-266	-216	-296	-241	-291	-276	0.51	0.52	0.56	0.54	0.53	
48	-812	-687	-842	-652	-852	-707	-287	-272	-317	-297	-317	-317	0.55	0.66	0.60	0.59	0.60	
65	-886	-716	-911	-681	-916	-761	-361	-301	-386	-326	-381	-371	0.69	0.73	0.74	0.71	0.72	
69	-880	-725	-915	-685	-920	-740	-355	-310	-390	-330	-385	-350	0.68	0.75	0.74	0.72	0.72	
71	-896	-741	-921	-701	-936	-756	-371	-326	-396	-346	-401	-366	0.71	0.79	0.75	0.75	0.75	
77	-879	-724	-904	-674	-914	-779	-354	-309	-379	-319	-379	-389	0.67	0.74	0.72	0.71	0.71	
85	-906	-746	-946	-711	-956	-806	-381	-331	-421	-356	-421	-416	0.73	0.80	0.80	0.79	0.78	
91	-920	-760	-960	-735	-970	-825	-395	-345	-435	-380	-435	-435	0.75	0.83	0.83	0.81	0.81	
100	-930	-760	-980	-745	-965	-865	-405	-345	-455	-390	-430	-475	0.77	0.83	0.87	0.80	0.82	
104	-939	-774	-999	-759	-994	-879	-414	-359	-474	-404	-459	-489	0.79	0.86	0.90	0.86	0.85	
116	-947	-787	-1022	-792	-1007	-922	-422	-372	-497	-437	-472	-532	0.80	0.90	0.95	0.88	0.88	
120	-951	-781	-1016	-801	-1021	-911	-426	-366	-491	-446	-486	-521	0.81	0.88	0.94	0.91	0.88	
127	-957	-782	-1022	-792	-1012	-907	-432	-367	-497	-437	-477	-517	0.82	0.89	0.95	0.89	0.89	
133	-924	-804	-1049	-839	-1069	-959	-399	-389	-524	-484	-534	-569	0.76	0.94	1.00	1.00	0.92	
148	-1071	-886	-1156	-871	-1066	-951	-546	-471	-631	-516	-531	-561	1.04	1.14	1.20	0.99	1.09	
155	-1046	-886	-1131	-896	-1046	-971	-521	-471	-606	-541	-511	-581	0.99	1.14	1.15	0.96	1.06	
168	-1084	-899	-1159	-939	-1104	-1024	-559	-484	-634	-584	-569	-634	1.06	1.17	1.21	1.06	1.13	
187	-1075	-870	-1120	-900	-1090	-995	-550	-455	-595	-545	-555	-605	1.05	1.10	1.13	1.04	1.08	
200	-1036	-856	-1106	-881	-1091	-991	-511	-441	-581	-526	-556	-601	0.97	1.06	1.11	1.04	1.05	
204	-1076	-916	-1151	-926	-1141	-966	-551	-501	-626	-571	-606	-576	1.05	1.21	1.19	1.13	1.15	
218	-1102	-927	-1137	-912	-1157	-987	-577	-512	-612	-557	-622	-597	1.10	1.23	1.17	1.16	1.17	

March creep using F5 shrinkage (Part 1 of Table)

Time (days)	DEMEC Reading (DR)						Measured creep strain ($\mu\text{m/m}$) $\epsilon_{\text{CST},i}$						Thermal/ Shrinkage strain ($\mu\text{m/m}$)
	1A	1B	2A	2B	3A	3B	1A	1B	2A	2B	3A	3B	
initial	0.043	0.041	0.035	0.034	0.039	0.032	0	0	0	0	0	0	-
0	-0.062	-0.042	-0.070	-0.037	-0.068	-0.046	-525	-415	-525	-355	-535	-390	0
4	-0.091	-0.067	-0.102	-0.067	-0.103	-0.081	-670	-540	-685	-505	-710	-565	-5
6	-0.092	-0.068	-0.104	-0.072	-0.102	-0.082	-675	-545	-695	-530	-705	-570	-7
14	-0.097	-0.070	-0.111	-0.071	-0.112	-0.089	-700	-555	-730	-525	-755	-605	-16
19	-0.105	-0.075	-0.122	-0.078	-0.119	-0.099	-740	-580	-785	-560	-790	-655	-21
22	-0.113	-0.085	-0.129	-0.088	-0.129	-0.102	-780	-630	-820	-610	-840	-670	-24
29	-0.108	-0.078	-0.123	-0.077	-0.120	-0.094	-755	-595	-790	-555	-795	-630	-31
33	-0.116	-0.086	-0.130	-0.086	-0.128	-0.102	-795	-635	-825	-600	-835	-670	-34
35	-0.110	-0.083	-0.126	-0.081	-0.123	-0.097	-765	-620	-805	-575	-810	-645	-36
39	-0.113	-0.084	-0.128	-0.084	-0.128	-0.099	-780	-625	-815	-590	-835	-655	-40
43	-0.116	-0.086	-0.130	-0.086	-0.127	-0.102	-795	-635	-825	-600	-830	-670	-43
48	-0.118	-0.095	-0.132	-0.095	-0.130	-0.108	-805	-680	-835	-645	-845	-700	-47
65	-0.140	-0.108	-0.153	-0.108	-0.150	-0.126	-915	-745	-940	-710	-945	-790	-60
69	-0.140	-0.111	-0.155	-0.110	-0.152	-0.123	-915	-760	-950	-720	-955	-775	-62
71	-0.134	-0.105	-0.147	-0.104	-0.146	-0.117	-885	-730	-910	-690	-925	-745	-64
77	-0.131	-0.102	-0.144	-0.099	-0.142	-0.122	-870	-715	-895	-665	-905	-770	-68
85	-0.145	-0.115	-0.161	-0.115	-0.159	-0.136	-940	-780	-980	-745	-990	-840	-72
91	-0.152	-0.122	-0.168	-0.124	-0.166	-0.144	-975	-815	-1015	-790	-1025	-880	-76
100	-0.161	-0.129	-0.179	-0.133	-0.172	-0.159	-1020	-850	-1070	-835	-1055	-955	-81
104	-0.160	-0.129	-0.180	-0.133	-0.175	-0.159	-1015	-850	-1075	-835	-1070	-955	-83
116	-0.173	-0.143	-0.196	-0.151	-0.189	-0.179	-1080	-920	-1155	-925	-1140	-1055	-89
120	-0.171	-0.139	-0.192	-0.150	-0.189	-0.174	-1070	-900	-1135	-920	-1140	-1030	-91
127	-0.175	-0.142	-0.196	-0.151	-0.190	-0.176	-1090	-915	-1155	-925	-1145	-1040	-94
133	-0.150	-0.128	-0.183	-0.142	-0.183	-0.168	-965	-845	-1090	-880	-1110	-1000	-97
148	-0.162	-0.127	-0.187	-0.131	-0.165	-0.149	-1025	-840	-1110	-825	-1020	-905	-103
155	-0.172	-0.142	-0.197	-0.151	-0.176	-0.168	-1075	-915	-1160	-925	-1075	-1000	-106
168	-0.185	-0.150	-0.208	-0.165	-0.193	-0.184	-1140	-955	-1215	-995	-1160	-1080	-111
187	-0.182	-0.143	-0.199	-0.156	-0.189	-0.177	-1125	-920	-1170	-950	-1140	-1045	-117
200	-0.172	-0.138	-0.194	-0.150	-0.187	-0.174	-1075	-895	-1145	-920	-1130	-1030	-122
204	-0.181	-0.151	-0.204	-0.160	-0.198	-0.170	-1120	-960	-1195	-970	-1185	-1010	-123
218	-0.179	-0.146	-0.194	-0.150	-0.194	-0.167	-1110	-935	-1145	-920	-1165	-995	-127

March creep using F5 shrinkage (Part 2 of Table)

Time (days)	Measured creep strain less shrinkage and thermal strain ($\mu\text{m/m}$) $\epsilon_{\text{Cre},i}$						True creep strain ($\mu\text{m/m}$) $\epsilon_{\text{Cr},i}$						Creep coefficient $\phi(t, t_0)$					
	1A	1B	2A	2B	3A	3B	1A	1B	2A	2B	3A	3B	1A	1B	2A	3A	Average	
0	-	-	-	-	-	-	0	0	0	0	0	0	0	0	0	0	0	0
4	-665	-535	-680	-500	-705	-560	-140	-120	-155	-145	-170	-170	0.27	0.29	0.30	0.32	0.29	
6	-668	-538	-688	-523	-698	-563	-143	-123	-163	-168	-163	-173	0.27	0.30	0.31	0.30	0.30	
14	-684	-539	-714	-509	-739	-589	-159	-124	-189	-154	-204	-199	0.30	0.30	0.36	0.38	0.34	
19	-719	-559	-764	-539	-769	-634	-194	-144	-239	-184	-234	-244	0.37	0.35	0.46	0.44	0.40	
22	-756	-606	-796	-586	-816	-646	-231	-191	-271	-231	-281	-256	0.44	0.46	0.52	0.53	0.49	
29	-724	-564	-759	-524	-764	-599	-199	-149	-234	-169	-229	-209	0.38	0.36	0.45	0.43	0.40	
33	-760	-600	-790	-566	-800	-636	-236	-186	-266	-211	-266	-246	0.45	0.45	0.51	0.50	0.47	
35	-729	-584	-769	-539	-774	-609	-204	-169	-244	-184	-239	-219	0.39	0.41	0.46	0.45	0.43	
39	-740	-585	-775	-550	-795	-615	-215	-170	-250	-195	-260	-225	0.41	0.41	0.48	0.49	0.45	
43	-752	-592	-782	-557	-787	-627	-227	-177	-257	-202	-252	-237	0.43	0.43	0.49	0.47	0.45	
48	-758	-633	-788	-598	-798	-653	-233	-218	-263	-243	-263	-263	0.44	0.53	0.50	0.49	0.49	
65	-855	-685	-880	-650	-885	-730	-330	-270	-355	-295	-350	-340	0.63	0.65	0.68	0.65	0.65	
69	-852	-698	-888	-658	-893	-713	-328	-283	-363	-303	-358	-323	0.62	0.68	0.69	0.67	0.67	
71	-821	-666	-846	-626	-861	-681	-296	-251	-321	-271	-326	-291	0.56	0.61	0.61	0.61	0.60	
77	-802	-647	-827	-597	-837	-702	-277	-232	-302	-242	-302	-312	0.53	0.56	0.58	0.57	0.56	
85	-867	-707	-907	-672	-917	-767	-342	-292	-382	-317	-382	-377	0.65	0.70	0.73	0.72	0.70	
91	-899	-739	-939	-714	-949	-804	-374	-324	-414	-359	-414	-414	0.71	0.78	0.79	0.77	0.76	
100	-939	-769	-989	-754	-974	-874	-414	-354	-464	-399	-439	-484	0.79	0.85	0.88	0.82	0.84	
104	-932	-767	-992	-752	-987	-872	-407	-352	-467	-397	-452	-482	0.77	0.85	0.89	0.84	0.84	
116	-991	-831	-1066	-836	-1051	-966	-466	-416	-541	-481	-516	-576	0.89	1.00	1.03	0.96	0.97	
120	-979	-809	-1044	-829	-1049	-939	-454	-394	-519	-474	-514	-549	0.86	0.95	0.99	0.96	0.94	
127	-995	-820	-1060	-830	-1050	-945	-470	-406	-536	-476	-515	-556	0.90	0.98	1.02	0.96	0.96	
133	-868	-748	-993	-783	-1013	-903	-343	-333	-468	-428	-478	-513	0.65	0.80	0.89	0.89	0.81	
148	-921	-736	-1006	-721	-916	-801	-397	-322	-482	-367	-382	-412	0.76	0.77	0.92	0.71	0.79	
155	-969	-809	-1054	-819	-969	-894	-444	-394	-529	-464	-434	-504	0.85	0.95	1.01	0.81	0.90	
168	-1029	-844	-1104	-884	-1049	-969	-504	-429	-579	-529	-514	-579	0.96	1.03	1.10	0.96	1.01	
187	-1007	-802	-1052	-832	-1022	-927	-482	-387	-527	-477	-487	-537	0.92	0.93	1.00	0.91	0.94	
200	-953	-773	-1023	-798	-1008	-908	-428	-358	-498	-443	-473	-518	0.82	0.86	0.95	0.88	0.88	
204	-997	-837	-1072	-847	-1062	-887	-472	-422	-547	-492	-527	-497	0.90	1.02	1.04	0.99	0.99	
218	-983	-808	-1018	-793	-1038	-868	-458	-393	-493	-438	-503	-478	0.87	0.95	0.94	0.94	0.93	

Third Loading

The third loading even corresponds to the instant at which the hinge supporting falsework in F5 was removed. In F4, the hinge supporting falsework was removed simultaneously with the falsework supporting the superstructure. For this reason, creep at third loading is only presented for the April and May concrete batches.

April creep (Part 1 of Table)

Time (days)	DEMEC Reading (DR)						Measured creep strain ($\mu\text{m/m}$) $\epsilon_{\text{CST},i}$						Thermal/Shrinkage strain ($\mu\text{m/m}$)
	1A	1B	2A	2B	3A	3B	1A	1B	2A	2B	3A	3B	
initial	0.004	0.009	0.012	0.012	0.008	0.005	0	0	0	0	0	0	0
0	-0.102	-0.083	-0.090	-0.102	-0.106	-0.091	-530	-460	-510	-570	-570	-480	0
6	-0.114	-0.093	-0.098	-0.108	-0.111	-0.101	-590	-510	-550	-600	-595	-530	-17
11	-0.120	-0.109	-0.105	-0.129	-0.118	-0.126	-620	-590	-585	-705	-630	-655	-46
15	-0.134	-0.114	-0.122	-0.143	-0.138	-0.136	-690	-615	-670	-775	-730	-705	-70
19	-0.140	-0.118	-0.127	-0.153	-0.146	-0.146	-720	-635	-695	-825	-770	-755	-40
31	-0.157	-0.134	-0.146	-0.173	-0.161	-0.164	-805	-715	-790	-925	-845	-845	-116
35	-0.156	-0.136	-0.143	-0.176	-0.159	-0.161	-800	-725	-775	-940	-835	-830	-76
42	-0.162	-0.136	-0.148	-0.180	-0.162	-0.166	-830	-725	-800	-960	-850	-855	-112
48	-0.147	-0.125	-0.135	-0.166	-0.152	-0.166	-755	-670	-735	-890	-800	-855	12
63	-0.149	-0.126	-0.138	-0.167	-0.161	-0.132	-765	-675	-750	-895	-845	-685	97
70	-0.164	-0.137	-0.150	-0.187	-0.163	-0.153	-840	-730	-810	-995	-855	-790	18
83	-0.174	-0.149	-0.162	-0.198	-0.173	-0.173	-890	-790	-870	-1050	-905	-890	-17
102	-0.170	-0.147	-0.159	-0.190	-0.172	-0.174	-870	-780	-855	-1010	-900	-895	18
115	-0.166	-0.142	-0.157	-0.186	-0.165	-0.170	-850	-755	-845	-990	-865	-875	56
119	-0.172	-0.150	-0.164	-0.191	-0.171	-0.164	-880	-795	-880	-1015	-895	-845	14
133	-0.165	-0.142	-0.152	-0.187	-0.161	-0.163	-845	-755	-820	-995	-845	-840	44

April creep (Part 2 of Table)

Time (days)	Measured creep strain less shrinkage and thermal strain ($\mu\text{m/m}$) $\epsilon_{\text{Cre},i}$						True creep strain ($\mu\text{m/m}$) $\epsilon_{\text{Cr},i}$						Creep coefficient $\phi(t_i, t_0)$							
	1A	1B	2A	2B	3A	3B	1A	1B	2A	2B	3A	3B	1A	1B	2A	2B	3A	3B	Average	
0	-530	-460	-510	-570	-570	-480	0	0	0	0	0	0	0	0	0	0	0	0	0	0
6	-572	-492	-532	-582	-577	-512	-42	-32	-22	-12	-7	-32	0.08	0.07	0.04	0.02	0.01	0.07	0.05	
11	-574	-544	-539	-659	-584	-609	-44	-84	-29	-89	-14	-129	0.08	0.18	0.06	0.16	0.02	0.27	0.13	
15	-620	-545	-600	-705	-660	-635	-90	-85	-90	-135	-90	-155	0.17	0.18	0.18	0.24	0.16	0.32	0.21	
19	-680	-595	-655	-785	-730	-715	-150	-135	-145	-215	-160	-235	0.28	0.29	0.28	0.38	0.28	0.49	0.33	
31	-689	-599	-674	-809	-729	-729	-159	-139	-164	-239	-159	-249	0.30	0.30	0.32	0.42	0.28	0.52	0.36	
35	-724	-649	-699	-864	-759	-754	-194	-189	-189	-294	-189	-274	0.37	0.41	0.37	0.52	0.33	0.57	0.43	
42	-717	-612	-687	-847	-737	-742	-188	-152	-177	-277	-167	-262	0.35	0.33	0.35	0.49	0.29	0.55	0.39	
48	-767	-682	-747	-902	-812	-867	-237	-222	-237	-332	-242	-387	0.45	0.48	0.47	0.58	0.43	0.81	0.54	
63	-862	-772	-847	-992	-942	-782	-332	-312	-337	-422	-372	-302	0.63	0.68	0.66	0.74	0.65	0.63	0.67	
70	-857	-747	-827	-1012	-872	-807	-327	-287	-317	-442	-302	-327	0.62	0.63	0.62	0.78	0.53	0.68	0.64	
83	-872	-772	-852	-1032	-887	-872	-342	-312	-342	-462	-317	-392	0.65	0.68	0.67	0.81	0.56	0.82	0.70	
102	-887	-797	-872	-1027	-917	-912	-357	-337	-362	-457	-347	-432	0.67	0.73	0.71	0.80	0.61	0.90	0.74	
115	-906	-811	-901	-1046	-921	-931	-376	-351	-391	-476	-351	-451	0.71	0.76	0.77	0.84	0.62	0.94	0.77	
119	-894	-809	-894	-1029	-909	-859	-364	-349	-384	-459	-339	-379	0.69	0.76	0.75	0.80	0.59	0.79	0.73	
133	-889	-799	-864	-1039	-889	-884	-359	-339	-354	-469	-319	-404	0.68	0.74	0.69	0.82	0.56	0.84	0.72	

May creep (Part 1 of Table)

Time (days)	DEMEC Reading (DR)						Measured creep strain ($\mu\text{m/m}$) $\epsilon_{\text{CST},i}$						Thermal/ Shrinkage strain ($\mu\text{m/m}$)
	1A	1B	2A	2B	3A	3B	1A	1B	2A	2B	3A	3B	
initial	0.012	0.001	0.015	0.020	0.013	0.006	0	0	0	0	0	0	-
0	-0.054	-0.113	-0.045	-0.111	-0.057	-0.115	-330	-570	-300	-655	-350	-605	0
6	-0.060	-0.121	-0.055	-0.122	-0.063	-0.129	-360	-610	-350	-710	-380	-675	-29
11	-0.067	-0.135	-0.059	-0.129	-0.074	-0.144	-395	-680	-370	-745	-435	-750	-56
15	-0.078	-0.148	-0.069	-0.152	-0.085	-0.157	-450	-745	-420	-860	-490	-815	-76
19	-0.080	-0.153	-0.070	-0.159	-0.087	-0.165	-460	-770	-425	-895	-500	-855	-34
31	-0.093	-0.171	-0.085	-0.183	-0.102	-0.182	-525	-860	-500	-1015	-575	-940	-102
35	-0.094	-0.172	-0.085	-0.182	-0.102	-0.181	-530	-865	-500	-1010	-575	-935	-75
42	-0.095	-0.174	-0.086	-0.186	-0.104	-0.188	-535	-875	-505	-1030	-585	-970	-89
48	-0.082	-0.162	-0.074	-0.170	-0.096	-0.171	-470	-815	-445	-950	-545	-885	17
63	-0.082	-0.165	-0.073	-0.176	-0.094	-0.168	-470	-830	-440	-980	-535	-870	82
70	-0.093	-0.176	-0.085	-0.191	-0.101	-0.186	-525	-885	-500	-1055	-570	-960	44
83	-0.102	-0.187	-0.096	-0.201	-0.114	-0.202	-570	-940	-555	-1105	-635	-1040	1
102	-0.099	-0.184	-0.093	-0.196	-0.113	-0.201	-555	-925	-540	-1080	-630	-1035	12
115	-0.093	-0.178	-0.084	-0.187	-0.106	-0.197	-525	-895	-495	-1035	-595	-1015	46
119	-0.102	-0.188	-0.090	-0.201	-0.111	-0.190	-570	-945	-525	-1105	-620	-980	10
133	-0.095	-0.182	-0.094	-0.192	-0.105	-0.190	-535	-915	-545	-1060	-590	-980	47

May creep (Part 2 of Table)

Time (days)	Measured creep strain less shrinkage and thermal strain ($\mu\text{m/m}$) $\epsilon_{\text{cre},i}$						True creep strain ($\mu\text{m/m}$) $\epsilon_{\text{cr},i}$						Creep coefficient $\phi(t_i, t_0)$							
	1A	1B	2A	2B	3A	3B	1A	1B	2A	2B	3A	3B	1A	1B	2A	2B	3A	3B	Average	
0	-	-	-	-	-	-	0	0	0	0	0	0	0	0	0	0	0	0	0	0
6	-331	-581	-321	-681	-351	-646	-1	-11	-21	-26	-1	-41	0.00	0.02	0.07	0.04	0.00	0.07	0.03	
11	-339	-624	-314	-689	-379	-694	-9	-54	-14	-34	-29	-89	0.03	0.09	0.05	0.05	0.08	0.15	0.07	
15	-374	-669	-344	-784	-414	-739	-44	-99	-44	-129	-64	-134	0.13	0.17	0.15	0.20	0.18	0.22	0.18	
19	-426	-736	-391	-861	-466	-821	-96	-166	-91	-206	-116	-216	0.29	0.29	0.30	0.31	0.33	0.36	0.32	
31	-423	-758	-397	-912	-472	-838	-93	-188	-98	-257	-123	-233	0.28	0.33	0.33	0.39	0.35	0.38	0.34	
35	-455	-790	-425	-935	-500	-860	-125	-220	-125	-280	-150	-255	0.38	0.39	0.42	0.43	0.43	0.42	0.41	
42	-446	-786	-416	-941	-496	-881	-116	-216	-116	-286	-146	-276	0.35	0.38	0.39	0.44	0.42	0.46	0.41	
48	-487	-832	-462	-967	-562	-902	-157	-262	-162	-312	-212	-297	0.48	0.46	0.54	0.48	0.61	0.49	0.51	
63	-552	-912	-522	-1062	-617	-952	-222	-342	-222	-407	-267	-347	0.67	0.60	0.74	0.62	0.76	0.57	0.66	
70	-569	-929	-544	-1099	-614	-1004	-239	-359	-244	-444	-264	-399	0.72	0.63	0.81	0.68	0.75	0.66	0.71	
83	-571	-941	-556	-1106	-636	-1041	-241	-371	-256	-451	-286	-436	0.73	0.65	0.85	0.69	0.82	0.72	0.74	
102	-567	-937	-552	-1092	-642	-1047	-237	-367	-252	-437	-292	-442	0.72	0.64	0.84	0.67	0.84	0.73	0.74	
115	-571	-941	-541	-1081	-641	-1061	-241	-371	-241	-426	-291	-456	0.73	0.65	0.80	0.65	0.83	0.75	0.74	
119	-580	-955	-535	-1115	-630	-990	-250	-385	-235	-460	-280	-385	0.76	0.68	0.78	0.70	0.80	0.64	0.73	
133	-582	-962	-592	-1107	-637	-1027	-252	-392	-292	-452	-287	-422	0.77	0.69	0.97	0.69	0.82	0.70	0.77	

Measured Data from Material Testing: Shrinkage

Shrinkage in concrete begins immediately upon the onset of hydration. The shrinkage for each batch of concrete was measured; however, the shrinkage in F4 concrete (October, November, and March) was not measured until the application of prestress. Shrinkage in F5 (April and May) was measured beginning at the start of drying.

October shrinkage from F4

Time (days)	DEMEC Reading (DR)				Measured shrinkage strain $\epsilon_{ST,i}$				Temp. (°C)	Thermal strain (m/m) $\alpha\Delta T$	True shrinkage strain (m/m) $\epsilon_{sh}(t_i, t_s)$				
	1A	1B	2A	2B	1A	1B	2A	2B			1A	1B	2A	2B	Average
0	0.014	0.022	0.017	0.008	0	0	0	0	14.5	0	0	0	0	0	
6	-0.002	0.004	-0.004	-0.010	-80	-90	-105	-90	15.0	6.0	-86	-96	-111	-96	-97
10	-0.009	-0.002	-0.011	-0.020	-115	-120	-140	-140	14.2	-3.6	-111	-116	-136	-136	-125
13	-0.018	-0.013	-0.023	-0.030	-160	-175	-200	-190	16.5	24.0	-184	-199	-224	-214	-205
17	-0.018	-0.020	-0.028	-0.036	-160	-210	-225	-220	16.6	25.2	-185	-235	-250	-245	-229
20	-0.028	-0.020	-0.028	-0.041	-210	-210	-225	-245	15.2	8.4	-218	-218	-233	-253	-231
24	-0.028	-0.022	-0.030	-0.042	-210	-220	-235	-250	16.5	24.0	-234	-244	-259	-274	-253
27	-0.015	-0.013	-0.020	-0.034	-145	-175	-185	-210	16.0	18.0	-163	-193	-203	-228	-197
31	-0.006	-0.031	-0.026	-0.044	-100	-265	-215	-260	16.0	18.0	-118	-283	-233	-278	-228
41	-0.032	-0.019	-0.033	-0.047	-230	-205	-250	-275	18.0	42.0	-272	-247	-292	-317	-282
45	-0.037	-0.021	-0.037	-0.047	-255	-215	-270	-275	20.4	70.8	-326	-286	-341	-346	-325
48	-0.035	-0.032	-0.038	-0.048	-245	-270	-275	-280	17.2	32.4	-277	-302	-307	-312	-300
55	-0.036	-0.026	-0.036	-0.046	-250	-240	-265	-270	16.0	18.0	-268	-258	-283	-288	-274
59	-0.040	-0.031	-0.042	-0.052	-270	-265	-295	-300	17.2	32.4	-302	-297	-327	-332	-315
73	-0.038	-0.029	-0.033	-0.050	-260	-255	-250	-290	18.5	48.0	-308	-303	-298	-338	-312
80	-0.041	-0.029	-0.038	-0.051	-275	-255	-275	-295	19.0	54.0	-329	-309	-329	-349	-329
85	-0.041	-0.036	-0.041	-0.053	-275	-290	-290	-305	21.0	78.0	-353	-368	-368	-383	-368
87	-0.047	-0.038	-0.045	-0.060	-305	-300	-310	-340	17.4	34.8	-340	-335	-345	-375	-349
92	-0.047	-0.039	-0.044	-0.060	-305	-305	-305	-340	19.0	54.0	-359	-359	-359	-394	-368
104	-0.050	-0.046	-0.048	-0.062	-320	-340	-325	-350	18.6	49.2	-369	-389	-374	-399	-383
106	-0.053	-0.044	-0.045	-0.062	-335	-330	-310	-350	18.0	42.0	-377	-372	-352	-392	-373
122	-0.042	-0.029	-0.036	-0.048	-280	-255	-265	-280	21.1	79.2	-359	-334	-344	-359	-349
135	-0.040	-0.037	-0.040	-0.051	-270	-295	-285	-295	21.2	80.4	-350	-375	-365	-375	-367
139	-0.047	-0.045	-0.046	-0.056	-305	-335	-315	-320	19.4	58.8	-364	-394	-374	-379	-378
149	-0.046	-0.039	-0.043	-0.054	-300	-305	-300	-310	22.0	90.0	-390	-395	-390	-400	-394
157	-0.049	-0.045	-0.044	-0.061	-315	-335	-305	-345	18.4	46.8	-362	-382	-352	-392	-372
164	-0.043	-0.038	-0.038	-0.052	-285	-300	-275	-300	20.0	66.0	-351	-366	-341	-366	-356
168	-0.046	-0.043	-0.043	-0.056	-300	-325	-300	-320	18.3	45.6	-346	-371	-346	-366	-357
178	-0.043	-0.042	-0.039	-0.055	-285	-320	-280	-315	17.2	32.4	-317	-352	-312	-347	-332
183	-0.047	-0.043	-0.042	-0.052	-305	-325	-295	-300	21.0	78.0	-383	-403	-373	-378	-384
200	-0.048	-0.045	-0.046	-0.057	-310	-335	-315	-325	17.8	39.6	-350	-375	-355	-365	-361
206	-0.042	-0.038	-0.037	-0.049	-280	-300	-270	-285	17.1	31.2	-311	-331	-301	-316	-315
212	-0.043	-0.036	-0.040	-0.045	-285	-290	-285	-265	17.0	30.0	-315	-320	-315	-295	-311
220	-0.059	-0.055	-0.052	-0.062	-365	-385	-345	-350	15.1	7.2	-372	-392	-352	-357	-368
226	-0.061	-0.059	-0.055	-0.068	-375	-405	-360	-380	16.0	18.0	-393	-423	-378	-398	-398
235	-0.064	-0.066	-0.065	-0.071	-390	-440	-410	-395	18.5	48.0	-438	-488	-458	-443	-457
239	-0.059	-0.058	-0.054	-0.064	-365	-400	-355	-360	18.0	42.0	-407	-442	-397	-402	-412
251	-0.079	-0.075	-0.072	-0.081	-465	-485	-445	-445	11.5	-36.0	-429	-449	-409	-409	-424
255	-0.070	-0.069	-0.069	-0.079	-420	-455	-430	-435	15.0	6.0	-426	-461	-436	-441	-441
262	-0.074	-0.069	-0.072	-0.081	-440	-455	-445	-445	11.4	-37.2	-403	-418	-408	-408	-409
268	-0.057	-0.053	-0.051	-0.062	-355	-375	-340	-350	17.5	36.0	-391	-411	-376	-386	-391
283	-0.059	-0.041	-0.027	-0.071	-365	-315	-220	-395	15.0	6.0	-371	-321	-226	-401	-330
290	-0.067	-0.053	-0.045	-0.075	-405	-375	-310	-415	10.0	-54.0	-351	-321	-256	-361	-322
303	-0.072	-0.072	-0.057	-0.083	-430	-470	-370	-455	11.0	-42.0	-388	-428	-328	-413	-389
322	-0.069	-0.067	-0.056	-0.079	-415	-445	-365	-435	13.0	-18.0	-397	-427	-347	-417	-397
335	-0.059	-0.064	-0.063	-0.074	-365	-430	-400	-410	18.9	52.8	-418	-483	-453	-463	-454
339	-0.079	-0.045	-0.079	-0.055	-465	-335	-480	-315	11.7	-33.6	-431	-301	-446	-281	-365
353	-0.051	-0.056	-0.055	-0.061	-325	-390	-360	-345	13.4	-13.2	-312	-377	-347	-332	-342

November shrinkage from F4

Time (days)	DEMEC Reading (DR)				Measured shrinkage strain $\epsilon_{ST,I}$				Thermal Temp. (°C)	Thermal strain (m/m) $\alpha\Delta T$	True shrinkage strain (m/m) $\epsilon_{sh}(t_i, t_s)$				
	1A	1B	2A	2B	1A	1B	2A	2B			1A	1B	2A	2B	Average
0	0.012	0.022	0.020	-0.002	0	0	0	0	14.5	0	0	0	0	0	
6	-0.006	0.001	-0.001	-0.022	-90	-105	-105	-100	15.0	6.0	-96	-111	-111	-106	-106
10	-0.016	-0.004	-0.012	-0.030	-140	-130	-160	-140	14.2	-3.6	-136	-126	-156	-136	-139
13	-0.027	-0.010	-0.020	-0.043	-195	-160	-200	-205	16.5	24.0	-219	-184	-224	-229	-214
17	-0.025	-0.020	-0.026	-0.048	-185	-210	-230	-230	16.6	25.2	-210	-235	-255	-255	-239
20	-0.036	-0.025	-0.020	-0.013	-240	-235	-200	-55	15.2	8.4	-248	-243	-208	-63	-191
24	-0.023	-0.038	-0.032	-0.057	-175	-300	-260	-275	16.5	24.0	-199	-324	-284	-299	-276
27	-0.025	-0.015	-0.021	-0.049	-185	-185	-205	-235	16.0	18.0	-203	-203	-223	-253	-220
31	-0.037	-0.018	-0.041	-0.042	-245	-200	-305	-200	16.0	18.0	-263	-218	-323	-218	-255
41	-0.048	-0.028	-0.044	-0.065	-300	-250	-320	-315	18.0	42.0	-342	-292	-362	-357	-338
45	-0.050	-0.031	-0.047	-0.069	-310	-265	-335	-335	20.4	70.8	-381	-336	-406	-406	-382
48	-0.052	-0.037	-0.050	-0.072	-320	-295	-350	-350	17.2	32.4	-352	-327	-382	-382	-361
55	-0.046	-0.033	-0.046	-0.070	-290	-275	-330	-340	16.0	18.0	-308	-293	-348	-358	-327
59	-0.054	-0.041	-0.055	-0.077	-330	-315	-375	-375	17.2	32.4	-362	-347	-407	-407	-381
73	-0.051	-0.041	-0.051	-0.076	-315	-315	-355	-370	18.5	48.0	-363	-363	-403	-418	-387
80	-0.058	-0.036	-0.056	-0.079	-350	-290	-380	-385	19.0	54.0	-404	-344	-434	-439	-405
85	-0.059	-0.042	-0.056	-0.082	-355	-320	-380	-400	21.0	78.0	-433	-398	-458	-478	-442
87	-0.065	-0.050	-0.063	-0.088	-385	-360	-415	-430	17.4	34.8	-420	-395	-450	-465	-432
92	-0.064	-0.051	-0.060	-0.086	-380	-365	-400	-420	19.0	54.0	-434	-419	-454	-474	-445
104	-0.063	-0.051	-0.067	-0.093	-375	-365	-435	-455	18.6	49.2	-424	-414	-484	-504	-457
106	-0.063	-0.051	-0.062	-0.089	-375	-365	-410	-435	18.0	42.0	-417	-407	-452	-477	-438
122	-0.051	-0.041	-0.059	-0.080	-315	-315	-395	-390	21.1	79.2	-394	-394	-474	-469	-433
135	-0.055	-0.043	-0.060	-0.083	-335	-325	-400	-405	21.2	80.4	-415	-405	-480	-485	-447
139	-0.062	-0.050	-0.065	-0.092	-370	-360	-425	-450	19.4	58.8	-429	-419	-484	-509	-460
149	-0.058	-0.048	-0.066	-0.092	-350	-350	-430	-450	22.0	90.0	-440	-440	-520	-540	-485
157	-0.069	-0.051	-0.073	-0.096	-405	-365	-465	-470	18.4	46.8	-452	-412	-512	-517	-473
164	-0.057	-0.042	-0.062	-0.085	-345	-320	-410	-415	20.0	66.0	-411	-386	-476	-481	-438
168	-0.066	-0.050	-0.067	-0.091	-390	-360	-435	-445	18.3	45.6	-436	-406	-481	-491	-453
178	-0.062	-0.044	-0.065	-0.087	-370	-330	-425	-425	17.2	32.4	-402	-362	-457	-457	-420
183	-0.060	-0.047	-0.063	-0.087	-360	-345	-415	-425	21.0	78.0	-438	-423	-493	-503	-464
200	-0.067	-0.055	-0.069	-0.096	-395	-385	-445	-470	17.8	39.6	-435	-425	-485	-510	-463
206	-0.063	-0.045	-0.055	-0.084	-375	-335	-375	-410	17.1	31.2	-406	-366	-406	-441	-405
212	-0.064	-0.044	-0.060	-0.087	-380	-330	-400	-425	17.0	30.0	-410	-360	-430	-455	-414
220	-0.074	-0.059	-0.071	-0.098	-430	-405	-455	-480	15.1	7.2	-437	-412	-462	-487	-450
226	-0.080	-0.065	-0.076	-0.104	-460	-435	-480	-510	16.0	18.0	-478	-453	-498	-528	-489
235	-0.086	-0.072	-0.084	-0.113	-490	-470	-520	-555	18.5	48.0	-538	-518	-568	-603	-557
239	-0.077	-0.064	-0.078	-0.108	-445	-430	-490	-530	18.0	42.0	-487	-472	-532	-572	-516
251	-0.091	-0.079	-0.097	-0.121	-515	-505	-585	-595	11.5	-36.0	-479	-469	-549	-559	-514
255	-0.087	-0.074	-0.094	-0.114	-495	-480	-570	-560	15.0	6.0	-501	-486	-576	-566	-532
262	-0.093	-0.079	-0.097	-0.117	-525	-505	-585	-575	11.4	-37.2	-488	-468	-548	-538	-510
268	-0.072	-0.060	-0.080	-0.097	-420	-410	-500	-475	17.5	36.0	-456	-446	-536	-511	-487
283	-0.060	-0.052	-0.060	-0.084	-360	-370	-400	-410	15.0	6.0	-366	-376	-406	-416	-391
290	-0.074	-0.070	-0.082	-0.102	-430	-460	-510	-500	10.0	-54.0	-376	-406	-456	-446	-421
303	-0.099	-0.078	-0.088	-0.107	-555	-500	-540	-525	11.0	-42.0	-513	-458	-498	-483	-488
322	-0.090	-0.072	-0.081	-0.105	-510	-470	-505	-515	13.0	-18.0	-492	-452	-487	-497	-482
335	-0.085	-0.062	-0.083	-0.101	-485	-420	-515	-495	18.9	52.8	-538	-473	-568	-548	-532
339	-0.084	-0.063	-0.063	-0.103	-480	-425	-415	-505	11.7	-33.6	-446	-391	-381	-471	-423
353	-0.074	-0.069	-0.067	-0.088	-430	-455	-435	-430	13.4	-13.2	-417	-442	-422	-417	-424

March shrinkage from F4

Time (days)	DEMEC Reading (DR)				Measured shrinkage strain $\epsilon_{ST,I}$				Thermal strain (m/m)		True shrinkage strain (m/m) $\epsilon_{sh}(t_i, t_s)$				
	1A	1B	2A	2B	1A	1B	2A	2B	Temp. (°C)	$\alpha\Delta T$	1A	1B	2A	2B	Average
0	-0.027	-0.002	-0.003	-0.020	0	0	0	0	14.5	0	0	0	0	0	0
6	-0.043	-0.013	-0.020	-0.037	-80	-55	-85	-84	15.0	6.0	-86	-61	-91	-90	-82
10	-0.056	-0.011	-0.031	-0.041	-145	-45	-140	-104	14.2	-3.6	-141	-41	-136	-100	-105
13	-0.064	-0.022	-0.026	-0.055	-185	-100	-115	-174	16.5	24.0	-209	-124	-139	-198	-167
17	-0.071	-0.027	-0.047	-0.060	-220	-125	-220	-199	16.6	25.2	-245	-150	-245	-224	-216
20	-0.079	-0.037	-0.052	-0.068	-260	-175	-245	-239	15.2	8.4	-268	-183	-253	-247	-238
24	-0.084	-0.041	-0.053	-0.074	-285	-195	-250	-269	16.5	24.0	-309	-219	-274	-293	-274
27	-0.078	-0.033	-0.047	-0.067	-255	-155	-220	-234	16.0	18.0	-273	-173	-238	-252	-234
31	-0.075	-0.022	-0.040	-0.065	-240	-100	-185	-224	16.0	18.0	-258	-118	-203	-242	-205
41	-0.090	-0.043	-0.063	-0.079	-315	-205	-300	-294	18.0	42.0	-357	-247	-342	-336	-320
45	-0.098	-0.052	-0.067	-0.082	-355	-250	-320	-309	20.4	70.8	-426	-321	-391	-379	-379
48	-0.100	-0.061	-0.076	-0.090	-365	-295	-365	-349	17.2	32.4	-397	-327	-397	-381	-376
55	-0.102	-0.061	-0.075	-0.090	-375	-295	-360	-349	16.0	18.0	-393	-313	-378	-367	-363
59	-0.109	-0.068	-0.085	-0.100	-410	-330	-410	-399	17.2	32.4	-442	-362	-442	-431	-420
73	-0.112	-0.071	-0.087	-0.097	-425	-345	-420	-384	18.5	48.0	-473	-393	-468	-432	-441
80	-0.114	-0.069	-0.087	-0.096	-435	-335	-420	-379	19.0	54.0	-489	-389	-474	-433	-446
85	-0.113	-0.074	-0.089	-0.099	-430	-360	-430	-394	21.0	78.0	-508	-438	-508	-472	-481
87	-0.126	-0.083	-0.095	-0.104	-495	-405	-460	-419	17.4	34.8	-530	-440	-495	-453	-479
92	-0.122	-0.080	-0.096	-0.106	-475	-390	-465	-429	19.0	54.0	-529	-444	-519	-483	-494
104	-0.133	-0.080	-0.102	-0.110	-530	-390	-495	-449	18.6	49.2	-579	-439	-544	-498	-515
106	-0.125	-0.084	-0.093	-0.109	-490	-410	-450	-444	18.0	42.0	-532	-452	-492	-486	-490
122	-0.116	-0.076	-0.089	-0.104	-445	-370	-430	-419	21.1	79.2	-524	-449	-509	-498	-495
135	-0.121	-0.080	-0.089	-0.108	-470	-390	-430	-439	21.2	80.4	-550	-470	-510	-519	-513
139	-0.127	-0.086	-0.097	-0.112	-500	-420	-470	-459	19.4	58.8	-559	-479	-529	-517	-521
149	-0.124	-0.083	-0.091	-0.108	-485	-405	-440	-439	22.0	90.0	-575	-495	-530	-529	-532
157	-0.130	-0.089	-0.098	-0.115	-515	-435	-475	-474	18.4	46.8	-562	-482	-522	-520	-521
164	-0.124	-0.081	-0.088	-0.110	-485	-395	-425	-449	20.0	66.0	-551	-461	-491	-515	-504
168	-0.130	-0.089	-0.094	-0.113	-515	-435	-455	-464	18.3	45.6	-561	-481	-501	-509	-513
178	-0.128	-0.086	-0.093	-0.113	-505	-420	-450	-464	17.2	32.4	-537	-452	-482	-496	-492
183	-0.126	-0.085	-0.093	-0.107	-495	-415	-450	-434	21.0	78.0	-573	-493	-528	-512	-526
200	-0.134	-0.091	-0.096	-0.119	-535	-445	-465	-494	17.8	39.6	-575	-485	-505	-533	-524
206	-0.127	-0.080	-0.083	-0.118	-500	-390	-400	-489	17.1	31.2	-531	-421	-431	-520	-476
212	-0.128	-0.081	-0.086	-0.115	-505	-395	-415	-474	17.0	30.0	-535	-425	-445	-504	-477
220	-0.136	-0.091	-0.094	-0.123	-545	-445	-455	-514	15.1	7.2	-552	-452	-462	-521	-497
226	-0.140	-0.096	-0.097	-0.128	-565	-470	-470	-539	16.0	18.0	-583	-488	-488	-557	-529
235	-0.147	-0.104	-0.104	-0.134	-600	-510	-505	-569	18.5	48.0	-648	-558	-553	-617	-594
239	-0.145	-0.099	-0.104	-0.130	-590	-485	-505	-549	18.0	42.0	-632	-527	-547	-591	-574
251	-0.151	-0.112	-0.121	-0.139	-620	-550	-590	-594	11.5	-36.0	-584	-514	-554	-558	-552
255	-0.150	-0.109	-0.116	-0.137	-615	-535	-565	-584	15.0	6.0	-621	-541	-571	-590	-581
262	-0.155	-0.111	-0.120	-0.137	-640	-545	-585	-584	11.4	-37.2	-603	-508	-548	-546	-551
268	-0.134	-0.096	-0.106	-0.114	-535	-470	-515	-469	17.5	36.0	-571	-506	-551	-505	-533
283	-0.105	-0.076	-0.070	-0.129	-390	-370	-335	-544	15.0	6.0	-396	-376	-341	-550	-416
290	-0.128	-0.092	-0.082	-0.138	-505	-450	-395	-589	10.0	-54.0	-451	-396	-341	-535	-431
303	-0.134	-0.100	-0.089	-0.139	-535	-490	-430	-594	11.0	-42.0	-493	-448	-388	-552	-470
322	-0.132	-0.101	-0.095	-0.129	-525	-495	-460	-544	13.0	-18.0	-507	-477	-442	-526	-488
335	-0.142	-0.092	-0.102	-0.112	-575	-450	-495	-459	18.9	52.8	-628	-503	-548	-511	-547
339	-0.112	-0.112	-0.078	-0.150	-425	-550	-375	-649	11.7	-33.6	-391	-516	-341	-615	-466
353	-0.130	-0.092	-0.089	-0.112	-515	-450	-430	-459	13.4	-13.2	-502	-437	-417	-445	-450

April shrinkage from F5

Time (days)	DEMEC Reading (DR)				Measured shrinkage strain $\epsilon_{ST,i}$				Temp. (°C)	Thermal strain (m/m) $\alpha\Delta T$	True shrinkage strain (m/m) $\epsilon_{sh}(t_i, t_s)$				
	1A	1B	2A	2B	1A	1B	2A	2B			1A	1B	2A	2B	Average
0	0.018	-0.023	0.025	0.028	0	0	0	0	20.0	0	0	0	0	0	
7	-0.014	-0.033	-0.005	0.012	-160	-50	-150	-80	14.0	-72.0	-88	22	-78	-8	-38
10	-0.029	-0.056	-0.021	-0.008	-235	-165	-230	-180	16.5	-42.0	-193	-123	-188	-138	-161
13	-0.034	-0.056	-0.019	-0.009	-260	-165	-220	-185	16.0	-48.0	-212	-117	-172	-137	-160
17	-0.033	-0.058	-0.020	-0.013	-255	-175	-225	-205	16.0	-48.0	-207	-127	-177	-157	-167
27	-0.066	-0.081	-0.049	-0.038	-420	-290	-370	-330	18.0	-24.0	-396	-266	-346	-306	-329
29	-0.067	-0.087	-0.052	-0.044	-425	-320	-385	-360	16.9	-37.2	-388	-283	-348	-323	-335
31	-0.069	-0.091	-0.059	-0.046	-435	-340	-420	-370	20.4	4.8	-440	-345	-425	-375	-396
34	-0.073	-0.093	-0.067	-0.048	-455	-350	-460	-380	17.2	-33.6	-422	-317	-427	-346	-378
38	-0.074	-0.093	-0.062	-0.045	-460	-350	-435	-365	19.7	-3.6	-457	-347	-432	-361	-399
38	-0.074	-0.093	-0.062	-0.045	-460	-350	-435	-365	19.7	-3.6	-457	-347	-432	-361	-399
41	-0.081	-0.102	-0.072	-0.059	-495	-395	-485	-435	16.0	-48.0	-447	-347	-437	-387	-405
45	-0.089	-0.107	-0.072	-0.069	-535	-420	-485	-485	17.2	-33.6	-502	-387	-452	-452	-448
59	-0.098	-0.114	-0.084	-0.071	-580	-455	-545	-495	18.4	-19.2	-561	-436	-526	-476	-500
66	-0.106	-0.117	-0.091	-0.083	-620	-470	-580	-555	19.0	-12.0	-608	-458	-568	-543	-545
71	-0.110	-0.123	-0.095	-0.080	-640	-500	-600	-540	21.0	12.0	-652	-512	-612	-552	-582
72	-0.115	-0.121	-0.094	-0.085	-665	-490	-595	-565	18.0	-24.0	-641	-466	-571	-541	-555
73	-0.118	-0.123	-0.095	-0.083	-680	-500	-600	-555	17.5	-30.0	-650	-470	-570	-525	-554
78	-0.117	-0.125	-0.102	-0.086	-675	-510	-635	-570	19.0	-12.0	-663	-498	-623	-558	-586
90	-0.124	-0.130	-0.111	-0.089	-710	-535	-680	-585	18.6	-16.8	-694	-519	-664	-568	-611
92	-0.129	-0.129	-0.104	-0.086	-735	-530	-645	-570	18.0	-24.0	-711	-506	-621	-546	-596
108	-0.113	-0.122	-0.096	-0.083	-655	-495	-605	-555	21.1	13.2	-669	-509	-618	-568	-591
125	-0.127	-0.132	-0.108	-0.094	-725	-545	-665	-610	19.4	-7.2	-718	-538	-658	-603	-629
135	-0.124	-0.129	-0.106	-0.092	-710	-530	-655	-600	22.0	24.0	-734	-554	-679	-624	-648
143	-0.131	-0.135	-0.117	-0.095	-745	-560	-710	-615	18.4	-19.2	-726	-541	-691	-596	-639
150	-0.133	-0.132	-0.113	-0.098	-756	-545	-690	-630	20.0	0.0	-756	-545	-690	-630	-655
154	-0.136	-0.139	-0.122	-0.104	-771	-580	-735	-660	18.3	-20.4	-750	-560	-715	-640	-666
164	-0.137	-0.134	-0.124	-0.099	-776	-555	-745	-635	17.2	-33.6	-742	-522	-712	-602	-644
169	-0.136	-0.145	-0.121	-0.103	-771	-610	-730	-655	21.0	12.0	-783	-622	-742	-667	-704
186	-0.142	-0.145	-0.135	-0.106	-801	-610	-801	-670	17.8	-26.4	-774	-584	-774	-644	-694
192	-0.117	-0.142	-0.142	-0.072	-675	-595	-836	-500	17.1	-34.8	-641	-561	-801	-465	-617
198	-0.121	-0.137	-0.123	-0.084	-695	-570	-740	-560	17.0	-36.0	-659	-534	-704	-524	-606
206	-0.140	-0.145	-0.137	-0.097	-791	-610	-811	-625	15.1	-58.8	-732	-552	-752	-567	-650
212	-0.144	-0.149	-0.140	-0.100	-811	-630	-826	-640	16.0	-48.0	-763	-582	-778	-592	-679
221	-0.156	-0.157	-0.146	-0.116	-871	-671	-856	-720	18.5	-18.0	-853	-653	-838	-702	-761
225	-0.148	-0.152	-0.139	-0.112	-831	-645	-821	-700	18.0	-24.0	-807	-621	-797	-676	-725
237	-0.168	-0.165	-0.152	-0.127	-931	-711	-886	-775	11.5	-102.0	-829	-609	-784	-673	-724
241	-0.155	-0.160	-0.143	-0.122	-866	-686	-841	-750	15.0	-60.0	-806	-626	-781	-690	-726
248	-0.163	-0.163	-0.155	-0.128	-906	-701	-901	-780	11.4	-103.2	-803	-597	-797	-677	-719
254	-0.140	-0.141	-0.125	-0.103	-791	-590	-750	-655	17.5	-30.0	-761	-560	-720	-625	-667
269	-0.136	-0.112	-0.095	-0.098	-771	-445	-600	-630	15.0	-60.0	-711	-385	-540	-570	-552
276	-0.148	-0.124	-0.109	-0.124	-831	-505	-670	-760	10.0	-120.0	-711	-385	-550	-640	-572
289	-0.155	-0.136	-0.127	-0.115	-866	-565	-760	-715	11.0	-108.0	-758	-457	-652	-607	-619
308	-0.148	-0.129	-0.120	-0.108	-831	-530	-725	-680	13.0	-84.0	-747	-446	-641	-596	-608
321	-0.141	-0.119	-0.123	-0.091	-796	-480	-740	-595	18.9	-13.2	-782	-467	-727	-582	-640
325	-0.116	-0.158	-0.112	-0.122	-670	-676	-685	-750	11.7	-99.6	-571	-576	-586	-651	-596
339	-0.131	-0.138	-0.126	-0.089	-745	-575	-755	-585	13.4	-79.2	-666	-496	-676	-506	-586

May shrinkage from F5

Time (days)	DEMEC Reading (DR)				Measured shrinkage strain $\epsilon_{ST,i}$				Thermal Temp. (°C)	Thermal strain (m/m) $\alpha\Delta T$	True shrinkage strain (m/m) $\epsilon_{sh}(t_i, t_s)$				
	1A	1B	2A	2B	1A	1B	2A	2B			1A	1B	2A	2B	Average
0	0.055	0.070	0.063	0.088	0	0	0	0	20.4	0	0	0	0	0	
3	0.024	0.031	0.032	0.046	-155	-195	-155	-210	17.2	-38.4	-117	-157	-117	-172	-140
7	0.019	0.025	0.026	0.039	-180	-225	-185	-245	19.7	-8.4	-172	-217	-177	-237	-200
7	0.019	0.025	0.026	0.039	-180	-225	-185	-245	21.7	15.6	-196	-241	-201	-261	-224
10	0.007	0.010	0.017	0.028	-240	-300	-230	-300	16.0	-52.8	-187	-247	-177	-247	-215
14	-0.007	-0.002	0.004	0.020	-310	-360	-295	-340	17.2	-38.4	-272	-322	-257	-302	-288
28	-0.027	-0.018	-0.016	0.003	-410	-440	-395	-425	18.5	-22.8	-387	-417	-372	-402	-395
35	-0.035	-0.022	-0.018	-0.005	-450	-460	-405	-465	19.0	-16.8	-433	-443	-388	-448	-428
40	-0.043	-0.037	-0.037	-0.015	-490	-535	-500	-515	21.0	7.2	-497	-542	-507	-522	-517
41	-0.042	-0.035	-0.033	-0.013	-485	-525	-480	-505	18.1	-27.6	-458	-497	-452	-477	-471
42	-0.046	-0.036	-0.038	-0.019	-505	-530	-505	-535	17.4	-36.0	-469	-494	-469	-499	-483
47	-0.045	-0.042	-0.037	-0.021	-500	-560	-500	-545	19.0	-16.8	-483	-543	-483	-528	-510
59	-0.061	-0.056	-0.052	-0.030	-580	-630	-575	-590	18.6	-21.6	-559	-609	-554	-568	-572
61	-0.055	-0.044	-0.039	-0.022	-550	-570	-510	-550	18.0	-28.8	-521	-541	-481	-521	-516
77	-0.051	-0.038	-0.036	-0.020	-530	-540	-495	-540	21.1	8.4	-539	-549	-503	-548	-535
94	-0.067	-0.058	-0.055	-0.037	-610	-640	-590	-625	19.4	-12.0	-598	-628	-578	-613	-604
104	-0.066	-0.055	-0.051	-0.036	-605	-625	-570	-620	22.0	19.2	-624	-644	-589	-639	-624
112	-0.073	-0.063	-0.060	-0.045	-640	-665	-615	-665	18.4	-24.0	-616	-641	-591	-641	-622
119	-0.074	-0.060	-0.061	-0.040	-645	-650	-620	-640	20.0	-4.8	-640	-645	-615	-635	-634
123	-0.079	-0.065	-0.066	-0.048	-670	-675	-645	-680	18.3	-25.2	-645	-650	-620	-655	-643
133	-0.081	-0.063	-0.069	-0.047	-680	-665	-660	-675	17.2	-38.4	-642	-627	-622	-637	-632
138	-0.079	-0.073	-0.068	-0.055	-670	-715	-655	-715	21.0	7.2	-677	-722	-662	-722	-696
155	-0.086	-0.075	-0.073	-0.058	-705	-725	-680	-730	17.8	-31.2	-674	-694	-649	-699	-679
161	-0.084	-0.062	-0.068	-0.049	-695	-660	-655	-685	17.1	-39.6	-656	-621	-616	-646	-634
167	-0.078	-0.061	-0.068	-0.051	-665	-655	-655	-695	17.0	-40.8	-624	-614	-614	-654	-627
175	-0.087	-0.074	-0.074	-0.064	-710	-720	-685	-760	15.1	-63.6	-647	-657	-622	-697	-655
181	-0.091	-0.079	-0.082	-0.070	-730	-745	-725	-790	16.0	-52.8	-678	-692	-672	-737	-695
190	-0.102	-0.090	-0.089	-0.079	-785	-800	-760	-835	18.5	-22.8	-763	-778	-738	-813	-773
194	-0.095	-0.080	-0.081	-0.070	-750	-750	-720	-790	18.0	-28.8	-722	-722	-691	-761	-724
206	-0.108	-0.095	-0.096	-0.082	-815	-825	-795	-850	11.5	-106.8	-709	-719	-689	-744	-715
210	-0.102	-0.091	-0.091	-0.075	-785	-805	-770	-815	15.0	-64.8	-721	-741	-706	-751	-729
217	-0.104	-0.093	-0.092	-0.081	-795	-815	-775	-845	11.4	-108.0	-687	-707	-667	-737	-700
223	-0.080	-0.072	-0.073	-0.060	-675	-710	-680	-740	17.5	-34.8	-640	-675	-645	-705	-667
238	-0.055	-0.073	-0.050	-0.055	-550	-715	-565	-715	15.0	-64.8	-485	-650	-500	-650	-572
245	-0.070	-0.080	-0.053	-0.061	-625	-750	-580	-745	10.0	-124.8	-500	-626	-455	-620	-550
258	-0.078	-0.080	-0.067	-0.073	-665	-750	-650	-805	11.0	-112.8	-552	-638	-537	-692	-605
277	-0.077	-0.076	-0.066	-0.070	-660	-730	-645	-790	13.0	-88.8	-571	-641	-556	-701	-618
290	-0.078	-0.069	-0.064	-0.051	-665	-695	-635	-695	18.9	-18.0	-647	-677	-617	-677	-655
294	-0.070	-0.091	-0.052	-0.078	-625	-805	-575	-830	11.7	-104.4	-521	-701	-471	-726	-605
308	-0.072	-0.066	-0.065	-0.058	-635	-680	-640	-730	13.4	-84.0	-551	-596	-556	-646	-587

Appendix B

Calculations

Determination of Moment of Inertia of Superstructure: Comparison of results of configuration approximations

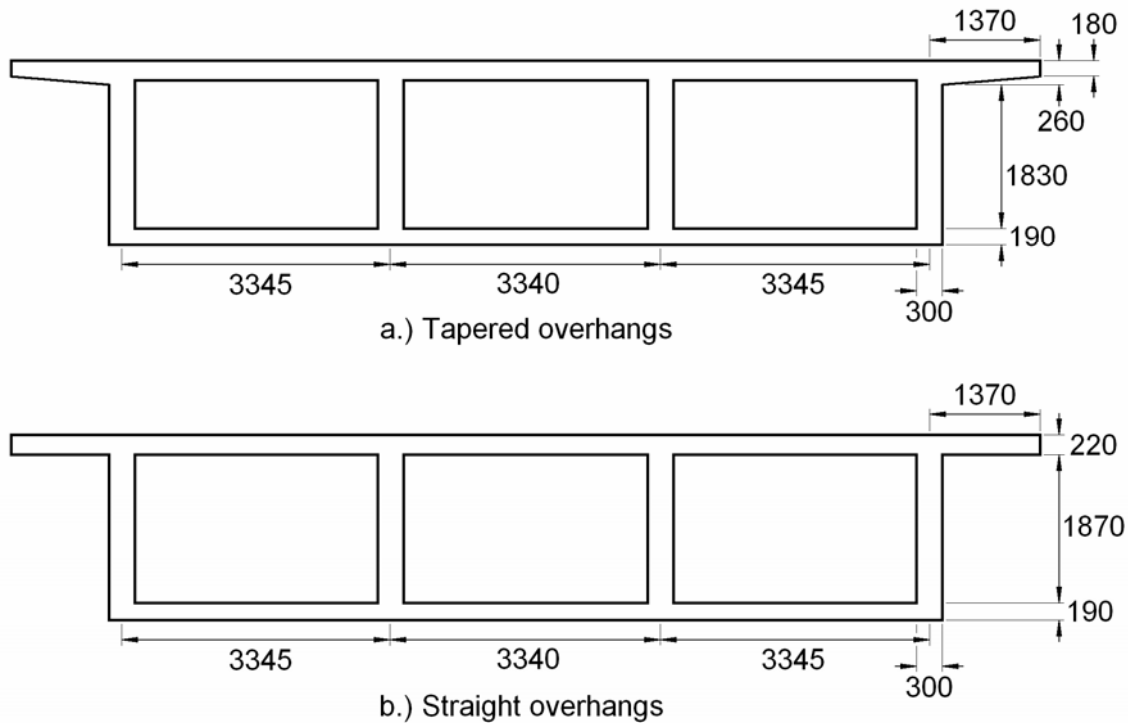


Figure B1: Bridge cross section in actual and idealized layouts (all units in mm).

Moment of inertia for superstructure with tapered overhangs

$$\bar{y} = \frac{\sum Ay}{\sum A}$$

$$\begin{aligned} & [220(10330)110] + [180(1220)(2)90] + \left[1220 \left(\frac{80}{2} \right) (2) \left(\frac{80}{3} + 180 \right) \right] \\ \bar{y} = & \frac{+ [1870(1200)1200] + [190(10330)2185]}{[220(10330)] + [180(1220)(2)] + [1220(80)] + [1870(1200)] + [190(10330)]} \\ \bar{y} = & \frac{[(0.250) + (0.040) + (0.020) + (2.592) + (4.288)](10^{12})}{[(2.273) + (0.439) + (0.098) + (2.244) + (1.963)](10^6)} \end{aligned}$$

$$\bar{y} = 1024.786 \text{ mm}$$

$$I = \sum AD^2 + I_0$$

$$\begin{aligned} \sum AD^2 = & [180(2440)(1024.786 - 90)^2] + \left[80(1220) \left(1024.786 - 90 - 2 \left(\frac{80}{3} \right) \right)^2 \right] \\ & + [220(10330)(1024.786 - 110)^2] + [1870(1200)(1155 - 1024.694)^2] \\ & + [190(10330)(2185 - 1024.694)^2] \end{aligned}$$

$$\sum AD^2 = [(0.384) + (0.076) + (1.902) + (0.038) + (2.642)] 10^{12}$$

$$\sum AD^2 = 5.041(10^{12})$$

$$\begin{aligned} I_0 = & \frac{80(2440)^3 + 80(2440)^2 1200 + 80(1220)^3 2440}{36} + \frac{2440(180)^3}{12} \\ & + \frac{10330(220)^3}{12} + \frac{1200(1870)^3}{12} + \frac{10330(190)^3}{12} \end{aligned}$$

$$I_0 = [(0.0242) + (0.0012) + (0.0092) + (653.92) + (5.904)] 10^9$$

$$I_0 = 0.694(10^{12})$$

$$I = \sum AD^2 + I_0 = (5.041 + 0.694)(10^{12})$$

$$I = 5.74(10^{12}) \text{ mm}^4$$

Moment of inertia for superstructure with straight overhangs

$$\bar{y} = \frac{\sum Ay}{\sum A}$$

$$\bar{y} = \frac{[220(12770)110] + [1870(1200)1200] + [190(10330)2185]}{[220(12770)] + [1870(1200)] + [190(10330)]}$$

$$\bar{y} = \frac{[(0.309) + (2.592) + (4.288)](10^{12})}{[(2.809) + (2.244) + (1.963)](10^9)}$$

$$\bar{y} = 1024.694 \text{ mm}$$

$$I = \sum AD^2 + I_0$$

$$\sum AD^2 = [220(12770)(1024.694 - 110)^2] + [1870(1200)(1155 - 1024.694)^2] \\ + [190(10330)(2185 - 1024.694)^2]$$

$$\sum AD^2 = [(2.3505) + (0.0381) + (2.6424)]10^{12}$$

$$\sum AD^2 = 5.031(10^{12})$$

$$I_0 = \frac{12770(220)^3}{12} + \frac{1200(1870)^3}{12} + \frac{10330(190)^3}{12}$$

$$I_0 = [(11.33) + (653.92) + (5.90)]10^9$$

$$I_0 = 0.671(10^{12})$$

$$I = \sum AD^2 + I_0 = (5.031 + 0.671)(10^{12})$$

$$I = 5.70(10^{12}) \text{ mm}^4$$

Moment of inertia for superstructure with non-prestressed reinforcement

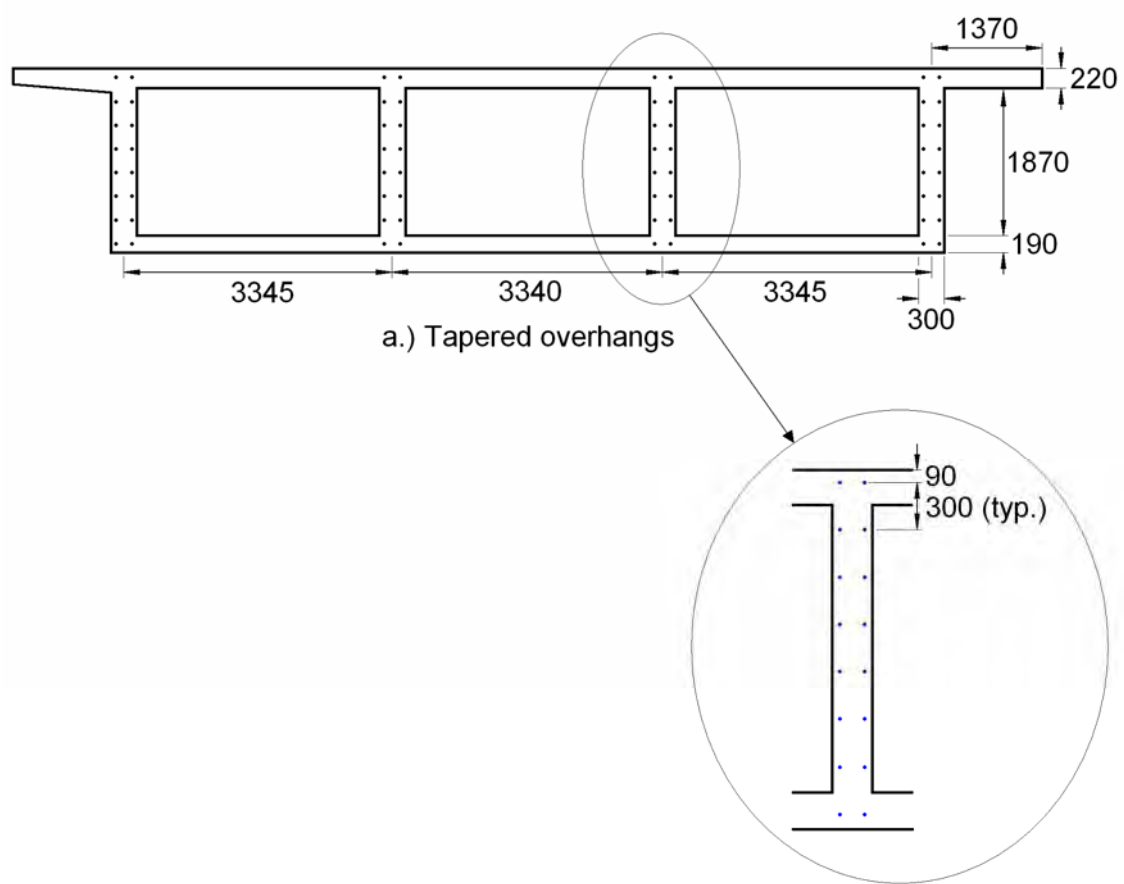


Figure B2: Bridge cross section showing addition of non-prestressed steel (all units in mm).

$$\bar{y} = \frac{\sum Ay}{\sum A}$$

$$\bar{y} = \frac{[220(12770)]110 + [1870(1200)]1200 + [190(10330)]2185 + \left[1064(90 + 390 + 690 + 990 + 1290 + 1590 + 1890 + 2190) \left(\frac{200}{32} - 1\right)\right]}{[220(12770)] + [1870(1200)] + [190(10330)] + \left[1064(8) \left(\frac{200}{32} - 1\right)\right]}$$

$$\bar{y} = \frac{[(0.309) + (2.592) + (4.288) + (0.051)](10^{12})}{[(2.809) + (2.244) + (1.963)](10^9) + (44.6)(10^3)}$$

$$\bar{y} = 1032.639 \text{ mm}$$

$$I = \sum AD^2 + I_0$$

$$\begin{aligned} \sum AD^2 = & [220(12770)(1024.694 - 110)^2] + [1870(1200)(1155 - 1024.694)^2] \\ & + [190(10330)(2185 - 1024.694)^2] \\ & + [5586((943)^2 + (643)^2 + (343)^2 + (43)^2 + (257)^2 + (557)^2 + (857)^2 + (1157)^2)] \end{aligned}$$

$$\sum AD^2 = [(2.3505) + (0.0381) + (2.6424) + (0.022)]10^{12}$$

$$\sum AD^2 = 5.053(10^{12})$$

$$I_0 = \frac{12770(220)^3}{12} + \frac{1200(1870)^3}{12} + \frac{10330(190)^3}{12}$$

$$I_0 = [(11.33) + (653.92) + (5.90)]10^9$$

$$I_0 = 0.671(10^{12})$$

$$I = \sum AD^2 + I_0 = (5.053 + 0.671)(10^{12})$$

$$I = 5.72(10^{12}) \text{ mm}^4$$

Calculations for idealization of horizontally curved bridge as plane

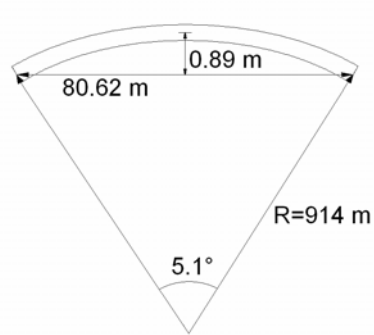


Figure B3: Layout and geometry of horizontal bridge curvature.

$$\frac{0.89}{80.62} = 1.11\% < 2.5\%$$

Appendix C

Monitored strains and temperatures

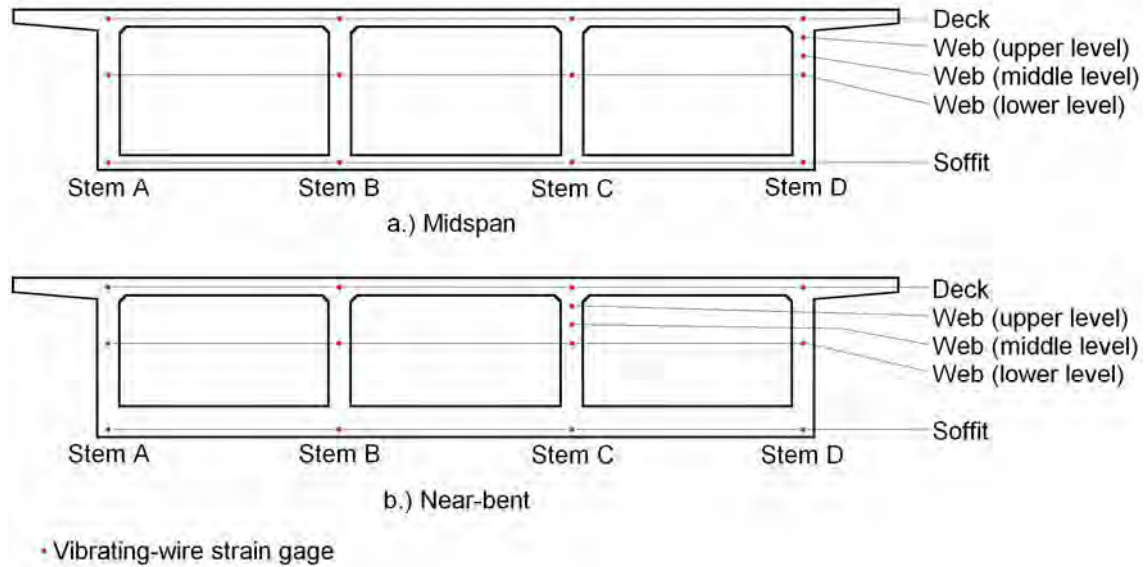


Figure C1: Locations of vibrating wire strain gages in representative bridge cross sections.

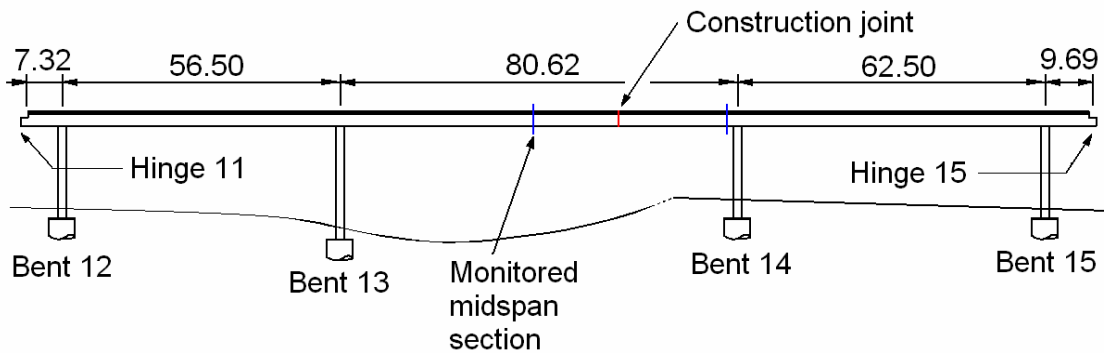
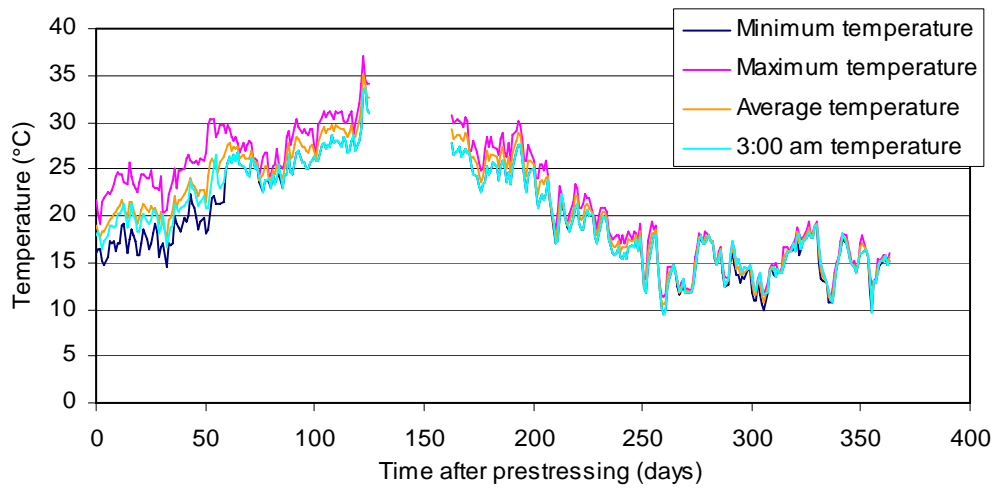
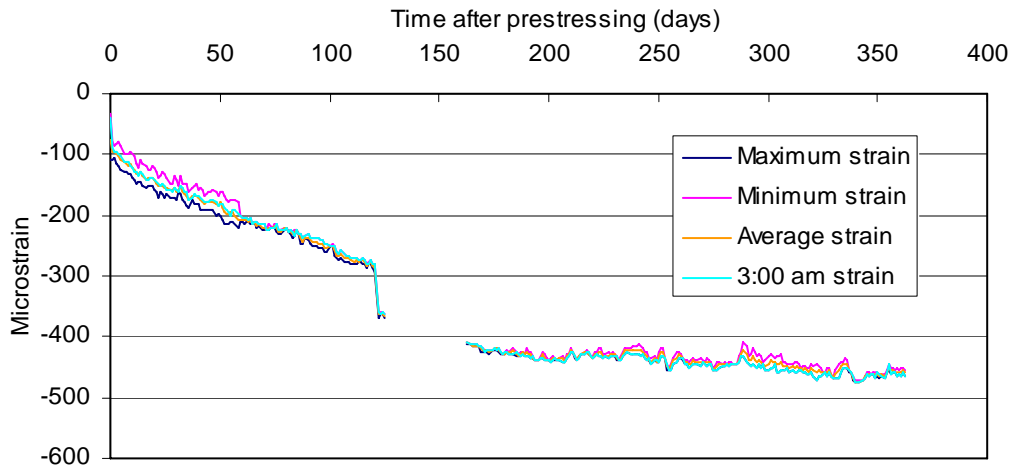


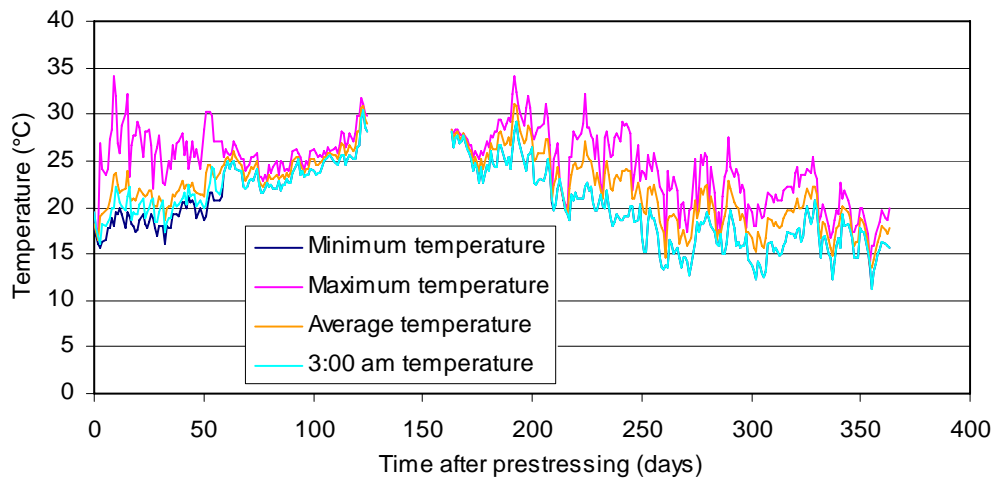
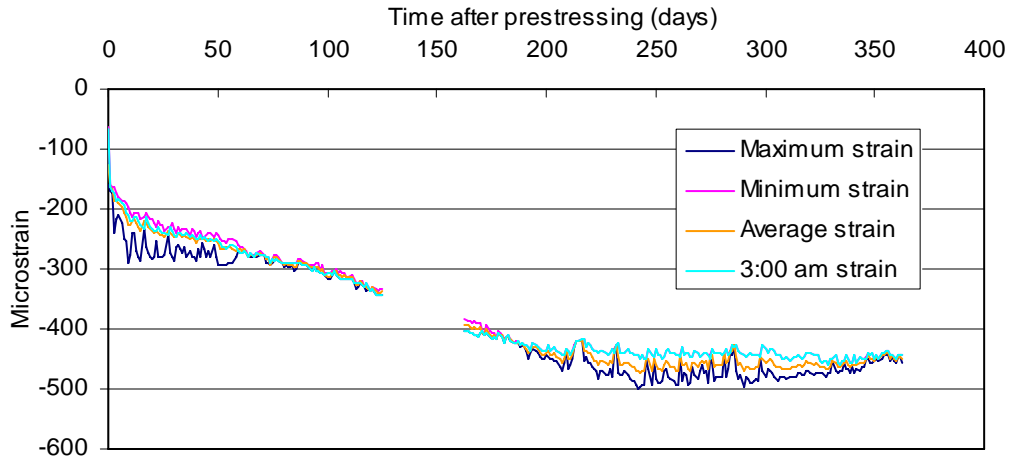
Figure C2: Location of gages at the midspan section in F4.

Frame 4 Midspan

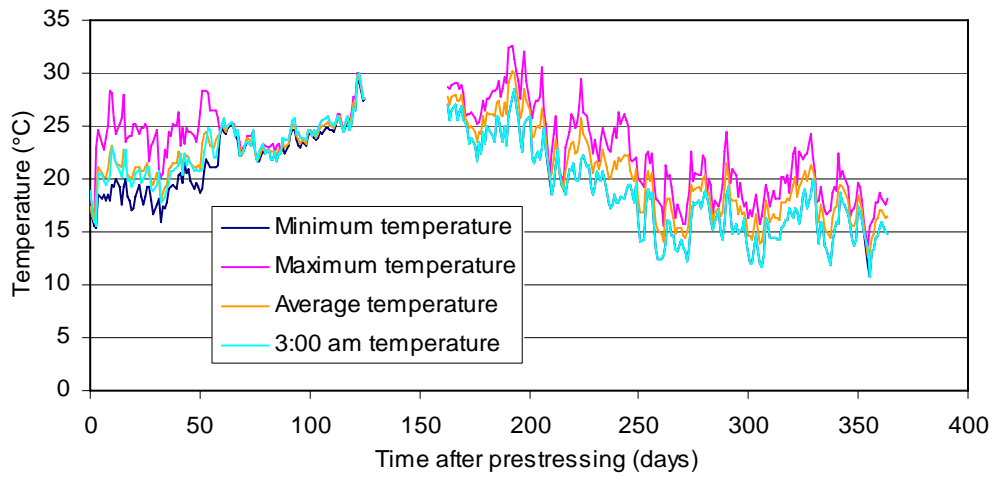
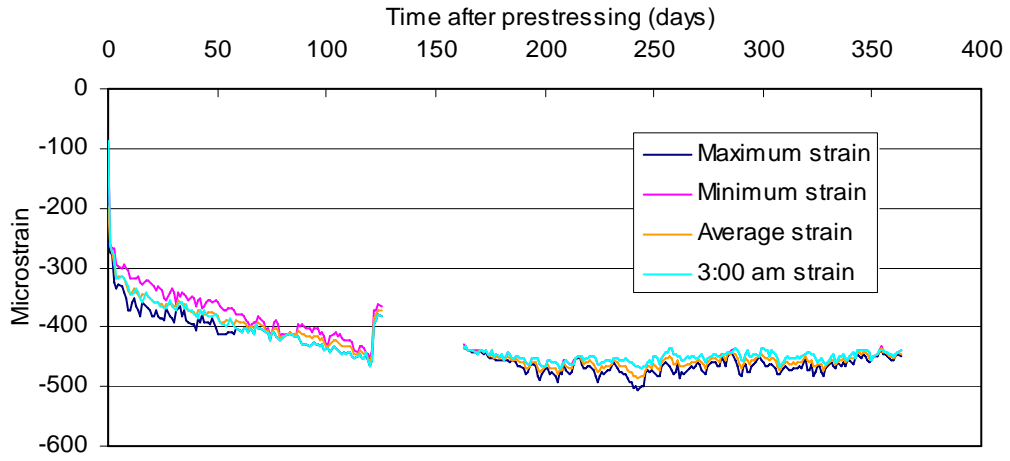
Stem A deck



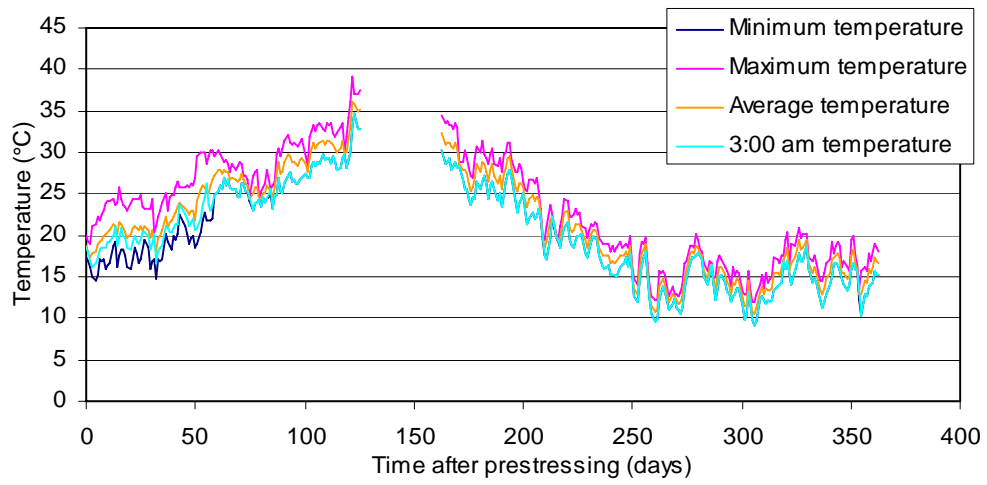
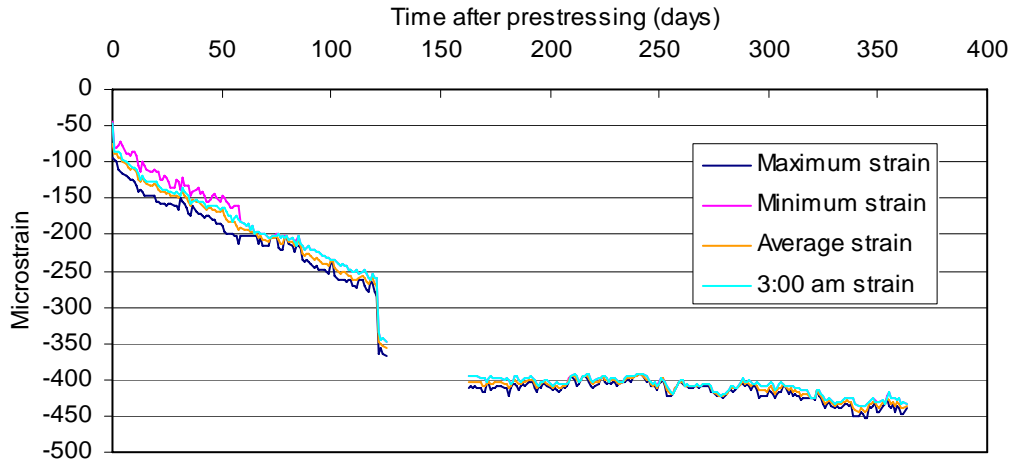
Stem A web



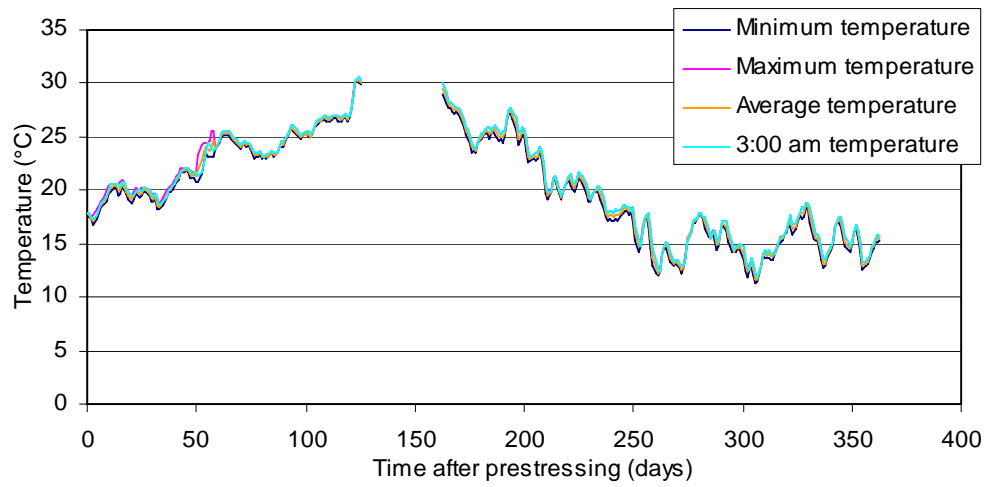
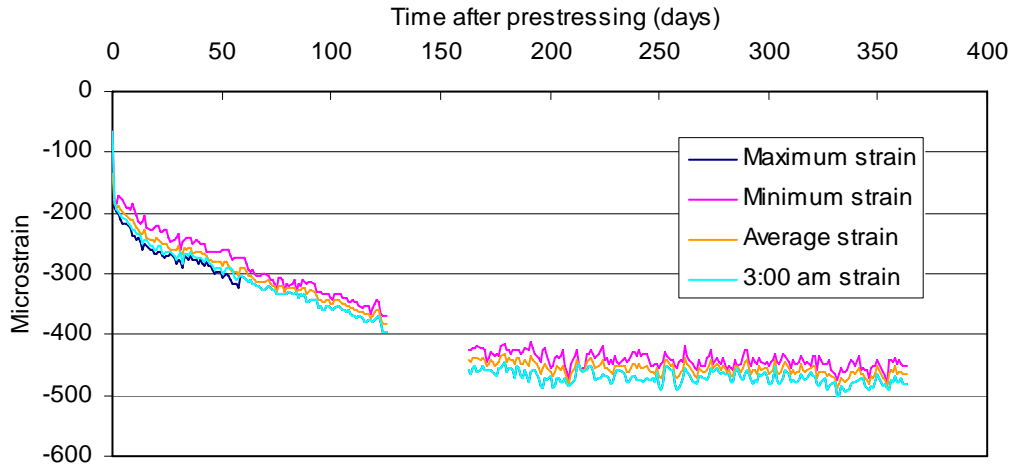
Stem A soffit



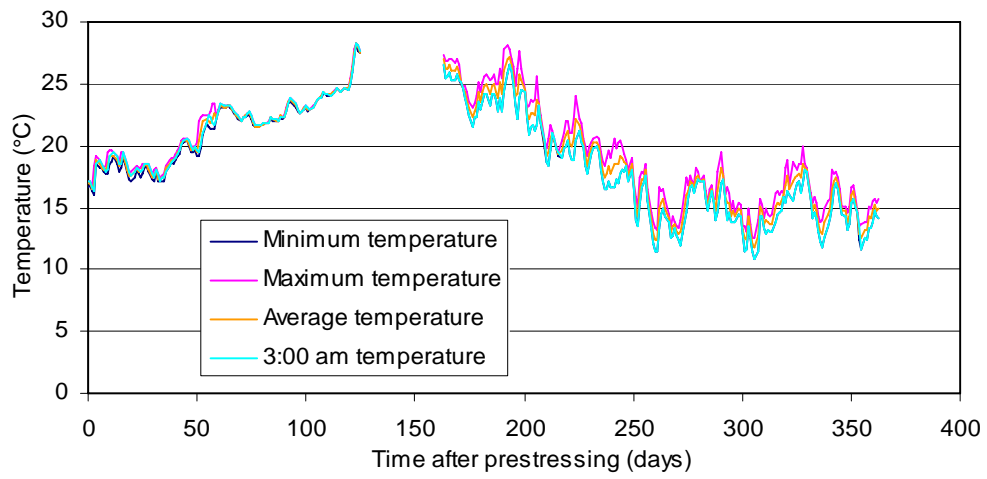
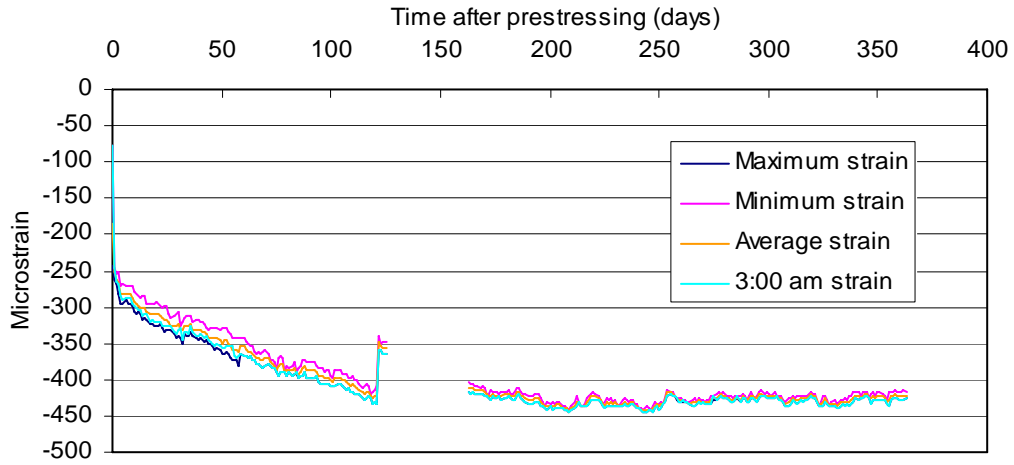
Stem B deck



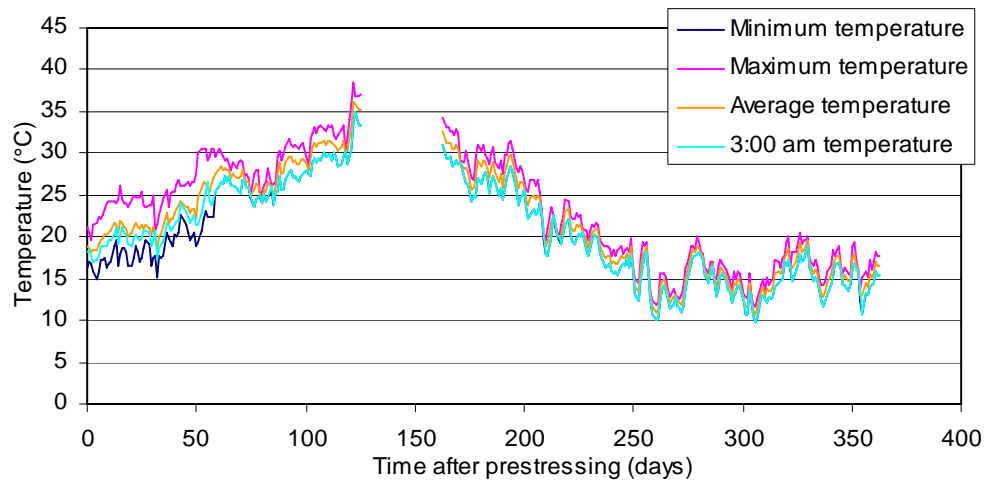
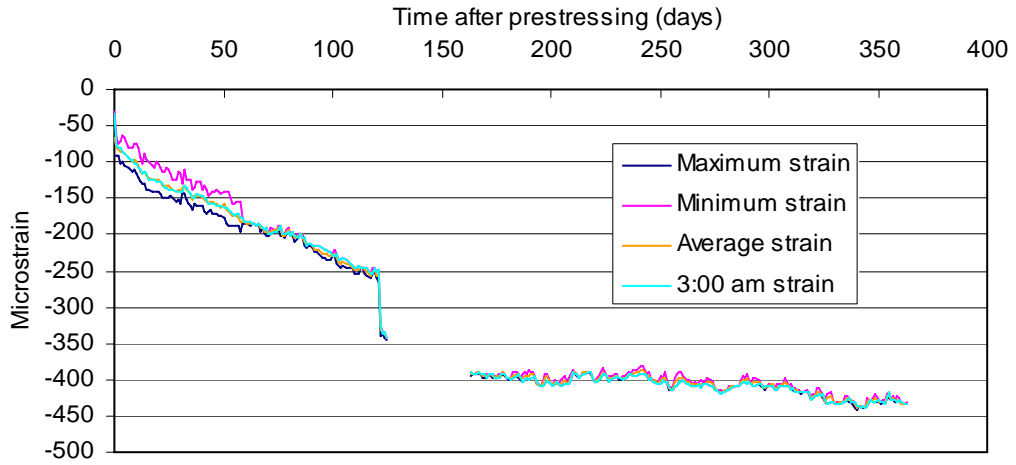
Stem B web



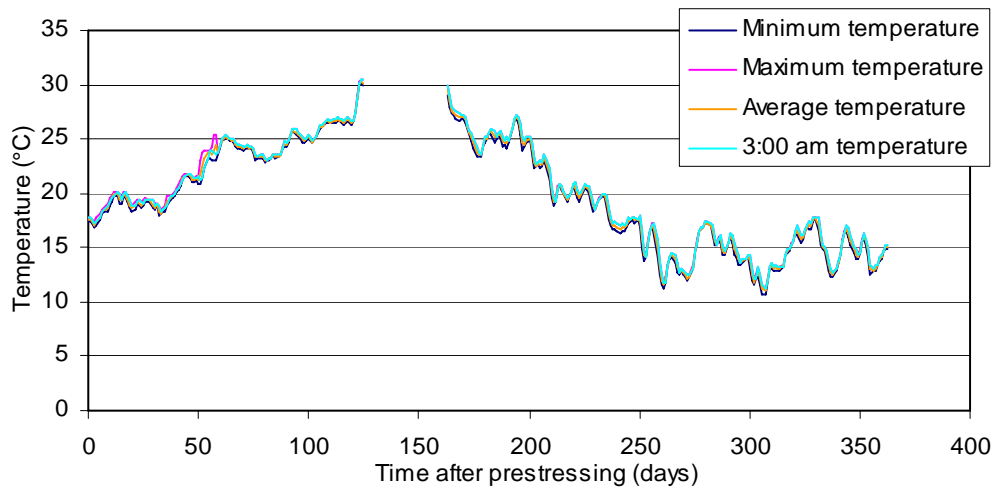
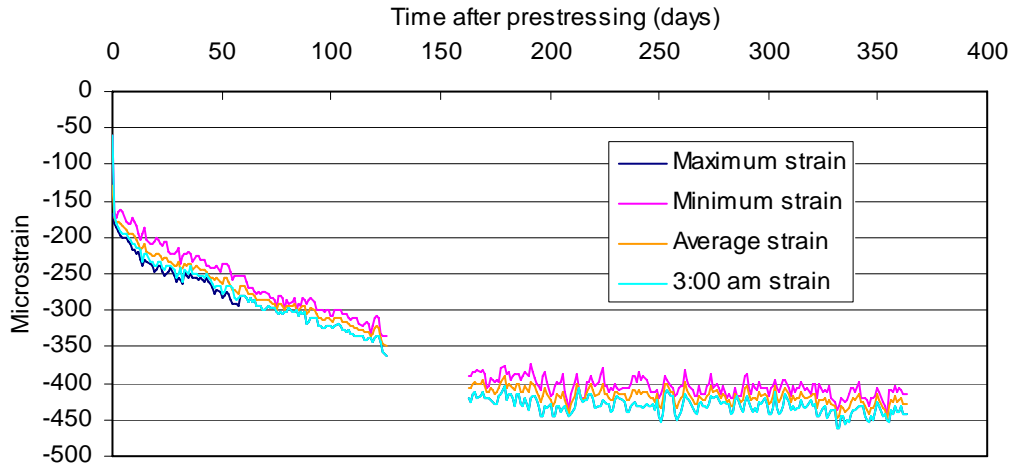
Stem B soffit



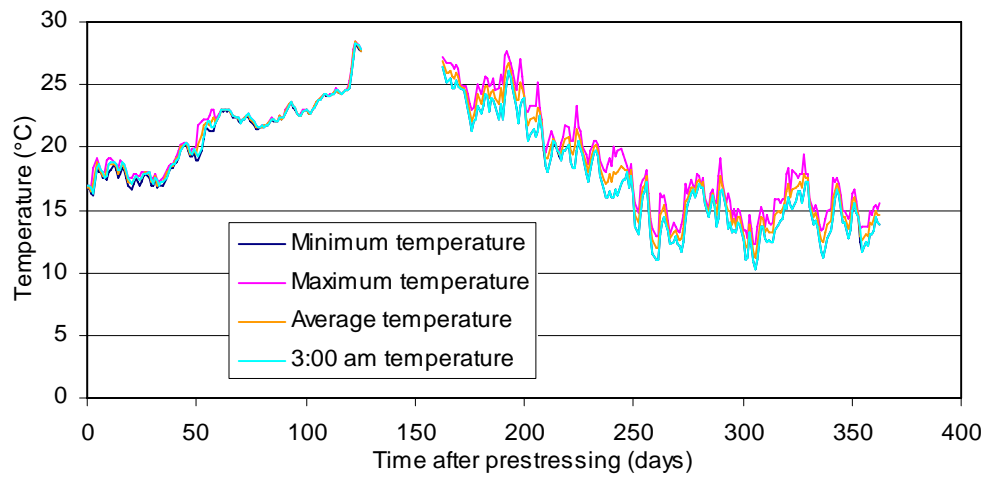
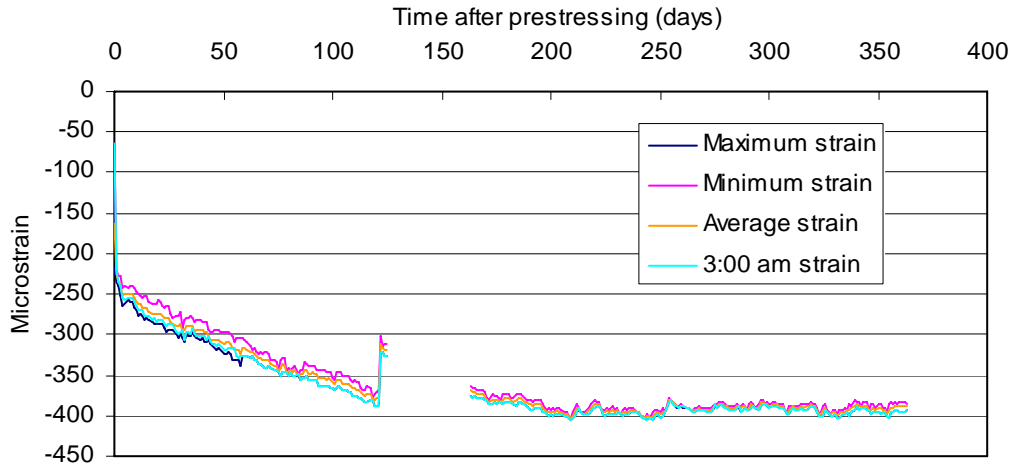
Stem C deck



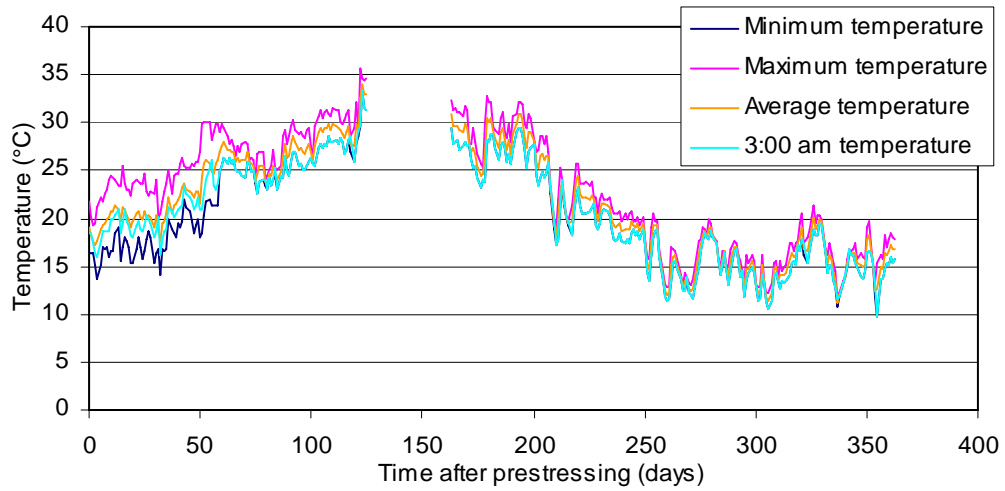
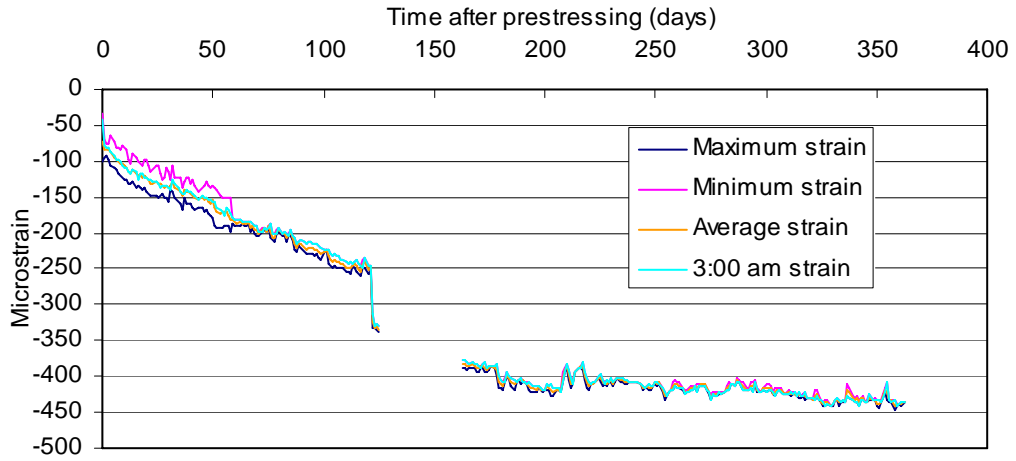
Stem C web



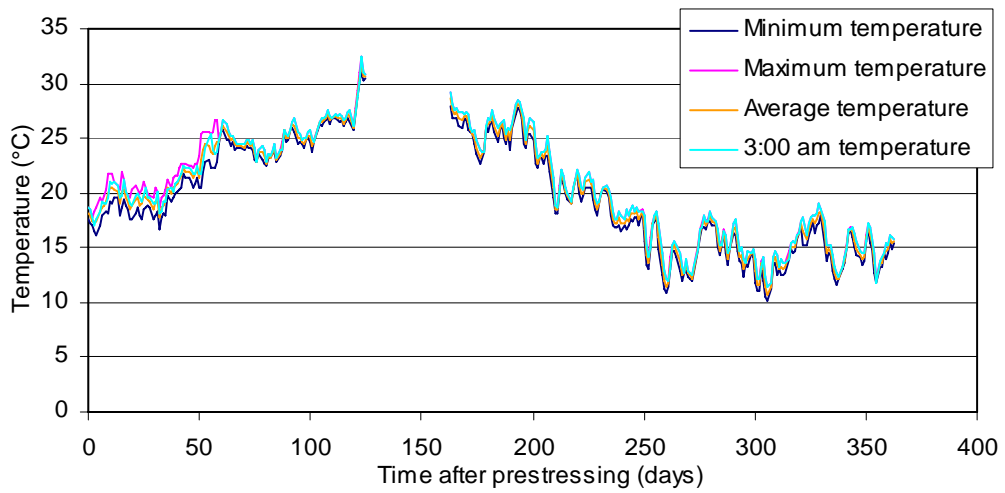
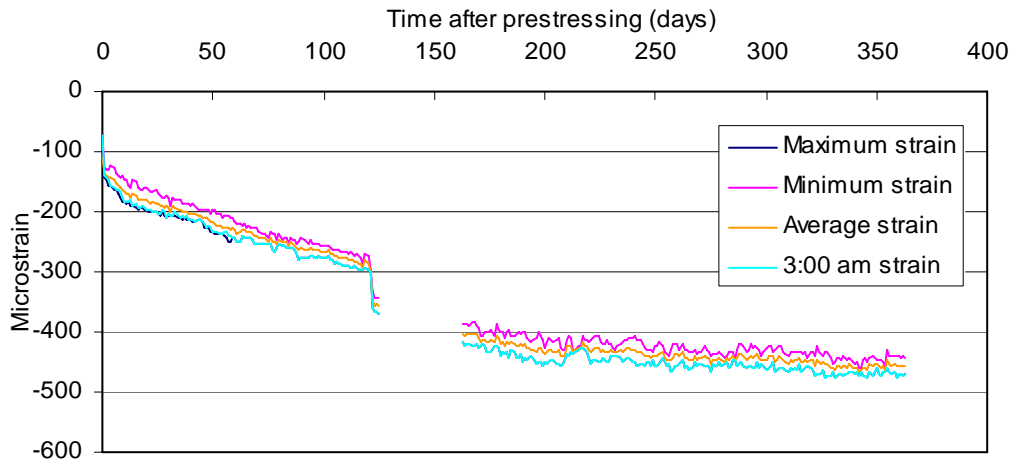
Stem C soffit



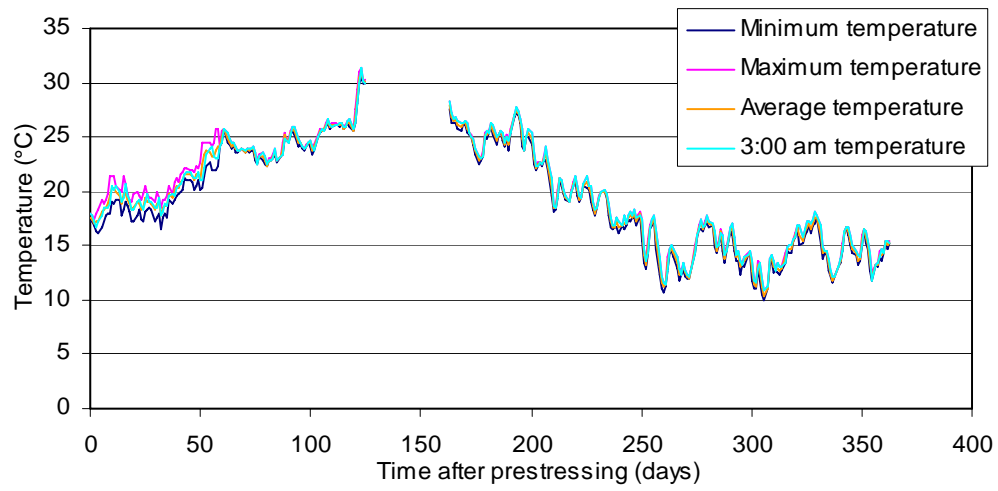
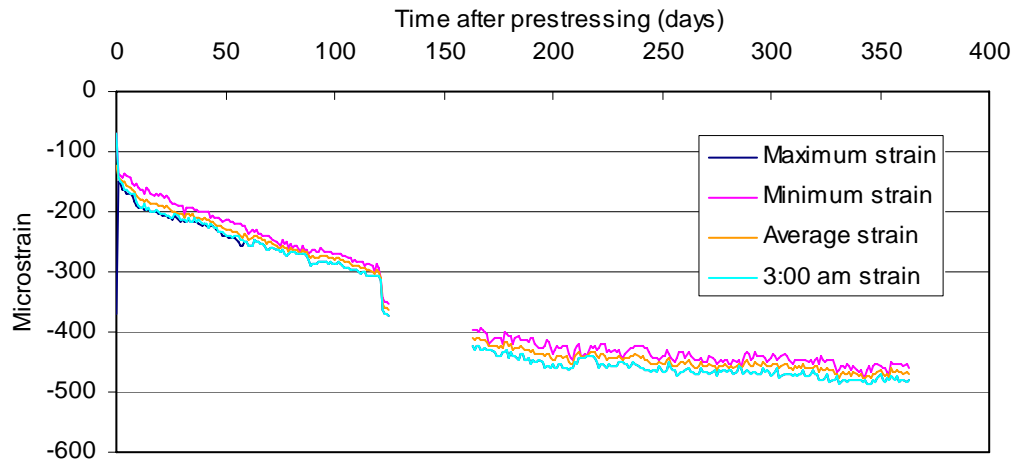
Stem D deck



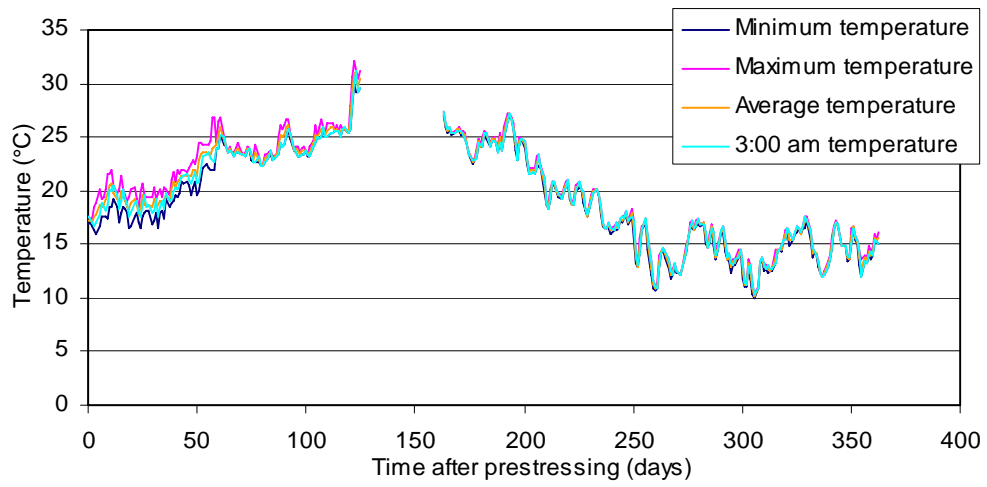
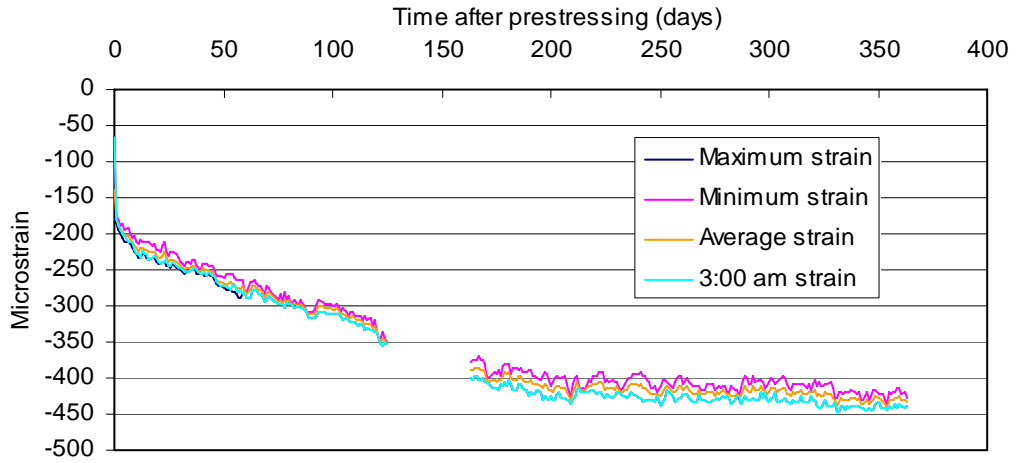
Stem D web (upper level)



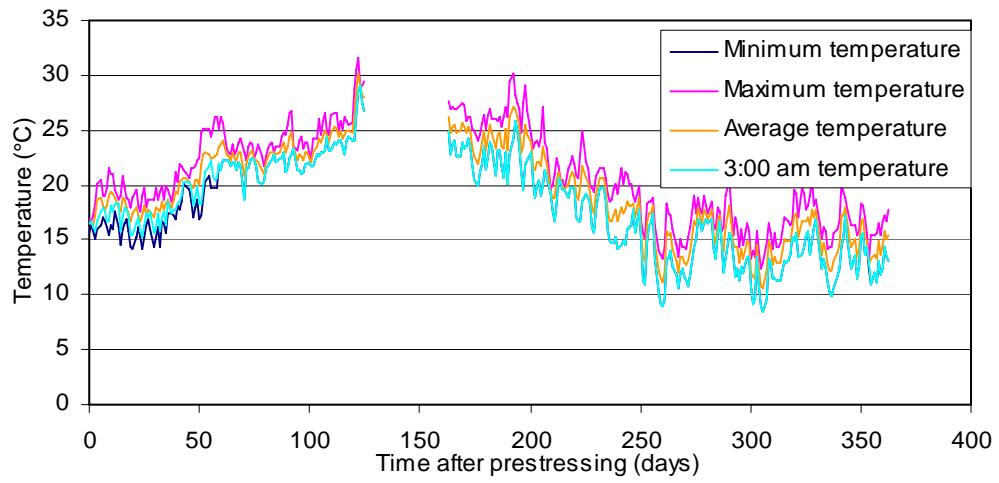
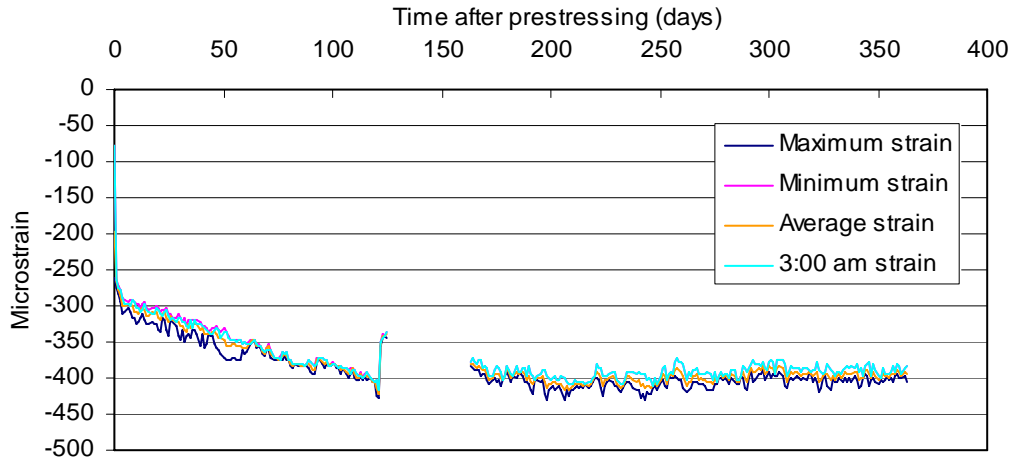
Stem D web (middle level)



Stem D web (lower level)



Stem D soffit



Frame 4 Near the Bent

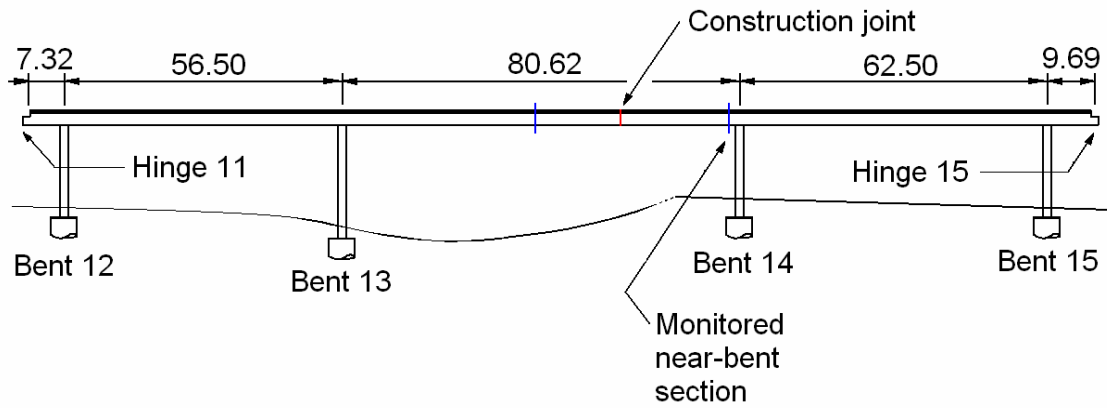
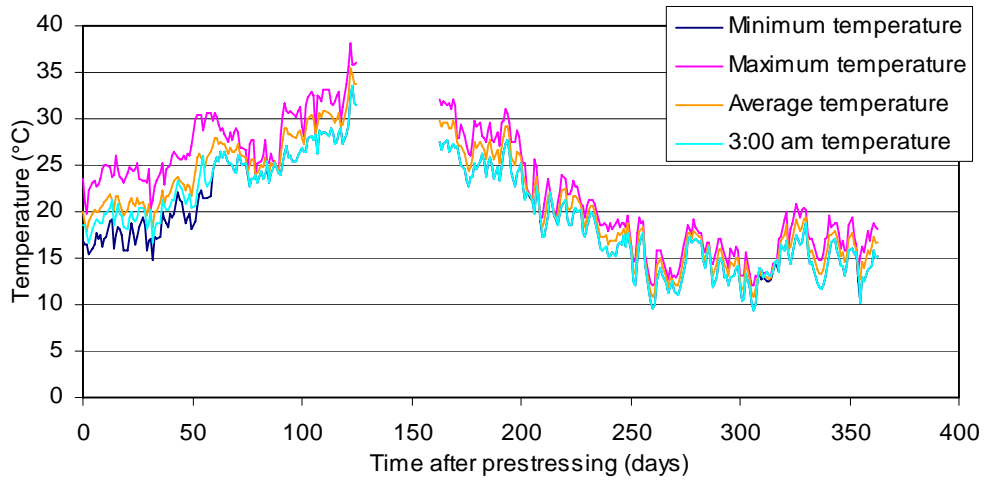
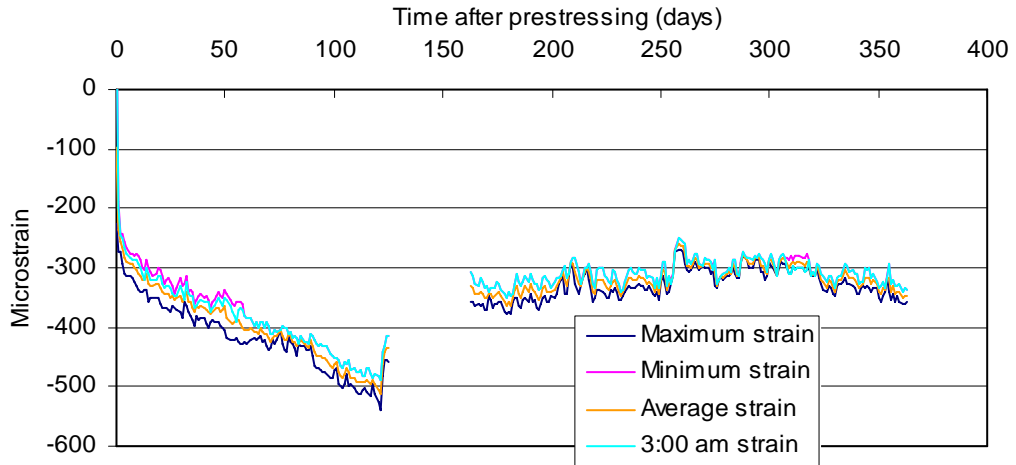
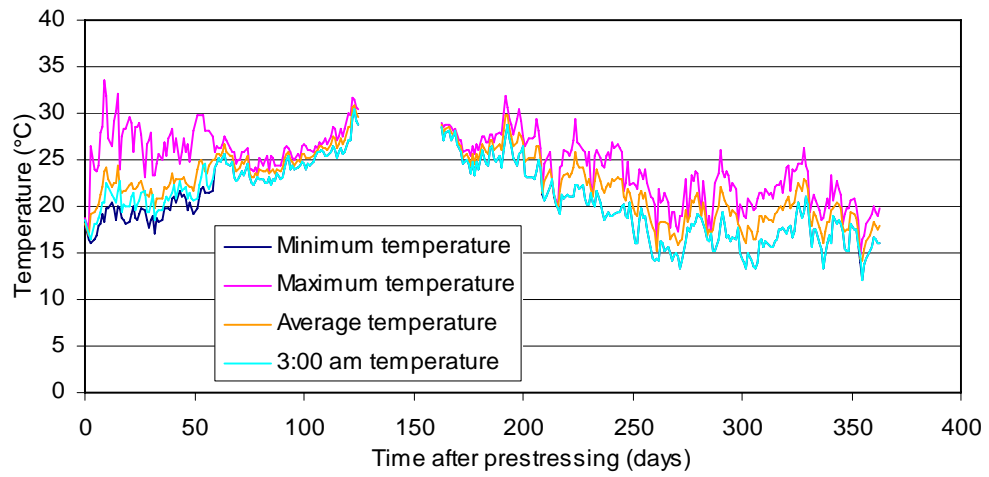
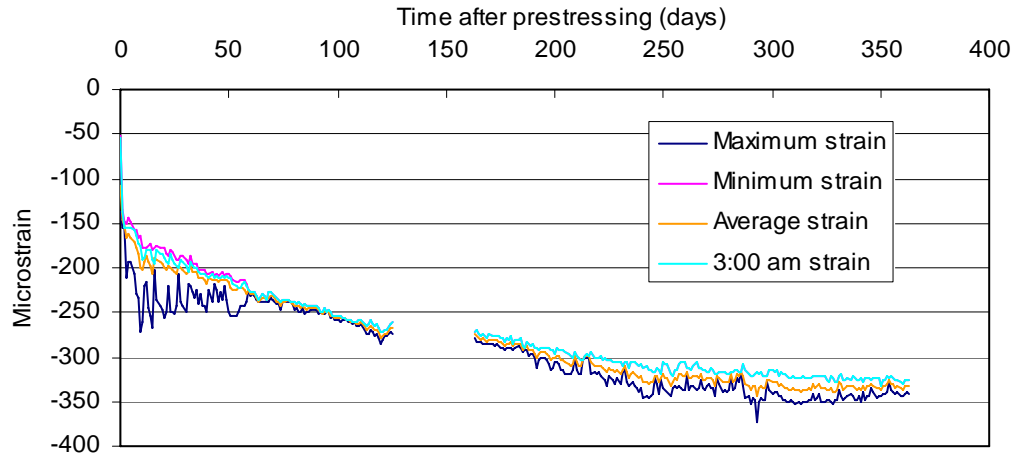


Figure C3: Location of gages at the near-bent section in F4.

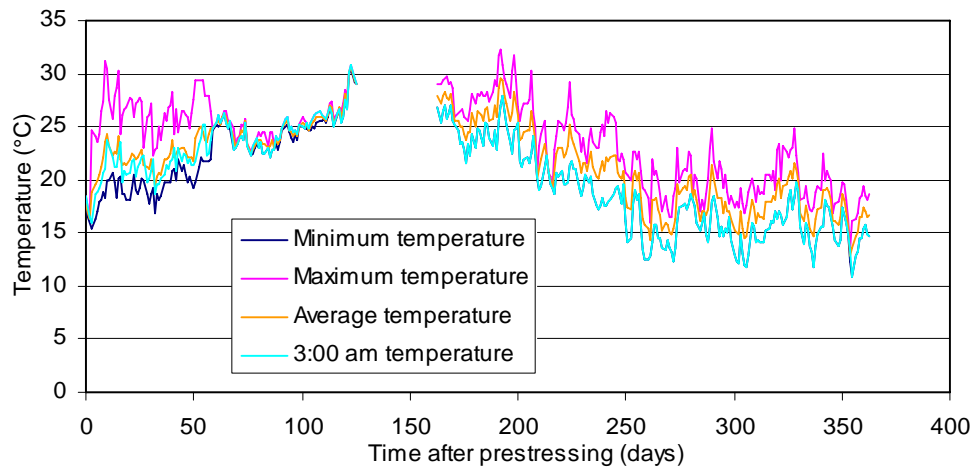
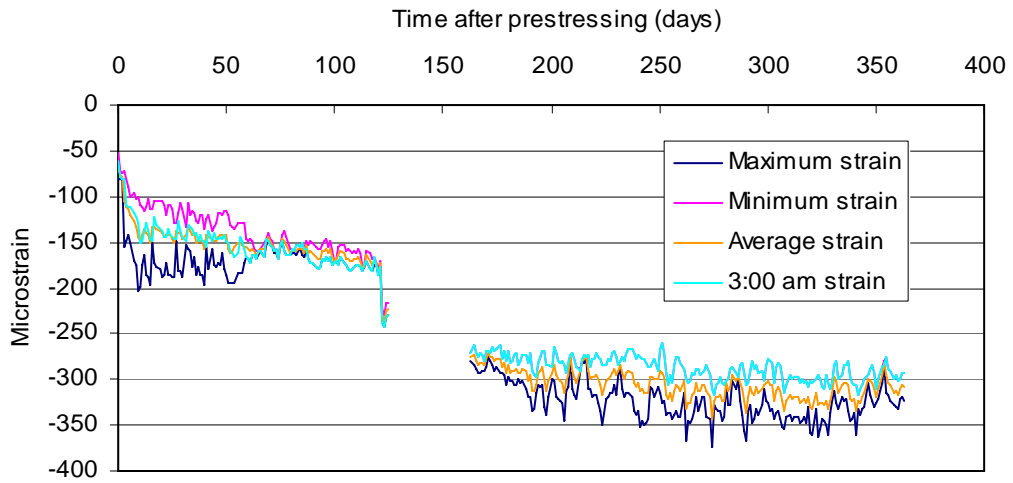
Stem A deck



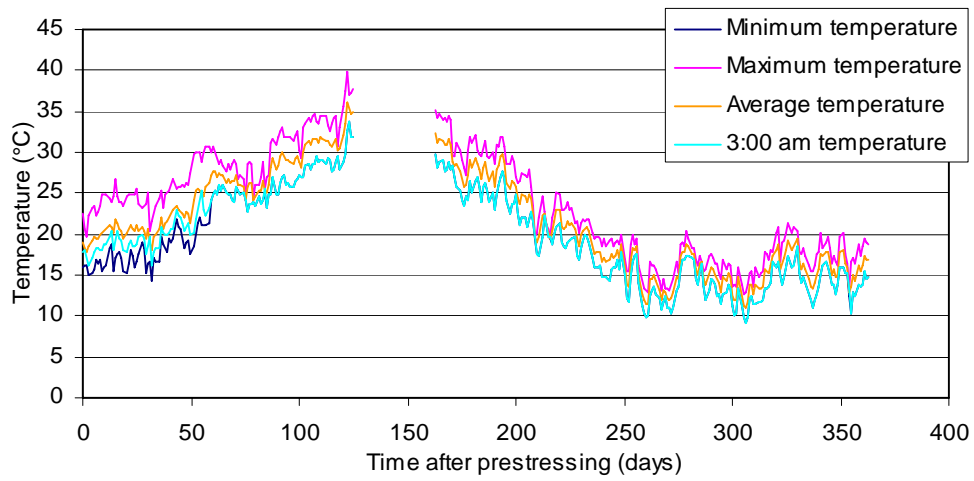
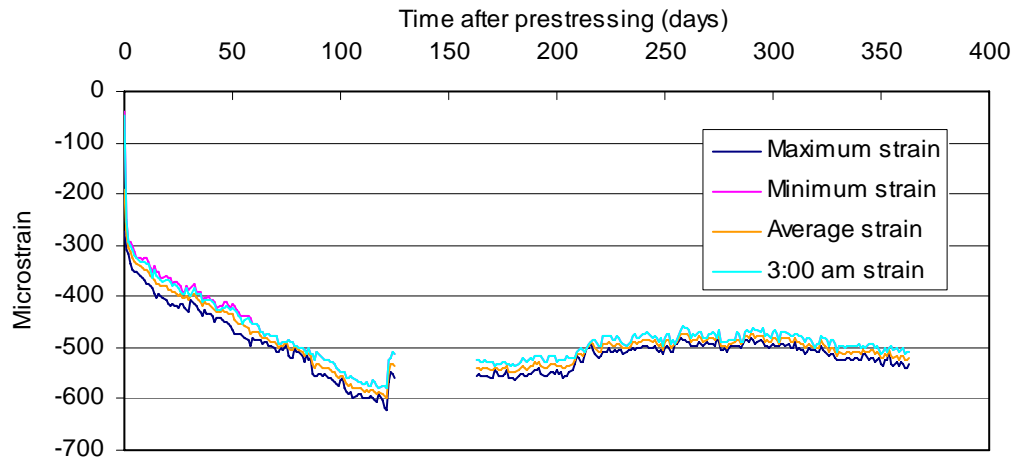
Stem A web



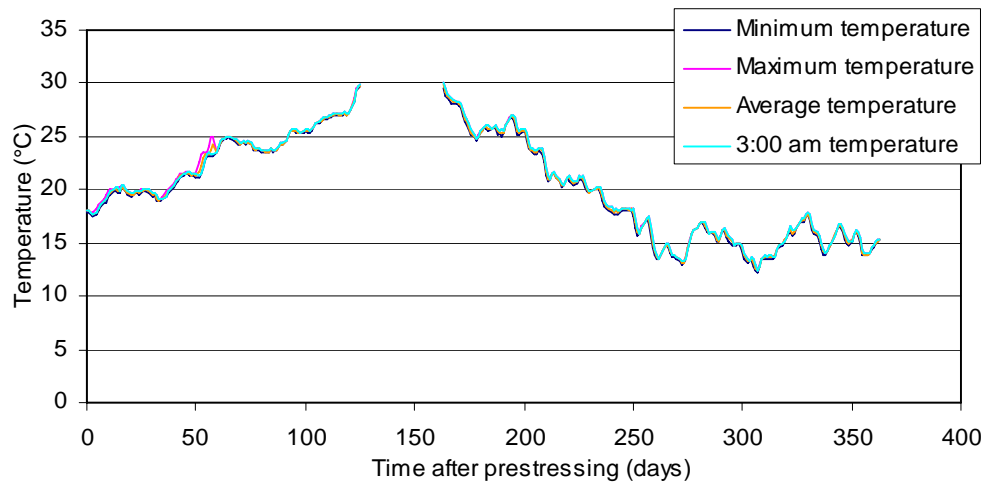
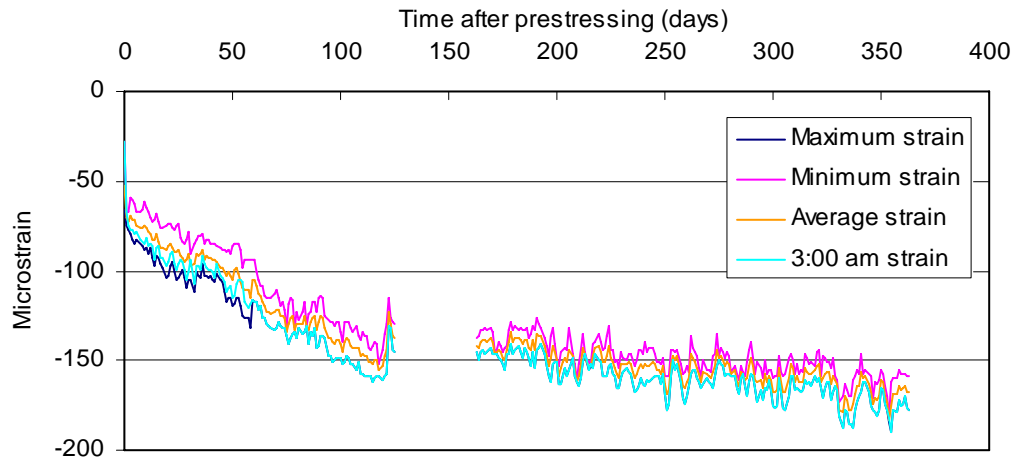
Stem A soffit



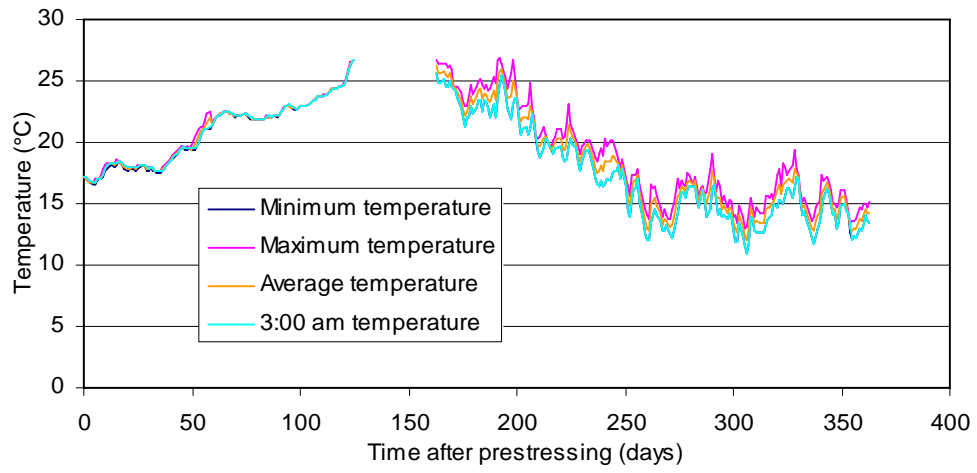
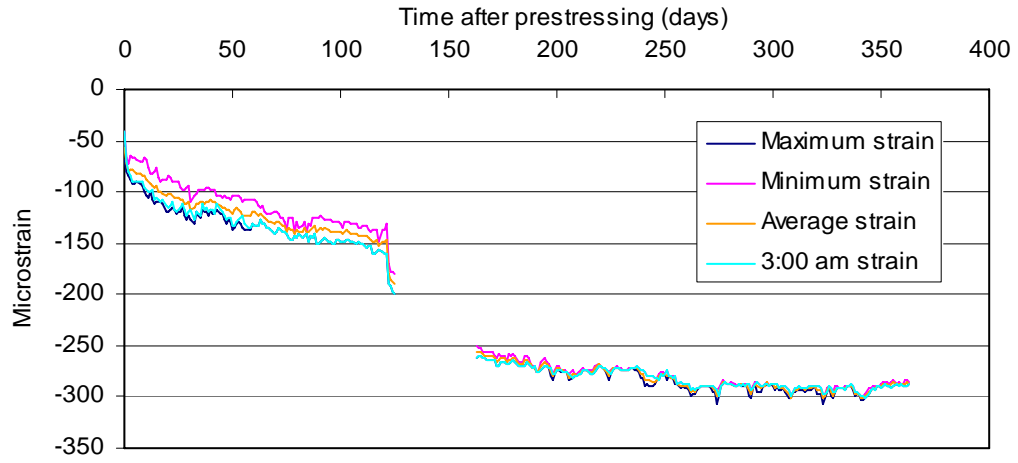
Stem B deck



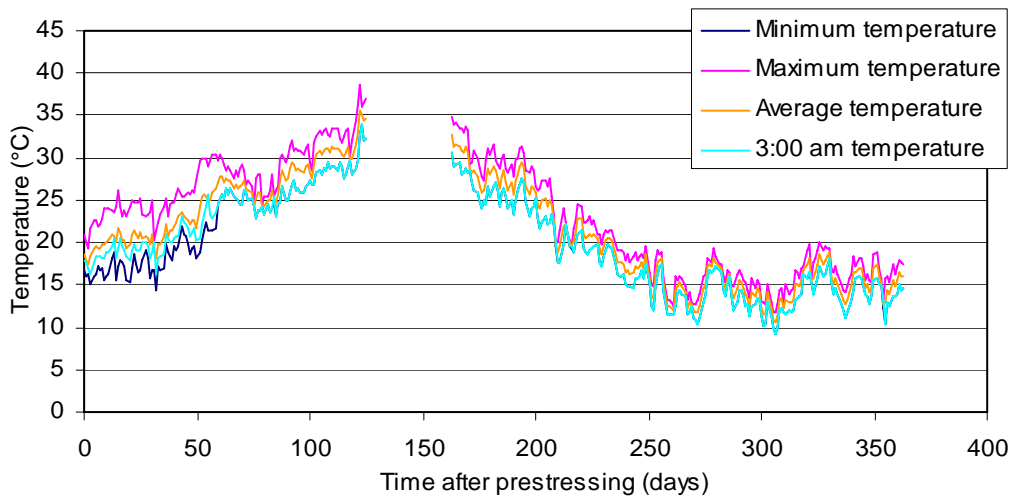
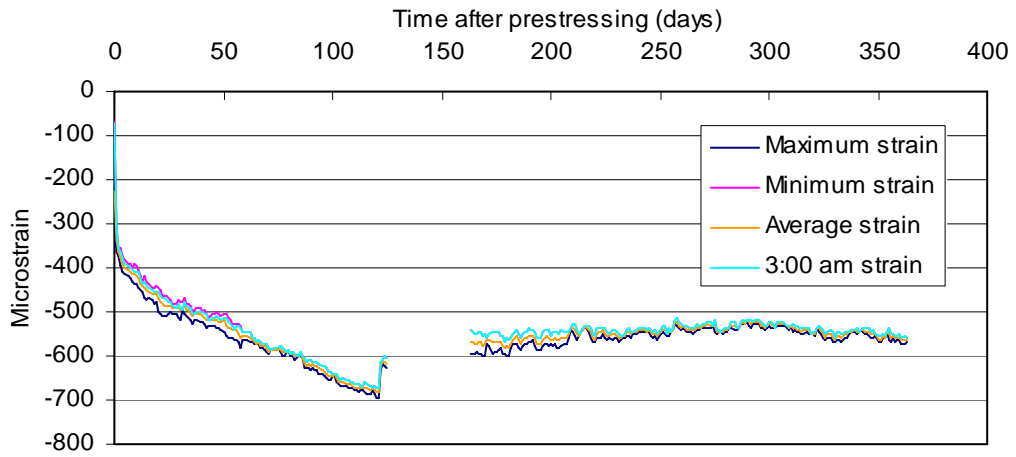
Stem B web



Stem B soffit

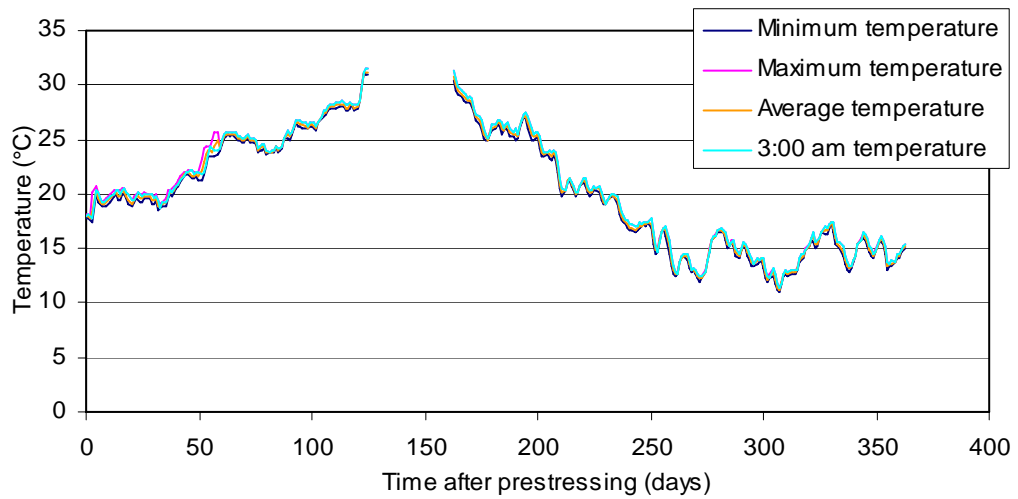


Stem C deck



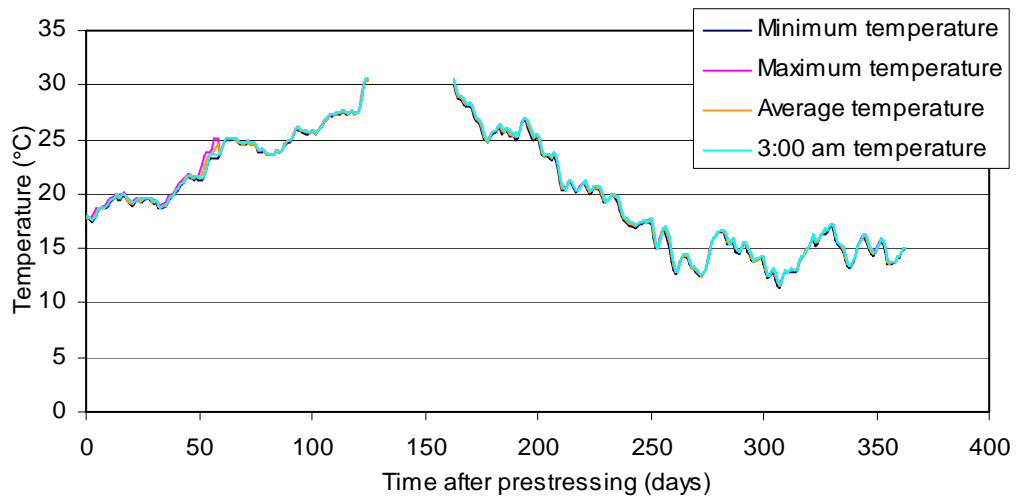
Stem C web (upper level)

No strain data available due to gage malfunction

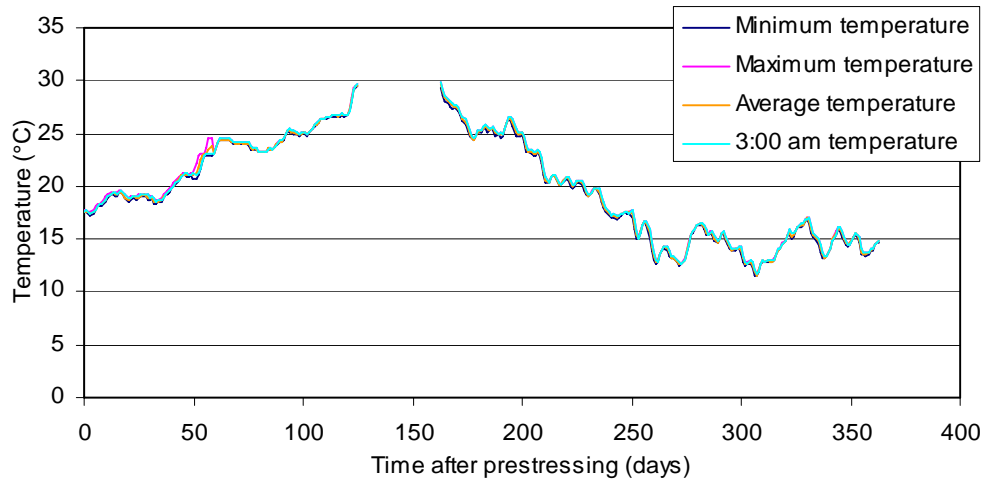
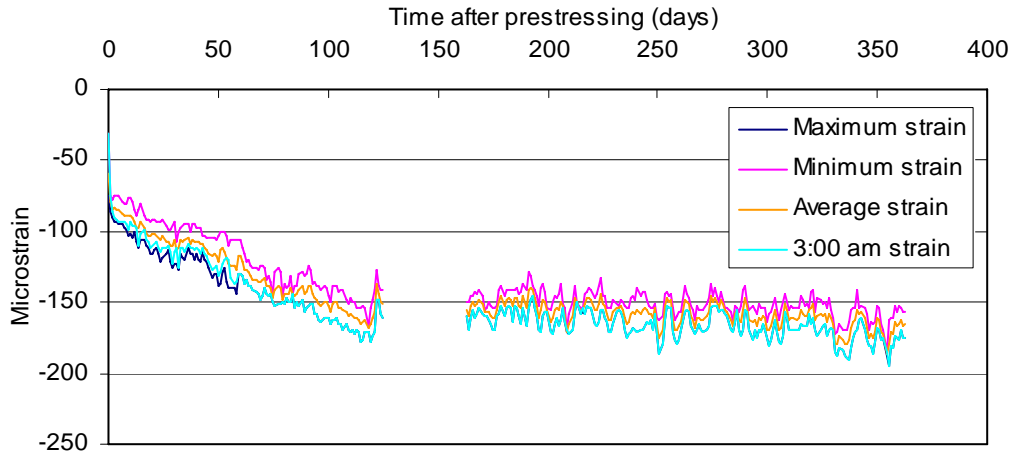


Stem C web (middle level)

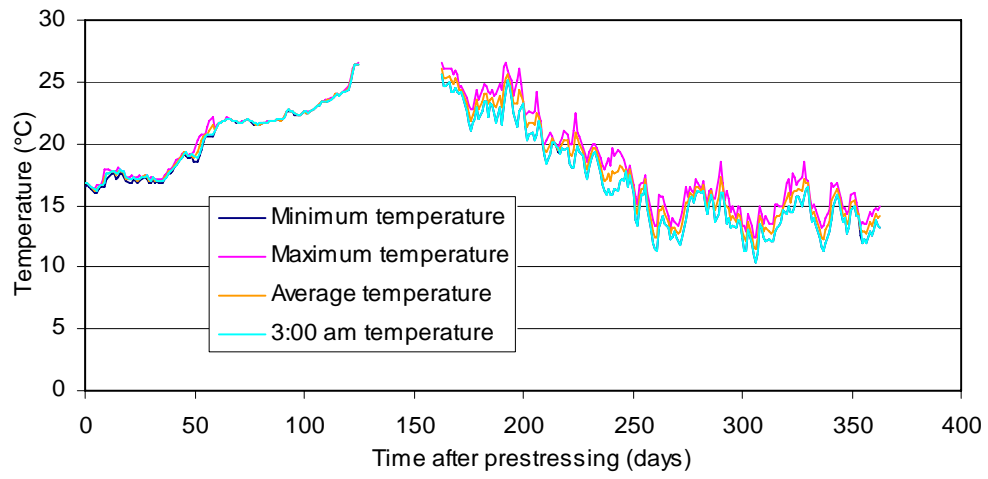
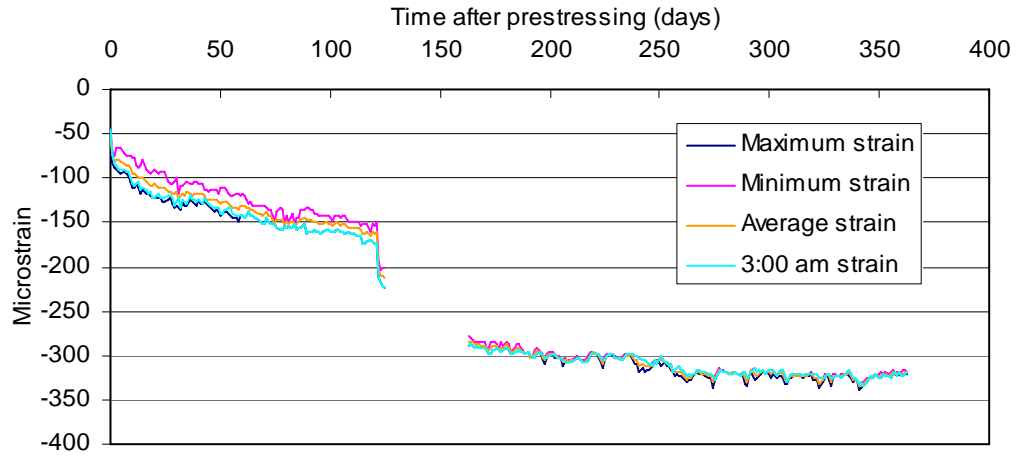
No strain data available due to gage malfunction



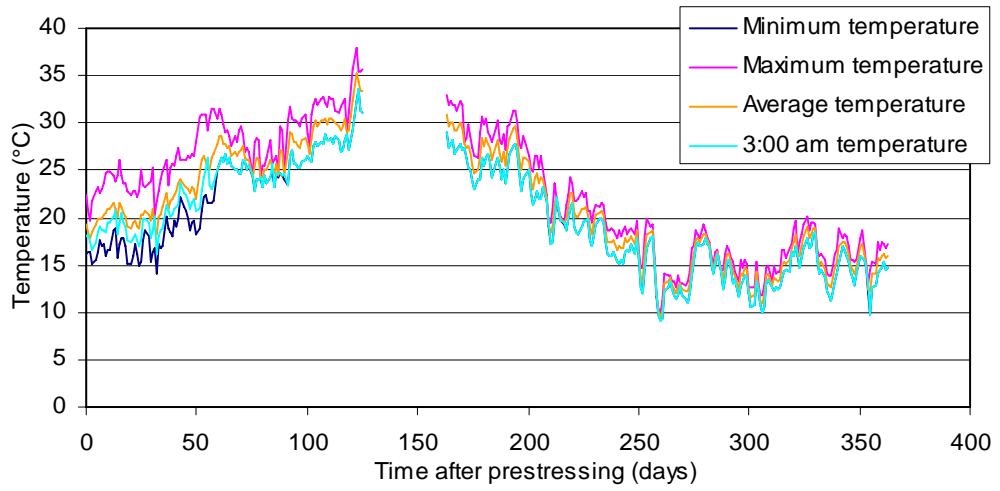
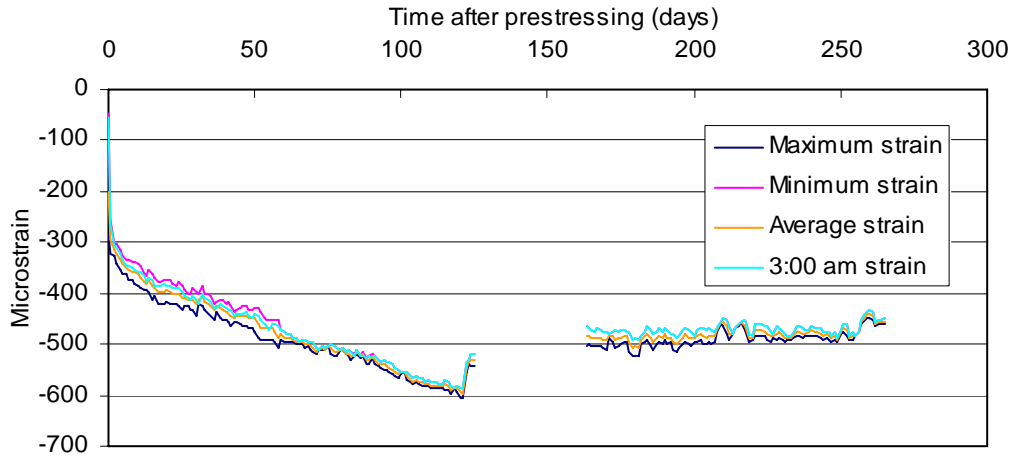
Stem C web (lower level)



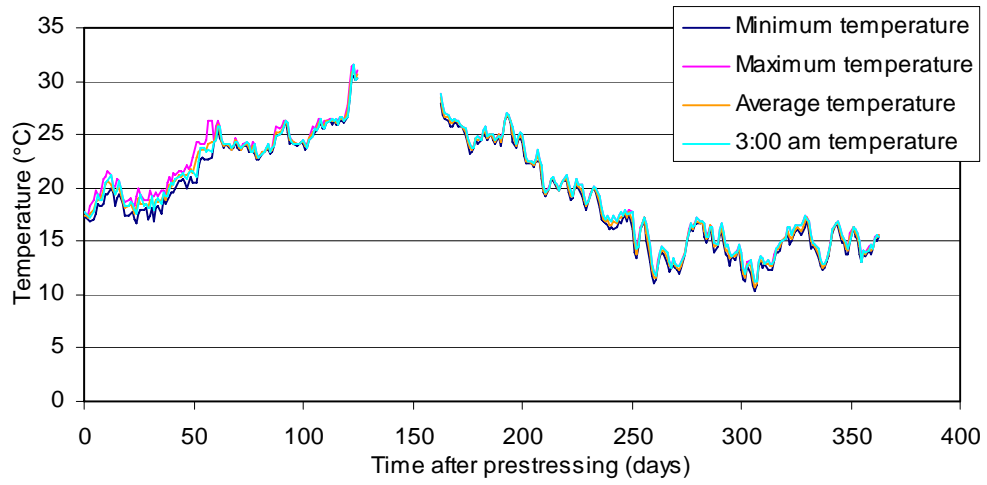
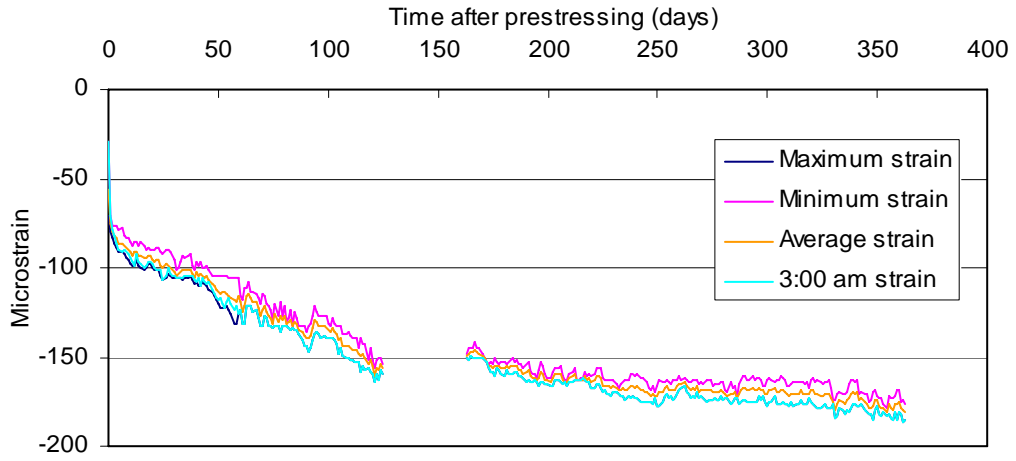
Stem C soffit



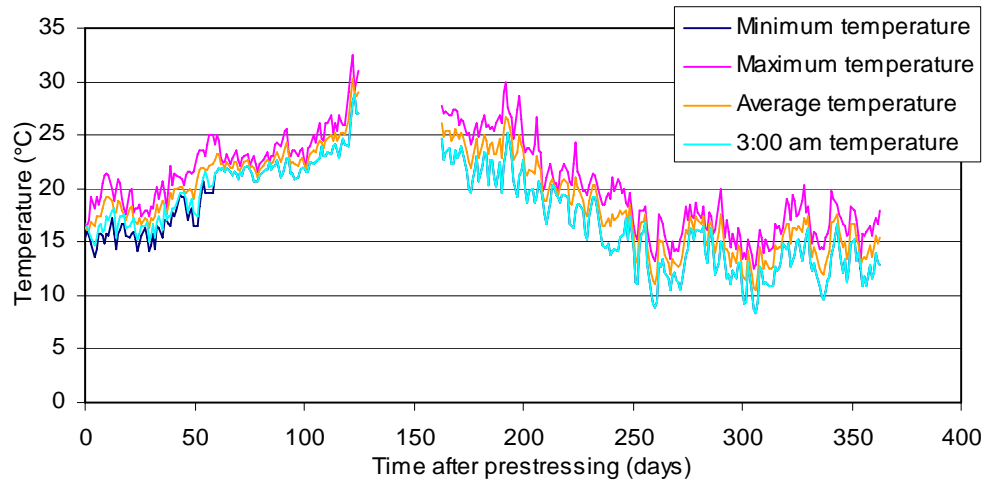
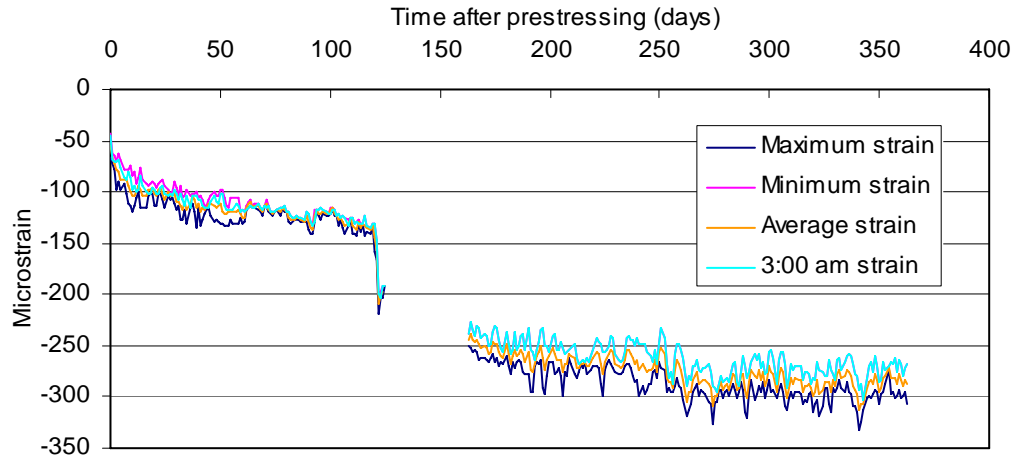
Stem D deck



Stem D web



Stem D soffit



Frame 5 Midspan

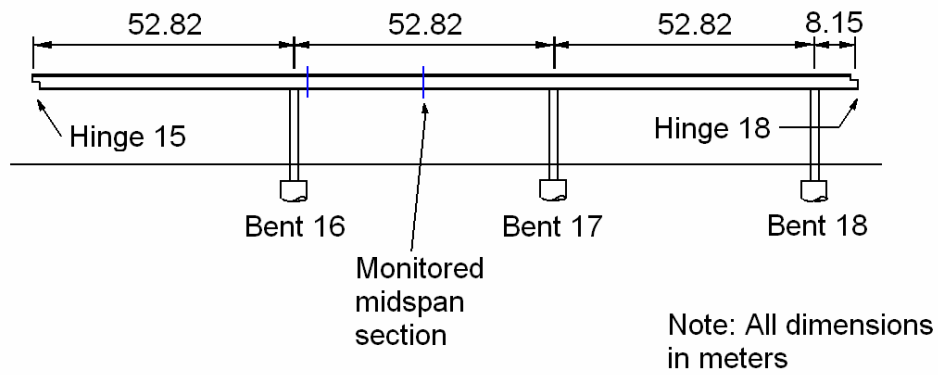
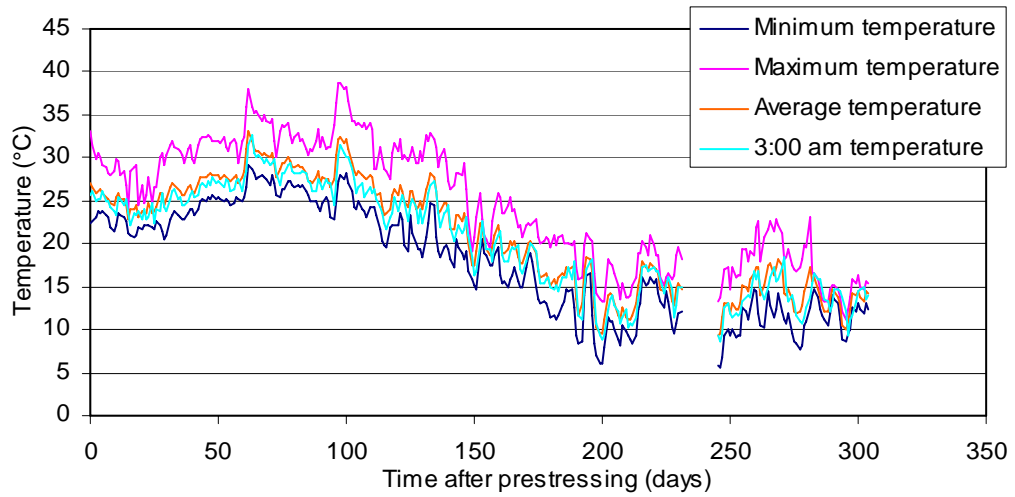


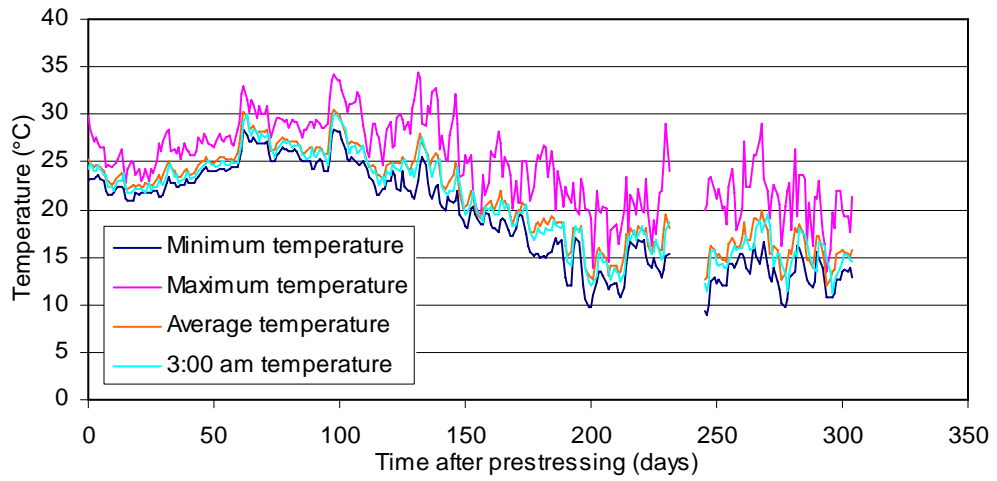
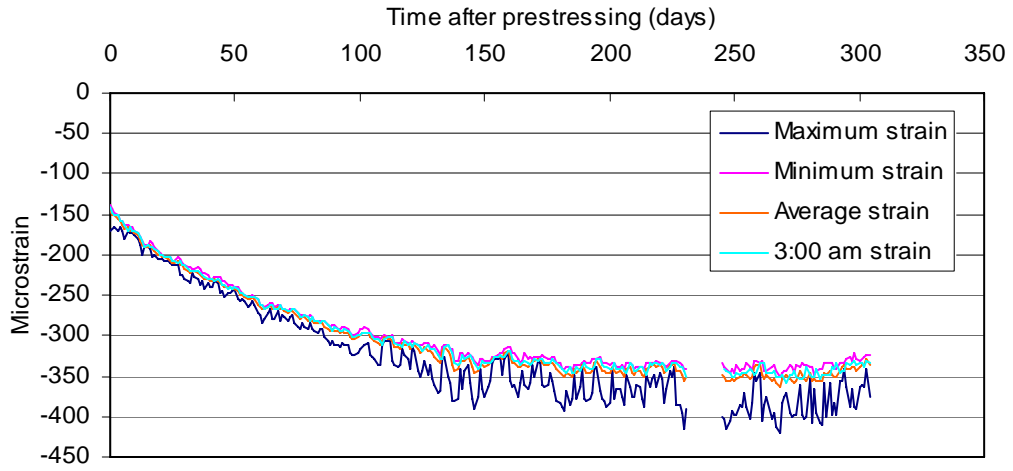
Figure C4: Location of gages at the midspan section in F5.

Stem A deck

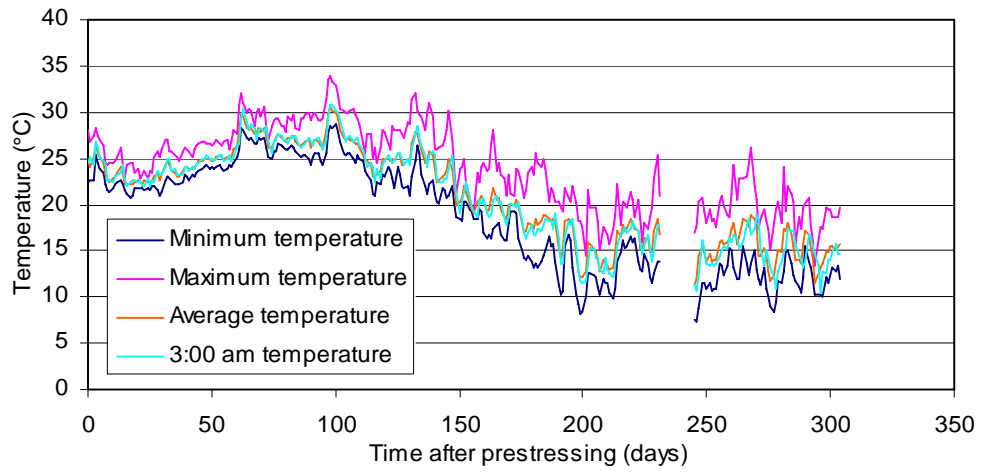
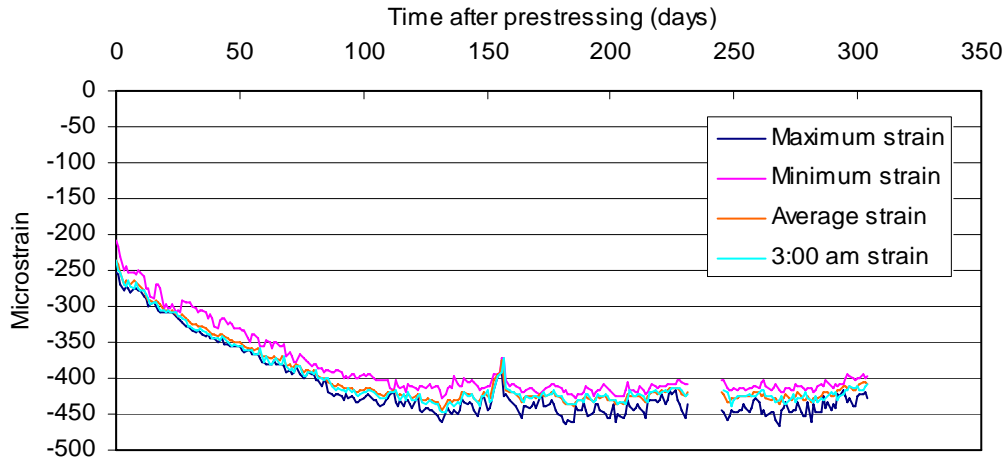
No strain data available due to gage malfunction



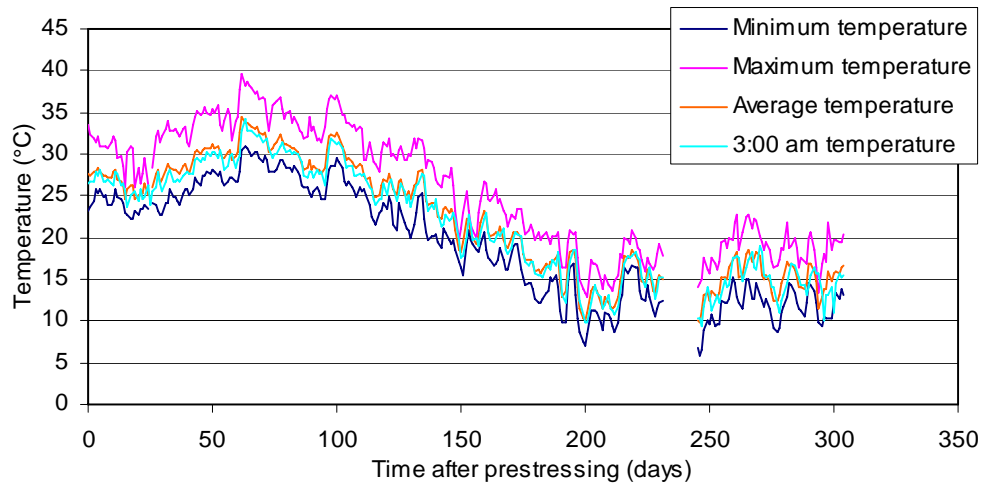
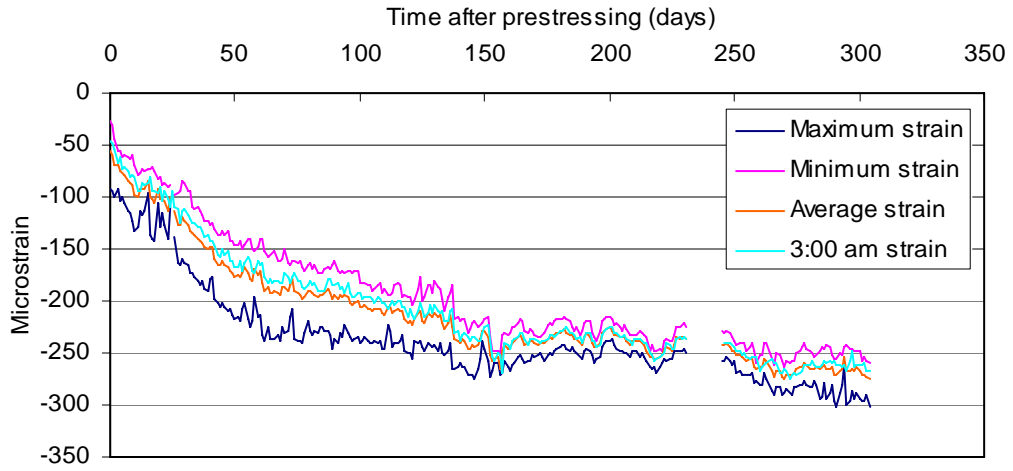
Stem A web



Stem A soffit

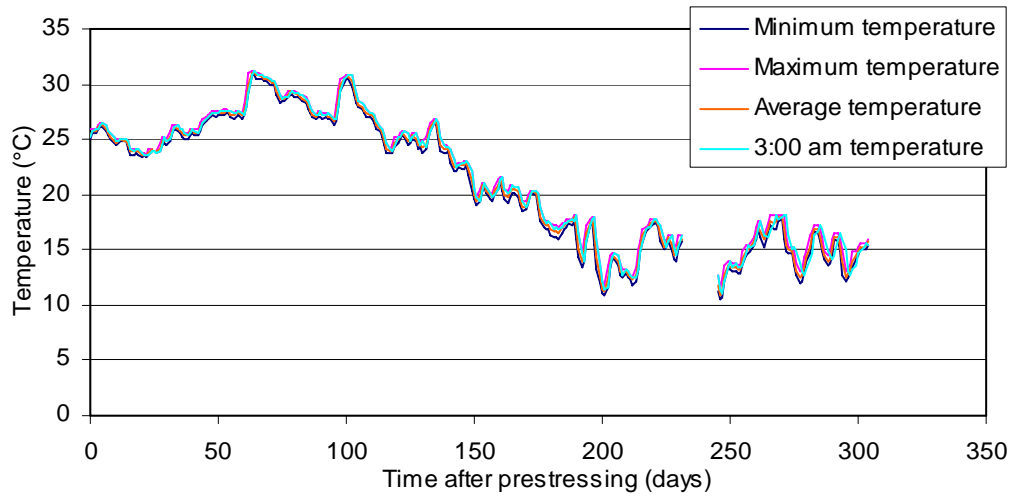


Stem B deck

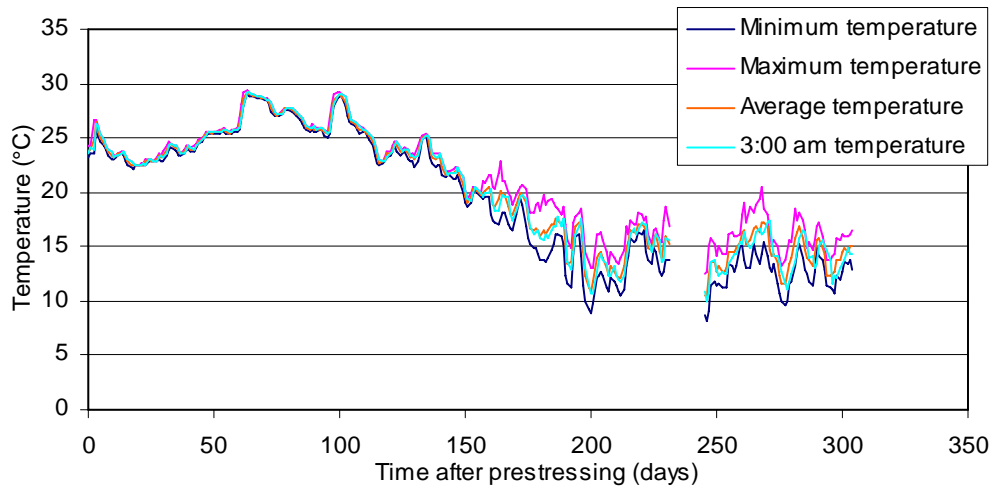
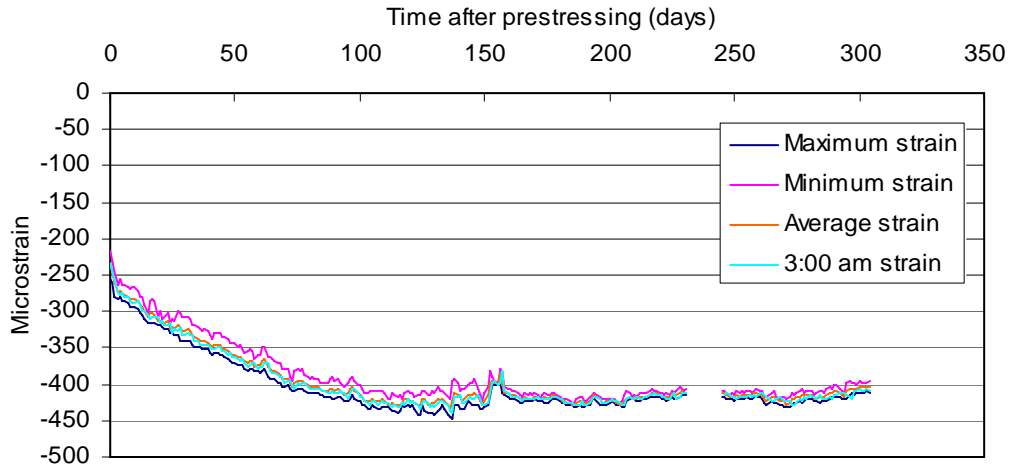


Stem B web

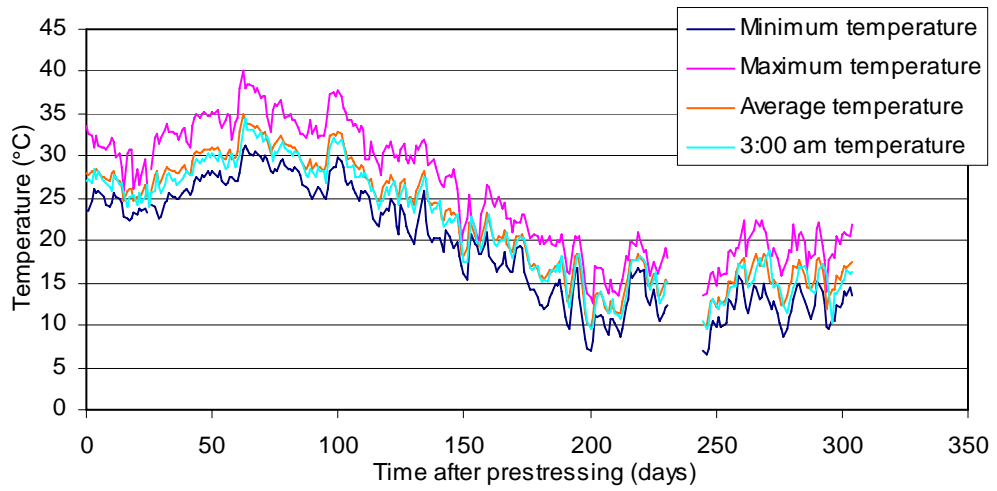
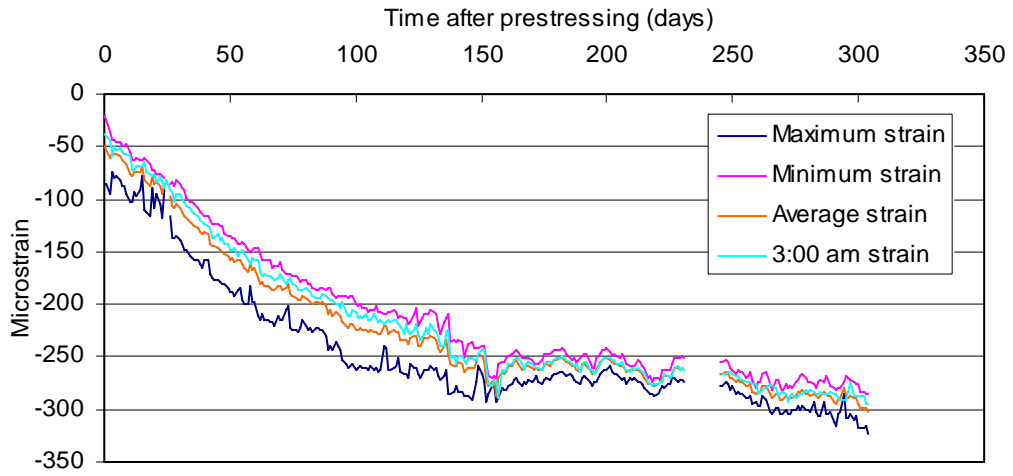
No strain data available due to gage malfunction



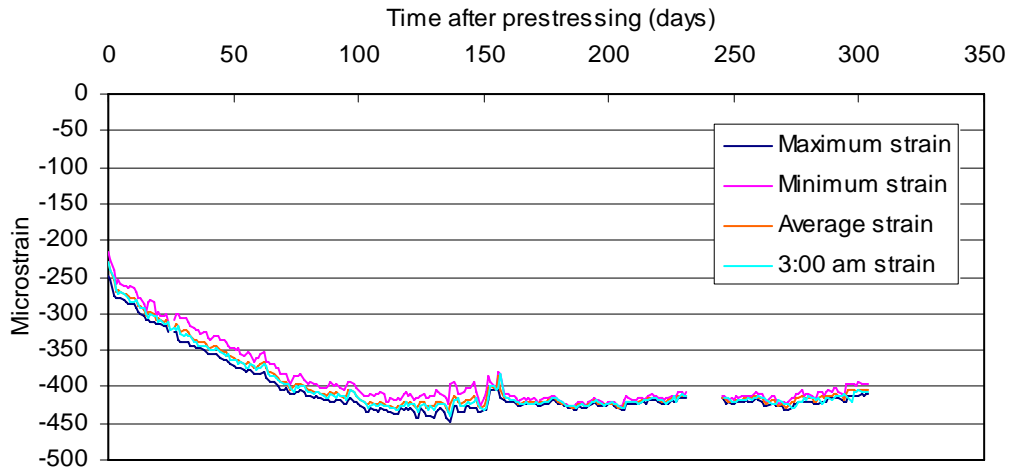
Stem B soffit



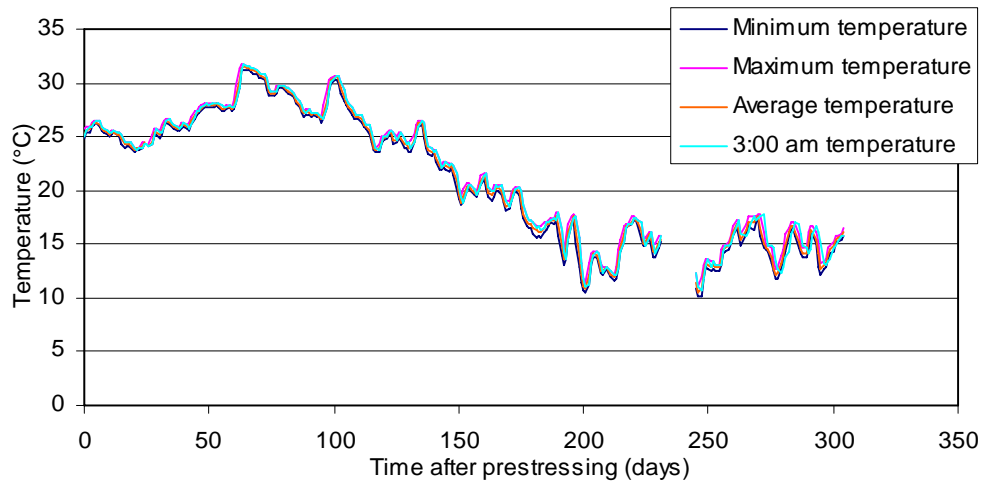
Stem C deck



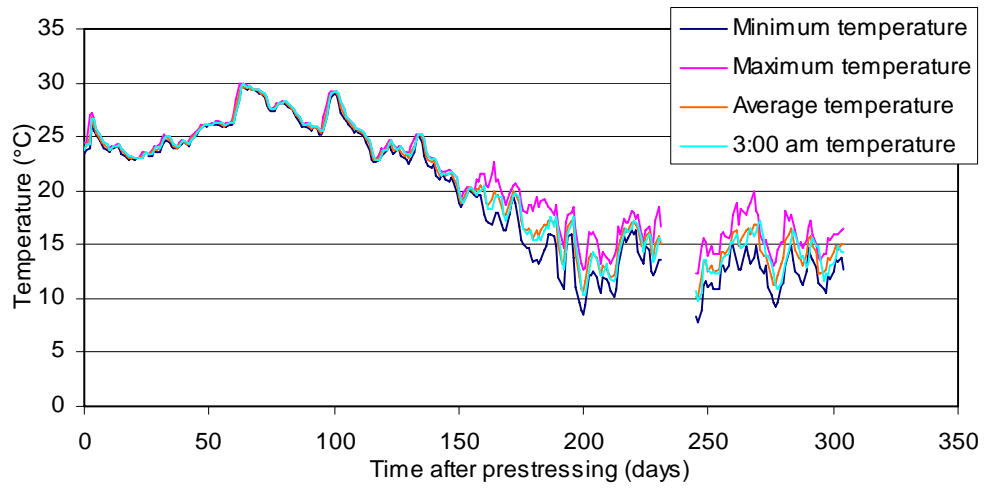
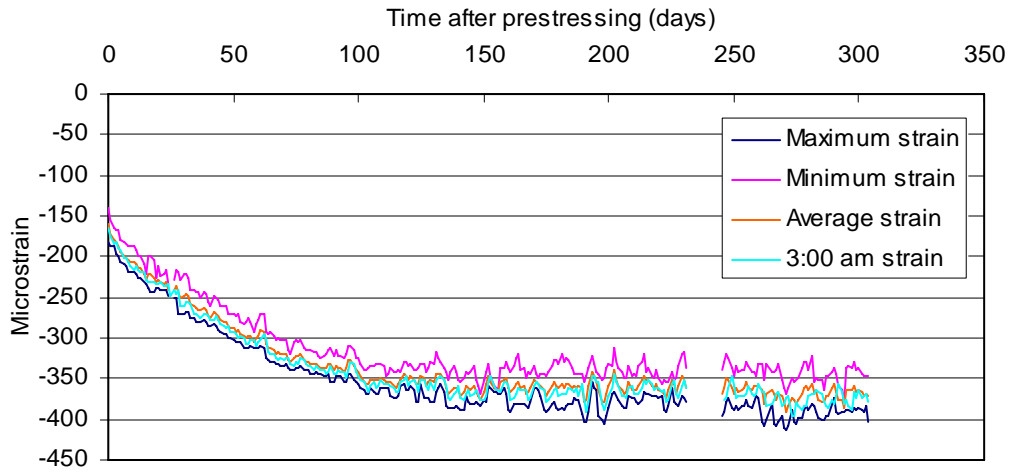
Stem C web



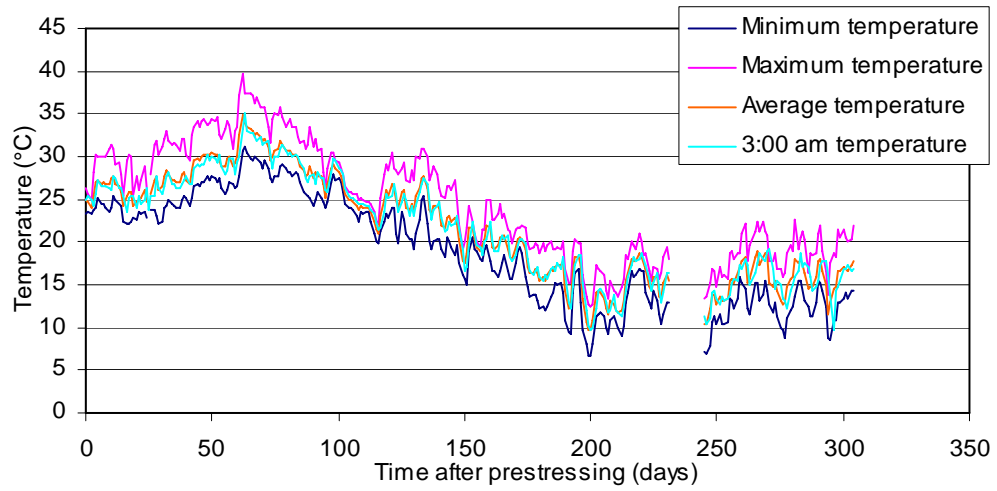
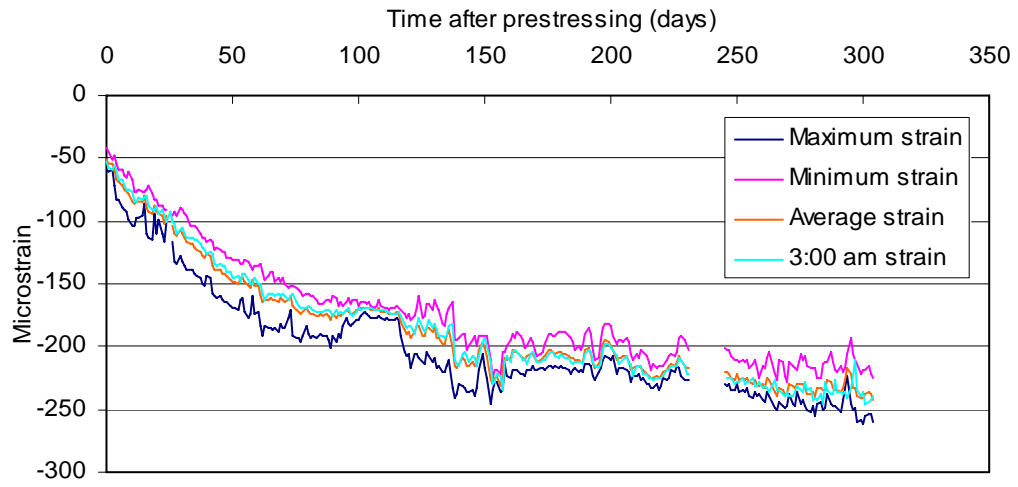
+



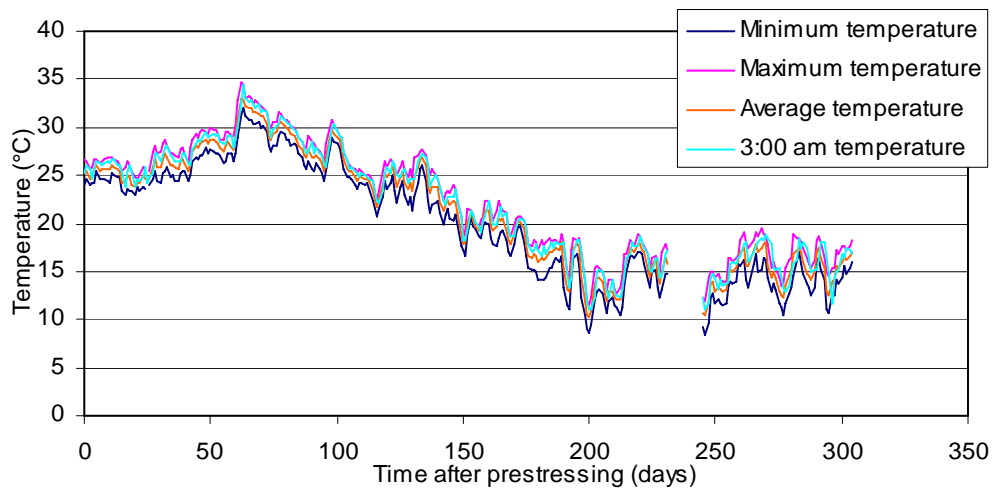
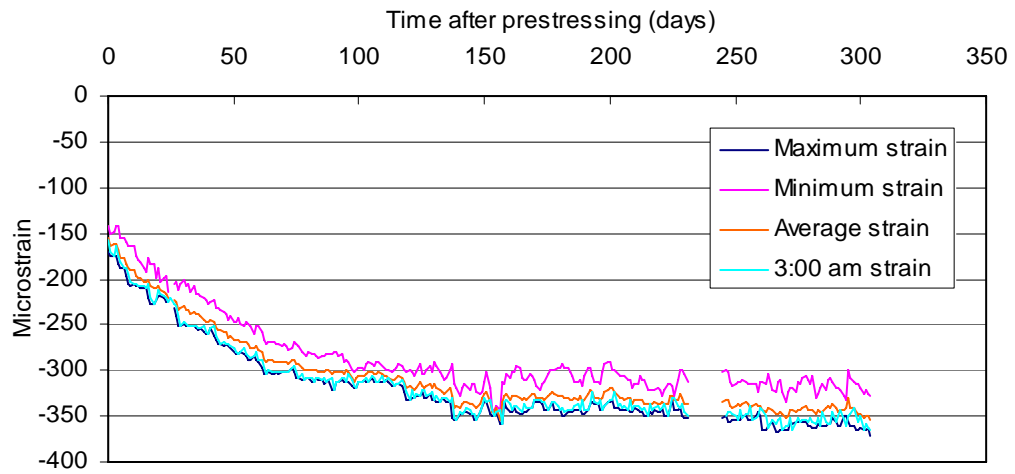
Stem C soffit



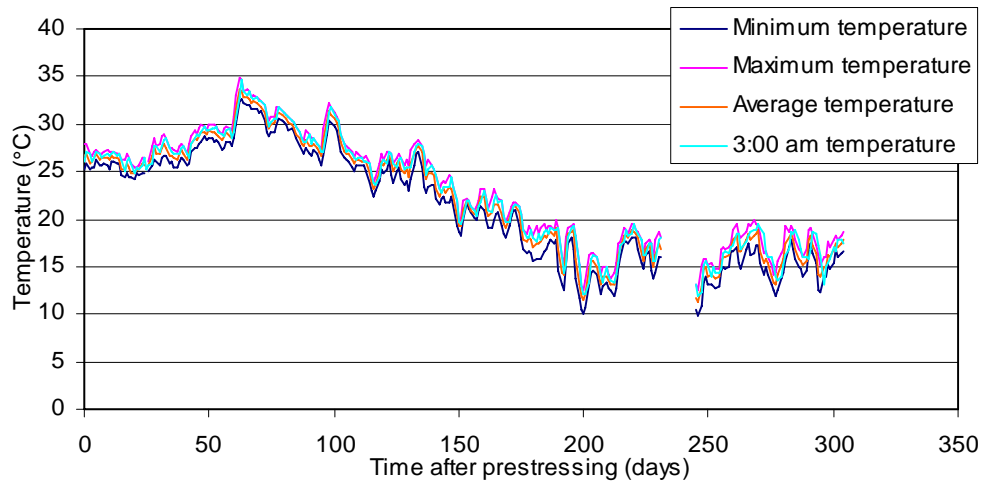
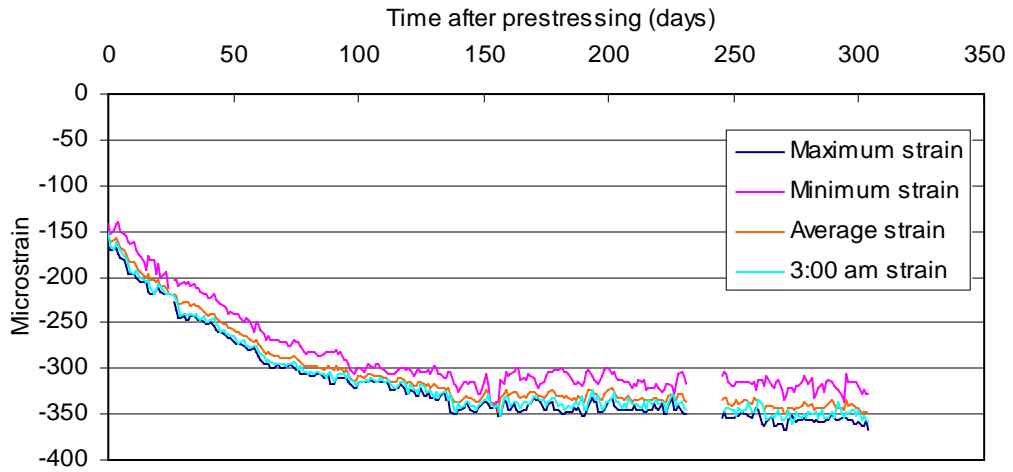
Stem D deck



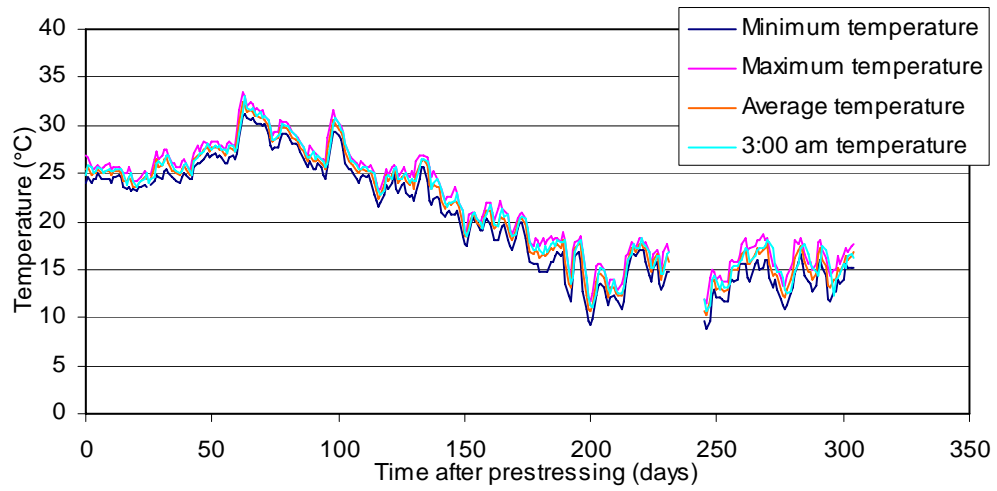
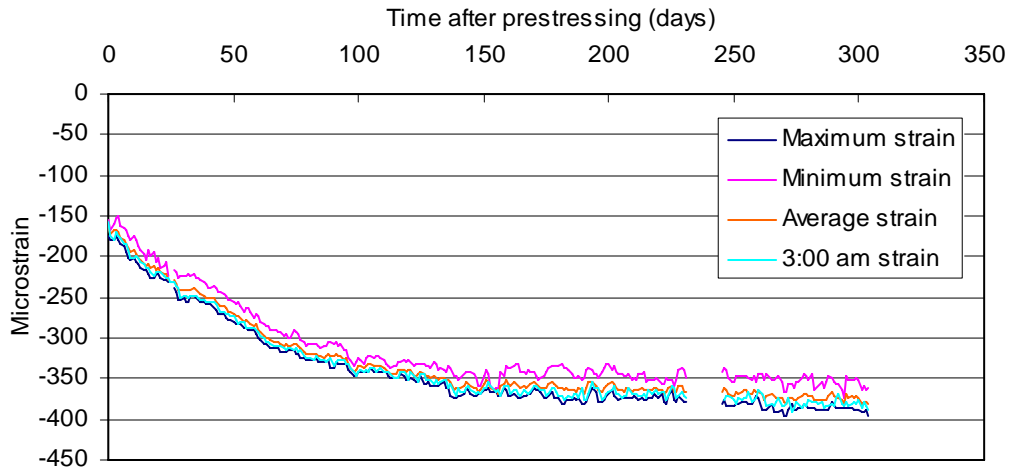
Stem D web (upper level)



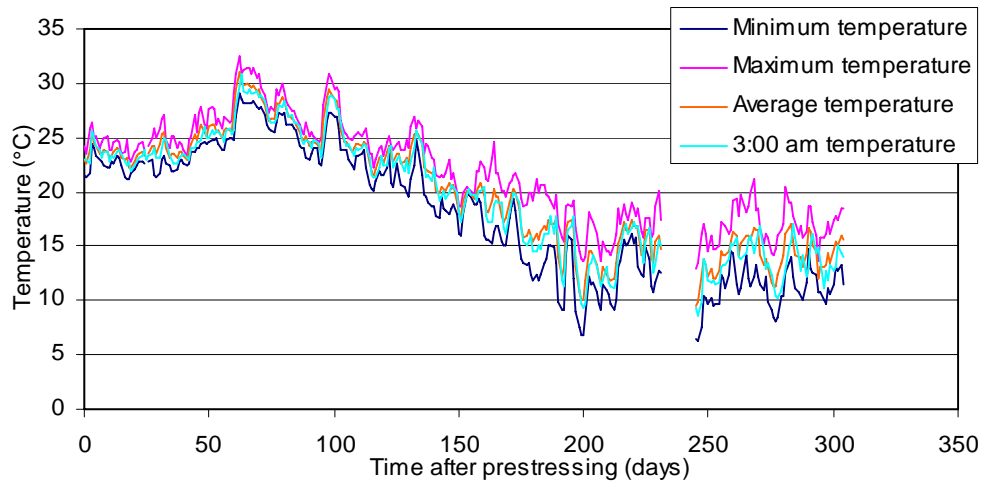
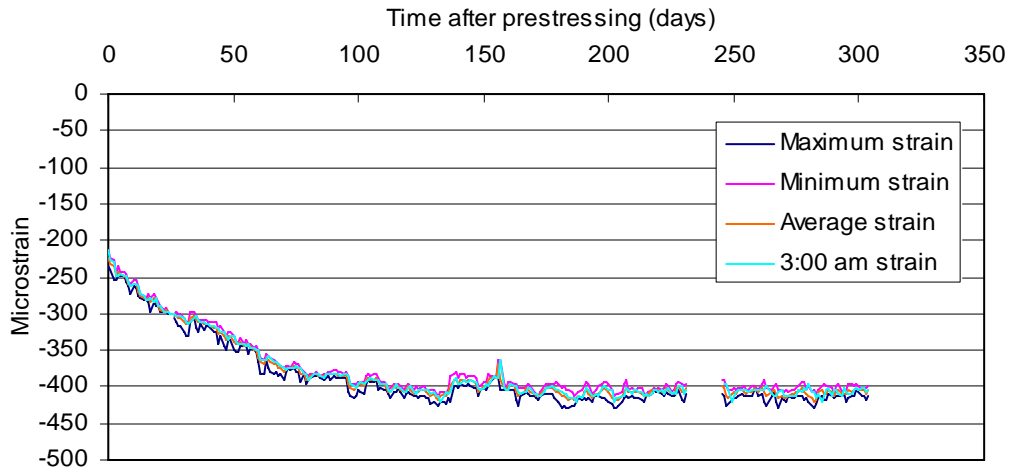
Stem D web (middle level)



Stem D web (lower level)



Stem D soffit



Frame 5 Near the Bent

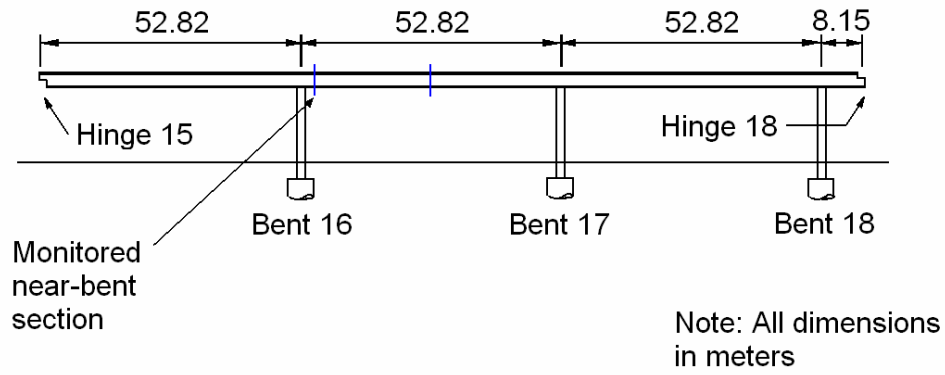
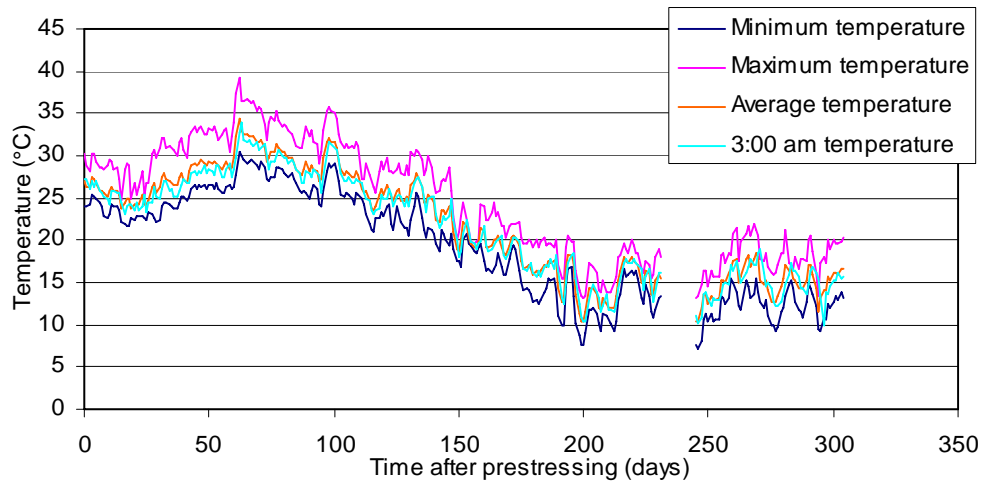
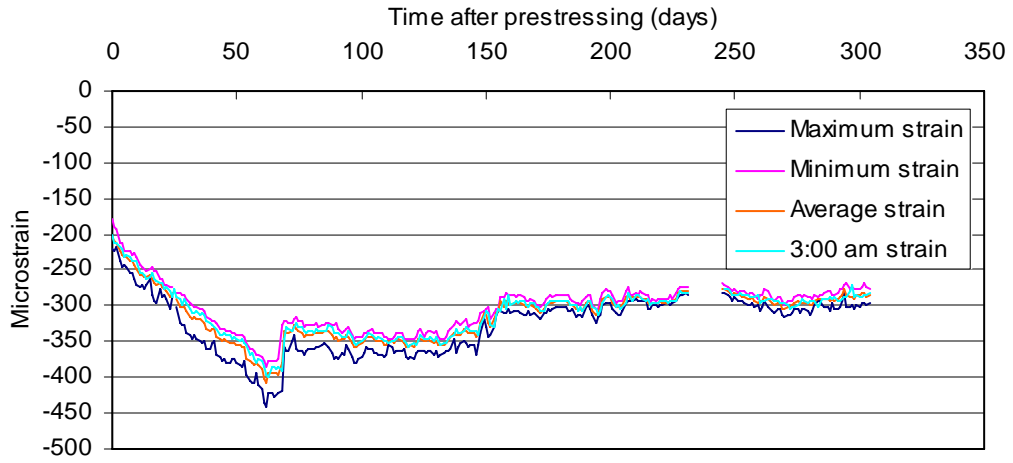
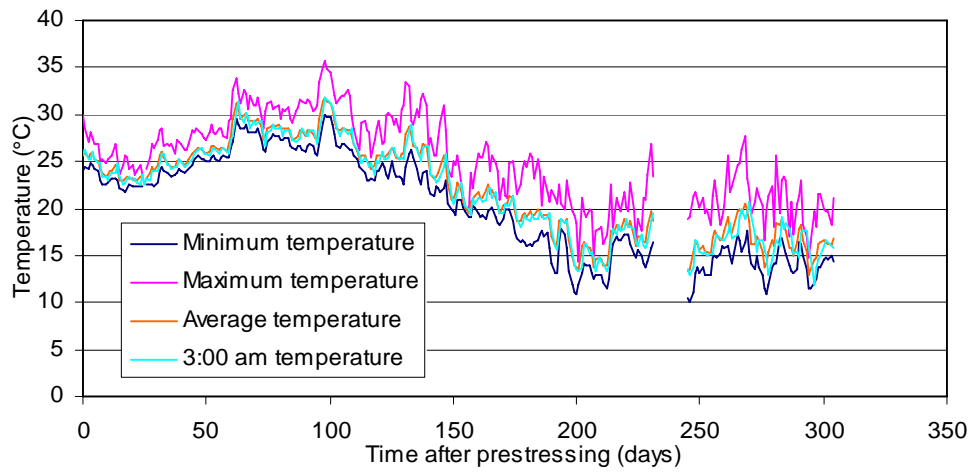
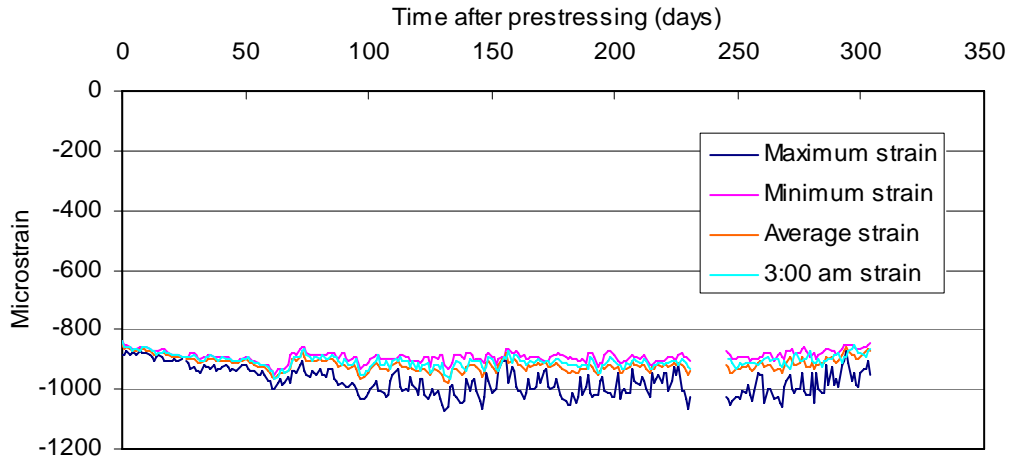


Figure C5: Location of gages at the near-bent section in F5.

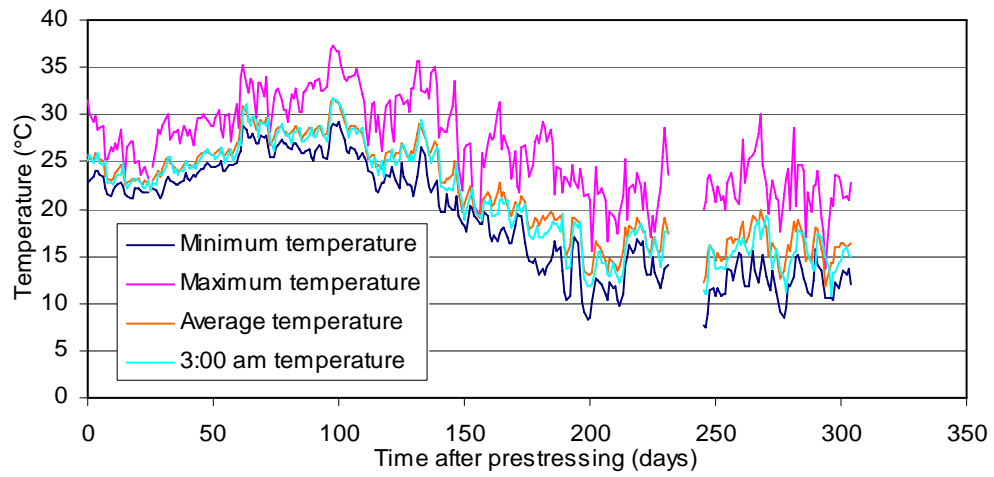
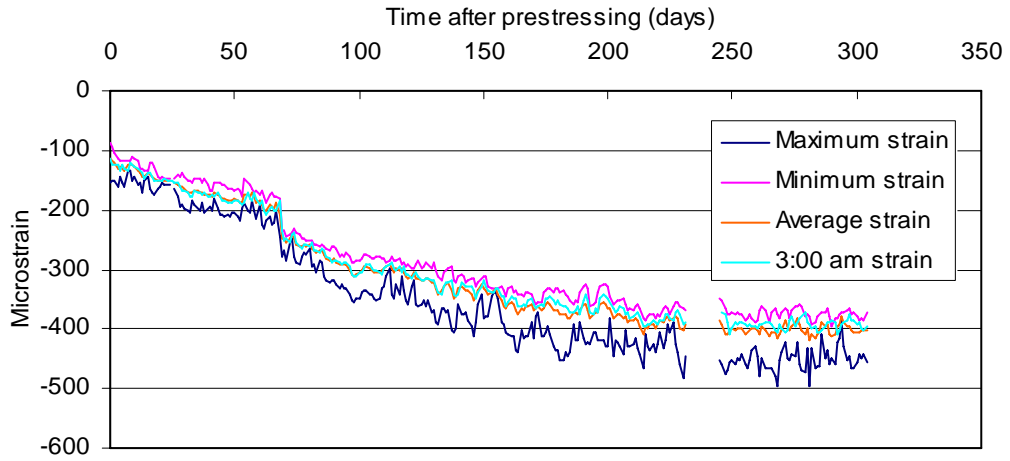
Stem A deck



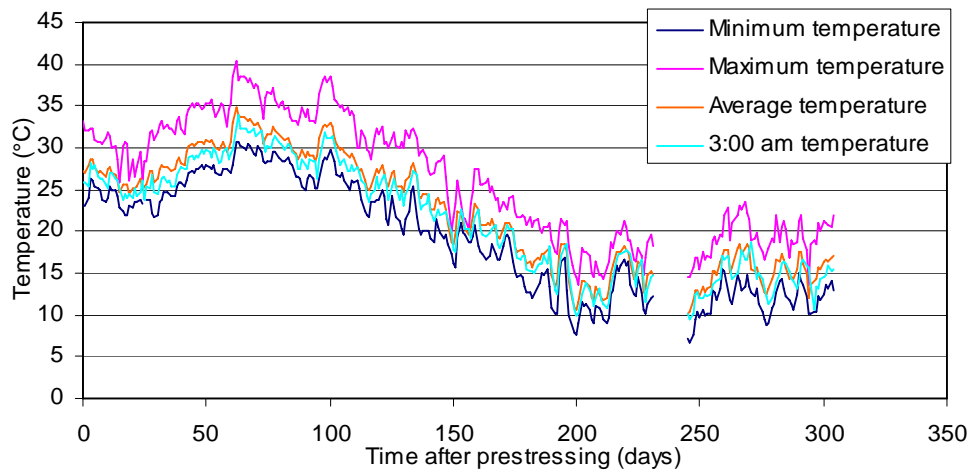
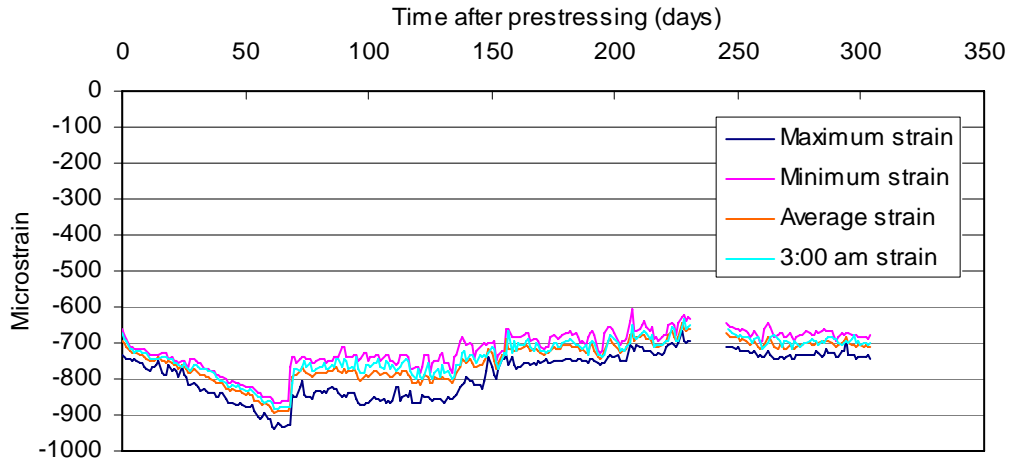
Stem A web



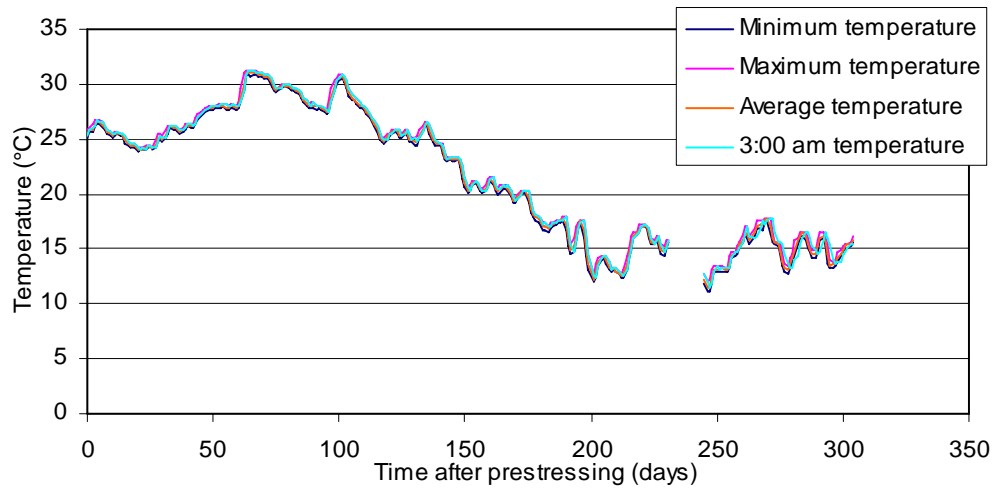
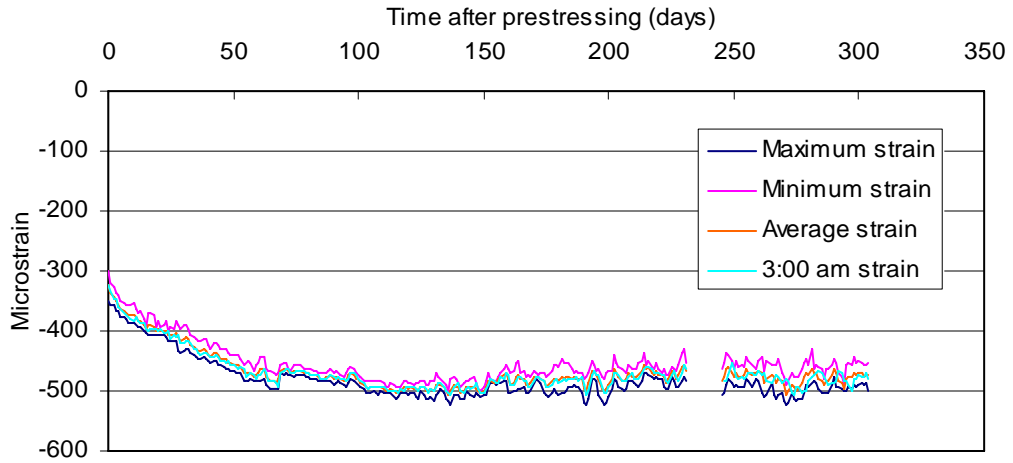
Stem A soffit



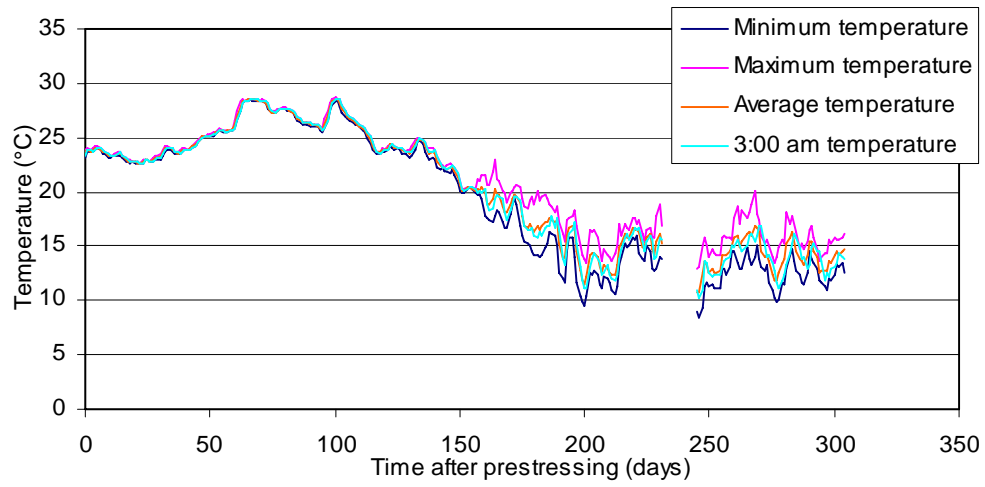
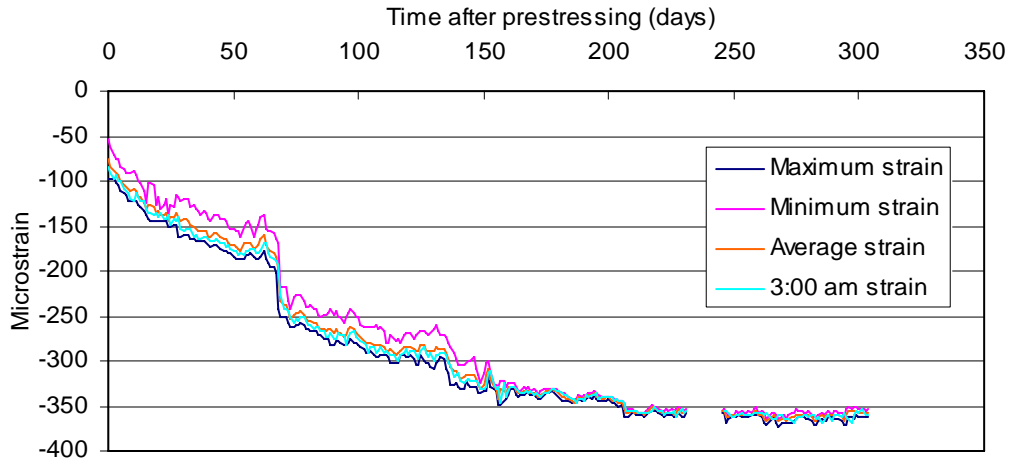
Stem B deck



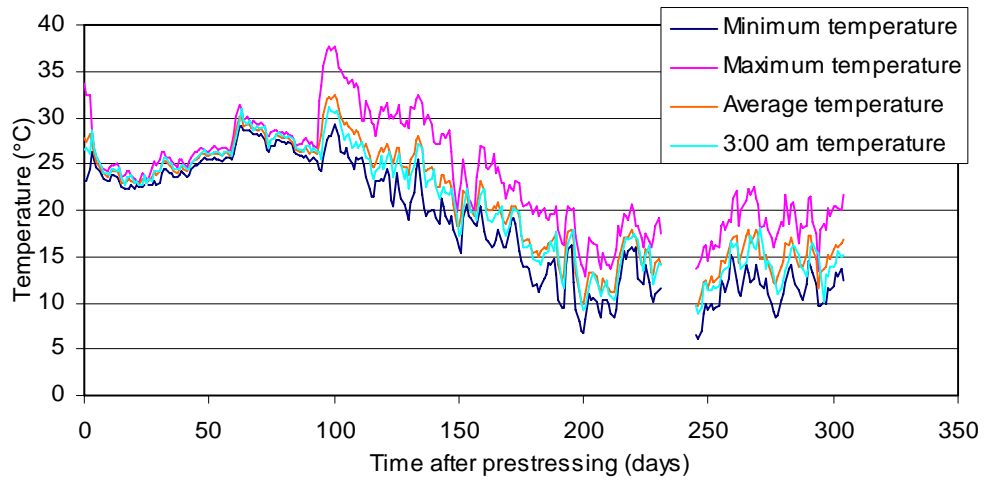
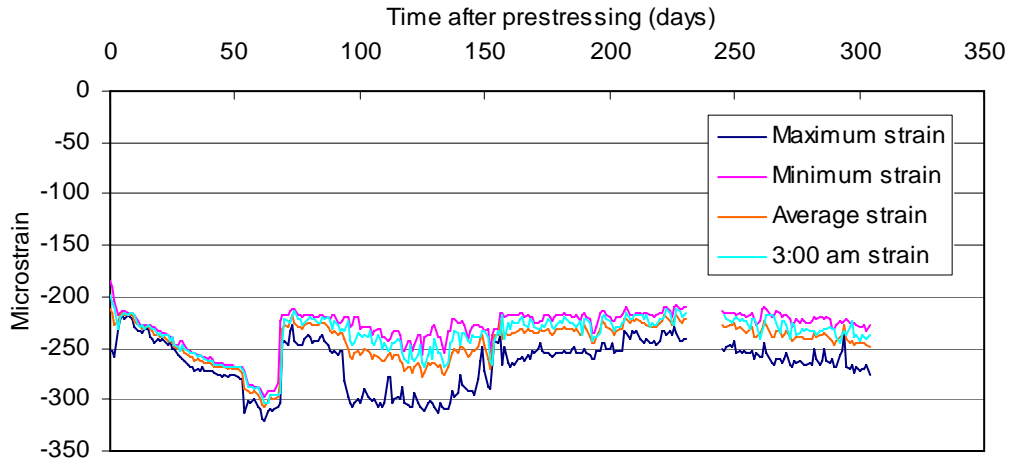
Stem B web



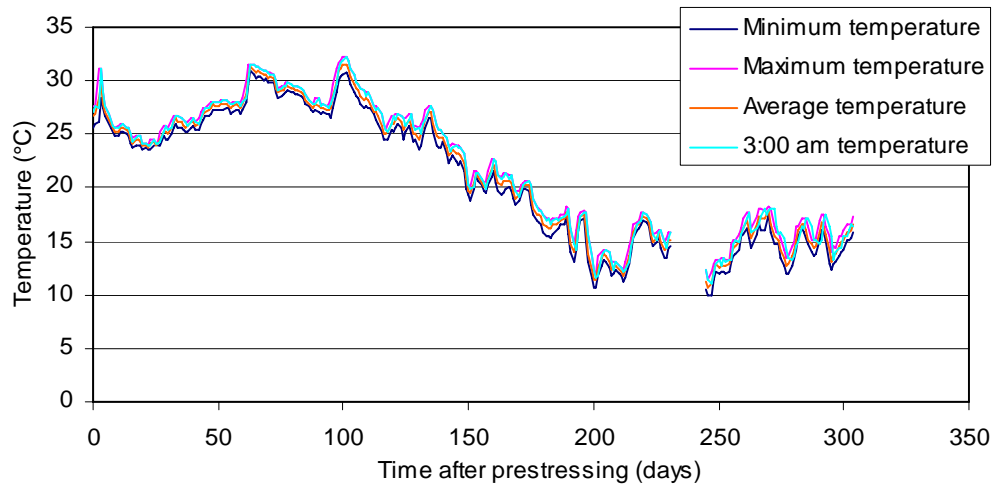
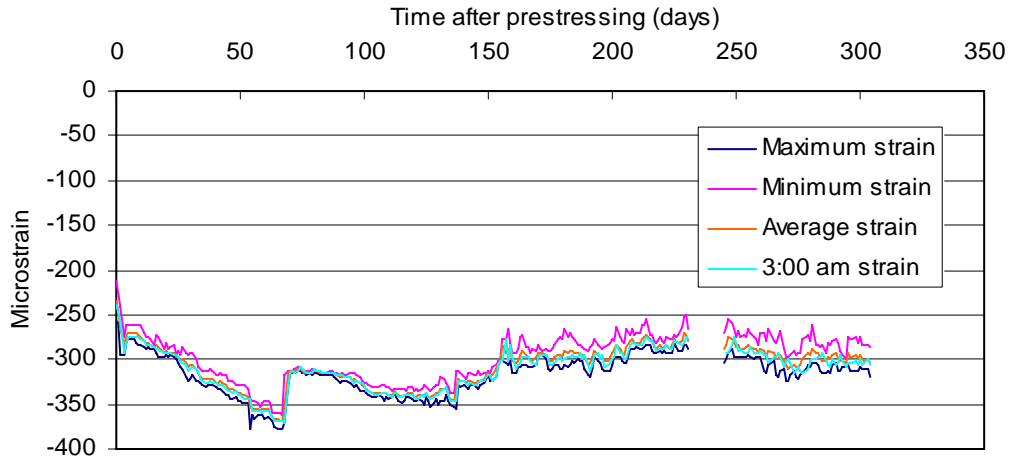
Stem B soffit



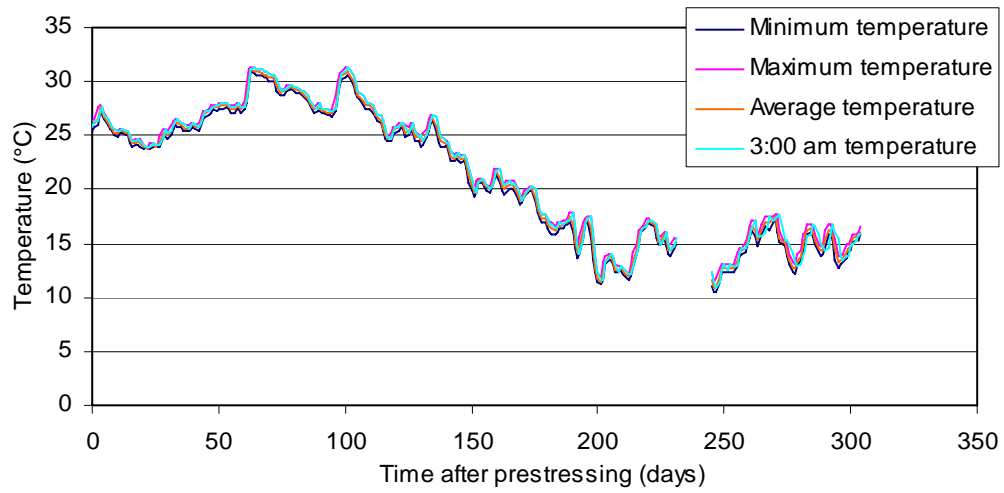
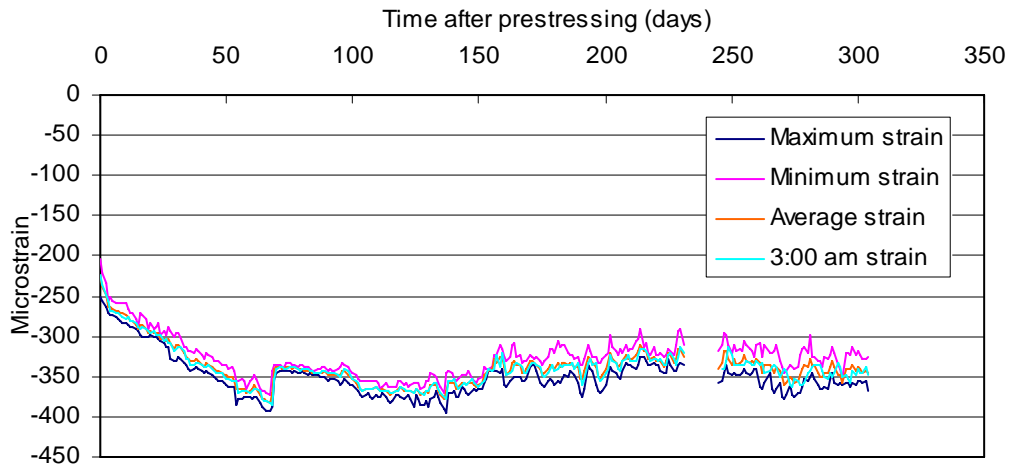
Stem C deck



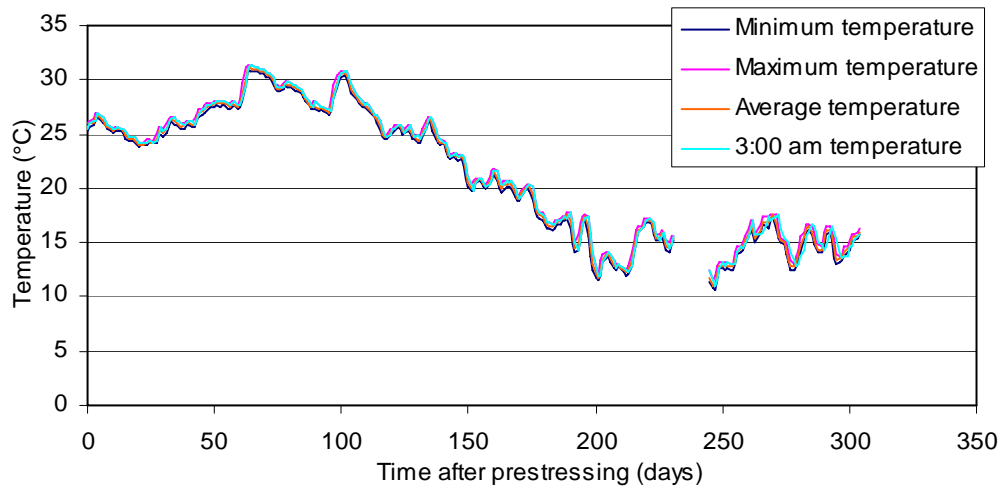
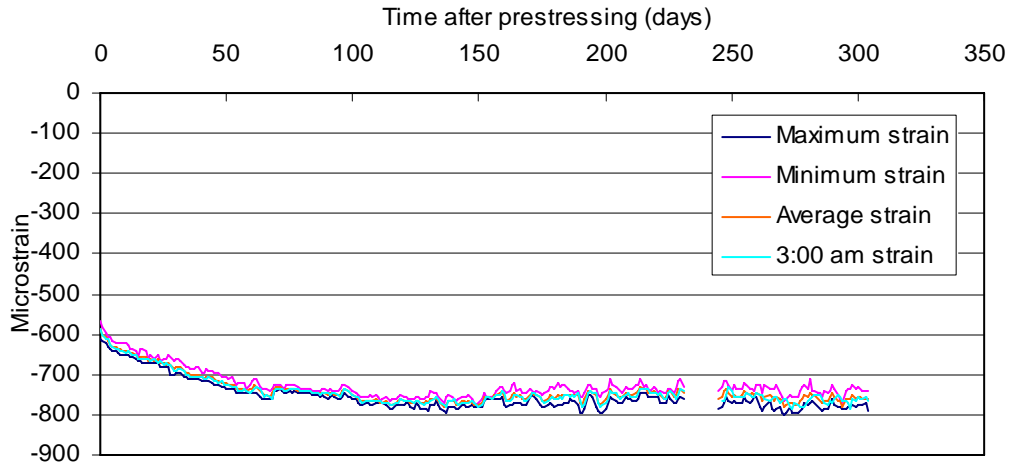
Stem C web (upper level)



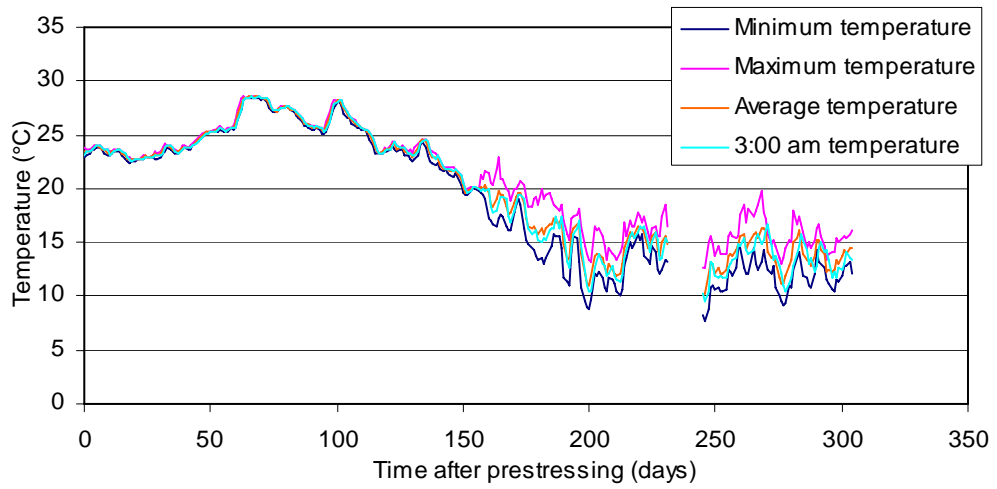
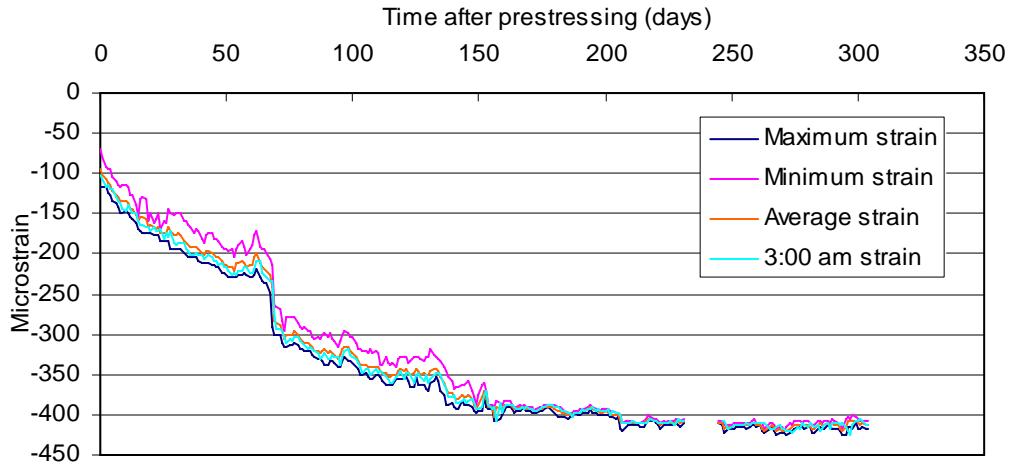
Stem C web (middle level)



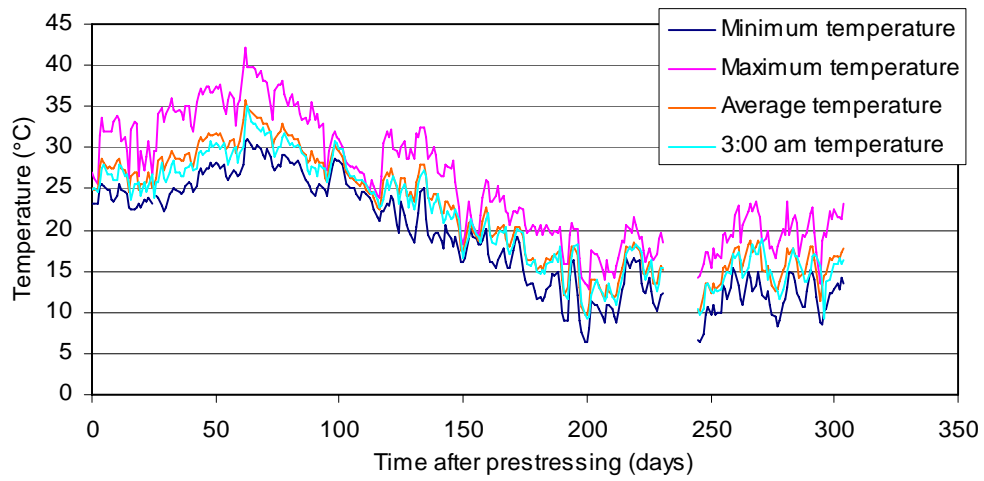
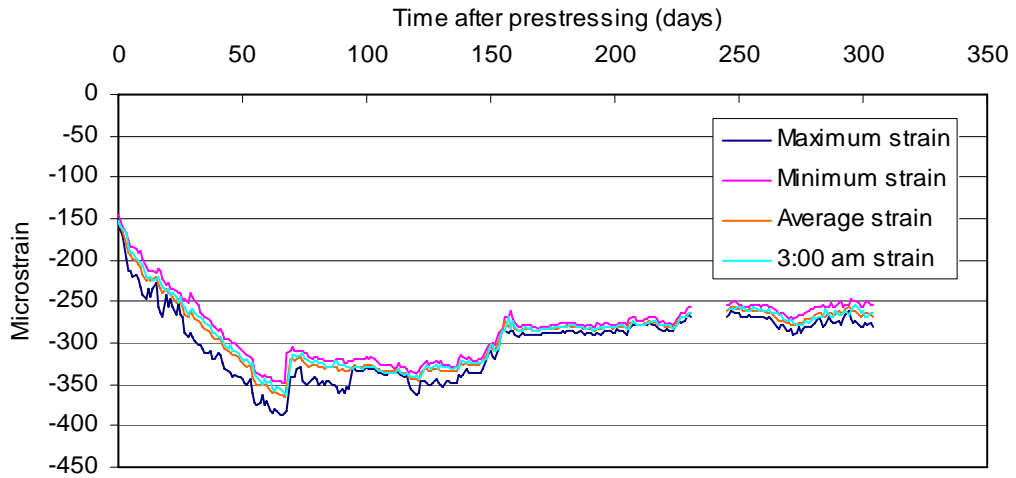
Stem C web (lower level)



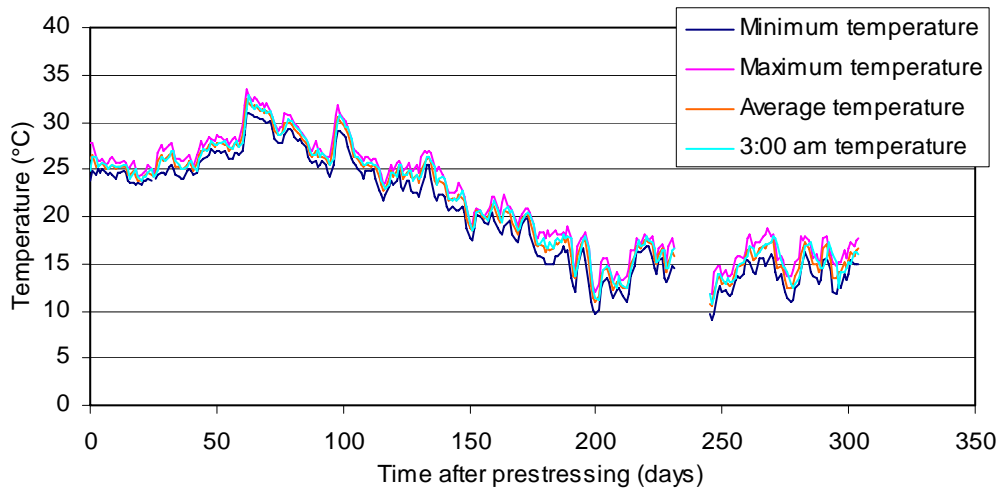
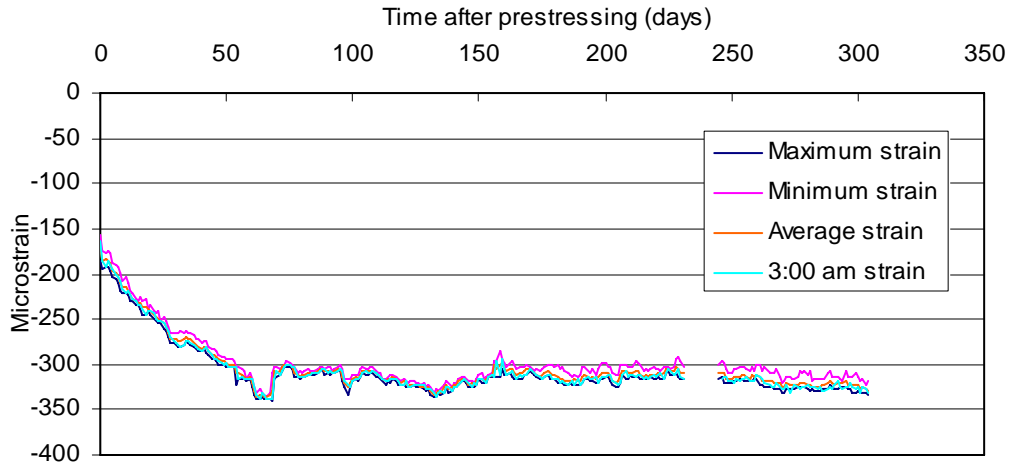
Stem C soffit



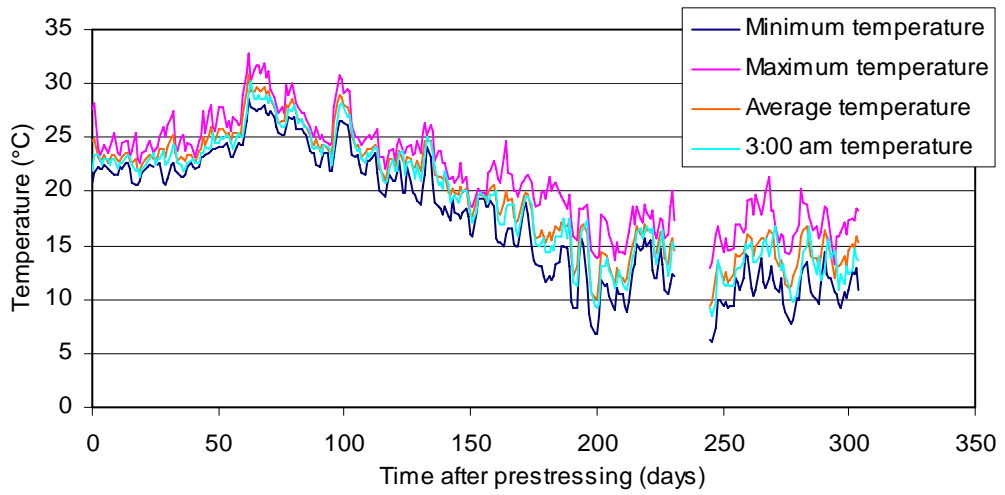
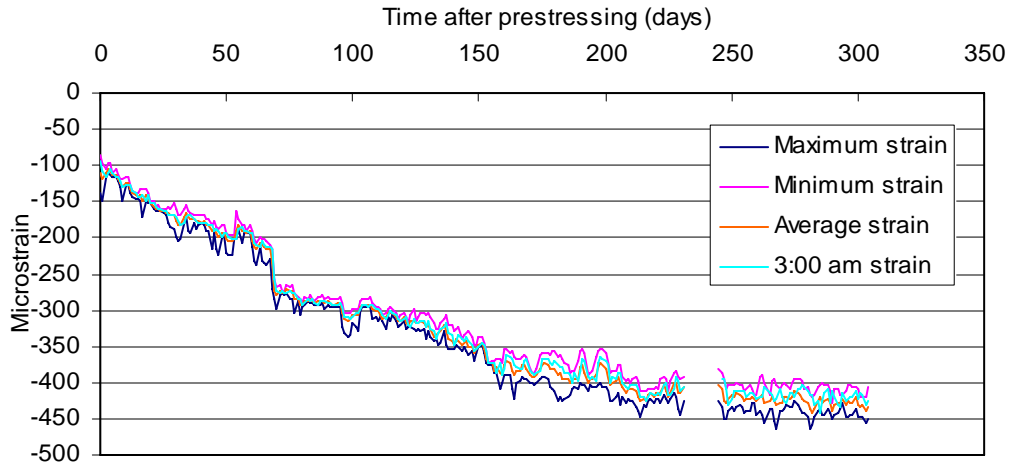
Stem D deck



Stem D web

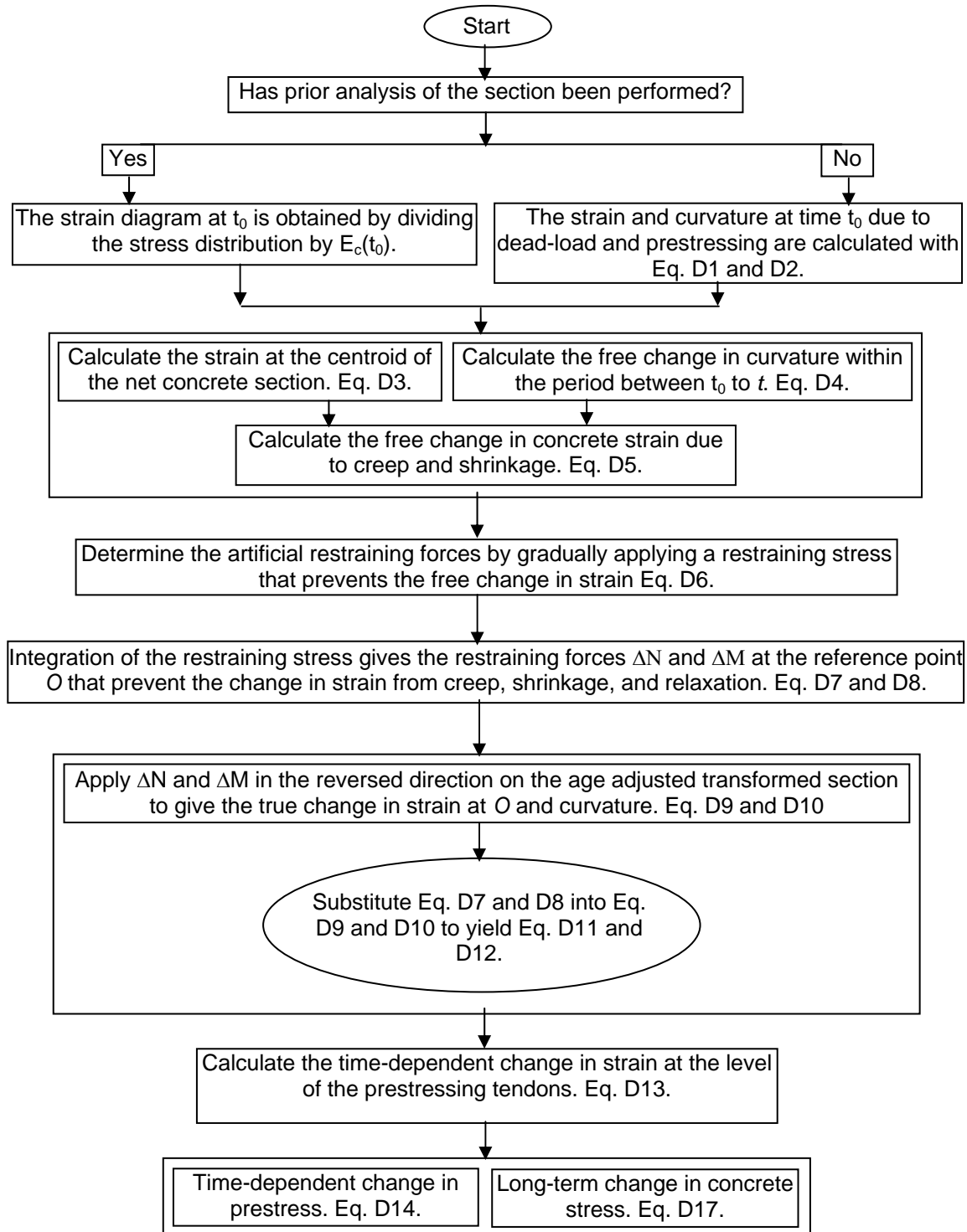


Stem D soffit



Appendix D

Steps of the Proposed Method



Sign Convention

Axial force N is positive when it is tensile. Bending moment M and its associated curvature ψ are positive when they produce tension at the bottom fiber of the cross section. Stress σ and strain ε are positive for tension and elongation. It follows that shrinkage ε_{sh} is a negative quantity; also, the relaxation in prestressing steel $\Delta\sigma_{pr}$ and the loss in tension due to combined effects of creep, shrinkage, and relaxation $\Delta\sigma_{ps}$ are negative. The analysis is considered for a prestressed concrete section with its centroidal principal y -axis in the vertical direction; the coordinate y of any concrete fiber or steel layer is measured downward from a reference point O (Figure D1).

List of Equations of the Proposed Method

$$\varepsilon_1(t_0) = \frac{N_D - P_{ps}}{A_1 E_c(t_0)} \quad (D1)$$

$$\psi(t_0) = \frac{M_D - P_{ps}(d_{ps} - d_1)}{I_1 E_c(t_0)} \quad (D2)$$

$$\varepsilon_{cc}(t_0) = \varepsilon_1(t_0) + (y_{cc} - y_1)\psi(t_0) \quad (D3)$$

$$\Delta\psi_{free} = \phi\psi(t_0) \quad (D4)$$

$$(\Delta\varepsilon_{cc})_{free} = \phi\varepsilon_{cc}(t_0) + \varepsilon_{sh} \quad (D5)$$

$$\sigma_r = -\bar{E}_c [(\Delta\varepsilon_{cc})_{free} + \Delta\psi_{free} y] \quad (D6)$$

$$\Delta N = -\bar{E}_c A_c (\Delta\varepsilon_{cc})_{free} + A_{ps} \Delta\bar{\sigma}_{pr} \quad (D7)$$

$$\Delta M = -\bar{E}_c I_c \Delta\psi_{free} - \bar{E}_c A_c (\Delta\varepsilon_{cc})_{free} y_{cc} + y_{ps} A_{ps} \Delta\bar{\sigma}_{pr} \quad (D8)$$

$$\Delta \varepsilon_O = -\Delta N / (\bar{E}_c \bar{A}) \quad (D9)$$

$$\Delta \psi = -\Delta M / (\bar{E}_c \bar{I}) \quad (D10)$$

$$\Delta \varepsilon_O = k_A (\Delta \varepsilon_{cc})_{free} - \frac{A_{ps}}{A} \frac{\Delta \bar{\sigma}_{pr}}{\bar{E}_c} \quad (D11)$$

$$\Delta \psi = k_I \Delta \psi_{free} + \frac{k_{cc}}{h} (\Delta \varepsilon_{cc})_{free} - \frac{A_{ps} y_{ps}}{\bar{I}} \frac{\Delta \bar{\sigma}_{pr}}{\bar{E}_c} \quad (D12)$$

$$\Delta \varepsilon_{ps} = \Delta \varepsilon_O + y_{ps} \Delta \psi \quad (D13)$$

$$\Delta \sigma_{ps} = E_{ps} (\Delta \varepsilon_O + y_{ps} \Delta \psi) + \Delta \bar{\sigma}_{pr} \quad (D14)$$

$$k_A = \frac{A_c}{A} \quad (D15a)$$

$$k_I = \frac{I_c}{I} \quad (D15b)$$

$$k_{cc} = \frac{A_c y_{cc} h}{I} \quad (D15c)$$

$$k_{ps} = 1 - \frac{E_{ps}}{\bar{E}_c} \left(\frac{A_{ps}}{A} + \frac{A_{ps} y_{ps}^2}{\bar{I}} \right) \quad (D15d)$$

Eq. D14 may also be represented by Eq. D16.

$$\Delta \sigma_{ps} = E_{ps} \left\{ k_A (\Delta \varepsilon_{cc})_{free} + y_{ps} \left[k_I \Delta \psi_{free} + k_{cc} (\Delta \varepsilon_{cc})_{free} / h \right] \right\} + k_{ps} \Delta \bar{\sigma}_{pr} \quad (D16)$$

$$\Delta \sigma = \bar{E}_c (\Delta \varepsilon_O - (\Delta \varepsilon_{cc})_{free} + y (\Delta \psi - \Delta \psi_{free})) \quad (D17)$$

List of Symbols used in the Proposed Method

E_{ps} = Modulus of elasticity of prestressing steel

E_{ns} = Modulus of elasticity of non-prestressed steel

$\bar{E}_c = \frac{E_c(t_0)}{(1 + \chi\phi)}$ = Age-adjusted elasticity modulus of concrete to account

for the creep effects of stresses applied gradually on concrete

$E_c(t_0)$ = Modulus of elasticity of concrete at time t_0

ϕ = Creep coefficient of concrete

χ = Aging coefficient

$\bar{\Delta}\sigma_{pr}$ = Reduced relaxation of prestressed steel, defined by $\chi_r \Delta\sigma_{pr}$

$\Delta\sigma_{pr}$ = Intrinsic relaxation of prestressed steel

χ_r = Reduced relaxation coefficient (0.7 ~ 0.8)

A_c = Area of net concrete section, that is gross concrete section minus
area of non-prestressed steel minus area of prestressing duct

A_{ps} = Area of prestressed steel

A_{ns} = Area of non-prestressed steel

A_1 = Area of the transformed section at t_0 composed of A_c plus

$$A_{ns} \left(\frac{E_{ns}}{E_c(t_0)} \right)$$

\bar{A} = Area of age-adjusted transformed section composed of A_c plus

$$A_{ns} \left(\frac{E_{ns}}{\bar{E}_c} \right) \text{ plus } A_{ps} \left(\frac{E_{ps}}{\bar{E}_c} \right)$$

I_c = Moment of inertia of A_c about its centroid

\bar{I} = Moment of inertia of \bar{A} about its centroid

y_{cc} = Depth of the centroidal axis of the net concrete section from O

y_{ps} = Depth of the centroid of prestressing tendons from O

y_1 = Depth of the centroidal axis of the transformed concrete section

h = Total thickness of section

$(\Delta\varepsilon_{cc})_{free}$ = Change in concrete strain if the creep and shrinkage were
unrestrained

$\Delta\psi_{free}$ = Change in concrete curvature if the creep and shrinkage were
unrestrained

$\varepsilon_{cc}(t_0)$ = Initial strain at the centroid of the net concrete section

ε_{sh} = Concrete shrinkage

$\psi(t_0)$ = Initial curvature of the concrete

$\varepsilon_1(t_0)$ = Initial strain in the concrete at the centroid of the transformed
section

$\Delta\varepsilon_O$ = Long-term change in strain at O

$\Delta\psi$ = Long-term change in curvature

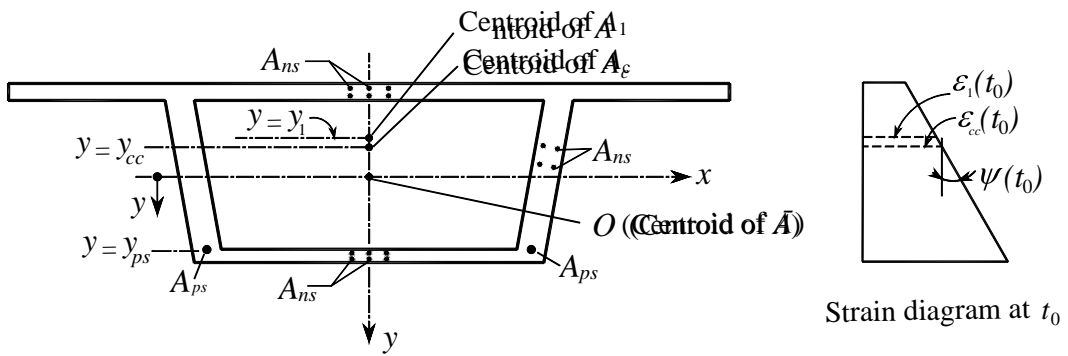


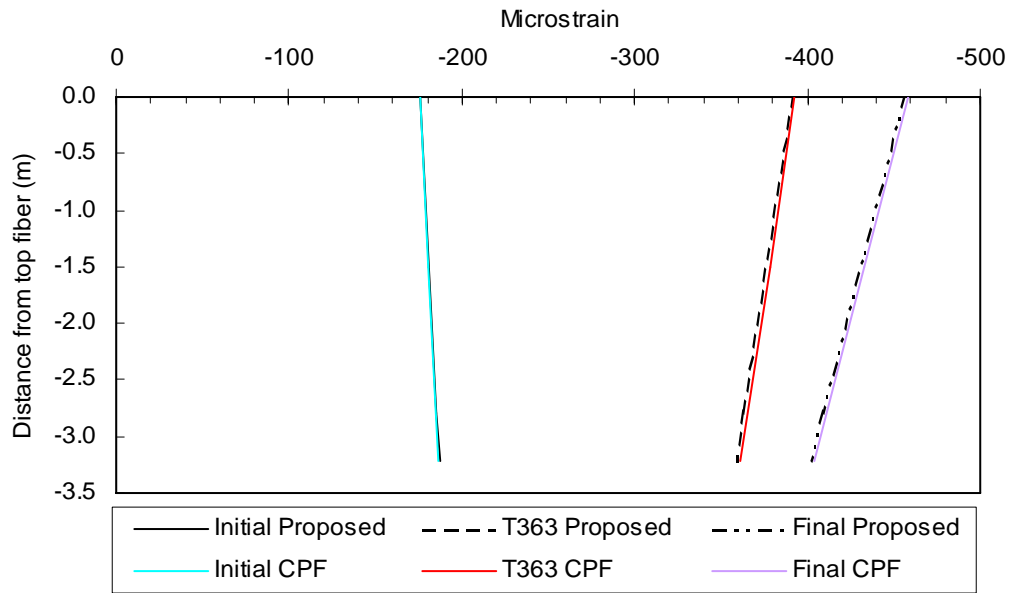
Figure D1: Typical prestressed concrete section and strain diagram immediately after prestressing.

Appendix E

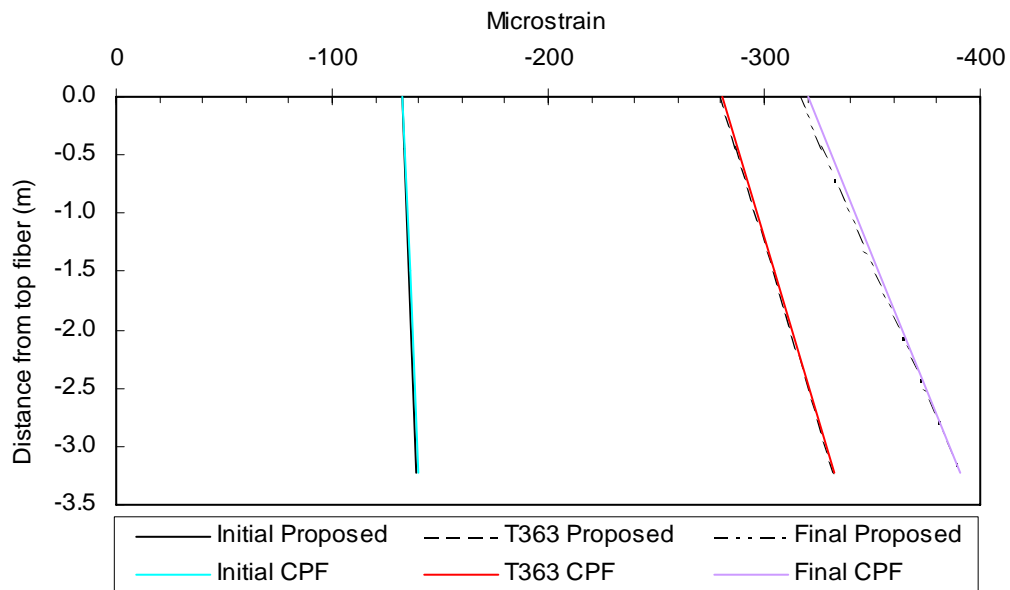
Comparison of Strains from CPF and the Proposed Method

Using ACI specified input data

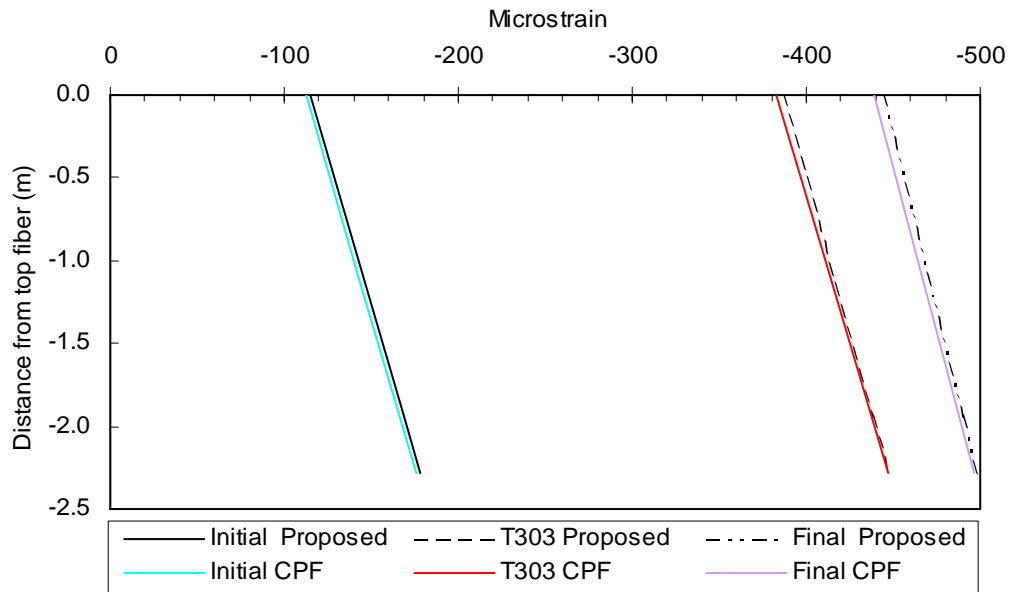
F4 at midspan



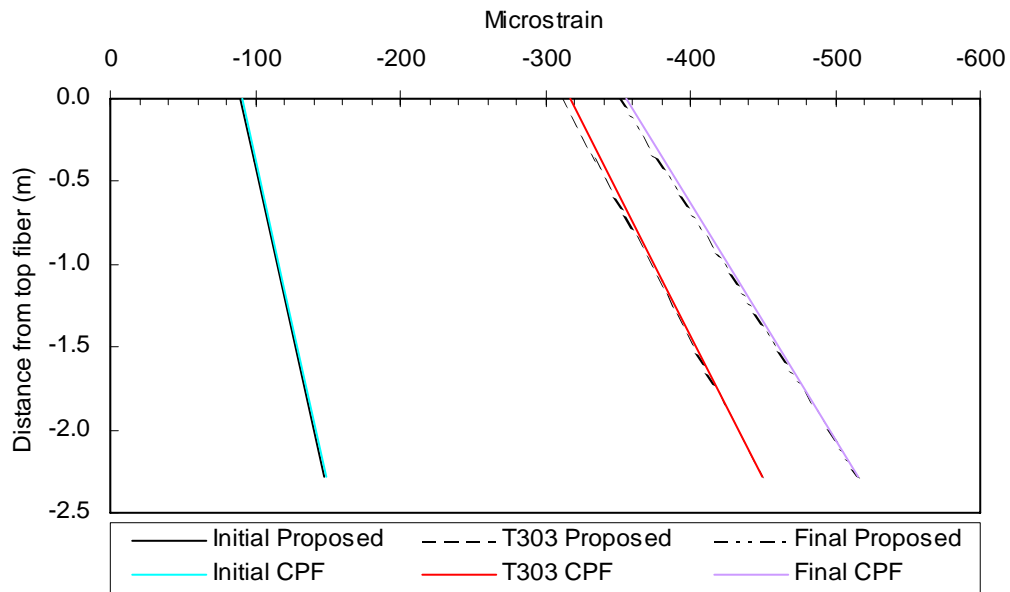
F4 near the bent



F5 at midspan

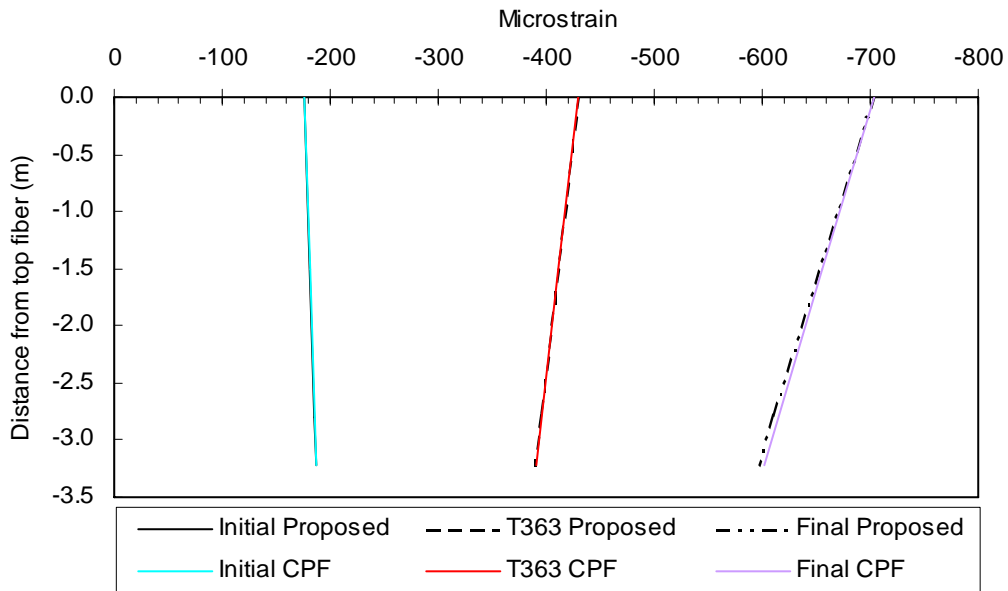


F5 near the bent

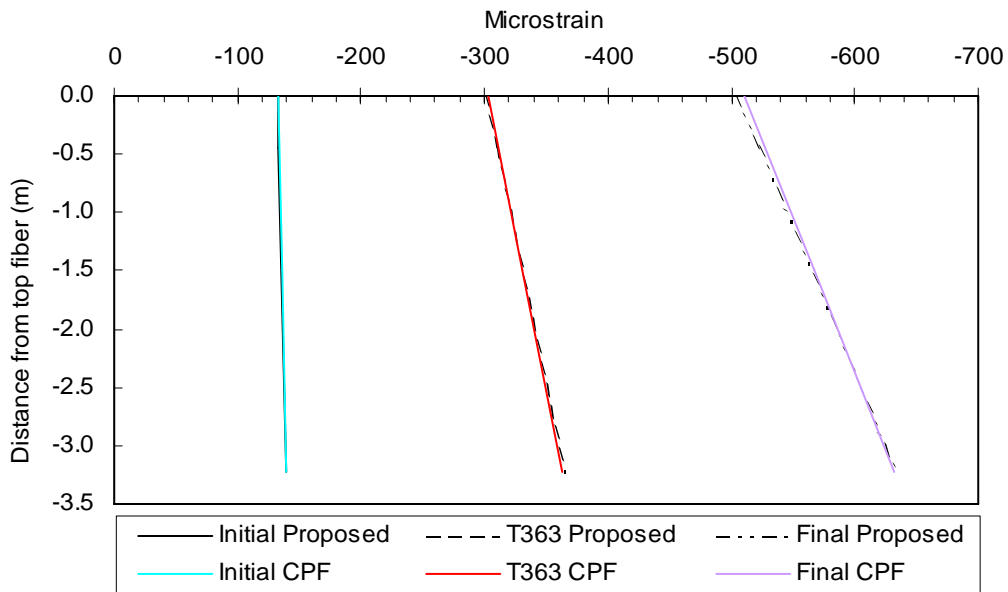


Using CEB-FIP specified input data

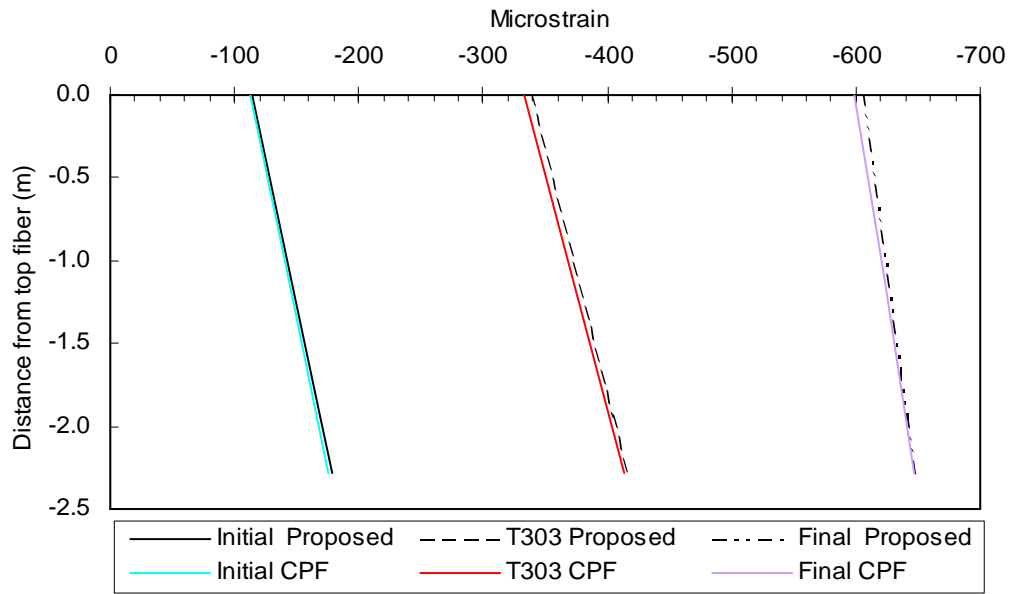
F4 at midspan



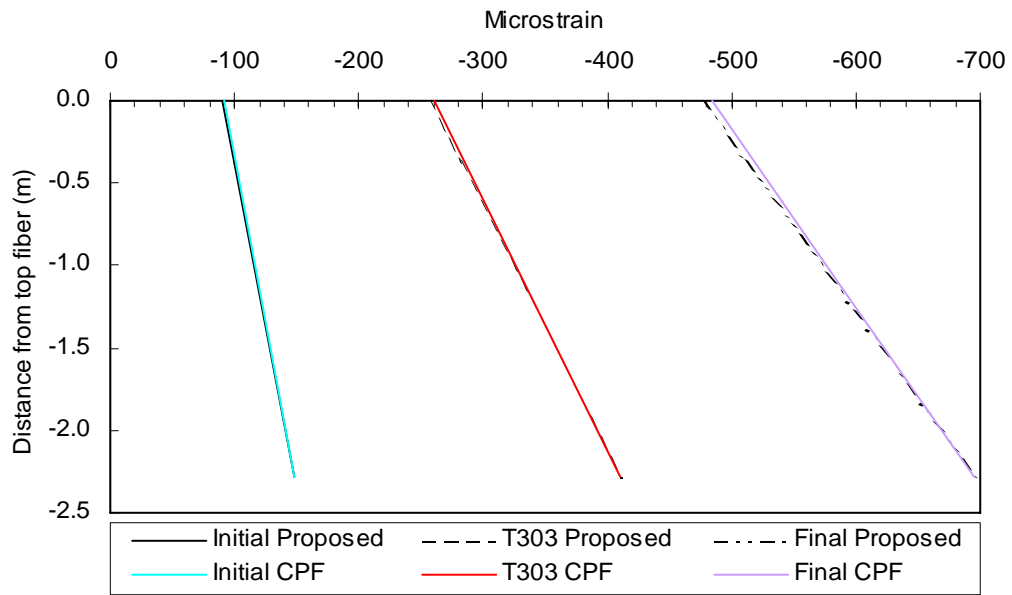
F4 near the bent



F5 at midspan

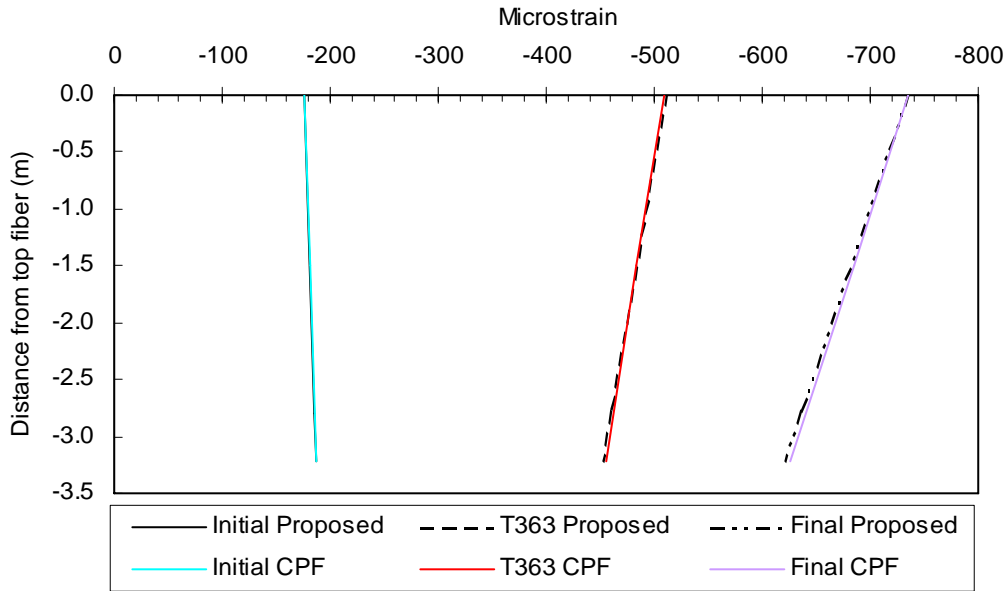


F5 near the bent

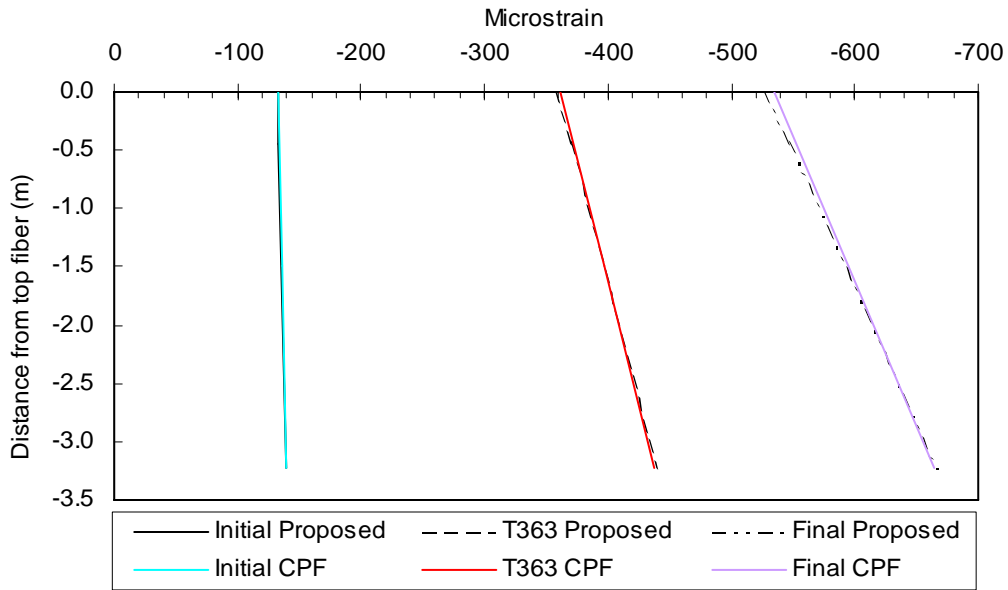


Using measured material properties as input data

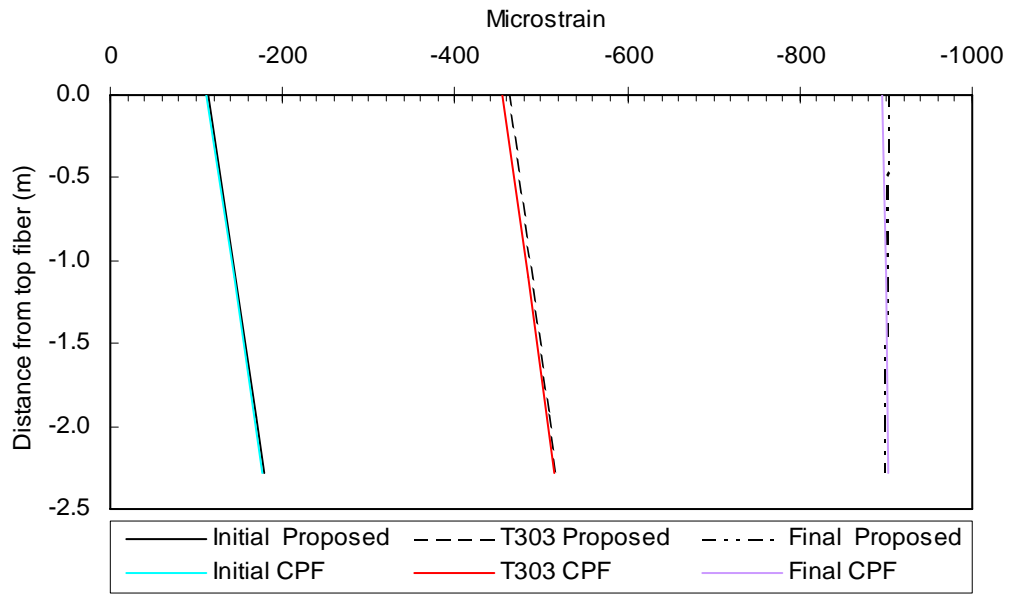
F4 at midspan



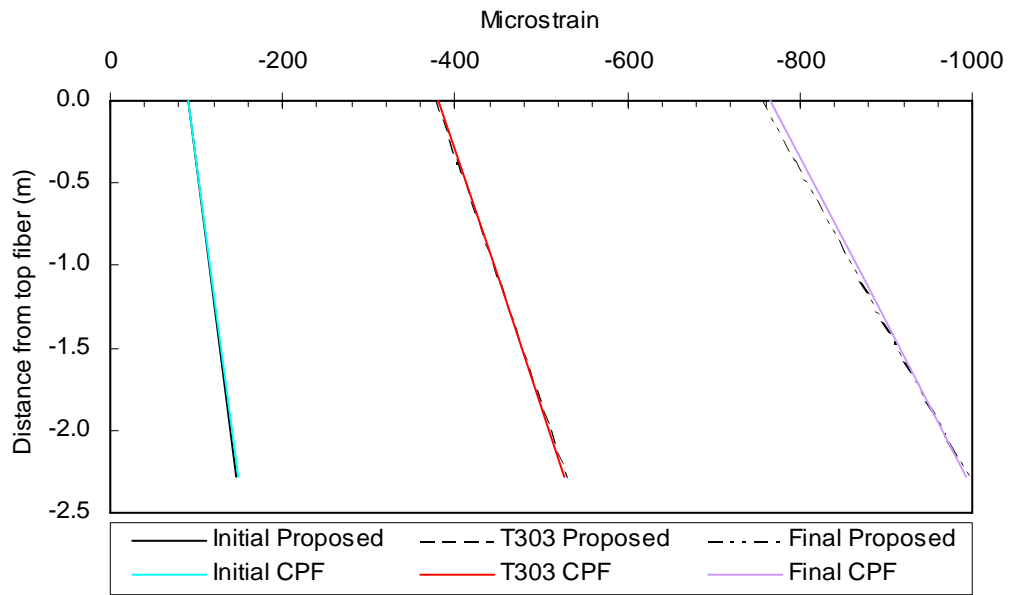
F4 near the bent



F5 at midspan



F5 near the bent

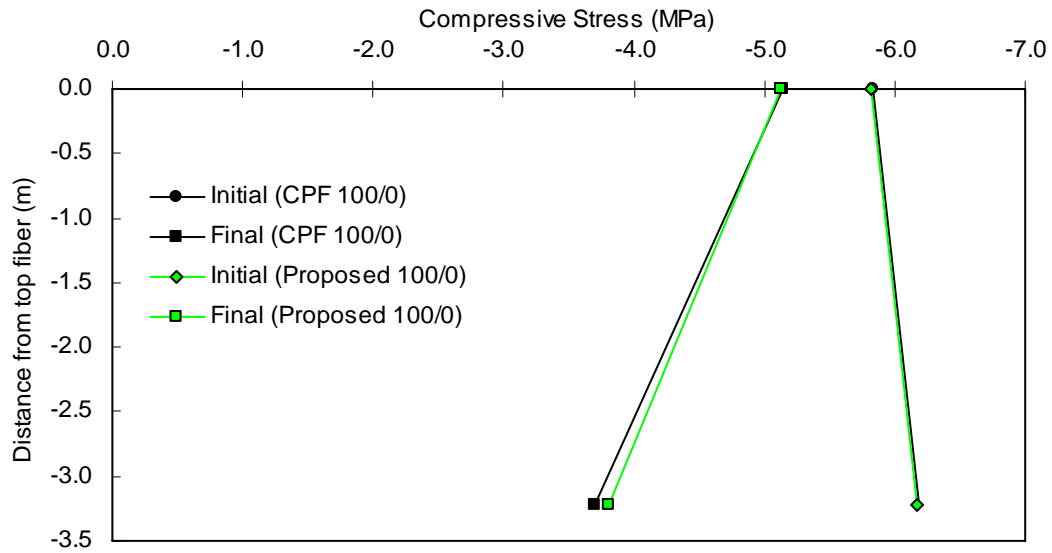


Appendix F

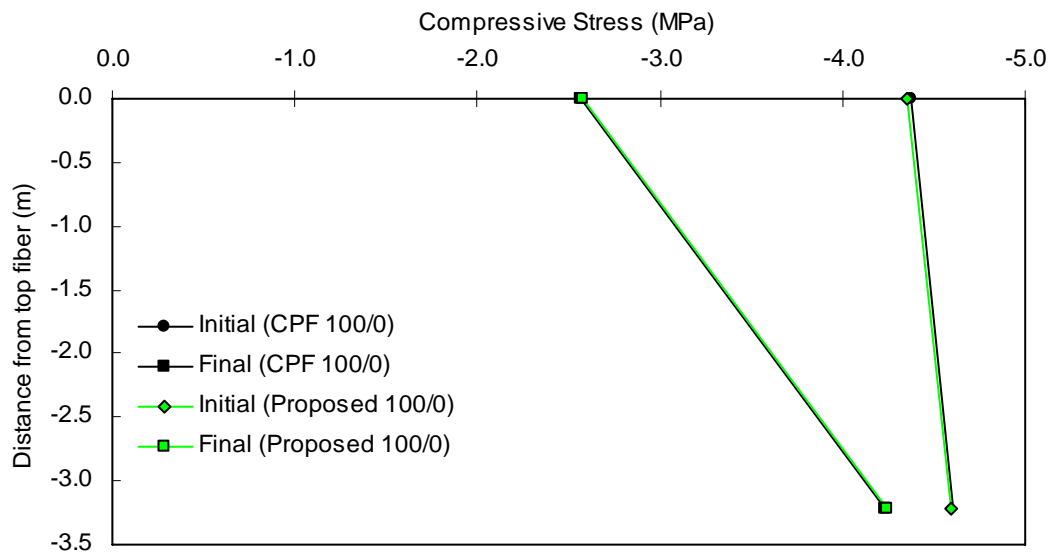
Comparison of Stresses from CPF and the Proposed Method

Using ACI specified input data

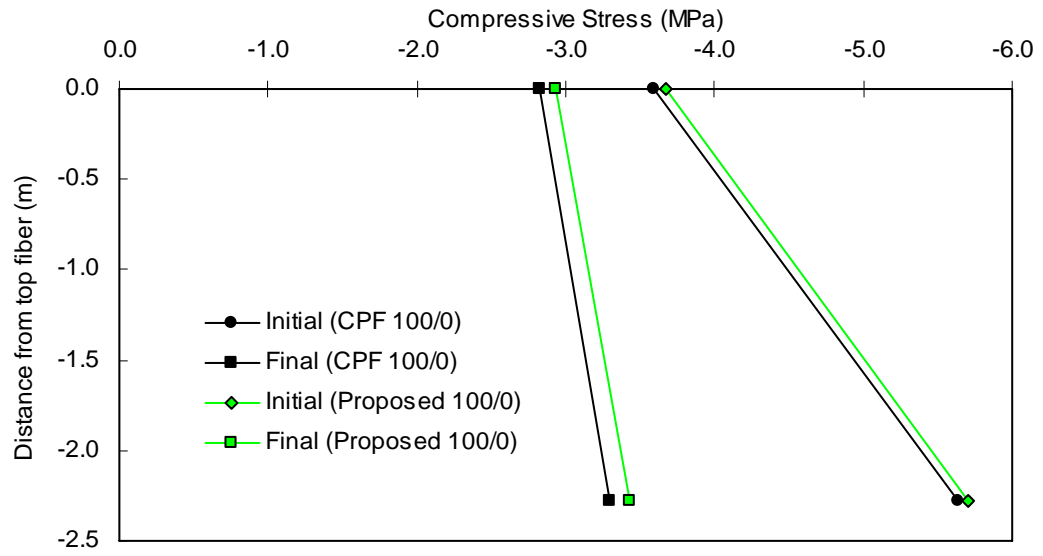
F4 at midspan



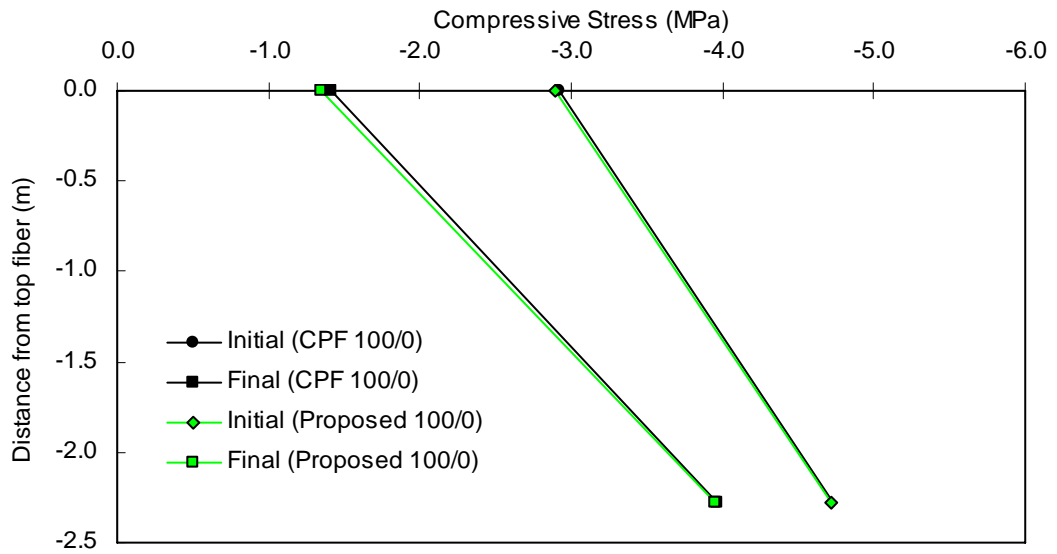
F4 near the bent



F5 at midspan

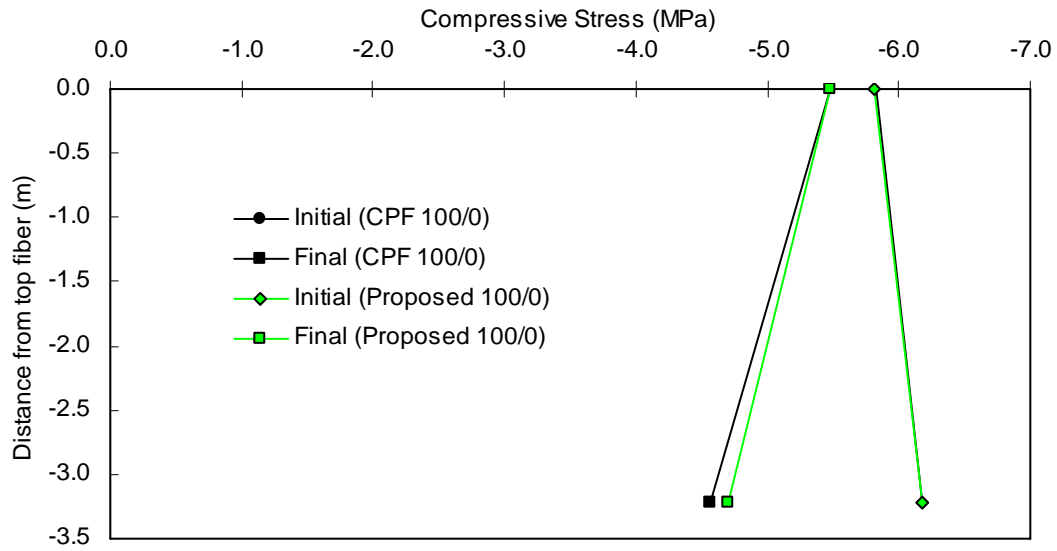


F5 near the bent

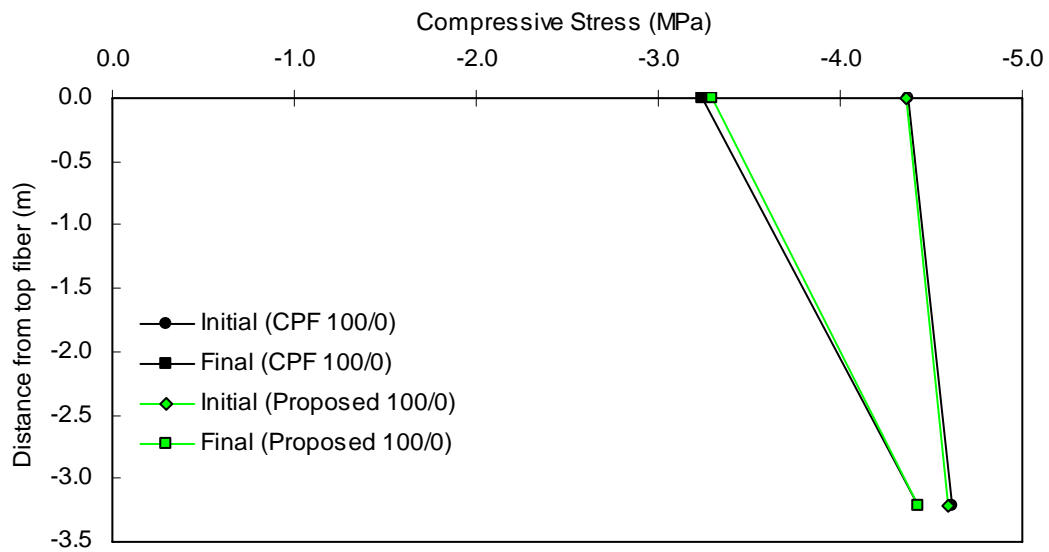


Using CEB-FIP specified input data

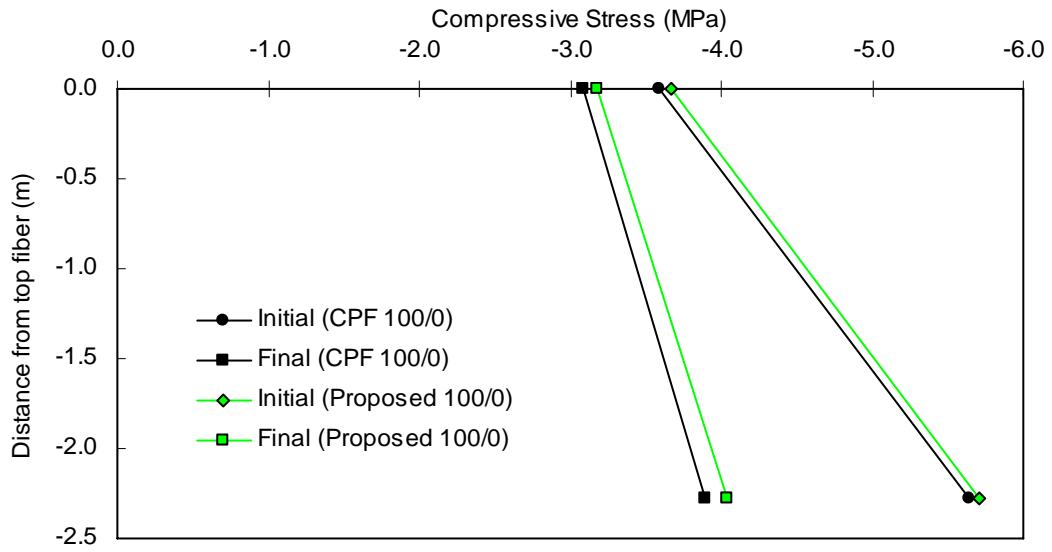
F4 at midspan



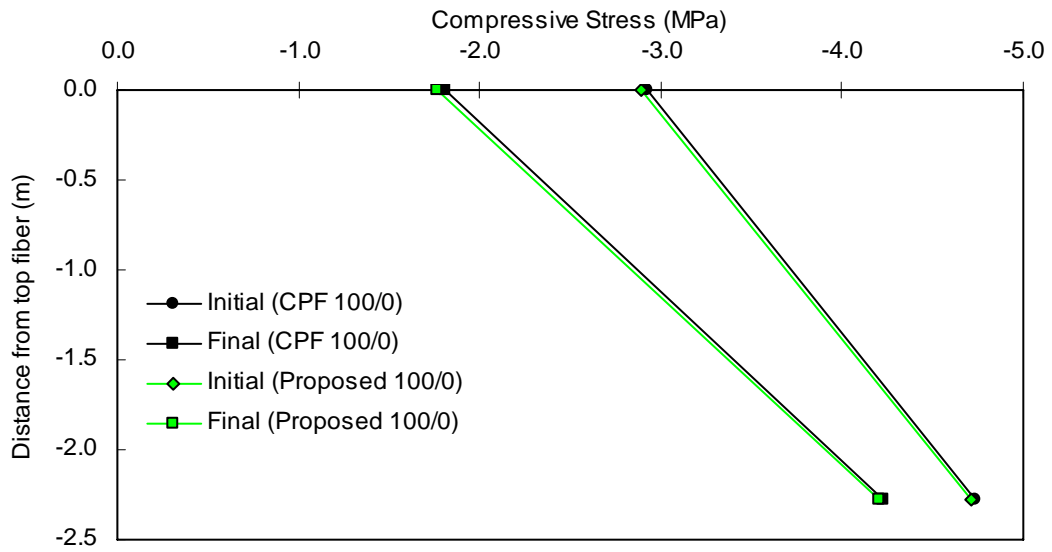
F4 near the bent



F5 at midspan

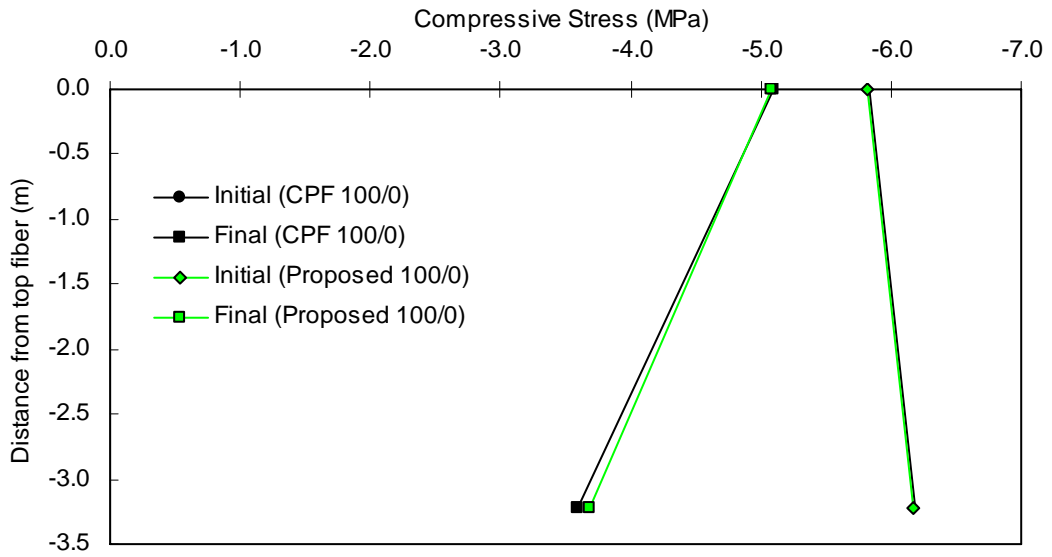


F5 near the bent

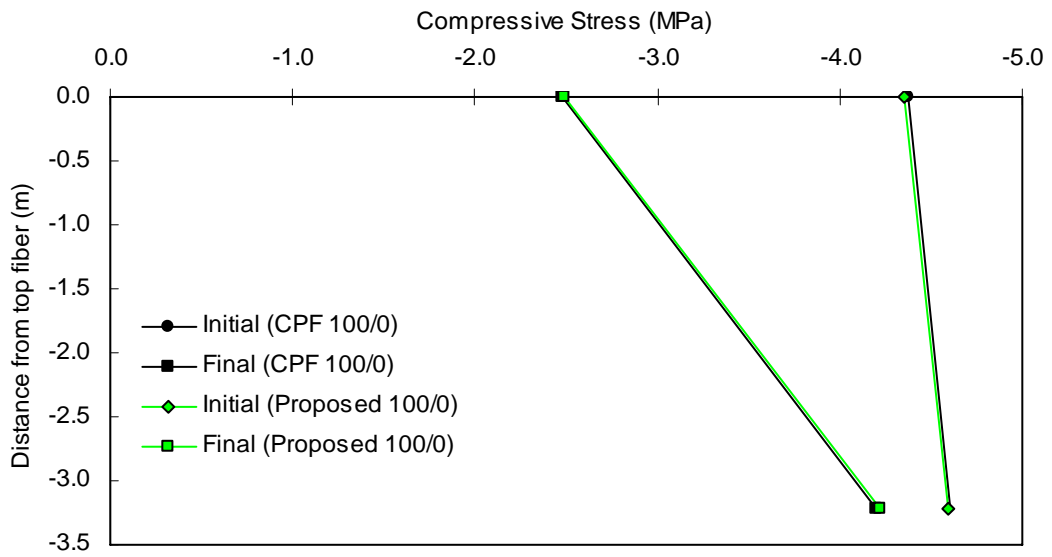


Using measured material properties as input data

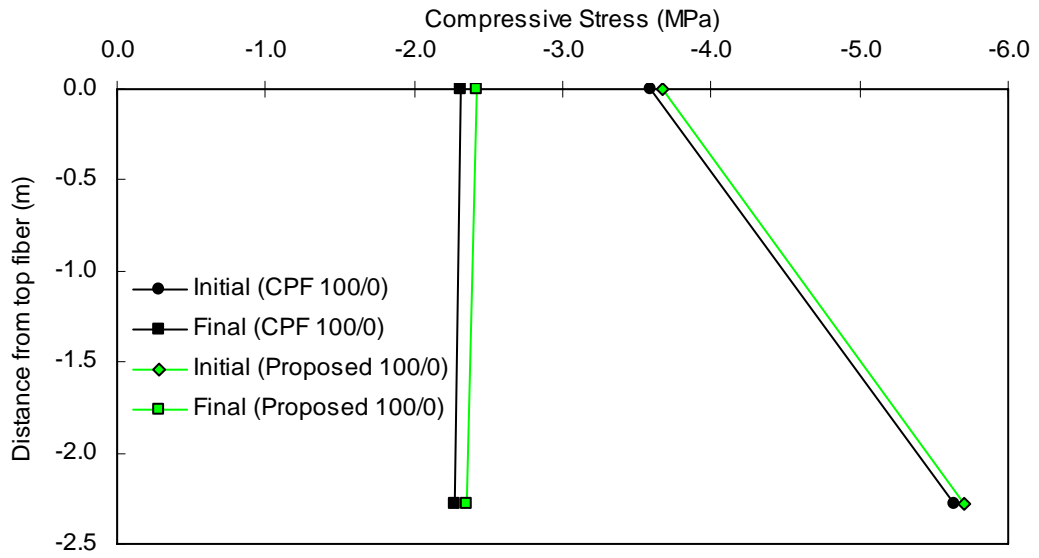
F4 at midspan



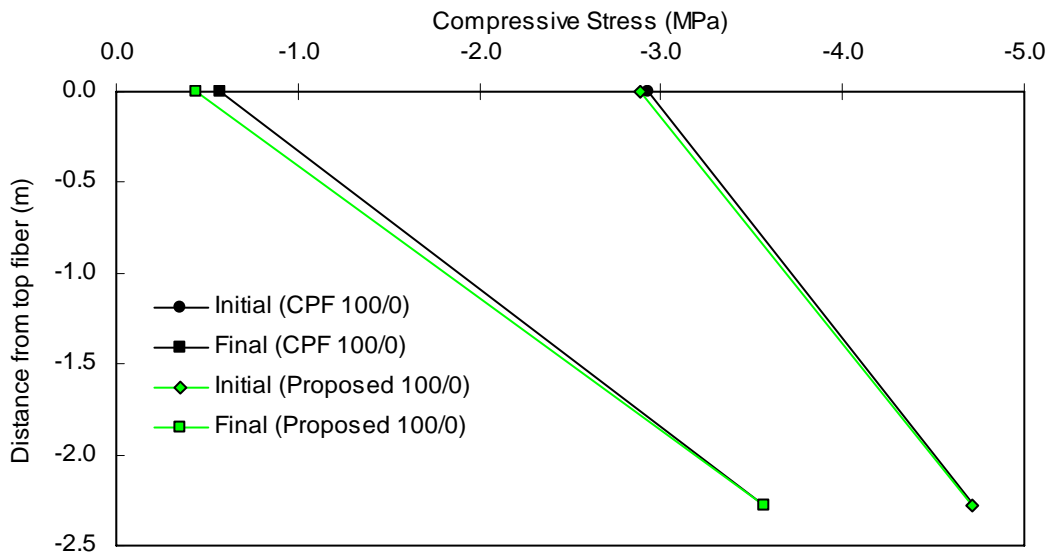
F4 near the bent



F5 at midspan



F5 near the bent



Appendix G

Example Input for CPF

Variables and parameters are as defined in [16].

TITLE: Frame 5 with LC50/50, CEB-FIP Material Properties

C**** SET 1: CONTROL PARAMETERS.

IOUT = 1

C** IOUT = program runs until completion

IUNITS = 1

C** IUNITS = indicator for type of units used

NPOIN = 10

C** NPOIN = total number of nodes (joints) in the structure

NELEM = 9

C** NELEM = total number of elements (members) in the structure

NSD = 10

C** NSD = total number of nodes with prescribed displacements including temporary supports

NCTYP = 3

C** NCTYP = total number of concrete types

NSTYP = 2

C** NSTYP = total number of reinforcing steel types

MNSC = 42

C** MNSC = largest number of sections in any member

MNCL = 3

C** MNCL = largest number of concrete layers in all sections

MNPSL = 2

C** MNPSL = total number of prestressed tendons in the structure

```

MNSL = 7
C**      MNSL = total number of Nonprestressed layers in the structure

NLSTG = 4
C**      NLSTG = total number of time intervals

IOWT = 0
C**      IOWT = indicator for calculation of self weight

IFRCT = 1
C**      IFRCT = indicator for calculation of friction losses in post-tensioned tendons

ITPND = 1
C**      ITPND = indicator for analysis of time-dependent effects

NONLIN = 1
C**      NONLIN = indicator for nonlinear analysis accounting for the effects of cracking

NITER = 10
C**      NITER = maximum number of iterations allowed per time interval

NORM = 0
C**      NORM = indicator for type of convergence criteria

TOLR = 0.01 0.01 0.01
C**      TOLR = tolerance ratios relating to the displacement components or nodal forces in global x,
C**      y, and z directions

IRELAX = 1
C**      IRELEX = indicator for calculation of time-dependent from relaxation of prestressed steel

ITDATA = 0
C**      ITDATA = indicator for generation of time-dependent concrete properties of concrete

C**** SET 2: MATERIAL PROPERTIES.

C**** FOR CONCRETE:

C**      I      ISTG      GAMA      ALFAT      FCT (N/m2)      FC28      T0      Ho

          1      1          0.0      0.0      100000000.0      GEN 1,3

          END-OF-GROUP

```

```

C** I = concrete type number
C** ISTG = the number of the time interval at the start of which concrete type I is introduced to
C** the structure
C** GAMA = specific weight (density) of concrete type I
C** ALFAT = coefficient of thermal expansion of concrete type I
C** FCT = tensile strength of concrete type I
C** FC28 = compressive strength of concrete type I at 28 days
C** T0 = age in days of concrete type I at time of first loading
C** Ho = notional thickness of concrete parts of type I

```

```

C**** FOR STEEL:

```

```

C** I      ES (N/m2)    BETAI    ALFAT

      1      200.E+9    1.0
      2      193.E+9    1.0
END-OF-GROUP

```

```

C** I = steel type number
C** ES = modulus of elasticity of steel type I
C** BETAI = coefficient for high bond reinforcing steel
C** ALFAT = coefficient of thermal expansion of steel type I

```

```

C** I      AMU      AK      DL

      2      0.20    0.0000000001    0.01
END-OF-GROUP

```

```

C** I = prestressed steel type number
C** AMU = curvature friction coefficient for steel type I
C** AK = wobble friction coefficient for steel type I
C** DL = magnitude of anchor slip for steel type I

```

```

C**** SET 3: COORDINATES OF NODES.

```

```

C** I      XI(I) (m)    YI(I) (m)

      1      0.0      14.78
      2      0.990    14.78
      3      52.815    14.78
      4      105.635    14.78

```

```

5      158.455      14.78
6      165.155      14.78
7      166.605      14.78
8      52.815       0.0
9      105.635      0.0
10     158.455      3.5      ! Locations of nodes are defined in Figure 4.8
END-OF-GROUP

```

```

C** I = node number
C** XI(I) = global x-coordinate of node I
C** YI(I) = global y-coordinate of node I

```

```

C**** SET 4: DATA FOR PRESTRESSING TENDONS.

```

```

1      2      1      2      5      3      ! I, (IPSTYP(I,J), J=1,5)

18587755.0 (kN) 18587755.0 0.01344 (m) 0.03871 (m) ! (PL(I,J), J=1,2), APSL(I)

1      2      3      ! (IPCT(I,J), J=1,NCTYP)

2      2      1      2      5      3      ! I, (IPSTYP(I,J), J=1,5)

19362245.0 (kN) 19362245.0 0.01400 (m) 0.03871 (m) ! (PL(I,J), J=1,2), APSL(I)

1      2      3      ! (IPCT(I,J), J=1,NCTYP)

```

```

END-OF-GROUP

```

```

C** I = prestressing tendon number
C** IPSTYP(I,1) = steel type number of tendon I
C** IPSTYP(I,2) = number of the time interval at the start of which tendon I is post-tensioned
C** IPSTYP(I,3) = number of the element which contains the "first" end of tendon I
C** IPSTYP(I,4) = number of the element which contains the "second" end of tendon I
C** IPSTYP(I,5) = identifier of the jacking end
C** PL(I,1) = jacking force at the "first" end of tendon I
C** PL(I,2) = jacking force at the "second" end of tendon I
C** APSL(I) = cross-sectional area of tendon I
C** DUCTL(I) = cross-sectional area of duct for post-tensioned tendon I
C** (IPCT(I,J), J = 1, NCTYP) = list of numbers of the concrete types through which tendon I passes

```

C**** SET 5: TOPOLOGY OF MEMBERS AND SECTION DIMENSIONS.

C**** MEMBER 1. Left Hinge (Span 15)

C**** CONTROL INFORMATION.

C** IE NOD(IE,1) NOD(IE,2) NSEC NCL NPSL NSL INTG ILSTG DO (m) SRM (m)

1 1 2 14 2 0 7 1 1 1.1 0.15

C** IE = member number

C** NOD(IE,1) = number of the starting node of member IE

C** NOD(IE,2) = number of the end node of member IE

C** NSEC = total number of sections in member IE

C** NCL = total number of divisions (layers) of the cross-section depth

C** NPSL = total number of prestressed tendons in member IE

C** NSL = total number of nonprestressed steel layers in member IE

C** INTG = indicator of integration scheme for displacement calculation

C** ILSTG = number of the time interval at the start of which member IE is introduced in the structure

C** DO = depth of the reference axis

C** SRM = average spacing between cracks

C** NC DX

4 0.089646

1 0.0

8 0.080177

C** NC = number of divisions of equal spacing between sections

C** DX = ratio of the length of one division to the total length of the member

C** IWSC(IE,I), I=1,NSEC

1 3 5 6 10 14

C** IWSC(IE,I), I=1,NSEC = list of the section numbers (in member IE) for which internal forces,

C** strains, and stresses in concrete and steel are to be printed out

C**** CONCRETE DIMENSIONS INFORMATION.

C** PART 1: NC ICTYP(1,1) ICTYP(1,2)

1 3 0

C** NSTRT NEND BTL (m) BBL (m) BTR BBR BTC BBC

```

          1          14          10.33          10.33
C**      NSTRT      NEND      DCTL (m) DL (m)      DCTR      DR      DCTC      DC
          1          14          0.0          1.380

```

```

C** PART 2: NC      ICTYP(1,1)      ICTYP(1,2)
          1          3          0

```

```

C**      NSTRT      NEND      BTL (m)      BBL (m)      BTR      BBR      BTC      BBC
          6          14          10.33          10.33

```

```

C**      NSTRT      NEND      DCTL (m) DL (m)      DCTR      DR      DCTC      DC
          6          14          1.380          2.750

```

END-OF-GROUP

```

C** NC = number of concrete layers (having the same thickness) in concrete part J
C** ICTYP(1,1) = concrete type number of part J
C** ICTYP(1,2) = indicator to which concrete section properties are given as data or calculated
C** by computer

```

```

C** NSTRT = section number at the beginning of a segment over which the width is constant or
C** varying linearly or parabolically
C** NEND = section number at the end of the same segment
C** BTL = width at the top of part J at the beginning of the segment
C** BBL = width at the bottom of part J at the beginning of the segment
C** BTR = width at the top of part J at the end of the segment
C** BBR = width at the bottom of part J at the end of the segment
C** BTC = width at the top of part J at the center of the segment
C** BBC = width at the bottom of part J at the center of the segment

```

```

C** NSTRT = section number at the beginning of a segment over which the width is constant or
C** varying linearly or parabolically
C** NEND = section number at the end of the same segment
C** DCTL = distance from the top fiber of the cross-section to the top fiber of part J at the
C** beginning of the segment
C** DL = depth of concrete part J at the beginning of the segment
C** DCTR = distance from the top fiber of the cross-section to the top fiber of part J at the
C** end of the segment
C** DR = depth of concrete part J at the end of the segment
C** DCTC = distance from the top fiber of the cross-section to the top fiber of part J at the
C** center of the segment
C** DC = depth of concrete part J at the center of the segment

```

C**** LAYOUT AND PROPERTIES OF NONPRESTRESSED STEEL LAYERS.

```

C** I INSTYP(I,1) INSTYP(I,2) NSTRT NEND ASL (m2) DSL (m) DSR DSC

```

1	1	1	1	14	0.0097	0.525
2	1	1	1	14	0.0097	0.881
3	1	1	1	14	0.0097	1.237
4	1	2	6	14	0.0097	1.593
5	1	2	6	14	0.0097	1.949
6	1	2	6	14	0.0097	2.305
7	1	2	6	14	0.0120	2.661

C** I = nonprestressed steel layer number
 C** INSTYP(I,1) = steel type number of layer I
 C** INSTYP(I,2) = number of the concrete later which includes the nonprestressed steel layer I
 C** NSTRT = number of the section at which layer I starts
 C** NEND = number of the section at which layer I ends
 C** ASL = cross-sectional area of layer I
 C** DSL = distance from the top face of the member to layer I at its start
 C** DSR = distance from the top face of the member to layer I at its end
 C** DSC = distance from the top face of the member to layer I at its center

C**** MEMBER 2. Left Cantilever, 52.82 m span (Span 15)

C**** CONTROL INFORMATION.

C** IE NOD(IE,1) NOD(IE,2) NSEC NCL NPSL NSL INTG ILSTG DO (m) SRM (m)

2	2	3	36	3	2	2	1	1	1.1	0.15
---	---	---	----	---	---	---	---	---	-----	------

C** NC DX

2	0.005789
1	0.0
4	0.02411925
1	0.0
6	0.0481588
1	0.0426932
9	0.046245
1	0.0
2	0.010564
1	0.0
1	0.002365
2	0.030150
1	0.033817
1	0.0
2	0.013242

C** IWSC(IE,I), I=1,NSEC

1 2 3 4 8 12 15 16 21 25 28 33 34 35 36

C**** CONCRETE DIMENSIONS INFORMATION.

C** PART 1: NC ICTYP(1,1) ICTYP(1,2)
1 2 0

C** NSTRT NEND BTL (m) BBL (m) BTR BBR BTC BBC
1 36 12.77 12.77

C** NSTRT NEND DCTL (m) DL (m) DCTR DR DCTC DC
1 36 0.0 0.22

C** PART 2: NC ICTYP(1,1) ICTYP(1,2)
1 1 0

C** NSTRT NEND BTL (m) BBL (m) BTR BBR BTC BBC
1 3 10.33 10.33
4 8 1.51 1.51 1.2 1.2
9 28 1.2 1.2
29 33 1.2 1.2 1.62 1.62
34 36 10.33 10.33

C** NSTRT NEND DCTL (m) DL (m) DCTR DR DCTC DC
1 3 0.22 2.34
4 25 0.22 2.34 0.22 1.92746
26 33 0.22 1.92746 0.22 1.76
34 36 0.22 1.76

C** PART 3: NC ICTYP(1,1) ICTYP(1,2)
1 1 0

C** NSTRT NEND BTL (m) BBL (m) BTR BBR BTC BBC
1 36 10.33 10.33

C** NSTRT NEND DCTL (m) DL (m) DCTR DR DCTC DC
1 3 2.56 0.19
4 25 2.56 0.19 2.14746 0.19
26 33 2.14746 0.19 1.98 0.3
34 36 1.98 0.3

END-OF-GROUP

C**** TENDON PROFILE.

C** IPSL(IE,I), I=1,NPSL

1 2

C**	NSTRT	NEND	DPSL (m)	DPSR (m)	DPSC (m)
	1	30	1.145	0.661	2.1322152
	30	36	0.661	0.296	0.38725

END-OF-GROUP

C**	NSTRT	NEND	DPSL (m)	DPSR (m)	DPSC (m)
	1	30	1.605	0.769	2.2582152
	30	36	0.769	0.384	0.48025

END-OF-GROUP

C** NSTRT = section number at the beginning of the segment over which the depth of the tendon is

C** constant or varying linearly or parabolically

C** NEND = section number at the end of the same segment

C** DPSL = depth of the tendon from the top face of the member at the beginning of the segment

C** DPSR = depth of the tendon from the top face of the member at the end of the segment

C** DPSC = depth of the tendon from the top face of the member at the center of the segment

C**** LAYOUT AND PROPERTIES OF NONPRESTRESSED STEEL LAYERS.

C**	I	INSTYP(I,1)	INSTYP(I,2)	NSTRT	NEND	ASL (m2)	DSL (m)	DSR	DSC
	1	1	1	1	36	0.035	0.11		
	2	1	3	1	36	0.031	2.66066		2.17206

C**** MEMBER 3. 52.82 m span (Span 16) ! Representative geometries of the monitored sections
! of Span 16 are located in Figure 4.9. Section 20 and 5
! of MEMBER 3 correspond to the monitored midspan and
! near-bent locations.

C**** CONTROL INFORMATION.

C**	IE	NOD(IE,1)	NOD(IE,2)	NSEC	NCL	NPSL	NSL	INTG	ILSTG	DO (m)	SRM (m)
	3	3	4	39	3	2	2	1	1	1.1	0.15

C**	NC	DX
	2	0.013
	1	0.0

1 0.005771
 1 0.018229
 1 0.05
 1 0.020668
 1 0.0
 2 0.010365
 1 0.0
 2 0.0078685
 1 0.0
 10 0.068573
 1 0.0
 2 0.0078685
 1 0.0
 2 0.010365
 1 0.0
 1 0.020668
 2 0.025
 1 0.024
 1 0.0
 2 0.013

C** IWSC(IE,I), I=1,NSEC

1 2 3 4 5 8 11 15 18 20 22 25 28 31 36 37 38 39

C**** CONCRETE DIMENSIONS INFORMATION.

C** PART 1: NC ICTYP(1,1) ICTYP(1,2)
 1 2 0

C** NSTRT NEND BTL (m) BBL (m) BTR BBR BTC BBC
 1 39 12.77 12.77

C** NSTRT NEND DCTL (m) DL (m) DCTR DR DCTC DC
 1 39 0.0 0.22

C** PART 2: NC ICTYP(1,1) ICTYP(1,2)
 1 1 0

C** NSTRT NEND BTL (m) BBL (m) BTR BBR BTC BBC
 1 3 10.33 10.33
 4 8 1.62 1.62 1.2 1.2
 9 31 1.2 1.2
 32 36 1.2 1.2 1.62 1.62
 37 39 10.33 10.33

C**	NSTRT	NEND	DCTL (m)	DL (m)	DCTR	DR	DCTC	DC
	1	3	0.22	1.76				
	4	11	0.22	1.76		0.22	1.87	
	12	28	0.22	1.87				
	29	36	0.22	1.87		0.22	1.76	
	37	39	0.22	1.76				

C**	PART 3:	NC	ICTYP(1,1)	ICTYP(1,2)
		1	1	0

C**	NSTRT	NEND	BTL (m)	BBL (m)	BTR	BBR	BTC	BBC
	1	39	10.33	10.33				

C**	NSTRT	NEND	DCTL (m)	DL (m)	DCTR	DR	DCTC	DC
	1	3	1.98	0.3				
	4	11	1.98	0.3		2.09	0.19	
	12	28	2.09	0.19				
	29	36	2.09	0.19		1.98	0.3	
	37	39	1.98	0.3				

END-OF-GROUP

C**** TENDON PROFILE.

C** IPSL(IE,I), I=1,NPSL

1 2

C**	NSTRT	NEND	DPSL (m)	DPSR (m)	DPSC (m)
	1	7	0.296	0.616	0.376
	7	33	0.616	0.616	1.877
	33	39	0.616	0.296	0.376

END-OF-GROUP

C**	NSTRT	NEND	DPSL (m)	DPSR (m)	DPSC (m)
	1	7	0.384	0.704	0.464
	7	33	0.704	0.704	2.003
	33	39	0.704	0.384	0.464

END-OF-GROUP

C**** LAYOUT AND PROPERTIES OF NONPRESTRESSED STEEL LAYERS.

C** I INSTYP(I,1) INSTYP(I,2) NSTRT NEND ASL (m2) DSL (m) DSR DSC

1	1	1	1	39	0.035	0.11
2	1	3	1	39	0.031	2.17206

C**** MEMBER 4. 52.82 m span (Span 17)

C**** CONTROL INFORMATION.

C** IE NOD(IE,1) NOD(IE,2) NSEC NCL NPSL NSL INTG ILSTG DO (m) SRM (m)

4	4	5	39	3	2	3	1	1	1.1	0.15
---	---	---	----	---	---	---	---	---	-----	------

C** NC DX

2	0.013
1	0.0
1	0.005771
1	0.018229
1	0.05
1	0.020668
1	0.0
2	0.010365
1	0.0
2	0.0078685
1	0.0
10	0.068573
1	0.0
2	0.0078685
1	0.0
2	0.010365
1	0.0
1	0.020668
2	0.025
1	0.024
1	0.0
2	0.013

C** IWSC(IE,I), I=1,NSEC

1 2 3 4 8 11 15 18 20 22 25 28 31 36 37 38 39

C**** CONCRETE DIMENSIONS INFORMATION.

C** PART 1: NC ICTYP(1,1) ICTYP(1,2)

1	2	0
---	---	---

C**	NSTRT	NEND	BTL (m)	BBL (m)	BTR	BBR	BTC	BBC
	1	39	12.77	12.77				

C**	NSTRT	NEND	DCTL (m)	DL (m)	DCTR	DR	DCTC	DC
	1	39	0.0	0.22				

C**	PART 2:	NC	ICTYP(1,1)	ICTYP(1,2)
		1	1	0

C**	NSTRT	NEND	BTL (m)	BBL (m)	BTR	BBR	BTC	BBC
	1	3	10.33	10.33				
	4	8	1.62	1.62	1.2		1.2	
	9	31	1.2	1.2				
	32	36	1.2	1.2	1.62		1.62	
	37	39	10.33	10.33				

C**	NSTRT	NEND	DCTL (m)	DL (m)	DCTR	DR	DCTC	DC
	1	3	0.22	1.76				
	4	11	0.22	1.76	0.22		1.87	
	12	28	0.22	1.87				
	29	36	0.22	1.87	0.22		1.76	
	37	39	0.22	1.76				

C**	PART 3:	NC	ICTYP(1,1)	ICTYP(1,2)
		1	1	0

C**	NSTRT	NEND	BTL (m)	BBL (m)	BTR	BBR	BTC	BBC
	1	39	10.33	10.33				

C**	NSTRT	NEND	DCTL (m)	DL (m)	DCTR	DR	DCTC	DC
	1	3	1.98	0.3				
	4	11	1.98	0.3	2.09		0.19	
	12	28	2.09	0.19				
	29	36	2.09	0.19	1.98		0.3	
	37	39	1.98	0.3				

END-OF-GROUP

C**** TENDON PROFILE.

C** IPSL(IE,I), I=1,NPSL

1 2

C**	NSTRT	NEND	DPSL (m)	DPSR (m)	DPSC (m)
-----	-------	------	----------	----------	----------

1	7	0.296	0.616	0.376
7	33	0.616	0.616	1.877
33	39	0.616	0.296	0.376

END-OF-GROUP

C** NSTRT NEND DPSL (m) DPSR (m) DPSC (m)

1	7	0.384	0.704	0.464
7	33	0.704	0.704	2.003
33	39	0.704	0.384	0.464

END-OF-GROUP

C**** LAYOUT AND PROPERTIES OF NONPRESTRESSED STEEL LAYERS.

C** I INSTYP(I,1) INSTYP(I,2) NSTRT NEND ASL (m2) DSL (m) DSR DSC

1	1	1	1	39	0.035	0.11		
2	1	1	26	39	0.0151	0.11		
3	1	3	1	39	0.031	2.17206		

C**** MEMBER 5. Right Cantilever, 8.15 m span (Span 18)

C**** CONTROL INFORMATION.

C** IE NOD(IE,1) NOD(IE,2) NSEC NCL NPSL NSL INTG ILSTG DO (m) SRM (m)

5	5	6	30	3	2	3	1	1	1.1	0.15
---	---	---	----	---	---	---	---	---	-----	------

C** NC DX

4	0.051212
1	0.0
8	0.036894
6	0.041045
1	0.0
6	0.027363
1	0.0
2	0.044776

C** IWSC(IE,I), I=1,NSEC

1 3 5 6 10 14 17 20 24 27 28 29 30

C**** CONCRETE DIMENSIONS INFORMATION.

```

C** PART 1: NC ICTYP(1,1) ICTYP(1,2)
              1      2          0

C**          NSTRT  NEND  BTL (m)  BBL (m)  BTR  BBR  BTC  BBC
              1      30    12.77   12.77

C**          NSTRT  NEND  DCTL (m)  DL (m)  DCTR  DR  DCTC  DC
              1      30     0.0     0.22

C** PART 2: NC ICTYP(1,1) ICTYP(1,2)
              1      1          0

C**          NSTRT  NEND  BTL (m)  BBL (m)  BTR  BBR  BTC  BBC
              1      5    10.33   10.33
              6      27    1.51    1.51
              28     30    10.33   10.33

C**          NSTRT  NEND  DCTL (m)  DL (m)  DCTR  DR  DCTC  DC
              1      30     0.22    1.76

C** PART 3: NC ICTYP(1,1) ICTYP(1,2)
              1      1          0

C**          NSTRT  NEND  BTL (m)  BBL (m)  BTR  BBR  BTC  BBC
              1      30    10.33   10.33

C**          NSTRT  NEND  DCTL (m)  DL (m)  DCTR  DR  DCTC  DC
              1      30     1.98    0.3

                                END-OF-GROUP

```

C**** TENDON PROFILE.

```

C** IPSL(IE,I), I=1,NPSL
      1      2

C** NSTRT  NEND  DPSL (m)  DPSR (m)  DPSC (m)
      1      30    0.296    0.980    0.467

      END-OF-GROUP

C** NSTRT  NEND  DPSL (m)  DPSR (m)  DPSC (m)
      1      30    0.384    1.440    0.648

      END-OF-GROUP

```

C**** LAYOUT AND PROPERTIES OF NONPRESTRESSED STEEL LAYERS.

C**	I	INSTYP(I,1)	INSTYP(I,2)	NSTRT	NEND	ASL (m2)	DSL (m)	DSR	DSC
	1	1	1	1	30	0.035	0.11		
	2	1	1	1	20	0.0151	0.11		
	3	1	3	1	30	0.031	2.17206		

C**** MEMBER 6. Right Hinge (Span 18)

C**** CONTROL INFORMATION.

C**	IE	NOD(IE,1)	NOD(IE,2)	NSEC	NCL	NPSL	NSL	INTG	ILSTG	DO (m)	SRM (m)
	6	6	7	15	3	0	7	1	1	1.1	0.15

C**	NC	DX
	6	0.087931
	1	0.0
	4	0.102586
	1	0.0
	2	0.031035

C**	IWSC(IE,I)	I=1,NSEC
	1 4 7 11 15	

C**** CONCRETE DIMENSIONS INFORMATION.

C**	PART 1:	NC	ICTYP(1,1)	ICTYP(1,2)
		1	3	0

C**	NSTRT	NEND	BTL (m)	BBL (m)	BTR	BBR	BTC	BBC
	1	3	10.33	10.33				
	4	15	0.001	0.001				

C**	NSTRT	NEND	DCTL (m)	DL (m)	DCTR	DR	DCTC	DC
	1	15	0.0	0.375				

C**	PART 2:	NC	ICTYP(1,1)	ICTYP(1,2)
		1	3	0

C**	NSTRT	NEND	BTL (m)	BBL (m)	BTR	BBR	BTC	BBC
	1	8	10.33	10.33				

	9	15	0.001	0.001					
C**	NSTRT	NEND	DCTL (m)	DL (m)	DCTR	DR	DCTC	DC	
	1	15	0.375	0.840					
C**	PART 3: NC	ICTYP(1,1)	ICTYP(1,2)						
	1	3	0						
C**	NSTRT	NEND	BTL (m)	BBL (m)	BTR	BBR	BTC	BBC	
	1	15	10.33	10.33					
C**	NSTRT	NEND	DCTL (m)	DL (m)	DCTR	DR	DCTC	DC	
	1	15	1.215	1.065					
			END-OF-GROUP						

C**** LAYOUT AND PROPERTIES OF NONPRESTRESSED STEEL LAYERS.

C**	I	INSTYP(I,1)	INSTYP(I,2)	NSTRT	NEND	ASL (m2)	DSL (m)	DSR	DSC
	1	1	2	1	8	0.0097	0.420		
	2	1	2	1	8	0.0097	0.713		
	3	1	2	1	8	0.0097	1.006		
	4	1	3	1	15	0.0097	1.299		
	5	1	3	1	15	0.0097	1.592		
	6	1	3	1	15	0.0097	1.885		
	7	1	3	1	15	0.0120	2.178		

C**** MEMBER 7. Column 1

C**** CONTROL INFORMATION.

C** IE NOD(IE,1) NOD(IE,2) NSEC NCL NPSL NSL INTG ILSTG DO (m) SRM (m)

7 3 8 5 1 0 0 1 1 1.0675 0.0

C** NC DX

4 0.25

C** IWSC(IE,I), I=1,NSEC

1 2 3 4 5

C**** CONCRETE DIMENSIONS INFORMATION.

C** PART 1: NC ICTYP(1,1) ICTYP(1,2)

1 3 1

C** NSTRT NEND DCTL (m) DL (m) DCTR DR DCTC DC

1 5 0.0 2.135

C** N AC YC AIC

1 3.58 1.0675 2.58 GEN 1,5

END-OF-GROUP

C** N = section number

C** AC = gross area of concrete part J

C** YC = height of the centroid of the gross area of concrete part J above its bottom fiber

C** ACI = gross moment of inertia of concrete part J about an axis through its own centroid

C**** MEMBER 8. Column 2

C**** CONTROL INFORMATION.

C** IE NOD(IE,1) NOD(IE,2) NSEC NCL NPSL NSL INTG ILSTG DO (m) SRM (m)

8 4 9 5 1 0 0 1 1 1.0675 0.0

C** NC DX

4 0.25

C** IWSC(IE,I), I=1,NSEC

1 2 3 4 5

C**** CONCRETE DIMENSIONS INFORMATION.

C** PART 1: NC ICTYP(1,1) ICTYP(1,2)
1 3 1

C** NSTRT NEND DCTL (m) DL (m) DCTR DR DTC DC
1 5 0.0 2.135

C** N AC YC AIC
1 3.58 1.0675 2.58 GEN 1,5

END-OF-GROUP

C**** MEMBER 9. Column 3, Bent

C**** CONTROL INFORMATION.

C** IE NOD(IE,1) NOD(IE,2) NSEC NCL NPSL NSL INTG ILSTG DO (m) SRM (m)
9 5 10 5 1 0 0 1 1 1.0675 0.0

C** NC DX
4 0.25

C** IWSC(IE,I), I=1,NSEC

1 2 3 4 5

C**** CONCRETE DIMENSIONS INFORMATION.

C** PART 1: NC ICTYP(1,1) ICTYP(1,2)
1 3 1

C** NSTRT NEND DCTL (m) DL (m) DCTR DR DCTC DC
1 5 0.0 2.135

C** N AC YC AIC
1 3.58 1.0675 2.58 GEN 1,5

END-OF-GROUP

END-OF-GROUP ! THIS TERMINATES DATA FOR ALL ELEMENTS.

C**** SET 6: TIME-DEPENDENT PARAMETERS.

C** INTERVAL NUMBER 1

C**** CONTROL PARAMETERS.

IBC = 1 ILOAD = 1 ITPND = 1 ITMP = 0 IFORM = 0 JOUT = 7 BETA2 = 1.0

C** IBC = indicator for introduction or change in boundary conditions at the start of interval LSTG

C** ILOAD = indicator for external applied loads

C** ITPND = indicator for analysis of time-dependent effects

C** ITMP = indicator for analysis of temperature effects in interval LSTG

C** IFORM = indicator for formwork adjustment in interval LSTG

C** JOUT = indicator for type of output required in interval LSTG

C** BETA2 = coefficient representing the influence of load duration and repetition

C**** BOUNDARY CONDITIONS.

C** NBC NBD(1) NBD(2) NBD(3) BD(1) BD(2) BD(3)
1 1 2 1 0.0 1000000000.0 0.0

2	1	1	1
3	1	1	1
4	1	1	1
5	1	1	1
6	1	1	1
7	1	1	1
8	0	0	0
9	0	0	0
10	0	0	0

END-OF-GROUP

C** NBC = number of node at which boundary conditions are introduced or changed
C** NBD(1) = indicator for the boundary condition in the global x-direction
C** NBD(2) = indicator for the boundary condition in the global y-direction
C** NBD(3) = indicator for the boundary condition in the global z-direction
C** BD(1) = value of the prescribed displacement in the x-direction or stiffness of elastic support
C** BD(2) = value of the prescribed displacement in the y-direction or stiffness of elastic support
C** BD(3) = value of the prescribed displacement in the z-direction or stiffness of elastic support

C**** TIME-DEPENDENT MATERIAL PROPERTIES.

C** FOR CONCRETE:

C** APRIL

C** I EC(T0) (N/m2)
1 32.0E+9

C** I = concrete type number

C** EC = modulus of elasticity of concrete type I at the start of the current time interval LSTG

C** PHI(T, T0)

0.81 ! PHI(T, T0) can be found in Table 5.5

C** PHI = creep coefficient of concrete for current time interval LSTG

C** CHI(T, T0) S(T, T0)

0.91 -39.0E-6 ! CHI(T, T0) and S(T, T0) can be found in Table 5.5

C** CHI = aging coefficient for concrete type I during interval LSTG

C** S = shrinkage of concrete type I during interval LSTG

C** MAY

C** I EC(T0) (N/m2)
2 30.0E+9

```

C** PHI(T, T0)
0.98

C** CHI(T, T0)    S(T, T0)
0.91            -59.0E-6           ! CHI(T, T0) and S(T, T0) can be found in Table 5.5

```

```

C** COLUMN
C** I    EC(T0) (N/m2)
3      34.0E+9

```

```

C** PHI(T, T0)
0.0

```

```

C** CHI(T, T0)    S(T, T0)
0.0              0.0

```

```

C** REDUCED RELAXATION OF STEEL:

```

```

C** I    RDRLX (N/m2)
1      -16340000.0    GEN 1,3    ! RDRLX can be found in Table 5.5

```

```

END-OF-GROUP

```

```

C** I = prestressing tendon number
C** RDRLX = reduced relaxation for tendon I during the current interval LSTG

```

```

DISTRIBUTED LOADS:

```

C**	IELEM	IDIR	DIST1	DIST2 (m)	QL (N/m)	QR	QC
	1	0	0.0	0.990	225000.0		
	2	0	0.0	0.600	341000.0		
	2	0	0.600	5.600	98000.0	88500.0	
	2	0	5.600	44.3575	88500.0		83500.0
	2	0	44.3575	50.4525	83500.0		103000.0
	3	0	1.3725	7.4675	103000.0		82500.0
	3	0	7.4675	45.3525	82500.0		
	3	0	45.3525	51.4475	82500.0		103000.0
	4	0	1.3725	7.4675	103000.0		82500.0
	4	0	7.4675	45.3525	82500.0		
	4	0	45.3525	51.4475	82500.0		103000.0

5	0	1.3725	6.100	103000.0
5	0	6.100	6.700	284000.0
6	0	0.0	1.450	225000.0

END-OF-GROUP

C** IELEM = member number on which the load is applied
C** IDIR = indicator for the direction of distributed load
C** DIST1 = distance along the local axis from the starting node of member IELEM to the beginning
of the segment to which distributed load is applied
C** DIST2 = distance along the local axis from the starting node of member IELEM to the end of the
segment
C** QL = load intensity at the beginning of the segment
C** QR = load intensity at the end of the segment
C** QC = load intensity at the center of the segment

! END OF DATA FOR INTERVAL NO. 1

C** INTERVAL NUMBER 2

C**** CONTROL PARAMETERS.

IBC = 0 ILOAD = 1 ITPND = 1 ITMP = 0 IFORM = 0 JOUT = 7 BETA2 = 1.0

C**** TIME-DEPENDENT MATERIAL PROPERTIES.

C** FOR CONCRETE:

C** APRIL

C** I EC(T0) (N/m2)
1 33.7E+9

C** PHI(T, T0)

1.00 0.70 ! PHI(T, T0) can be found in Table 4.4

C** CHI(T, T0) S(T, T0)

0.91 -33.0E-6 ! CHI(T, T0) and S(T, T0) can be found in Table 5.5

C** MAY

C** I EC(T0) (N/m2)
2 33.5E+9

C** PHI(T, T0)

1.20 0.74 ! PHI(T, T0) can be found in Table 5.5

C** CHI(T, T0) S(T, T0)

0.90 -37.0E-6 ! CHI(T, T0) and S(T, T0) can be found in Table 5.5

C** COLUMN

C** I EC(T0) (N/m2)
3 34.0E+9

C** PHI(T, T0)

0.0

C** CHI(T, T0) S(T, T0)

0.0 0.0

C** REDUCED RELAXATION OF STEEL:

C** I RDRLX (N/m2)

1 -1800000.0 GEN 1,3 ! RDRLX can be found in Table 5.5
END-OF-GROUP

C**** APPLIED LOADS.

DISTRIBUTED LOADS:

C**	IELEM	IDIR	DIST1	DIST2 (m)	QL (N/m)	QR	QC
	1	0	0.0	0.990	225000.0		
	2	0	0.0	0.600	341000.0		
	2	0	0.600	5.600	98000.0	88500.0	
	2	0	5.600	44.3575	88500.0	83500.0	
	2	0	44.3575	50.4525	83500.0	103000.0	
	3	0	1.3725	7.4675	103000.0	82500.0	
	3	0	7.4675	45.3525	82500.0		
	3	0	45.3525	51.4475	82500.0	103000.0	
	4	0	1.3725	7.4675	103000.0	82500.0	
	4	0	7.4675	45.3525	82500.0		
	4	0	45.3525	51.4475	82500.0	103000.0	
	5	0	1.3725	6.100	103000.0		
	5	0	6.100	6.700	284000.0		
	6	0	0.0	1.450	225000.0		

END-OF-GROUP

! END OF DATA FOR INTERVAL NO. 2

C** INTERVAL NUMBER 3

C**** CONTROL PARAMETERS.

IBC = 0 ILOAD = 1 ITPND = 1 ITMP = 0 IFORM = 0 JOUT = 7 BETA2 = 1.0

C**** TIME-DEPENDENT MATERIAL PROPERTIES.

C** FOR CONCRETE:

C** APRIL

C** I EC(T0) (N/m2)
1 33.8.0E+9

C** PHI(T, T0)

1.15 0.90 0.72 ! PHI(T, T0) can be found in Table 5.5

C** CHI(T, T0) S(T, T0)
0.90 -35.0E-6

! CHI(T, T0) and S(T, T0) can be found in Table 5.5

C** MAY

C** I EC(T0) (N/m2)
2 33.7.0E+9

C** PHI(T, T0)

1.38 0.95 0.74 ! PHI(T, T0) can be found in Table 5.5

C** CHI(T, T0) S(T, T0)
0.89 -38.0E-6

! CHI(T, T0) and S(T, T0) can be found in Table 5.5

C** COLUMN

C** I EC(T0) (N/m2)
3 34.0E+9

C** PHI(T, T0)

0.0

C** CHI(T, T0) S(T, T0)
0.0 0.0

C** REDUCED RELAXATION OF STEEL:

C** I RDRLX (N/m2)

```
1      -1460000.0    GEN 1,3      ! RDRLX can be found in Table 5.5
END-OF-GROUP
```

```
C**** APPLIED LOADS.
```

```
JOINT LOADS:
```

```
C**  NODE    FRCX (N)  FRCY (N)  FRCZ (N)
     7      0.0      3820000.0
```

```
END-OF-GROUP
```

```
C**  NODE = the number of node at which joint loads are applied
C**  FRCX = force in the global x-direction
C**  FRCY = force in the global y-direction
C**  FRCZ = force in the global z-direction
```

```
! END OF DATA FOR INTERVAL NO. 3
```

C** INTERVAL NUMBER 4

C**** CONTROL PARAMETERS.

IBC = 0 ILOAD = 0 ITPND = 1 ITMP = 0 IFORM = 0 JOUT = 7 BETA2 = 1.0

C**** TIME-DEPENDENT MATERIAL PROPERTIES.

C** FOR CONCRETE:

C** APRIL

C** I EC(T0) (N/m2)
1 34.5E+9

C** PHI(T, T0)

1.59 1.33 1.19 ! PHI(T, T0) can be found in Table 5.5

C** CHI(T, T0) S(T, T0)
0.88 -237.0E-6

! CHI(T, T0) and S(T, T0) can be found in Table 5.5

C** MAY

C** I EC(T0) (N/m2)
2 34.5E+9

C** PHI(T, T0)

1.91 1.40 1.22 ! PHI(T, T0) can be found in Table 5.5

C** CHI(T, T0) S(T, T0)
0.85 -244.0E-6

! CHI(T, T0) and S(T, T0) can be found in Table 5.5

C** COLUMN

C** I EC(T0) (N/m2)
3 34.5E+9

C** PHI(T, T0)

0.0

C** CHI(T, T0) S(T, T0)
0.0 0.0

C** REDUCED RELAXATION OF STEEL:

C** I RDRLX (N/m2)

1 -9230000.0 GEN 1,3 ! RDRLX can be found in Table 5.5

END-OF-GROUP

! END OF DATA FOR INTERVAL NO. 4

Appendix H

Recommendations for Improvement of Experimental Procedures

- Since the actual bridge structure varies significantly from the test cylinders in both size (V/S) ratio and shape, the effects of environmental conditions are likely to be different. While adjustments can be made to consider this difference through the use of reduction factors applied to the measured material properties the results are gross approximations and do not provide accurate estimates. In the current study this was done by multiplying the measured values by a reduction factor, calculated by taking the ratio of the CEB-FIP [10] produced material properties for the bridge and test specimen. This method intrinsically assumes that the specifications can provide accurate predictions of creep and shrinkage, or that both methods provide the same level of error. The use of specimens with larger V/S ratios would provide the most straight-forward solution and it is recommended that a pilot study be conducted to accurately determine the difference in response based on specimen size and configuration, especially as a function of environmental exposure conditions.
- If specimens of the same size as those used in this investigation are to be used in further research, it is recommended that a set of specimens be sealed immediately after their removal from the forms so as to effectively create a set of specimens with an infinite V/S . As the influence of V/S ratio decreases with size, this set would provide creep and shrinkage that is more indicative of the actual materials characteristics in the bridge. The additional use of a set of unsealed specimens would provide the other extreme set of bounds on the maximum creep and shrinkage that could occur.
- In order to eliminate error due to the manual operation of DEMEC gauges, use of long gauge resistance strain gages bonded to the concrete or other automated methods of measurement are recommended.

- Measurement using an automated system which would enable taking a greater number of data points at pre-set intervals is also recommended for future use. This would not only reduce the level of uncertainty regarding changes between operators but would also provide for greater tracking of changes with changes in environment (temperature, humidity etc.) and age.
- Measurement devices should be used to enable acquisition of changes in materials characteristics right from the outset. Although shrinkage occurring prior to prestressing does not influence the prestress loss, it is an important component of the total amount of shrinkage that occurs during the life of the concrete and does induce stresses in the concrete due to the restraints imposed by the existence of reinforcement, and hence needs to be considered.
- Instrumentation placed in the bridge should be activated to monitor the strains from a period beginning with the pouring of concrete. The temperatures developed in the concrete during hydration should be also be monitored. Although these high temperatures are significantly more influential on the loss of prestress in pre-tensioned members the acquisition of these temperatures could be useful in subsequent research on long-term response. Similarly, the strain that develops in the member prior to loading should also be determined. The reinforcement in a bridge provides restraint to the shrinking of concrete, limiting the amount of shrinkage that occurs. Careful selection of the placement of the gages in the bridge would provide data on the magnitude of strain that does occur, allowing a better understanding of materials response on structural behavior.
- Wooden, concrete, or plastic standoffs rather than Styrofoam should be used for the placement of gauges since the Styrofoam is easily dislodged and damaged during pouring of concrete.

References

1. Aboumoussa, W., Iskander, M. "Thermal Movements in Concrete: A Case Study of Multistory Underground Car Park," *Journal of Materials in Civil Engineering*, V. 15, No. 6, November-December 2003, pp.545-553.
2. American Association of State Highway and Transportations Officials, "AASHTO-LRFD Bridge Design Specifications," Third Edition, Washington, DC, 2004.
3. ACI Committee 209, "Prediction of Creep, Shrinkage and Temperature Effects in Concrete Structures (ACI 209R-92)," American Concrete Institute, Farmington Hills, Michigan, 1997.
4. Bažant, Zdenek P., Wang, Tong-Sheng, "Practical Prediction of Cyclic Humidity Effect in Creep and Shrinkage of Concrete," *Materials and Structures*, No. 106, 1985, pp. 247-252.
5. Bažant, Zdenek P., "Creep and Shrinkage Prediction Model for Analysis and Design of Concrete Structures - Model B3," *Materials and Structures*, RILEM, Paris, V. 28, No. 180, 1995, pp. 357-365.
6. Bažant, Zdenek P., "Justification and Refinements of Model B3 for Concrete Creep and Shrinkage – 1: Statistics and Sensitivity," *Materials and Structures*, RILEM, Paris, V. 28, No. 181, 1995, pp. 415-430.
7. Bažant, Zdenek P., "Justification and Refinements of Model B3 for Concrete Creep and Shrinkage – 2: Updating and Theoretical Basis," *Materials and Structures*, RILEM, Paris, V. 28, No. 182, 1995, pp. 488-495.
8. Caltrans Bridge Design Specifications, April 2000.
9. Canadian Highway Bridge Design Code, CAN/CSA-S6-00, Rexdale, Canada, 2000.
10. Comite Euro-International du Beton – Federation Internationale de la Precontrainte, "Model Code for Concrete Structures," CEB-FIP MC 90, London, UK, 1993.
11. CR10X Data Acquisition System, Campbell Scientific, Inc.
12. Gardner, N. J. and Lockman, M. J., "Design Provisions for Drying Shrinkage and Creep of Normal-Strength Concrete," *ACI Materials Journal*, V. 98, No. 2, March-April 2001, pp. 159-167.
13. Ghali, A. "A Unified Approach for Serviceability Design of Prestressed and Nonprestressed Reinforced Concrete Structures," *Journal of the*

- Prestressed Concrete Institute*, V. 30, No. 2., March-April 1986, pp. 118-137.
14. Ghali, A., "Monitoring of Deflections of the Confederation Bridge," *Proceedings of the Annual Conference of the Canadian Society for Civil Engineering*, Sherbrooke, Quebec, V. 1, 1997, pp. 161-166.
 15. Ghali, A., Megally, S., Azarnejad, A., Elbadry, M., "Monitoring of Concrete Creep and Shrinkage of the Confederation Bridge," *Proceedings of the Annual Conference of the Canadian Society for Civil Engineering*, Regina, Saskatchewan, V. 4., 1999, pp. 141-150.
 16. Ghali, A., Elbadry, M. M., *Manual for Computer Program Crack*, Research Report No. CE85-1, 1985 Department of Civil Engineering, The University of Calgary, Alberta, Canada.
 17. Ghali, A., Elbadry, M., Megally, S., "Two-year deflections of the Confederation Bridge," *Canadian Journal of Civil Engineering*, V. 27, 2000, pp. 1139-1149.
 18. Ghali, A., Favre, R., and Elbadry, M. M., "Concrete Structures: Stresses and Deformations," Third Edition, Spon Press, London and New York, 2002.
 19. MacGregor, James G., Wight, James K., *Reinforced Concrete: Mechanics and Design*, Fourth Edition, Prentice Hall, New Jersey, 2004.
 20. Massicotte, B., Picard, A., "Monitoring of a Prestressed Segmental Box Girder Bridge During Strengthening," *PCI Journal*, V. 39, No. 3, May-June 1994, pp. 66-80.
 21. NCHRP Report 496, "Prestress Losses in Pretensioned High-Strength Concrete Bridge Girders," Washington, D. C., 2003.
 22. Nilson, A. H., *Design of Prestressed Concrete*, Second Edition, John Wiley and Sons, New York, 1987
 23. Precast/Prestressed Concrete Institute, "Precast/Prestressed Concrete Bridge Design Manual," Sixth Edition, Illinois, 2003.
 24. Russell, H. G., Shiu, K. N., Gamble, W. L., Marshall, V. L., "Evaluation and Verification of Time-Dependent Deformations in Posttensioned Box-Girder Bridges," *Transportation Research Record 871*, National Academy of Sciences, Washington, D. C., 1982.
 25. Saiidi, M. S., Shields, J., O'Connor, D., Hutchens, E., "Variation of Prestress Force in a Prestressed Concrete Bridge During the First 30 Months," *PCI Journal*, V. 41, No. 5, September-October 1996, pp. 66-72.

26. Shahawy, M. A., Arockiasamy, M. "Analytical and Measured Strains in Sunshine Skyway Bridge I," *Journal of Bridge Engineering*, V. 1, No. 2, May 1996, pp. 76-86.
27. Shahawy, M. A., Arockiasamy, M. "Analytical and Measured Strains in Sunshine Skyway Bridge II," *Journal of Bridge Engineering*, V. 1, No. 2, May 1996, pp. 87-97.
28. VW Embedment Strain Gage, 52650199, Slope Indicator Company, February 5, 2003.
29. Youakim, S. A., Karbhari, V. M., Ghali, A., Hida, S. E., "Prediction of Long-Term Prestress Losses," *PCI Journal*, V. 52, No. 2, 2007, pp. 116-130 (Also SSRP2006/21 titled "A Simplified Method for Prediction of Long-Term Pre-Stress Loss in Post-Tensioned Concrete Bridges")